Cybernetics of tunnel-in-the-sky displays

Max Mulder

Cybernetics of
Tunnel-in-the-Sky Displays

PROEFSCHRIFT

ter verkrijging van de graad van doctor
aan de Technische Universiteit Delft,
op gezag van de Rector Magnificus, prof. ir K.F. Wakker,
in het openbaar te verdedigen ten overstaan van een commissie,
door het College voor Promoties aangewezen,

op dinsdag 30 november 1999 te 16.00 uur

door

Max MULDER

vliegtuigbouwkundig ingenieur

geboren te 's-Hertogenbosch

Dit proefschrift is goedgekeurd door de promotoren:
Prof. dr ir J.A. Mulder
Prof. dr ir H.G. Stassen

Samenstelling promotiecommissie:

Rector Magnificus,	voorzitter
Prof. dr ir J.A. Mulder,	Technische Universiteit Delft, promotor
Prof. dr ir H.G. Stassen,	Technische Universiteit Delft, promotor
Prof. ir F.J. Abbink,	Nationaal Lucht- en Ruimtevaart laboratorium, Amsterdam
Prof. dr J.M. Flach,	Wright State University, USA
Prof. dr ir A.J. Grunwald,	Technion Haifa, Israel
Prof. dr J.J. Koenderink,	Universiteit Utrecht
D.T. McRuer P.E.,	Systems Technology Inc., USA
dr ir P.A. Wieringa,	Technische Universiteit Delft, reserve

Welk voordeel heeft de werker van datgene waarvoor hij zich aftobt?

voor Hans

Summary

The increasing number of air traffic control related delays in Europe and the United States indicates a *capacity problem* of the Air Traffic Management (ATM) system that is currently operational. A much more efficient use of airspace is required to handle the present and future volumes of commercial air traffic. An important step towards a flexible system that utilizes the airspace more efficiently would be to abandon the principle of fixed airways. Aircraft should be allowed to follow basically *any* trajectory as long as separation between aircraft is assured. To guarantee flight safety, these trajectories must be followed with a high level of precision in four dimensions including time. Tracking four-dimensional trajectories will put additional task demand load on the pilot and demands adequate levels of pilot situation awareness. Presently, research is ongoing to develop an improved cockpit human-machine interface that supports the crew in conducting the 4-D aircraft navigation, guidance and control tasks of future air traffic management systems.

Consensus is growing that the flexibility gained with the introduction of programmable cockpit displays in the 1980s must be exploited to the full extent. The current practice to have different two-dimensional presentations of the aircraft guidance and navigation situation must be abandoned. A future primary flight display presents the aircraft guidance and navigation situation in a way that is intuitively understandable, that supports the pilots' situation awareness, and that is compatible with the various tasks imposed by the future ATM system. A strong candidate is the *Tunnel-in-the-Sky display*, a perspective flight-path display that shows the reference trajectory in a synthetic three-dimensional world. The usefulness of the tunnel display in the pilot manual control task of guiding the aircraft along the curved trajectories of the future is the subject of this thesis.

The mainstream of tunnel display research is confined to empirical comparisons of the tunnel display with conventional displays in terms of pilot performance and workload. The approach taken in the present theoretical and experimental study of the tunnel display is original and new as it is conducted from the perspective of *cybernetics*. A four-stage methodology is followed to study the fundamental characteristics of pilot/display interaction, centered around a theoretical analysis of information, in particular the information used for control. The *first* stage of the approach consists of an analysis of a pilot's tasks and the information needs to fulfil these tasks. The *second* stage investigates the optical cues conveyed by the display that, theoretically, are available to the pilot and that, practically, can be used by the pilot. The *third* stage consists of empirical studies into

the relative effectiveness of the various cues. The *fourth* stage attempts to describe the experimentally measured pilot behaviour with mathematical models.

The task analysis reveals that, basically, two tasks can be distinguished in the pilot manual control task of following a complex trajectory. First, in the *regulation* task the trajectory remains the same, there is no need for anticipating any changes, and the only pilot concern is to maintain a stationary tunnel image, i.e. compensate for changes in this image. The two main reference conditions are the aircraft stationary flight conditions of *recti-linear* and *curvi-linear* motion. Second, in the *anticipation* task the trajectory changes and the pilot must conduct a transition manoeuvre between the two reference conditions.

The information analysis is conducted within the paradigm of Gibson's ecological approach to visual perception. The principal hypothesis is that *the main stimulus of the pilot when moving through a limited environment as depicted by the tunnel display is that of an approach to a surface.* The information conveyed by the tunnel display is analyzed for the recti-linear and curvi-linear motion conditions. In both conditions the aircraft position and attitude relative to the trajectory can be perceived through the *static* optical cues of *linear perspective.* The aircraft flight-path, velocity, and temporal status relative to the trajectory can be perceived through the *dynamic* cues of *motion perspective.* The most important cues conveyed by the tunnel display are those of *optical splay* and *optical density.* A generic method is developed which allows mathematical expressions to be derived that describe the optical cues in terms of the properties of the tunnel geometric design, the properties of the perspective projection, and the aircraft motion states. The characteristics of the cues in presenting the aircraft state to the pilot can then be examined, providing insight into which cues are important to the pilot and which cues are not.

The theoretical task and information analyses provide substantial insight into how the tunnel display geometric design variables could affect pilot behaviour. The hypothesized relationships resulting from this analysis can be extremely useful in the definition of human-centered tunnel display design guidelines. To examine the validity of the theoretical hypotheses and to provide empirical evidence for them, a number of pilot-in-the-loop *experiments* are conducted. In each experiment, the objective is to obtain an understanding on how manipulating a selected set of tunnel display design variables affect pilot behaviour, and they are designed to allow this behaviour to be analyzed not only in terms of performance, but also in a more control-theoretical sense. This is not a trivial procedure. The pilot model identification methods are limited to determining only the pilot loop closures of the aircraft attitude, flight-path and position, yielding a minimal representation of pilot control behaviour. The model-based analysis focuses on examining the *adaptation* of the pilot models to the different experimental conditions: the models are used as *tools* to study the effects of varying tunnel display designs on pilot control behaviour.

Three experiments are described that examine the effects of manipulating some of the main tunnel display design variables, such as the *tunnel size*, the *viewing volume* and the presence of *flight-path vector* symbology. Another three experiments are described that investigate the fundamental characteristics of the *tunnel geometrical design* in the two pilot regulation tasks of following a trajectory that is either straight or circular, and in

the pilot anticipation task of conducting a transient curve-interception manoeuvre.

The *tunnel size* display design variable scales the magnitude with which the aircraft position error relative to the trajectory is presented on the display. It is shown that reducing the tunnel size yields an improved path-following performance at the cost, however, of higher levels of pilot control activity and workload. A model-based analysis shows that a tunnel that is too small yields an ill-damped control situation, and it is recommended that robustness margins should be incorporated in the choice of a tunnel size, based on the tradeoff between path-following performance and closed loop stability.

The tunnel display presents preview information about the reference trajectory to be flown. Limiting the display *viewing volume* to a particular viewing distance forces pilots to focus on that restricted part of the trajectory. The dynamics of the presented part of the trajectory ahead change as a function of two variables, the viewing distance and the aircraft velocity, forcing pilots to *adapt* their control behaviour as a function of these two variables. The experimental data confirm the hypotheses that, first, dependent on the aircraft velocity, pilots *prefer* a particular viewing distance over others, and second, that the preferred viewing distance increases for larger velocities.

An advantage of electronic displays is that they can be augmented with synthetic symbology designed to improve pilot performance. The *flight-path vector* (FPV) symbol presents the aircraft direction of motion. Without the FPV, pilots are found to be unable to perceive the direction of motion relative to the tunnel trajectory well enough to use this information for purposes of control. When the FPV symbol is presented, pilots adopt a direct feedback of the flight-path angle error, yielding improved path-following performance and lower effort ratings. A pilot's use of the FPV is harmed, however, when the bandwidth of the turbulence component acting on the aircraft flight-path increases.

The relative usefulness of the main optical information sources depicting the aircraft position error, *optical splay* and *optical density*, is investigated in the pilot regulation task of controlling the aircraft recti-linear motion along a straight trajectory. It is shown that whereas performance with a display conveying only optical splay information is unaffected by the aircraft longitudinal motion along the trajectory, it decreases when both the aircraft vertical and lateral motion must be controlled simultaneously. In contrast, performance with a display conveying only optical density information decreases when the aircraft traversing motion was active, whereas the effects of the control task dimensions are smaller than for the splay-only display. The principal virtue of the optical splay relative to the optical density is concluded to be the fact that the splay angle is a property of the *whole* line: it has a constant *gain* independent of where the pilot is looking at.

In a companion study the effectiveness of splay and density information in the task of controlling the aircraft curvi-linear motion along a circular trajectory is investigated. It is shown that since the quality of the optical information in curved tunnels is worse as compared to that in straight tunnels, the task of controlling the aircraft along circular trajectories is markedly more difficult. The aircraft direction of motion *must* be perceived from the cues of motion perspective, at smaller viewing distances. The optical splay angles are found to be important for the perception and control of the aircraft flight-path relative

to the trajectory. Due to the trajectory curvature, the aircraft position and heading relative to the trajectory is not accurately presented by the display. These *presentation biases* are large in particular for the splay angles and it is found that the density information is essential for the perception and control of the aircraft position relative to the trajectory. The aircraft transition manoeuvre between a straight and a curved section of the trajectory is the only *anticipation* task addressed in this thesis. The investigation is centered around the pilot *timing* of the manoeuvre. Two hypotheses are stated. First, pilots could use time-to-contact (TTC) information from the expanding tunnel frames, a *time*-based approach. Second, pilots could focus on the motion of an emergent feature of the tunnel outline, the tangent point, a *distance*-based approach. These hypotheses could both be confirmed experimentally. Since the TTC information is independent of the geometric properties of the tunnel as well as those of the curve, the TTC-strategy is context-independent and results in a robust pilot strategy to time the curve-interception manoeuvre.

The experiments show that the cybernetic, information-centered approach is successful in pin-pointing the important characteristics of pilot/display interaction. The use of models provides additional insight into the manner in which pilots adapt their control behaviour to the experimental conditions, complementing the traditional performance and workload-oriented analysis of human behaviour. Nonetheless, the limitations of adopting a model-based approach are clearly identified. First, only the *integral* pilot response to the optical cues conveying an aircraft motion referent can be determined. Since a generic tunnel display always shows redundancy in the optical information, the added value of using models in determining cue dominance hierarchies is small. Second, in multi-loop vehicular control tasks the number of ways in which pilots can adapt their control behaviour is large. This often results in considerable differences between pilots in their control behaviour, especially in the inner loops, which makes it hard to generalize the results.

Although the research focuses on the tunnel display, this thesis provides an overview of the ins and outs of adopting a model-based approach. An experimental methodology is developed in an attempt to *integrate* the model-based approach with the approach of collecting mainly pilot performance-related data. It describes how experiments must be designed with the objective of collecting data which can be used for a control-theoretic analysis. The limitations of the non-parametric identification methods in multi-axis, multiple loop tracking tasks are described. It is shown that the bias and variance of the estimated pilot frequency responses can be computed analytically only for single-axis tracking tasks with a parallel pilot model structure. The use of criterion functions, in both the frequency and the time domain, in the parametric identification methods is exemplified. A method to compute the Cramer-Rao lower bound of the variance in the estimated pilot model parameter vector is derived. The application of two prominent modelling techniques, a multi-loop version of the crossover model and the optimal control model, is described. It is shown that the over-parameterization of the latter model hampers its use considerably.

Contents

Chapter 1

Introduction

1.1 The future of air traffic management

The management of air traffic will change radically in the near future. The increasing number of air traffic control related delays in Europe and the United States is symptomatic for the *capacity problem* of the Air Traffic Management (ATM) system that is currently operational. With a predicted 200-300% increase in passenger transportation volume before 2015 this problem will become a threat for the aviation community from both an economic and a safety point of view (Abbink, 1996). The main cause of the capacity problem is the *inflexibility* of the present air traffic management system. This system dates from the 1950s and was developed to handle the air traffic at much lower density levels than there are today. It consists of a network of fixed routes called *airways* that, in most cases, connects the ground-based radio-navigation beacons. En-route as well as near large airports the air traffic is channeled by the Air Traffic Control (ATC) authorities along these fixed routes with a prescribed vertical and lateral *separation*, minimizing the potential for conflicts.[1] As a consequence, the current system requires compliance of all airspace users to a concept of fixed airways and reporting points, with aircraft often flying at prescribed velocities from one fix to the next, and with only a limited number of available standardized flight levels.

In contrast to the inflexibility of the present air traffic management system stands the increased functionality of the on-board computer systems of modern commercial aircraft. The majority of these aircraft is equipped with Area Navigation (RNAV), a function of the Flight Management System (FMS). RNAV operations allow aircraft to fly *efficient*

---

[1]En route aircraft follow *airways*. Departing aircraft follow a Standard Instrument Departure (SID) connecting the takeoff runway with the appropriate airway. Approaching the airport, aircraft follow a Standard Terminal Arrival Route (STAR) to the landing runway. The final leg of a STAR at the final approach fix may often be guided by the Instrument Landing System (ILS) that marks a single straight-in approach path to the runway. In a *precision approach*, *all* incoming aircraft must intercept and follow the fixed ILS approach path, Fig. 1.1.
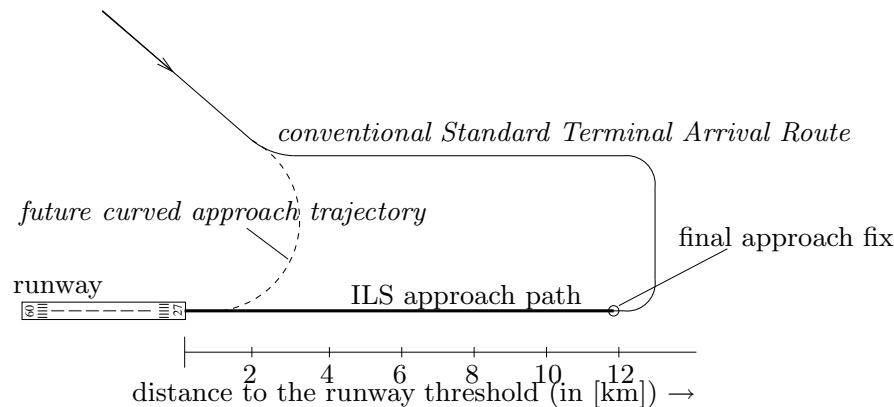
Figure 1.1: Top view of a conventional STAR followed by a straight-in ILS final approach path, and a curved approach path of the future (adopted from Jensen (1978)).

(fuel/time/economy) trajectories directly to their point of destination, in any airspace within prescribed accuracy tolerances (Kayton & Fried, 1997). In practice, however, in most cases nowadays the execution of the efficient and direct FMS trajectories is frustrated by interventions from the ATC authorities. It is obvious that the flexibility to operate efficiently in much of the world's airspace is sacrificed for purposes of safety (separation). A number of measures is currently under investigation that provide the air traffic control much more freedom in managing the flow of air traffic. An important objective is to abandon the principle of fixed airways. En route, the new system should allow aircraft to basically fly *any* trajectory, as computed by the FMS RNAV functions, as long as the separation between aircraft is assured. This is known as *Free Flight* (RTCA, 1995). Near airports, the new system should also allow aircraft to follow efficient arrival procedures, for instance by intercepting the final approach segment just shortly before the runway threshold (Fig. 1.1). Following such *efficient* trajectories, however, *safety* must still be guaranteed, not only with respect to the own and nearby planes but also with respect to the ATM situation as a whole. Efficiency and safety are the keywords of the **Future Air Navigation System** (FANS) that is being advocated by the ICAO countries.

Technological advances in the fields of Communication, Navigation and Surveillance (CNS) are developed to allow the introduction of an ATM system that satisfies the current and future demands of efficiency, safety and capacity. The two principal technologies of the future CNS-ATM system are the *satellite-based* CNS technologies providing global coverage, and the application of *digital data-links*. With data-link the airborne FMS computers and the ground-based ATM computers may then be connected, allowing these computers to literally *negotiate*, in real-time, all details about a certain trajectory, in both space and time, that best satisfy the demands from the own aircraft (economy, passenger comfort) and the constraints imposed by ATM (separation from the other traffic, airspace capacity). This so-called *Trajectory-Negotiation Process* (TNP) yields optimal trajectories for all airspace users. To comply with – and if possible, to reduce the constraints of

– the separation demands between aircraft, it is foreseen that in following the planned trajectory, the constraint of *time* will be of much more importance than so far, allowing a much closer sequencing of approaching aircraft. The future ATM environment incorporates *4-D Navigation*, where aircraft obtain clearance for manoeuvering within a limited volume of airspace, the *aircraft performance shell* or *bubble-in-the-sky*, that moves along the prescribed trajectory in time. Although the time constraints themselves are not new, a stricter compliance to these constraints can be expected. When the ATM situation as a whole is carefully planned, perhaps even hours or days ahead in time, and accurately controlled in space *and* in time, the ATC can be dealt with on a *strategic* level. Then, aircraft would indeed be allowed to follow the efficient FMS trajectories, while at the same time satisfying the constraints due to the other traffic.

The technology needed to implement the 4-D future air navigation system is available and a global effort is conducted to make it operational before 2015 (Galotti Jr., 1998). With the introduction of the FANS technologies the efficiency of air traffic management is expected to increase considerably. Allowing more flexible trajectories to be flown and reducing the separation between aircraft yields an increase in the capacity of the available airspace. Safety must be enhanced through a well-considered implementation and an accurate execution of the 4-D trajectories. An improved cockpit Human-Machine Interface (HMI) will have to be introduced that presents the data in an organized and intuitive way, supporting the crew's situation awareness. It should allow the crew to quickly understand the consequences of the trajectory negotiation process and it should support them in executing the prescribed 4-D trajectories, either manually or as supervisors of the automatic flight control systems (De Vriendt, Mulder, & van Paassen, 1999).

1.2 The human factor

The introduction of flexible 4-D navigation procedures in the future CNS-ATM environment has considerable impact on all members of the aviation community, not in the least the pilots (Galotti Jr., 1998). It is common knowledge that, even without the dramatic changes in future ATM demands, considerable problems already exist in the modern cockpit environment (Billings, 1997). Therefore, before discussing the optional developments, first the current status of the cockpit HMI will be discussed.

Flight crew error   "*The majority of worldwide, commercial jet transport accidents from 1959 through 1991 have involved multiple causes. Flight crew error was the most dominant cause and persisted in about 65 percent of fatal crashes.*" (RAND, 1993). The statistics of air transportation accidents further show that not all phases of flight are equally safe. Fig. 1.2, charting the percentage of fatal accidents against the percentage of total flight time, shows that although operations *near the ground* take less than 20% of flight time, they account for more than 75% of all fatal accidents. Apparently, this is where the most critical – i.e. less error-tolerant – aircraft manoeuvres are executed. Not surprisingly, the phase of flight and the occurrence of unexpected events like system
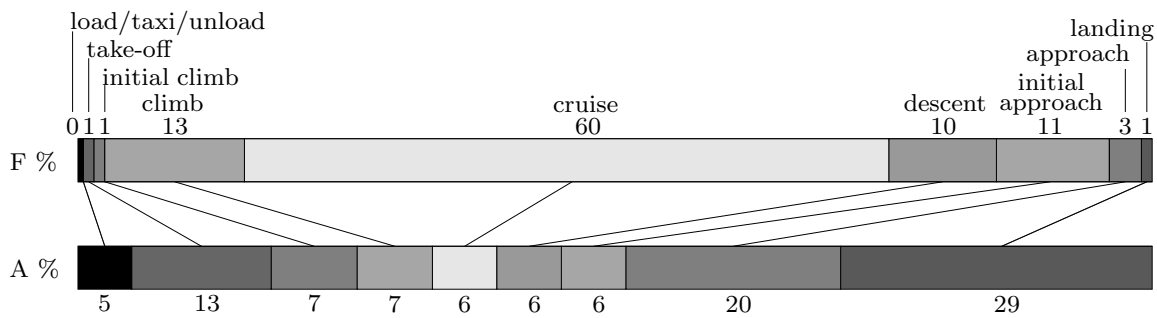
Figure 1.2: Percentage of fatal accidents (A%) of civil jet aircraft versus flight phase percentage (F%) of an average flight duration of 1.5 hour. Period: 1959-1991 (RAND, 1993). Accidents caused by terrorism, sabotage or military actions are excluded.

failures, constitute the two principal factors affecting the task demand load and the pilot mental workload (Wiener, 1985; Ritter, 1993).

The origins of flight-crew error *"The traditional dream ... has been to solve the problem of human error by eliminating its source."* (Wiener & Curry, 1980). With the progress of technology, many of the functions on the flight-deck of commercial aircraft that were previously performed manually have become automated. The introduction of increasing levels of automation has shifted the pilot's role to that of a system *supervisor* and the nature of the pilot tasks has shifted from manipulative tasks to cognitive tasks.[2] The philosophy behind automating the pilot's skill-based and rule-based control and manipulation tasks is twofold. First, automatons can perform these tasks faster and more accurate with all its benefits in terms of reliability, performance, economy and safety. Second, by automating parts of the pilot's task the task demand load reduces considerably, allowing pilots to allocate their resources to conduct tasks at the knowledge-based level of cognitive control, such as flight planning and problem solving. The division of tasks between humans and automated systems is not a trivial matter (Sheridan, 1991).

Consider the two types of automation that are currently operational on the flight-deck that affect the pilot's guidance and navigation tasks. In the baseline situation, illustrated in Fig. 1.3(a), a pilot is in direct *manual* control of the vehicle. The mismatch between the current and the desired flight situation determines the pilot control strategy and the control actions applied to the aircraft. The pilot mentally constructs the present and future guidance situation from the cockpit displays, a task that is – with the current generation of displays – rather difficult, contributing to the pilot mental workload, and leading to an

---

[2]A widely accepted framework for describing the mechanisms humans have for processing information is the Skills-Rules-Knowledge (SRK) paradigm of (Rasmussen, 1983). According to the SRK-taxonomy, information can be interpreted in three mutually exclusive ways – signals, signs and symbols – and the way in which information is interpreted determines which of the three levels of cognitive control is activated: (i) *Skill-Based* Behaviour (SBB), a repertoire of automated behavioural patterns; (ii) *Rule-Based* Behaviour (RBB), a set of cue-action mappings, and (iii) *Knowledge-Based* Behaviour (KBB), describing problem solving operations on a symbolic representation (Vicente & Rasmussen, 1992).
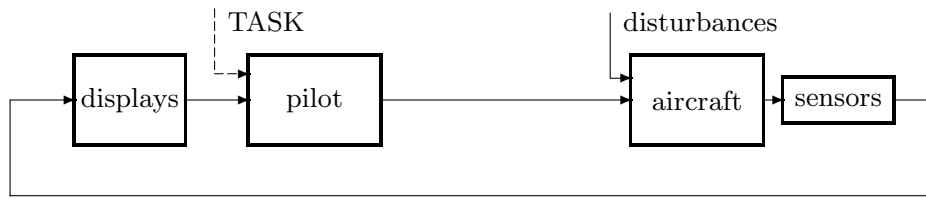
(a) manual control, no augmentation
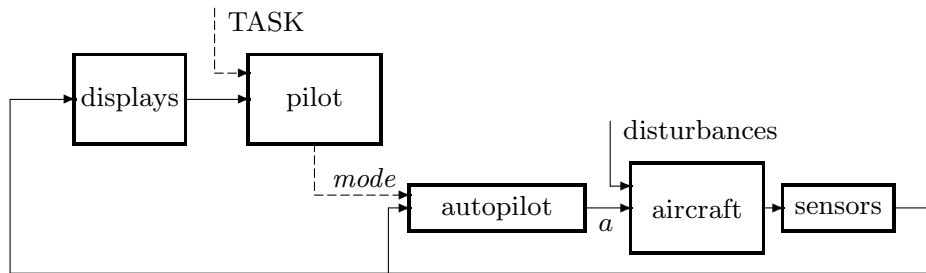
(b) supervisory control, *control augmentation*
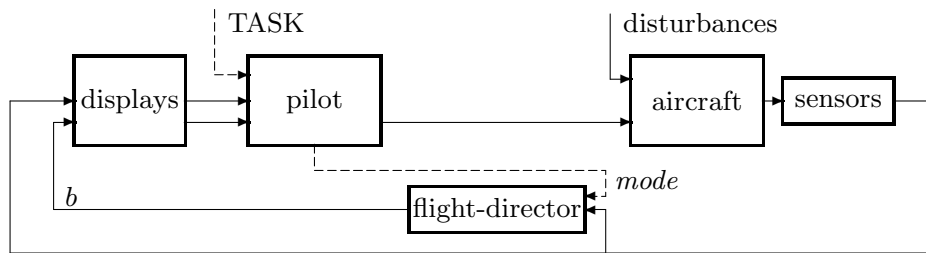
(c) manual control, *display augmentation*

Figure 1.3: Different types of flight guidance automation.

unsatisfactory path-following performance (Wilckens, 1971; Wiener, 1985; Oliver, 1990; Foyle, Ahumada, Larimer, & Sweet, 1992). To increase performance and to reduce mental workload, the pilot has two alternatives, both involving automated systems. When the Autopilot (AP) is engaged (Fig. 1.3(b)), the pilot only has to decide upon the most appropriate AP-mode and setting for the given guidance task demands, i.e. the pilot defines the set-points of the automatic controllers. The control of the aircraft is handed over to the autopilot, the functioning of which is monitored by the pilot. This situation is referred to as *control augmentation* (Kelley, 1967) and is similar to the common modes of automation found in industrial plants. The alternative of using the autopilot is the Flight-Director (FD) which can be regarded as a hybrid form of automation that is a rather unique feature of the cockpit. Again, the pilot engages the FD and decides upon the most appropriate FD-mode and setting for the guidance sub-task at hand. The FD has the same functionality as the AP. However, whereas the AP output signals (*a* in Fig. 1.3(b)) are used to control the aircraft control surfaces, those of the FD (*b* in Fig. 1.3(c)) are *steering commands* that are presented to the pilot. When the pilot successfully follows these commands

by moving the control manipulator, the constraints of the guidance sub-task as specified with the engaged FD-mode are satisfied. This situation is referred to as *display augmentation*. By engaging the FD in a given mode, the pilot orders an automaton to assemble and process all information relevant to the task into a set of steering commands that can be directly applied to the aircraft, without any cognitive processing. Today, most approaches and landings of large commercial aircraft are conducted either manually, using the flight-director, or automatically, using the autopilot while the FD is used for monitoring.[3]

In recent years, concerns are growing about whether the original cockpit automation objectives are achieved, but also about the desirability of these objectives in the first place. It appears as if automation has indeed reduced the pilots' manual workload, at the cost, however, of increasing their *mental* workload (Tanaka & Matsumoto, 1986; Sheridan, 1991). Regretfully, it has become clear that humans do not perform very well in monitoring tasks (Wiener & Curry, 1980). The changing role of pilots is also suspected to *remove them from the control loop*, decreasing their ability to keep track of the aircraft current situation – a phenomenon coined *Situation Awareness* (SA) (Endsley, 1995) – and the aircraft future situation with respect to the navigation constraints – known as *Navigation Awareness* (NA). Another concern is the loss in pilot proficiency in conducting his task manually when automation fails (Wiener & Curry, 1980). Furthermore, such failures of automation – known as the *automation deficit* – lead to peak levels of pilot mental workload (Sheridan, 1991). Finally, several studies reveal that the flight-deck automation has reached a level of complexity that makes it difficult for a pilot to understand the functional structure underlying the automated system's actions (Sarter, 1991). Pilots are often unaware of – or even surprised by – transitions between different automation modes, a phenomenon coined *Mode Awareness* (MA) (Sarter & Woods, 1994). Thus, although there are many benefits to be derived from automation, the experience gathered in the last two decades indicates that new and unanticipated human factors problems emerge: *"It is highly questionable whether total system safety is always enhanced by allocating functions to automatic devices rather than human operators, and there is some reason to believe that flight-deck automation may have already passed its optimum point."* (Wiener & Curry, 1980).

Human-centered automation   Recent developments in automation have eliminated some causes of human error at the cost, however, of introducing others. Since it is not foreseen in the near future that pilots will be eliminated from the flight-deck, future developments should lead to automation that is *robust* – error-resistant and error-tolerant including technical and human errors – and concerned about the specific capabilities and deficiencies of the human pilot. This is known as *Human-Centered Automation* (HCA) (Billings, 1991), of which the main guidelines are collected in Table 1.1. In a human-centered interface design, the crew is the central element in control and management of the system, and automation is present to assist it (ICAO, 1992). Examining these guidelines

---

[3]In this respect, the company philosophy of Royal Dutch Airlines (KLM) is that of all flights one-third of the landings should be done manually (i.e. using the FD), one-third by the automated systems, and one-third by choice. Informal communication with KLM pilots, however, reveals that – under the guise of maintaining their flying skills – at least 90 percent of all landings are still conducted *manually*.

Table 1.1: Guidelines of human-centered automation (Billings, 1991).

Humans must remain in command of flight and air traffic operations
Automation can assist by providing a range of management options
Human operators must remain involved
Automation can assist by providing better and more timely information
Human operators must be better informed
Automation can assist by providing explanations of its actions and intentions
Human operators must do a better job of anticipating problems
Automation can assist by monitoring trends and providing decision support
Human operators must understand the automation provided to them
Designers can assist by providing simpler, more intuitive information
Human operators must manage all of their resources effectively
Properly designed and used, automation can be their most useful resource

make clear that the role of the pilot as a system monitor must become less passive and more interactive with the automated systems. The HCA guidelines strongly suggest that future developments in cockpit automation must be *directed towards methods of bringing pilots back into the loop* (Wiener, 1985). One of the main avenues to improve current cockpit interfaces is to provide information that supports the pilot in remaining on top and ahead of the situation (NASA/DoD/FAA, 1995). The cockpit human-machine interface should be re-designed to allow and support HCA. In this respect, a design philosophy that is gaining support for interface designs of complex work environments is that of Ecological Interface Design (EID). EID is based on Rasmussen's SRK-paradigm and has two goals. First, *the interface should not contribute to the difficulty of the task* by forcing a higher level of cognitive processing than required by the task demands. Second, *the interface should support the entire range of activities that operators are faced with*, i.e. it should support all three levels (SBB/RBB/KBB) of cognitive control (cf. Vicente & Rasmussen, 1992). These principles are also relevant in the aviation context. First, the cockpit displays should be re-designed to support the perception and action compatibility of humans in SBB and RBB tasks. If pilots have difficulty in constructing a coherent mental picture of the overall flight situation from the displays (causing a lack in SA) it indicates that these displays force them to apply higher levels of cognitive processing than needed for the elementary SBB task of controlling the aircraft. Second, in the automated environment the principal pilot task is that of coping with unanticipated events which requires KBB. For this purpose, the interface should allow for the development, by pilot training, of an adequate internal representation at all levels of cognitive control. The experienced level of complexity of the automated systems and the occasional failure of the pilot to track and to understand what these systems are doing (a lack of MA) indicates that the current cockpit interfaces do not satisfy the EID principles.

Summarizing, the status of pilot/flight-deck interaction indicates that many improvements need to be realized before the future ATM environment can be introduced. From a safety perspective, the persistent nature of human error provides little comfort in light of the expected growth and complexity of aviation operations. It goes without saying that the

4-D navigation procedures of the future will put additional task demand load on the pilot. The flexibility in air traffic handling inevitably demands the high-precision control of relatively complex, curved trajectories demanding levels of pilot situation and navigation awareness that exceed the current needs considerably. Solving these problems by simply enhancing flight-deck automation is a viable option but contradicts, however, the need to bring pilots back into the loop with a more active role in the operation of their vehicles. So, if this approach is being taken, it should adopt the principles of HCA. A second avenue that should be followed in parallel to the first, aims at improving the management and transfer of information to the pilot (NASA/DoD/FAA, 1995). In the next section the current status and future developments in the cockpit HMI are discussed.

1.3 The cockpit human-machine interface

The cockpit can be regarded as the physical location where the pilot interacts with the aircraft. The flight-deck systems form the human-machine interface designed to support the crew in flight mission management and control. The cockpit HMI is certainly not the end-product of some integrated design effort. Rather, as aerospace developments progressed new systems were continually being added to improve flight performance and mission capability (Lovesey, 1977). Cockpit instrumentation gradually filled all the available space in the cockpit, and the number of cockpit controls and displays has grown exponentially since World War II. An important breakthrough has been the introduction of *electronic* displays into the cockpit around the early 1980s, replacing most of the electro-mechanical cockpit input and output devices. The programmable electronic display devices, either Cathode Ray Tubes (CRT) or flat panel technology displays, allowed the introduction of Multi-Function Displays (MFD) that provide enormous flexibility and versatility to the flight crew – and the cockpit designer – with resultant improvements in flight management performance. With a significant portion of the instrument panel covered by the electronic displays, modern cockpits are referred to as *glass cockpits* (AGARD, 1996). The flexibility of modern display technology allows the design and implementation of virtually *any* display format, or: "*The point has been reached where the question is no longer what can be displayed, but what should be displayed and how we should display it.*" (Oliver, 1990). Below, the current status and future developments in the cockpit instrumentation will be discussed, emphasizing those displays that are relevant in the context of the current and future ATM systems, i.e. the displays that present the guidance and navigation information concerning the aircraft motion states relative to a prescribed trajectory.

1.3.1 Modern cockpit instrumentation

The Electronic Flight Instrument System (EFIS) displays

The current generation of commercial transport aircraft is equipped with the Electronic Flight Instrument System (EFIS). The main flight and navigation information is presented

①	artificial horizon
②	fixed aircraft symbol
③	airspeed (in [knots])
④	altitude (in [ft])
⑤	vertical speed (in 100 [ft/min])
⑥	pitch ladder
⑦	bank indicator
⑧	FD command bars
⑨	automation modes
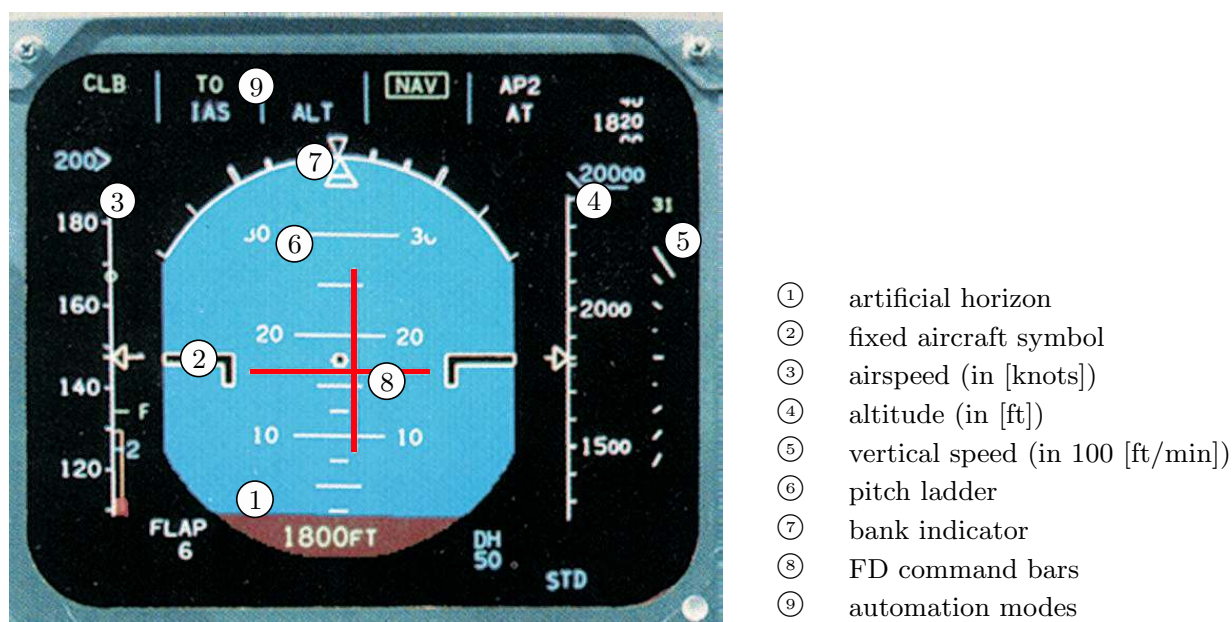
Figure 1.4: The Primary Flight Display (Fokker 100 version).

on two colour CRTs, the Primary Flight Display (PFD) and the Navigation Display (ND).

The Primary Flight Display   The PFD is an electronic analog of the electro-mechanic Attitude Director Indicator (ADI) and presents primarily aircraft guidance information, Fig. 1.4. Central on the PFD, the artificial horizon shows the aircraft attitude. The linear tapes to the left and right of the artificial horizon depict the aircraft velocity and altitude, respectively. The vertical speed is shown on the extreme right of the display. When the Flight-Director is engaged, the horizontal and vertical FD command bars appear on the artificial horizon. In the upper part of the display the active modes of the aircraft automated systems are shown (Pallett & Coombs, 1997).

The Navigation Display   The ND presents navigation information in two modes. In Compass Mode (ND-CM) the ND is an electronic analog of the electro-mechanic Horizontal Situation Indicator (HSI), a compass rose showing the aircraft heading and the lateral deviation from a selected radio beacon radial or the ILS localizer. The ND in Map Mode (ND-MM) depicts the aircraft position on a moving map in relation to airports, en-route fixes or waypoints, and the intended course or track, Fig. 1.5 (Pallett & Coombs, 1997).

Comments on the EFIS displays

The current PFD and ND-CM can be regarded as electronic *copies* of the electro-mechanical instruments that were developed even before WW-II, with some additional functionality. The information the display elements present is merely *status*, and most of the indicators convey only one signal. Some successful efforts were done to *integrate* more than one signal into a single display element. For instance, the artificial horizon presents both the aircraft pitch and the roll attitude angles in a way that is compatible to the visual hori-

①	fixed aircraft symbol
②	compass rose
③	heading
④	planned trajectory (track)
⑤	waypoint + waypoint-ID
⑥	distance circles (in nautical miles)
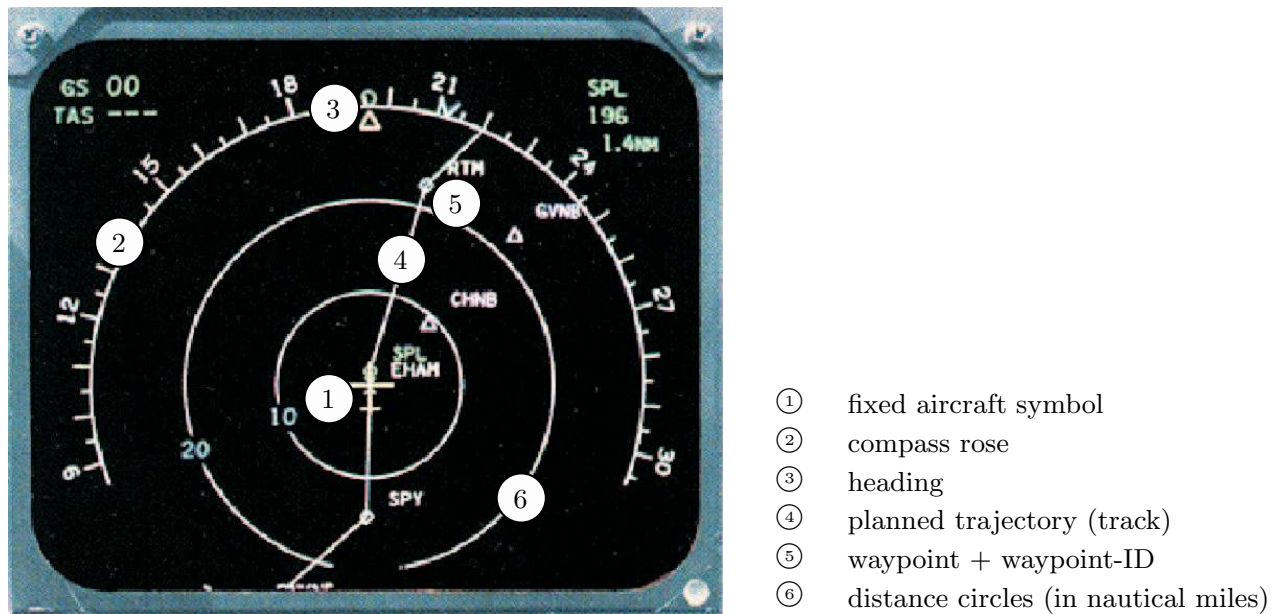
Figure 1.5: The Navigation Display, in Map Mode (Fokker 100 version).

zon when looking through the cockpit windshield. Integrating components of information on the display reduces the need for scanning, reducing visual workload (Roscoe, 1968). Nonetheless, the most persistent information processing task of pilots using conventional displays is *still* that of integrating the information from different sources (Roscoe, Corl, & Jensen, 1981). In this respect the only *real* improvement of the EFIS displays over their mechanical predecessors is the ND in Map Mode, where the horizontal navigation situation is shown as a pictorial representation that is very intuitive: "...*at a glance, the crew knows the aircraft's position and its relation to all relevant navigational points within the map's range*" (Oliver, 1990). The improvement in awareness of the lateral situation, however, does not hold for the vertical situation and the vertical flight-path. Some preliminary designs have been developed for the Vertical Situation Display (VSD), showing a pictorial representation of the vertical flight profile similar to that of the ND-MM. These VSDs, however, are currently not installed in commercial aircraft. The only indication of the present vertical path deviation is presented in numerical form on the FMS.

The current EFIS displays are *planar* representations of the aircraft's spatio-temporal situation. The PFD shows the aircraft attitude and the ND shows a top-view of the horizontal navigation situation. Neither one of these displays represent any information about the dimension not explicit in the display (Prevett & Wickens, 1994). The orthogonal displays represent the three-dimensional situation with two two-dimensional pictures, a representation that is incompatible with the 'natural' way humans perceive their 3-D environment (Haskell & Wickens, 1993). To become aware of the current flight situation the pilot must mentally integrate a considerable amount of information from a set of (semi-) integrated or individual displays from several spatial locations on the instrument panel. The difficulty of pilots in mentally reconstructing the flight situation from the

planar EFIS displays, especially in high-workload situations, is certainly one of the main causes of the occasional lack of situation awareness. Furthermore, although the ND-MM shows intuitive information about the current and future horizontal navigation situation, the pilot is unable to achieve the necessary trajectory-following performance with these EFIS displays (Foyle et al., 1992). When precise flight manoeuvering is required, pilots are forced to either engage and use the flight-director steering command system or engage the auto pilot, Fig. 1.3. In the first case the pilot is in the control loop but must do what the FD computer tells him to do, whereas in the second case the pilot is out of the control loop and acts as a system supervisor. In *both* situations the information processing task is performed by the computer, and not – at least, not necessarily, although pilots *are* trained to 'see-through' the automated systems – by the pilot.

Considering the future ATM demands, there have been several studies that indicate that flying complex, curved approaches *can* be conducted manually with conventional EFIS displays (Erkelens & Dronkelaar, 1990; Knox, 1992), at least when the flight-director is engaged. These studies, however, examined the tracking of *fixed* curved airways only and were mainly concerned about the path-following performance, *not* with pilot situation awareness. The fact that current systems can, in principle, be enhanced to comply with the future precise navigation demands do not take away the growing concern about the suitability of these systems from a pilot's perspective. For instance, the flight director does not present *any* information about the current nor the future aircraft motion status with respect to the trajectory. So, the pilot is not able to judge the importance of the actual path deviation from the FD command bars. Furthermore, it is inevitable that some pilots follow the FD needles more accurately than others, resulting in path-following performance differences which can not be tolerated in an ATM environment where an aircraft received clearance only for a certain volume of airspace moving along the negotiated trajectory. Clearly, other forms of presenting the 3-D/4-D guidance information should be developed. Consensus in the aviation community is growing that, at last, the flexibility gained with the introduction of programmable electronic displays must be exploited to the full extent. This could mean a truly radical change towards the design of displays that take advantage of humans' unique strengths in visual processing: "*The goal of a smart approach to interface design would be to provide the information needed for controllability in a form that exploits the power of perception.*" (Vicente & Rasmussen, 1990).

1.3.2 Future cockpit instrumentation

Guiding an aircraft along a trajectory near the earth's surface is a task that is similar to every-day locomotion as walking or driving a car. With respect to walking the aerial locomotion is guided by manipulating a machine instead of our own limbs; the vehicle acts as some interim between the bodily motion and the locomotion itself. With respect to car driving it are the restricted car kinematics and the less complex car dynamics that are different. Despite these differences the task of manual aircraft control is of similar difficulty, at least *when visual contact with the environment is continuously available*, i.e.
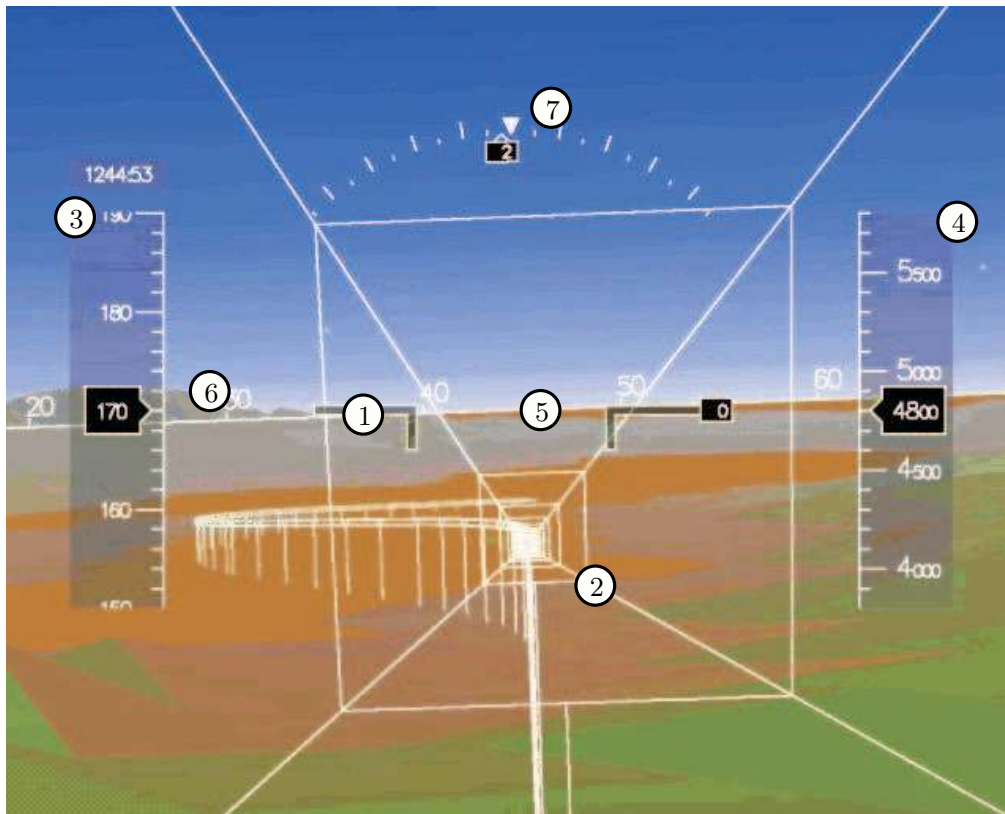
Figure 1.6: The Tunnel-in-the-Sky display. In this figure, ① depicts the aircraft symbol, ② the tunnel geometry, ③ the aircraft velocity (in [knots]), ④ the aircraft altitude (in [ft]), ⑤ the horizon line, ⑥ the heading angle indicators and ⑦ the bank angle indicator.

under Visual Meteorological Conditions (VMC) (Naish, 1971; Wilckens, 1971). When the visual contact with the environment is not available, i.e. under Instrument Meteorological Conditions (IMC), and the pilot has to rely on the cockpit displays, the task rapidly becomes more difficult. Why is that? The aircraft characteristics remain the same, and so do the pilot properties. Apparently, whereas the out-of-the-windshield visual information about the 3-D environment leads to an immediate awareness of the flight situation, the current displays do not (Wilckens, 1971): they make the task more difficult than it is.

Perspective flight-path displays

The introduction above, although roughly stated, exemplifies the growing consensus in the aviation community about what the primary flight display of the future should look like. That is, it should present the aircraft spatio-temporal navigation and guidance situation in a manner that is *intuitively understandable*, i.e. requiring minimal cognitive processing, that *enhances the pilot's situation awareness* during all phases of flight, and that is *compatible with and among the various pilot's control and monitoring tasks* to be performed. A suitable candidate that could satisfy these demands in the current and the

future air navigation system is a *perspective flight-path display* such as the *Tunnel-in-the-Sky display* (TIS). A perspective flight-path display is a pictorial display that shows the trajectory to be flown in a synthetic three-dimensional world similar to and compatible with the contact analog, Fig. 1.6. It presents the aircraft 3-D guidance situation with respect to the trajectory to be followed in an integrated fashion through a spatial, 3-D, representation of that situation. It allows a *direct* spatial orientation of the aircraft's position, attitude and motion relative to a fixed landmark – the tunnel geometry – in the environment. Hence, the spatio-temporal flight situation with respect to the environment is presented in a way that is compatible with the way in which humans naturally perceive their environment, allowing pilots to use their perceptual system in an *ecological* fashion (van Paassen & Mulder, 1998b). The display allows and supports pilots to rely on the same perception and action cycles they use in their activities of daily life. It frees pilots from mentally re-constructing the flight situation from an array of planar, quasi-spatial displays and allows them to literally perceive the flight situation in a glance. Because the pilot's guidance and navigation task itself is spatio-temporal, the perspective tunnel display is highly compatible to the pilot's internal representation (Mulder, 1994). The tunnel display maps the task-related variables onto a visual pattern that directly represents the variables of the task domain. Because of this, the task domain variables can be defined and, most importantly, *controlled* in terms of the properties of the visual pattern itself, not requiring *any* transformation between task and information domains at all (Mulder, Stassen, & Mulder, 2000). The success of the tunnel display can be predicted on the basis of the so-called Proximity Compatibility Principle (PCP) (Wickens & Andre, 1990), which states that the way humans process the information is related to the nature of task information processing characteristics. That is, a task that requires mental integration of sources of information, *close mental proximity*, will best be suited by more proximate displays, whereas tasks that require focused attention on those sources will be harmed by close proximity (Wickens & Andre, 1988). The tunnel display allows pilots to utilize their extremely proficient processes of perception and pattern recognition instead of requiring them to utilize the cognitively intensive processes of integration and inference (Bennett & Flach, 1992). It takes advantage of the processing efficiency of lower levels, especially the skill-based level, of cognitive control (Vicente & Rasmussen, 1992).

A perspective flight-path display is *not* a new concept. *Contact analog* displays have been propagated before and after WW-II (Poppen, 1936; Roscoe, 1948; Jones, Schrader, & Marshall, 1950; Fogel, 1959; Roscoe, Hasler, & Dougherty, 1966). *Pictorial* displays have been operational for decades in various vehicles such as submarines and space-craft (Kelley, 1967; McLane & Wolf, 1968). The promising contact analog display concepts that have been propagated since the 1950s, however, could not be implemented effectively with the contemporary technology. This changed with the advent of analog and digital computers in the late 1960s, resulting in several successful demonstrations of various forms of pictorial, perspective cockpit displays (Wilckens & Schattenmann, 1968; Wempe & Palmer, 1970; van Houtte, 1970; Palmer & Wempe, 1971; Wilckens, 1971, 1973; Eisele, Williges,

& Roscoe, 1976; Knox & Leavitt, 1977; Adams & Lallman, 1978; Jensen, 1978; Grunwald, Robertson, & Hatfield, 1980, 1981; Roscoe & Jensen, 1981; Jensen, 1981). Some of the findings of those investigators who are considered here as the main innovators of and contributors to the development of the tunnel-in-the-sky display are discussed in detail in Chapter 2. Recently, research in perspective flight-path displays is booming, and these research efforts provide increasing evidence for the hypotheses that presenting flight guidance information through a perspective flight-path display *enhances situation awareness* (Andre, Wickens, Moorman, & Boschelli, 1991; Dorighi, Ellis, & Grunwald, 1991; Dorighi, Grunwald, & Ellis, 1992; Haskell & Wickens, 1993; Parrish, Busquets, Williams, & Nold, 1994; Prevett & Wickens, 1994; Below, von Viebahn, & Hammer, 1995; Regal & Whittington, 1995), is *compatible with and among a variety of pilot control and monitoring tasks* (Wilckens, 1973; Roscoe et al., 1981; Oliver, 1990; Barfield & Rosenberg, 1992; Funabiki, 1997), and *allows pilots to manually conduct complex, curved precision approach and landing procedures with an accuracy comparable to that of their automatic counterparts* (Grunwald et al., 1980; Roscoe & Jensen, 1981; Watler & Logan, 1981; Grunwald, 1984; Reising, Barthelemy, & Hartsock, 1989; Haskell & Wickens, 1993; Theunissen, 1993b; Parrish et al., 1994; Prevett & Wickens, 1994; Regal & Whittington, 1995; Grunwald, 1996b) *without an appreciable raise in pilot mental workload* (Dorighi et al., 1991; Ineson, 1994; Below et al., 1995). With the tunnel display the pilot is in *direct* command of the flight operation (cf. Fig. 1.3(a)) with a suitable level of situation and navigation awareness. It is a very promising candidate to become the primary flight display of future aircraft cockpits, and it forms the subject of this thesis.

1.4 Motivation of the research project

Research at the Delft University of Technology

In 1990, the DELft Program for Hybridized Instrumentation and Navigation Systems (DELPHINS) was initiated at the Faculty of Electrical Engineering of the Delft University of Technology (DUT). The main goal of this project was to develop advanced presentation methods for 4-D navigation and guidance information in the cockpit and resulted in an implementation of the tunnel-in-the-sky display (Theunissen, 1997). In 1992 another project was initiated, at the Faculty of Aerospace Engineering of the DUT. The main goal of this project was to examine the *fundamental* properties of pilot/display interaction with a general tunnel-in-the-sky display, and its results are the subject of this thesis.

Towards a fundamental analysis of the tunnel-in-the-sky display

The introduction of a perspective primary flight display on the flight-deck has tremendous implications. Although large number of design aspects is or could be important in the development of a new display, the most important criteria are that it yields a *high performance*, supports a *high level of situation awareness*, and results in a *suitable level*

of mental workload (Hettinger, Nelson, Brickman, Haas, & Roumes, 1995). Obviously, the most important issue concerning the replacement of an existing display with another would be to assess their *relative* performance in meeting these three demands. And indeed, such a comparison has been the main objective of many previous attempts to study the effectiveness of the tunnel display format with respect to conventional displays (e.g. Wilckens & Schattenmann, 1968; Haskell & Wickens, 1993; Flohr & Huisman, 1997). As has been stated above, the tunnel display often showed its superiority over conventional instrumentation. But 'why is that?', or, 'where does this superiority come from?'. These questions were frequently stated at the start of the current research project and led to a rather different project perspective. In an attempt to *complement* the mainstream of tunnel display investigations, the scope of the current project is strictly limited to an in-depth analysis of the *fundamental* characteristics of a generic tunnel display as a means for presenting the aircraft guidance information to the pilot. In this respect, the thesis front page design, showing an extreme close-up of the display and revealing the screen's pixels, acts as a metaphor of the scope of the project. A second objective was to assess a research method, discussed below, that provides knowledge about pilot/display interaction that can be used for improving the tunnel display design. The task of the pilot considered here will be that of *manual* control of an aircraft through the tunnel along a planned trajectory. The reason for the emphasis on the manual control task is twofold. First, as has been stated above, pilots persist in conducting some of the most crucial flight phases manually and there are no indications that this will change in the near future. Second, the trend in developing new cockpit HMIs is indeed to support manual control, in the philosophy of the HCA principles of *pilot-in-the-loop* and *pilot-in-control*.

Adopting a *cybernetic* approach

The presentation of the guidance information by means of a pictorial, perspective tunnel display has important consequences. Whereas the pilot *task* of following a trajectory in space remains the same, the *information* is presented in a completely different fashion. Instead of perceiving and mentally integrating the guidance information from a number of instruments, the same information is presented as a pictorial representation of the visual contact, enhanced with additional synthetic guidance information. Then, the question arises: what are the effects of the 3-D tunnel presentation on pilot information processing and pilot behaviour? And how does this affect the analysis of the pilot/display interaction? The research presented here originates from these two questions. As the title of the thesis explains, the approach taken here is rooted in *cybernetics*.[4] The *cybernetic approach* adopted in this thesis, studies the fundamental properties of pilot/display interaction centered around *information* (Owen & Johnson, 1992), in particular the *information used for control*. It is an integrated, multi-disciplinary approach to study the perception and control behaviour of pilots interacting with the spatial tunnel display (Warren, 1988). It

---

[4]The term cybernetics originates from the Greek word for *steerman* ($\chi\upsilon\beta\epsilon\rho\nu\acute{\eta}\tau\eta\varsigma$) and was used in (Wiener, 1961) to coin the scientific discipline handling the control and communication theory.

consists of four stages. In the **first** stage an analysis of the pilots' tasks and an inventory of their information needs to fulfil these tasks are conducted. The **second** stage involves an investigation of the visual cues that, theoretically, are *available to* and, practically, are *used by* the pilot. The **third** stage consists of a number of empirical studies into the relative effectiveness in terms of perception and control of the various sets of optical cues . When a human operator is required to act as a part of a closed loop control system it is essential to investigate the behaviour of that operator in the control or monitoring tasks. The knowledge obtained in this way can lead to guidelines for the design of *all other* components in the loop, in this case the aircraft and, most importantly, the display. A model-based approach suits this purpose very well and, since the use of models *forces* the theoretical hypotheses to be described mathematically, a model-based investigation could guide future research. Therefore, the **fourth** and final stage of the cybernetic approach involves attempts to capture the empirically measured pilot behavioural characteristics with mathematical models. Note, however, that the cybernetic methodology is a model-based approach in the sense that it applies mathematical pilot modelling efforts as a *tool* for analyzing the effects of varying tunnel display designs on pilot behaviour. The pilot models themselves are *not* the main results. Rather, pilot modelling is a means to accomplish the primary objective of this thesis, which is *to obtain an understanding of the interaction of a pilot and the tunnel-in-the-sky display* that can be used for improving the design of the tunnel display from a human-centered perspective.

1.5   Outline of the thesis

With the motivation and goals of the research project being elaborated in the previous section, the contents and structure of the underlying thesis can be described below.

What does this thesis *not* contain?

In the definition of the motivation for this PhD project discussed above, a number of rather comprehensive assumptions has been made already. Concerning the potential technological problems and developments necessary to implement the intended future cockpit environment, such as the accuracy and update rate of the aircraft position measurement avionics, it is assumed that all these problems have been *solved*. Hence, the current research starts at the moment when the trajectory negotiation process has resulted in a trajectory to be followed that is presented to the pilot with the tunnel-in-the-sky display. The pilot task is to *manually* control the aircraft along this commanded trajectory; the use of the display for monitoring task purposes will not be discussed. The effects of *time* constraints in trajectory-following are not addressed; the tasks are essentially 3-D and not 4-D. Finally, only the *classical* manual control of aircraft is considered, consisting of the pilot feedback of the aircraft attitude, flight-path and position relative to the prescribed trajectory presented by the display. The potential benefits of forms of aircraft control augmentation, such as rate-command/attitude-hold control modes, are not included.
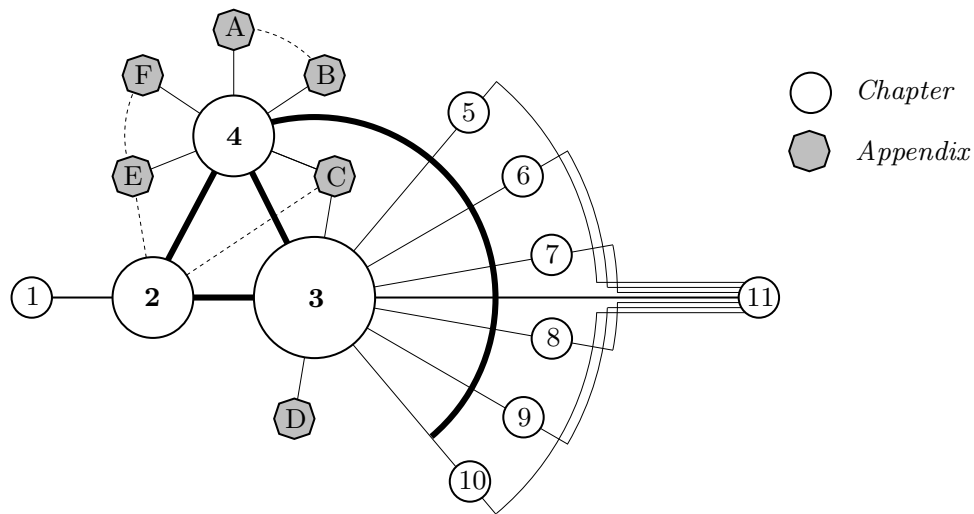
Figure 1.7: Stylized depiction of the structure of this thesis.

The subject of the research is a *generic* tunnel display design based on the formats that were applied in earlier investigations (e.g. Wilckens & Schattenmann, 1968; Grunwald et al., 1980; Theunissen, 1997). Some tunnel display design issues, such as the choice of the frame of reference, the field of view, etc., remain untouched, generally because these design issues have been solved in an almost identical fashion in the previous tunnel display implementations. So, apparently, considerable consensus already exists what the tunnel display should look like, and a further discussion of these issues seems to be almost trivial. The current research focuses on the design of the basic elements of the *tunnel geometry* (② in Fig. 1.6) and does not address the more 'conventional' display components such as the velocity and altitude indicators. The thesis does not contain any comparison between the tunnel display and conventional EFIS displays. Furthermore, of all sources of information available to the pilot only the *visual* channel is examined here: effects of vestibular, haptic and aural stimuli are neglected. If considered to be relevant, the consequences of neglecting these effects will be commented on in the text. Finally, the experimental efforts will be mainly concerned about the effects of various tunnel display geometrical designs on pilot *performance* and pilot *control behaviour*. Situation awareness, task demand load and mental workload are only addressed in the research through the use of pilot questionnaires.

Structure of the thesis

Fig. 1.7 shows the structure of this thesis pictorially. The thesis consists of two parts. Chapters 2 to 4 discuss the theoretical part of the research. Chapters 5 to 10 describe the experiments that have been carried out to investigate the theoretical considerations. The main results of this thesis are summarized in the retrospective, Chapter 11.

Theoretical background Chapter 2 entails a *task analysis* of the pilot task of manually guiding the aircraft along a planned trajectory, with the tunnel-in-the-sky display as

the primary flight instrument. Some important findings of earlier tunnel display research efforts are discussed first, followed by a survey of investigations into related areas. The discussion in this chapter will focus on issues of *control*, addressing questions like 'what are the tasks of pilots?' and 'what information do they need in conducting these tasks?'. The chapter ends with a first definition of the cybernetic approach.

The tunnel-in-the-sky display as a means to present the aircraft guidance information to the pilot is the subject of Chapter 3. The investigation is concentrated on a theoretical study of this *information*, addressing two intimately related topics namely that of *information transfer*, i.e. 'what information does the display provide?', and that of *information processing*, i.e. 'how is the information used by the pilot?'. Based on an extensive review of the literature, especially the literature concerned about human visual motion processing, the interaction characteristics of the tunnel display are analyzed and an attempt is done to put them into a theoretical framework.

In Chapter 4 the findings obtained in the *control* chapter, 2, and the *information* chapter, 3, are investigated from an experimental point of view, i.e. 'how are the theoretical considerations on pilot/display interaction going to be assessed experimentally?'. As will become clear, the guiding philosophy behind the various experimental validation efforts is to maintain the unique human perception and action compatibility supported by the tunnel display. The initial definition of the cybernetic approach of Chapter 2 will be refined in the sense that, first of all, it utilizes classical model-based techniques as a *tool* to increase our understanding of the pilot perception and action cycles. Second, the approach is extended with the use of *pilot questionnaires* to collect subjective pilot comments about their interaction with the experimental tunnel-in-the-sky display formats.

Summarizing, the theoretical chapters together form the backbone of this thesis. Many different techniques and a large variety of knowledge from numerous research disciplines are applied in an attempt to get a grip on the tunnel display design variables that affect pilot/display interaction. Most of the background information necessary to comprehend the full scope of the research presented here is included in Appendices A to F.

Experimental validation   The theoretical analysis conducted in Chapters 2 to 4 requires a thorough experimental validation. Six experiments, labelled X1 to X6, will be reported in this thesis in Chapters 5 to 10, respectively. Each experiment is defined to investigate a specific set of tunnel display design variables and their effects on pilot/display interaction. The experiments can be regarded as *case studies* that investigate a limited scope of theoretical issues brought up in Chapters 2 and 3. Whereas the task conducted in each experiment originates from the task or control-related analysis of Chapter 2, the variables that are varied experimentally originate from the information-related analysis of Chapter 3. The experimental results are investigated to increase the insight into the various effects of the different tunnel geometrical design variables on pilot performance and control behaviour, a matter of an in-depth *analysis*. These insights can then be used to define specific tunnel design guidelines, to guide future theoretical investigations, and to (re-)direct the experimental research, all of which can be regarded as *synthesis* efforts.

Chapter 2

Background, related research and the cybernetic approach

2.1 Introduction

The first step in the cybernetic approach is an analysis of a pilot's tasks and information needs to fulfil theses tasks. In this chapter such an analysis will be conducted from the perspectives of control and observation theory.

"Few problems are truly new." (Kelley, 1967). Therefore, all investigations should start with a study of literature that could be important to the research objectives at hand. Such a literature survey, conducted at the start of this project (Mulder, 1994), indicated that although the number and variety of relevant investigations conducted in the past is impressive, only a few of them address the cybernetic issues important here in the same specific context. As far as the tunnel display research is concerned, the contributions of Wilckens and Schattenmann and certainly the investigations of Grunwald must be reviewed here. The research of these pioneers is described in §2.2, a discussion which at the same time provides a selected overview of tunnel display developments since the late 1960s. The pilot task of manually controlling the aircraft along the *curved* trajectories of the future, with a tunnel-in-the-sky display, is the subject of §2.3. Based on the findings from the literature survey the pilot tasks will be analyzed and described as the concatenation of a number of sub-tasks. The task analysis leads to a number of specific questions which has up until now not been addressed in aerospace research. One of the outcomes of the literature survey, however, was that in addressing these questions much can be learned from investigations conducted in the context of *automobile driving* research. These issues are the subject of §2.4. In §2.5 the various bits of knowledge obtained in this chapter will be collected and put in perspective of the present research.

2.2   History of the tunnel display: a selected overview

The concept of so-called *contact analog displays* is old. Since WW-II various attempts to emulate the out-of-the-windshield visual contact with the cockpit instruments have been reported (Roscoe, 1948), and the first perspective flight-path display formats emerged in the early 1950s. At that time the available technology posed severe limitations and most of these early concepts have never reached farther than the designer's drawing table. The advance of computer technology led to a revival of perspective display research in the late 1960s and has since then expanded significantly. For a literature review on pictorial display formats and perspective flight-path displays the reader is referred to Quinn (1982) and Theunissen (1991), respectively. In this section the works of two tunnel-in-the-sky pioneers, Wilckens & Schattenmann and Grunwald, will be discussed. These pioneers have laid the foundation for most of the *innovative* tunnel display research since the late 1960s.

2.2.1   The Kanal display of Wilckens and Schattenmann

Since 1968, Wilckens and Schattenmann have reported several studies on the effectiveness of their Kanal – channel – display for all-weather landing purposes. They are regarded pioneers because they were the first to provide a scientific basis for the potential of perspective flight-path displays as a means to improve the cockpit HMI.

Kanal display design philosophy   In the 1960s considerable effort was conducted to solve the problem of aircraft landing under all-weather conditions (Wilckens & Schattenmann, 1968). Whereas the manual control of aircraft ILS approach and landings constituted no serious problems in good visibility conditions (in VMC), problems *did* occur in bad weather conditions (in IMC). Here, pilots had no visual contact with the outside world and had to rely completely on their instruments. The approach taken, symptomatic for the cockpit HMI developments, has been to extend the functionality of the *automated* systems to allow automated landings. The pilot task is then to monitor the safe operation of the autopilot and, in the case of a system failure or unsatisfactory performance, to abort the procedure and perform a go-around manoeuvre. The reason for extending the capability of the autopilot to the all-weather landing situation was the belief that conducting manual landings during these conditions was beyond human capabilities (Wilckens, 1971). Wilckens, a test-pilot himself, strongly opposed this claim and stated that it is not the pilot, but the inferior design of the cockpit instruments that had to be blamed for the unsatisfactory performance in IMC: *"...the root of the problem is a poor display."* (Wilckens, 1973). In a visionary paper (Wilckens, 1973), Wilckens predicted that the consequences of automating the pilot out of the control loop were the loss of pilot proficiency, the lack of pilot awareness of the flight situation and the probability of excessive mental workload in case the autoland or ILS navigation systems would fail.

In Wilckens (1973) the evolution of cockpit display design is sketched in order to explain the fallacy of the conventional designs. The aggregation of several cockpit displays across the instrument panel yields a more efficient pilot scanning pattern (Roscoe, 1968). The

available instrument indicators in principle provide sufficient aircraft *status* information for the landing task in IMC. The manual approach and landing control task during Cat II and III approaches, however, *demands continuous scanning and mental integration of the numerous status indicators into a coherent mental picture.* This is a task beyond pilot capabilities, at least as far as this mental picture should act as a basis for *high-precision* path-following that would be acceptable for routine operations. The Flight-Director (FD) reduces the need for scanning and information integration by providing the pilots a set of *command* signals that they must obey in order to fly the precision approach path. Wilckens argued that the FD *masks* the problem by reducing the pilot's role to that of a *stick actuator* (Wilckens & Schattenmann, 1968). The pilot cannot derive an overall view of the situation from the FD command information alone, i.e. this information is not *transparent* (Wilckens, 1973). The flight situation *can* be assessed by scanning in addition the other status instruments, especially the Horizontal Situation Indicator (HSI) display, at the cost, however, of decreasing path-following performance and higher mental workload. Wilckens concludes that the current cockpit instrumentation is too abstract in nature and makes it difficult for the pilot to stay on top of the flight situation.

The solution advocated by Wilckens was to offer the pilot a *synthetic* visual presentation of the outside view by developing a head-down contact analog display of the through-the-windshield visual information, independent of visibility conditions. Arguments to restore the visual contact scene are the intuitive spatial orientation on the one hand and the resulting ease and naturalness of control on the other (as in approach and landings during good visibility). For adequate guidance *precision* Wilckens reasoned that, in addition, the commanded trajectory should be presented on the display, enhancing the level of quantitative guidance information (Wilckens, 1971). This trajectory is shown through the perspective representation of a *channel*, a common and intuitive geometrical entity for humans. The Kanal display, Fig. 2.1(a), is similar as the tunnel display, except that the top plane is not shown. The channel is shown by means of dots that mark the lateral and vertical path constraints. Wilckens and Schattenmann were the first to report a qualitative attempt to *relate the changes in the perspective channel presentation, i.e. the optical information presented to the pilot, to the aircraft flight situation* (Schattenmann & Wilckens, 1973; Wilckens, 1973). As indicated in Fig. 2.1(b), both the aircraft attitude (ψ, θ, ϕ) and the aircraft position (y, h) with respect to the trajectory are shown by pure pictorial means through the perspective projection on the tunnel geometry.

Empirical Kanal display simulation studies   In the 1966-1972 period Wilckens and Schattenmann conducted a number of empirical evaluations of their Kanal display at the fixed-base flight simulator of the German national aerospace laboratory DLR. In a first set of experiments the Kanal display was compared with the conventional ILS instrumentation (no Flight-Director) in an ILS approach and landing task (Wilckens & Schattenmann, 1968). The results indicated that the channel display, which in fact only shows *status* information, *inherently provides command information*, allowing pilots to intercept the localizer and glidepath from any particular position offset on an asymptotic track. The *precision* of

(a) channel format   (b) perspective relations
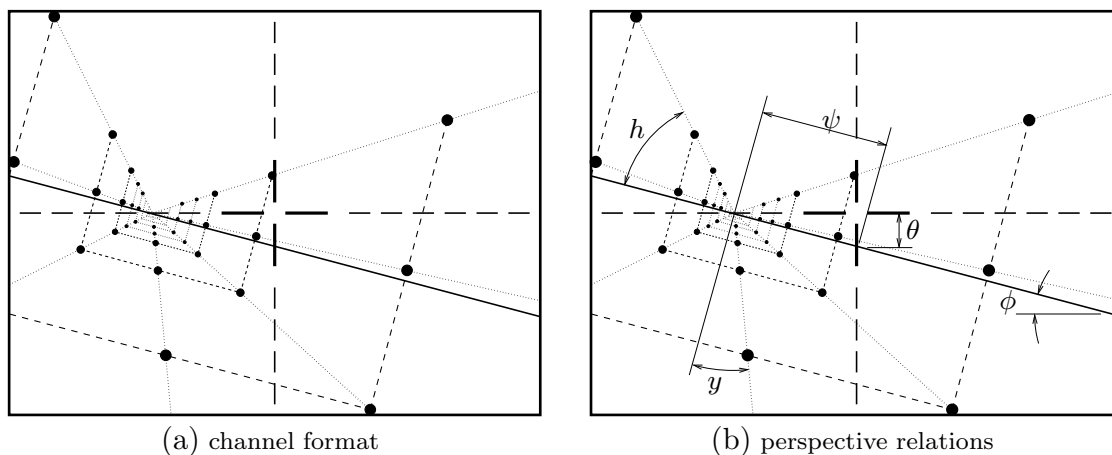
Figure 2.1: The Kanal display format (left) and the relations between the perspective projection
and the aircraft flight situation (right) (adopted from (Schattenmann & Wilckens,
1973)). The Kanal display was presented through an oscilloscope CRT. It consists
of an array of dots marking the projection of the channel boundaries. The thick
dashed lines show the display center; the continuous line depicts the horizon line.
All other lines shown are included here to accentuate the channel geometry.

intercepting and tracking this command information, however, is completely determined
by the pilot himself. The presentation of *tolerance regions* around the prescribed flight
path allowed pilots to reduce their gain (aileron, elevator, *not* throttle) as soon as the
aircraft is 'settled' inside of these regions. The sensitivity in pictorially presenting the
guidance information inspired pilots to perform better than usual and allowed them to
perceive much more directly the dynamic responses of the aircraft to control inputs. In
a later experiment the channel display was compared with three conventional types of
instrumentation – 'ILS standard', 'ILS integrated', and a Flight-Director – in a similar
ILS approach and landing task (Wilckens, 1973; Schattenmann & Wilckens, 1973). The
displays were analyzed in terms of the performance (path-following accuracy) and pilot
control behaviour. Results showed that performance with the channel display and the FD
display were similar, whereas performance with the other two display designs was signif-
icantly less. Again, it was found that the path-following responses (in terms of accuracy
and smoothness) with the channel display were similar to those of the FD display. As a
result, Wilckens showed analytically that the channel display inherently provides informa-
tion (through the changes in the projected tunnel geometry, see Fig. 2.1(b)), similar to
the Flight-Director (Wilckens, 1973). The use of a Flight-Director *forces* pilots to act as a
high-bandwidth servo-controller that must obey *all* FD commands by applying immediate
and small control inputs. The channel display, however, presents guidance information
through a perspective projection, allowing the pilot to perceive *all* elements of the flight
situation (attitude, flight-path and position) and to act on these elements accordingly.
The use of the channel display allows pilots to conduct well co-ordinated manoeuvres to
track the localizer and the glidepath as effectively as in visual flight. Furthermore, whereas
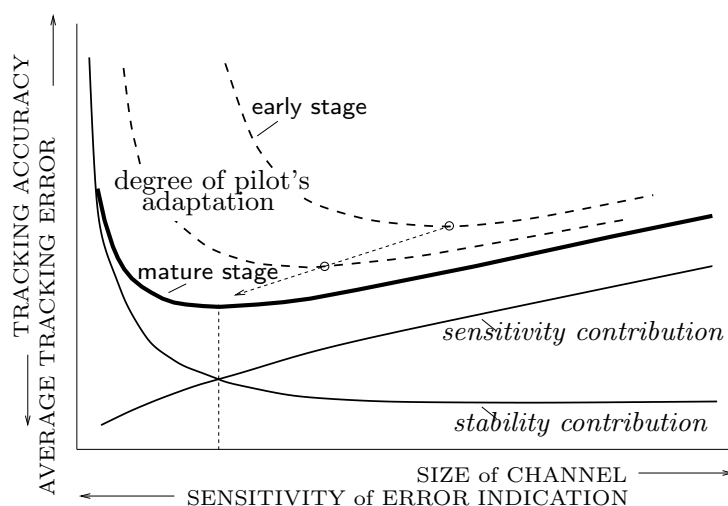
Figure 2.2: Relation between the channel size and the pilot tracking accuracy (Wilckens, 1973). The figure shows the influence of the pilot proficiency on the tracking accuracy, from the early learning stage to a mature stage.

the Flight-Director integrates the guidance information according to a fixed set of rules, the channel display allows pilots to choose their own strategy to intercept and track the prescribed path. So, the channel display concept offers flexibility where the FD reduces the pilot's role to that of a servant strictly following commands.

Wilckens and Schattenmann were the first to notice the effectiveness of the channel *size* as a way to manipulate the level of path-following accuracy adopted by pilots. The relation between the channel size and tracking accuracy can be exemplified in a qualitative diagram, Fig. 2.2, which shows that the tracking accuracy is limited on the one hand by the size of the channel (large sizes), the *sensitivity contribution*, and on the other hand by the closed loop dynamic stability (small sizes), the *stability contribution* (Wilckens, 1973). Hence, an *optimal tunnel size* is hypothesized to exist, depending on the level of pilot adaptation, i.e. pilot proficiency, with the channel display.

Conclusive remarks   The channel display was claimed by Wilckens and Schattenmann to be a dramatic improvement in 'information transfer' to the pilot, solving many of the problems caused by the inappropriate conventional cockpit instrumentation designs. Many of the implications they reported involving the design of their Kanal display are still very relevant today. The disadvantages of the Flight-Director display as compared to the contact analog display has been clearly addressed by them. Wilckens and Schattenmann showed that both the displays present command information, either explicit (Flight-Director) or implicit (channel). The *explicit* command information of the FD is non-transparent and forces the pilot to act as just a servo-controller. It does not provide *any* information about the current nor the future status of the flight condition: it is a *ghost* (Wilckens, 1973). The *implicit* command information of the perspective display allows spontaneous and intuitive orientation, a high level of manual precision control, and

a 'natural' and therefore effective use of the available controls. By making use of the unique capabilities of humans to plan and anticipate future situations, the channel display is considered to be superior for not only manual guidance but for supervisory monitoring tasks as well, allowing smooth manual take-over from automatic control systems whenever necessary. Many problems with the cockpit HMI of present generations of transport aircraft, in terms of situation awareness, mode awareness and pilot proficiency, were foreseen by Wilckens and Schattenmann almost thirty years ago.

2.2.2   The Tunnel-in-the-Sky display of Grunwald

Grunwald may be seen as a pioneer in the research of perspective displays in general, and the tunnel-in-the-sky display in particular. His investigations of manual control with perspective displays were based on a sound control-theoretic approach and have been a strong motivation for the cybernetic approach adopted in the current research project.

Control-related information in perspective displays and display augmentation

Grunwald successfully bridged the views from psychology and human engineering regarding the issue of how humans use the information in the visual world for the purpose of vehicular control. In two landmark articles Grunwald examined the availability and use of control-related information in spatial visual displays (Grunwald & Merhav, 1976), as well as methods to improve control performance by *augmenting* the abstract visual information in those displays (Grunwald & Merhav, 1978). In the task of guiding a Remotely Piloted Vehicle (RPV) along a straight trajectory, Grunwald showed the importance of the *preview* of the desired trajectory laying ahead. Subjects were reported to use a span of forward looking distances to extract higher-order information about their motion condition from the visual field, allowing them to predict the future path (Grunwald & Merhav, 1976). This process can be enhanced further by superimposing *synthetic* symbolic elements on the visual display. For instance, a *Flight-Path Vector* (FPV) shows the instantaneous direction, the tangent, of forward motion, whereas presenting the predicted vehicle path conveys information about the change in the direction of motion, the curvature, in the future. The symbolic display augmentation presents information compatible to the motion condition that must normally be perceived in the visual field itself. It presents extremely useful *predictive feedback information*, allowing pilots to *anticipate* for potential errors and to initiate corrections even before these errors actually occur (Kelley, 1967).

Design philosophy of the tunnel-in-the-sky display

Grunwald reported the design and evaluation of a perspective tunnel display for 3-D helicopter approaches (Grunwald et al., 1980, 1981) and for 4-D aircraft approaches (Grunwald, 1984). The pictorial *through-the-windshield* visual contact augmented with the three-dimensional commanded trajectory presented as a tunnel was reported to be extremely useful for following a curved trajectory: "...*a winding and descending tunnel in the sky*

(a) basic tunnel display format   (b) tunnel-and-predictor display format
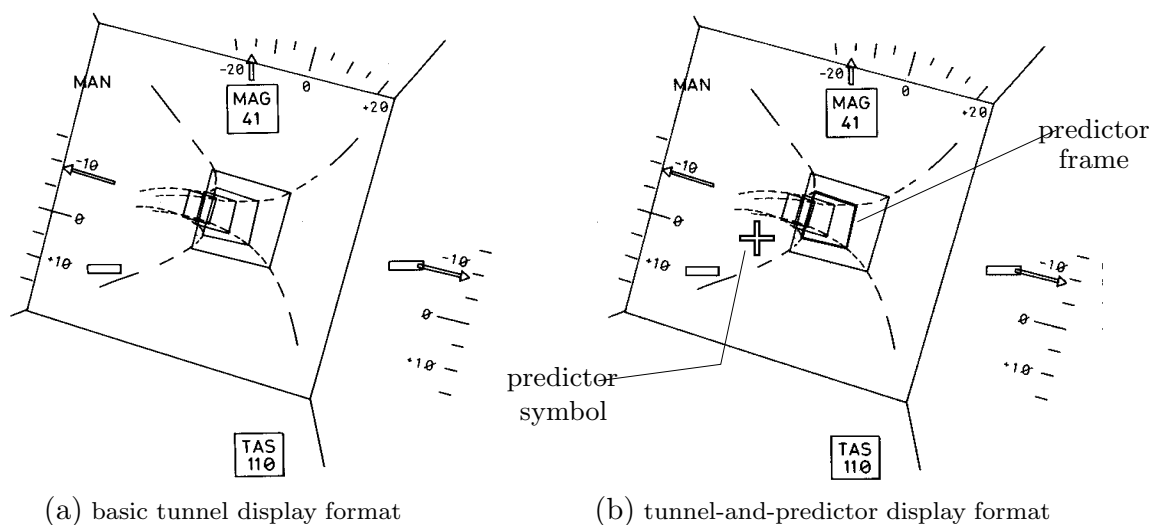
Figure 2.3: The tunnel-in-the-sky display format of (Grunwald et al., 1980, 1981) (left) and the tunnel-and-predictor combination (right).

which combines both preview of the trajectory as well as the necessary control information in one display format." (Grunwald et al., 1981). Whereas Wilckens and Schattenmann evaluated their Kanal display only for the ILS landing task, Grunwald examined pilot performance with the tunnel display in curved approaches. Grunwald's baseline tunnel display is illustrated in Fig. 2.3(a). The experiments revealed considerable performance limitations with the basic tunnel display due to badly damped pilot responses, accompanied by a considerable level of workload. Directed by experience from his earlier research, Grunwald attributed these problems to the use of only a small-sized CRT to present the optical information. Due to the lack of peripheral vision the rate cues providing system damping could not be perceived appropriately.

The flight-path predictor symbol In (Grunwald et al., 1980, 1981) it is shown analytically as well as experimentally that a *Flight-Path Predictor* (FPP) symbol, flying ahead and showing the *predicted* aircraft position, can restore damping and provides useful control information for following complex curved trajectories. The tunnel-and-predictor combination, Fig. 2.3(b), outperformed conventional displays in its abilities to follow a curved path in the presence of turbulence, to re-enter the path from an off-set position, as well as to monitor the automated flight (Grunwald et al., 1980, 1981). The success of the tunnel-and-predictor display was attributed to the fact that whereas the tunnel image compensates for predictor errors, the FPP compensates for the lack of tunnel display rate cues (Grunwald et al., 1981). The design and evaluation of rules to predict the future aircraft position, *predictor laws*, are reported in (Grunwald, 1985) and (Mulder, 1992).

Qualitative evaluation of the tunnel geometry In (Grunwald et al., 1980, 1981) a qualitative attempt is reported of how control-related information can be perceived from

the basic tunnel geometry. To illustrate the procedure, Fig. 2.4(a) shows the cues to be derived from the tunnel display, whereas Fig. 2.4(b) shows the situation from above. Line A–A represents the horizon and the roll angle ϕ can be estimated from the inclination of A–A with respect to the monitor reference frame $C_y C_z$. Point C is the center of the image and represents the vehicle axis. Point S is the center of the nearest tunnel square, whereas point F indicates the instantaneous desired trajectory direction that can be estimated by extending the four tunnel corner lines nearby to a point at infinity. The F_y and F_z axes are defined as parallel and perpendicular to the horizon, and provide lateral and vertical position deviation information with the distances between F and S in F_y and F_z direction, respectively. The vehicle attitude with respect to the tunnel can be estimated from the deviation of F from the center C, as well as the lateral and vertical interception angles. The downslope Γ_t of the trajectory follows from the deviation between F and line A–A. Trajectory preview is displayed explicitly with the tunnel section F at a fixed distance D ahead of the vehicle. At the same distance D, point R is located on the line FS. The distance between R and T in F_y and F_z direction provides an indication of the trajectory curvature and the change in vertical downslope, respectively. Velocity cues are conveyed by the speed of passing tunnel elements. A predictor symbol cross P can be explicitly shown at a distance D ahead, presenting the predicted aircraft position. The lateral and vertical deviations ϵ_l and ϵ_v between P and T represent the *predicted* future position error.

The task with and without a predictor symbol   Without the predictor symbol all control-related information must be perceived from the basic tunnel geometry. When the predictor is presented the control task, defined as staying inside the displayed tunnel, is simplified drastically. This can be explained as follows. With a predictor, minimizing the errors ϵ_l and ϵ_v between the predictor P and the reference frame T *automatically* yields path-following, the precision of which dependent on the accuracy of the predictor. This exemplifies the augmentation of the basic tunnel presentation via pure *predictive* information: the predictor does *not* tell the pilot what to do (like a Flight-Director), but only shows what will happen when the pilot does not change the instantaneous flight condition. With the predictor the pilot task essentially becomes an elementary two-axis *pursuit* tracking task (McRuer & Jex, 1967).

Providing 4-D guidance information   Grunwald extended his tunnel-and-predictor concept to allow accurate control of the aircraft forward velocity in a 4-D guidance task (Grunwald, 1984). This is accomplished by presenting the predictor symbol related to the *actual* forward speed as well as a reference frame in the tunnel, ahead of the own plane, related to the *desired* forward speed. By matching the predictor symbol in the lateral and vertical dimensions the pilot optimizes the path-following accuracy. By matching the predictor symbol with the tunnel reference frame in the longitudinal direction, the pilot can minimize errors in the forward velocity. Hence, all information for accurate 4-D path-following is presented *centrally* in the display through the use of a single symbol. Experiments showed that accurate velocity control was achieved with moderate throttle
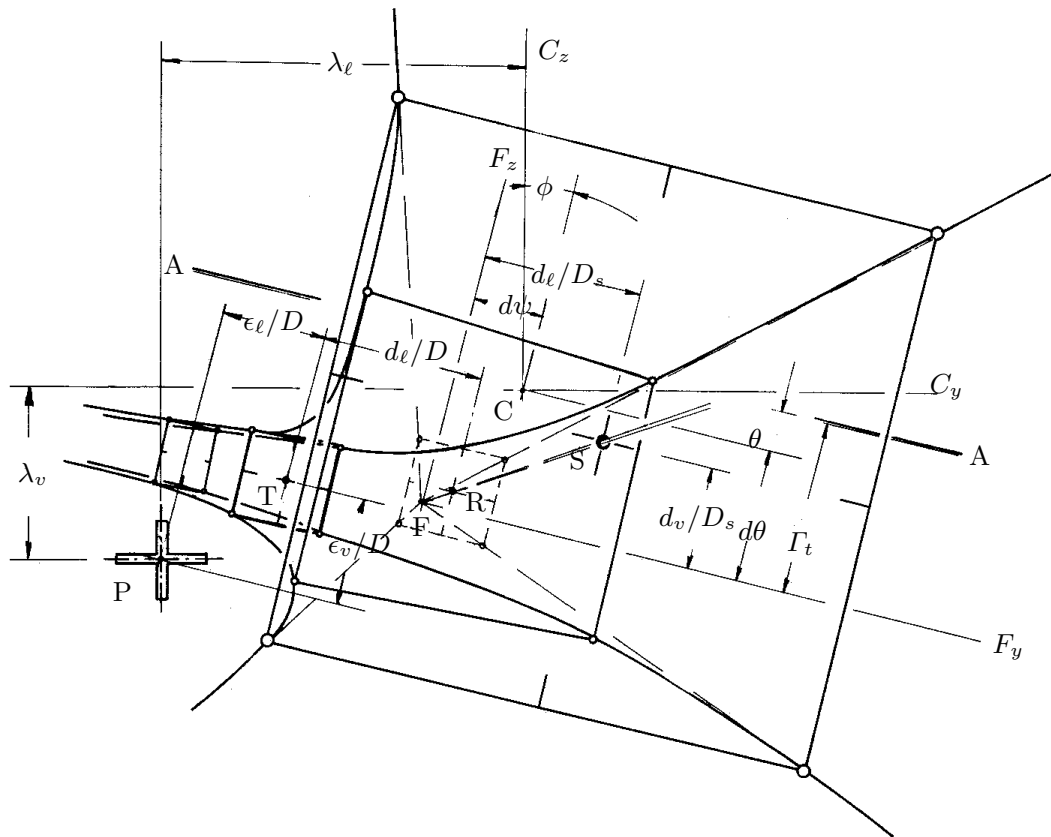
(a) control-related information in the tunnel-and-predictor display
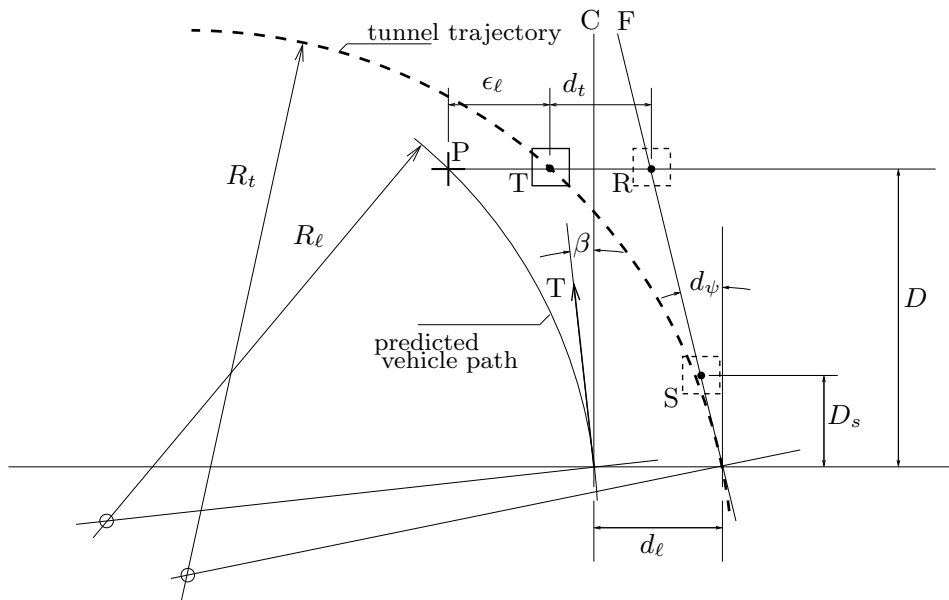
(b) top view of the situation

Figure 2.4: Control-related information conveyed by the basic tunnel geometry and the predictor symbol (Grunwald et al., 1980, 1981). The notations and symbols applied in this figure are explained in the text.

activity and without affecting the path-following performance (Grunwald, 1984).

Rotating the tunnel geometry   In following a curved tunnel segment with constant radius and without effects of wind, an aircraft conducts a stationary curve by rotating its wings with a fixed angle of bank. Grunwald investigated the potential usefulness of rotating the tunnel geometry as a whole to depict aircraft roll angle *command* information (Grunwald et al., 1981; Grunwald, 1984). The results were not successful: no performance differences were observed between the rotated and non-rotated tunnels were reported (Grunwald et al., 1981). In Grunwald (1984) the same conclusions were drawn, with the additional comment that rotating the tunnel geometry was confusing during transients between straight and curved sections of the trajectory. Improvements to solve these problems during curve-transition manoeuvres were reported (Grunwald, 1996a, 1996b).

Conclusive remarks

The pioneer tunnel-in-the-sky display investigations of Wilckens & Schattenmann and Grunwald illustrate the main developments in this display very well. The *preview* of the short-term guidance constraints was found to be one of the principal virtues of the display. The superiority of the information transfer to the human pilot as compared to the conventional instruments has been unequivocally reasoned by Wilckens and Schattenmann. An important advantage of the *synthetic* contact analog representation is that the visual information can be *enhanced* with elements that are not available in the outside world: a computer-generated display allows the designer to emphasize or augment those display elements that convey clear and unambiguous guidance information. The research of Grunwald has shown the tremendous gains to be achieved by augmenting the display with entities presenting higher-order guidance information such as the flight-path vector and the flight-path predictor. In conclusion, the main innovative developments in designing perspective flight-path displays have been conducted more than two decades ago. Of course, many other research groups have implemented their own implementation of a tunnel/channel/pathway/highway or whatever-in-the-sky display. But none of these designs have led to any substantial advancements over the classic designs of the pioneers.

2.3   A first analysis of the pilot's guidance task

Applying the SRK-taxonomy to the pilot guidance and navigation task

A classification of pilot behaviour according to Rasmussen's SRK taxonomy is reported in (Tanaka & Matsumoto, 1986), Fig. 2.5. The mission of a transport aircraft pilot is to bring the aircraft from one airport to another following a pre-determined flight plan. The pilot supervisory task is the judgement of whether the current flight condition is in accordance with the nominal plan. In case of unexpected situations, such as changing weather conditions or system failures, pilots must decide upon the navigation alternatives. This is a decision-making task that falls in the category of *knowledge-based behaviour*, where
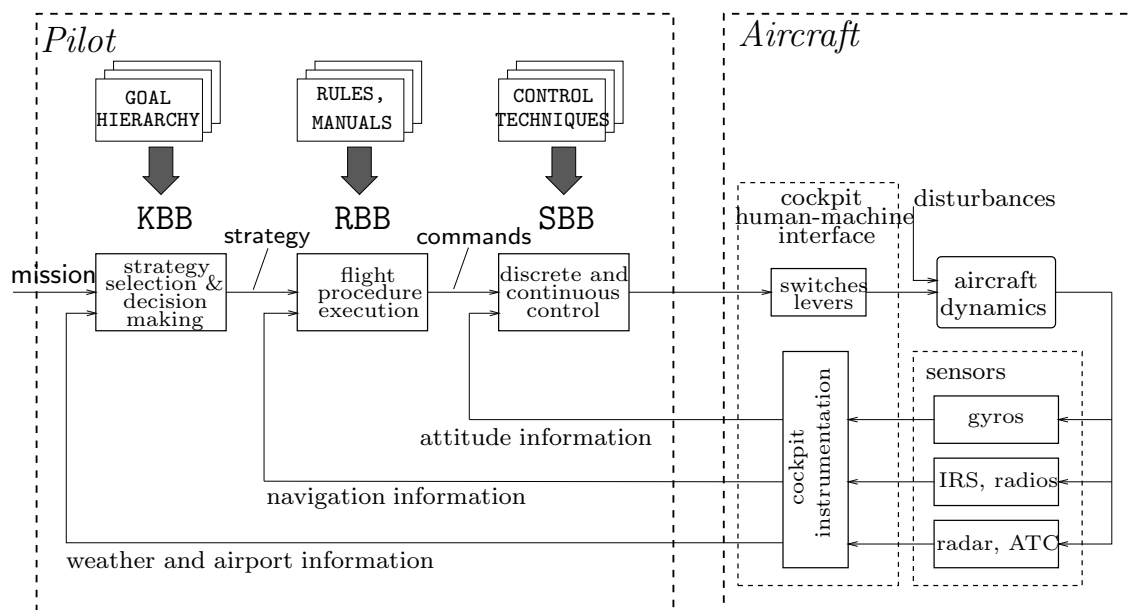
Figure 2.5: Describing the pilot's guidance and navigation tasks following Rasmussen's three levels of cognitive control (adapted from (Tanaka & Matsumoto, 1986)).

pilot experience plays an important role in determining the next procedure. Pilots are trained to deal with unexpected events in a systematic, procedural manner. Aircraft operation manuals are provided wherein all tasks are described sequentially, together forming a procedure for each flight phase. The selected strategy is composed of a sequence of procedures and the behaviour stemming from these explicit procedures falls in the category of *rule-based behaviour*. At this level, various tasks are activated that are composed of simpler units of perception and action, such as reading the airspeed indicator and moving the control manipulators. These units of behaviour are classified at the lowest level of cognitive control, *skill-based behaviour*. The categorization of 'cognitive control' can be viewed as a *hierarchical control system* consisting of three levels: KBB at the top, RBB in the middle and SBB is at the bottom level Fig. 2.5. A basic assumption of this thesis, as in most of the earlier tunnel display investigations (Wilckens, 1971; Grunwald et al., 1980; Theunissen, 1997), is that all issues initiating pilot cognitive behaviour at the two higher levels are neglected. That is, the current investigation starts where the higher level navigation tasks involving pilot knowledge-based and rule-based behaviour discussed above, have yielded an optimal 3-D or 4-D trajectory to be flown. The focus is on pilot skill-based control behaviour, involving low-level cognitive perception and action cycles.

Defining a 3-D or 4-D trajectory

The on-board Flight Management System (FMS) computers contain algorithms for computing efficient (fuel/time/economy) flight profiles that satisfy all boundary conditions defined by e.g. passenger comfort and the aircraft flight envelope. These profiles demand

(a) definition of way-points   (b) the FMS trajectory
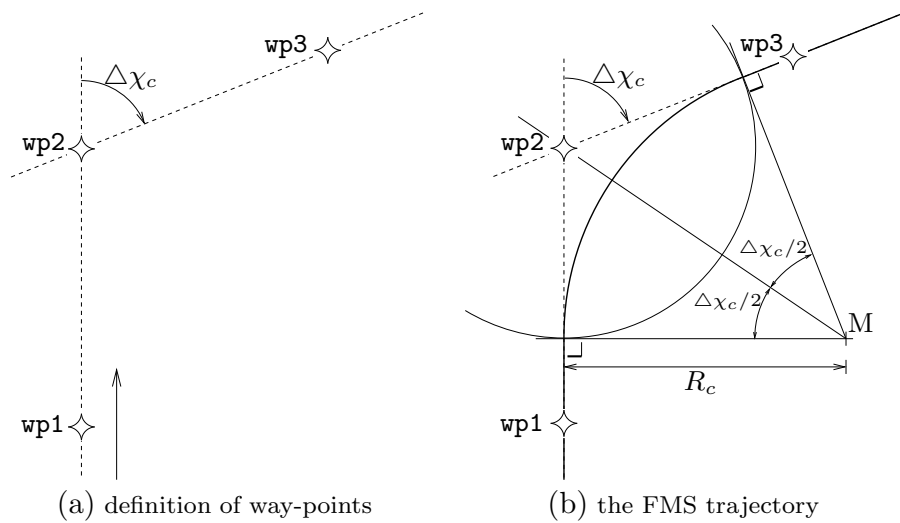
Figure 2.6: The computation by the aircraft Flight Management System computers of a curved trajectory, starting from a set of route-fixes or way-points.

high-precision aircraft guidance and are usually flown by the autopilot or with the Flight-Director engaged. FMS trajectories are defined by means of *way-points*, marking a fixed geographical position (Brockhaus, 1994). Basically, two sorts of way-points are used, i.e. those that must be overflown with a pre-defined track (wp1, wp3) and those which do not have to be overflown (wp2), Fig. 2.6(a). As this figure shows, way-point wp2 marks the cross-point of two straight lines with different track angles; the lay-out of the way-points *commands* a change in track angle $\triangle\chi_c$. Because aircraft cannot instantaneously change their track angle, a circle segment is used for a smooth transient manoeuvre, Fig. 2.6(b). The radius R_c of the circle segment is determined by the airspeed and a maximum roll angle of 25 to 30 [deg]. Given the curve radius, the FMS computes the curved section of the trajectory, resulting in a *candidate* trajectory connecting way-points wp1 and wp3. Next, the FMS applies fast-time simulation (FTS) techniques to test whether this candidate trajectory satisfies all constraints. Repeating the FTS method for various other trajectories yields a trajectory that satisfies all constraints best. This is the final, *optimal*, trajectory that forms the reference for computing an array of set-points for the automatic controllers (AP and FD). When approaching (following a STAR) or leaving (SID) an airport usually strict velocity constraints hold. In the future, it can be expected that the airborne FMS computers, negotiating with the ATC computers on the ground, will further impose strict time constraints on the aircraft approach and departure manoeuvres. To generate 4-D trajectories a similar procedure as discussed above can be used, enhanced with functionality to deal with the time constraints. Fig. 2.7 shows a provisional approach plate for a curved MLS approach, used by pilots in their preparation of the approach and landing with conventional instruments. From the discussion above it is clear that the curved trajectories that are computed in FMS computers are *piecewise continuous* and *consist of a concatenation of straight and circular segments*.
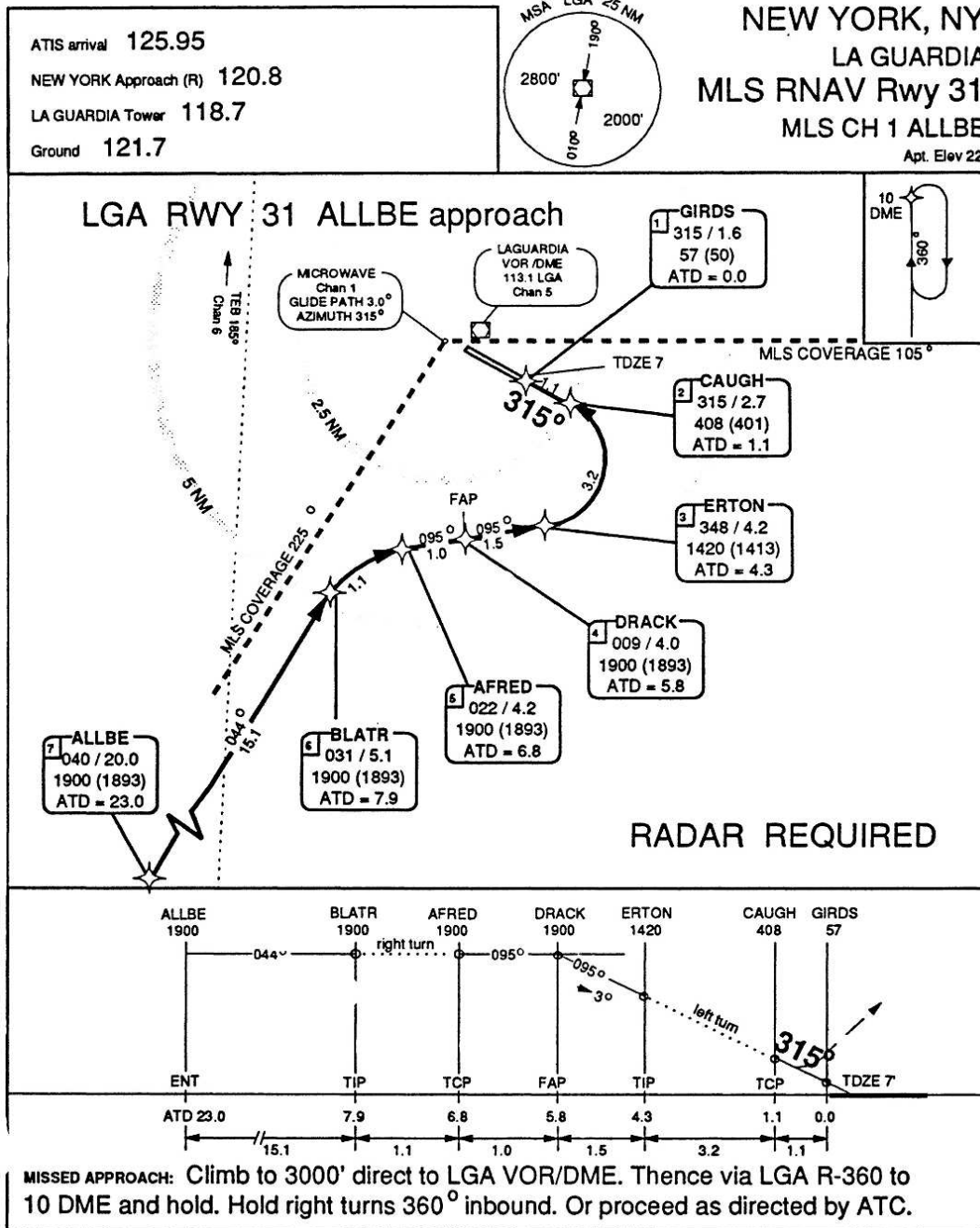
Figure 2.7: Proposed approach plate for a curved approach to New York's La Guardia airport (Erkelens & Dronkelaar, 1990). The star symbols labelled 'CAUGH', 'ERTON', etc. are way-points. The *top* of this plate shows the identification of the arrival and the frequencies to be used for communication and surveillance. The *middle* and *bottom* sections illustrate the horizontal and vertical approach geometry, respectively. A pilot must intercept the approach profile at 'ALLBE' with a track of 44° [deg]. After a right hand turn the 3° [deg] glidepath is intercepted at 'DRACK'.
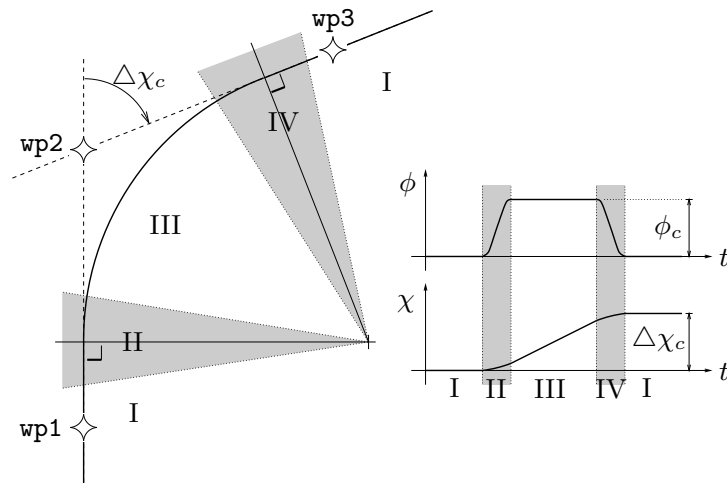
Figure 2.8: Analysis of the pilot's guidance task of following a FMS trajectory that is a concatenation of straight and circular segments (left). The right hand figure shows time histories of the aircraft roll angle ϕ and the track angle χ.

The pilot's guidance task

The 3-D reference trajectories as evaluated in the present work are assumed to consist of straight sections and approximately circular segments in the horizontal and vertical plane. This has also been the case for the majority of previous tunnel display investigations (Wilckens, 1973; Grunwald et al., 1981; Grunwald, 1984; Wickens, Haskell, & Harte, 1989; Grunwald, 1996a; Theunissen, 1997). The consequences for pilot behaviour of following a prescribed trajectory that consists of a concatenation of straight and circular sections were analyzed in (Mulder, 1995). To exemplify the analysis, the aircraft manoeuvre in the horizontal plane, Fig. 2.6(b), is repeated in Fig. 2.8, also including the time histories of two main aircraft asymmetric state elements, the roll angle ϕ and the track angle χ (Appendix C). Four stages are distinguished: (I) following a straight section; (II) anticipating and intercepting the circular segment; (III) following a circular section, and (IV) anticipating and intercepting a straight segment again. Hence, following the reference trajectory means that the pilot must either maintain a certain stationary (steady) flight condition, or execute a transition manoeuvre between these steady conditions. The two stationary flight conditions are the aircraft *recti-linear* motion, in straight tunnel segments, and the aircraft *curvi-linear* motion, in circular tunnel segments (Appendix C). Transition manoeuvres are needed for an aircraft to change its track angle (usually in the horizontal plane), resulting in the transition from rect-linear to curvi-linear motion, or to change its flight-path angle (vertical plane), resulting in the transition between two recti-linear motion conditions. This has consequences for investigating pilot control behaviour. Maintaining a certain steady reference condition in the presence of disturbances is known as a *regulation* task. Controlling a transition between two reference conditions is markedly different, both from a control as a perceptual point of view, and is referred

to as an *anticipation* task (Mulder, 1995). From the perspective of investigating pilot control behaviour in these two tasks, a literature survey (Mulder, 1994) indicated that much can be learned from the findings in automobile driving research. Therefore, some investigations in automobile driving will be discussed in the next section. In §2.5 both the vehicular control research domains will be linked together again.

2.4   Research in automobile driving

Why is automobile driving research important here?

The striking resemblances between the task of guiding an aircraft along a trajectory in space with a perspective flight-path display and that of controlling an automobile along a road were mentioned first in (Wilckens & Schattenmann, 1968). The principal similarities that are relevant in the current research context were identified in (Mulder, 1994):

- The *preview* of the trajectory ahead conveys the current and future guidance constraints, allowing the driver or pilot to anticipate changes in the oncoming trajectory.
- The task objective is not necessarily to minimize all guidance errors. A *boundary control* task is executed in which the guidance errors are kept within the constraints presented by the road or tunnel boundaries.
- The control-related information is perceived from the out-of-the-window visual scene or from a synthetic representation of that scene. The effects of the control inputs immediately lead to changes in the visual scene. Hence, the human perception and action skills are supported through the *representation of both perception and action in the same spatial format*.
- Both are *vehicular control* tasks: a multi-dimensional vehicle state must be perceived and controlled such that stability is guaranteed and performance goals are met.

There are also some important differences. The control of an aircraft is more difficult due to the larger number of degrees of freedom, the less favourable dynamics, and the higher velocities involved. Furthermore, whereas an automobile driver usually has an almost unobscured view on the outside world, with a tunnel display the pilot is confronted with a *synthetic representation* of that world on only a small-sized CRT.

Behavioural and control-theoretic automobile driver models

Validated driver models exist for driving tasks such as lane keeping and lane-change manoeuvres (Crossman & Szostak, 1968; Weir & McRuer, 1968; Weir, Heffley, & Ringland, 1972; McRuer, Allen, Weir, & Klein, 1977; Donges, 1978; Reid, Solowka, & Billing, 1981; Reid, 1983). In these investigations the principal interest is the way in which drivers extract the control-related information from the visual scene (McRuer et al., 1977). The usefulness of these visual cues are usually examined in the following ways:

- By considering the *guidance and control requirements* of the human-vehicle system, a system **controllability** analysis, yielding a set of vehicle motion states that must be sensed and control actions that must be initiated to satisfy the guidance demands.

- By determining the *availability and functionality of the visual cues* in the visual field, a system **observability** analysis, yielding a set of vehicle motions that can be sensed and used for control, on various levels of usefulness.

- By performing *eye-movement experimental studies*, which could lead to an identification of the most utilized visual cues.

Some of the main representants and findings of these three approaches are discussed below.

Effects of trajectory preview   Central in most driver-modelling attempts is the notion of *duality* of information conveyed by the view of the road ahead (Donges, 1978). First, the visual field provides *preview* information on the instantaneous and future course of the road, the *forcing function*, which is used for vehicle *guidance*. Second, static and dynamic visual cues contain information on the instantaneous deviations between the vehicle's path and the reference trajectory. These visual cues are used to *stabilize* the vehicle motion. Therefore, the automobile driver is generally modelled on two *levels* of control. The high level represents the utilization of the preview of the future trajectory, yielding an open loop *anticipatory* control activity. The anticipatory control mode represents the driver's guidance response to the *deterministic* forcing function, the road ahead. The lower level represents the continuous control of the position and heading of the vehicle, yielding a closed loop *compensatory* control activity. The compensatory control mode represents the driver's control response to the *stochastic* control errors, the perturbations by wind (Donges, 1977). A driver, who is controlling the compensatory inner loops, occasionally switches to the anticipatory control level, a strategy referred to as *intermittent* control.

Perceptual studies   Perceptual studies usually start with a mathematical analysis of the elements in the visual scene that could provide the control-related information (Gibson, 1950; Gordon, 1965, 1966a, 1966b). Experiments are then conducted, e.g. using eye-trackers, in an attempt to relate the driver's steering responses to the features in the environment being looked at. These experiments generally support the duality in the available information stated above. Eye-movement patterns reveal that drivers use the *entire* view of the road ahead for automobile guidance (Gordon, 1966b). An intermittent visual attention allocation, yielding observation of the entire range of preview ahead, is required by the needs for *anticipation* and *vehicular alignment*. The need for *anticipation* requires the driver to look farther ahead to obtain a general idea of conditions (the road curvature) that have to be met in the near future. Close-up viewing results from the need to *align* the vehicle with the road. In following a curved section of the road, the driver looks into the curve at a shorter range of viewing distances than when following a straight section (Kondo & Ajimine, 1968). An experienced car driver has an accurate internal representation of the vehicle handling qualities and the disturbances acting on the vehicle, but also in terms of perceived changes in the future trajectory. In eye-movement

studies of Kondo and Ajimine (1968) and Shinar, McDowell, and Rockwell (1977), it is found that drivers exhibit anticipatory lateral eye movements some time before the change in trajectory started. In what is referred to as the *curve negotiation* process, drivers estimate from the road ahead the trajectory changes in terms of curvature and roadway characteristics. Based on this information and their internal representation, drivers initiate an anticipatory control action to intercept the curve.

Control-theoretic models The division of the driver behaviour into anticipatory and compensatory control is a well-established theoretical hypothesis. The way in which the two control levels are modelled, however, shows some alternative viewpoints, especially for the anticipatory mode. Many possible ways exist in which the use of the preview information can be modelled. Do drivers fixate at a single point ahead of the road, do they look at a fixed angle into a roadway curve, or do they use an interval of future errors? In addition, do they act on perceived changes in future position, or heading, or road curvature? In general, using a one-point looking distance approximation of the effect of the previewed road ahead can lead to satisfactory results (McRuer et al., 1977; MacAdam, 1981; Guo & Fancher, 1983). The modelling attempts reported in (Grunwald & Merhav, 1976), however, showed that it takes at least a two-point looking distance model to describe human control behaviour properly. This is confirmed in (Hess, 1981; Hess & Modjtahedzadeh, 1989) where this fact is attributed to a driver's need to estimate the *trend* in the forcing function, which is impossible with a single-point looking model. Yet, it is the trend that makes the preview worthwhile, because it allows an *inversion* of the low-frequency vehicle dynamics, yielding a *perfect* feed forward controller (Hess, 1981). Almost all modelling attempts consider the *road curvature* as the primary perceptual cue for anticipatory control (McRuer et al., 1977; Donges, 1978; Reid et al., 1981; Reid, 1983).

Error-neglecting control The control-theoretic driver models are based on the assumption that drivers control their vehicles in a continuous error-correction mode. Godthelp (1984), however, pointed out that, because of the boundary control nature of a driver's task, drivers do not need to minimize the guidance errors per se. Rather, these errors can be *neglected* up to that moment the driver decides to act on them again, yielding a different control strategy referred to as *error-neglecting control*. Godthelp showed that the driver's internal representation allows the estimation of a *temporal* rather than a spatial range with respect to the road boundaries, the so-called Time-to-Line Crossing (TLC) variable. In error-neglecting control, drivers can neglect the path errors up to the moment the temporal range, the TLC, drops below a certain threshold. The preview of the trajectory ahead allows the driver to maintain a *temporal region of safety*, similar to the *field-of-safe-travel* concept reported by Gibson and Crooks (1938). Blaauw (1984) describes a way to model the driver's error-neglecting control behaviour.

Research implications

The relevance of the automobile driving investigations for the present research is unequivocal. In both the guidance tasks the trajectory to be followed is the *deterministic* forcing

function of the human/vehicle control system. The disturbances (wind, control inaccuracies) that act continuously on the vehicle are the main *stochastic* inputs. The task of following the trajectory presented in a spatial format, allowing *preview* of the forcing function, is *dual*. First, the operator must keep the vehicle aligned with the trajectory in the presence of disturbances. Second, the operator must anticipate oncoming changes in the trajectory. The *boundary control* task allows the human controller to act in different ways, i.e. more than one control strategy applies. The task of staying within the space-restricted trajectory yields a continuum between the strategy of continuously compensating for all guidance errors and that of neglecting all errors as long as the – spatial and/or temporal – guidance constraints are satisfied. Obviously, the freedom in adopting or selecting a strategy within this continuum depends strongly on the *task* of the human controller.

2.5   Taking a cybernetic approach

2.5.1   Re-examining the pilot's guidance task

The definition of the pilot's guidance task, §2.3, will be re-examined in the light of the findings of the previous section.

Error-neglecting control?   A perspective flight-path display allows pilots to adopt a control strategy that suits them best in satisfying their task objectives (Wilckens, 1973). When the path-following constraints are low, i.e. for large tunnel sizes, pilots might be tempted to relax the guidance activities and put their attention temporarily to other tasks. This could result in periods of *error-neglecting* control similar to those observed in automobile driving. Indeed, a temporal variable similar to that of the TLC, the Time-to-Wall-Crossing (TWC) variable, has been proposed in (Mulder, Theunissen, & van der Vaart, 1995). Although this type of behaviour is certainly relevant in the present context, it is considered to be of only secondary importance. One of the main motivations for developing the tunnel display in the first place has been to allow *high-precision* manual trajectory-following. Secondly, in flight the guidance constraints especially when approaching the landing runway are much higher than on the road and will certainly not allow pilots to temporarily neglect (for more than a very short while) the guidance task. Third, there is the matter of passenger comfort: it is very uncommon that an aircraft is allowed to *waggle* its way along the trajectory; at least the aircraft roll angle must be kept constant during an approach to landing. Therefore, it is hypothesized that the most important part of pilot behaviour will be that of high-precision manual guidance and control, requiring considerable attention from the pilot. The present work focuses on the pilot *error-correcting* task of *flying the aircraft through the tunnel as accurately as possible* (Mulder, 1995).

Preview   The preview of the trajectory ahead allows pilots to anticipate future changes in the trajectory. The task analysis of §2.3 identified two types of tasks: *regulation tasks*, i.e. following straight or circular trajectories, and *anticipation tasks*, i.e. controlling the transient manoeuvres between straight and circular sections. In the **regulation tasks**

the trajectory type remains the same and there is no need for anticipating any changes. The only concern of the pilot is to maintain a stationary tunnel image and compensate for perturbations in this image. "*When the vehicle is aligned with a straight or regularly curved highway, the road assumes a steady state appearance. The borders and lane markers remain almost stationary in the driver's field of view. The driver's problem in lateral guidance, ..., may be to maintain an acceptable steady state condition and to null deviations from the steady condition by utilizing visual feedback information.*" (Gordon, 1966a). This statement is adopted to be one of the main hypotheses of this thesis and will be elaborated further in Chapter 3. So, in the task of precisely following a time-invariant trajectory, the question remains: 'what is the added value of preview after all?' There is no need for anticipating changes in the trajectory and the guidance constraints remain the same. Preview of the trajectory ahead shows a spatial representation of the commanded trajectory and the motion condition itself. It allows the operator to *directly perceive* the errors in vehicular guidance and to establish *spatial* feedback loops compatible to those applied in every-day locomotion. For instance, if the aircraft direction of motion is aligned with the trajectory but it is not positioned on the trajectory, a control action is needed to bring the aircraft back on track. When the aircraft is positioned towards one of the sides of the tunnel but its motion is directed towards the center, there is no need for a control action. But this has nothing to do with *error-neglecting* control, it is simply the operation of a well-damped feedback system: a Flight-Director in principle uses the same feedbacks to generate the command signals (Wilckens, 1973). The tunnel, however, allows pilots to close the control loops themselves and to choose their own particular feedback gains.

In the **anticipation tasks** the desired trajectory changes abruptly (even discontinuously) and so do the aircraft *reference* states such as the roll angle. The pilot anticipation task is to control the transient manoeuvres between the two reference conditions of *recti-linear* and *curvi-linear* motion. When anticipating a curve the aircraft is still on a straight section immediately preceding the curve. Here, preview is essential: pilots must estimate the oncoming change in trajectory curvature and, based on their internal representation, initiate an open-loop *feed forward* control action to start the manoeuvre. The aircraft will start to develop the required lateral acceleration to follow the oncoming curvature. Hence, the pilot anticipation task involves the *timing* of the feed forward control action and the estimation of the required *amplitude* of this control action. During the transient manoeuvre the pilot checks the validity of the feed forward control action by compensating for errors in this action through feedback. Methods to model this type of behaviour are discussed in (Mulder, 1994, 1995). In this thesis the pilot anticipation task of conducting a curve transition manoeuvre will be analyzed in qualitative terms in Chapter 10.

2.5.2   Towards a mathematical description of the regulation task

A multiple-axis, multi-loop regulation task   The main working hypothesis in this thesis is that *the pilot controls the aircraft along the trajectory as accurately as possible*, or, equivalently, *the pilot continuously compensates for the effects of the disturbances*. This
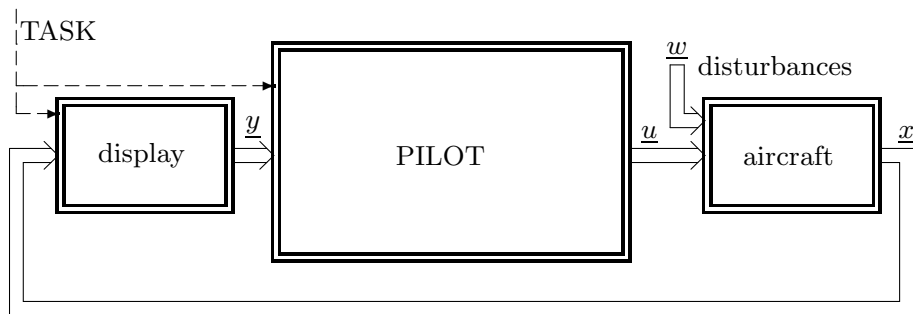
(a) the general non-linear aircraft control situation
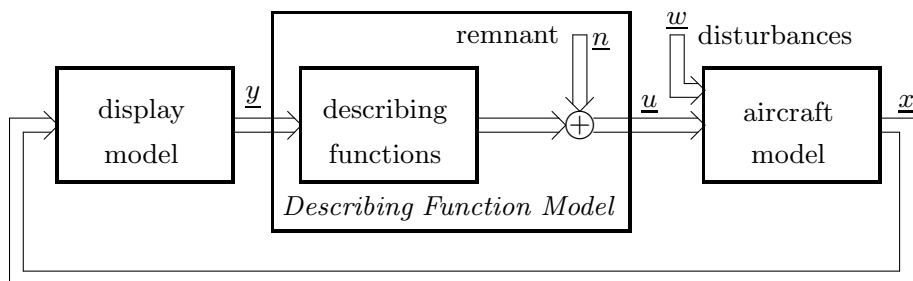
(b) the general situation after linearization of all components
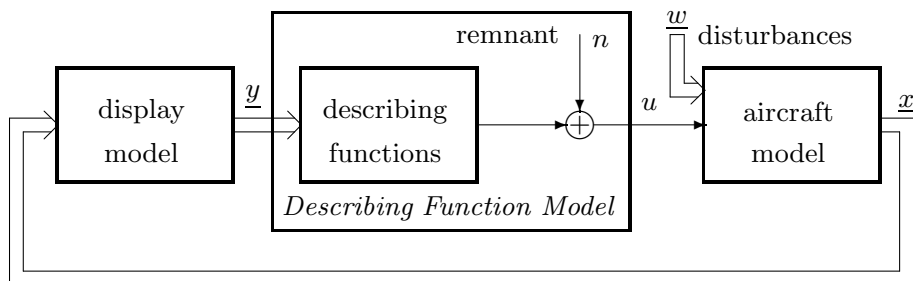
(c) the single-axis, multi-loop aircraft regulation task

Figure 2.9: The general pilot-in-the-loop situation considered in this thesis, and the consequences of the various simplifying assumptions. In this figure $\underline{x}$ and $\underline{w}$ represent the aircraft state vector and the atmospheric disturbance vector, respectively. The aircraft state vector is transformed in the display block into a set of optical cues, depicted by $\underline{y}$, that are observed by the pilot. The pilot responds to these cues with control actions $\underline{u}$. The pilot control behaviour can be described as the sum of the output of a set of linear describing functions and a remnant signal vector $\underline{n}$.

results in the multiple-axis, multi-loop regulation task of Fig. 2.9(a). A pilot controls ($\underline{u} \in \mathcal{R}^{\ell}$) the aircraft, disturbed with atmospheric turbulence ($\underline{w} \in \mathcal{R}^s$), along the tunnel trajectory. The aircraft state ($\underline{x} \in \mathcal{R}^n$) is presented with the tunnel display.[1] Perturbations (i.e. attitude and position errors) from the reference trajectory yield a set of optical cues ($\underline{y} \in \mathcal{R}^m$) which allow pilots to perceive the aircraft state with respect to the trajectory.[2] The aircraft dynamics, the effects of the atmospheric turbulence, the pilot control behaviour and the display transformations are all in principle *non-linear*. Since the analysis of non-linear systems is difficult and not many techniques exist for their evaluation, much can be gained by linearizing the elements in the control loop:

- The <u>aircraft dynamics</u> can be linearized well around any stationary flight condition (Etkin, 1972). An obvious choice would be the flight condition that is appropriate for the reference trajectory, i.e. a recti-linear or curvi-linear aircraft flight condition. The linearized aircraft models are described in Appendix C.

- The <u>display transformations</u>, describing the relation between the aircraft state and the optical cues, can also be linearized. In conjunction with the linearization of the aircraft dynamics, an attractive operating point of linearization is the situation of zero aircraft position and attitude errors with respect to the reference trajectory. The display *model* then consists of the linearized expressions for the set of optical cues, i.e. $\underline{y} = \mathcal{T}(\underline{x})$. This description will be the subject of Chapter 3.

- The <u>human pilot</u> can be modelled according to the *describing function method*, which decouples pilot control behaviour into a causal mathematical description and a remnant model (McRuer, Graham, Krendel, & Reisener Jr., 1965). The implications of this method are discussed in §2.5.3 and in Appendix E.

The linearization yields a closed loop system that is linear, Fig. 2.9(b).

The single-axis, multi-loop regulation task In most cases in this thesis the pilot has only one output signal, $\ell = 1$. In controlling an aircraft this means that the pilot either controls the so-called *asymmetric* or horizontal aircraft motions or the *symmetric* or vertical aircraft motions (Appendix C). This yields the control task that is the starting point of the analysis here: the *single-axis, multi-loop aircraft regulation task* of Fig. 2.9(c).

The linear aircraft model Linear dynamic models can be obtained that are representative for the aircraft symmetric and asymmetric motions (Etkin, 1972). The simplified linear models, depicted in Fig. 2.10, consist of a cascade combination of three transfer functions connecting the main elements of the aircraft state vector: the attitude angles ϕ (roll) and θ (pitch), the flight-path angle errors χ_e and γ_e (defined relative to the trajectory), and the position errors x_e and v_e (relative to the trajectory). The transfer functions are described in Appendix C. In each channel three loops must be closed by a

---

[1] The TASK variable affecting the display reflects the properties of the reference trajectory. It is assumed that these properties are *time-invariant*: the trajectory is either straight or circular.

[2] As has been stated in Chapter 1 all sources of information other than those presented by the visual display, such as motion cues, are neglected in this study.
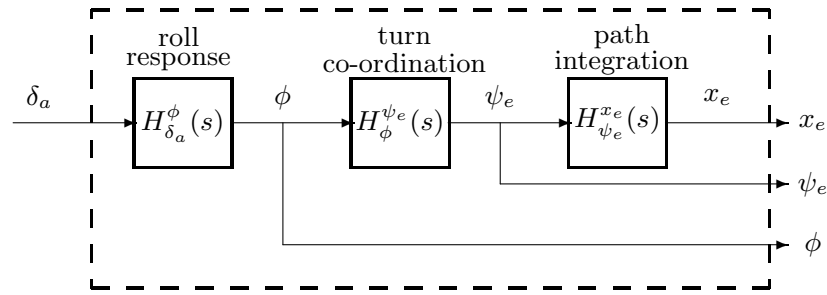
(a) asymmetric aircraft dynamics (simplified)
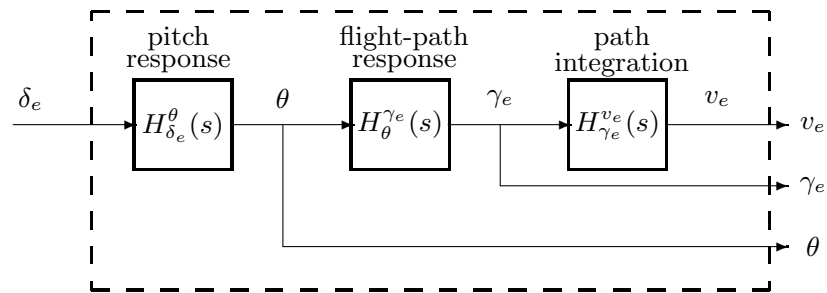
(b) symmetric aircraft dynamics (simplified)

Figure 2.10: The simplified linearized aircraft dynamics. The aircraft states for the *asymmetric* motion are the roll angle ϕ, the flight-path angle error χ_e (which equals the heading angle error ψ_e in the no-slip condition) and the lateral position error x_e. The aircraft states for the *symmetric* motion are the pitch angle θ, the flight-path angle error γ_e and the vertical position error v_e. The aileron δ_a and elevator δ_e controls are the inputs of the asymmetric and symmetric channels, respectively.

pilot, which are referred to as the *inner loop* (aircraft attitude), the *middle loop* (aircraft flight-path angle error, the direction of motion with respect to the track) and the *outer loop* (the aircraft position with respect to the track). Although not shown in Fig. 2.10 the aircraft disturbances are essential in the experimental analysis, Chapter 4.

The linear display model   The display model consists of a set of linearized expressions relating the aircraft state, $\underline{x}$, with the optical cues conveyed by the spatial display: $\underline{y} = \mathcal{T}(\underline{x})$. Fig. 2.11 shows a number of *static* screen shots of the tunnel geometry, presenting a straight trajectory, for several combinations of the lateral position error x_e and the heading angle error ψ_e. In case of perfect alignment of the aircraft with the trajectory the tunnel image is *symmetric*, and any deviation from the trajectory yields a distortion of this symmetrical condition (Theunissen & Mulder, 1994). The optical deviations from any particular aircraft reference condition can be used for control purposes because they reflect deviations from the ideal situation (Mulder, 1995). Hence, it can be hypothesized that the pilot perceives the aircraft motion state relative to the trajectory through the

$$\psi_e \ [\text{deg}] \rightarrow$$
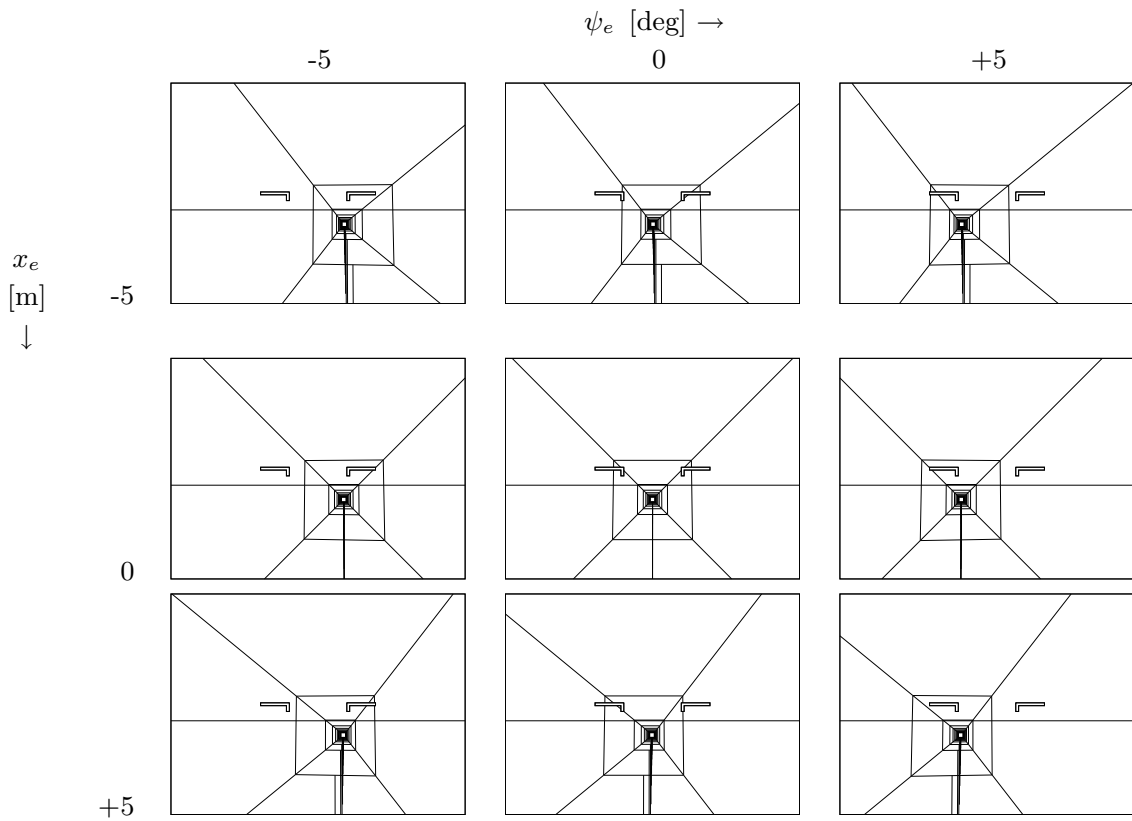
Figure 2.11: Distortion of the symmetry in the geometry of a generic tunnel-in-the-sky display. x_e and ψ_e represent the lateral position error and the heading angle error with respect to the trajectory, respectively.

optical changes in the tunnel geometry: $\hat{\underline{x}} = \mathcal{T}^{-1}(\underline{y})$. Two intimately related questions are important here, i.e. 'what information does the pilot perceive for purposes of control?', and 'how is the information presented on the display?'. These topics, referred to as *information processing* and *information transfer*, respectively, are the subject of Chapter 3.

2.5.3 Modelling the human pilot

Many attempts have been conducted in the past to obtain a mathematical description of human control behaviour for numerous applications. A short retrospective will be given below, for a more detailed discussion the reader is referred to Appendix E.

The quasi-linear pilot model The human controller is a complex control and information processing system. Human controllers are time-varying, adaptive, often non-linear, and the control behaviour is essentially stochastic (McRuer & Jex, 1967). Such systems are difficult to be characterized in mathematical terms. Research in the two decades after WW-II resulted in the successful application of *quasi-linear* describing function theory to the problem of modelling human control behaviour in the single-axis compensatory tracking task (Krendel & McRuer, 1960). The resulting pilot model, referred to as the

quasi-linear pilot model Fig. 2.9(b), operates in the frequency domain.

Classical control theory: *descriptive* **(structural-isomorphic) pilot models**   The describing function modelling technique was applied by McRuer and his colleagues in the late 1950s and the early 1960s in their research into compensatory control tasks (Krendel & McRuer, 1960). The model structure and model parameters obtained experimentally by using the quasi-linear describing function models had predictive significance *only* in applications that were similar to the experimental conditions. No attempt was conducted to relate the model structure or model parameters with the task variables. This changed with the publication of McRuer et al. (1965), a landmark report that described the phenomenon that human controllers *systematically adapt* their control behaviour to the dynamics of the system to be controlled and the bandwidth of the disturbances. This systematic adaptation of human control behaviour was generalized in the so-called *Crossover Model* (COM) theorem, §E.2, that relates the structure and parameters of the *causal* part of the quasi-linear pilot model to the task variables. This theorem allows human control behaviour to be *predicted*. Attempts to parameterize the causal model yielded the development of the so-called structural-isomorphic models such as the *precision model* and the *simplified precision model* (McRuer & Jex, 1967). The model parameters can be determined from the so-called *verbal adjustment rules* which relate them to the task variables. The descriptive models are widely used in human-machine studies.

Modern control theory: *algorithmic* **pilot models**   The advance of modern control theory in the mid-1960s resulted in the concepts of optimal filtering (LQG) and optimal control (LQR) (Kwakernaak & Sivan, 1972). One of the first attempts to describe human control behaviour in the paradigm of optimal control and estimation theory yielded the *Optimal Control Model* (OCM) (Kleinman, Baron, & Levison, 1970b, 1970a), see §E.3. Here, the input-output relation of the human operator is compared with an *optimal* controller, instead of only a *stabilizing* controller. The algorithmic model consists of an optimal *observer*, generating an optimal state estimate of the system to be controlled, and a deterministic *regulator* which transfers the estimated state into the optimal output, Fig. E.6. In contrast with the structural models which *describe* what the pilot is doing, the optimal control model is a *normative* model, i.e. it describes what the pilot *should* be doing given the inherent limitations and the task variables at hand. The OCM was believed to be suitable for a more general application area, having a wider objective than the describing function models (Kok & van Wijk, 1978; Wewerinke, 1989). In spite of this, however, the algorithmic model has not become as widely used as the structural models, which can be attributed primarily to the fact that the algorithmic model is over-parameterized (van Wijk & Kok, 1977), hampering the model validation significantly.

Modelling approach in this thesis

Manual control studies of human-machine systems have been mainly focused on the single-input single-output (SISO) control task. In the aircraft control case studied here, the operator has to perceive and control more than one variable at a time. The number of

applications of multi-loop operator models has been relatively small (Stapleford, McRuer, & Magdaleno, 1967; Stapleford, Craig, & Tennant, 1969; Weir & McRuer, 1972; Weir et al., 1972; van Lunteren, 1979; Reid, 1983). A reason for this could be that, since the identification of the describing function for single-axis tasks is already a tedious procedure, these difficulties are tremendous when multiple-loop tasks are considered.

The Multi-Loop Model and the Optimal Control Model   The goal of this thesis is *not* to develop yet another control-theoretic pilot model. Rather, the analysis focuses on the applicability of the two pilot modelling approaches introduced above. A multi-loop structural model, referred to as the *Multi-Loop Model* (MLM), is applied to represent the classical modelling approach. It is defined in the frequency domain using elementary transfer functions that consist of basic elements such as gains, lead/lag filters and a time delay. Generally, developing a MLM pilot model resembles the development of an automatic controller for the system under control, extended by incorporating the main human limitations, such as the time delay and the neuromuscular dynamics (McRuer & Jex, 1967). The MLM is described in detail in §E.2. Second, the *Optimal Control Model* (OCM) is applied to represent the modelling approach rooted in modern control and estimation theory. The MLM and OCM models are described in §E.2 and E.3, respectively.

OCM and MLM outputs   The frequency domain MLM and the time domain OCM models both provide model outputs in both the frequency and the time domain. The frequency domain results are the model descriptions of the various feedback loop closures of the human pilot, i.e. a set of transfer functions. The OCM also results in a prediction of the spectrum of the pilot's remnant signal. The time domain results are the model predictions of the variances of all signals in the closed loop pilot/aircraft system. The methods to calculate the MLM and OCM outputs are described in Appendices E and F.

Model validation   Validation efforts aim at comparing the model outputs with the experimental data. The data that are easiest to obtain are the statistics of all measurable signals in the loop, and many validation attempts of especially the OCM have been based only on the time domain data (e.g. Grunwald & Merhav, 1976; Wewerinke, 1976). This can be attributed to the difficulty of obtaining estimates of the pilot frequency responses, especially in multi-loop cases. In this thesis it is attempted to use the experimental data in *both* the domains in the model validation procedure. For this purpose, the pilot describing functions determining the loop closures depicted in Fig. 2.9(c) must be estimated, a procedure which is discussed further in Chapter 4. The extensive model validation efforts of both the MLM and the OCM models will be one of the principal themes of this thesis.

2.5.4   Another model-based approach?

The pilot's guidance task of following a curved trajectory has been analyzed in this chapter. A number of sub-tasks can be distinguished that fall in the category of either a *regulation* task or an *anticipation* task (Mulder, 1995). The tunnel display acts as a medium that shows the guidance information pilots need in performing the task, enabling them to

Table 2.1: List of experiments described in this thesis. In this table the task can be either a **R**egulatory or an **A**nticipatory control task. The control dimension is either **L**ateral or **V**ertical aircraft control, or both.

experiment	thesis chapter	control task	control dimension	subject of investigation
X1	5	**R**	**L**	the effects of the tunnel size
X2	6	**R**	**L**	the effects of the viewing distance
X3	7	**R**	**L & V**	optical cues in straight tunnel sections
X4	8	**R**	**L**	optical cues in curved tunnel sections
X5	9	**R**	**L**	symbology: a flight-path vector
X6	10	**A**	**L**	curve initiation

interact with the aircraft appropriately. The results of the control actions immediately result in changes in the tunnel image that allow the pilot to obtain an estimate of the vehicle motion through the synthetic three-dimensional world. The *coupling of perception and action* in the tunnel display stands central in the next two chapters.

Active psychophysics There are many different ways to examine pilot behaviour. The approach adopted here puts special interest on describing pilot behaviour with mathematical models. The ultimate goal of modeling the pilot behaviour is *not* the model itself. Rather, the modeling techniques are used to act as a *tool* to gain insight on how the tunnel display geometrical design variables affect pilot behaviour as seen from both a perception and a control perspective. More specifically, the models are used to examine the *changes* in pilot behaviour that result from applying different tunnel *geometrical* designs. A similar approach, referred to as *active psychophysics*, emerged in the late 1980s in other investigations (Flach, 1991).

Experimental studies The theories discussed in this chapter and the following two chapters are evaluated in a total number of 6 experiments, labelled X1 to X6, listed in Table 2.1. The experiments can be seen as *case studies* in the attempt to get a grip on pilot/display interaction with a generic tunnel-in-the-sky display format. All experiments investigate pilot behaviour in the aircraft regulation task, except for Experiment X6 that examines anticipation task of intercepting a curved section of the trajectory. The experiments have in common that the tunnel geometrical design acts as the main experimental variable that is being manipulated. The only exception is Experiment X5 in which the effect of the *flight-path vector* symbol, introduced in §2.2.2, is analyzed. Attention is focused on the effects of these different tunnel display designs on pilot performance, control behaviour and workload. The specific topics addressed in the experiments all originate from the findings discussed in the theoretical part of this thesis, in particular Chapter 3.

Chapter 3

Information transfer and information processing

3.1 Introduction

An investigation of the applicability of a display interface between a human and a machine must account for the properties of their interaction. In performing the guidance and control tasks of flying through the tunnel, pilots need information about the aircraft's motion state in terms of its attitude, flight-path angle and position, all relative to the trajectory, and about the trajectory to be followed. The previous chapter addressed the interaction from the perspective of the pilot's *task*. In this chapter the properties of the tunnel display as a means for providing the control-related information to the pilot will be discussed. This constitutes the second stage of the cybernetic approach.

Transformation of information   The tunnel display shows the aircraft motion state, $\underline{x}$, by means of an array of optical cues, $\underline{y}$, Fig. 2.9(c). A complex transformation exists between both variables: $\underline{y} = \mathcal{T}(\underline{x})$. In conventional, planar, cockpit displays that show the aircraft state through a set of individual indicators, this transformation is simply a one-to-one mapping. The pilot can pick up the information by scanning the cockpit instruments. In the tunnel display the aircraft status variables are shown in an *integrated* fashion through the projection of a regular geometrical shape on a picture plane, and the transformation is far more complex. The pilots' ease in using the perspective display versus the conventional, planar, displays in controlling their aircraft seems contradictory when considering the relative complexity in the transformation $\mathcal{T}$ applied in both the presentation methods. Apparently, the perspective tunnel display conveys the control-related information in a way that is *compatible* to a human perceptual system, and pilots seem to pick up this information *immediately* from the array of optical cues. Some refer to this phenomenon as *holistic perception* (Wickens, 1992) a term that seems to stem from the philosophical standpoint of *direct perception* in ecological psychology (Gibson, 1986).

But what does this mean? To answer this question two intimately related cybernetic issues must be dealt with: information transfer and information processing.

Information transfer and information processing   These terms do *not* indicate stages in perception. Rather, they are used here to distinguish between those properties of pilot-display interaction that can be described in mathematical terms and those that can not. *Information processing* deals with the question of how pilots perceive and use the information presented in conducting their task. It focuses on the perceptual and cognitive mechanisms of the human observer and is rooted in the research disciplines of psychology and physiology. The knowledge collected in these domains guides the selection and analysis of the most informative optical cues conveyed by the display, i.e. what cues are important and what cues are not. *Information transfer* refers to a mathematical description of the characteristics of the optical cues in terms of the aircraft motion state, the display design variables, and the properties of the perspective projection. In short, information transfer is a matter of *geometry*, whereas information processing is a matter of *psychology*. The first issue can be solved analytically, the second one can not (Warren & Owen, 1982).

In the tunnel display context the most important issue in investigating human information processing is the visual perception of three-dimensional scenes in motion. The earliest developments in this field were conducted by perceptual psychologists, most notably Gibson, who focused on the empirical question of *what is* the mechanism by which humans perceive visual motion (Gibson, 1950). Later, the computational vision scientific community addressed the issue from both a normative (*what should be* the mechanism) and a theoretical (*what could be* the mechanism) standpoint (Singh, 1991), in order to formulate a theory of visual motion perception that can be used in an automaton, i.e. machine vision. Results of a literature survey in the research domains of psychology, physiology, human engineering and computational vision, summarized in §3.2 form the basis of this chapter. For a preliminary study, the reader is referred to (Mulder, 1994).

Recti-linear and curvi-linear motion   In accordance with the analysis of the pilot's guidance and control tasks, conducted in §2.3, the information conveyed by the tunnel display is analyzed for the two elementary aircraft stationary flight conditions:

1. **recti-linear motion**, the motion along a *straight* trajectory, and
2. **curvi-linear motion**, the motion along a *circular* trajectory.

In both cases[1] the discussion starts with a mathematical analysis, information transfer, of potential optical cues (§3.4 and §3.6), with the goal of investigating how small deviations from the two reference flight conditions are coded in the perspective display. Then, the pilot's perception and use, information processing, of a selected set of optical cues in order to control the aircraft in the two motion conditions will be discussed (§3.5 and §3.7). Here, the functionality of the optical cues for the pilot's task is analyzed at the hand of the findings reported in literature in conjunction with their characteristics revealed by the mathematical analysis. Summarizing, the chapter starts with a survey of literature on

---

[1]The *transition* between straight and curved sections in the trajectory will be discussed in Chapter 10.

human visual motion perception in §3.2 (the *human*-side of the HMI) followed by a brief introduction of perspective projection methods in §3.3 (the *machine*-side of the HMI). The two aircraft reference flight conditions of recti-linear and curvi-linear motion are analyzed in §3.4 to §3.7. The chapter concludes with a retrospective of the main findings, §3.8.

3.2 *Human* – Human visual motion perception

A short introduction of human visual motion perception, in particular the ecological approach, will be given in §3.2.1. To clarify the theoretical issues an example is provided in §3.2.2, which will prove to be very relevant in the tunnel display context. The determination of the functionality of a source of optical information is the subject of §3.2.3.

3.2.1 Ecological optics and the visual perception of egomotion

The question 'how do humans perceive their environment' has puzzled scientists for centuries. The visual system, in particular the eye, has long been regarded as an organic analog of a camera. The eye's pupil serves as the center of projection of all incoming light rays, projecting the three-dimensional world onto a two-dimensional surface, the retina. Because in this projection one dimension, depth, was lost, the primary issue in visual perception was the reconstruction of the 'lost' dimension, i.e. 'how do humans perceive depth?' It was hypothesized that perception started with *form*, a static representation of the environment. Then, a number of cues for depth could be used to 'add' the third dimension: the *monocular* depth cues of linear perspective, apparent size, light and shade, relative motion, aerial perspective and accommodation, and the *binocular* depth cues of binocular disparity and convergence. During WW-II the psychologist Gibson assisted the USAF in developing their pilot selection and training programs. Equipped with the theory of depth perception, tests were developed with the objective to predict the success or failure of a student pilot in tasks as landing an aircraft. None of these tests were successful, disappointing Gibson to the point that he believed that "*the whole theory of depth perception was false*" (Gibson, 1986). In the decades that followed Gibson developed a radically different theory of visual perception. He noted that "*optical rest is a special case of optical motion, and <u>not</u> the other way around*" (Gibson, 1955). Therefore, the "*psychology of aircraft landing does not consist of the classical problems of space perception and the cues for depth. It is a psychology of locomotion, that occurs in time as well as in space, and the problems are those of the judgements required for the control of locomotion. The fundamental visual perception is that of approach to a surface*" (Gibson, Olum, & Rosenblatt, 1955). And "*What gives rise to the perception of motion ... it is not the motion of light over the retina ... but something that happens in ambient light. This is not easy to specify and measure, but it is surely a change in the structure of the array*" (Gibson, 1968). Now we know that Gibson discovered the optic flow field, or, as Koenderink (1986) puts it, "*Gibson was the first to notice that the deformation of the retinal image due to egomotion ... is not just a nuisance but actually a rich source of information concerning*

the world." Gibson recognized that during locomotion the cues of *motion perspective –* the gradients of velocities in the visual field corresponding to the elements of a physical surface – carry information about one's locomotion as well as information about the surface itself (Gibson, 1954). The optic flow field is considered the *ecological stimulus* for vision because it is a stimulus that is inherently *spatio-temporal* (Lee, 1980b): it reveals information about the environment to a larger degree than static optic arrays do (e.g. Lee, 1974, 1980a; Clocksin, 1980; Longuet-Higgins, 1984; Koenderink, 1986). Conversely, perception is necessary to guide movements of the body. This *reciprocity of perception and action* leads to the ecological axiom that both constitute the same functional unit (Rieger, 1983). "*The active observer (during locomotion) ... controls the flow and thus objectifies his information in a sense that is impossible in the static case*" (Koenderink, 1986).

Principles of ecological optics   Ecological optics is the study of the information available in light (Gibson, 1961). The principles of ecological optics relevant in the study of visual perception of locomotion are (Warren & Owen, 1982):

- The light coming to a moving point of observation is *structured* owing to the structure of the environment and the observer's travel.

- The optical structure is *constantly changing*, owing to the observer's travel and to events in the environment.

- Over the changing structure or transformation of optical structure, there remain properties that do not change and that are thus *invariant over the transformation*.

The latter properties, referred to as *optical invariants*, are claimed to form the basis of the information used by active observers to control their locomotion through the environment. An example is the visual angle subtended between the optic horizon and the aim point during an approach along a straight line to a surface (Lintern & Liu, 1991).

The visual perception of egomotion

Gibson (1968) postulated that for the control of locomotion two types of information are needed: (i) *exterospecific* information about the layout of the surfaces in the environment, and (ii) *propriospecific* information about the human's own body movements. To capture the *relativistic* nature of the perception and action cycle, Lee and Lishman (1977) proposed a third type of information, labelled *expropriospecific* information, marking information about the position, orientation and movement of the body relative to the environment. Expropriospecific information is necessary to *guide* the body through the environment, allowing the observer to foresee his motion relative to the environment (Lee & Lishman, 1977). These types of information are in principle contained in the optic flow field (Lee, 1980b, 1980a; Koenderink & van Doorn, 1981; Rieger, 1983; Koenderink, 1986).

The components of optic flow   The optic flow field is the optical concomitant of the observer's egomotion through the environment (Warren, 1976). It consists of four basic

components (Koenderink, 1986): (i) *translation*, resulting from movement in a plane perpendicular to the viewing axes, (ii) *isotropic expansion/contraction*, resulting from movement along the viewing axis, (iii) *rotation*, resulting from a rotation along the viewing axis, and (iv) *shear*, resulting from a rotation perpendicular to the viewing axis. Whereas translation and rotation do not result in a deformation of the visual field, the other components *do*. Translation leads to a *lamellar* (parallel) flow pattern, rotation leads to a *rotary* pattern, expansion/contraction leads to a *radial* pattern and shear leads to a deformed pattern. The pattern of the *total* changing optic array is determined by the addition of the components that are specific for the locomotion and structure of the environment.

Information in optic flow fields The structure of the optic array is determined by the layout of the environment and the locomotion of the observer. Locomotion of the observer yields information about the *segmentation* of the visual field into coherent entities and of the visual world into coherent objects (Gestalt law of 'common fate') (Koenderink, 1986). Two types of locomotion are commonly studied: recti-linear and curvi-linear motion (Gordon, 1965, 1966b). Recti-linear motion with respect to a surface results in a radial expansion pattern when looking in the direction of motion. The *direction of motion* is specified in the optic flow field by the *focus of radial outflow* (FRO), i.e. the point in the optic array that does not move relative to the observer (Gibson, 1950). Hence, the FRO is an optical invariant of the optic flow field, the perception of which can aid the moving observer in judging the heading of the locomotion with respect to the environment (Gibson, 1950). When the FRO is positioned on the optical horizon, the locomotion is parallel to the ground surface. When the FRO is positioned below the horizon, the observer will collide into the ground plane at the point in the visual field specified by the FRO. In principle, this could be the strategy of pilots in estimating their touchdown point when conducting a landing (Gibson et al., 1955). But there is still more to it.

Again, it was Gibson who suggested that *"the length of time before touching down seems to be given by the optical information in an univocal manner"* (Gibson et al., 1955). It has been convincingly shown in many studies (Lee, 1974; Lee & Lishman, 1977; Lee, 1980a; Lee & Reddish, 1981) that observers can indeed perceive *temporal* cues in the optic flow field. These temporal cues, e.g. *Time-To-Contact* (TTC), provide information for *timing* actions relative to the environment. Examples exist of the successful use of a time-to-contact cue in the recti-linear approach of planar surfaces under different angles (Lee, 1980a; Lee & Reddish, 1981; Regan & Vincent, 1995; Mulder, Pleijsant, van der Vaart, & van Wieringen, 1999) and also for angular or rotational approaches (Lee, Young, & Rewt, 1992). Temporal information can also be extracted from the optic flow field when the observer is *not* on a collision course with some element of the environment (Kaiser & Mowafy, 1993). These are referred to as *Time-To-Passage* (TTP) cues.

Related topics

Peripheral and central stimulation The 'normal' viewing condition is that of unlimited viewing of the total optic array, stimulating both the foveal and peripheral vision.

With a tunnel display the viewing onto the synthetic three-dimensional world is restricted to a small 'window' (the display screen). Hence, because only foveal vision is stimulated, an important issue is whether this affects human visual motion perception. In the past it was generally agreed that peripheral vision dominates the perception and control of egomotion and that central vision is relatively insensitive to information specific to egomotion. This is known as the *peripheral dominance hypothesis* (Brandt, Dichgans, & Koenig, 1973). Psychophysical experiments show that motion discriminations in the peripheral field have larger thresholds (Johnson & Leibowitz, 1976) and result in smaller reaction times (Hosman, 1996). Furthermore, research applicable to virtual reality applications showed that restricting the field of view leads to perceptual and visuomotor decrements when performing tasks such as reaching for and grasping objects (Alfano & Michel, 1990). More recent research proved the inadequacy of the peripheral dominance hypothesis. Information about egomotion *can* be perceived with central vision (Andersen & Braunstein, 1985), and judgements about ego-heading are even more accurate when conducted with central rather than peripheral vision (Warren & Kurtz, 1992). A consideration of the ecology of retinal flow during self-motion reveals that central flow can have a variety of patterns (radial, rotary, lamellar), whereas peripheral flow is almost always locally lamellar (Warren & Kurtz, 1992). This led Warren and Kurtz (1992) to state the *functional specificity hypothesis*, in which central and peripheral vision are differentially sensitive to the information that is characteristic of each retinal region. The finding that central vision is more sensitive to radial flow patterns and peripheral vision more sensitive to lamellar-specific flow has also been reported in Crowell and Banks (1993). Time-to-contact estimates in foveal vision are reported *robust* under various conditions, whereas these estimations in peripheral vision are not (Regan & Vincent, 1995). In conclusion, with a small display there is certainly a loss of information due to the absence of peripheral stimulation. Recent findings in literature, however, show that heading judgements (Warren & Kurtz, 1992) and temporal judgements (Regan & Vincent, 1995) are consistent and more accurate with central vision than with peripheral vision.

Visual motion processing in the brain   Motion, which used to be considered a mere by-product of segmenting static sequences of images by using form and color cues, has come to be regarded as a *separate* perceptual channel (Ballard & Kimball, 1983). The *transformation* of stimuli is considered visual information itself, and the task of the brain is to extract the constant, invariant features of objects from the changing array of information it receives from them (Regan, Beverly, & Cynader, 1979). Recent neurophysiological and psychophysical work supports the concept of a *functional specialization* in the visual cortex, that supposes that color, form, motion and other attributes of the visual environment are processed separately (Zeki, 1992). In (Nakayama & Loomis, 1974) it is hypothesized that motion-sensitive cells exist in the visual system that operate on the optic flow pattern on the retina, structuring the visual field in terms of distinct surfaces at varying distances from the observer. This reasoning was taken a step further in Koenderink (1986), who suggested that the physiological mechanisms processing optic flow fields could be based

on *logic consequences* from the extraction of information from optic flow. Thus, the visual system consists of mechanisms that are sensitive to specific flow gradients, e.g. *motion* detectors (translation, rotation) and *looming* detectors (expansion, contraction).

Computational vision   The information richness of the optic flow field forms the basis of the research in computational vision (Prazdny, 1980, 1981). Movement through the environment *maps* environmental characteristics on the optic flow pattern. In Lee (1974) it was suggested that it should be possible to derive information about the environment and the locomotion of the observer when given the optic flow pattern. This would mean deriving an *inverse mapping* (Clocksin, 1980). The determination of (i) the locomotion through the environment and (ii) the environment itself from the optic flow generated by a sequence of camera images could allow the development of machines that can *see*. The first problem is referred to as the *passive navigation* problem (Bruss & Horn, 1983). Computer vision approaches typically formulate the egomotion and environmental shape estimation problem as a mathematical optimization problem in three stages: (i) the computation of the optic flow field from the changing camera image, (ii) the estimation of egomotion based on the optic flow, and (iii) the estimation of a map of relative depth (or impact-time) of the environment (Bajcsy & Lieberman, 1976; Horn & Schunk, 1981; Zacharias, Caglayan, & Sinacori, 1985b, 1985a; Zacharias, Miao, & Warren, 1995). The computational vision community has substantiated many of the mere philosophical ideas from (ecological) psychology (Singh, 1991).

3.2.2   Example: control of altitude as a function of optical texture

Control of altitude above a flat ground surface   In the 1980s a number of empirical studies was conducted to investigate the potential sources of information for altitude control (Wolpert, Owen, & Warren, 1983; Wolpert & Owen, 1985; Bennett, Johnson, Perrone, & Phatak, 1986; Wolpert, 1988; Johnson, Bennett, O'Donnel, & Phatak, 1988; Johnson, Tsang, Bennett, & Phatak, 1989; Owen, 1990). In these experiments, subjects actively controlled their altitude during locomotion above a flat ground surface. Three ground textures were examined: lines *parallel* to the direction of motion (Fig. 3.1, top), lines *perpendicular* to the direction of motion (Fig. 3.1, bottom), and the combination of both textures. Disturbances were introduced as velocities perpendicular and parallel to the direction of motion. The attitude of the observer with respect to the ground surface remained constant. The projection on the viewplane of the lines parallel to the direction of motion makes *optical splay angle* information available (Biggs, 1966; Naish, 1971; Wewerinke, 1978). The projection of the lines perpendicular to the direction of motion conveys *optical depression angle* information, also referred to as *optical density*. Both variables are isolated components from the global optical expansion pattern that results from an approach to a flat ground surface (Gibson, 1950; Gibson et al., 1955). Texture parallel to the viewing direction isolates the *perspective gradient* whereas texture perpendicular to the viewing direction isolates the *compression gradient* (Cutting & Millard, 1984). The main
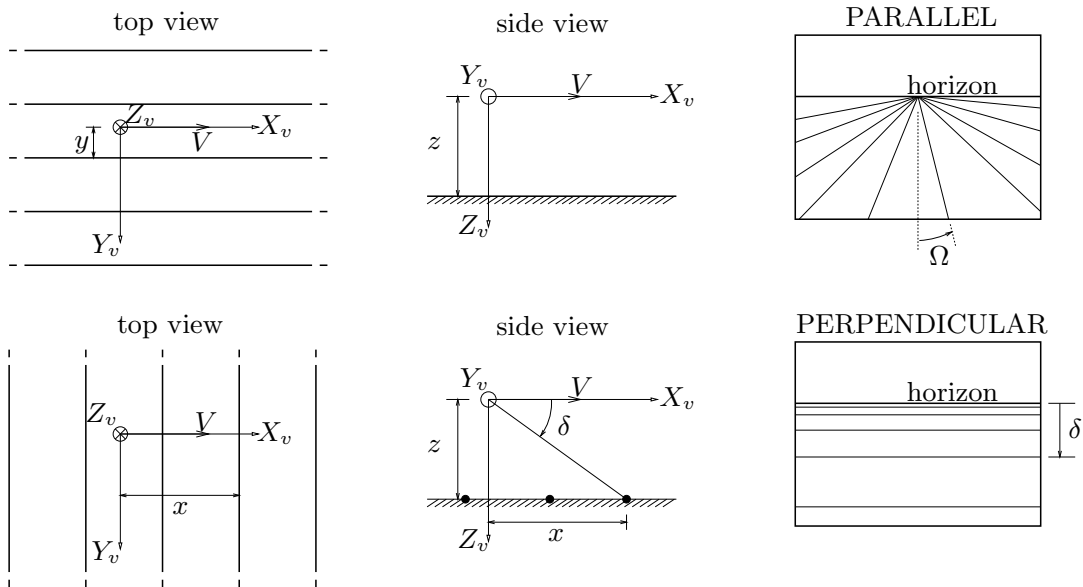
Figure 3.1: Parallel (top row) and perpendicular (bottom row) texture used in the altitude control experiments summarized in Flach et al. (1992).

interest in the experiments listed above was which source of optical information proved to be the most useful one for the control of altitude above a surface. The experimental results were rather contradictory: in (Wolpert et al., 1983; Wolpert & Owen, 1985; Wolpert, 1988) it was concluded that optical splay angle was the functional variable in altitude control, whereas in (Bennett et al., 1986; Johnson et al., 1988) it was found that the optical density led to the best performance. In an attempt to connect these experimental results and take away the controversy, additional experiments were conducted by Flach, Hagen, and Larish (1992). Prior to these experiments a mathematical analysis of the optical cues was conducted, discussed below, at the hand of (Flach et al., 1992).

Mathematical analysis   The following expression holds for the optical splay angle of the projection of a line segment on the display screen, Fig. 3.1:

$$\Omega = \arctan\left(\frac{y}{z}\right), \tag{3.1}$$

with z the height above the ground and y the lateral distance between the observer and the particular line segment (both in [m]). The splay *rate* is defined by:

$$\dot{\Omega} = -\underbrace{\left(\frac{\dot{z}}{z}\right)\cos\Omega\sin\Omega}_{\substack{\text{changes in} \\ \text{altitude}}} + \underbrace{\left(\frac{\dot{y}}{z}\right)\cos^2\Omega}_{\substack{\text{changes in} \\ \text{lateral position}}}, \tag{3.2}$$

an expression that specifies changes in splay angle resulting from changes in altitude and lateral position. Both terms are scaled by the height above the ground surface, z. The $(\dot{z}/z)$-term represents the fractional change in altitude (reciprocal to the time-to-contact

of (Lee, 1974)). The sine and cosine terms define the dependence of the splay rate on optical location, i.e. the splay angle itself. The contribution of the first term (change in altitude) will be zero for splay angles of 0° (perpendicular to the horizon) and 90° (the horizon), and will be maximal for a splay line of 45°. The contribution of the second term (changes in lateral position) is zero for a splay angle of 90° (the horizon) and maximal for a line perpendicular to the horizon ($\Omega = 0°$). These characteristics were already reported by Wewerinke (1978). The same holds for the optical depression angle of a line segment:

$$\delta = \arctan\left(\frac{z}{x}\right), \tag{3.3}$$

with z the height above the ground and x the longitudinal distance between the observer and the particular line segment (both in [m]). The depression angle *rate* is given by:

$$\dot{\delta} = \underbrace{\left(\frac{\dot{z}}{z}\right)\cos\delta\sin\delta}_{\substack{\text{changes in}\\\text{altitude}}} \quad \underbrace{-\left(\frac{\dot{x}}{z}\right)\sin^2\delta}_{\substack{\text{changes in}\\\text{longitudinal position}}} \quad . \tag{3.4}$$

The first and second terms specify changes in δ due to changes in altitude and longitudinal position, respectively, both scaled with altitude. The $(\dot{x}/z)$-term is referred to as the *global optical flow rate* (Warren, 1982). Similar to the optical splay angle, the sine and cosine terms show the dependence of the depression angle rate on the optical location, i.e. the depression angle itself. The contribution of the first term is maximal for a depression angle of 45° below the horizon and zero for a depression angle of 0° (the horizon) and 90° (below the observer). The contribution of the second term is zero for a depression angle of 0° (the horizon) and maximum for a depression angle of 90° (below the observer).

The mathematical analysis proved to be extremely useful in explaining the contradictory results in literature (Flach et al., 1992). Consider the situation in which the observer can only move in vertical direction ($\dot{x} = \dot{y} = 0$). In this case the optical splay and density cues provide identical information about fractional changes in altitude ($\dot{z}/z$). When a longitudinal velocity disturbance is added ($\dot{x} \neq 0$, $\dot{y} = 0$) this only affects the density and *not* splay. In the altitude control task this means a clear advantage of using splay in this situation. When a lateral velocity disturbance is added ($\dot{x} = 0$, $\dot{y} \neq 0$), however, this only affects splay and not density, yielding superior performance when using the latter variable. When all disturbances except $\dot{z}$ are set to zero and longitudinal (forward) motion is active ($\dot{x} = -V$, with V the velocity of locomotion) this means that with perpendicular texture the observer must detect a change in depression angle due to a change in altitude *on top of* the optic flow created by the forward motion. This could lead to poorer performance. For the display showing the parallel lines, the forward motion has no effect at all: the *optic splay angles create no optic flow information specifying forward motion* (Crowell & Banks, 1996). The example shows that a sound pre-experimental mathematical analysis of the available optical cues, besides reducing the number of experiments, could help distinguish between valuable experimental findings and those that are mere artifacts caused by an inappropriate experimental design. Flach et al. (1992) states that the question of what

type of texture is superior to others in terms of altitude regulating performance is stated inappropriately. Rather, "*the amount of optical activity associated with changes in altitude (= signal) relative to the amount of activity associated with changes other than altitude (= noise)*" should be investigated. The issue of functionality of an optical cue for a certain task will be discussed further below. Besides the importance of the altitude regulation example from a theoretical perspective, in the remainder of this chapter it will be shown that there is more to it. The control of *distance with respect to a planar surface* is very relevant in the task of guiding the aircraft through a tunnel. Following the reference trajectory simply means to stay within the center of the tunnel. The tunnel walls limit the lateral (left/right) and vertical (top/bottom) motion of the aircraft. Except for the theoretical case of *perfect* guidance along the trajectory, the aircraft will *always* approach two of the tunnel planes. Because the tunnel is presented by means of a perspective wireframe the same cues as introduced above – optical splay and optical density, or, equivalently, the gradients of perspective and compression – could well be important.

3.2.3   The functionality of sources of optical information

Although a spatial visual scene conveys a substantial number of potentially informative cues that allows the perception and control of locomotion, "*it is possible for two cues to specify the same referent equally in a geometric sense, but not be equally useful to a pilot*" (Warren, 1988). An important question is which optical variables are selected and used by the human observer. A straightforward approach to infer a human's strategy or cue utilization would be the use of a questionnaire. Visual motion perception, however, is a skill-based activity which happens unconsciously, significantly reducing the effectivity of interviews. A well-designed questionnaire could provide clues to what cues are used, narrowing-down the options (Johnson & Phatak, 1990a).

Ecological functionalism   In ecological optics, investigating the phenomena of persistence and change in optical information, attention focuses on optical invariants. These invariants can be either *static* (a constant (visual) angle or distance) or *dynamic* (characteristics of optic flow, e.g. the focus of radial outflow). Research into optical invariants aims at assessing the usefulness of an invariant by showing mathematically that it is capable of specifying its source. Then, the actual use of that invariant is examined empirically. In (Warren & Owen, 1982) the *ecological functionalism* concept is advocated to address the problem of how to study the sensitivity to optical invariants. In the context of the perception and action paradigm of (Gibson, 1986) (the reason for perception is to guide actions and the goal of all behaviour is to control what is perceived), a fundamental principle exists, i.e. that of *perceptual learning*: the easier the parameters of an event are to *detect*, the easier they are to *control* (Owen, 1990; Johnson & Phatak, 1990a). Furthermore, a correspondence exists between sensitivity and effectiveness in *sustained control*, i.e. what is easier to detect *initially*, is easier to control *subsequently* (Owen, 1990). In (Warren & Riccio, 1985) the existence of a *cue dominance hierarchy* is postulated. When faced with a large amount of information the observer's initial task would be to determine what

sources of information are the most useful to the task at hand. Performance improves to the extent that the observer uses the appropriate cues. The perceptual learning process indicates that strong cues are learned faster than weak cues.

Functional and contextual variables   Based on these findings and on an extensive body of empirical data (Wolpert et al., 1983; Wolpert & Owen, 1985; Bennett et al., 1986; Wolpert, 1988; Johnson et al., 1988), Owen (1990) suggested that two classes of event variables exist that influence sensitivity of visually perceiving changes in locomotion:

1. *Functional variables*: variables of an optical flow pattern that are used to select and guide a control action.
2. *Contextual variables*: optical properties that merely influence the sensitivity of a functional variable.

The operational distinction between the two classes is assumed to become evident in the structure of the psychophysical functions (Owen, 1990): functional variables have an *asymptotic* effect on performance, whereas contextual variables reveal an *optimum* level (quadratic form) of performance. Contextual variables are related to the operating characteristics of the sensory system supporting sensitivity to functional variables (Owen, 1990). Although this is an intellectually attractive theory, Owen himself pointed out that whether an optical variable is functional or contextual depends also on the task (Owen, 1990; Johnson & Phatak, 1990b): the *characteristics of the perceptual mechanism depends on the task*. In this respect, the example of §3.2.2 illustrated that the functional value of visual information must be considered in the context of an event. Flach et al. (1992) argue that in comparing alternative visual scenes conveying various sorts of optical information, two factors are important: (i) the *specificity* of the information to the task, and (ii) the level at which the visual system is *tuned* to the optical information sources: "*the perceptual system ... may be designed simply to resonate to specificity*". What matters is the amount of optical activity associated with changes in the variables it specifies (and that is important to the task performance) with respect to the amount of activity in that optical variable that is *not* specific to the variable to be controlled (Flach et al., 1992). An *ideal* observer regulates the locomotion with optical variables that vary solely with the degree of freedom to be regulated (Johnson & Phatak, 1990a).

Ideal observer models   The performance of human observers as a function of different visual stimuli depends on several stimulus properties, some of which cannot be manipulated or isolated experimentally. A disadvantage of psychophysical experiments is that they measure the performance of the visual system as a whole. The observation that a change in stimulus properties leads to a change in performance does not yield a simple interpretation. Do these results tell us something about the information in the displays or about the perceptional mechanisms of the observer? The classification of visual cues as functional and contextual is an attractive but difficult to apply concept, that is per definition a posteriori. An interesting approach could be the development of so-called *ideal observer models* (Crowell & Banks, 1996) that quantify the informativeness of an optical stimulus.

The observer models are not meant to mimic human behaviour, but only to assess the information content in optical stimuli. It is shown that these models can handle the question whether changes in performance are attributable to either the informativeness of the optical stimulation or to the more efficient neural mechanism of processing it.

Pre-experimental analysis The functionality of an optical source of information can be addressed before experimental testing through a mathematical analysis of its characteristics (Warren & Owen, 1982). Although the classification of a cue as a functional or a contextual variable depends on the task as well, the analysis of Flach et al. (1992) proved to be very useful. Based on the literature survey a number of questions can be stated that can guide the (mathematical) analysis of the characteristics of an optical cue:

1. 'is the cue – i.e. the variable it represents, the *motion referent* – important for the task at hand?': *task-specificity*;

2. 'is the cue easy to detect/identify?': *detectability*;

3. 'is the cue conveyed by a single display element or through the combination of several elements?': *observability*;

4. 'what are the degrees of freedom of a cue?': *kinematics*;

5. 'is the cue easy to use? For instance, what are the *dynamic* relationships of changes in the cue with respect to the observer's control signal?': *dynamics*;

6. 'does the cue depend only on one variable/referent or is it a function of more than one variable?': *specificity*;

7. 'when the cue is a function of more than one variable, what are the relative contributions of these variables to that particular cue?': *signal-to-noise ratio*.

Besides these questions, two other properties are important in the tunnel display context. First, the characteristics of the optical cues depend on the tunnel geometrical design and the properties of the perspective projection. Second, in the control of an aircraft more than one motion state needs to be controlled simultaneously. This makes the application of the guidelines stated above essentially multi-dimensional, increasing the importance of investigating the relations between the (characteristics of) the cues.

Categorization of optical cues A categorization that will prove to be useful for the tunnel display investigation is to distinguish between *static* and *dynamic* optical cues. Static cues are defined as those sources of information that are conveyed by a single snap-shot or *frozen* image of the display. For instance, all tunnel figures of this thesis convey static cues. Dynamic cues, on the other hand, are defined as those sources of information that are conveyed by the *animated* picture resulting from the motion through the tunnel. These dynamic cues can be categorized one step further. First, there are the *time derivatives* of the static optical cues that are labelled *indirect* dynamic cues. Second, the cues resulting from the optic flow of the animated image are labelled *direct* dynamic sources of information. Before applying the knowledge obtained in this section to analyze the characteristics of information transfer and information processing of the tunnel display, attention will be dedicated to the properties of the perspective projection.
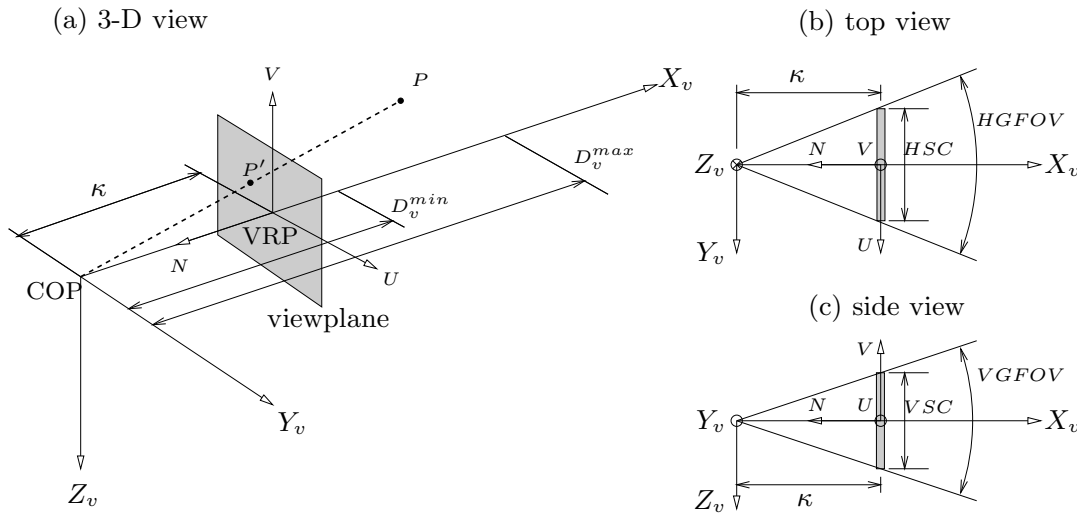
Figure 3.2: The perspective projection method and the principal terminology.

3.3 *Machine* – Perspective projection methods

Perspective projection methods are treated extensively in many books on computer graphics (e.g. (Foley, van Dam, Feiner, & Hughes, 1992)). At the hand of Fig. 3.2 the main terminology will be introduced in §3.3.1, followed by a mathematical description in §3.3.2.

3.3.1 Terminology

The 3-D world is projected on the *viewplane* defined by the Viewing Reference co-ordinate system[2] $\mathcal{F}^{vr}$ with axes U, V and N (the *viewplane normal*). The origin of $\mathcal{F}^{vr}$, the View-Reference Point (VRP), is the center of the viewplane. The Center Of Projection (COP) is the point in which all projectors coincide. The COP lies on the N axis at a distance κ, the so-called *distance-to-the-screen*, from the VRP (in [m]). This parameter is determined by the screen size (horizontal HSC; vertical VSC (in [m])) and the geometrical Field Of View (FOV) of the projection (horizontal $HGFOV$; vertical $VGFOV$ (in [deg])):

$$\kappa \;=\; \frac{HSC}{2\tan(HGFOV/2)} \;=\; \frac{VSC}{2\tan(VGFOV/2)} \tag{3.5}$$

The COP is the origin of the *Viewing* co-ordinate system $\mathcal{F}^v$, that is defined with its longitudinal axis – the *central viewing axis* – along the viewplane normal but in opposite direction: $X_v = -N$. The Y_v and Z_v axes are positive in the direction of U and $-V$, respectively. The part of the 3-D world that is projected on the viewplane is determined by the *view volume*. A finite view volume is defined by two planes parallel to the viewplane, a *front* and a *back clipping plane* at *minimum* and *maximum viewing distances* D_v^{min} and D_v^{max}, respectively. Anything outside of the pyramidal view volume is clipped out.

---

[2]All co-ordinate systems applied in this thesis are orthogonal and right-handed.

3.3.2   Properties of the perspective mapping

Perspective projection procedure   In a perspective tunnel display the center of projection COP can be positioned in the aircraft center of gravity. The Viewing axes are then fixed and aligned with the aircraft Body axes, i.e. $\mathcal{F}^v \equiv \mathcal{F}^b$. The attitude of the Body axes is determined by the three Euler angles (ψ, θ and ϕ) that relate $\mathcal{F}^b$ to the Geodetical axes $\mathcal{F}^g$ (Appendix C). The Geodetical axes move along with the aircraft, its attitude fixed relative to the Earth. The World axes $\mathcal{F}^w$ are defined similarly as $\mathcal{F}^g$, except that its position is *fixed* with respect the Earth. The co-ordinates of the aircraft center of gravity, i.e. the COP, in $\mathcal{F}^w$ is referred to as $\underline{x}_{COP}^w$. An arbitrary point P in $\mathcal{F}^w$ is mapped onto the viewplane with the perspective projection. First, the co-ordinates of this point in $\mathcal{F}^v$ ($\equiv \mathcal{F}^b$) must be computed, which is conducted in two steps (Appendix D):

$$\underline{x}_p^v = \underbrace{R_X(\phi)R_Y(\theta)R_Z(\psi)}_{\substack{\text{rotation of } \mathcal{F}^w \text{ to} \\ \text{align } \mathcal{F}^w \text{with } \mathcal{F}^v}} \cdot \underbrace{\left(\underline{x}_p^w \; - \; \underline{x}_{COP}^w\right)}_{\substack{\text{translation of} \\ \mathcal{F}^w \text{ to the COP}}}, \tag{3.6}$$

with R_X, R_Y and R_Z the orthogonal rotation matrices defined in Appendix C. Eq. 3.6 is a *rigid-body* transformation (Foley et al., 1992). When the co-ordinates of a point P are known in $\mathcal{F}^v$ ($=\mathcal{F}^b$), the projection onto the viewplane is given by (using similar triangles):

$$u_p \; = \; \kappa\left(\frac{y_p^v}{x_p^v}\right); \quad v_p \; = \; -\kappa\left(\frac{z_p^v}{x_p^v}\right). \tag{3.7}$$

Effect on the roll angle on the projection   An important property of the perspective projection is that the final rotation in Eq. 3.6 is conducted along the aircraft longitudinal Body axis X_b ($\equiv X_v$). Hence, the aircraft rotation ϕ along X_b yields an orthogonal transformation *within the viewplane*, preserving angles and distances (Appendix D):

$$u_p = u_p|_{\phi=0} \cos\phi - v_p|_{\phi=0} \sin\phi, \quad \text{and} \quad v_p = u_p|_{\phi=0} \sin\phi + v_p|_{\phi=0} \cos\phi. \tag{3.8}$$

Any relation that is defined with respect to the display horizon is independent of the aircraft roll angle, a property that simplifies the computation of many cues.

Derivatives of the perspective projection co-ordinates   A first – heuristic – analysis of the *dynamic* properties of a projection point can be conducted by differentiating the static relationship between a point P and its projection, Eq. 3.7:

$$\dot{u}_p \; = \; \kappa\left(\frac{\dot{y}_p^v}{x_p^v}\right) - u_p\left(\frac{\dot{x}_p^v}{x_p^v}\right); \quad \dot{v}_p \; = \; -\kappa\left(\frac{\dot{z}_p^v}{x_p^v}\right) - v_p\left(\frac{\dot{x}_p^v}{x_p^v}\right). \tag{3.9}$$

The velocity of the projection of a point on the screen is *scaled* by the distance of that point to the COP. Because $\dot{x}_p^b < 0$ and $x_p^b > 0$ for all visible points, the velocity in the viewplane will generally be positive for the right and top half of the viewplane (and vice versa), illustrating the *radial* flow. Eq. 3.9 exemplifies the fact that forward motion is amplified for points located farther from the display center (u_p and v_p large). Lateral and vertical motion perpendicular to the viewing axis yields an equal velocity component for *all* points on the screen. These findings will be elaborated further in the next sections.

(a) bird's eye view (the pilot's task)   (b) pilot's view (the tunnel image)
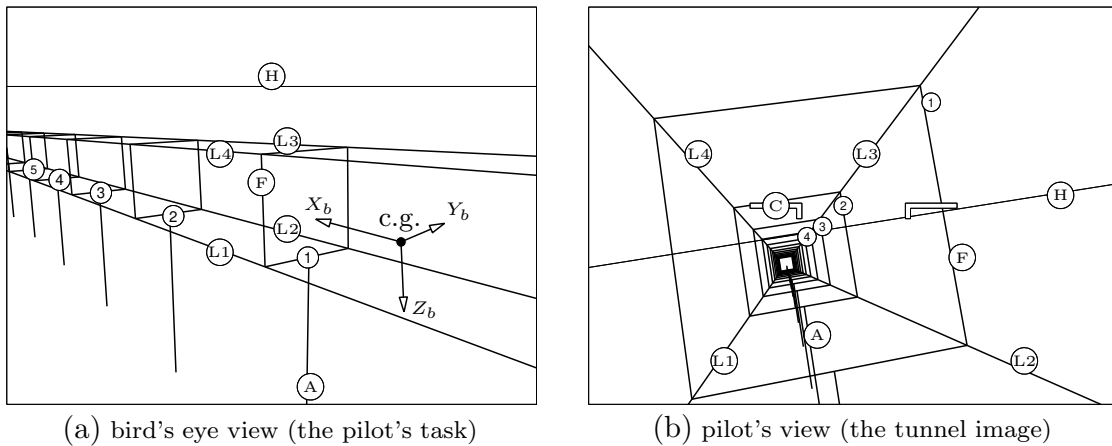
Figure 3.3: The general situation of flying through a straight tunnel section.

3.4 Information in straight tunnel sections

The potential sources of information conveyed by the tunnel display for the pilot task of following straight trajectories are discussed in this section (Mulder, Mulder, & Stassen, 1999b). A generic tunnel geometry is defined in §3.4.1. The static cues conveyed by a single snap-shot of the tunnel display are discussed in §3.4.2. The dynamic cues resulting from the animated picture when moving through the tunnel are discussed in §3.4.3.

3.4.1 Definition of the situation

The general situation considered here is illustrated in Fig. 3.3(a) that shows a bird's eye view of the aircraft – represented by its Body axes $\mathcal{F}^b$ – flying through a straight tunnel. Fig. 3.3(b) shows the corresponding (instantaneous) tunnel display image. In the tunnel, three elements can be distinguished: (i) the tunnel *frames* (marked Ⓕ) that are positioned in longitudinal direction; (ii) the *longitudinal frame lines* Ⓛᵢ (i=1–4) connecting the vertices of the tunnel frames, and (iii) the *altitude poles* Ⓐ that connect each individual frame with the Earth's surface. As one can see from the position of the far end of the tunnel with respect to the horizon Ⓗ, the trajectory has a non-zero downslope.

Mathematical description   A mathematical description of a generic tunnel geometry can be obtained at the hand of Fig. 3.4. Here, the straight tunnel is shown from the left-hand side, including an inset that shows a tunnel cross-section (view A–A). The tunnel has a width W_t and a height H_t (both in [m]), a ground slope Γ_t (in [rad], defined positive when downward) and a reference track angle χ_t (in [rad]). To facilitate the analysis χ_t is assumed to be zero. The tunnel frames are positioned at intermediate distances $\triangle D$ (in [m]) and are numbered 1, 2, ... starting from the first visible frame.

The aircraft is positioned in the tunnel with an arbitrary position and attitude with respect to the tunnel centerline. The attitude of the aircraft is defined with respect to $\mathcal{F}^g$ by means of the three Euler angles. The origin of the World reference frame $\mathcal{F}^w$ is positioned on the

view A–A of cross-section
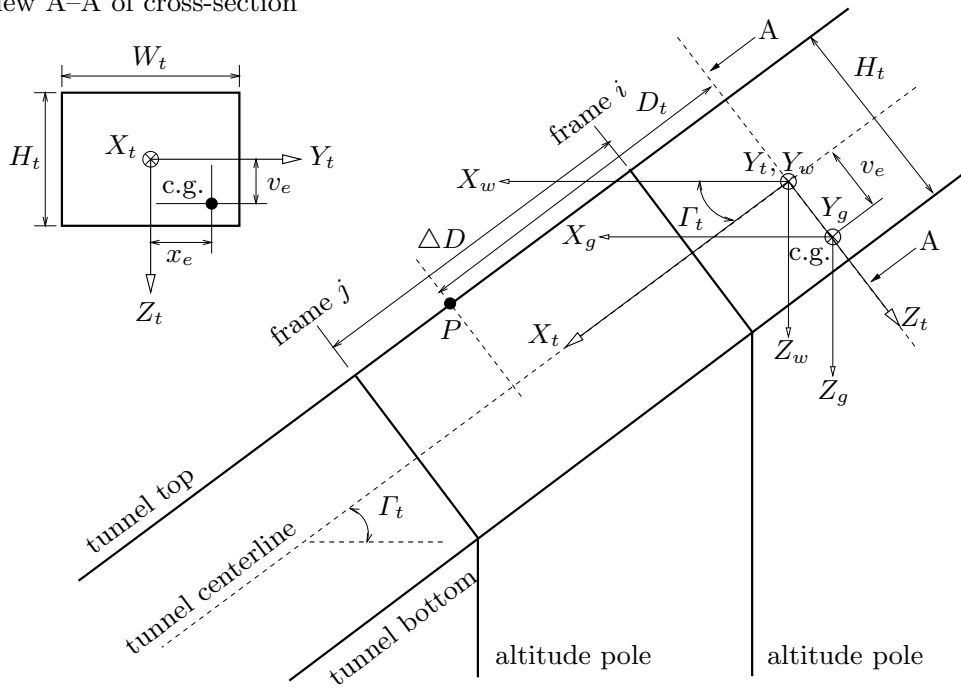
Figure 3.4: Generic tunnel geometry used in the analysis (side view).

cross-point of the tunnel centerline and a plane perpendicular to this centerline through the aircraft center of gravity. The X_w axis is defined along the direction of the horizontal projection of the tunnel centerline. Another useful reference frame is the *Tunnel* frame of reference $\mathcal{F}^t$, the origin of which coincides with that of $\mathcal{F}^w$. The longitudinal axis is aligned with the tunnel centerline: $\mathcal{F}^t$ is similar to $\mathcal{F}^w$ except that it is rotated around Y_w with the downslope angle Γ_t. The aircraft position *error* can now be defined relative to $\mathcal{F}^t$ in lateral, x_e, and vertical, v_e, direction (in [m]). A longitudinal position error is defined zero in the analysis. The inset of Fig. 3.4 (view A–A) shows that x_e and v_e are defined positive when the aircraft is positioned to the right and below the tunnel centerline.

Perspective display mapping The position of an arbitrary point P of the tunnel can be defined in $\mathcal{F}^t$ at a distance D_t into the tunnel, measured along X_t. After transforming this point from $\mathcal{F}^t$ to $\mathcal{F}^w$ the perspective mapping procedure (Eqs 3.6-3.7, Appendix D) yields the projection of that particular point P on the viewplane: (u_p, v_p).

3.4.2 Static optical cues

Cue inventory

When the aircraft is positioned in the generic tunnel of Fig. 3.4, with an arbitrary position and attitude with respect to the trajectory, the display image will resemble that of Fig. 3.3(b). The main static cues in this image are described at the hand of Figs 3.5 to 3.7 which show three subsets of cues (defined in $\mathcal{F}^{vr}$) resulting from the projection of the

longitudinal, vertical and lateral elements of the tunnel geometry. The aircraft attitude angles θ and ϕ are directly coded in the display, Fig. 3.5. The following cues are defined:[3]

1. The position of the *infinity point* (u_∞, v_∞), defined as the projection on the viewplane of an arbitrary point of the tunnel when the distance D_t into the tunnel goes to infinity (Fig. 3.5).

2. The *optical splay angles* Ω_i (i=1–4), defined as the angles of the longitudinal frame lines with respect to the horizon. Another optical splay angle can be defined for the 'virtual' line connecting the tops of all altitude poles (Ω_5) (Fig. 3.5).

3. The *lateral displacements* ϵ_i (left) and η_i (right) of the vertical frame lines (frame i) with respect to the rotated viewplane centerline V'. The lateral displacements π_i of the altitude poles are similar cues (Fig. 3.6).

4. The *relative lateral displacements* ϵ_{ij} (left), η_{ij} (right) and π_{ij} of the vertical frame lines and the altitude poles of frames i and j (Fig. 3.6).

5. The *quotient* of the relative lateral displacements ϵ_{ij} and η_{ij}, a quantity that is referred to as the *lateral compression ratio* (Fig. 3.6).

6. The *vertical frame line angles* ζ_i (left) and ξ_i (right) of the vertical frame lines with respect to V (Fig. 3.6).

7. The *vertical displacements* μ_i (bottom) and ν_i (top) of the lateral frame lines (frame i) with respect to the rotated viewplane centerline U' (Fig. 3.7).

8. The *relative vertical displacements* μ_{ij} (bottom) and ν_{ij} (top) of the lateral frame lines of frames i and j (Fig. 3.7).

9. The *quotient* of the relative vertical displacements μ_{ij} and ν_{ij}, a quantity that is referred to as the *vertical compression ratio* (Fig. 3.7).

10. The *lateral frame line angles* ρ_i (bottom) and σ_i (top) of the lateral frame lines with respect to U (Fig. 3.7).

Mathematical expressions can be derived that relate the optical cues to the aircraft position and attitude with respect to the trajectory. These expressions, listed in Appendix D, are in principle non-linear and must be linearized for later use. A suitable linearization point that is applied throughout the analysis is the situation of zero position errors and small attitude angles. The latter assumption allows the application of the small angle equivalents of geometric functions. The linearized expressions, discussed below[4], can be used to study the effects of (small) deviations from the linearization point on the tunnel image.

(1) The position of the *infinity point*   The position on the viewplane of the infinity point, marking the projection of the trajectory at infinity, can be approximated by:

$$
\begin{aligned}
u_\infty\Big|_{\phi=0} &= -\kappa\left(\tan\psi\frac{1}{\cos\theta}\right) &\approx& -\kappa\left(\psi\right); \\
v_\infty\Big|_{\phi=0} &= -\kappa\left(\tan\left(\theta+\Gamma_t\right)\right) &\approx& -\kappa\left(\theta+\Gamma_t\right).
\end{aligned}
\tag{3.10}
$$

---

[3]Cues resulting from intersections of the tunnel geometry with the viewplane borders are neglected.

[4]The angular cues (6) and (10) are less important and are discussed in Appendix D.
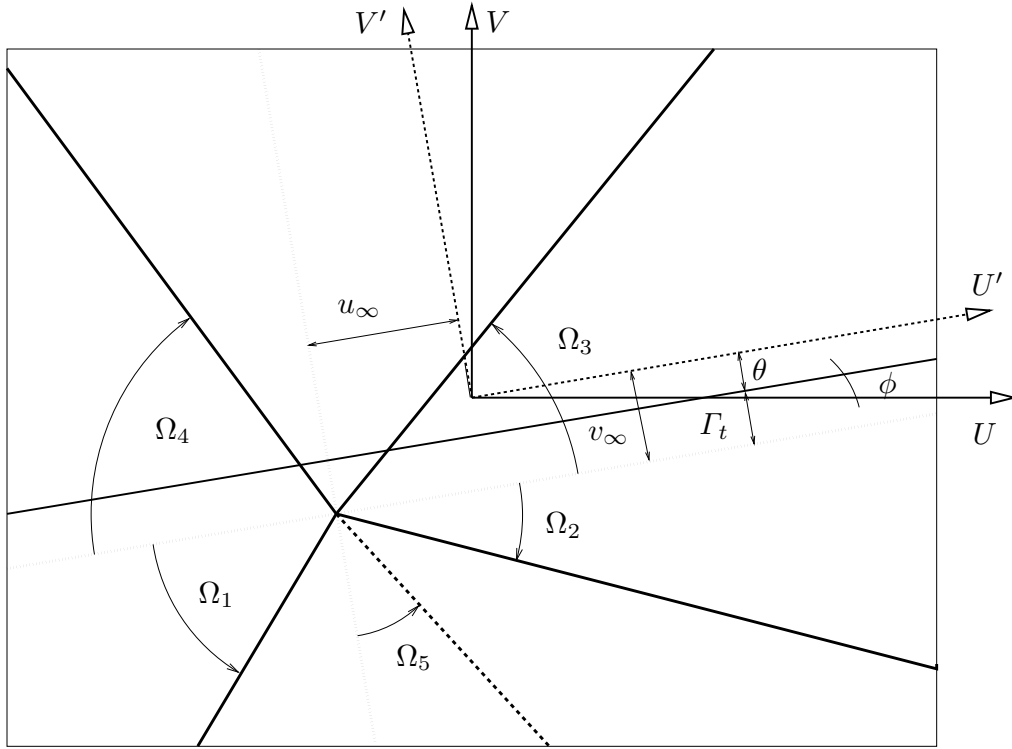
Figure 3.5: The first subset of static optical cues in a straight tunnel section: the *longitudinal* tunnel cues (1)–(2). All symbols are explained in the text.

As has been discussed in §3.3.2, the roll angle ϕ results in an orthogonal transformation with respect to the origin of $\mathcal{F}^{vr}$. The co-ordinates of the infinity point for a non-zero ϕ can therefore be computed using Eq. 3.8. The position of the infinity point in lateral and vertical direction represents the lateral (ψ) and vertical ($\Gamma_t + \theta$) *angular difference* between the aircraft longitudinal axis X_b and the tunnel centerline X_t. Its position is independent of the aircraft position error. Extending the planes of the top and bottom tunnel walls into the distance results in a horizontal *pseudo-horizon* located -$\kappa\Gamma_t$ below the true horizon, Fig. 3.5. Similarly, extending the planes of the left and right tunnel walls into the distance yields a second – vertical – pseudo-horizon, perpendicular to the true horizon. The infinity point is the crosspoint of both pseudo-horizons. The importance of the two pseudo-horizons, depicted by the dotted lines in Fig. 3.5, will become clear below.

(2) The *optical splay angles* The non-linear relations for the optical splay angles $\Omega_1 \ldots \Omega_5$, Eqs D.5, are linearized to obtain expressions for the *change* in splay angle ω_i from the reference condition Ω_{0_i}:

$$\omega_1 \quad = \quad -\left(\frac{2W_t}{W_t^2 + H_t^2}\right) v_e - \left(\frac{2H_t}{W_t^2 + H_t^2}\right) x_e; \tag{3.11}$$

$$\omega_2 \quad = \quad -\left(\frac{2W_t}{W_t^2 + H_t^2}\right) v_e + \left(\frac{2H_t}{W_t^2 + H_t^2}\right) x_e; \tag{3.12}$$
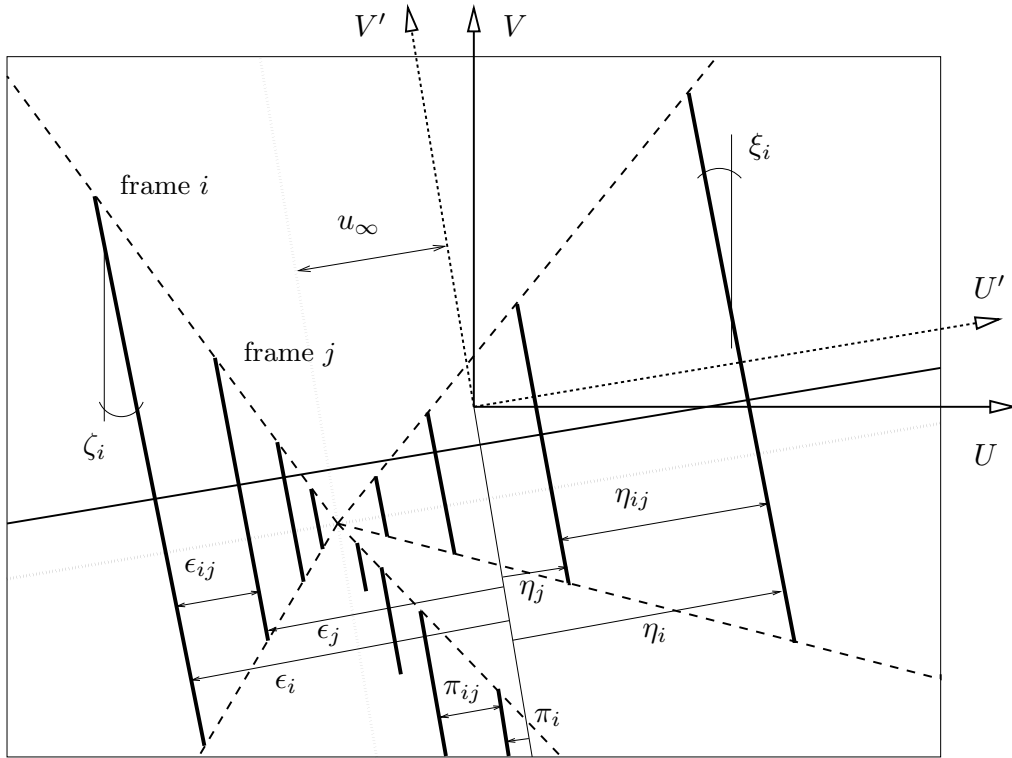
Figure 3.6: The second subset of static optical cues in a straight tunnel section: the *lateral* tunnel cues (3)–(6).

$$\omega_3 = +\left(\frac{2W_t}{W_t^2 + H_t^2}\right) v_e + \left(\frac{2H_t}{W_t^2 + H_t^2}\right) x_e; \qquad (3.13)$$

$$\omega_4 = +\left(\frac{2W_t}{W_t^2 + H_t^2}\right) v_e - \left(\frac{2H_t}{W_t^2 + H_t^2}\right) x_e; \qquad (3.14)$$

$$\omega_5 = -\left(\frac{2}{H_t}\right) x_e. \qquad (3.15)$$

These expressions – as in the non-linear case – are independent of the perspective projection (κ), the aircraft attitude (ψ, θ, ϕ) and the distance D_t into the tunnel. The reference condition of the splay angles of the longitudinal frame lines and the 'virtual' splay angle Ω_5 are equal to $\arctan(H_t/W_t)$ and 0, respectively. In other words, when the position errors are zero and the tunnel is square ($W_t = H_t$), the reference condition is that of two perpendicular lines at 45° of the horizon. The splay angles are only a function of the position error with respect to the trajectory and the tunnel size. They provide strong cues for *symmetry*, especially when either the vertical or lateral position error is zero. This yields *symmetrical* conditions with respect to the horizontal and vertical pseudo-horizons, respectively. When neither x_e nor v_e are zero the situation is not symmetric and all splay angles are rotated due to the effects of *both* position errors. Hence, the position errors are shown in a *coupled* fashion. The effects of a lateral and vertical position error can be distinguished by computing $\omega_1 + \omega_2$ (or $\omega_3 + \omega_4$) to obtain v_e and $\omega_2 + \omega_3$ (or $\omega_1 + \omega_4$)
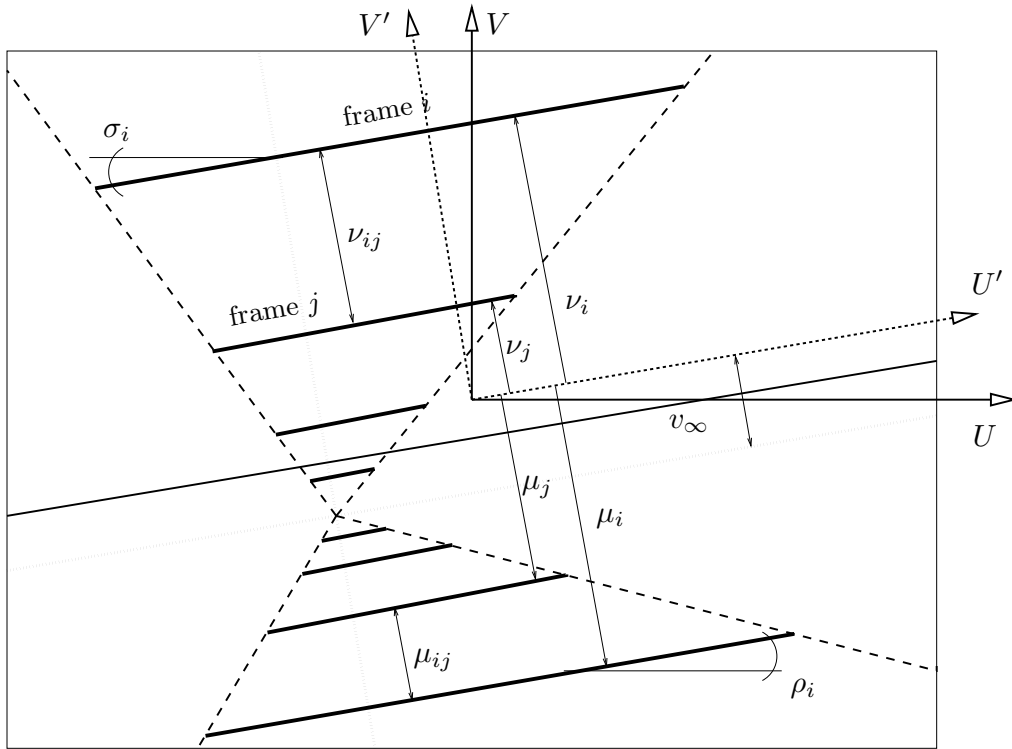
Figure 3.7: The third subset of static optical cues in a straight tunnel section: the *vertical* tunnel cues (7)–(10).

to obtain x_e. The splay angle of the virtual line connecting the altitude poles, however, is only a function of the lateral position error. When v_e is zero and the tunnel is square, the *change* in this splay angle for a non-zero x_e is twice as large as for any other splay angle.

(3)–(5) The *lateral displacement* cues   The vertical lines of the tunnel frames that convey the lateral tunnel cues (3)–(6) are illustrated in Fig. 3.6. All displacement cues are derived in the rotated $\mathcal{F}^{vr}$ frame of reference. For a small heading angle ψ and when the distance to the frame D_i is large relative to $(W_t + 2x_e)$, the following linearized expressions hold (Appendix D):

$$\epsilon_i = \kappa \left[\psi + \left(\frac{W_t + 2x_e}{2D_i} \right) \right] ; \eta_i = -\kappa \left[\psi - \left(\frac{W_t - 2x_e}{2D_i} \right) \right] ; \pi_i = \kappa \left[\psi + \frac{x_e}{D_i} \right]. \quad (3.16)$$

The *relative* lateral displacements ϵ_{ij} (left frame lines) are defined as $\epsilon_{ij} = \epsilon_i - \epsilon_j$. Similar expressions hold for η_{ij} and π_{ij}. Linearized expressions for all lateral displacement cues are collected in Table 3.1, showing their values in the linearization point and the relative change in these variables due to small deviation(s) from this point (i.e. ϵ_{0_i} and $\delta\epsilon_i$).

(7)–(9) The *vertical displacement* cues   The lateral lines of the tunnel frames that convey the vertical tunnel cues (7)–(10) are illustrated in Fig. 3.7. The derivation of the

vertical displacement cues is similar to that of their lateral counterparts, yielding:

$$\mu_i = \kappa \left[(\theta + \Gamma_t) + \left(\frac{H_t - 2v_e}{2D_i} \right) \right] ; \quad \nu_i = -\kappa \left[(\theta + \Gamma_t) - \left(\frac{H_t + 2v_e}{2D_i} \right) \right] . \quad (3.17)$$

All other vertical displacement cues are listed in Table 3.1.

The displacement cues show the aircraft attitude and the position errors in an *uncoupled* fashion: the lateral expressions are independent of the variables in the vertical dimension and vice versa. The displacements of a frame i on the display (Eqs 3.18 and 3.21) are due to two components: (i) the attitude with respect to the tunnel, and (ii) the position error. The contribution of the position error is *scaled* with the distance to the frame D_i. When the distance goes to ∞, the lateral/vertical displacement of the infinity point is obtained (Eq. 3.10). The relative displacements of two tunnel frames i and j only depend on the position error and a compression factor (Eqs 3.19 and 3.22). The compression factor is the same for both dimensions and is determined by the distances to the frames involved. The quotient of the relative displacements (Eqs 3.20 and 3.23), the *compression ratio*, is only a function of the position error and the tunnel size. When the infinity point is taken as the reference, the vertical displacement of a lateral frame line with respect to this point – or, equivalently, with respect to the horizontal pseudo-horizon – is similar to the depression angle introduced in §3.2.2. Consider Fig. 3.6. A position error to the left of the trajectory leads to a compression of the 'texture' of the left tunnel wall, composed by the vertical lines of the tunnel frames at the left of the vertical pseudo-horizon, and an expansion of the 'texture' of the right tunnel wall, composed by the vertical lines of the tunnel frames at the right of the vertical pseudo-horizon:

$$\epsilon_{i\infty} = \epsilon_i - \epsilon_\infty = \kappa \left(\frac{W_t + 2x_e}{2D_i} \right) ; \quad \eta_{i\infty} = \eta_i - \eta_\infty = \kappa \left(\frac{W_t - 2x_e}{2D_i} \right) . \quad (3.24)$$

The same holds in the vertical dimension, Fig. 3.7:

$$\mu_{i\infty} = \mu_i - \mu_\infty = \kappa \left(\frac{H_t - 2v_e}{2D_i} \right) ; \quad \nu_{i\infty} = \nu_i - \nu_\infty = \kappa \left(\frac{H_t + 2v_e}{2D_i} \right) , \quad (3.25)$$

for the compression of the 'texture' on the bottom and top tunnel walls, respectively. The two pseudo-horizons serve as the main reference for the compression of the texture elements, the lateral and vertical lines of the tunnel frames, composing the tunnel walls. Summarizing, the *static* optical cues can be categorized in cues that represent the gradient of optical perspective, the splay angles, and those that represent the optical compression gradient, the relative displacements. The aircraft attitude with respect to the trajectory is conveyed by the infinity point. The position of the aircraft with respect to the trajectory is conveyed, in a coupled fashion, by the splay angles, and, in an uncoupled fashion, by the relative displacements of the tunnel frame lines with respect to the vertical and horizontal pseudo-horizons. Thus, the cues in a tunnel display are essentially the same as those reported in §3.2.2. The discussion shows clearly that the static cues in principle do *not* convey any information about the aircraft *relative motion* with respect to the trajectory.

Table 3.1: Expressions for the linearized displacement cues in straight tunnels.

	Lateral displacement cues	

(3)   lateral displacements of frame i (3.18)

$$\epsilon_{0_i} = \kappa \frac{W_t}{2D_i} \qquad\qquad \delta\epsilon_i = \kappa\left(\psi + \frac{x_e}{D_i}\right)$$
$$\eta_{0_i} = \kappa \frac{W_t}{2D_i} \qquad\qquad \delta\eta_i = -\kappa\left(\psi + \frac{x_e}{D_i}\right)$$
$$\pi_{0_i} = 0 \qquad\qquad\qquad \delta\pi_i = -\kappa\left(\psi + \frac{x_e}{D_i}\right)$$

(4)   relative lateral displacements of frames i and j (3.19)

$$\epsilon_{0_{ij}} = \kappa \frac{W_t}{2}\left(\frac{D_j - D_i}{D_i D_j}\right) \qquad\qquad \delta\epsilon_{ij} = \kappa x_e \left(\frac{D_j - D_i}{D_i D_j}\right)$$
$$\eta_{0_{ij}} = \kappa \frac{W_t}{2}\left(\frac{D_j - D_i}{D_i D_j}\right) \qquad\qquad \delta\eta_{ij} = -\kappa x_e \left(\frac{D_j - D_i}{D_i D_j}\right)$$
$$\pi_{0_{ij}} = 0 \qquad\qquad\qquad\qquad\qquad \delta\pi_{ij} = -\kappa x_e \left(\frac{D_j - D_i}{D_i D_j}\right)$$

(5)   quotient of relative lateral displacements of frames i and j (3.20)

$$\left(\frac{\epsilon_{ij}}{\eta_{ij}}\right)_0 = 1 \qquad\qquad\qquad \delta\left(\frac{\epsilon_{ij}}{\eta_{ij}}\right) = \frac{4x_e}{W_t}$$

	Vertical displacement cues	

(7)   vertical displacements of frame i (3.21)

$$\mu_{0_i} = \kappa\left(\Gamma_t + \frac{H_t}{2D_i}\right) \qquad\qquad \delta\mu_i = \kappa\left(\theta - \frac{v_e}{D_i}\right)$$
$$\nu_{0_i} = -\kappa\left(\Gamma_t - \frac{H_t}{2D_i}\right) \qquad\qquad \delta\nu_i = -\kappa\left(\theta - \frac{v_e}{D_i}\right)$$

(8)   relative vertical displacements of frames i and j (3.22)

$$\mu_{0_{ij}} = \kappa \frac{H_t}{2}\left(\frac{D_j - D_i}{D_i D_j}\right) \qquad\qquad \delta\mu_{ij} = -\kappa v_e \left(\frac{D_j - D_i}{D_i D_j}\right)$$
$$\nu_{0_{ij}} = \kappa \frac{H_t}{2}\left(\frac{D_j - D_i}{D_i D_j}\right) \qquad\qquad \delta\nu_{ij} = \kappa v_e \left(\frac{D_j - D_i}{D_i D_j}\right)$$

(9)   quotient of relative vertical displacements of frames i and j (3.23)

$$\left(\frac{\mu_{ij}}{\nu_{ij}}\right)_0 = 1 \qquad\qquad\qquad \delta\left(\frac{\mu_{ij}}{\nu_{ij}}\right) = \frac{4v_e}{H_t}$$

3.4.3 Dynamic optical cues

Definition of a recti-linear flight condition

Definition The *recti-linear* flight condition is most relevant for the analysis of straight tunnel sections. In this condition the aircraft travels along a straight line: the aircraft velocity vector is constant in direction (with respect to the World) and magnitude.[5]

Aircraft kinematics In Appendix C it is shown that the aircraft velocity vector is aligned with the longitudinal axis X_a of the *Aerodynamic* reference frame $\mathcal{F}^a$. The attitude of $\mathcal{F}^a$ relative to $\mathcal{F}^b$ is determined by two aerodynamic angles: the *angle of attack* α and the *angle of slip* β. The aircraft velocity vector and the rotation vector are defined within $\mathcal{F}^b$ with $\underline{V}^b = (u^b, v^b, w^b)$ and $\underline{\Omega}^b = (p^b, q^b, r^b)$, respectively. The direction of motion with respect to $\mathcal{F}^w$ can be determined by transforming the velocity vector from $\mathcal{F}^a$, via $\mathcal{F}^b$ and $\mathcal{F}^g$, to $\mathcal{F}^w$. In recti-linear motion, the rotation vector can be neglected: $\underline{\Omega}^b = \underline{0}$.

Flight-path angle and flight-path angle error The aircraft *flight-path angle* determines the aircraft direction of motion in $\mathcal{F}^w$. In the simplified – but representative – case of small aircraft attitude and aerodynamic angles, the following relations hold:

$$u^w \; = \; V_{tas}; \quad v^w \; = \; V_{tas} \underbrace{(\psi + \beta)}_{\chi^w}; \quad w^w \; = \; V_{tas} \underbrace{(\theta - \alpha)}_{\gamma^w}. \tag{3.26}$$

Here, χ^w is defined as the *flight-path azimuth* angle and γ^w the *angle of climb*. V_{tas} is the velocity. The direction of motion relative to $\mathcal{F}^t$ – the tunnel centerline, i.e. the reference trajectory (Fig. 3.3) – can then also be defined using two angles:

$$\chi^t \; = \chi^w; \qquad \gamma^t \; = \; -\left(\Gamma_t + \gamma^w\right). \tag{3.27}$$

Following the straight reference trajectory implies that the aircraft velocity vector must remain aligned with X_t. Hence, the latter two angles constitute the *flight-path angle error*: $\chi_e = \chi^t$ and $\gamma_e = \gamma^t$. When the flight-path angle error is small, the following equations hold for the derivatives of the position errors x_e and v_e in $\mathcal{F}^t$:

$$\dot{x}_e \; = \; V_{tas}\chi_e; \qquad \dot{v}_e \; = \; V_{tas}\gamma_e. \tag{3.28}$$

Derivatives of the static optical cues: *indirect* dynamic cues

The static cues of §3.4.2 are conveyed by a *frozen* tunnel image. When moving through the tunnel the magnitudes of these cues change in time, and the derivatives of these essentially *local* cues form the first category of dynamic cues, the *indirect* dynamic cues.

The position of the *infinity point*, Eq. 3.10, is determined by the aircraft attitude (lateral ψ, vertical $(\theta + \Gamma_t)$) relative to the tunnel centerline X_t. The motion of this point on the display is therefore a function of the aircraft angular velocities ($\dot{\psi} \approx r^b$ and $\dot{\theta} \approx q^b$, see Appendix C) which are assumed zero. Hence, in recti-linear motion the position of the

---

[5]It is assumed that the atmosphere is calm, neglecting effects of turbulence and wind.

infinity point on the display remains the same: it does not convey *any* information about the direction of motion with respect to the trajectory. The derivatives of the *splay angles*, Eqs 3.12 - 3.15, are a function only of the derivatives of the position errors, determined by the flight-path angle error χ_e and γ_e (Eq. 3.28). E.g. for the splay rate $\dot{\omega}_1$:

$$\dot{\omega}_1 = -\left(\frac{2W_t}{W_t{}^2 + H_t{}^2}\right) V_{tas}\gamma_e - \left(\frac{2H_t}{W_t{}^2 + H_t{}^2}\right) V_{tas}\chi_e. \tag{3.29}$$

The direction of motion relative to the tunnel trajectory is coded by means of the rotation velocities of the splay angles. Similar to the splay angles themselves, the splay rates show the lateral and vertical direction of motion in a *coupled* fashion: a change in any splay angle can be due to a lateral or a vertical flight-path angle error, or both. An interesting property of the splay angles is that when the flight-path angle error is zero, so are the splay rates, and the splay angles remain constant. Now consider the relative *displacements* of the tunnel frames. Whereas the positions of the frames on the viewplane are a function of both the attitude and the position relative to the tunnel, the relative displacements are only a function of the position errors. Comparing the velocity of a frame and the stationary infinity point conveys information about the flight-path angle error. The derivatives of the lateral displacements relative to the vertical pseudo-horizon (Eq. 3.24) are:

$$\dot{\epsilon}_{i\infty} \;\; = \;\; + \;\; \underbrace{\left(\frac{\dot{x}_e}{W_t/2 + x_e}\right)}_{\substack{\text{fractional change} \\ \text{in distance to the} \\ \text{left tunnel wall}}} \;\; \epsilon_{i\infty} \;\; + \;\; \underbrace{\left(\frac{V_{tas}}{W_t/2 + x_e}\right)}_{\substack{\text{global optical} \\ \text{flow rate}}} \;\; \epsilon_{i\infty}^2/\kappa;$$

$$\dot{\eta}_{i\infty} \;\; = \;\; - \;\; \underbrace{\left(\frac{\dot{x}_e}{W_t/2 - x_e}\right)}_{\substack{\text{fractional change} \\ \text{in distance to the} \\ \text{right tunnel wall}}} \;\; \eta_{i\infty} \;\; + \;\; \underbrace{\left(\frac{V_{tas}}{W_t/2 - x_e}\right)}_{\substack{\text{global optical} \\ \text{flow rate}}} \;\; \eta_{i\infty}^2/\kappa, \tag{3.30}$$

for the left and right tunnel walls, respectively. The same holds for the derivatives of the vertical displacements with respect to the horizontal pseudo-horizon:

$$\dot{\mu}_{i\infty} \;\; = \;\; - \;\; \underbrace{\left(\frac{\dot{x}_e}{H_t/2 - v_e}\right)}_{\substack{\text{fractional change} \\ \text{in distance to the} \\ \text{bottom tunnel wall}}} \;\; \mu_{i\infty} \;\; + \;\; \underbrace{\left(\frac{V_{tas}}{H_t/2 - v_e}\right)}_{\substack{\text{global optical} \\ \text{flow rate}}} \;\; \mu_{i\infty}^2/\kappa;$$

$$\dot{\nu}_{i\infty} \;\; = \;\; + \;\; \underbrace{\left(\frac{\dot{v}_e}{H_t/2 + v_e}\right)}_{\substack{\text{fractional change} \\ \text{in distance to the} \\ \text{top tunnel wall}}} \;\; \nu_{i\infty} \;\; + \;\; \underbrace{\left(\frac{V_{tas}}{H_t/2 + v_e}\right)}_{\substack{\text{global optical} \\ \text{flow rate}}} \;\; \nu_{i\infty}^2/\kappa. \tag{3.31}$$

The rates of the relative displacements with respect to the appropriate pseudo-horizon are a function of the flight-path angle error in each dimension. These equations show the additive properties of two elements of flow (Flach et al., 1992). The first terms on the right-hand side show the fractional change in distance to the appropriate tunnel wall, i.e. the

temporal cue of *time-to-contact* with that particular wall. The second terms on the right-hand side show the relationship with the global optical flow rate. The flow components are both *scaled* with the displacement *relative* to the infinity point, or, equivalently, the two pseudo-horizons. Eqs 3.30 and 3.31 also show the influence of the relative distance between the pseudo-horizon and the local tunnel feature itself. When this distance is large, the effect of the second component on the right-hand side of the equations is amplified, whereas for smaller distances to the pseudo-horizons it is especially the effect of the first component that is strong. These phenomena will be discussed further in §3.5.

The optic flow field: *direct* optical cues

Computational aspects   The velocities of the projected points of the tunnel on the viewplane constitute an *optic flow pattern*. The optic flow equations are a function of the position and the velocity of an arbitrary point P in $\mathcal{F}^b$. The position of this point in $\mathcal{F}^b$ ($\underline{x}_p^b$) is known through the perspective mapping formulas. The velocity of this point (fixed to $\mathcal{F}^w$) in $\mathcal{F}^b$ can be computed with the following expression (Etkin, 1972):

$$\underline{V}_p^b \;=\; -\underline{V}^b \;-\; \underline{\Omega}^b \times \underline{x}_p^b, \tag{3.32}$$

with $\underline{V}^b$ and $\underline{\Omega}^b$ the aircraft velocity and rotation vector in $\mathcal{F}^b$ (Appendix C). Substituting the vector components in this equation yields the *image field equations* (Singh, 1991):

$$\dot{u}_p \;=\; \underbrace{\left(-\kappa v^b + u_p u^b\right)/x_p^b}_{\dot{u}_p^T} + \underbrace{\left(-\kappa^2 r^b - \kappa v_p p^b - u_p v_p q^b - u_p^2 r^b\right)/\kappa}_{\dot{u}_p^R}; \tag{3.33}$$

$$\dot{v}_p \;=\; \underbrace{\left(+\kappa w^b + v_p u^b\right)/x_p^b}_{\dot{v}_p^T} + \underbrace{\left(-\kappa^2 q^b + \kappa u_p p^b - u_p v_p r^b - v_p^2 q^b\right)/\kappa}_{\dot{v}_p^R}. \tag{3.34}$$

The velocity of a projected point on the viewplane consists of a *translational* component $(\dot{u}_p^T, \dot{v}_p^T)$ and a *rotational* $(\dot{u}_p^R, \dot{v}_p^R)$ component (Longuet-Higgins & Prazdny, 1980).

The focus of radial outflow   In the recti-linear flight condition studied here the assumption was that the aircraft rotation vector can be neglected: $\underline{\Omega}^b = \underline{0}$. The velocity of a projected point on the viewplane can then be expressed in the translational components in Eqs 3.33 and 3.34 only. The *focus of radial outflow* (FRO) marks the origin of the radial expansion pattern resulting from recti-linear motion (Gibson, 1950). The position of the FRO on the viewplane can be computed with:

$$\begin{aligned}
\dot{u}_p = 0 \;\longrightarrow\; u_p = u_p^0 \;&=\; +\kappa\left(\frac{v^b}{u^b}\right) \;=\; +\kappa\frac{\tan(\beta)}{\cos(\alpha)} \;\approx\; +\kappa(\beta); \\
\dot{v}_p = 0 \;\longrightarrow\; v_p = v_p^0 \;&=\; -\kappa\left(\frac{w^b}{u^b}\right) \;=\; -\kappa\tan(\alpha) \;\approx\; -\kappa(\alpha).
\end{aligned} \tag{3.35}$$

For small angles the position (u_p^0, v_p^0) of the FRO on the viewplane is determined by the aircraft aerodynamic angles α and β. Thus, the FRO shows the direction of the velocity

vector with respect to the aircraft Body axes: i.e. it shows the attitude of $\mathcal{F}^a$ in $\mathcal{F}^b$.

The radial expansion pattern   In (Longuet-Higgins & Prazdny, 1980) it is shown that, with the position of the FRO known, the optic flow pattern resulting from the recti-linear flight can be described as straight radial lines through the FRO:

$$\dot{u}_p = \left(u_p - u_p^0\right) \frac{u^b}{x_p^b}; \quad \dot{v}_p = \left(v_p - v_p^0\right) \frac{u^b}{x_p^b}. \tag{3.36}$$

Fig. 3.8 shows the radial expansion pattern resulting from recti-linear flight. The velocity vector of an arbitrary point is determined by: (i) the distance between the position of the FRO and the projection of that particular point on the viewplane: close to the FRO all velocities diminish; (ii) the distance with respect to the COP: points that are positioned farther away move not as fast as points closer to the viewpoint (motion parallax), and (iii) the velocity of the locomotion: when the velocity increases the magnitude of all flow vectors increase. Hence, the radial expansion pattern provides information about translation *and* relative depth (Bruss & Horn, 1983). The future path, when the current state of motion remains the same, is specified in the optic flow pattern by the *locomotor flow line*, i.e. the flow line passing directly below the observer (Lee & Lishman, 1977), see Fig. 3.8.

Effects of a flight-path angle error and a position error   The expressions for the position and the velocity of a point in $\mathcal{F}^b$ can be substituted in Eqs 3.33 and 3.34. In the following, it is assumed that the aircraft position errors, the attitude angles and the aerodynamic angles are small. In this simplified – but representative – situation the following expressions can be derived for the velocities of points positioned on the left $(^l)$, right $(^r)$, top $(^t)$ and bottom $(^b)$ walls of the tunnel:

$$\begin{aligned}
\dot{u}_p^l &= - \kappa\chi_e \left(\frac{V_{tas}}{D_t}\right) - \kappa\left(\frac{W_t + 2x_e}{2D_t}\right)\left(\frac{V_{tas}}{D_t}\right); \\
\dot{u}_p^r &= - \kappa\chi_e \left(\frac{V_{tas}}{D_t}\right) + \kappa\left(\frac{W_t - 2x_e}{2D_t}\right)\left(\frac{V_{tas}}{D_t}\right);
\end{aligned} \tag{3.37}$$

and:

$$\begin{aligned}
\dot{v}_p^t &= + \kappa\gamma_e \left(\frac{V_{tas}}{D_t}\right) + \kappa\left(\frac{H_t + 2v_e}{2D_t}\right)\left(\frac{V_{tas}}{D_t}\right); \\
\dot{v}_p^b &= + \kappa\gamma_e \left(\frac{V_{tas}}{D_t}\right) - \kappa\left(\frac{H_t - 2v_e}{2D_t}\right)\left(\frac{V_{tas}}{D_t}\right).
\end{aligned} \tag{3.38}$$

These formulas are in principle identical to those derived for the relative displacements, Eqs 3.30 - 3.31. They illustrate that the flight-path angle error (χ_e, γ_e) results in an *equal* contribution of flow for all points on the display, scaled by their distance to the COP. The effect of a position error is scaled twice by the distance, indicating that the contribution in flow asymmetry due to a position error is strongest for those points on the tunnel that are close to the COP. Deriving the flow pattern characteristics from the *local* properties of the tunnel geometry and from the *global* optic flow equations yields identical properties.

Cues specifying temporal information

The optic flow pattern equations as well as those describing the derivatives of local properties of the tunnel display, contain elements specifying temporal cues. For instance, setting
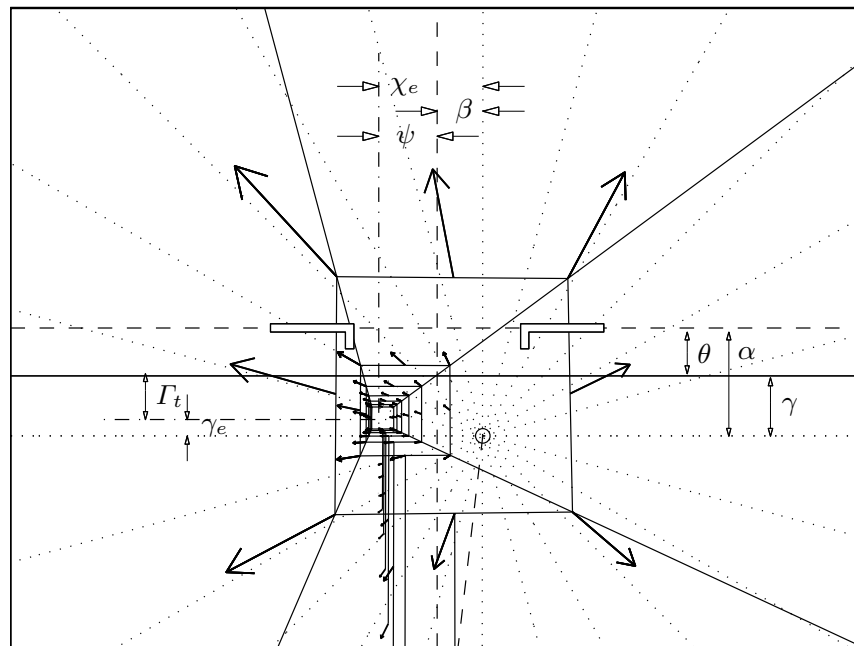
(a) recti-linear flight with a non-zero flight-path angle error
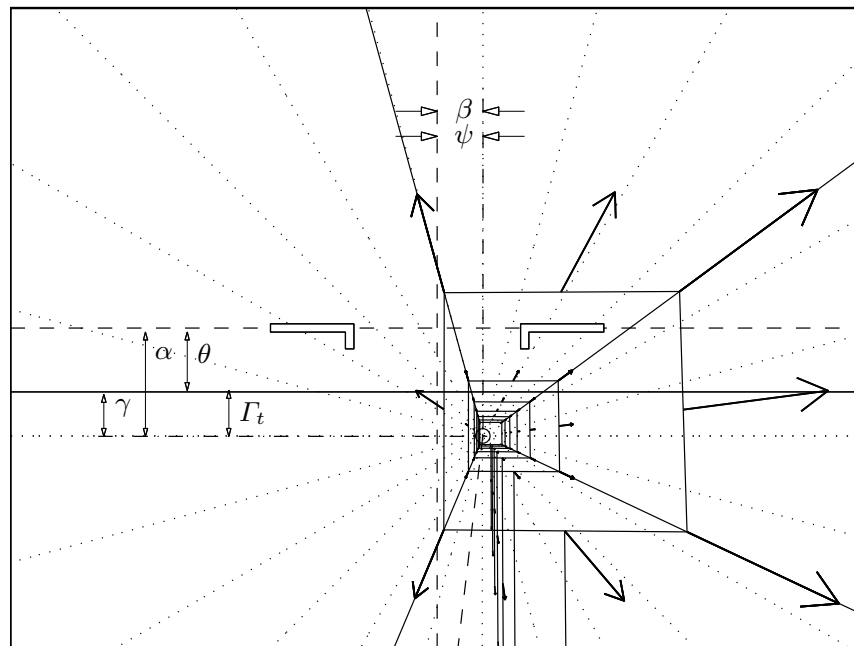
(b) recti-linear flight with a zero flight-path angle error

Figure 3.8: Radial flow pattern in recti-linear motion. In this figure, the dotted lines show the theoretical radial flow pattern originating from the focus of radial outflow (circle). The dashed lines show the viewplane centerlines. The dash-dot lines mark the position of the infinity point. The thick dashed line shows the locomotor flow line, projected on the bottom tunnel wall. The arrows show the velocities of the tunnel frame elements on the viewplane. The aircraft attitude angles (ψ, θ), aerodynamic angles (α, β) and flight-path angles (χ, γ) are as indicated. The following state is plotted: $W_t = H_t = 45$ [m]; $\Gamma_t = 3°$; $V_{tas} = 70$ [m/s]; $\beta = +3°$; $\alpha = +7°$; $\psi = +4°, -3°$; $\theta = +3°, +4°$; $\gamma_e = +1°, 0°$; $\chi_e = +7°, 0°$; $x_e = -15$ [m]; $v_e = +5$ [m].

the optical velocities to zero in Eqs 3.37 and 3.38, i.e. when considering the FRO, yields:

$$\left(\frac{\dot{x}_e}{W_t/2+x_e}\right) = \left(\frac{\dot{v}_e}{H_t/2+v_e}\right) = \left(\frac{V_{tas}}{D_t}\right) = 1/TTC.$$

The location of the FRO with respect to the tunnel geometry yields information about time-to-contact with the tunnel walls when continuing the recti-linear motion. The impact point is *locally* specified by the FRO, but also by the *entire* radial expansion pattern. Consider Fig. 3.8(a). Crossing the vertical flow line emerging from the FRO with the right tunnel wall shows the location of impact with that wall. The same holds for crossing the horizontal flow line emerging from the FRO with the bottom tunnel wall. When the FRO is put at the infinity point, Fig. 3.8(b), the flight-path angle error is set to zero and the recti-linear motion is aligned with the tunnel centerline: TTC $\rightarrow \infty$. The position error shows through the *asymmetry* of the optic flow pattern. The 'texture' compression rates in the lateral, Eq. 3.30, and vertical, Eq. 3.31, dimensions convey similar, and uncoupled, temporal cues in terms of the fractional change in distance to the tunnel walls. The greater the magnitude of the fractional change in distance, the larger the flight-path angle error, and the smaller the time before impact with one of the tunnel walls.

3.5 Perception and control of recti-linear motion

In recti-linear motion all rotation effects are neglected and the aircraft travels through the world along a straight line. This is a simplified abstraction of reality. Recti-linear motion is nothing but a special case of curvi-linear motion, discussed in §3.6, namely that case in which the radius of circular motion is extremely large. The recti-linear motion condition is important in the analysis of optical cues because many concepts can be derived for this elementary state of locomotion. Guided by the findings reported in literature (§3.2) the tunnel display has been analyzed mathematically in §3.4. In this section the sources of optical information are studied from the perspective of the pilot. The principal hypothesis – rooted in the early work of (Gibson et al., 1955) – is that the *main stimulus of a pilot in controlling recti-linear motion through a straight tunnel is that of an approach to a plane.* Instead of only one plane limiting the motion in one direction, the tunnel consists of four planes, limiting the motion in four directions. The discussion is categorized with respect to the perception of the motion referents that are important for controlling the aircraft along the trajectory. These referents, defined with respect to the reference trajectory, are: (i) the aircraft attitude and, (ii), position, (iii) the relative motion (flight-path), the forward velocity and the temporal situation. The first three referents represent the variables necessary for the control of the aircraft inner, outer and middle loops, respectively (Chapter 2). The characteristics of the optical cues conveying information about a motion referent are analyzed with the guidelines of §3.2.3 in mind.

(i) The aircraft attitude

The attitude of the aircraft serves as the inner loop variable necessary for aircraft control. The attitude of the aircraft Body axes $\mathcal{F}^b$ with respect to the *world*, $\mathcal{F}^w$, is determined by the three Euler angles. The aircraft roll angle ϕ and pitch angle θ are shown by the tunnel display in similar fashion as in conventional primary flight displays, i.e. through the translation and rotation of the horizon with respect to the display center. For a discussion of the mechanisms of perceiving a moving horizon display, the reader is referred to (Hosman & Mulder, 1997). The attitude of the aircraft with respect to the *tunnel* is conveyed by the tunnel display through the *infinity point*, marking the projection of the reference trajectory at infinity. As indicated in Fig. 3.5 the two parallel lateral tunnel planes and the two parallel vertical tunnel planes at infinite distance yield two perpendicular axes, the pseudo-horizons, which are rotated with the aircraft roll angle ϕ with respect to $\mathcal{F}^{vr}$. The downslope Γ_t of the tunnel trajectory results in a vertical displacement of the horizontal pseudo-horizon with which the vertical attitude with respect to the tunnel, $\theta + \Gamma_t$, can be perceived. The vertical pseudo-horizon marks the lateral attitude – the heading ψ – of the aircraft with respect to the tunnel trajectory. The perception of aircraft attitude is hypothesized to be *direct*. The presentation is not influenced by the tunnel geometry itself. Limiting the viewing volume (i.e. the minimum and maximum viewing distances D_v^{min} and D_v^{max}, §3.3.1), however, could deteriorate the perceivability of the infinity point. These issues are studied in Experiment X2, discussed in Chapter 6.

(ii) The aircraft position

The aircraft position with respect to the trajectory is conveyed by the tunnel display through the gradients of optical perspective and optical compression.

The gradient of optical perspective   The *splay angles* are a function of the aircraft lateral and vertical position errors and the tunnel size, Eqs 3.12-3.15. A clear disadvantage of the splay angles is that a change in any splay angle can be due to a lateral or a vertical position error, or both. In the automobile driving research in which the potential use of splay angles is advocated (Biggs, 1966; Riemersma, 1981, 1984; Beall & Loomis, 1996) this disadvantage does not occur because the automobile motion is limited to the horizontal plane (v_e=0). The fact that the splay angles show the position referents v_e and x_e in a *coupled* fashion led to inferior performance in several altitude control studies in which both lateral and vertical velocity disturbances were present (Bennett et al., 1986; Johnson et al., 1988, 1989). Although it is possible that the pilot can mentally distinguish between the effects of a lateral and a vertical position error on splay, §3.4.2, this requires cognitive processing. The splay angles also have some important virtues. First, because it is a property of the entire line the change in splay angle is the same for all points on the line: the splay *gain* is independent on which part of the line is being perceived (Beall & Loomis, 1996). Second, the splay angles are unaffected by the aircraft longitudinal motion. Third,

the splay angles are unaffected by the attitude of the aircraft relative to the tunnel.

The gradient of optical compression The displacements of the tunnel frame lines with respect to the two pseudo-horizons convey optical density information, Eqs 3.24 and 3.25. An advantage of the compression gradient cues is that they show the information in both dimensions in an *uncoupled* fashion. The relative position with respect to the four tunnel walls is shown through the relative *compression* of the 'texture' – the lines of the tunnel frames in the appropriate planes – in the two planes that are being approached, and through the relative *expansion* of the 'texture' in the two planes that recede from the pilot. The relative change in compression and expansion of the tunnel frame elements with respect to the pseudo-horizons, however, also depends on the position of the particular elements that are perceived. Hence, the *gain* in presenting the position error referent depends on the distance to the local element perceived, an important disadvantage. Another disadvantage of the fact that *relative* displacements must be perceived is that these displacements themselves are affected by the longitudinal motion, and a pilot must perceive a change in these displacements between frames *on top* of the displacements of these frames due to the forward motion (Crowell & Banks, 1996). This could have been the reason why splay angles were found superior in some of the altitude control studies (Wolpert et al., 1983; Wolpert & Owen, 1985; Wolpert, 1988). A final comment must be made. Considering the relative position of the tunnel walls as such, i.e. perceiving the walls as *walls* instead of the concatenation of tunnel frames, with respect to the pseudo-horizons, is not affected by the forward motion. It can be hypothesized that when enough tunnel frames are presented (the intermediate frame distances $\triangle D$ are small), the percept will be that of a global density instead of merely a local relative displacement, improving the effectivity of the compression gradient.

Concluding, there are two main sources of optical information that specify a position error. Both are *static* cues. There also exists an asymmetry in the optic flow pattern for a non-zero position error, especially for those frames close by (§3.4.2). The projection of the tunnel geometry conveys such salient and informative cues by itself, however, that it can be hypothesized that the flow field cues can be regarded as contextual rather than functional. The functional cues are those of optical splay and optical compression. Both have their specific virtues and it depends on the characteristics of the task and the display which of the cues is most effective in specifying the position error referent. This is one of the main themes of Experiment X3, described in Chapter 7.

(iii) The flight-path

The attitude of the aircraft does *not* reveal the direction of locomotion with respect to the trajectory. The aerodynamic angles α (vertical) and β (lateral) depict the direction of the aircraft velocity vector with respect to the aircraft Body axes $\mathcal{F}^b$ ($\equiv \mathcal{F}^v$). Together with the aircraft attitude angles θ and ψ these angles determine the direction of motion with respect to the World, i.e. the flight-path (γ^w, χ^w). According to literature and supported

by the analysis of §3.4.3 there are two ways of perceiving the aircraft direction of motion.

The perception of flight-path from the global optic flow field   Recti-linear motion results in a radial optic flow pattern, Fig. 3.8. Since the direction of motion is specified by the focus of radial outflow, Gibson postulated that the FRO serves as an optical basis for the perception of heading (Gibson, 1950). However, it is not the (local) FRO per se that specifies the direction of motion, but rather the *global* flow pattern (Warren, Morris, & Kalish, 1988). The direction of motion is implicit everywhere in the flow field, even when the FRO is not in view (Warren, 1976). This is illustrated in Fig. 3.8, showing that the *magnitudes* of the optic flow field velocity vectors depend on the distances to the environmental objects, whereas the *directions* of these vectors are completely determined by the direction of locomotion. The future path is specified in the locomotor flow line. In the past, research focused on determining the accuracy with which observers are able to perceive the FRO. One of the first studies, investigating the accuracy of estimating heading during the approach to a fronto-parallel plane, reported that accuracy was lacking (Johnston, White, & Cumming, 1973). More recent findings, however, investigating the accuracy of estimating the impact point during motion parallel to a plane, confirm Gibson's hypothesis. The optical flow patterns provide sufficient basis for motion direction judgements during recti-linear motion at a level prerequisite for the control of locomotion (Warren et al., 1988), irrespective of eye movements (Warren & Hannon, 1990), and independent on the fact whether the FRO is visible or not (Warren, 1976). A Grunwald and Kohn (1993) reported experiments in which subjects had to estimate the flight-path during passive recti-linear and curvi-linear motion over different types of texture. Results indicated that the accuracy in estimating the direction of recti-linear motion increased and estimation times decreased with the global optical flow rate. It was also concluded that the far visual field as opposed to the near visual field is essential in estimating the flight-path. This was attributed to the larger local expansion rates of the optic flow – defined as the change in flow vector direction per unit angular distance – in the far visual field. Due to the smaller magnitudes of the flow field velocities in the far visual field, however, estimation times became larger.

The perception of flight-path from local gradients   The *splay angle rates* are a function of the flight-path angle error in both the lateral (χ_e) and vertical (γ_e) direction, Eq. 3.29. The characteristics of these rates are similar to those of the splay angles themselves. A clear disadvantage is that the splay rates are affected by both the lateral and vertical referents of relative motion. The splay rate *gain*, however, is the same for the entire line and the splay rates are unaffected by the longitudinal motion. Another property of the splay rates is that the forward velocity itself acts as a gain: when the velocity increases, so do the splay rates for the same flight-path angle error. Most importantly, when the flight path angle error is zero, so are the splay rates and the splay angles remain constant: the splay angles coincide with the directions of the radial flow lines (Gordon, 1966b; Lee & Lishman, 1977). Hence, the splay angles could act as an optical invariant for the relative distance to any of the four tunnel walls. The *displacements* of the tunnel frame

lines with respect to the two pseudo-horizons are only a function of the lateral and vertical position errors. The derivatives of these displacements, Eqs 3.30-3.31, in each dimension are only a function of the flight-path angle error in that particular dimension. This is an important virtue. Similar to the relative displacements themselves, and probably even worse, is that the *rates* of the changes in relative displacements must be perceived on top of the motion of the local tunnel elements due to the forward motion (§3.2.2). Again, when enough frames are positioned to give the impression of a 'wall' instead of just a set of frames receding in the distance, this disadvantage could become less important.

The *redundancy* in optical information specifying flight-path could be one of the key issues in explaining the relative success of using the tunnel display for aircraft guidance tasks. It is hypothesized, however, that the *local* gradient cues of perspective and compression are more important than the cues of the *global* optic flow pattern. This assumption originates from the observation that the tunnel display does not contain *any* elements (such as texture) that can 'carry' the flow, except for the tunnel geometry itself. This is a fundamentally different stimulus situation than those applied in the experiments listed above where the visual field presented was information-rich, consisting of fields of random texture elements. The discussion above clearly showed that the changing tunnel geometry provides strong cues for the flight-path relative to the trajectory. Thus, why would a pilot bother about the location of the FRO when the changing tunnel geometry *itself* conveys the task-relevant information? Results of automobile driving experiments support this hypothesis (Biggs, 1966; Gordon, 1966b; Fry, 1968; Riemersma, 1981, 1984; Beall & Loomis, 1996; Kappé, 1997). Some of these issues are investigated in Experiment X5, discussed in Chapter 9.

The perception of the velocity of recti-linear motion

A subject of interest that has not been addressed in this chapter before is the pilot perception of the velocity of the recti-linear motion. In automobile driving, a generally acknowledged finding is that the major sensation of speed experienced by the driver is due to the streaming of the peripheral visual field across the periphery of the retina (Gordon, 1966a; Salvatore, 1968; Denton, 1980; Hills, 1980). With a small display, however, stimulating only foveal vision, other perceptual mechanisms must apply. Generally, two aspects of the optic array are identified that affect the perception of the velocity of motion: *optical edge rate* and *global optical flow rate* (Larish & Flach, 1990). Optical edge rate is defined as the rate at which *local* discontinuities cross a fixed point of reference in the observer's field of view (Warren, 1982). The effectiveness of optical edge rate has been demonstrated in automobile driving, where placing stripes at exponentially decreasing intervals on roads approaching traffic roundabouts (yielding the perpendicular texture of Fig. 3.1) resulted in a significant reduction in speed (Denton, 1980). Global optical flow rate, introduced in §3.2.2 and defined as the ratio of the velocity of motion and the altitude above the ground surface, Eq. 3.4 and Eqs 3.30-3.31, is a *global* multiplier that affects every point in

the visual array, independent of the surface texture. When the distance to the surface becomes smaller, the global optical flow rate increases, whereas the optical edge rate remains constant. Results in literature suggest that optical edge rate is the *functional* variable for the perception and control of forward velocity, whereas the global optical flow rate acts as a contextual variable (Denton, 1980; Owen, Warren, Jensen, Mangold, & Hettinger, 1981; Awe, Johnson, & Schmitz, 1989; Larish & Flach, 1990).

Concerning the tunnel display, it is clear that the splay angles and splay rates do not convey any information about forward motion, not to mention its magnitude. The approaching tunnel frames, on the other hand, *do* provide the edge rate and global optical flow rate cues introduced above. Eqs 3.30-3.31 show the relationships between the compression rate gradient and the pilot's recti-linear motion. These equations show that smaller tunnels yield an increase in the global optical flow rate and could lead to an illusive perception of increasing forward velocity. A secondary effect is that a position error leads to a (small) increase in the global optical flow rate of the texture at the near wall and to a (small) decrease in this quantity of the texture elements of the opposite wall. The effect of the global optical flow rate decreases at larger distances. Hence, an equilibrium state exists in the velocities of the local texture elements (a restatement of the flow *asymmetry* of §3.4.3). Perceiving the velocity of the frame elements at some fixed location on the viewplane – the optical edge rate – could well be the pilot's strategy to determine the perception of forward velocity. When the intermediate distances between frames is constant, a change in optical edge rate always depicts a change in velocity, independent of a change in position relative to the plane in which the frame elements lie.

Temporal cues

Temporal cues form the basis of all anticipatory behaviour (Lee, 1974; Lishman, 1981). In the tunnel display the main temporal cues are those conveying information about time-to-collision with the four tunnel walls *and* the fronto-parallel planes of the approaching tunnel frames. The discussion above shows that the tunnel frames are essential for the perception of forward velocity. In a recti-linear flight condition through a straight tunnel section the direction of motion is generally almost perpendicular to the tunnel frames and the resulting isotropic expansion of the frames conveys information about time-to-contact (Lee, 1980b, 1980a). When the aircraft forward velocity and the distance between frames is constant, the passing frames constitute a *temporal unit*, which could form the basis of all pilot's spatio-temporal behaviour (Lee, 1980b; Rieger, 1983), including for instance the anticipation of oncoming changes in the trajectory. This is studied in Experiment X6, discussed in Chapter 10. The temporal cues conveying information about time-to-collision with a tunnel wall provide information about the future aircraft trajectory relative to the spatial constraints. In this respect, the use of a temporal cue labelled the *time-to-wall-crossing* (TWC) variable, similar to the time-to-line-crossing (TLC) variable of Godthelp (1984) (Chapter 2), has been hypothesized to specify the temporal distance between the aircraft and a tunnel wall (Mulder et al., 1995). The TWC is based on an extrapolation

of the future aircraft path, which is assumed to be either straight or circular yielding a first and second order TWC, respectively. The first order TWC equals the conventional TTC specified by the optic flow and can be considered most relevant in the study of recti-linear motion. In automobile driving the use of the quotient of the splay angle and the splay angle rate for temporal purposes has been hypothesized (TLC = TTC = $\Omega_i/\dot{\Omega}_i$) in (Kappé, 1997). In the context of the tunnel display, however, the use of splays for this purpose is questionable, essentially because the splay angles and their derivatives are affected by the motion referents in *both* the lateral and vertical dimension. Whereas the splay angles can in principle be de-coupled, this will involve cognitive processing. The same – and probably even worse – holds for the splay rates. Hence, it is questionable if, when both the splays and the splay rates are processed this way, pilots use the quotient of these relatively uncertain quantities to estimate TTC with the tunnel wall. Another important argument for the rejection of the functionality of splay for temporal purposes is the availability of another powerful temporal cue, namely that of the optical compression gradient. The relative displacements of the tunnel frame elements with respect to the pseudo-horizons provide information about the position relative to the tunnel walls in an *uncoupled* fashion. Furthermore, the rates of the optical compression gradients in lateral and vertical dimension directly convey temporal information about *time-to-contact* with the tunnel walls, Eqs 3.30 - 3.31. Thus, it is hypothesized that the main temporal cues for the estimation of time-to-collision with any of the four tunnel walls are the optical compression rates, and *not* those of splay as suggested in (Theunissen, 1997).

3.6   Information in curved tunnel sections

The potential sources of optical information conveyed by the tunnel display for the pilot task of following circular tunnel trajectories are studied in this section (Mulder, Mulder, & Stassen, 1999a). A generic tunnel geometry is defined in §3.6.1. The discussion of the static and dynamic cues in §3.6.2 and §3.6.3 is similar to those in straight tunnel sections.

3.6.1   Definition of the situation

A bird's eye view of the situation is shown in Fig. 3.9(a), whereas Fig. 3.9(b) shows the corresponding tunnel image. The optical cues originate from the projection of the main elements of the tunnel geometry – the frames Ⓕ , the altitude poles Ⓐ and the longitudinal lines Ⓛ connecting the frames – on the viewplane. An important difference between the current situation and the case of straight tunnels is that, when looking farther into the tunnel, the tunnel geometry does not vanish to infinity but bends off towards one of the sides of the viewplane. This has major consequences for the optical information.

Mathematical description   A generic geometrical definition of a right curve[6] is illustrated in Fig. 3.10, showing a top view of the situation in Fig. 3.9. To facilitate the

---

[6]Below, only trajectories curved to the right are discussed; left curves lead to similar results.

(a) bird's eye view (the pilot's task)   (b) pilot's view (the tunnel image)
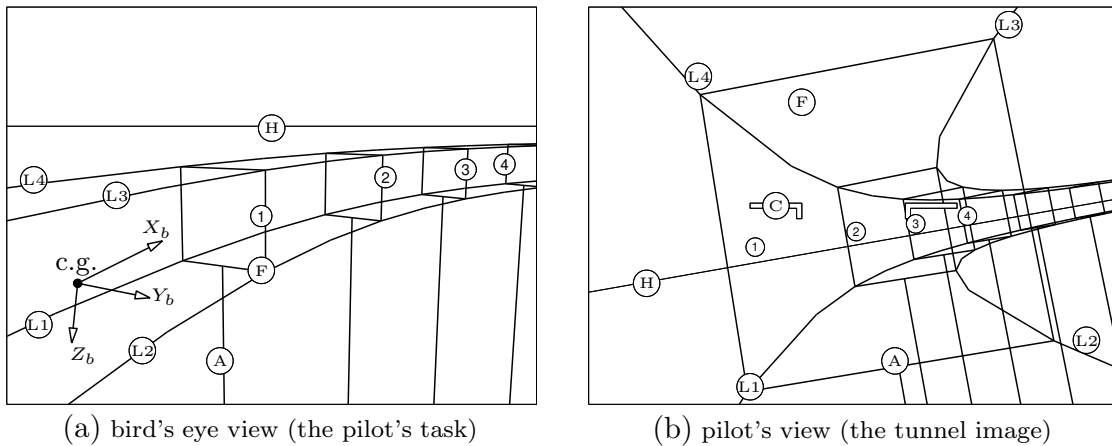
Figure 3.9: The general situation of flying through a curved tunnel section.

analysis, it is assumed that the downslope Γ_t of the circular trajectory is zero. As can be seen from Fig. 3.10, the circular tunnel is approximated by a concatenation of straight *segments* bridging an angular distance – measured along the tunnel centercircle – of $\triangle S^s$, corresponding with a fixed angle $\triangle\Psi$: $\triangle S^s = R_t \triangle\Psi$. The vertices of a tunnel segment s_i are positioned on the tunnel inner and outer (top and bottom) circular boundaries. The tunnel *frames* are placed at every c^{th} quadruple of these vertices: the angular distance $\triangle S^f$ between frames equals $c \triangle S^s$. The aircraft is positioned in the tunnel (width W_t, height H_t) with an arbitrary position and attitude with respect to the tunnel centercircle. The origin of the World reference frame $\mathcal{F}^w$ lies on the cross-point of the tunnel centercircle and a plane perpendicular to the centercircle through the aircraft center of gravity. The X_w axis is tangential to the centercircle and the Y_w axis points to the center of the circular trajectory. Because the tunnel downslope angle Γ_t is zero, the tunnel frame of reference $\mathcal{F}^t$ is identical to $\mathcal{F}^w$. The aircraft position error is defined similarly as for straight tunnels (view A–A of Fig. 3.4). The aircraft attitude is defined with respect to $\mathcal{F}^g$ with the Euler angles ψ, θ and ϕ, of which the heading angle ψ is defined with respect to the (instantaneous) tangent of the tunnel centercircle. The perspective display mapping is identical to that of straight tunnel sections, with the exception that now the *angular distance* S_t (measured along the tunnel centercircle) is used instead of D_t.

3.6.2   Static optical cues

Cue inventory

Positioning the aircraft with an arbitrary position error and attitude with respect to the trajectory results in a tunnel image similar to that of Fig. 3.9(b). The primary static cues are described at the hand of Fig. 3.11 showing two subsets of cues (defined in $\mathcal{F}^{vr}$) resulting from the projection of the longitudinal (Fig. 3.11(a)) and vertical (Fig. 3.11(b))
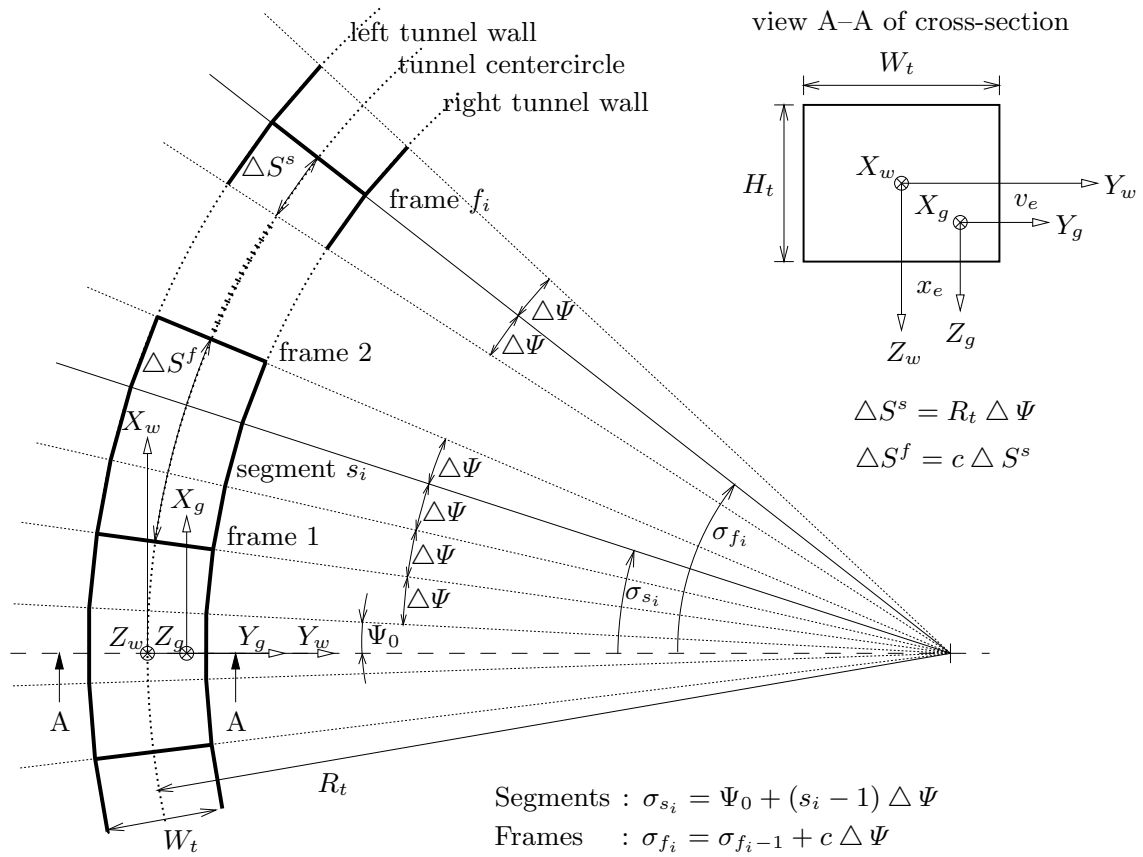
Figure 3.10: Generic circular tunnel geometry used in the analysis (top view).

elements of the tunnel geometry.[7] The following cues can be defined:

1. The *distance* into the tunnel S_t^{max} (angular distance σ^{max}), defined as the maximum distance along the tunnel centercircle that is visible on the viewplane (Fig. 3.11(a)).

2. The position of the *infinity points* $(u_\infty, v_\infty)_{s_i}$ that result from extrapolating the four longitudinal segment lines – for each segment s_i – to infinity (Fig. 3.11(a)).

3. The *relative distances* between the infinity points $(\triangle u_\infty, \triangle v_\infty)_{s_i, s_j}$ of segments s_i and s_j (Fig. 3.11(a)).

4. The *optical splay angles* $(\Omega_{1\ldots4})_{s_i}$ defined as the angles of the longitudinal segment lines of segment s_i with the horizon (Fig. 3.11(a)).

5. The *lateral displacements* ϵ_{f_i} (left), η_{f_i} (right) and π_{f_i} (poles) of the vertical frame lines and the altitude poles of frame f_i with respect to the rotated viewplane centerline V' (Fig. 3.11(b)).

6. The *relative lateral displacements* $\epsilon_{f_i f_j}$ (left), $\eta_{f_i f_j}$ (right) and $\pi_{f_i f_j}$ (poles) of the vertical frame lines and the altitude poles of frames f_i and f_j (Fig. 3.11(b)).

---

[7]The cues resulting from the projection of the lateral elements of the tunnel geometry – the *vertical displacement cues* – are similar to those of straight trajectories (§3.4.2 with $\Gamma_t{=}0$).
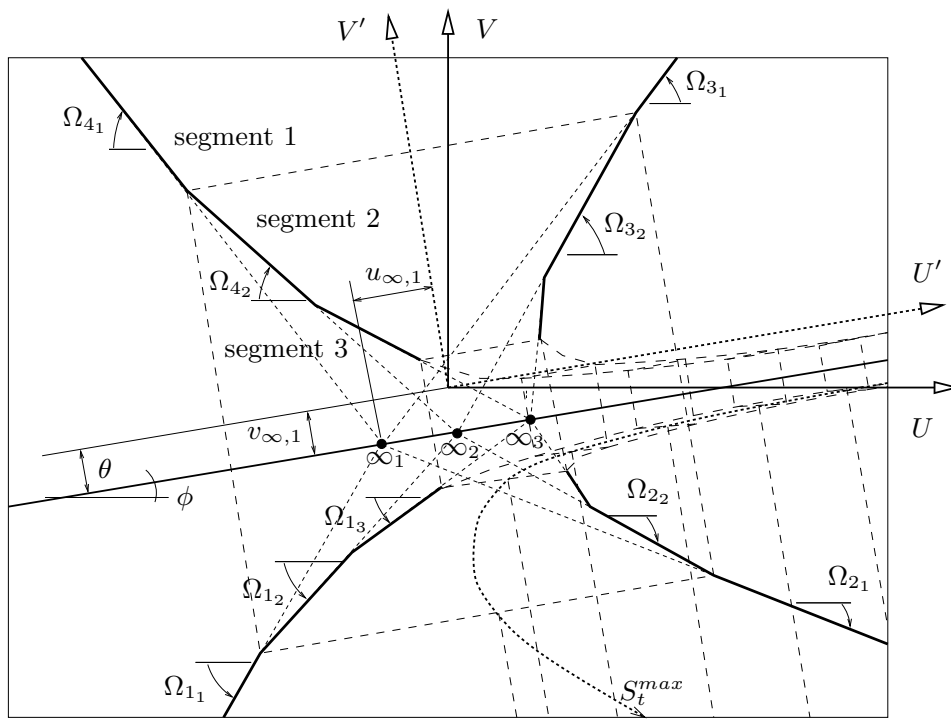
(a) the longitudinal tunnel cues (1)–(4).
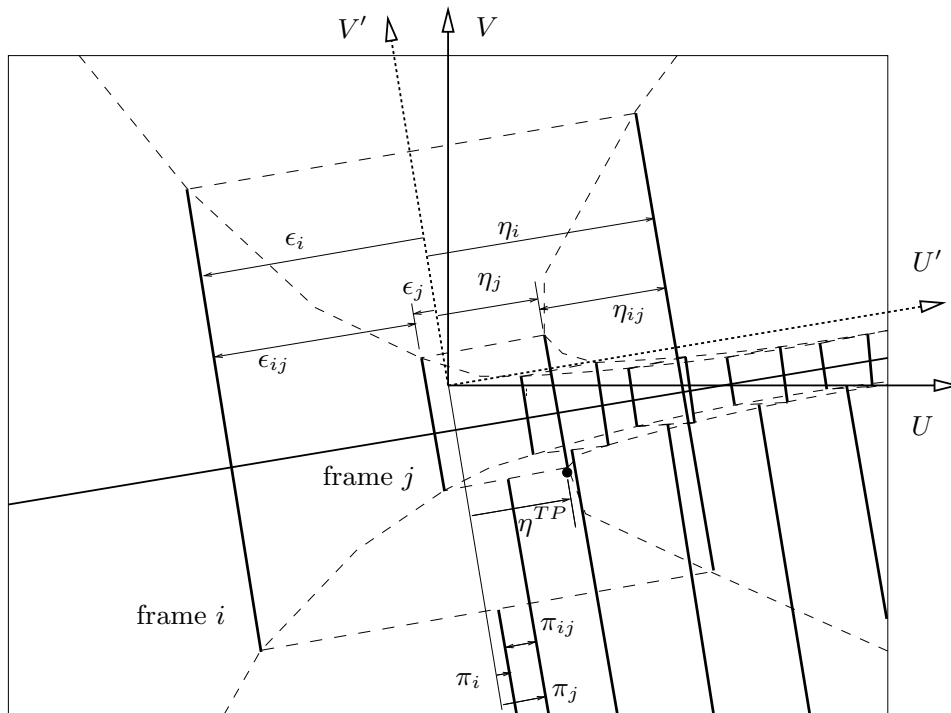
(b) the lateral tunnel cues (5)–(7).

Figure 3.11: Two subsets of static optical cues in a circular tunnel section. The top figure shows the elements of the tunnel geometry that convey the longitudinal cues with continuous lines and the elements that convey the lateral and vertical cues with dashed lines. In the bottom the elements conveying the lateral cues are shown with continuous lines. All symbols are explained in the text.

7. The position of the *tangent point* on the viewplane, defined as that point of the inner curve tunnel wall that has the smallest lateral displacement η (Fig. 3.11(b)).[8]

An important difference with the inventory of static cues for straight tunnels is that instead of only one infinity point and one set of splay angles, the curved trajectory yields similar quantities but now for *all* tunnel segments s_i. Furthermore, because the circular trajectory is shown through a concatenation of planes, no pseudo-horizons emerge in the display. Rather, every segment introduces its own pseudo-horizon, which makes the situation fairly complicated. Mathematical expressions are derived that relate the optical cues to the aircraft attitude and position with respect to the circular tunnel trajectory (Appendix D). The linearization point is the situation of zero position errors and small attitude angles. The aircraft roll angle, however, *can* have a considerable non-zero value.

(1) The (angular) distance into the tunnel The maximum distance into the curve, along the tunnel centercircle, that is visible on the viewplane is given by:

$$S_t^{max} = R_t \sigma^{max} = R_t(2\psi + HGFOV). \tag{3.39}$$

For a certain perspective projection ($HGFOV$) the maximum distance depends only on the radius of the circular trajectory and the aircraft heading with respect to the centercircle.

(2)–(3) The positions of the infinity points The co-ordinates of the infinity point of segment s_i can be approximated by:

$$u_{\infty_{s_i}}\big|_{\phi=0} = \kappa\left[\tan(\sigma_{s_i} - \frac{\triangle\Psi}{2}) - \left(1 + \tan^2(\sigma_{s_i} - \frac{\triangle\Psi}{2})\right)\psi\right]; \tag{3.40}$$

$$v_{\infty_{s_i}}\big|_{\phi=0} = -\kappa\left(\theta\right). \tag{3.41}$$

For the relative positions of the infinity points of two consecutive segments s_i and $s_i + 1$ the following expressions hold:

$$\triangle u_{\infty_{s_i s_i+1}}\big|_{\phi=0} \approx \kappa \triangle\Psi; \qquad \triangle v_{\infty_{s_i s_i+1}}\big|_{\phi=0} = 0. \tag{3.42}$$

The location of the infinity points of segments s_i are – as in the case of straight tunnels – only a function of the aircraft attitude with respect to the trajectory. The relative positions of the infinity points mark the angular difference $\triangle\Psi$ of the consecutive segments s_i and $s_i + 1$. They are unaffected by the aircraft attitude and position relative to the trajectory.

(4) The optical splay angles Analytic expressions for the splay angles $\Omega_1 \ldots \Omega_4$ of segment s_i are collected in Appendix D. Linearizing these relations yields expressions for the change in splay angle $\omega_{j_{s_i}}$ from the reference condition $\Omega_{j_{s_i}}$ ($j = 1 \ldots 4$):

$$
\begin{aligned}
\omega_{1_{s_i}} &= - K_{V_{s_i}^1} v_e - K_{X_{s_i}^1} x_e; \\
\omega_{2_{s_i}} &= - K_{V_{s_i}^2} v_e + K_{X_{s_i}^2} x_e; \\
\omega_{3_{s_i}} &= + K_{V_{s_i}^3} v_e + K_{X_{s_i}^3} x_e; \\
\omega_{4_{s_i}} &= + K_{V_{s_i}^4} v_e - K_{X_{s_i}^4} x_e.
\end{aligned}
\tag{3.43}
$$

---

[8]Actually, the tunnel conveys a tangent *line* segment.

The *gains* relating x_e and v_e with the changes of the four splay angles are listed in Appendix D. The splay angle changes are a function of the position error only, and are independent of the attitude with respect to the trajectory. Similar to the situation of straight tunnels, the splay angles show the position errors in a *coupled* fashion. There are two important differences. First, there exists *no* symmetric condition for the lateral dimension. As one can see in Fig. 3.11(a) the splay angles of the outer curve tunnel wall always remain positive and go to 0° for segments at a larger distance S_t. The splay angles of the inner curve wall are small for small S_t's, approximate 90° near the tangent point, and become 180° when the distance S_t becomes large. Second, it is shown in Appendix D that the splay gains $K_{V_{s_i}^1}$, etc., are a function of the angular viewing distance σ_{s_i}, Eqs D.13. Fig. D.1 illustrates that the splay angle gains decrease for larger viewing distances: the splay angles convey information for a position error *only at smaller viewing distances.*

(5)–(7) The lateral displacement cues   The lateral displacements ϵ_{f_i}, η_{f_i} and π_{f_i} of the vertical frame lines and the altitude poles can be computed and linearized similarly as for the straight tunnel sections (Appendix D). The linearized expressions are summarized in Table 3.2, showing the values of the cues in the linearization point and the change in these variables that result from a change in the aircraft state. Due to the curvature of the tunnel geometry, two situations must be distinguished: (i) frames close to the aircraft $(\sigma_{f_i} < 30°)$[9], and (ii) frames farther away into the tunnel $(\sigma_{f_i} > 30°)$. As one can see from Table 3.2, the expressions resemble those of straight tunnel sections, especially for small angular distances S_t. The vertical displacement cues are the same as those for straight tunnels, Eqs 3.21-3.23 with $\Gamma_t=0$ and D_i replaced by S_{f_i}. Similar to straight tunnels, the linearized displacement cues show the aircraft attitude and position errors in an *uncoupled* fashion: the lateral expressions are independent of the aircraft and/or tunnel characteristics in the vertical dimension and vice versa. The curvature of the trajectory only affects the lateral displacement cues. For small distances S_{f_i} the displacement of a frame f_i from its reference condition, Eq. 3.45, is due to the aircraft attitude and position with respect to the tangent of the centercircle. The effect of the position error is scaled with the angular distance to the frame. For large distances, Eq. 3.46, only the heading angle with respect to the centercircle tangent is presented. The relative displacements of two consecutive frames f_i and $f_i + 1$ for small angular distances depend on the position error only, scaled by a compression factor that is similar to that of straight tunnels, Eq. 3.48. For large viewing distances the effects of the aircraft attitude and position error on the change in relative displacements vanish completely, Eq. 3.49. Rather, these relative displacements mark the angular heading difference $c\triangle\Psi$ of the consecutive frames.

The tangent point, of which the initial position on the inner curve wall is determined by the tunnel geometry, W_t and R_t, and shows the lateral attitude and position error in a way similar to the other lateral displacement cues. The effect of a position error on the change in position of the tangent point is scaled by the tunnel width.

---

[9]These limits are mere indications.

Concluding, the static optical cues in curved tunnels resemble those of straight tunnels. The splay angles of the curve segment lines and the lateral and vertical displacements of the tunnel frames show information about the aircraft attitude and position with respect to the centercircle. There are three important differences. First, in curved trajectories there exists *no vertical pseudo-horizon* that could act as a reference for the lateral displacements of the tunnel frames. Second, due to the trajectory curvature in the lateral dimension no *symmetric* condition in splays nor in lateral displacement cues is available in this dimension. Third, the displacement cues *and* the splay angles convey information about a position error only at small viewing distances σ_{s_i}.

3.6.3 Dynamic optical cues

Definition of a curvi-linear flight condition

Definition   The curvi-linear flight condition in which the aircraft travels along a circular trajectory is most relevant for the analysis of circular tunnel sections. Because the downslope Γ_t of the reference trajectory is zero, the curvi-linear flight condition studied here is a stationary, horizontal turn. The aircraft velocity vector is constant in magnitude but rotates within the horizontal plane with an angular velocity of V_{tas}/R_t (in $\mathcal{F}^w$).

Aircraft kinematics   The aircraft makes a turn by rotating its wings with a roll angle ϕ with respect to the horizon. For a stationary horizontal turn with velocity V_{tas} and a curve radius R_t the reference bank angle Φ_t[10] equals $\arctan(g_0 R_t/V_{tas}^2)$, with g_0 the gravitational acceleration (9.80665 [m/s^2]). The rotation vector in $\mathcal{F}^b$ is then given by:

$$\underline{\Omega}^b = \left(\frac{g_0}{V_{tas}}\right)\left(-\sin\theta\tan\phi_t \quad \cos\theta\tan\phi_t\sin\phi_t \quad \cos\theta\sin\phi_t\right)^T. \tag{3.51}$$

Flight-path angle error and yaw rate error   Here, the same properties hold as in straight tunnels (§3.4.3). The direction of the aircraft velocity vector in $\mathcal{F}^b$ can be defined with the attitude of the Aerodynamic reference frame $\mathcal{F}^a$. The direction of motion with respect to $\mathcal{F}^w$, however, must be corrected for the aircraft roll angle (Appendix C):

$$\begin{aligned}
\alpha &= -(\chi^w - \psi)\cos\gamma\sin\phi &+& \quad (\theta - \gamma^w)\cos\phi; \\
\beta &= \underbrace{(\chi^w - \psi)}_{\beta^w}\cos\gamma\cos\phi &+& \quad \underbrace{(\theta - \gamma^w)}_{\alpha^w}\sin\phi.
\end{aligned} \tag{3.52}$$

Because $\mathcal{F}^w = \mathcal{F}^t$ the flight-path angle errors χ_e and γ_e equal χ^w and γ^w, respectively. In the horizontal turn studied here γ_e equals zero. Note that for curvi-linear motion, yet another variable determines the success in following the trajectory. As indicated above, the radius of the stationary turn depends on the aircraft roll angle: when the roll angle is not equal to the reference roll angle ϕ_t the trajectory curvature is not correct. Hence,

---

[10]When the aircraft pitch angle is small, the bank angle equals the roll angle: $\Phi_t = \phi_t$.

Table 3.2: Expressions for the linearized lateral displacement cues in circular tunnels.

(5)   lateral displacements of frame f_i (3.44)

$$\epsilon_{0_{f_i}} = \epsilon_{01_{f_i}} + \epsilon_{02_{f_i}} \qquad \delta\epsilon_{f_i} = \delta\epsilon_{f_i}^X + \delta\epsilon_{f_i}^{\psi 1} + \delta\epsilon_{f_i}^{\psi 2}$$

$$\epsilon_{01_{f_i}} = -\kappa\tan(\tfrac{\sigma_{f_i}}{2}) \qquad \delta\epsilon_{f_i}^X = \kappa\frac{x_e}{R_t\sin(\sigma_{f_i})}$$

$$\epsilon_{02_{f_i}} = \kappa\tan(\tfrac{W_t}{2R_t\tan(\sigma_{f_i})}) \qquad \delta\epsilon_{f_i}^{\psi 1} = \kappa\psi$$

$$\delta\epsilon_{f_i}^{\psi 2} = \kappa\psi\tan^2(\tfrac{\sigma_{f_i}}{2})$$

$$\eta_{0_{f_i}} = \eta_{01_{f_i}} + \eta_{02_{f_i}} \qquad \delta\eta_{f_i} = \delta\eta_{f_i}^X + \delta\eta_{f_i}^{\psi 1} + \delta\eta_{f_i}^{\psi 2}$$

$$\eta_{01_{f_i}} = \kappa\tan(\tfrac{\sigma_{f_i}}{2}) \qquad \delta\eta_{f_i}^X = -\kappa\frac{x_e}{R_t\sin(\sigma_{f_i})}$$

$$\eta_{02_{f_i}} = \kappa\tan(\tfrac{W_t}{2R_t\tan(\sigma_{f_i})}) \qquad \delta\eta_{f_i}^{\psi 1} = -\kappa\psi$$

$$\delta\eta_{f_i}^{\psi 2} = -\kappa\psi\tan^2(\tfrac{\sigma_{f_i}}{2})$$

small viewing distances $(\sigma_{f_i} < 30°)$ (3.45)

$$\epsilon_{0_{f_i}} = -\kappa\left(\tfrac{\sigma_{f_i}}{2} - \tfrac{W_t}{S_{f_i}}\right) \qquad \delta\epsilon_{f_i} = \kappa\left(\psi + \tfrac{x_e}{S_{f_i}}\right)$$

$$\eta_{0_{f_i}} = \kappa\left(\tfrac{\sigma_{f_i}}{2} + \tfrac{W_t}{S_{f_i}}\right) \qquad \delta\eta_{f_i} = -\kappa\left(\psi + \tfrac{x_e}{S_{f_i}}\right)$$

large viewing distances $(\sigma_{f_i} > 30°)$ (3.46)

$$\epsilon_{0_{f_i}} = -\kappa\tan(\tfrac{\sigma_{f_i}}{2}) \qquad \delta\epsilon_{f_i} = \kappa\left(1 + \tan^2(\tfrac{\sigma_{f_i}}{2})\right)\psi$$

$$\eta_{0_{f_i}} = \kappa\tan(\tfrac{\sigma_{f_i}}{2}) \qquad \delta\eta_{f_i} = -\kappa\left(1 + \tan^2(\tfrac{\sigma_{f_i}}{2})\right)\psi$$

(6)   relative lateral displacements of frames f_i and $f_i + 1$ (3.47)

small viewing distances $(\sigma_{f_i} < 30°)$ (3.48)

$$\epsilon_{0_{f_i f_i+1}} = \kappa\frac{W_t}{2}\left(\frac{S_{f_i+1} - S_{f_i}}{S_{f_i}S_{f_i+1}}\right) \qquad \delta\epsilon_{f_i f_i+1} = \kappa x_e\left(\frac{S_{f_i+1} - S_{f_i}}{S_{f_i}S_{f_i+1}}\right)$$

$$\eta_{0_{f_i f_i+1}} = \kappa\frac{W_t}{2}\left(\frac{S_{f_i+1} - S_{f_i}}{S_{f_i}S_{f_i+1}}\right) \qquad \delta\eta_{f_i f_i+1} = -\kappa x_e\left(\frac{S_{f_i+1} - S_{f_i}}{S_{f_i}S_{f_i+1}}\right)$$

large viewing distances $(\sigma_{f_i} > 30°)$ (3.49)

$$\epsilon_{0_{f_i f_i+1}} = -\kappa\left(c\tfrac{\triangle\Psi}{2}\right) \qquad \delta\epsilon_{f_i f_i+1} = 0$$

$$\eta_{0_{f_i f_i+1}} = \kappa\left(c\tfrac{\triangle\Psi}{2}\right) \qquad \delta\eta_{f_i f_i+1} = 0$$

(7)   tangent point of the inner curve wall (3.50)

$$\eta_0^{TP} = \kappa\sqrt{\frac{W_t}{R_t}} \qquad \delta\eta^{TP} = -\kappa\left(\psi + \sqrt{\frac{W_t}{R_t}}\frac{x_e}{W_t}\right)$$

Note: the lateral displacement cues of the altitude poles are the same as those
listed with η, except for the following initial conditions:
$\pi_{02_{f_i}} = 0$, $\pi_{0_{f_i f_i+1}} = 0$ and $\pi_{0_{f_i}} = \kappa\left(\sigma_{f_i}/2\right)$ for small viewing distances.

$$r_e^w = 0, \chi_e^w < 0 \qquad\qquad r_e^w \neq 0, \chi_e^w = 0 \qquad\qquad r_e^w < 0, \chi_e^w < 0$$
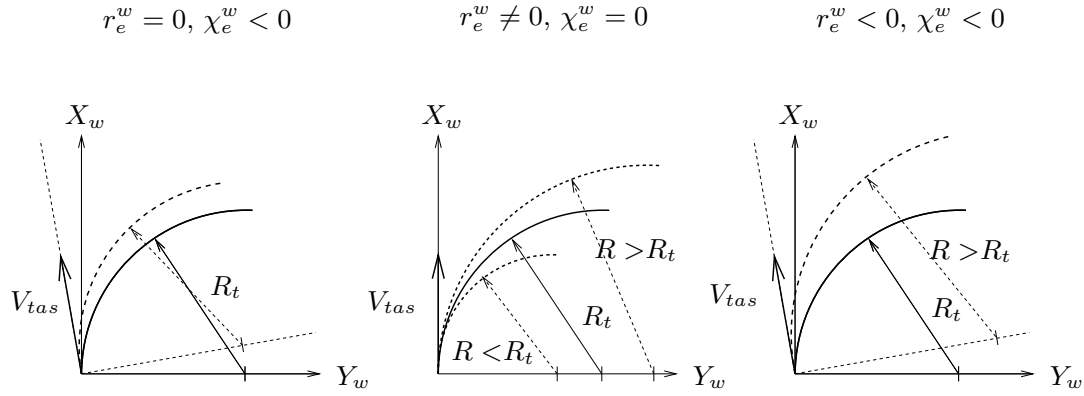
Figure 3.12: The effects of a yaw rate error r_e^w and a flight-path angle error χ_e^w on following a horizontal, circular tunnel trajectory.

even when the velocity vector is (instantaneously) aligned with the tunnel centercircle, an incorrect roll angle results in another path error, labelled the *yaw rate error*:

$$r_e^w \;=\; r^w - r_t^w \;=\; V_{tas}/R - V_{tas}/R_t \;=\; V_{tas}/R_t \left(\frac{\tan \phi_t}{\tan \phi} - 1 \right). \qquad (3.53)$$

For small attitude angles the yaw rate approximates the heading angle rate ($r^w \approx \dot{\psi}$). Combinations of a flight-path angle error and a yaw rate error are illustrated in Fig. 3.12.

Derivatives of the static optical cues: *indirect* dynamic cues

The derivatives of the static cues provide information about the flight-path and the radius of curvi-linear motion. A yaw-rate error can be regarded as the difference between the translational velocity of the complete tunnel geometry on the viewplane with respect to its reference translational velocity. When the radius is too small, the tunnel geometry sweeps across the viewplane at a rate that is higher than desired and vice versa.

The flight-path angle error is conveyed by similar cues as in straight tunnel sections. For small viewing distances S_t the derivatives of the splay angles and the relative lateral displacements of the tunnel frames are only a function of the flight-path angle error. The virtues of these cues are discussed before. An important difference between the condition of straight tunnels, however, is that in curved trajectories no (stationary) vertical pseudo-horizon exists that could facilitate the use of the relative lateral displacement cues.

The optic flow field: *direct* dynamic cues

Computational aspects   Now, both the rotational and the translational components of the velocity of a point on the viewplane are present in the image field equations, Eqs 3.33-3.34. Due to the curvi-linear motion the *radial* optical expansion pattern changes into a *hyperbolic* optic flow pattern that is quite complicated. Heuristically (Prazdny, 1981; Rieger, 1983), it can be stated that each of the three components of the rotation vector

$\underline{\Omega}^b$, p^b, q^b, r^b, adds a component to the optic flow velocity vectors, Eqs 3.33 and 3.34. The rotation along X_b (p^b), parallel to the viewplane, leads to a circular flow pattern (rotary flow): $(\dot{u}_p^R, \dot{v}_p^R) = (-v_p, u_p)p^b$. The rotation along Y_b (q^b), perpendicular to the viewplane, leads to a hyperbolic flow pattern (translation and shear) in the direction of $-V$: $(\dot{u}_p^R, \dot{v}_p^R) = (-u_p v_p, -\kappa^2 - v_p^2)q^b/\kappa$. Similar, the rotation along Z_b (r^b), also perpendicular to the viewplane and the most relevant here, leads to a hyperbolic flow pattern in the direction of $-U$: $(\dot{u}_p^R, \dot{v}_p^R) = (-\kappa^2 - u_p^2, -u_p v_p)r^b/\kappa$. A further study of these rotations reveals that the rotational component of the optic flow velocities on the viewplane is independent of the geometry of the 3-D world. Rather, the component only depends on the position of the projected points on the viewplane itself. The flow field provides no information about (relative) depth of the environment, but only of the rotation with respect to the World (Bruss & Horn, 1983). It can be shown that, essentially because $\mathcal{F}^v \equiv \mathcal{F}^b$, the optic flow pattern on the viewplane is independent of the aircraft roll angle ϕ. Hence, this variable yields a rigid body transformation not only of the position field (the optic array), stated in §3.3.2, but also of the velocity field (the optic flow).

The FRO and the optic flow pattern   The curvi-linear motion condition leads to a hyperbolic flow field that can be seen as the sum of two components, i.e. a *translational* component resulting in the *radial* expansion pattern, and a rotational component, yielding a *solenoidal* flow pattern (Gordon, 1965; Prazdny, 1981; Warren, Mestre, Blackwell, & Morris, 1991). The addition of both the flow patterns implies that *no focus of radial outflow is present in the flow field* (Gordon, 1965, 1966b). Rather, the entire flow field is curved into the direction of the curvi-linear motion, Fig. 3.13. The curvi-linear field resembles the radial field near the observer where the effects of the translation are large. For larger viewing distances the rotational effects overshadow those of translation (Gordon, 1966b). In the hyperbolic flow field two elements require some explanation. Similar to the straight tunnels the future path of the curvi-linear motion is specified by the *locomotor flow line* (Lee & Lishman, 1977), the streamline that passes directly below the observer. Second, as was discovered by (Gordon, 1966b), the hyperbolic flow field of the elements on the inside of the path show an interesting property: they reverse their lateral direction of motion on the viewplane. The line connecting these elements is referred to as the *reversal boundary* (Warren et al., 1991; Raviv & Herman, 1994).

Effects of a flight-path angle error and a yaw rate error   Fig. 3.13 illustrates the effects of a flight-path angle error χ^w and a yaw rate error r_e^w on the optic flow field. To exemplify the pattern of the optic flow field the theoretical flow lines are shown of an array of points located on the horizontal plane of the bottom tunnel wall. The reference condition is shown in the center, illustrating the fact that in this situation the locomotor flow line follows the trajectory while the reversal boundary lies in the inner side of the curve, crossing the tangent or reversal point (Raviv & Herman, 1994). The flow velocities of the tunnel elements are all perfectly aligned with the circular tunnel trajectory. When the yaw rate becomes too large ($r_e^w > 0$, the left column of Fig. 3.13) all flow velocities of the tunnel elements increase in magnitude and the whole geometry sweeps across the
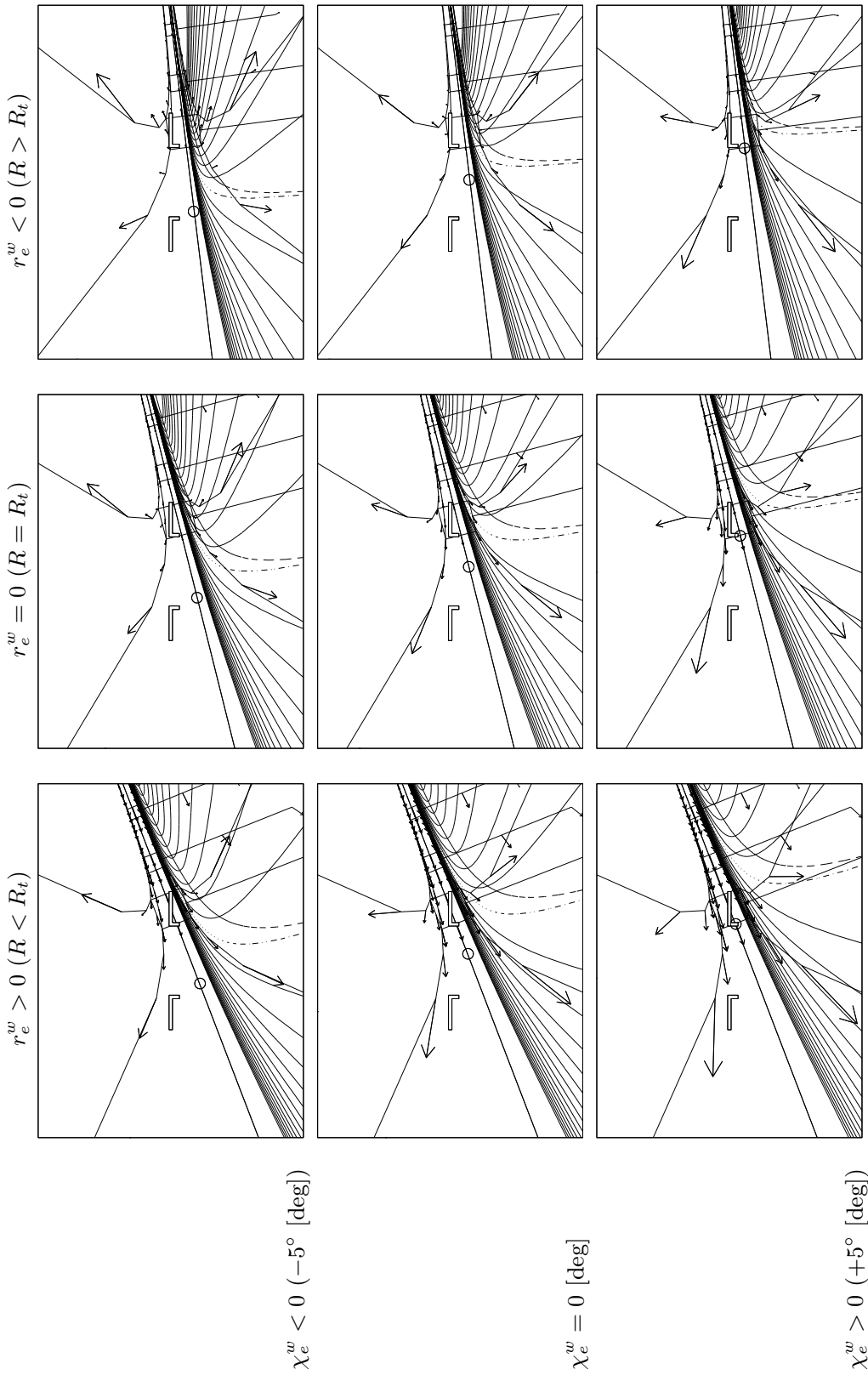
Figure 3.13: The optic flow field for several conditions of a yaw rate error and a flight-path angle error. The circle shows the direction of the velocity vector with respect to the World. The thin lines, the dash-dot line and the dashed line show the theoretical flow pattern, the *locomotor flow line* and the *reversal boundary* (these are explained in the text), respectively. The following state is plotted: R_t=2000 [m]; W_t=H_t=45 [m]; V_{tas}=70 [m/s]; χ_e=−5°, 0°, +5°; γ_e=0°; ψ=0°; θ=0°; ϕ = 21° (left), 14° (middle), 7° (right); x_e=v_e=0 [m].

screen. When the yaw rate is too small, the flow velocities decrease in magnitude, especially for larger viewing distances S_t: the tunnel image does not show the desired translatory motion and the percept will be one of going off the trajectory. The effects of a flight-path angle error are especially salient near the observer, e.g. by the location of the locomotor flow line and the reversal boundary near the bottom border of the screen. Fig. 3.13 shows that the effects of errors in yaw rate and in flight-path angle can either amplify or attenuate each other, exemplifying the difficulty of conceptualizing the flow in curvi-linear motion.

3.7 Perception and control of curvi-linear motion

The study of curvi-linear motion is far more complex than that of the rather elementary recti-linear motion condition. In the previous section the tunnel display was analyzed mathematically in order to investigate how the aircraft motion referents are presented. Based on a literature survey and the findings of the former sections, the sources of optical information are examined below from the perspective of the pilot. Similar to the study of recti-linear motion in §3.5, the investigation is categorized with respect to the motion states that must be perceived to control the aircraft along the circular trajectory.

(i) The aircraft attitude The aircraft roll angle ϕ and pitch angle θ can be perceived from the horizon. In contrast to the situation of straight tunnels where the heading angle ψ with respect to the trajectory is conveyed by the infinity point, the trajectory curvature prevents the use of this feature. Rather, the aircraft heading angle must be perceived through the lateral translation of the tunnel geometry as a whole on the viewplane with respect to a reference condition. This is not a simple task, especially in a situation in which the pilot must continuously compensate for the effects of turbulence. Furthermore, one should realize that, due to the projection method, the part of the trajectory located directly near the aircraft is not shown on the display. In a right curve with zero position and heading errors with respect to the centercircle, the first visible part of the tunnel is translated somewhat to the inner side of the curve (Fig. 3.11). Hence, the heading conveyed by this part of the tunnel is to the right, even when the instantaneous heading is correct (Eq. 3.40), resulting in a *bias* in the perception of heading directed to the outer curve wall (Appendix D). In straight tunnels this problem does not occur because the tunnel heading is constant (it does not depend on the viewing distance).

(ii) The aircraft position Similar to straight tunnels, the position of the aircraft with respect to the trajectory is conveyed by the splay angles – in a coupled fashion – and the relative displacements of the tunnel frames – in an uncoupled fashion. Both the cues are only useful at small viewing distances. Due to the trajectory curvature in the lateral plane, no vertical pseudo-horizon is present in the display, impeding the use of the relative lateral displacement cues for the perception of the lateral position error x_e considerably. The property that the most nearby part of the curved trajectory is not shown by the display also has its consequences for the perception of a position error. As discussed in §3.6, no symmetric condition exists for the splay angles and displacement cues in curved tunnels.

The distortion in symmetry, even for zero position and attitude errors, with respect to the 'natural' condition, i.e. that of straight tunnels, results in a bias in the perception of the position error. For curves to the right the display conveys a small lateral position error to the right, i.e. towards the inner curve wall. These *presentation biases* are discussed in Appendix D and are one of the themes of Experiment X4 (Chapter 8).

(iii) The flight-path   Similar to recti-linear motion there are in principle to ways to perceive the instantaneous direction of curvi-linear locomotion: (i) via the global optic flow field, and (ii) through the gradients of local elements in the visual field. Not many studies in literature have investigated the curvi-linear motion condition. Warren et al. (1991) studied the perception of the future course of movement on circular paths, referred to as *circular* heading as opposed to the *tangential* heading of the motion, from optical flow. Three sources of information about circular heading were identified: (i) the locomotor flow line; (ii) the reversal boundary, and (iii) the vector normals specifying the location of the rotation axis. Experimental findings led Warren et al. (1991) to conclude that local features of the flow pattern – (i) and (ii) – are unnecessary for the judgement of circular heading, and that this variable is specified by the motions of only a few elements. Observers could distinguish circular from tangential heading and could perceive the former with an accuracy sufficient for the control of locomotion (thresholds of 1.2°).

In a series of experiments of (Grunwald & Kohn, 1993) subjects were asked to estimate their flight-path – tangential heading – while being passively flown in curvi-linear motion above a flat textured surface. It was concluded that in curvi-linear motion, the flight-path is considerably more difficult to estimate than for straight motion, and that judgements are more sensitive to the level of global optical flow rate. Obscuring the near part of the visual field – small S_ts – led to considerably larger flight-path estimation errors than when the far part of the visual field was obscured, at least for low levels of the global optical flow rate. When the latter variable increased, the estimation errors when using the far visual field decreased and those of using the near visual field increased. In both cases, estimation times decreased with global optical flow rate. Furthermore, the presence of a constant, randomly chosen, unknown sideslip angle increased the flight-path estimation errors and estimation times when the near part of the visual field was obscured. Grunwald suggests that for the perception of a sideslip angle especially the near field is used – to estimate the location of the locomotor flow line – whereas the far field could be used to obtain an estimate of the reversal boundary. According to Grunwald and Kohn (1993), the key issue in explaining the relative difficulty with respect to recti-linear motion (the estimation errors were approx. 5°) lies in the fact that the curved flight-path estimates must rely on the entire flow pattern, whereas for recti-linear motion the estimate can be based on the distant field only. This statement is supported by the analysis in this chapter.

The experiments cited above both applied information-rich displays, conveying salient optic flow patterns. Similar to the situation of straight tunnels it is questionable whether the tunnel display presents the same level of flow pattern stimuli. The display does not contain units of texture other than the elements of the tunnel geometry itself. Recall that

in Fig. 3.13 the flow properties such as the locomotor flow line and the reversal boundary could be shown only after including a whole array of texture elements that are normally not there. The only 'normal' flow originates from the motion of the segment vertices and the tunnel frames shown by the arrows in Fig. 3.13. It is a safe assumption that the flow properties other than those conveyed by the changing tunnel geometry cannot be perceived and are useless. Therefore, it is hypothesized that especially the *local gradients of motion perspective form the basis of flight-path perception.* In this respect, similar cues play a role as in straight tunnels, i.e. the splay rates and the compression rates. An important difference with the case of straight tunnels, however, is that only for smaller viewing distances these cues are useful. Furthermore, the compression rates cannot be perceived relative to a pseudo-horizon (at least, in the lateral dimension) because of the trajectory curvature. Hence, it is hypothesized that the splay angle rates are the main cue for the perception of flight-path relative to the trajectory in curved tunnels.

(iv) The yaw rate error   Probably the easiest way to determine the yaw rate error is to estimate the difference between the actual and the reference roll angle. For a given curve radius and aircraft velocity, the roll angle ϕ_t to achieve the required yaw rate, is constant. The reference roll angle can be presented with some bug on the bank angle indicator, or by rotating the tunnel frames with the reference roll angle. This feature, invented by Grunwald et al. (1981), and others are studied in Experiment X4, discussed in Chapter 8.

The yaw rate error can also be perceived from the optic flow pattern (Fig. 3.13). When the yaw rate is too large, the whole tunnel geometry sweeps across the screen at a velocity that is too large. When the yaw rate is too small, the curvature of the aircraft flight path is too shallow and the flow field shows only a marginal lateral velocity on the viewplane, especially for points located farther into the curve: here, the translational component of the flow dominates. When the yaw rate and flight-path angle errors are zero, the tunnel geometry maintains a steady-state condition (Gordon, 1966b; Lee & Lishman, 1977).

Velocity and temporal cues   The cues conveying information about forward velocity are probably the same as in straight tunnels. The tunnel frames that approach and pass the observer when moving through the tunnel allow the use of optical edge rate, while the tunnel size manipulates the subjective velocity through the global optical flow rate. When the curvi-linear motion condition is correct and the frames are positioned at equal distances, the optical expansion of the passing frames – allowing the perception of time-to-contact – constitute a temporal unit.

Concerning the temporal situation with respect to the tunnel boundaries one should distinguish between the vertical dimension – that is essentially the same as in straight tunnels – and the lateral dimension – which is quite different. In assessing the spatio-temporal situation of approaching the inner or outer curve walls, whereas in curvi-linear motion, the observer must incorporate some component that is of higher order than those that are used in the recti-linear motion. In other words, besides the flight-path that determines the instantaneous *direction* of the motion, also the yaw rate component should be incor-

porated that determines the rotation of the velocity vector with respect to the World, i.e. the change in the direction of motion in time. This is a relatively unexplored area of research. In (Lee et al., 1992) it was shown that besides the conventional translational time-to-contact cues, also *angular* time-to-contact cues exist that e.g. allow somersaulters to judge the time before contact with the ground. As has been discussed in §3.5, the use a first and second order time-to-wall crossing variable has been analyzed in (Theunissen & Mulder, 1995a) in straight tunnels. Because the second order TWC is based on the assumption that the future aircraft path is circular, it could be a useful variable to describe pilot anticipatory behaviour. The problem, however, is that it can not be linked with any source of optical information: *no optical concomitant* exists for the perception of the second order TWC. Theunissen (1997) argued that this variable can be estimated by the pilot by computing the quotient of a splay angle and its *predicted* value, the prediction based on splay, splay rate and the splay acceleration. Hence, a rather difficult relation is suggested that inevitably demands cognitive processing. But this could well be besides the point. With only little imagination many relations among individual optical cues can be conceived that could, in theory, be used by pilots. The strength of e.g. the time-to-contact cue, however, lies in the fact that it is linked to an optical invariant, namely the *relative dilation* of the visual image on the retina (Lee, 1980b; Lee & Reddish, 1981), that allows a *direct* perception of this variable. To 'prove' that 'in principle' optical information exists for the estimation of higher order temporal cues by simply combining a bunch of individual cues into a single referent does not seem to make much sense. The origin and use of temporal cues in curved tunnel sections remains a subject of future research.

3.8   Retrospective

The findings in this chapter illustrate the fact that with the tunnel display the same *low-level* perceptual mechanisms can be applied as in *ordinary* locomotion tasks. Hence, with the application of the perspective tunnel display the *ecology is brought back* in the cockpit. With this in mind, the main findings are summarized below, and an approach is chosen that will guide the experimental efforts discussed in the remainder of this thesis.

Information transfer and information processing

In controlling an aircraft, pilots need information about the state of their vehicle with respect to some reference. The tunnel display presents this information through the transformation of a regular geometrical object in a synthetic 3-D world. The stimulus array that results from this transformation is compatible to the stimuli that emerge during every-day locomotion through the environment. All human goal-directed behaviour involves perception and action in space and time (Gibson, 1986). Hence, the *ecological* stimulus for vision is that of the optic flow field which is inherently spatio-temporal (Lee, 1980a). The changing pattern of light that enters the eye during locomotion is *structured* and conveys information about the structure of the environment, the nature of the locomotion and the

temporal situation relative to the environment (Lee & Lishman, 1977). The information-richness of the optic flow field allows observers to control their locomotion using vision only, a highly proficient perception and action cycle.

The tunnel display has been analyzed for the two most important stationary flight, recti-linear and curvi-linear motion. In both conditions the effects of acceleration have been neglected, yielding *stationary* flow fields. Although actual flight conditions cannot be perfectly stationary, the assumption of stationary flight conditions served well to exemplify the sources of information from tunnel displays. Based on a literature survey in the domains of psychology, physiology, computational vision and human engineering, the cybernetic issues of information transfer ('how is the information presented?') and information processing ('how is the information used?') are treated. The main hypothesis, adopted from the ecological approach to visual perception of (Gibson, 1986), was that the main pilot stimulus when moving through a bounded environment as depicted by the tunnel display is that of an approach to a surface. In both recti-linear and curvi-linear motion the aircraft position and attitude relative to the trajectory can be perceived through the cues of *linear perspective*, cues that emerge from a *static* tunnel image. The aircraft flight-path, velocity, and temporal situation are conveyed by the changing tunnel geometry through the cues of *motion perspective*, cues that are essentially *dynamic*. It is hypothesized that essentially the *local* cues conveyed by the dynamic transformation of the tunnel image are used to control locomotion. This hypothesis originates from the fact that the display does not present any information other than the tunnel geometry itself, which makes it questionable whether the *global* cues of the optic flow field (such as the FRO) are used. Concluding, probably one of the key issues in assessing the relative ease in using the tunnel display for aircraft guidance is that the information conveyed by the display is highly *redundant*. Almost all aircraft motion states can be perceived through a set of optical cues. The tunnel display conveys all information needed for controlling the aircraft in a truly *ecological* fashion (Mulder et al., 2000).

The remainder of this thesis

The goal of the remainder of this thesis is to obtain an understanding of the relation between the visual information conveyed by the tunnel display for the pilot's *perception* of the aircraft motion through the tunnel, and the pilot's *use* of that information in controlling the locomotion. The redundancy in optical information about the status of the locomotion is one of the main virtues of the perspective tunnel display. Warren (1988) pointed out, however, that although sources of optical information can specify the same referent in a geometrical sense, they may not be equally useful to the pilot. Ecological functionalism (Warren & Owen, 1982) is a paradigm with which these issues can be investigated in a theoretical and practical sense. The theoretical issues have been studied in this chapter. Central in the empirical evaluation that follows is that the pilot perception and action cycles remain intact. Hence, the experiments will be *interactive* in the sense that pilots perform a continuous task of adjusting their locomotion through

the environment using the same perceptual and activation mechanisms as they would apply in real flight. This approach resembles *active psychophysics* (Owen & Warren, 1982; Flach, 1991). Irrespective of the approach taken, the redundancy of optical information in spatial displays such as the tunnel display is a difficult entity to test empirically. The main problem in testing the *relative functionality* of a set of redundant cues is that these cues can not be *isolated*. For instance, in the tunnel display the global flow pattern (specifying the FRO) and the derivatives of local elements (e.g. splays) cannot be separated. Hence, experiments designed to assess the utilization of different optical cues in visual displays are often subject to alternate interpretation, facing the experimenter with problems of determining which of the, redundant, sources of information is actually responsible for the pilot's performance (Warren & Owen, 1982; Owen & Johnson, 1992). In this respect, recall that in the introduction of this chapter the process of information transfer was symbolized as $\underline{y} = \mathcal{T}(\underline{x})$, i.e. a transformation of the aircraft state into a set of optical cues. Whereas the former, i.e. $\underline{x}$, can be considered *extrinsic to the self-motion event* the latter, optical, variables are definitely *intrinsic to the self-motion event* (Owen, 1990). In assessing the inverse of this process, i.e. estimating the aircraft state from the display, it is important to stand still at the specific nature of this state estimation. Are pilots *really* interested in the state variables themselves or is it the information conveyed by the transforming visual array that is important? Engineering approaches generally assume the former, i.e. that humans rely on optical variables to retrieve *estimates* of the state variables, $\underline{\hat{x}} = \mathcal{T}^{-1}(\underline{y})$, that are, in turn, used for control (Johnson & Phatak, 1990a). The study in this chapter revealed that both the extrinsic and the intrinsic variables are coupled in the transforming visual array and that *an inverse transformation is not needed*: pilots can use the information conveyed by the optical cues *directly* for control. Hence, in evaluating the sources of information it is important to keep in mind that although the environmental variables – that usually form the independent measures in experimental testing – are manipulated, it are really the optical variables – the effects of the environmental variables on the visual array – that are important (Owen, 1990). The direct manipulation of optical variables could allow for inferences to be made *directly* from those that are manipulated instead of implying them from indirect relations among environmental variables (Larish & Flach, 1990; Owen & Johnson, 1992).

Chapter 4

Philosophy of the experimental method

4.1 Introduction

In the previous two chapters the pilot manual control task with a perspective tunnel-in-the-sky display has been analyzed from both a control-oriented and an information-oriented perspective. These *theoretical* investigations constitute the first two steps of the cybernetic approach (§1.4), and attempt to understand the manner in which the tunnel display design affects pilot behaviour. The third and fourth steps of the approach concern *experimental* studies addressing the hypothesized relations, and attempts to model the pilot control behaviour, respectively. The experiments must be defined such to allow an evaluation of the data in both a psychological as a control-theoretical sense. This is not a trivial procedure. During the course of the research and based on the experiences reported in similar areas of research, a structured methodology of experimenting has been developed that provides as much support as possible to the cybernetic evaluation. This method has been applied for all experiments and forms the subject of the current chapter.

Purpose of the experiments

The experiments discussed in this thesis, listed in Table 2.1, are aimed at improving the understanding of the interaction between the pilot and the tunnel display. The optical cues resulting from the projection of the tunnel geometry convey information about the aircraft's attitude, flight-path, and position with respect to the tunnel. These are the motion states the pilot needs to control the aircraft along the designated path and it is his primary task to perceive them from the optical cues. To examine the characteristics of this observation process the experiments will systematically vary the amount and nature of the optical information. The main objective of the experiments is *to obtain specific knowledge on* how *and* why *the various tunnel display design variables affect pilot perfor-*

mance, control behaviour, and workload. The ultimate goal in obtaining this knowledge is to specify the tunnel display design guidelines from a human-centered perspective.

Alternative experimental approaches

Passive modes of interaction   Various ways exist to examine a human-machine interface. A legitimate and popular approach is to conduct psychophysical experiments in an attempt to correlate the psychological responses to the physical dimensions of a stimulus. In passive *Stimulus-Response* (SR) tasks the *perceivability* of a specific source of information is measured in terms of observation accuracies, thresholds and time delays. These experiments have over the years resulted in a vast amount of human response data (Boff, Kaufman, & Thomas, 1986). Despite the fact that this data can provide useful insights into the perceivability of a certain aircraft motion state from the tunnel display, it is difficult to apply the data in a *real* control situation (Bennett et al., 1986; Wewerinke, 1989). Although it is true that in most cases the *perceivability* of a variable affects its *usability*, the SR-data are often of less avail in situations where the pilot must *use* that variable in an *active* fashion. Examples exist of pilot strategies that are completely different when studying the behaviour in an active rather than a passive fashion (Johnson & Kaiser, 1991). The domination of the passive interaction modes in psychological research has often led to inappropriate generalizations (Flach, 1991).

Active psychophysics   A useful starting point in the analysis here would be the principal assumption of ecological psychology: perception is essentially a matter of *interaction* between the observer and the environment (Gibson, 1986). The pilot's task of controlling an aircraft with a tunnel display fits well in this theory. It is a condition of continuous observation of the environment by means of an ecological display, and a continuous manipulation of the (ego-) motion through that environment. The pilot is closing the loop through the optical array. So, instead of taking the pilot out of the control loop and examining only his (passive) observation characteristics, an ecological approach requires that the interaction properties are studied in an *active* fashion. This approach is referred to as *active psychophysics* (Johnson & Phatak, 1990a, 1990b), "...*a study of human performance that does justice to the intimate coupling between perception and action.*" (Flach, 1991).

The notion of dynamics   Many experimental studies focus the research interests on the characteristics of the visual scene and neglect the notion of *dynamics* completely. The dynamics of the vehicle to be controlled, however, can significantly alter the set of visual cues that a human might use in conducting the task. A study of human control behaviour cannot neglect the fundamental *feedback* structure. In the current analysis considerable attention will be given to the effect of the aircraft dynamics. This could facilitate the extrapolation of the experimental findings to the practical in-flight control situation.

Taking a model-based approach   The methodology of the experiments described in this thesis is related to active psychophysics, in which theories of ecological psychology are coupled with concepts of control theory. In conjunction with the discussion in §2.5.2 and

§2.5.3, an attempt is made to describe the pilot manual control situation in mathematical terms. An essential step in the investigation is the *validation* of the pilot models. In §4.2 the model identification and validation procedure is described that is applied in this thesis. Some of the consequences of taking a model-based approach are discussed in §4.3. In §4.4 the experimental method and the main data-processing flows are discussed that result from the model-based approach. The Human-Machine Laboratory is described in §4.5. The findings of this chapter are summarized in the retrospective, §4.6.

4.2 Pilot model identification techniques

4.2.1 The two-stage identification method

In the single-axis, multi-loop pilot regulation task, illustrated in Fig. 2.9(c), all elements except the pilot 'block' are known and can be described in mathematical terms. In order to conduct a control-theoretical analysis of the closed loop pilot/aircraft system, an objective estimate of the pilot control characteristics must be obtained.

Problem statement Although methods for identifying the human element in closed loop tracking tasks have been known since the early applications of (Krendel & McRuer, 1960), it took until the late 1970s until these methods were formalized mathematically in (van Lunteren, 1979). The main problems encountered in the identification of the human control behaviour in the single-axis, multi-loop tracking tasks considered here, are:

- The pilot is operating <u>in closed loop fashion</u>, resulting in undesirable correlations between the various signals due to the feedback loops.

- The pilot uses <u>more than one input signal</u>, which requires the identification of a *multi-loop* feedback system.

- The <u>observation time is limited</u> due to, for example, pilot fatigue or boredom.

Another difficulty, i.e. that the human operator is essentially a non-linear system, is solved by applying the describing function theory introduced in §2.5.2. The non-linear pilot dynamics are replaced by a multi-dimensional linear describing function model including a stochastic remnant signal, see Fig. 2.9(c). A generic method that can handle these difficulties in a satisfactory manner is developed by van Lunteren (1979). This method is discussed below in general terms. For a formal description the reader is referred to Appendix F.

A two-stage identification method What has become common practice in human-machine systems research is the identification of the human control behaviour in two stages. The first stage in this procedure is the application of a *non-parametric identification* method, discussed in §4.2.2, which yields an estimation of the multi-loop pilot describing function, the so-called *frequency responses*. The second stage in the identification procedure is the application of a *parameter estimation* method, discussed in §4.2.3.

4.2.2   Non-parametric identification

The instrumental variable method

Consider the general single-axis, multi-loop regulating task of Fig. 2.9(c). When the aircraft disturbances are set zero, all stochastic effects in the closed loop are caused by the pilot's remnant signal n. An *open loop* identification method would use the signals u and $\underline{y}$ (m inputs) to estimate the multi-loop pilot describing function $\underline{H}_p(1 \times m)$, yielding an estimate $\underline{\hat{H}}_p$. It can be shown that this estimate is considerably biased because, due to the feedback, the pilot output signal and the input signals are all correlated with the pilot's remnant signal (van Lunteren, 1979). This problem can be solved by inserting measurable input signals in the loop that are uncorrelated with the pilot noise (and with each other). Such a method is known as the *Instrumental Variable* (IV) method (Söderström & Stoica, 1989). The main advantage of this method is that it can be applied with a minimum amount of a priori knowledge about the system to be identified. It dictates that *for each frequency response to be estimated an uncorrelated input signal, a forcing function, must be inserted in the closed loop* (van Lunteren, 1979). This means that m forcing functions must be applied here. The insertion of a forcing function signal leads to some disturbance in the closed loop that could otherwise be non-existing. Reasonable questions would then be where these signals must be inserted, and, what do they look like?

Inserting the forcing function signals   Fig. 2.9(c) shows that the forcing functions can be inserted in the *display* model, or in the *aircraft* model, or in both models. Introducing these signals in the display model, however, means that the relation between the aircraft state and the optical information is disturbed. This is highly undesirable because it disturbs the *interfacing properties* of the display that are essentially the subject of investigation here. Another, more feasible option would be to insert the forcing functions in the aircraft model. A satisfactory solution would be to 'use' the aircraft atmospheric disturbances for this purpose, as this would lead to a realistic pilot task, namely that of controlling an aircraft along the tunnel trajectory in the presence of turbulence.

Type of the forcing function signals   The forcing functions must appear *random*. If they were predictable, the human controller would inevitably make use of this property, leading to a totally different situation from the regulating task defined here (Krendel & McRuer, 1960; McRuer & Jex, 1967). An obvious choice would be to insert m mutually uncorrelated random noise signals in the loop with well-chosen properties. Common practice in human-machine studies, however, is the use of signals that each consist of a *sum of sinusoids*. There are several reasons for this practice. Most importantly, sinusoidal signals are *deterministic* and *periodic*, which means that they excite the (non-linear) system in a deterministic and reproducible way. This also means that, given the periodic character of the input signal, *time-averaging* can be used to attenuate the effects of the noise, without affecting the deterministic input-output behaviour of the system to be identified.

The signal-to-noise ratio   Support for the use of sinusoidal input signals can also be given heuristically. Consider Fig. 2.9(c), initially assuming the SISO case. The aircraft dis-

turbances are replaced by a single forcing function consisting of a sum of sinusoids acting at a particular set of frequencies. Now, when it is assumed that all systems in the loop are linear and that the pilot's noise signal is zero, the superposition principle of linear system theory dictates that all signals in the control loop are deterministic and consist of a sum of sinusoids with power at the same set of frequencies as the forcing function. An unbiased estimate of the pilot's describing function can now be obtained by simply computing the quotients of the Fourier coefficients of the operator's output and input signals at those frequencies. The only problem with this *open loop* method is that in reality the pilot's noise signal is *not* zero. A common assumption is that this stochastic remnant signal has a continuous spectrum: it contains energy at all frequencies. Then, all signals in the loop, except of course the forcing function, become *stochastic* and contain energy at *all* frequencies, i.e. also at those frequencies not belonging to the set of frequencies of the forcing function. In case of a well-designed forcing function the contribution of this deterministic forcing function to the energy of an arbitrary signal at those frequencies of the forcing function's frequency-set is generally larger than the contribution of the stochastic noise signal to the energy of that signal. The ratio of these two contributions at a particular frequency is known as the *Signal-to-Noise Ratio* (SNR). The SNR is usually small at those frequencies that do not belong to the set of frequencies of the forcing function. At those frequencies that *do* belong to this set, the SNRs can be expected to be large enough to obtain a useful estimate of the operator's describing function at those frequencies. Hence, only estimates of the describing function are obtained at the set of frequencies of the sinusoids of the forcing function. The uncertainty in an estimate at a particular frequency is reciprocal to the SNR computed at that frequency: a large SNR leads to an good estimate and vice versa. The concept of the SNR and its use for computing the uncertainty of estimates of the pilot describing function is formalized in Appendix F.

The use of sinusoidal forcing functions is advantageous in cases where one wants frequency response estimates at discrete frequencies in the presence of random noise process noise (present case) or measurement error signals. If a random signal would be used, the energy of the forcing function is 'spread' over the frequency range of interest, and the uncertainties of the frequency response estimates at selected discrete frequencies are larger. A disadvantage of the use of sinusoids is that the frequency responses can only be estimated at a limited set of frequencies. However, one can shift frequencies in different experiments to explore the shape of the frequency response in order to be sure that no peaks are overseen, or one can add more frequencies. What to do is a matter of experience.

How many forcing functions can be applied?   In order to identify the pilot model one uncorrelated forcing function must be inserted in the closed loop for each model input. The number of forcing functions that can be inserted is limited, however, because:

- Each forcing function signal must be compensated for by the pilot: it increases the task demand load.
- To increase the number of forcing function signals in the loop without increasing the pilot workload, one could decrease the amplitudes of all occurring forcing functions

in the loop. This also leads, however, to decreasing SNRs and will therefore lead to larger uncertainties in the obtained estimates.

- The insertion of forcing function signals could perturb the 'normal' relationships between the variables in the loop. This affects the realism of the simulated task that might lead to a deterioration of a subject's motivation and performance.

- The limited observation time restricts the number of frequencies in each disturbance signal to be used, in particular in the low-frequency region, see Appendix F.

In conclusion, the number of forcing functions that can be applied simultaneously in the regulating task is limited: *only a limited amount of signal power can be inserted in the closed loop.* The necessity that the SNRs remain sufficiently large prevent the division of this energy over too many frequencies, or, equivalently, over too many forcing functions.

Constraints on model validation; restatement of the general situation

The fact that the number of forcing functions that can be applied is limited, restricts the possibilities of pilot model identification. Although often several model properties can be determined using only a single estimated describing function, the fact remains that the number of describing functions that can be determined is rather small. In the experiments described in this thesis, it was found that the maximum number of forcing functions that can be used is three, but in most cases this number is reduced to two. The identification constraints force a restatement of the ambitious model validation proposal of §2.5.2. Reconsider Fig. 2.9(c). The aircraft state vector ($\underline{x} \in \mathcal{R}^n$) for a linearized stationary flight condition generally consists of 3 to 6 elements (Etkin, 1972). From the tunnel display the pilot can perceive a number of states directly, e.g. the aircraft's attitude from the horizon. Other states, such as the aircraft position relative to the tunnel, can be estimated using a *set* of cues. Hence, the number of elements of the observation vector, $\underline{y} \in \mathcal{R}^m$, the pilot input, is larger than that of the state vector: $m \gg n$. It would be a challenge to identify all feedback loop closures of the observation vector, a procedure that would allow an analysis of which elements of the observation vector are important and which ones are not. From the discussion above, however, it is clear that this is very difficult. Given the fact that only two or three loop closures can be identified, all that can be achieved would be the identification of the *primary* pilot feedback loops of aircraft attitude, flight-path and position. This will be the approach followed here, its consequences discussed in §4.3.

Restatement of the general situation A general definition of the closed loop control situation is shown in Figs 4.1 and 4.2 for the case of three and two parallel feedback loops, respectively. The situation is generalized to allow the identification method to be applied for both the asymmetric and the symmetric aircraft motion. The **pilot model** can have a *parallel* multi-loop model structure, Fig. 4.1(a), in which all feedback loops are closed simultaneously, or a *serial* model structure, Fig. 4.1(b), in which all feedback loops are closed sequentially. For a discussion of these two model structures the reader is referred to Appendices E and F. The **aircraft model** represents the generalized linear cascaded

(a) parallel model structure

(b) serial model structure
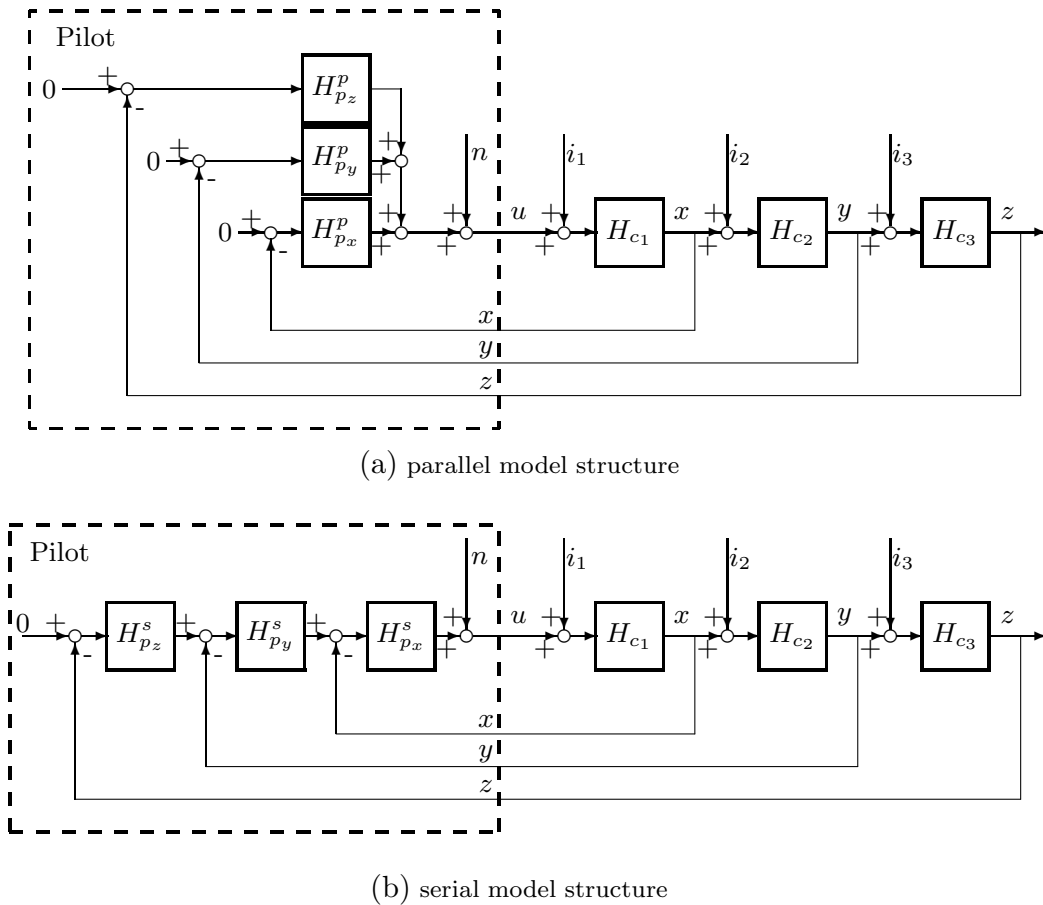
Figure 4.1: Generalized pilot describing function model for three input signals in a disturbance task. In this figure, H_{c_1}, H_{c_2} and H_{c_3} represent the inner, middle and combined outer loop aircraft dynamics, respectively (Fig. 2.10). In (a) $H_{p_x}^p$, $H_{p_y}^p$ and $H_{p_z}^p$ are the inner, middle and outer loop describing functions of a *parallel* pilot model, whereas in (b) the pilot is modelled through their *serial* counterparts $H_{p_x}^s$, $H_{p_y}^s$ and $H_{p_z}^s$. The forcing function signals i_1, i_2 and i_3 are inserted before the feedback of the inner, middle and outer loop signals x (attitude), y (flight-path) and z (position).

model structure illustrated in Fig. 2.10. The **display model** seems to have disappeared completely, which is only partly true. Recall that the situation illustrated in Fig. 4.1(a) is an abstraction of reality. The display model, i.e. the set of linearized equations transforming the elements of the aircraft state into a set of optical cues, is included in the pilot observation model which in turn is *hidden* in the set of describing functions. It depends on the modelling approach whether the observation process is explicitly modelled, as in the OCM, or not, the MLMs. The **aircraft disturbances** are inserted for each state variable *before* the hypothesized pilot feedback of that variable. The manner in which the forcing functions disturb the aircraft motion is an abstraction of reality. Especially the insertion

of disturbance signal i_3 requires some further attention, for the following reason.

The disturbance on the aircraft flight-path angles   The addition of a disturbance signal to the aircraft flight-path angle, i.e. i_3 on y in Fig. 4.1, disturbs the relation between the aircraft's direction of motion and its attitude with respect to the trajectory: the direction of the aircraft's motion is not fixed any more with respect to the aircraft's Body axes. Chapter 3 revealed that this could have important consequences for the pilot's use of the tunnel display. Without the disturbance on flight-path, the aircraft direction of motion is conveyed *explicitly* by the display through the infinity point. With the disturbance on flight-path, the aircraft direction of motion is displayed *implicitly* by the display via the cues of motion perspective. This exemplifies how the insertion of forcing functions affects the pilot's task and could conflict with other experimental factors.

Identifying three loops with two input signals   In the experiments described in this thesis the tasks are restricted to the condition in which the aircraft motion is *fixed* with respect to its Body axes. The only exception is Experiment X5, investigating the effects of a flight-path vector (Chapter 9). This restriction conflicts with the necessity of inserting the disturbance signal i_3 to identify the pilot feedback of the aircraft position error. A possible solution for this problem is granted by the structure of the simplified aircraft model. Consider the aircraft asymmetric motion. In the absence of i_3, i.e. no side-slip, the relation between the aircraft's position and heading error with respect to the trajectory is that of an integrator with a gain: $\dot{x}_e = V_{tas}\psi_e$. Both the feedback loops can then be identified as one *combined* feedback loop, assuming that the pilot response to this *combined* signal consists of a proportional and a differential component. The estimation of the combined middle and outer loop feedback results in the control situations illustrated in Fig. 4.2. The combined feedback describing function can be estimated through either the use of the middle loop signal (y, the aircraft's flight-path angle), Fig. 4.2(a), or the outer loop signal (z, the aircraft position), Fig. 4.2(b). This method, discussed further in §F.4.4, is applied in all experiments of this thesis, except in Experiment X5. The generalized models of Figs 4.1(a) and 4.2 are the starting points of the formal description of the non-parametric identification method in Appendix F. Below, the results of the method will be discussed for the situation with two forcing functions as depicted in Fig. 4.2(b). The situation for three forcing functions is similar.

Definition of the measurement method

Consider Fig. 4.1(a). During a single measurement run, that lasts T_m [s], all measurable signals of interest, u, x, y and z. are sampled with a sample frequency f_s [Hz]. This results in data arrays of all variables with N elements, where $N = T_m/f_s$, e.g. $u(k;\zeta), k = 1, \ldots, N$ (a ζ indicates that a variable is a *realization* of a stochastic process). Conducting a discrete-Fourier transform (DFT) for these signals results in complex arrays representing the Fourier coefficients of these signals at discrete frequencies, i.e. $U(\nu_k;\zeta), k = 1, \ldots, N/2$. The minimum frequency is referred to as the *ground frequency* ν_0 and is determined by the length of the measurement interval: $\nu_0 = 1/T_m$ [Hz]. Due to the use of a DFT all

(a) estimation of the combined outer loop using the middle loop signal

(b) estimation of the combined outer loop using the outer loop signal
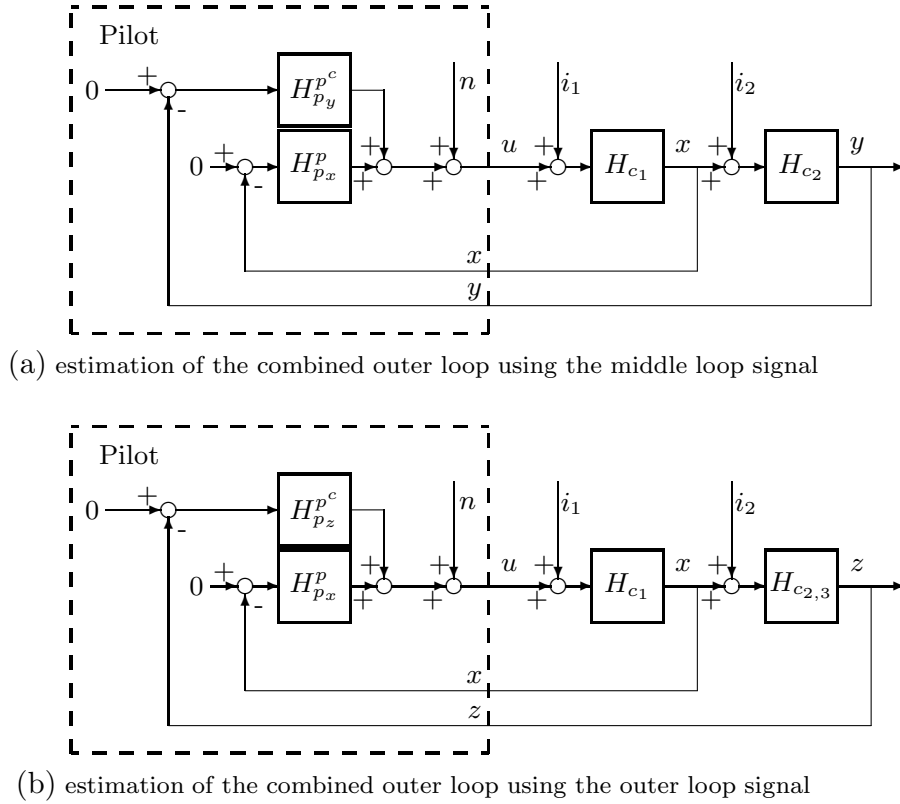
Figure 4.2: Generalized parallel describing function model for two input signals in a disturbance task. In these figures, H_{c_1}, H_{c_2} and $H_{c_{2,3}}$ represent the inner, middle and combined outer loop dynamics of the aircraft. $H_{p_x}^p$ is the inner loop describing function. $H_{p_y}^{p^c}$ and $H_{p_z}^{p^c}$ are the describing functions representing the *combined* outer loops using the middle and outer loop signals, respectively. The forcing functions i_1 and i_2 are inserted before the feedback of the inner and middle loop variables x and y.

other frequencies are an integer multiple of the ground frequency, i.e. $\nu_k = k\nu_0$.

Definition of the forcing functions The forcing functions i_1 and i_2 are each defined as a sum of sinusoids that have power at a limited set of frequencies, e.g. i_1 is defined as:

$$i_1(t) = \sum_{j=1}^{j=N_f} A_{1_j} \sin\left(k_{1_j}\nu_0 t + \phi_{1_j}\right), \tag{4.1}$$

with A_{1_j} and ϕ_{1_j} the amplitude and phase component of i_1 at the jth frequency component, N_f representing the number of frequencies in the signal. Each sinusoid period in the forcing function fits an integer number of times in the measurement interval T_m. Hence, when discrete-Fourier transformed, the forcing functions i_1 and i_2 contain power only at the pre-defined sets of frequencies:

$$\underline{\nu}_{i_1} = \underline{k}_1\nu_0 = \left\{\nu_{1_1}, \nu_{1_2}, \ldots, \nu_{1_{N_f}}\right\}; \text{ and } \underline{\nu}_{i_2} = \underline{k}_2\nu_0 = \left\{\nu_{2_1}, \nu_{2_2}, \ldots, \nu_{2_{N_f}}\right\},$$

with ν_0 the ground frequency, and

$$\underline{k}_1 \;=\; \left\{ k_{1_1}, k_{1_2}, \ldots, k_{1_{N_f}} \right\}, \quad \text{and} \quad \underline{k}_2 \;=\; \left\{ k_{2_1}, k_{2_2}, \ldots, k_{2_{N_f}} \right\},$$

the indices of the discrete Fourier coefficients.

Estimation of the describing functions

The generalized parallel pilot model for two inputs in a disturbance task is shown in Fig. 4.2(b). The linear part of the pilot's control behaviour is characterized by the describing functions $H_{p_x}^p$ and $H_{p_z}^{p^c}$ that give the contribution to the control signal u resulting from the feedback of the inner and outer loop system outputs x and z, respectively. The non-linear part of the control behaviour is represented by the stochastic remnant signal n. In Appendix F it is described how the pilot frequency responses can be estimated from the discrete-Fourier transformed data, at the two sets of frequencies of the forcing functions i_1 and i_2: $\hat{H}_{p_x}^p(\nu_k; \zeta)$ and $\hat{H}_{p_z}^{p^c}(\nu_k; \zeta)$ for $\nu_k \in \left[\underline{\nu}_{i_1} \cup \underline{\nu}_{i_2} \right]$. The principal assumption that is made in the estimation procedure is that at these frequency sets the contribution of the pilot remnant noise to a signal is small relative to the contribution of the forcing function. The uncertainty in the estimated describing functions depends on the validity of this assumption. In Appendix F *analytic* expressions are derived for the *bias* and *variance* of the estimated frequency responses, which depend on the dynamics of the various elements in the closed loop (the aircraft *and* the pilot). Most importantly, they are a function of the *signal-to-noise ratios* introduced above. It can be stated that, generally, as these signal-to-noise ratios are larger, the estimation bias and variance will be smaller.

Crossover frequencies and phase margins   After transforming the estimated frequency responses of the parallel pilot model to their serial counterparts, the serial pilot describing functions can be *combined* with the cascade aircraft dynamics of Fig. 2.10. This allows a computation of the *bandwidth* and *stability* of all feedback loops, variables that are referred to as the *crossover frequency* and *phase margin*, respectively. Whereas the phase margin reflects the notion of *stability*, the crossover frequency reflects the *performance* of the closed loop system. In general, these variables are *antagonistic*. From a performance perspective, the crossover frequencies should be as high as possible. Due to the human's limitations, in particular the processing time delay, the crossover frequency cannot become too large, for this would lead to an unacceptably low level of system stability.

The multi-loop aircraft control situations described here have a clear loop-for-loop feedback structure, starting from the inner loop outwards to the outer loops. Generally, the crossover frequencies of the outer loops can be expected to be lower than the bandwidth of the inner loops. This reflects the fact that in closing more loops the operator's limitations and especially his time delay, lump together (McRuer & Jex, 1967). This decreases the phase margin (i.e. system stability) that can only be recovered by lowering the crossover frequency. Heuristically, one could also state that it makes no sense to have an outer loop crossover frequency that exceeds the inner loop closed loop bandwidth, for in that case the equivalent inner loop system would be too slow for the outer loop controller.

As has been discussed in §2.5.2, three elementary loops are closed in the control of the aircraft motion. These three loops result in three pairs of crossover frequencies and phase margins: $(\omega_c^{in}, \varphi_m^{in})$, $(\omega_c^{mid}, \varphi_m^{mid})$ and $(\omega_c^{out}, \varphi_m^{out})$. In the identification method described here, however, the middle and outer loops are identified as a *combined* outer loop. The latter two pairs cannot be determined from the estimated frequency responses alone, and a parameterization is necessary to distinguish between these two loops (§4.2.3). The crossover frequency and phase margin of the combined outer loop frequency response $(\omega_c^{out^c}, \varphi_m^{out^c})$, which *can* be computed from the data, have a limited physical meaning. This is a disadvantage of the method using only two forcing functions.

4.2.3   Model parameter estimation

The identifiability of the parameters   The non-parametric identification procedure has led to the estimation of the linear part of the pilot's control behaviour at a limited set of frequencies. The frequency responses serve as objective building blocks for the validation of the two modelling approaches proposed in §2.5.3: the MLM and OCM models. The non-parametric method does not make any assumption about the model structure $\mathcal{M}(\underline{\theta})$, nor the parameter vector $\underline{\theta}$. When identifying the parameters in a model structure $\mathcal{M}(\underline{\theta})$, an important issue is the *identifiability* of the parameters: does the identification of the parameter vector $\underline{\theta}$ from experimental data lead to a unique result? The identifiability of the parameters is a property of a model structure, and some methods exist to test this property of certain classes of model structures (Söderström & Stoica, 1989). During the parameter estimation procedure a model may appear to be either too simple (*under*parameterized) or too complex (*over*parameterized). The OCM suffers from the problem of overparameterization (Phatak, Weinert, Segall, & Day, 1976; Kok & Stassen, 1980). According to van Wijk and Kok (1977) either the OCM weighting matrices, the *regulator* variables, or the OCM observation and motor noise ratios, the *observer* variables, can be identified. So, problems can be expected in applying the OCM.

Parameter estimation and the minimization of criteria   The parameter estimation techniques are essentially *optimization* problems: a criterion J is minimized that quantifies the mismatch between the results of the parameterized model and the experimental data:

$$\hat{\underline{\theta}} = \arg \min_{\underline{\theta}} J(\underline{\theta}). \tag{4.2}$$

The definition of a loss function J is not trivial and depends on experience in parameter estimation and a priori knowledge on the model's characteristics. In Appendix F three criterion functions are described that are used in this thesis. These are referred to as J_F and J_T, that operate on the frequency and time domain data, respectively, and J_{FT}, a criterion that combines both the domains. In these criterion functions the mismatch in modelling the experimental data is squared and weighted with the uncertainty in obtaining the experimental data. The application of such quadratic criterion functions leads to a

weighted least-squares estimate of the parameter vector $\underline{\theta}$.

The uncertainty in the estimated parameters   Minimizing a criterion $J(\underline{\theta})$ leads to an estimate $\hat{\underline{\theta}}$ of the true parameter vector $\underline{\theta}_0$, Eq. 4.2. Additional information can be gained about the validity of the estimated parameters. For instance, there exists a *theoretical lower bound* for the covariance of an estimated parameter:

$$\mathrm{E}\left\{(\hat{\underline{\theta}} - \underline{\theta}_0)(\hat{\underline{\theta}} - \underline{\theta}_0)^T\right\} \geq M_{\underline{\theta\theta}}^{-1}, \tag{4.3}$$

which is known as the *Cramer-Rao lower bound* (Söderström & Stoica, 1989). In this expression $M_{\underline{\theta\theta}}$ represents the *Fisher information matrix*, which is defined as:

$$M_{\underline{\theta\theta}} = \mathrm{E}\left\{\frac{\partial^2 J(\underline{\theta})}{\partial\underline{\theta}\partial\underline{\theta}}\right\}\bigg|_{\hat{\underline{\theta}} \,=\, \underline{\theta}_0}. \tag{4.4}$$

In Appendix F a method is derived that allows a computation of the Fisher information matrix and the Cramer-Rao lower bound for a frequency domain criterion J_F. In all parameter estimation applications described in this thesis the uncertainty in the estimated parameters is computed with the Cramer-Rao lower bound.

4.3   Consequences of including a model-based analysis

4.3.1   Model identification constraints

The nature of the perspective tunnel display, with its multiply confounded set of optical variables hampers an isolation of cues which could facilitate the analysis. It are essentially the elements of the aircraft motion state that are needed for control. It can be hypothesized that, generally, when the presentation of one of these elements is improved (and everything else remains constant), it facilitates the pilot perception. This, however, cannot be directly measured but must be inferred from the pilot's overt behaviour. The effect of changing a presentation must be examined by investigating the hypothesis that it affects pilot control behaviour, pilot performance and pilot workload. From the discussion in the previous section, it is clear that it is not possible to identify the pilot's feedback of the complete set of optical cues. Rather, only the pilot feedbacks of the main aircraft motion states can be determined, yielding a *minimal representation* of pilot control behaviour. In the parameterization stage this does not mean, however, that the number of model parameters needs to be decreased. One could for instance estimate the outer loop feedback (position error) frequency response and parameterize this response by summing up all individual contributions of a set of optical cues for this position error. This would be similar to the approach in studies determining models for the pilot's use of motion stimuli (van der Vaart, 1992; Hosman, 1996). In those studies, however, a *physical interpretation* could be given to all contributions based on a priori knowledge of the human vestibular system. This knowledge is not available here, however, and it is questionable whether such data is extractable at all. Furthermore, this approach would lead to a considerable increase

in the number of parameters that needs to be estimated, which stands diametral to the common policy of parameter economy in model identification. It can also be expected that in this case the uncertainty in the parameter estimates increases significantly. Note that the limitation of extracting the effects from individual contributions of the total set of optical cues to a variable under control, is universal. It is not just a disadvantage of the *cybernetic* perspective adopted here but an impossibility of *any* method, at least, when examining pilot behaviour in an *active* rather than a *passive* manner.

4.3.2   The pilot adaptation process

The non-parametric identification method allows the determination of the main aircraft state feedback loop closures. Such a *minimal representation* of pilot control behaviour can be parameterized with the data following this identification procedure, resulting in a particular set of parameters for the experimental condition that is studied. By repeating this modelling procedure for all experimental conditions, a parameterized model is obtained for each of these conditions. The set of parameter vectors that is determined provides knowledge into how one should change the parameters of the model in order to describe the changing pilot's control behaviour for the experimental conditions. When assuming that the model truly reflects the control behaviour, this approach allows an understanding of the manner in which pilots *adapt* their control behaviour to the experimental conditions. In other words, insight is gained into the pilot's *adaptation process.*

In a way, studying the adaptation process is both a direct as an indirect method. It *directly* examines the adaptation process of the *regulator*-side of the pilot addressing the question of *how* the pilot adapts as a function of some experimental variable. It examines the *observer*-side of the pilot in an *indirect* fashion, quite simply because the observer process cannot be measured. In other words, the method does not address the question of *why* the human controller adapts, simply because the answer to this question is hidden in the observer model. The cause(s) for the adaptation must be inferred from studying the characteristics of the set of optical cues that are present on the display, an analysis of which the foundation has been laid in the previous chapter. The determination of the adaptation of the (modelled) pilot's control behaviour allows a study of pilot behaviour that extends common methods which mainly address the *performance*-related time domain variables. These methods, however, do not say much about the constraints originating from the fact that a *dynamic* system is controlled. A model-based analysis provides knowledge about the *stability* of the system and allows a control-theoretic analysis to be conducted of the close loop pilot/aircraft system (van Paassen & Mulder, 1998a). The antagonism of performance and limitations can then be studied in a quantitative fashion.

4.3.3   Design of the experiment

The model identification that is essential for such an approach has a great impact on the design and definition of an experiment. In particular the non-parametric identification

procedure puts some strict demands on the experimental definition. Some of these issues, such as the choice of the aircraft dynamic model and design guidelines for the input signals, are discussed in Appendices C, E and F.

Averaging of time histories The modelling and identification efforts require that many replications are needed for each experimental condition. First, these replications are needed to obtain consistent estimates of the empirical data of the experiment such as the variances. Second, repeating the same condition allows a *time-averaging* procedure of the measured time histories. Averaging the time histories attenuates the remnant effects, which in turn yields a significant increase in the signal-to-noise ratios. Repeating the experimental conditions is therefore beneficial from an identification perspective. Because the available time for experimenting is limited (availability of pilots and apparatus), however, the need for repeating the same experimental condition restricts the total number of experimental conditions.

Isolation of cues Studying the pilot adaptation process is an *indirect* method of examining the effects of varying levels of information in the tunnel display. To increase the chance of success of determining the adaptation to such a varying optical source of information, the experiments must attempt to decrease the degrees of freedom in other sources of information that are possibly related. Because an ecological display such as the tunnel is inherently confounded, this is often a difficult task. It forces a well-considered choice of *free* optical variables to be studied.

Realism of the task The use of a simplified aircraft model and the insertion of forcing function signals are essential for model identification purposes. The most important drawback of this demand is that it could affect the *realism* of the pilot's task environment. Naturally, one would rather use a full-scale simulation environment incorporating extensive non-linear aircraft and atmospheric disturbance models. This is not possible here. When the level of realism of the environment, however, is insufficient, it can be questioned whether the results of the experiments are applicable for the practical in-flight situation. In this context it is important to realize that the research objectives addressed in this thesis require a laboratory approach. It is impossible to infer such fundamental pilot/display interaction characteristics from the *real* environment. The highest level of realism must be attempted to be realized within the constraints of the laboratory environment.

4.4 Methodology of the experiments

4.4.1 METHOD

The experimental method is illustrated in Fig. 4.3. Four stages can be distinguished.

Stage I: DESIGN The goal of the experiments is to examine the effects of varying a tunnel display design variable on pilot performance, control behaviour and workload. The experimental variables are typically a mixture of display-centered and aircraft-centered variables, a combination that should allow an examination of how the display affects
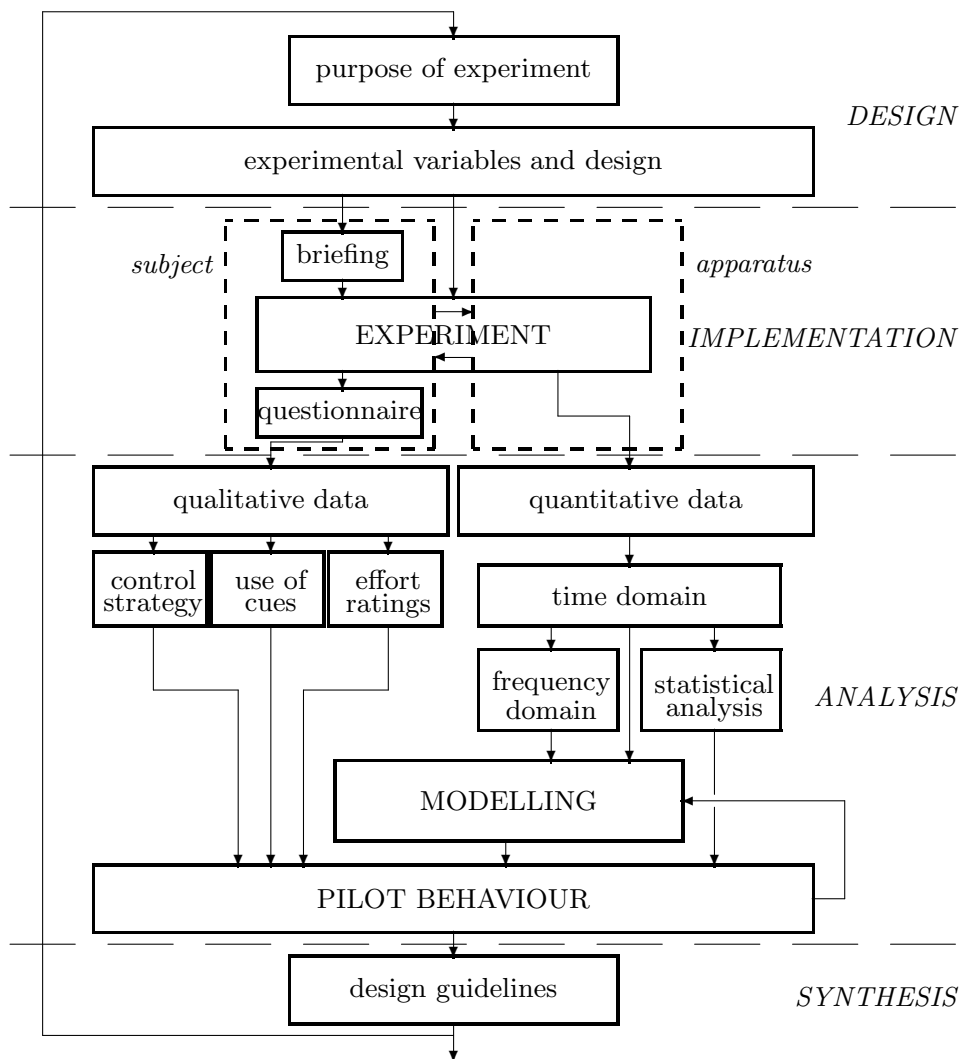
Figure 4.3: The experimental method applied in the cybernetic approach, starting with a definition of the purpose of the experiment (DESIGN), and ending with a transition of the knowledge obtained to the practical situation (SYNTHESIS).

pilot behaviour and also whether this depends on characteristics of the aircraft to be controlled. The independent measures follow from a pre-experimental evaluation, rooted in the information-analysis of Chapter 3, addressing the specific levels of the stimuli to be investigated. Finally, hypotheses are stated concerning the possible outcomes of the experiment, i.e. 'how do the independent measures affect the dependent measures?'.

Stage II: IMPLEMENTATION   The actual experiment itself is referred to as the implementation stage, in which three sub-stages can be distinguished.

Pilot briefing   Several days before the start of an experiment, all subjects received a pilot briefing, which contained information on the purpose of the experiment, the experimental variables, the task(s) to be performed and an experiment time schedule. Before the experiment was started the main instructions were verbally repeated to a subject.
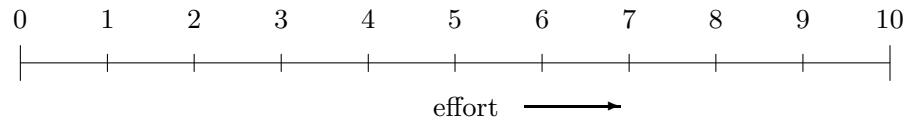
Figure 4.4: The effort scale used in the experiments (McDonnel, 1968).

Experiment   During the experiment, subjects interacted with the laboratory apparatus. All experiments consisted of two phases: (i) a *learning* phase, in which the subjects were getting accustomed to the experiment. This phase leads to a relatively constant level of performance and control activity, as expressed by their variances: (ii) a *measurement* phase, in which all data are measured and recorded. Generally, the learning phase required about 30–50% of the available time, depending on the subject and the experiment.

Pilot questionnaire   When all experimental trials were done, the subjects were requested to complete a pilot questionnaire. The questionnaire aims at collecting *subjective* or qualitative data that can substantiate the quantitative data. It contains a list of specific questions on the experiment, motivating subjects to put their comments on paper. The questions generally address the control strategy, the effect of the varying experimental conditions, the experienced realism of the simulation and the level of effort subjects experienced in conducting the task. The effort ratings were collected through the use of a 0–10 scale (Fig. 4.4), which was selected from the available effort scales for its simplicity. The ratings are used to discriminate between the experimental conditions on the basis of *effort*. The purpose is *not* to obtain some *general* effort rating parameter for the tunnel display, but only to allow an examination of the *differences* in the experienced effort. To reduce the two main effects of inter-subject variation, central tendency and leniency (Wewerinke, 1989), the ratings were transformed into Z-scores. Here, the set of ratings collected for a subject for all experimental conditions are transformed to an array of Z-scores having a mean of zero and a standard deviation of one.
A representative example of a pilot briefing and questionnaire is given in Appendix B.

Stage III: ANALYSIS   After completion of the experiment two sets of data are available: (i) the *qualitative* data, consisting of the pilot questionnaire and occasionally some additional pilot comments, and (ii) the *quantitative* data, i.e. the time histories of all variables of interest. The data-processing flows of the second set of data are discussed in §4.4.2. The data must be analyzed for the experimental condition under investigation to obtain an understanding of the observed pilot behaviour. The qualitative data directly provide some insight into this behaviour and can serve as *a priori knowledge* in the modelling procedure. The quantitative data are analyzed statistically before they are used in the pilot modelling efforts, discussed in §4.2. These efforts are expected to provide objective evidence for the manner in which the pilot *adapts* his control behaviour to the varying experimental conditions.

Stage IV: SYNTHESIS   The analysis stage in principle provides insight into how the experimental conditions have affected pilot behaviour with the tunnel display. This knowledge can then be used to define guidelines for specific tunnel display design issues. The transformation of the experimental insights into design guidelines, however, is non-trivial. Results of experiments in general do not lead to clear-cut and unequivocal solutions to a certain problem. They are sometimes ambiguous and could even lead to a whole set of other useful experiments. Hence, the development of design guidelines for an (ecological) display is essentially an *iterative* procedure (Roscoe et al., 1981; Wickens et al., 1989), which is illustrated by the 'feedback' loop in Fig. 4.3.

4.4.2   Data-processing flows of the quantitative data

The elementary data-processing flows of the quantitative data are illustrated in Fig. 4.5.

The time domain results   Starting point in the analysis are the time histories of all measured variables. The experimental condition is repeated R times, yielding R recordings of each variable. The statistics of a particular time history, e.g. variable $x^r(k; \zeta)$ for replication r, can be computed, resulting in for instance an estimate of the standard deviation (STD) of that variable for that replication: $\hat{\sigma}_x^r$. Repeating this procedure R times yields an array of measured STDs: $\hat{\sigma}_x^1 \ldots \hat{\sigma}_x^R$. Because this set represents the statistics of a variable for the repetition of the *same* experimental condition, they can be averaged, resulting in $\hat{\mu}_{\sigma_x}$ and $\hat{\sigma}_{\sigma_x}$. These quantities are the main results in the time domain. They are analyzed with statistical tests such as an Analysis of Variance (Hicks, 1982).

Averaging of time histories   The forcing function signals are the same for each experimental condition. Because they are *deterministic*, the time histories can be *averaged* in the time domain. This yields an averaged time history for each variable $(x^a(k; \zeta))$, attenuating the effects of the pilot's remnant considerably. The statistics of this averaged time domain response $(\hat{\sigma}_x^a)$ are therefore significantly *smaller* than the averaged statistics of the individual responses, i.e. $\hat{\sigma}_x^a < \hat{\mu}_{\sigma_x}$. They *do* show the same trends, however.

Frequency domain results   In principle, all time histories can be discrete-Fourier transformed $(x^r(k; \zeta) \rightarrow X^r(\nu_k; \zeta))$. The frequency domain data can be used to obtain estimations of the pilot's describing functions, i.e. $\hat{H}_{p_x}^{p^r}(\nu_k; \zeta)$ and $\hat{H}_{p_z}^{p^{c^r}}(\nu_k; \zeta)$, with the non-parametric identification method discussed in §4.2.2. Combining these estimates with the aircraft dynamics for that particular experimental condition allows a computation of the inner loop and *combined* outer loop crossover frequencies and phase margins, $(\omega_c^{in^r}, \varphi_m^{in^r})$ and $(\omega_c^{out^{c^r}}, \varphi_m^{out^{c^r}})$, for that condition. Repeating this procedure for all R replications allows a computation of their averages: $(\hat{\mu}_{\omega_c^{in}}, \hat{\sigma}_{\omega_c^{in}})$, $(\hat{\mu}_{\varphi_m^{in}}, \hat{\sigma}_{\varphi_m^{in}})$, etc. A drawback of using the *raw* time histories is that they contain the unattenuated pilot remnant. The estimated crossover frequencies and phase margins based on the frequency responses of the raw data can therefore be expected to be not very good. This problem was countered in two ways. First, a least-squares algorithm was used to estimate these quantities from the open loop
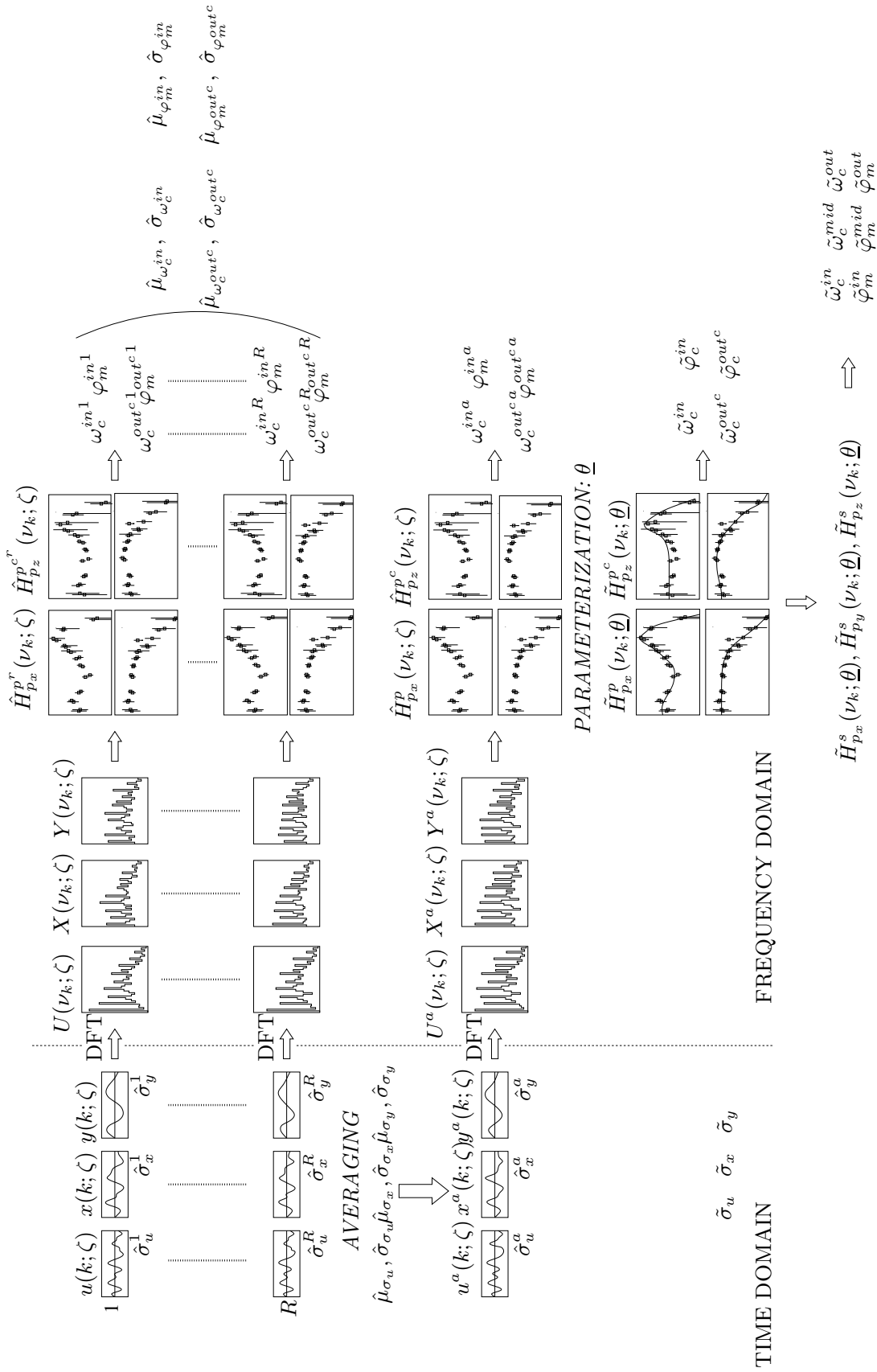
Figure 4.5: Elementary data-processing flows of the main quantitative experimental data. Note that this figure shows the data obtained for *one* subject for *one* experimental condition using the identification method with two forcing functions.

frequency responses, which reduced the variance in the estimates considerably (Appendix F). Second, by averaging the results the variation is further decreased.

The estimate of the frequency response to be used for the modelling purposes, is based on the *averaged* time histories $(x^a(k;\zeta) \rightarrow X^a(\nu_k;\zeta))$. The time domain averaging significantly attenuates the pilot remnant, yielding better results than when using the *raw* time histories. The inner loop and the combined outer loop bandwidths and stability margins can be computed: $(\omega_c^{in^a}, \varphi_m^{in^a})$, $(\omega_c^{out^{c\,a}}, \varphi_m^{out^{c\,a}})$. Note that the time-averaging procedure does *not* change the bandwidths and stability margins of the estimates. Hence, these quantities *can* be compared with those obtained by averaging the raw responses, i.e. $\omega_c^{in^a}$ should in principle be the same as $\hat{\mu}_{\omega_c^{in}}$.

Model parameterization The estimated pilot describing functions $\hat{H}_{p_x}^{p^a}(\nu_k;\zeta)$ and $\hat{H}_{p_z}^{p^{c\,a}}(\nu_k;\zeta)$, based on the averaged time histories, serve as the building blocks of the model parameterization. By minimizing some criterion function an optimal parameter is found which determines the modelled describing functions $\tilde{H}_{p_x}^{p}(\nu_k;\underline{\theta})$ and $\tilde{H}_{p_z}^{p^c}(\underline{\theta})$, allowing the modelled inner and combined outer loop bandwidth and stability quantities $(\tilde{\omega}_c^{in}, \tilde{\varphi}_m^{in})$, $(\tilde{\omega}_c^{out^c}, \tilde{\varphi}_m^{out^c})$ to be computed. A parameterization allows the computation of the middle and outer loop transfer functions of the *serial* pilot model, yielding $\tilde{H}_{p_x}^{s}(\nu_k;\underline{\theta})$, $\tilde{H}_{p_y}^{s}(\nu_k;\underline{\theta})$, and $\tilde{H}_{p_z}^{s}(\nu_k;\underline{\theta})$. Combining these transfer functions with the aircraft dynamics yields the modelled crossover and phase margin quantities for the inner, middle and outer loops: $(\tilde{\omega}_c^{in}, \tilde{\varphi}_m^{in})$, $(\tilde{\omega}_c^{mid}, \tilde{\varphi}_m^{mid})$, and $(\tilde{\omega}_c^{out}, \tilde{\varphi}_m^{out})$. Besides the determination of these frequency domain crossover and phase margin variables, the parameterized pilot models also allow a computation of the time domain variances of all signals in the loop, i.e. $\tilde{\sigma}_x$, etc.

4.5 The Human-Machine Laboratory

All experiments were conducted in the Human-Machine Laboratory (Appendix A). The components of this real-time simulation environment and the main flows of information will be discussed in §4.5.1. In §4.5.2 the test pilots are introduced who participated in the experiments, followed by a brief discussion of the experimental time schedule.

4.5.1 Elements of the real-time simulation environment

Fig. 4.6 illustrates the main flows of information in the simulation environment for the single-axis multi-loop regulating task of Fig. 2.9(c). The only 'new' element is the *side-stick* manipulator. The aircraft motions, described by the model of §2.5.2, are perturbed a set of forcing function signals, $\underline{i}$. The aircraft state $\underline{x}$ is displayed by the tunnel display through a set of optical cues $\underline{y}$. The pilot response signal is the *force* f applied on the side-stick. The stick *simulation* yields a new position of the stick, s, which, together with the set of forcing functions, serves as the input signal for the aircraft model. All components of the simulation environment are controlled by digital computers. The only physical elements that determine the pilot interaction with the environment are the display monitor and the
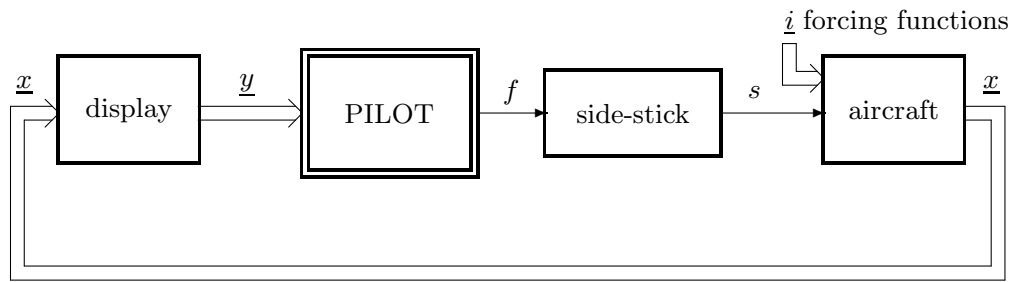
Figure 4.6: The main elements and information flows between these elements in the real-time
simulation environment of the Human-Machine Laboratory.

side-stick manipulator. The components are described in detail in Appendix A.

The side-stick manipulator   The side-stick is a two-axis, electro-hydraulic, servo-controlled stick. It is not a common stick in the sense that the force applied on the stick determines the stick position. Rather, this force is measured and serves as the input of a side-stick simulation program running on a digital computer. The output of this program is the updated position of the stick, which is sent to the servo-controller that puts the stick the commanded position. The characteristics of the stick are completely determined by the simulation software. The stick applied in the experiments is simulated as having the properties of an ordinary *passive* manipulator (van Paassen, 1994). The side-stick dynamics are simulated by means of a linear mass-spring-damper system, which properties are defined by a mass m, a linear spring constant k and a linear damping constant c. No non-linear stick properties, such as a breakout force or friction and stiction forces are simulated, yielding linear stick dynamics with an equivalent transfer function:

$$H_F^s(s) = \frac{1}{k + cs + ms^2}, \tag{4.5}$$

an ordinary second order low-pass filter with bandwidth $\sqrt{\frac{k}{m}}$ and damping $\frac{c}{2\sqrt{mk}}$. The side-stick properties for the roll (left/right) and pitch (forward/backward) rotation axes of the stick are summarized in Table 4.1. Not that from the discussion in §4.2 it follows that the *position* of the stick, s, and not the pilot force f is considered as the output signal of the pilot. This means that the estimated pilot frequency responses *include* the side-stick dynamics. Because the bandwidth of the stick is relatively high with respect to the measured pilot control behaviour and because the stick dynamics are deterministic, it can be hypothesized that this does not affect the identification procedure.

The aircraft model   The aircraft selected to be simulated in Experiments X1 to X5 is the Cessna Citation 500, a small two-engine business jet. Experiment X6 required a different simulation method and aircraft model (Chapter 10). The Citation satisfies the demands, stated in Appendix C, that an aircraft must fulfil for the identification procedure: it is a high-bandwidth aircraft with pleasant flying characteristics over a broad range of velocities. A considerable amount of data is available for analyzing the Citation dynamics (van der Linden, 1996). The simplified linearized cascade aircraft dynamics of Fig. 2.10

Table 4.1: Side-stick properties, defined for a point 90 [mm] above the stick rotation axis.

| | mass-spring-damper | | | bandwidth | damping | position | | |
| | m | k | c | ω_s | ζ_s | neutral | min. | max. |
	[kg]	[N/m]	[Ns/m]	[rad/s]	[-]	[deg]	[deg]	[deg]
roll	1.5	400	26.10	16.33	0.533	0	-27	+27
pitch	4.0	400	56.56	10.00	0.707	0	-21	+21

were simulated for a number of velocity conditions. The velocity conditions also determine the aircraft flying characteristics, which is discussed in Appendix C.

The forcing function signals The forcing functions are defined as a sum of sinusoids, Eq. 4.1, of which the frequencies, amplitudes and phases need to be specified beforehand. These are chosen at the hand of the *design rules* of §F.2.6. The **frequencies** of the sinusoids are defined as an integer multiple of the ground frequency ν_0 that depends on the length of the measurement interval T_m and the sample frequency f_s. The **phases** of the components of each forcing function are chosen random from a uniform distribution ($\sim \mathcal{U}(-180, 180)$ [deg]). They remain fixed over the experiment. The **amplitudes** of the sinusoids are determined by the choice of a *shaping filter* and the *intensity* of the white noise input of that shaping filter. For all experiments the same shaping filters are used. Here, only the shaping filters for the asymmetric aircraft motion will be discussed. The shaping filters for the symmetric aircraft motion are discussed in Chapter 7. The shaping filter of the inner loop forcing function i_1, Fig. 4.1(a), is defined as:

$$H_{w_1}^{i_1}(s) = \left(\frac{1 + \tau_\phi s}{K_\phi} \right) \left(\frac{\omega_1^2}{\omega_1^2 + 2\zeta\omega_1 s + s^2} \right), \tag{4.6}$$

an ordinary second order low-pass filter (ω_1=5 [rad/s] and ζ=0.8 [-]), compensated for the low-pass characteristics of the aircraft roll response, Appendix C. This eliminates the forcing function attenuation by the aircraft dynamics which is beneficial for pilot model identification. The shaping filter of the middle loop forcing function i_2 is defined as:

$$H_{w_2}^{i_2}(s) = \frac{1}{1 + \tau_2 s}, \tag{4.7}$$

an ordinary first order low-pass filter ($\tau_2 = 0.5$ [s]). Because the use of only a first order filter yielded sufficient power in the middle-frequency range, a compensation for the (combined) outer loop aircraft dynamics was not applied. The *intensities* $W1$ and W_2 of the shaping filter white noise input signals w_1 and w_2 are set at 10 [deg^2]. W_1 was set at 4.54 [deg^2] in Experiment X3 in order to reduce the task demand load. The shaping filter of the third forcing function i_3 is discussed in Chapter 9.

The display The tunnel display is shown in a highly abstracted fashion. All elements depicting status information, such as the speed tape, altitude tape, bank indicator, horizon heading indicator, pitch indicator, see Fig. 1.6, are removed. The tunnel geometry is shown as a grey wireframe on a black background. The aircraft reference symbol is a light-green

Table 4.2: Various data concerning the experiments of this thesis

		X1	X2	X3	X4	X5	X6
display update-rates and simulation time delays							
update-rate f_{EFIS}	[Hz]	17	25	20	15	17	15
time delay τ_{sim}	[s]	0.088	0.060	0.075	0.100	0.088	0.100
experiment measurement times and other properties							
run-in time T_i	[s]	20	20	15	20	15	5
measurement time T_m	[s]	81.92	81.92	105	81.92	105	30
# data points N	[-]	4096	4096	5250	4096	5250	1500
# conditions	[-]	12	12	18	20	18	20
# runs (# measurements)	[-]	8(5)	8(5)	14(6)	12(6)	10(6)	12(8)
# day shifts	[-]	2	2	5	4	4	2

outline. The display monitor is a 17 inch cathode ray tube (CRT) colour monitor with a refresh-rate[1] range of 55–70 [Hz]. The display hardware and software limited the display update-rate.[2] Even for the wireframe tunnel display the update-rate, referred to as f_{EFIS} (in [Hz]), and summarized in Table 4.2 was limited to about 15–25 [Hz]. These update-rates are near the lower bound for spatial data displays (Batson, Harris, & Houck, 1992).

The existence of time delays in the simulation   In Appendix A the origin and consequences of time delays in the simulation environment are analyzed in detail. This analysis revealed that because the simulation frequency f_{sim}, fixed at 2000 [Hz], is very high, the majority of the components yields only negligible time delays. The limited update-rate of the tunnel display results in a considerable simulation time delay equal to $\tau_{sim} \approx \frac{3}{2}\frac{1}{f_{EFIS}}$ (Eq. A.5). In Table 4.2 the values of the simulation time delay for all experiments are summarized. The existence of a time delay in the closed loop has important consequences for the non-parametric identification procedure, see §F.4.2.

4.5.2   Test pilots and experiment time schedule

Subjects   Three professional airline pilots (A–C) and one student pilot (D) participated in all experiments. For experiment X6 the population was extended with one additional student pilot (E). In the discussion of the pilot questionnaires only the results of the three professional pilots will be discussed, because their comments are considered to be most relevant. The experience and main characteristics of the test pilots are summarized in Table 4.3. The subjects were not paid for their co-operation. They received a compensation for their travel expenses, and, at the end of each experiment, a small gift.

The experiment time schedule   Each *experimental trial* consisted of two parts, starting with a run-in period of T_i (in [s]), followed by the actual measurement interval of T_m (in

---

[1]The *refresh-rate* is a hardware property defined as the rate at which the video monitor redraws the information being displayed, independent of the update-rate.

[2]The display *update-rate* is defined as the rate at which a new display image can be computed by the display software and hardware.

Table 4.3: Characteristics of the experimental test subjects. The coding of these subjects (A–E) is maintained in this thesis.

subject	year of birth	vision[a]	hand[b]	flying hours	experience
A	1966	U	R	1600	Single-engine, Citation, Metro, Fokker 100, Boeing 767
B	1963	U	R	4000	Single-engine, Boeing 767, MD-11
C	1966	C	R	1600	Single-engine, Citation, Metro, Fokker 100, Boeing 737
D	1967	U	R	50	Cessna Citation 500 (flight-simulator)
E	1973	U	R	150	Single-engine

[a]: U=uncorrected, C=corrected
[b]: L=left-handed, R=right-handed

[s]). During the run-in time a subject can get accustomed to the task, attenuating effects of operator non-linearity. The simulation frequency f_{sim} is fixed at 2000 [Hz] and the data-recording frequency f_s is set at 50 [Hz]. A measurement time T_m results in $N = T_m f_s$ data points. The values of these variables for all experiments are listed in Table 4.2. The experimental conditions are repeated a number of times (8–14) for each subject. The regulating tasks required the full attention of subjects and the experiments were quite demanding. To alleviate the subject's workload the time schedule provided considerable resting times between runs. An experiment was divided into *blocks*, each block consisting of 6 to 8 runs. During a block of runs, subjects stayed within the laboratory. In-between runs subjects had approximately 20 to 30 [s] to relax. When a block was finished, subjects were allowed to leave the laboratory for a period of approximately 5 to 10 minutes. After the completion of three to four blocks, the experiment was paused for 30 to 45 minutes. After this resting period the procedure was repeated. The total amount of time needed to conduct an experiment depended on the number of experimental conditions, the number of replications, and the time needed for each experimental run, see Table 4.2. Each experiment required approximately one to two and a half days for each subject to complete.

4.6 Retrospective

The objective of the theoretical analysis and the practical evaluation of the tunnel display described in this thesis is to obtain an understanding of *how* and *why* the various tunnel display geometric design variables affect pilot behaviour. This knowledge is needed for the specification of tunnel display design guidelines from a human-centered design perspective. The experiments are carefully designed to allow an evaluation of the pilot behaviour in a representative manual control task in both a psychological and a control-theoretical sense (§4.1). An important step in the model-based analysis, the fourth and final step of the cybernetic approach of §1.4 is the validation of the pilot models. A survey of the available model identification methods (§4.2) revealed that the pilot's use of only a limited subset of

the total array of visual information sources can be identified at the same time. This limits the complexity of the pilot model considerably. The model validation methods also put rather strict demands on the definition and the design of the experiment itself (§4.3). The modelling approach allows the determination of *how* pilots adapt their control behaviour as a function of the various experimental conditions. Because these conditions mainly affect the pilot's observation process, the model of which is difficult to identify experimentally, it can be expected that the hypotheses *why* the pilot adapts must still be inferred. During the course of this research project and based on the experiences reported in similar areas of research, a methodology of experimenting has been developed that provides as much support as possible to the cybernetic evaluation. In other words, the experiments aim at providing a maximum amount of quantitative data, extending the potential evidence with which the pre-experimental hypotheses can be tested. This methodology, discussed in §4.4, and illustrated in Fig. 4.3, is applied for all experiments, allowing the experiments and the experimental results to be discussed in a structured and consistent manner.

What can be expected to be achieved?

The validation of an extensive and complete model of pilot behaviour with a tunnel display is too ambitious. This setback has mainly two causes:

- The information conveyed in the tunnel display cannot be described by a set of *parallel* streams of information. The visual cues are entangled and can not be isolated without severely damaging the tunnel geometry (Chapter 3).
- The pilot model identification efforts show that only the main two or three pilot loop closures can be determined experimentally. The estimation of all individual pilot feedbacks is a utopian dream (Chapter 4).

Both problems can be considered insoluble. The impossibility of isolating the visual cues of the display is simply due to the nature of the perspective tunnel display. The impossibility of identifying all feedback loop closures is due to the characteristics of the human controller. The impossibility of validating an extensive pilot model on the basis of objective experimental data has a number of consequences. Most importantly, it will be impossible to obtain a model that exactly describes (and predicts) what the effects are (or will be) of a certain changing tunnel display variable on pilot behaviour. Instead of this, these effects can only be determined for rather elementary situations. Hence, in order to successfully address *what's going on*, the experiments must examine elementary concepts in which basic design aspects of the display are varied.

Chapter 5

The effects of the tunnel size

5.1 Introduction

In this chapter the first *case study* is described, Experiment X1, in which the effects of one of the main tunnel display design variables, the *tunnel size*, are investigated. The tunnel size issue has been addressed before in earlier studies (Wilckens, 1973; Grunwald, 1984; Theunissen, 1995) and it is examined again for a number of reasons. First, the investigation of the tunnel size yields an elementary experiment that is well-suited to test the modelling efforts as a whole and the applicability of specific pilot models in particular. Second, because it has been addressed before in literature the present results provide a benchmark for the cybernetic approach. The discussion in this chapter, and the following chapters, is divided into sections corresponding with Fig. 4.3. Guided by the findings in the previous chapters, first some background information is provided on the specific issue of interest, §5.2, followed by a statement of the research objectives that lead to an experiment design, §5.3. The qualitative pilot comments and the empirical performance-related experimental data are described in §5.4, followed by a discussion of the model-based analysis in §5.5. These findings are used to obtain insight in the ways in which the experimental variables affected the pilot behaviour, the *analysis*, followed by an attempt to put these findings into the perspective of display design, the *synthesis* (§5.6).

5.2 Background

Earlier studies: performance and workload

The tunnel size is one of the main tunnel display design variables. By limiting the airspace volume in which the aircraft may fly, the tunnel size *commands* the level of path-following accuracy. Increasing the tunnel size decreases this level, allowing pilots to reduce their control gains and to lower their level of attention allocated for the guidance task, yielding a more relaxed control strategy. Smaller tunnels command a higher level of trajectory-
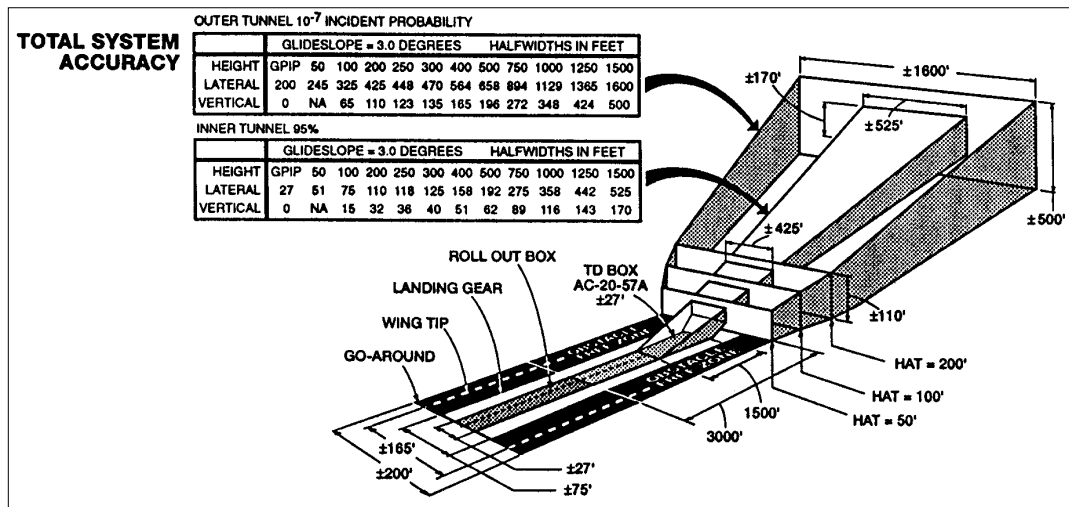
(a) RNP for a Cat IIIa precision approach and landing (Kelly & Davis, 1994)
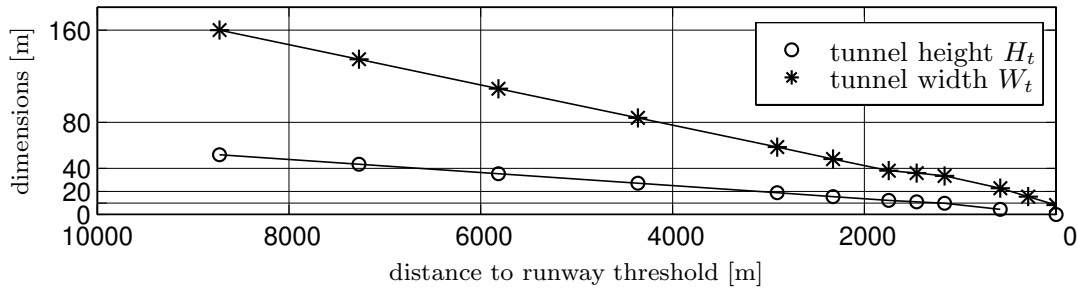
(b) inner tunnel dimensions for the RNP example in (a)

Figure 5.1: Required navigation performance (RNP) tunnels.

following precision, demanding more pilot attention for the guidance task. The tunnel size is an excellent example of a design *tradeoff* between performance and workload.

Required navigation performance   From an air-traffic control perspective the size of the tunnel should be small, allowing an efficient use of the airspace. In (Kelly & Davis, 1994) a methodology is described to determine the Required Navigation Performance (RNP) for aircraft precision approach and landing under Instrument Meteorological Conditions (IMC). The RNP defines an aircraft containment surface about the nominal flight-path, (in our context confusingly) called the *tunnel*, that specifies the approach and landing flight-path limits. In fact, two tunnels are specified: the inner and the outer tunnel. The dimensions of the aircraft containment surface define the outer tunnel, whereas the inner tunnel dimensions specify the allowed 95% aircraft deviations from the assigned flight-path. Fig. 5.1(a) shows the RNP tunnel for a Cat IIIa precision approach and landing, illustrating that performance must increase significantly when approaching the runway threshold, not only in the horizontal but especially in the vertical plane.

Earlier tunnel size studies   Not surprisingly, the tunnel size played an important role in almost all tunnel display investigations. In (Wilckens, 1973; Schattenmann &

Wilckens, 1973) the effects of different tunnel sizes (range 20-400 [m]) on pilot performance and control activity were investigated in a task of following a straight trajectory. It was concluded that control activity increased monotonously with decreasing tunnel size. The same holds for the performance, but only to a certain level: further reducing the tunnel size led to reduced closed loop stability and decreasing performance, as indicated in the qualitative diagram of Fig. 2.2. Wilckens recommended an *optimal* tunnel size to be established based on aircraft handling characteristics and pilot workload. Grunwald (1984) investigated the use of two tunnel sizes (300 and 450 [ft], i.e. 91 and 137 [m]) for curved approaches with the tunnel-and-predictor display (§2.2). Again, an increasing performance and control activity for the smaller tunnel was found. This experiment was repeated by Theunissen (1995). Besides the effect of tunnel size (22.5, 45 and 90 [m]) another issue was to distinguish between straight and curved sections of the trajectory. It is not reported in (Theunissen, 1995), nor in (Theunissen, 1997), however, *how* these different trajectory-following phases were separated from each other. Most probably, these phases were differentiated at the transitions between straight and curved sections. As will be discussed in Chapters 8 and 10, this procedure leads to considerable biases in the results because it includes the aircraft curve transition manoeuvre. This casts serious doubts upon the validity of the conclusions, and it was considered essential to re-examine the effects of the tunnel size in a well-considered manner. Therefore, Experiments X2 (Chapter 6), X4 (Chapter 8) and X6 (Chapter 10) were designed to, among others, investigate further the tunnel size parameter effects in following straight and curved sections and conducting straight-to-curved transitions, respectively.

An analysis of the visual sources of information

The sources of information in the tunnel display were studied in detail in Chapter 3. The discussion below focuses on the role of the tunnel size on the characteristics of some of these cues in *straight* tunnel sections. The analysis is limited to the lateral dimension and examines especially the presentation of the heading angle error ψ_e and the lateral position error x_e. It is assumed that the side slip angle β is small enough to be neglected: $\beta \approx 0$.

Cues for a position error   Figs 5.2(a) and 5.2(b) show the tunnel images for tunnel sizes of 20 and 40 [m], respectively. Both the figures show the situation of a zero and a non-zero lateral position error (x_e=+5 [m]), and a zero heading angle error. A smaller tunnel size allows a pilot to obtain a better estimate of the center of the tunnel frames and therefore of the location of the reference trajectory. The figures illustrate the main cues for a position error, i.e. the displacements of the tunnel frames ($\delta\epsilon_i$, $\delta\eta_i$) and the optical splay angles of the longitudinal frame lines (ω_i). Starting with the latter variables, it follows from the discussion in Chapter 3 that (Eqs 3.43, with H_t=W_t and v_e=0):

$$\omega_1 \;=\; \omega_4 \;=\; -\frac{x_e}{W_t}\;;\quad \omega_2 \;=\; \omega_3 \;=\; +\frac{x_e}{W_t}\;;\quad \omega_5 \;=\; -2\frac{x_e}{W_t}. \tag{5.1}$$

The tunnel size acts as a scaling factor, a *gain* for the change in splay angle caused by a position error. This scaling effect was originally reported in (Wilckens, 1973) and led
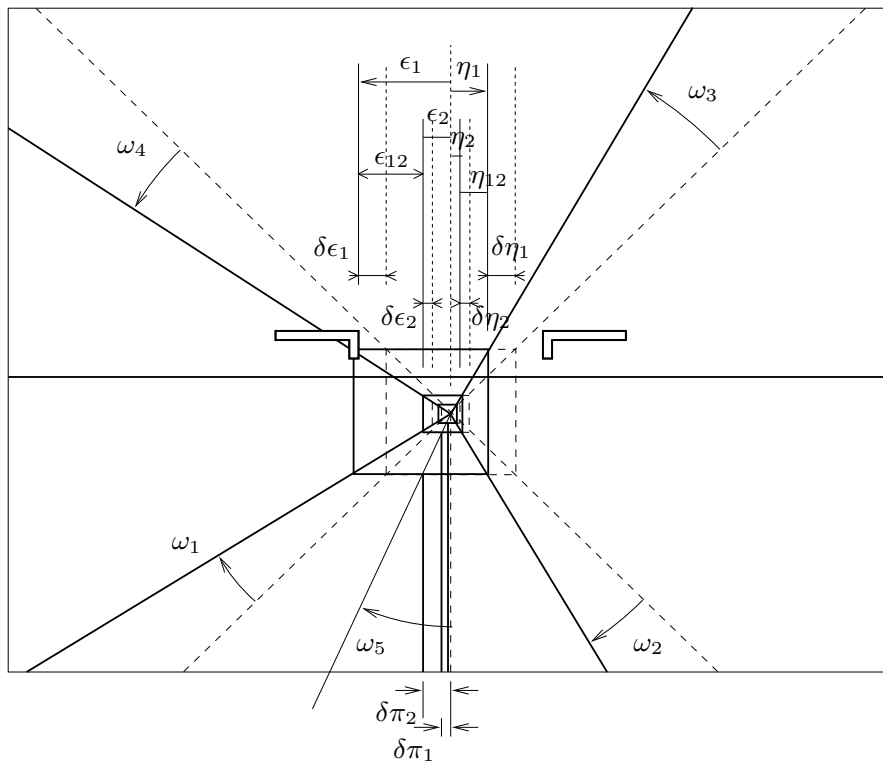
(a) $W_t = 20$ [m]
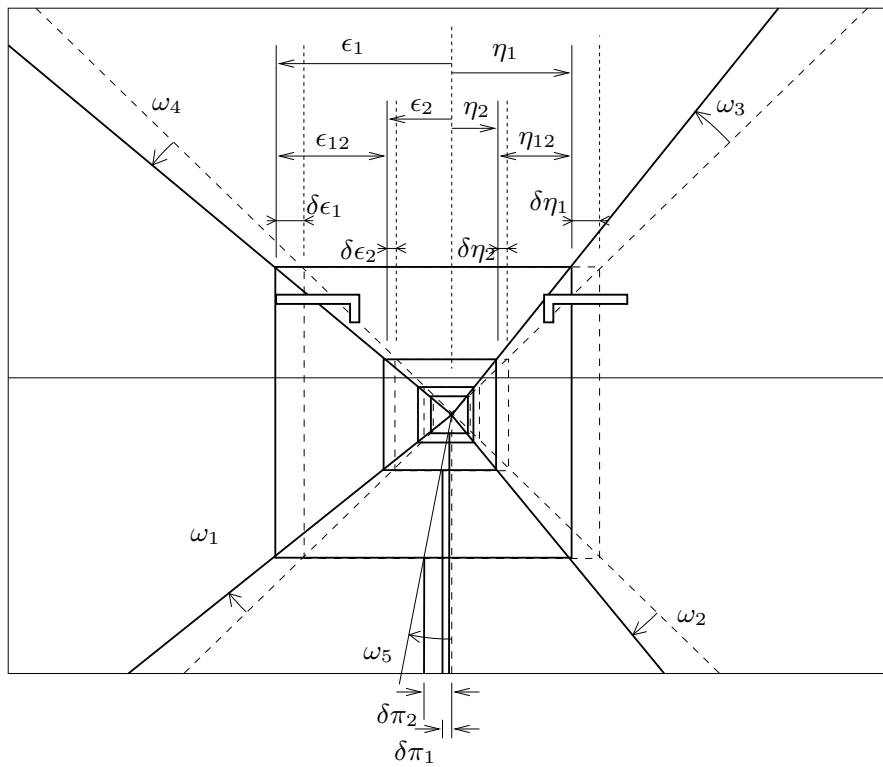
(b) $W_t = 40$ [m]

Figure 5.2: Static optical cues for a lateral position error x_e in straight tunnel sections. The dashed and continuous lines show the tunnel image for a zero and a non-zero ($+5$ [m]) lateral position error, respectively. The heading angle error ψ_e is zero.

Theunissen (1993b) to allocate the term *error gain* to the tunnel size. The 'virtual' line connecting the end-points of the altitude poles supporting the frames also yields a splay angle, with a 'gain' that is twice as large. The displacement cues are *independent* of the tunnel size, an effect which can be seen from Fig. 5.2 when comparing the values of these cues ($\delta\epsilon_i$, $\delta\eta_i$) for both tunnel sizes. The *relative* displacements (ϵ_{12}, η_{12} etc.), however, *do* appear larger in relation to the size of the frames themselves, for smaller tunnels. Decreasing the tunnel size leads to a situation in which the first visible frame is smaller and seems to be positioned farther away. The subsequent frames are even smaller and appear considerably cluttered on the display, leading to a situation where the relative displacements become difficult to perceive. The relative displacements of the altitude poles, however, remain visible and are unaffected by the tunnel size.

Cues for a heading angle error   The heading angle error ψ_e can be perceived from the translation of the *infinity point* with respect to the center of the screen marked by the aircraft reference symbol, a translation that is independent of the tunnel size. In the absence of side slip the aircraft heading angle error ψ_e equals the track angle error χ_e, the direction of motion relative to the trajectory. Hence, differentiating the splay angles of Eq. 5.1 yields a second potential cue for the heading angle error:

$$\dot\omega_1 \; = \; \dot\omega_4 \; = \; -\frac{V_{tas}}{W_t}\psi_e \; ; \quad \dot\omega_2 \; = \; \dot\omega_3 \; = \; +\frac{V_{tas}}{W_t}\psi_e \; ; \quad \dot\omega_5 \; = -2\frac{V_{tas}}{W_t}\psi_e. \tag{5.2}$$

Hence, the heading angle error is also coded in the display by the *splay angle rates*, scaled by the aircraft velocity and the size of the tunnel.

The subjective velocity   The discussion in Chapter 3 revealed that the tunnel size also affects the subjective sense of forward velocity. The higher subjective egomotion for smaller tunnels can be attributed to the V_{tas}/W_t ratio, the *global optical flow rate*, introduced in Chapter 3. Theunissen (1997) labelled this phenomenon the *velocity gain*.

Discussion   The heading angle error can be perceived from: (i) the position of the infinity point on the display, a cue that is *independent* of the tunnel size; and (ii) the angular velocities of the splay angles, that are larger for smaller tunnels. A position error can be perceived from the relative displacements of the tunnel frames and the altitude poles, cues that are independent of the tunnel size. Decreasing the tunnel size, however, deteriorates the usefulness of these cues, except for the relative displacements of the tunnel altitude poles. Because the relative displacement cues must be perceived while travelling forward through the tunnel, this could hamper their perceivability once more, especially for those frames close-by. The frames that are positioned farther away are located closer to the center of the screen, and because the relative motion of the display elements in that area is much lower, their perceivability remains satisfactory. Other powerful cues for the position error are the optical splay angles. These are a function of the lateral position error only, and are *scaled* by the tunnel size. The perceivability of the splay angles is unaffected by the aircraft forward motion, which could be an important virtue. The virtual line connecting the tops of the altitude poles conveys a splay angle with a gain that is twice as large as that of the other splays, which could make it an alternative cue for large tunnels.

Table 5.1: Experimental conditions (X1).

		1	2	3	4	5	6	7	8	9	10	11	12
V_{tas}	[m/s]	50	50	50	50	70	70	70	70	100	100	100	100
W_t	[m]	80	40	20	10	80	40	20	10	80	40	20	10

Concluding, the tunnel size affects mainly the presentation of the position error, by *scaling* the amplitude with which it is presented on the display. The principal cues are probably the splay angles, especially for smaller tunnels. For larger tunnels, the relative linear displacements of the frames and the altitude poles could be an alternative. It is clear that the tunnel size influences the perceivability of the visual cues which in turn affects the pilot control strategy. The significance of a cue depends on the tunnel size, the forward velocity and probably also on the pilot control and observation strategy.

5.3 Experiment X1

Experiment X1 investigates the effects of the tunnel size on pilot performance, control behaviour, and workload. The tunnel size commands the path-following accuracy, and its functionality for this purpose has been shown in earlier investigations. These studies, however, investigated the effects of the tunnel size on pilot behaviour using performance-related data alone. The current methodology, centered around a quantitative determination of the pilot control behaviour *adaptation* process, allows a re-examination of the mere qualitative claims of Wilckens (1973) concerning closed loop stability and performance.

METHOD

Subjects and instructions to subjects   Four subjects (A - D) participated in the experiment. They were instructed to control the aircraft through the tunnel as accurately as possible, i.e. all occurring attitude and position errors must be minimized.

Apparatus   The Human-Machine Laboratory was used, described in Appendix A.

Independent variables   Two independent variables were varied in the experiment:

  (i) The *tunnel size* W_t (4 levels): 80, 40, 20 and 10 [m].
  (ii) The *aircraft velocity* V_{tas} (3 levels): 50, 70 and 100 [m/s].

The aircraft velocity determines the velocity with which the aircraft moves through the environment and also affects the handling characteristics (Appendix C).

Experimental design   A full-factorial within-subjects design was applied, consisting of a total of 12 conditions (Table 5.1). The conditions were randomized over the experiment. Each subject conducted three familiarization sessions (36 runs) before completing five replications of all experimental conditions (60 runs) that served as the measurements.

Table 5.2: Definition of input signals i_1 and i_2 (X1). The amplitudes and phases are shown for the V_{tas}=70 [m/s] condition.

	input signal i_1				input signal i_2			
	k_{1_i}	ω_{1_i}	A_{1_i}	ϕ_{1_i}	k_{2_i}	ω_{2_i}	A_{2_i}	ϕ_{2_i}
i	[-]	[rad/s]	[deg]	[deg]	[-]	[rad/s]	[deg]	[deg]
1	4	0.3068	0.5859	-8.7396	5	0.3835	2.1309	161.0276
2	11	0.8437	0.6160	-131.0308	12	0.9204	1.9710	-112.8963
3	17	1.3039	0.6593	-123.4390	18	1.3806	1.7856	113.1471
4	25	1.9175	0.7299	150.6975	26	1.9942	1.5364	111.9376
5	31	2.3777	0.7836	-149.1154	32	2.4544	1.3706	108.8338
6	37	2.8379	0.8312	26.5673	38	2.9146	1.2276	91.4982
7	47	3.6049	0.8856	-42.8377	49	3.7583	1.0192	53.4347
8	61	4.6786	0.9009	153.3283	62	4.7553	0.8412	44.0517
9	82	6.2893	0.8319	-62.1594	83	6.3660	0.6503	-19.6409
10	107	8.2068	0.7109	-59.7727	109	8.3602	0.5048	40.2383
11	149	11.4282	0.5445	12.8682	151	11.5816	0.3692	-145.7304
12	197	15.1097	0.4218	-143.8011	199	15.2631	0.2819	-123.6679

Procedure   During the course of one day a subject conducted 96 experimental runs, divided in twelve blocks of eight runs each. A single run lasted 101.92 [s], consisting of a run-in time T_i of 20.0 [s] and a measurement time T_m of 81.92 [s]. The pace of the experiment was such to allow sufficient time for subject preparation and to prevent fatigue.

Dependent measures   Three categories of performance variables were selected as dependent measures: (i) pilot *control activity*, i.e. the aileron (δ_a) and aileron-rate ($\dot{\delta}_a$); (ii) pilot *inner loop activity*, i.e. the aircraft roll angle (ϕ) and roll-rate ($\dot{\phi}$); and (iii) *path-following accuracy*, i.e. the track-angle error (ψ_e) and cross-track error (x_e). The standard deviations of these variables represent the experimental results in the time domain.

Description of the experiment simulation

Tunnel display geometry   A generic tunnel was used consisting of square frames ($H_t = W_t$) positioned on altitude poles, connected with longitudinal lines. The reference trajectory was straight and had a downslope Γ_t of 3 [deg]. The intermediate frame distance $\triangle D$ was fixed at 350 [m]. No flight-path vector or other symbology was presented.

Aircraft models   The asymmetric motions of a Cessna Citation I were simulated at the three velocity conditions introduced above (Appendix C). The aircraft velocity vector was fixed relative to the aircraft Body axes representing a zero-slip condition. The symmetric motion referents were fixed to their initial condition values (Appendix C). Thus, the aircraft moved in a plane with downslope 3 [deg] through the vertical center of the tunnel.

Atmospheric disturbances   To satisfy the pilot model identification demands two independent forcing functions were inserted in the control loop (i_1 and i_2 in Fig. 4.2). These signals consisted of a sum of twelve sinusoids, the frequencies and amplitudes of

Table 5.3: Pilot questionnaire (X1): realism of the simulation.

How would you describe the level of *realism* of the simulated aircraft *dynamics*?					
	very realistic	realistic	average	unrealistic	very unrealistic
$V_{tas}=$ 50 [m/s]	·	1	·	2	·
$V_{tas}=$ 70 [m/s]	·	2	1	·	·
$V_{tas}=$ 100 [m/s]	·	3	·	·	·

How would you describe the level of *realism* of the simulated aircraft *disturbances*?					
	very realistic	realistic	average	unrealistic	very unrealistic
$V_{tas}=$ 50 [m/s]	·	·	1	2	·
$V_{tas}=$ 70 [m/s]	·	1	1	1	·
$V_{tas}=$ 100 [m/s]	·	·	·	3	·

which were chosen by the input signal design rules of Appendix F. To allow a comparison between the aircraft velocity conditions, the input signal spectra were compensated for the aircraft model characteristics. The signal definitions are summarized in Table 5.2.

Initial condition Before the start of each run, the aircraft was positioned in the center of the tunnel with zero position and attitude errors. The initial longitudinal position of the aircraft on the tunnel reference trajectory was randomized.

Experiment hypotheses

In the experiment the only factor that affects the *display* is the tunnel size, determining especially the magnitude with which the aircraft position error is presented. Whereas the presentation of the heading angle error depends less on the tunnel size, the presentation of all other aircraft motion states remains unaffected. Guided by the findings reported in literature, it is hypothesized that reducing the tunnel size leads to an increasing control activity, an improved path-following performance and higher pilot workload. Furthermore, it is hypothesized that aircraft control becomes less gradual and increasingly 'jerky' with smaller tunnels. Concerning the effects of the *aircraft velocity* it is hypothesized that, first, because the aircraft becomes easier to control for the higher velocity conditions, pilot control activity and workload are lower for these conditions. Second, because for higher aircraft velocities the same heading angle error yields larger position error rates, it is hypothesized that control of aircraft heading becomes more important for these conditions.

5.4 Results

5.4.1 The pilot questionnaire

After the experiment, subjects were requested to complete a pilot questionnaire. Because subject D was involved in the definition and set-up of the experiment, only the comments
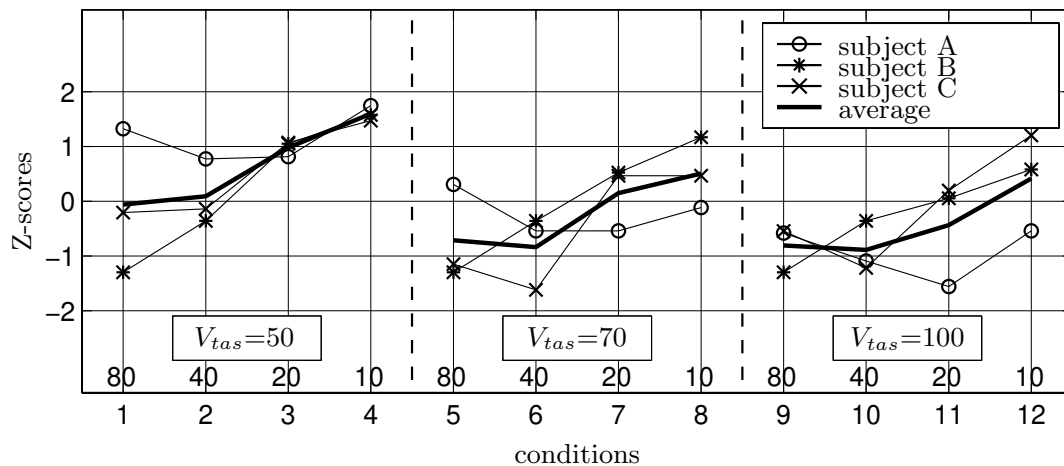
Figure 5.3: Z-scores of the effort ratings for all 12 conditions of Experiment X1. In this figure and in the following, the insets show the three velocity conditions (in [m/s]), the numbers 80-10 in the bottom of the figure indicate the tunnel size (in [m]) and the numbers 1-12 below the figure indicate the experimental configurations of Table 5.1.

of subjects A to C will be discussed.

Realism of the simulation   Subjects judged the simulation of the higher two velocity conditions satisfactory and the low-velocity condition as too sluggish, Table 5.3. They commented on the lack of increasing stick-stiffness for higher velocities. The level of realism of the simulated aircraft disturbances was judged rather poor. In particular the magnitude of the low-frequency turbulence component was found to be too strong.

Sources of information and control strategies   Subjects were asked to explain how they fulfilled their task and what elements of the display provided useful information. They stated that, for large tunnels, especially the displacements of the altitude poles were useful. For smaller tunnels, they commented on using more and more the splay angles. Subjects did not report any differences in control strategy when the aircraft velocity increased, except for the fact that when the aircraft velocity increased, the usefulness of the frames and altitude poles became less important for smaller tunnels. In the low-velocity condition subjects regarded the motion of the tunnel image on the screen annoying, which could be caused by the rather large pitch angle for this condition (Appendix C).

Effort ratings   The Z-scores of the pilot effort ratings increase for smaller tunnels, especially when the tunnel becomes very small (Fig. 5.3). The ratings are higher for the low-velocity condition, which corresponds well with the pilot comments stated above.

5.4.2   Time domain data: statistical analysis

A full-factorial mixed-model Analysis of Variance was conducted for the time domain data. The independent measures were the aircraft velocity (V) (3 levels) and the tunnel size (W) (4 levels). The ANOVA results are summarized in Table 5.4.

Table 5.4: Results of a full-factorial ANOVA (X1) on the dependent measures involving control activity, inner loop measures and path-following accuracy (in this table '★★', '★' and '○' represent chance levels of $p \leq 0.01$, $0.01 < p \leq 0.05$ and $0.05 < p \leq 0.10$, respectively).

	control activity		*inner loop measures*		*path-following performance*	
	δ_a	$\dot{\delta_a}$	$\dot{\phi}$	ϕ	ψ_e	x_e
main effects						
V	★★	★★	·	·	★★	·
W	★★	★★	★★	★★	·	★★
2-way interaction						
V×W	★	·	·	★	★★	★

(a) aileron

(b) aileron derivative

(c) roll angle

(d) roll angle derivative

(e) track-angle error

(f) cross-track error

Figure 5.4: The means and 95% confidence limits of the STDs of the dependent measures (all subjects).

Pilot control activity The pilot control activity increases for smaller tunnels (δ_a: $F_{3,9}$=17.871, p <0.01; $\dot{\delta}_a$: $F_{3,9}$=12.612, p <0.01) and decreases for larger velocities (δ_a: $F_{2,6}$=121.251, p <0.01; $\dot{\delta}_a$: $F_{2,6}$=106.443, p <0.01), Figs 5.4(a) and 5.4(b). A Newman-Keuls (NK) post-hoc analysis (p=0.05) revealed that tunnel size only had a significant effect on aileron for the low-velocity condition, causing the significant V×W-interaction. Only the values for the low and the high-velocity conditions were significantly different, independent of the tunnel size.

Inner loop measures Figs 5.4(c) and 5.4(d) indicate that the roll angle and the roll-rate increase for smaller tunnels (ϕ: $F_{3,9}$=34.846, p <0.01; $\dot{\phi}$: $F_{3,9}$=23.189, p <0.01). The velocity has not a significant effect. Post-hoc tests (NK, p=0.05) showed that the differences between the magnitudes of roll and roll-rate become less significant for the high-velocity conditions. Only for the smallest tunnel there was a significant difference from the other sizes, irrespective of the velocity.

Path-following performance The track-angle error (Fig. 5.4(e)) is only affected by the aircraft velocity ($F_{2,6}$=48.949, p <0.01), whereas the cross-track error (Fig. 5.4(f)) is only affected by the tunnel size ($F_{3,9}$=14.467; p <0.01). Post-hoc analyses (NK, p=0.05) revealed that for the high-velocity condition all differences in cross-track error between tunnel sizes were significant. For the other two velocity conditions all differences in x_e were also significant, except those between the two largest tunnels. A post-hoc analysis (NK, p=0.05) of the track-angle error showed that the differences due to the aircraft velocity were indeed all significant, independent of the tunnel size.

5.4.3 Frequency domain data

The frequency domain data form the principal source of information for the pilot modelling efforts. Furthermore, they can provide additional insight into the time domain results.

Relative noise ratios The relative noise ratio (RNR) of a signal depicts the relative amount of noise of that signal at a particular set of frequencies (Appendix F). The RNRs of the control signal δ_a and the inner loop (ϕ) and outer loop (x_e) signals are shown in Fig. 5.5 for the averaged data sets of one subject. The pilot's output signal δ_a is acting primarily at frequencies of i_1 (less than 25% of the signal at these frequencies is noise), whereas the outer loop signal (x_e) variance is distributed over both sets of frequencies. The distribution of the signal variances varies as a function of the independent variables. The RNRs computed for both sets of frequencies simultaneously (i_1&i_2), however, remain fairly constant and show that, generally, the pilot noise has only a small effect (less than 15-20% of the total signal variance). The same was found for all other subjects.

Frequency responses The estimated frequency responses are the main building blocks for the pilot modelling efforts. Fig. 5.6 shows some typical results, i.e. the inner loop and
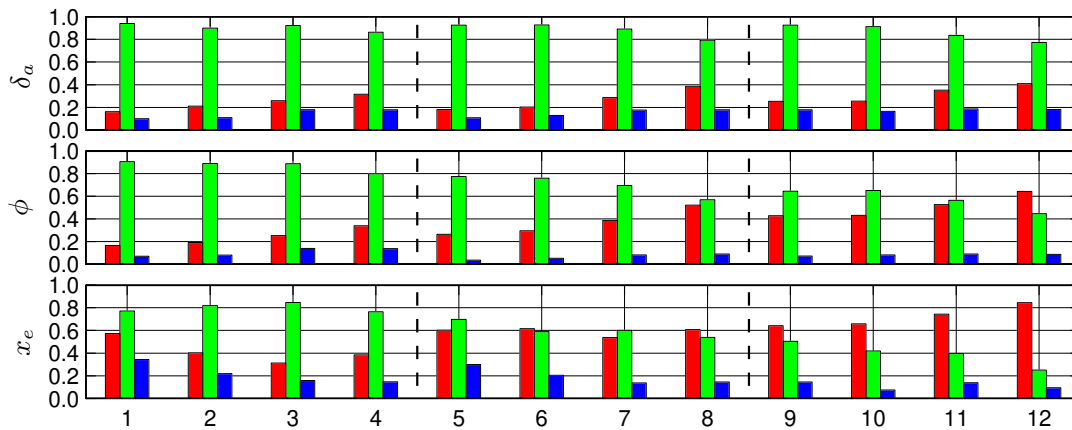
Figure 5.5: Relative noise ratios (one subject, all conditions). The three bars for each condition represent the RNRs computed at frequencies i_1 (left), i_2 (middle) and $i_1\&i_2$ (right).

the *combined* outer loop[1] frequency responses, for a *parallel* pilot model structure. The standard deviations show that the uncertainty of the estimates is rather small, especially in what will appear to be the inner and combined outer loop crossover regions. The estimation variances are quite large for the very low and the high frequency components. The uncertainty in the estimate of the combined outer loop frequency response is larger than the uncertainty in the inner loop estimate. Generally, the estimates at those frequencies that show a large variance are also considerably biased. The parallel pilot frequency responses are used for the model parameterization efforts, discussed later.

Crossover frequencies and phase margins The pilot frequency responses can be combined with the aircraft models to compute the crossover frequencies and phase margins. Fig. 5.9 (on page 135) shows these quantities for the inner loop and the combined outer loop for all subjects (vertical) and all configurations (horizontal). The figure shows an increasing inner loop crossover frequency ω_c^{in} for smaller tunnels as well as for larger aircraft velocities. The trend in the inner loop phase margin φ_m^{in} depends more on the subject. The combined outer loop crossover frequencies and phase margins clearly show the effect of the tunnel size: irrespective of the subject and the aircraft velocity, the crossover frequency $\omega_c^{out^c}$ increases and the phase margin $\varphi_m^{out^c}$ decreases sharply for smaller tunnels. The increasing $\omega_c^{out^c}$ for smaller tunnels requires an increasing inner loop crossover frequency ω_c^{in}. The fact that this does not always result in a decreasing φ_m^{in} could be attributed to a pilot strategy to offer more outer loop phase margin $\varphi_m^{out^c}$ to maintain sufficient inner loop stability. The smaller inner loop crossover frequencies ω_c^{in} for the lower velocity conditions correspond well with the pilot comments on the *sluggish* handling characteristics of those lower velocity models. Although the combined outer loop quantities correspond

---

[1]Recall that because only two forcing function signals (i_1 and i_2) are inserted the frequency response of the outer loop variable (x_e) includes the response of the middle loop variable (ψ_e). Therefore, the measured frequency response of the outer loop variable is referred to as the *combined* outer loop (§4.2.2).

(a) inner loop   (b) combined outer loop
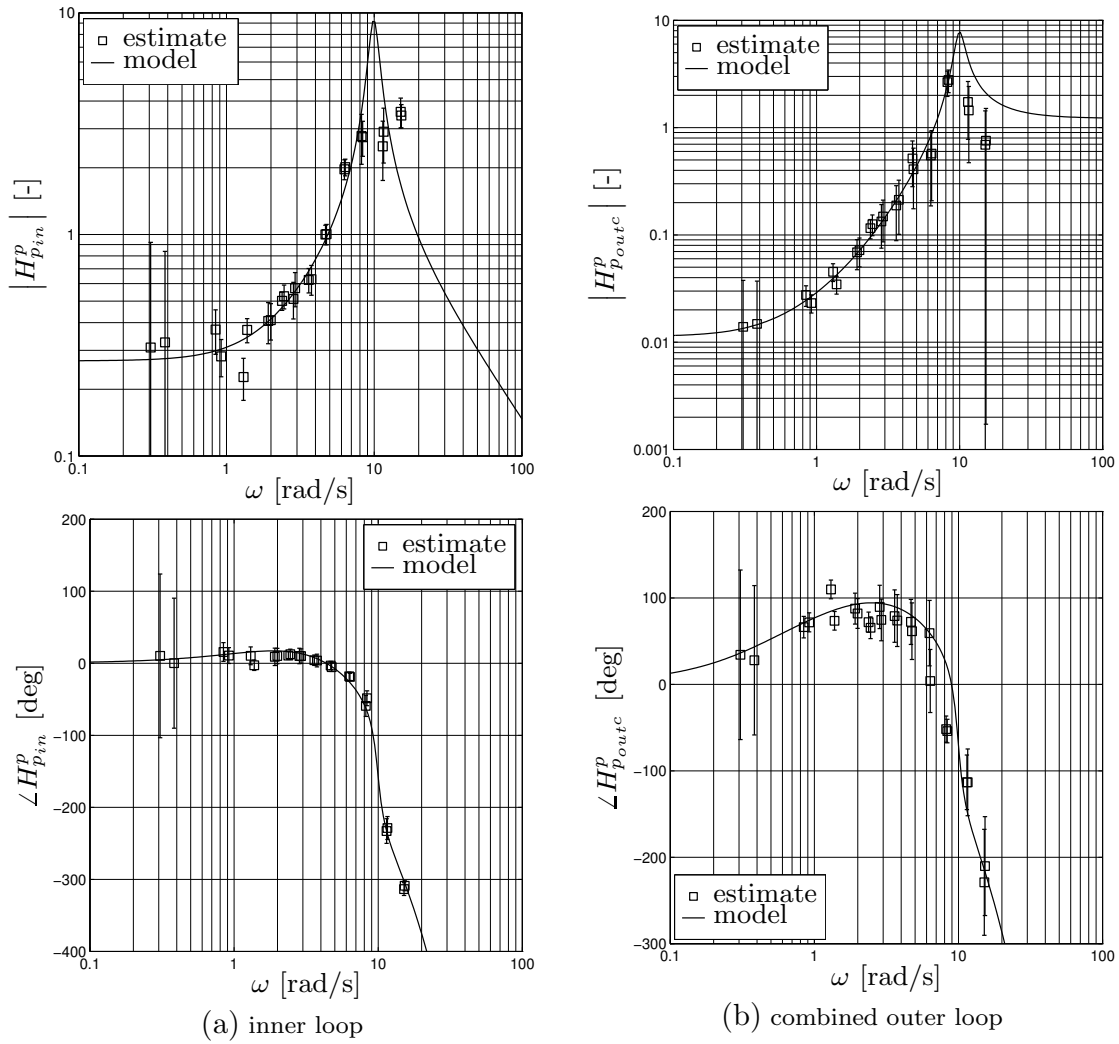
Figure 5.6: Estimated pilot frequency responses for a *parallel* pilot model structure (one subject, one configuration). The lines show the modelled pilot frequency function, using the MLM pilot model (§5.5).

well with the hypotheses, a model parameterization is needed to distinguish between the middle and outer loop closures, i.e. the feedbacks of ψ_e and x_e, respectively.

5.5   Modelling efforts

A mathematical model must be able to describe the trends in the time domain data resulting from the *total* pilot-vehicle system. The estimated frequency responses provide information about the structure and parameterization of the *pilot*-element in the closed loop. The results of two modelling approaches will be described, i.e. the Multi-loop model and the Optimal control model, introduced in Chapter 4, focusing on their applicability.

5.5.1 Multi-loop model

MLM model structure The frequency domain multi-loop pilot model, introduced in §2.5.3, explicitly represents the pilot loop-by-loop feedback. The MLM model for the control of the asymmetric aircraft motion consists of three aircraft loop closures: (i) the roll angle ϕ (*inner* loop), (ii) the heading angle error ψ_e (*middle* loop), and (iii) the lateral position error x_e (*outer* loop) (Appendix E). It is hypothesized that all pilot equalization is present in the inner loop feedback, and that all subsequent outer loops are closed with a proportional gain. Hence, the model structure as such is fixed. The model parameters for each condition are computed using the parameterization method described in Appendix F. Repeating this procedure for all conditions provides insight into the *adaptation* of the modelled pilot control behaviour to the experimental conditions.

MLM parameters The results of the MLM-parameter estimation procedure are illustrated in Figs 5.7 and 5.8 for the inner and outer loops, respectively. Although the pilot *limitation* variables seem to be rather scattered, some trends are apparent, Fig. 5.7(a). For increasing aircraft velocities there is a trend of a lower time delay τ, a higher neuromuscular (nm) bandwidth ω_n and a lower nm damping ζ_n. This indicates that pilots increase or maintain their inner loop phase margin for these conditions. The tunnel size yields a clear trend for the time delay and the nm damping, which both decrease for smaller tunnels. Again, this can be attributed to a pilot strategy of maintaining a sufficient inner loop phase margin. The inner loop lead $\tau_{L_{in}}$ and gain $K_{p_{in}}$ variables, depicting pilot inner loop *equalization*, also show some trends, Fig. 5.7(b). The decreasing lead for larger velocities can be attributed to the decreasing aircraft roll subsidence lag (τ_ϕ) for these conditions, indicated with the shaded areas in Fig. 5.7(b). In Appendix E it is shown that it is advantageous to maintain an inner loop lead that is higher than the inner loop aircraft lag. The decreasing pilot inner loop gain $K_{p_{in}}$ for larger velocities can be attributed to the higher aircraft inner loop gain (K_ϕ) for these conditions. The *antagonism* of the equalization is evident. For the low-velocity conditions, subjects A and B increase their lead and decrease their gain for smaller tunnels, whereas the opposite holds for subjects C and D, marking an inter-subject variation of the inner loop control strategy. The effect of the tunnel size depends on the subject as well as the velocity conditions. A smooth trend is apparent for the larger tunnels, a trend that is interrupted for the smallest tunnel size for all subjects and almost all conditions. This can also be seen, but less convincing, in the pilot limitation variables. The changes in pilot inner loop equalization could indicate a different control strategy for the smallest tunnels.

The parameters determining the outer loops loop closures show clear and identical trends for all subjects (Fig. 5.8). The middle loop gain $K_{p_{mid}}$ determines the bandwidth with which the pilot closes the aircraft heading angle error loop. Two trends are clear. First, the middle loop gain increases for smaller tunnels. Second, they are larger for the higher velocity conditions. The latter effect can be expected because for higher velocities the aircraft middle loop gain decreases, requiring a larger pilot gain to achieve the same band-
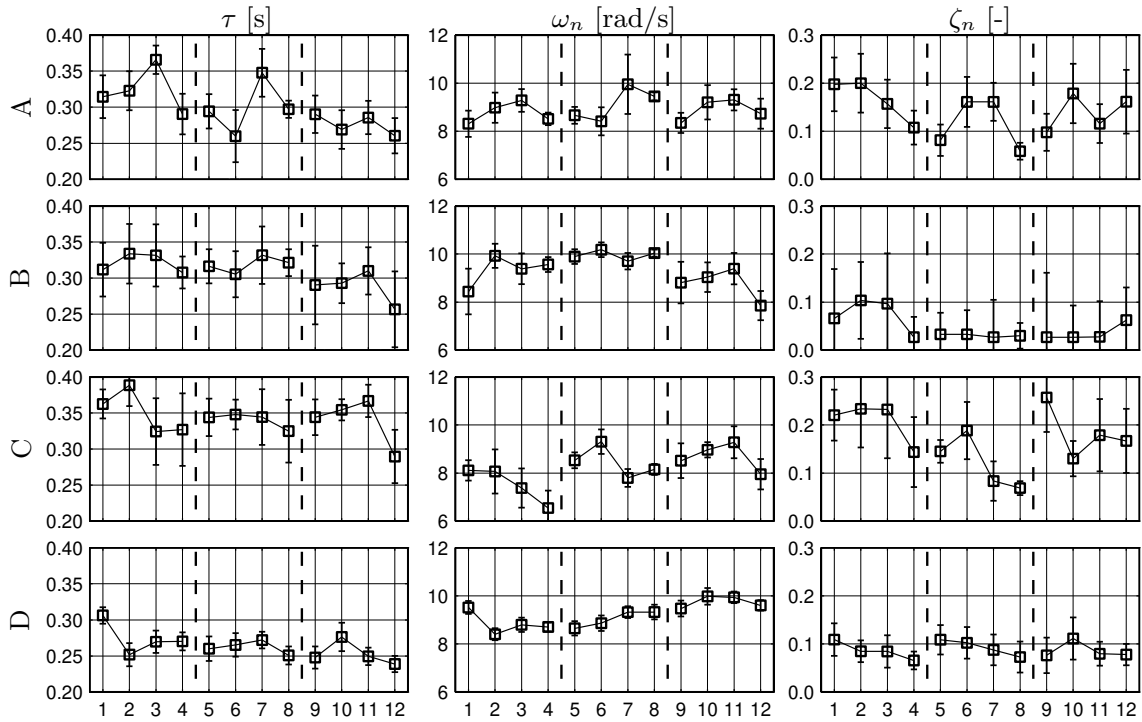
(a) time delay, neuromuscular bandwidth and damping
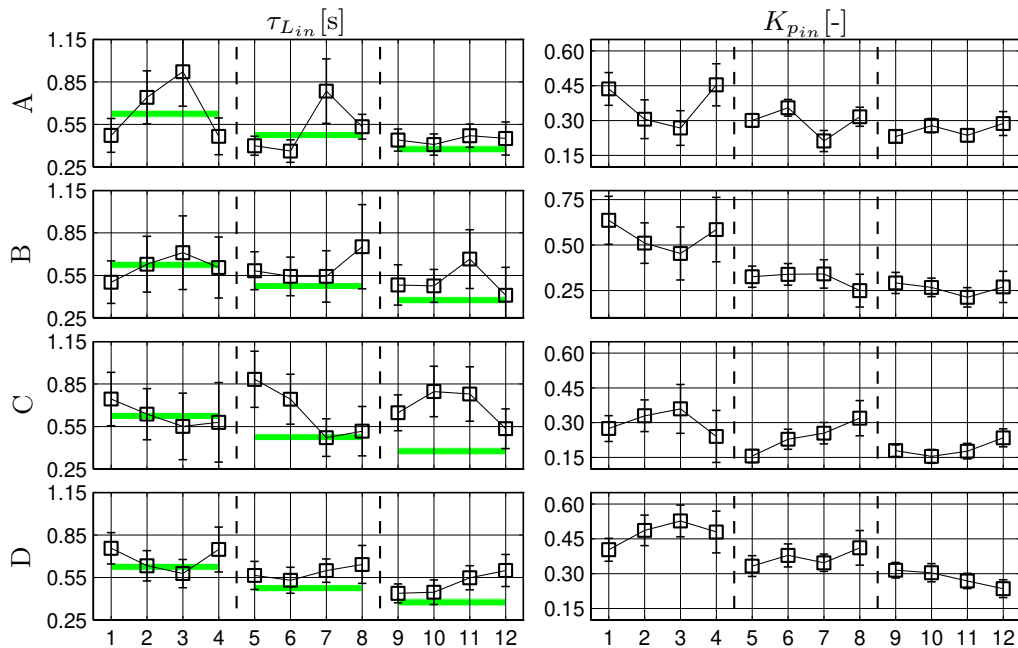
(b) inner loop lead and gain

Figure 5.7: Inner loop MLM pilot model variables (all subjects, all conditions). Here, and in the following, the cross-hairs show the parameter estimation uncertainties according to Cramer-Rao. In the bottom left figure, the horizontal shaded areas show the values of the aircraft roll subsidence lag time constant, τ_ϕ.
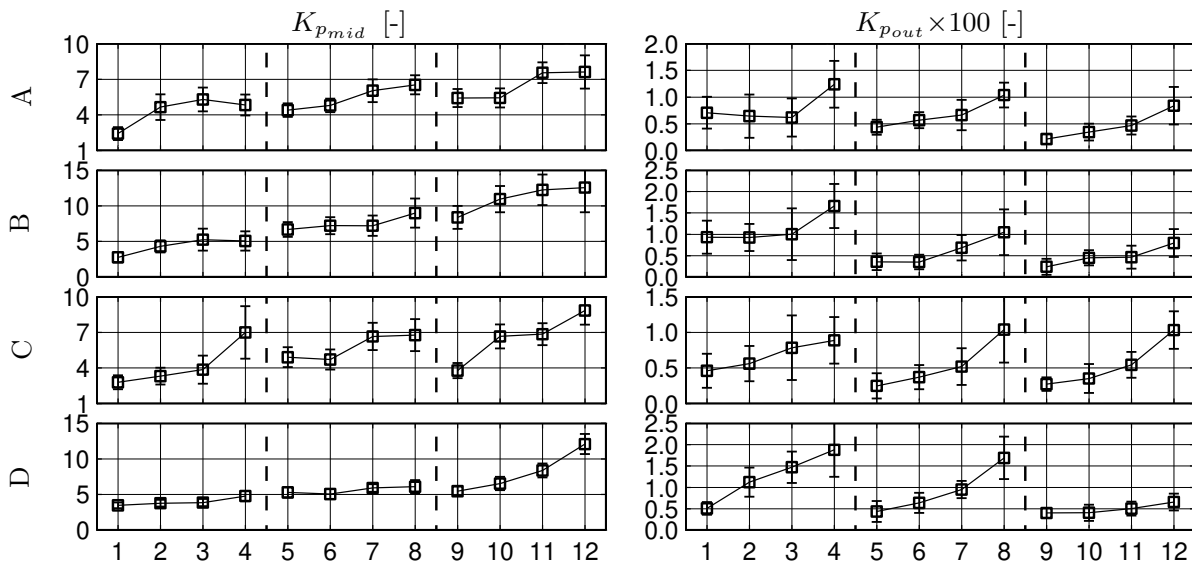
Figure 5.8: The middle and outer loop MLM gains (all subjects, all conditions).

width. The outer loop gain $K_{p_{out}}$ determines the bandwidth with which the pilot closes the aircraft position error loop. Again, two trends are clear. First, it increases rapidly for smaller tunnels. Second, the outer loop gains become smaller for the higher velocity conditions. The latter effect can be expected because for higher velocities the aircraft outer loop gain increases, requiring a smaller pilot gain to achieve the same bandwidth.

Summarizing, the pilots adapt to *all* experimental conditions. Whereas similar effects are found for the outer loop variables, the inner loop results show more inter-subject variation. This can be attributed to two different causes. First, the inner loop mainly serves the outer loops and there exist several ways to do this. Second, the pilot *task* of following the trajectory as accurately as possible mainly affects the outer loop feedbacks.

MLM results: crossover frequencies and phase margins   The parameterized MLMs are combined with the aircraft models to determine the bandwidth and stability characteristics of the closed loop pilot-vehicle system. Figs 5.9(a) and 5.9(b), showing the crossover frequencies and phase margins for the inner and combined outer loops, respectively, illustrate that the MLMs describe the trends in the measured data quite well, especially for the combined outer loop. The parameterization allows the middle and outer loop closures to be reconstructed from the single estimated combined outer loop frequency response. The resulting middle and outer loop crossover frequencies and phase margins are shown in Fig. 5.10. The trends of the crossover frequencies ω_c^{mid} and ω_c^{out} are similar to those observed for the middle and outer loop gains, respectively, Fig. 5.8. The increasing outer loop crossover frequency for smaller tunnels requires a considerable increase in the middle loop bandwidth. Especially for the smallest tunnel the difference between ω_c^{mid} and ω_c^{out} becomes very small, indicating that in these conditions the heading angle error feedback and the position error feedback become equally important. Whereas the increasing
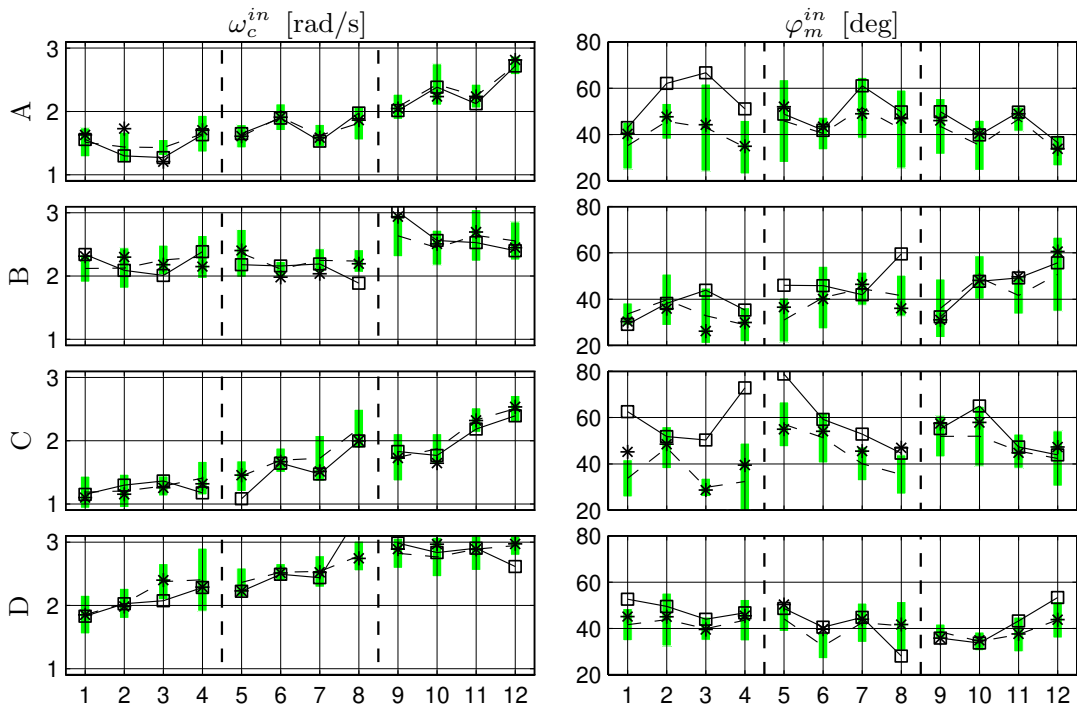
(a) inner loop
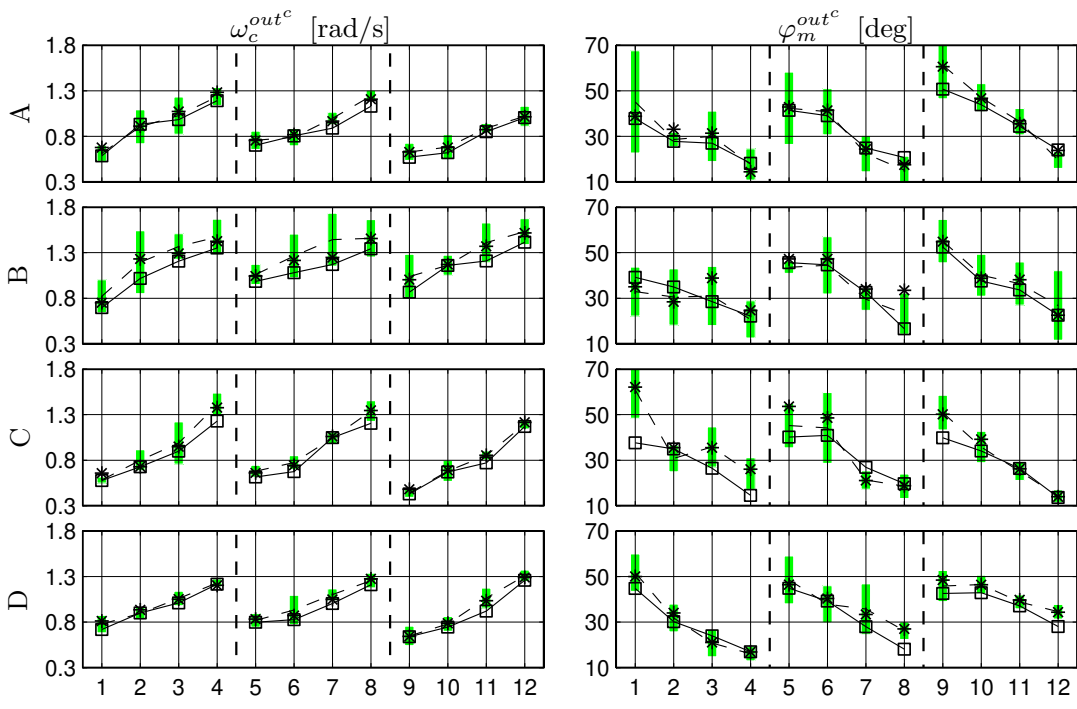
(b) outer loop (combined)

Figure 5.9: Crossover frequencies and phase margins (all subjects, all conditions). The shaded areas show the uncertainty regions of the *raw* frequency response data, their averages connected with the dashed line. The '*'-symbols show the quantities for the *averaged* frequency responses, whereas the squares show them for to the MLMs.
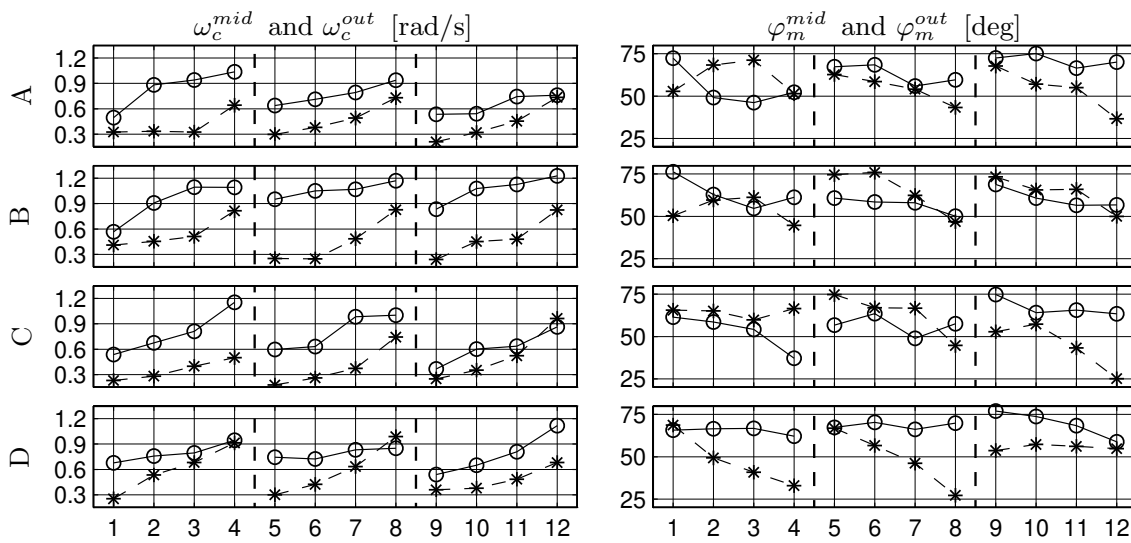
Figure 5.10: Crossover frequencies and phase margins of the middle ('o') and outer ('*') loops, following the MLM analysis (all subjects, all conditions).

crossover frequencies are accompanied by a sharp reduction in phase margin for the outer loop, the middle loop phase margin remains more or less constant.

Concluding, the outer loop position error feedback becomes of higher bandwidth when the tunnel size is reduced. This requires a higher bandwidth of the middle and inner loop feedbacks. The data shows that this requirement is fulfilled while at the same time the operator tries to maintain sufficient stability in the inner and middle loop closures. The potential problem of instability occurs mainly in the outer loop feedback.

MLM results: time domain data   Once the MLM parameters are computed, the total pilot-aircraft system can be simulated (including the disturbances, but without the pilot remnant) to obtain results in the time domain. Fig. 5.11 shows the time histories of some of the aircraft motion referents that result from this procedure, together with those that were actually measured in the experiment. Generally, the MLM time responses mimic those that are measured experimentally, especially for the outer loop variables ψ_e and x_e. The finding that the aileron control signal does not resemble the measured responses very well can be attributed to the assumption that pilot remnant is zero in the MLM simulation. Hence, the figure illustrates clearly that the effects of pilot remnant are attenuated when moving from the inner to the outer loop signals. The computation of the model time histories provides a method for determining the STDs of all signals in the closed loop. Another procedure is to compute these quantities directly in the frequency domain, a much faster method that is applied here (Appendix F). Because the frequency domain data is obtained by discrete-Fourier transforming the *averaged* time histories, reducing the remnant contribution to the signal variance, the STDs do not resemble those measured in the experiment, but rather those of the *averaged* time domain data .

(a) aileron   (b) roll angle   (c) track-angle error   (d) cross track error
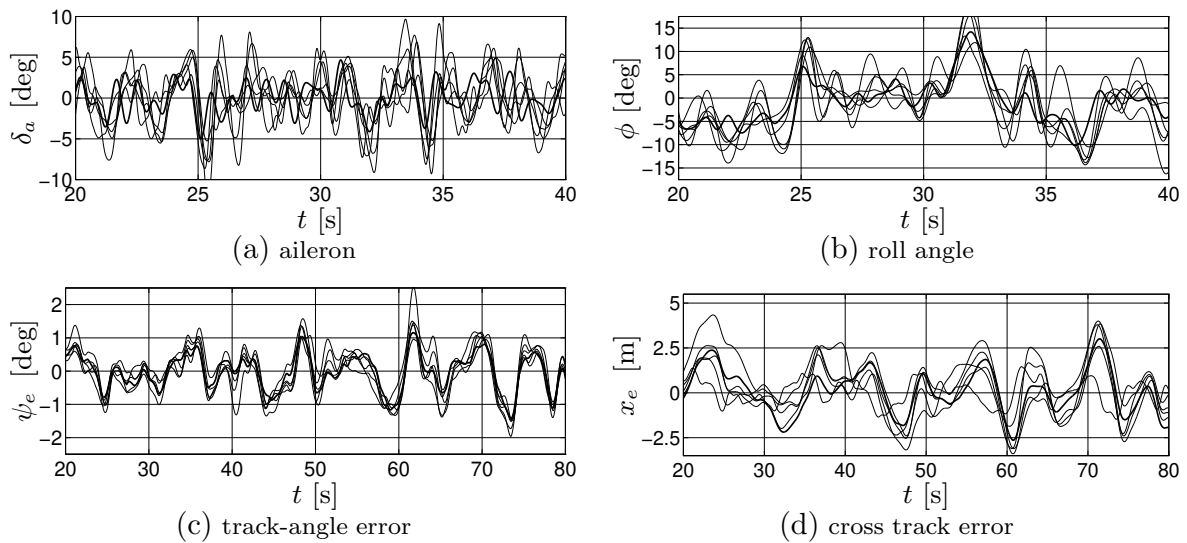
Figure 5.11: Time histories example (one subject, one condition). The thin lines show the 5 measured responses; the thick line shows the response of the MLM model.

5.5.2   Optimal control model

OCM model structure   The OCM pilot model has one output signal (δ_a) and two input signals: the roll angle ϕ and the lateral position error x_e. The implicit OCM-assumption that pilots also perceive the derivatives of these quantities yields a four-element observation vector. The OCM consists of a rather large number (twelve) of parameters: the time delay τ, the neuromuscular lag τ_N, the motor noise ratio ρ_u, four observation noise ratios ρ_{y_i}, the control input weighting R and the four elements of the weighting matrix Q_{y_i}. The OCM model parameters are determined using the same parameter estimation procedure as used before. In addition to the use of the estimated pilot frequency responses, the optimization procedure also incorporated the time domain data (i.e. the variances), resulting in an extended minimization criterion (Appendix F). Despite these efforts to increase the amount of empirical a priori information, the OCM parameter estimation procedure turned out to be quite problematic. It was impossible to obtain a consistent estimate of the whole set of OCM parameters, and the number of free parameters had to be decreased considerably.

Limiting the number of OCM model parameters   The motor noise ratio ρ_u was the first parameter to be fixed.[2] Furthermore, because the task of the pilot was to optimize the path-following performance, the weightings on the inner loop observations (ϕ and $\dot{\phi}$) were set to zero. This selection is not according to the 'common' method of setting the elements of the weighting matrix equal to the reciprocal values of what are considered the 'maximum allowed' variances. The question seems justified what these 'maximum allowed' variances are for these conditions. The trend in these variances are actually one of the

---

[2]To -25 [dB], which is a typical value used in most of the OCM applications (Innocenti, 1988).
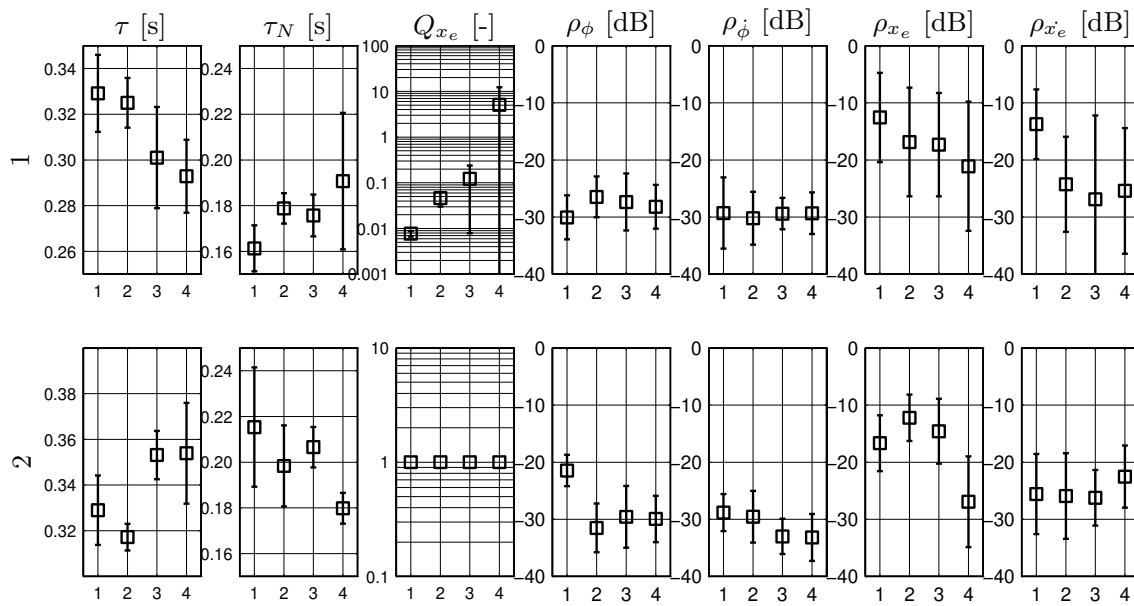
Figure 5.12: The main OCM variables for the two a priori parameter estimation Assumptions 1 (top) and 2 (bottom). The data are shown for one subject, conditions 1–4.

main *outcomes* of the experiment. Anyway, with this as a new starting point – nine free parameters – the procedure was repeated. The attempts were still in vain.

Limiting the number of OCM model parameters once more Extensive parameter sensitivity studies indicated that the *regulator* and the *observer* part of the OCM could both account for the trends in the experimental data. This is consistent with one of the main findings of a theoretical assessment of the identifiability of the OCM parameters (van Wijk & Kok, 1977). The finding that pilots increase their outer loop gains for smaller tunnels could be accounted for in the OCM in two ways: (i) by fixing the observer variables (noise ratios) at constant 'typical' levels and increasing the regulator weighting on the lateral position error; (ii) by fixing the regulator weightings and increasing the observation noise ratios on the observed lateral position and its derivative. Both the assumptions led to a description of the measured data with approximately the same level of accuracy. Similar to the conclusions in (van Wijk & Kok, 1977) it was reasoned that to improve the chance of success of the parameter estimation procedure, the remaining variables in either the OCM regulator or the observer were to be fixed beforehand. It was hypothesized that fixing the elements in the weighting matrix Q would be the best alternative, allowing the observation noise ratios to vary freely, which could allow a computation of the attentional fractions allocated to the various displayed variables. Numerous assumptions can be made on how a pilot subjectively or objectively sets the observation and control input weighting matrices Q and R. The discussion below will be limited to two cases (with $Q_{\dot{x}_e}=0$): (1) $R=1$, Q_{x_e} is free, yielding seven free parameters (τ, τ_N, Q_{x_e} and ρ_{y_i}); and (2) $R=0$, $Q_{x_e}=1$, yielding six free parameters (τ, τ_N and ρ_{y_i}). The parameter estimation procedure worked

satisfactory this time (Fig. 5.12). The parameter estimates for Assumption 1 show that especially the weighting Q_{x_e} increases for smaller tunnels, indicating a larger emphasis on minimizing the position errors. The outer loop observation ratios also increase for smaller tunnels. The uncertainty in the estimated parameters[3], however, is rather large, which is an indication of the insensitivity of the OCM parameters for the experimental data. The results for Assumption 2 show that, generally, all variables change and, most importantly, show different trends. The inner loop variables show opposite trends with respect to Assumption 1. The outer loop observation noise ratios do show the anticipated trend of becoming smaller for decreasing tunnels (i.e. smaller observation errors). The OCM allows a computation of the so-called total level of attention to the task (ρ_0) and the fractions of attention to the displayed variables (f_i), a procedure that is usually conducted the other way around (Appendix E). The nominal level of attention was rather high ($\rho_0 \approx$ -30 [dB]) compared to the typically reported range of -18 to -25 [dB] (Wewerinke, 1989), and remains almost constant. The fractions of attention indicated that virtually *all* attention is allocated to the inner loop observations (ϕ and $\dot{\phi}$), whereas the attention to the position error remains remarkably small, even for smaller tunnels.

Conclusion The application of the OCM provided evidence, albeit heuristic, for its over-parameterization characteristics. Although it is often suggested that the OCM parameters can be found using the parameter-setting procedures as proposed in (Kleinman & Baron, 1971), it is certainly not true that these parameters simply 'evolve' from the type of the experiment and the pilot's task. The experimenter must initialize and limit the model parameters according to some *inevitably subjective* assumption(s) (Kok & Stassen, 1980). Imposing constraints on the model parameters, however, also significantly affects the outcomes of the OCM. Although this is a trivial statement, it marks the heart of the problem encountered here: how far can one go in pre-defining a model to obtain the 'desired' model results, and, moreover, what does this say about the *predictive* qualities of that particular model? Here, two different a priori assumptions led to different sets of parameter estimates that could *both* describe the experimental data *adequately*. This puts serious doubts upon the applicability of the OCM to the experiment described in this section and a further elaboration was considered to be a waste of time.

5.6 Retrospective

5.6.1 Discussion of the results

Analysis

The experimental hypotheses could all be validated successfully, again showing the functionality of the tunnel size in manipulating the level of path-following accuracy. Independent of the aircraft velocity a reduction in tunnel size yields improved path-following performance, increases pilot control activity (Fig. 5.4) and leads to higher levels of pilot

---

[3]The computation (Cramer-Rao) of these uncertainties were based on the frequency domain data only.

workload (Fig. 5.3). The variation in aircraft velocity leads to different levels of control activity, roll angle variations and heading angles (Fig. 5.4). The trends in these levels correspond well with the pilots' judgements that the higher velocity conditions were easier to control than the low-velocity condition. Pilot comments regarding the control strategy and the use of the optical cues corresponded well with the pre-experimental cue analysis. The frequency domain data generally support the time domain results (Fig. 5.9).

MLM results The MLM application can be considered to be successful. A simple model consisting of only seven parameters could describe the experimental data satisfactory. The parameters could all be estimated from the available data with a reasonable accuracy. The course of the MLM parameters as a function of the experimental conditions showed that some of the adaptation could be accounted for (and can also be predicted, Appendix E), by the properties of the aircraft dynamics. The adaptation in the outer two loops was consistent and showed similar trends for all subjects (Fig. 5.8). This can be attributed to the task, which emphasized path-following performance. Smaller tunnels yield higher levels of position error feedback bandwidth, leading to increasing bandwidths of the inner loop (roll angle) and middle loop (heading angle error) loop closures. Whereas the stability margins of the latter loop closures remain fairly constant, a decreasing tunnel size leads to a significant reduction in the position error feedback stability (5.9 and 5.10). The inner loop equalization parameters showed more inter-subject variation, indicating that more ways exist to provide a well-chosen attitude control loop (Fig. 5.7). The inner loop variables indicate a pilot strategy of maintaining a relatively constant phase margin (i.e. stability) for the control of attitude, independent of tunnel size. For the smallest tunnels the bandwidth of the position error feedback becomes equal or even larger than that the heading angle error feedback (Fig. 5.10), which suggests that the pilot strategy changes from successively closing a number of loops to a controller that uses heading angle and position errors in a *parallel* fashion.

Cue dominance effects The MLM parameters mainly determine the bandwidth and stability of the pilot loop closures. They do not give information about the perceivability or usability of the various optical cues. E.g., consider the heading angle error feedback. The cue analysis revealed that this variable can be perceived either from the location of the infinity point – a cue that does not depend on tunnel size – or from the splay angle rates – a cue that does depend on tunnel size. The performance data show that the STDs of the heading angle error remain relatively *constant* for all tunnel sizes. The modelling data show that the bandwidth of the heading angle error feedback *increases* for smaller tunnels whereas the phase margin remains the same. These results can be explained by hypothesizing that pilots do not minimize the heading angle error as such, but rather *use* this variable in their attempts to minimize the lateral position error. Consequently, the *relative* importance of the two sources of information can *not* be inferred from the present data. Evidence for possible cue-dominance can only be examined when either manipulating one of these cues or by re-defining the pilot's task. The same holds for the inter-cue dominance concerning the cues conveying a position error. The data suggest

that its perceivability increases when the size of the tunnel is reduced. The cue analysis revealed that the relative lateral displacements of the tunnel frames and the altitude poles were independent of the tunnel size. These variables, however, are difficult to perceive for small tunnels. In these conditions the splay angles – scaled by the tunnel size – are the most effective indicators for a position error because of the higher gain. For larger tunnels the splay gains decrease, which, together with the improving perceivability of the displacement cues, could mean that in these cases the pilots prefer the latter cues, together with those conveyed by the altitude poles. The data suggest that the functionality of the splays reduce for larger tunnels and that the other tunnel cues become equally or even more attractive.

OCM modelling results   Even for the elementary experiment considered here the application of the OCM was not successful. Its application required fundamental a priori assumptions concerning the model parameters. Furthermore, because the model could describe the experimental data in two essentially different ways, a further analysis was abandoned. This is a setback, especially because it was expected beforehand that the OCM could incorporate the tunnel size effects in a conceptual manner. The experience with the MLMs, failing to assess a cue-dominance hierarchy, puts more doubts upon the *need* for using another pilot model. Assume that the OCM application *would* have been successful, resulting in for instance the intellectually attractive trend of a decreasing position error observation noise ratio for smaller tunnels. The question of what this means for the set of optical cues remains justified. Isn't it just another way of stating that the position error feedback bandwidth increases? And does this really say anything more about the dominance of certain cues over others? The answer is no. *In theory*, one could increase the observation vector of the OCM with some of the individual cues for a position error. *In theory*, the OCM could then discriminate between these cues, indicating which cues are important and which cues are not. When considering the significant identification problems that are already encountered when *only* modelling the *main* feedback loops, it is clear that this would be an unfeasable option.

Summarizing, the MLM and the OCM modelling approaches *fail* in determining the *relative usability* of the set of optical cues. Theoretically, the cue-dominance could be analyzed by incorporating the individual loops in the model structure. The identifiability of the resulting increasing set of parameters, however, would be impossible. Thus, although the models allow insight into *how* a pilot adapts his control behaviour, the question *why* this adaptation happens must still be *inferred* from the data. The cybernetic approach does result, however, in a considerably larger amount of quantitative evidence on which this inference can be based. E.g., the increasing importance of the heading angle error feedback loop for smaller tunnels (Fig. 5.10) is unexpected when considering the course of their STDs (Fig. 5.4(e)). Another finding is that the adaptation of control behaviour is not the same for all pilots, even when considering such a straightforward experimental variable as the tunnel size. Whereas the outer loops are closed in a consistent manner, the pilot inner loop equalization is conducted according to different strategies. This is disappointing from
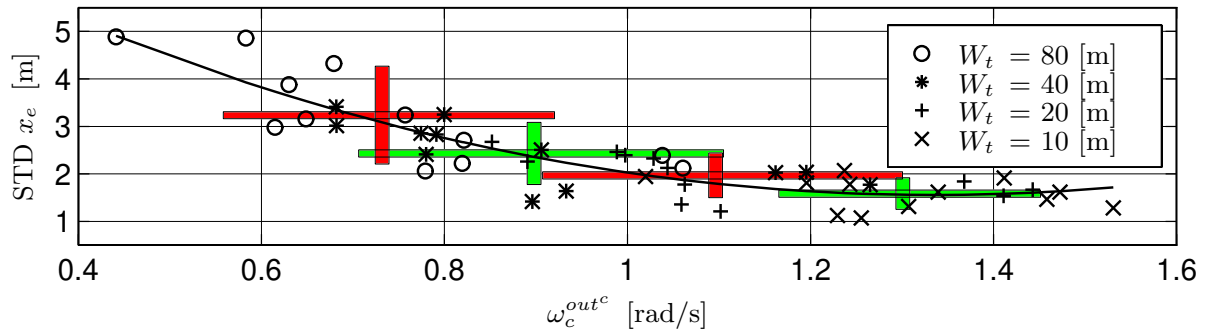
(a) performance vs. the combined outer loop crossover frequency
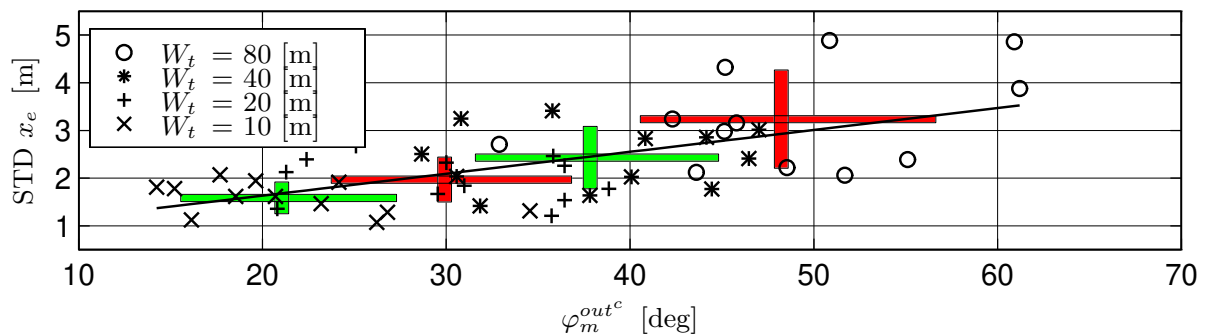
(b) performance vs. the combined outer loop phase margin

Figure 5.13: Path-following performance vs. combined outer loop bandwidth and stability (all subjects, all conditions). The filled rectangles show the mean and standard deviation of the variables shown on the ordinate and abscissa.

the perspective of generalizing the results found in the experiment, but exemplifies the difficulty of generalizing human behaviour.

Synthesis

The experimental findings reported in literature (Wilckens, 1973; Grunwald, 1984; Theunissen, 1995) are consistent in their statements concerning the tradeoffs between performance, pilot workload and system stability. These findings are all based on performance-related data. Pilot workload has not been assessed explicitly, nor has there been a control-theoretic analysis of pilot control behaviour for the varying tunnel size conditions. Moreover, an important question remains unanswered, i.e. what are the *limits* in defining a particular tunnel size? The RNP example (Fig. 5.1(a)) shows that limitations are put on the required path-following performance. Experiments confirm the statement that there is a direct relation between the path-following accuracy and the tunnel size. The performance data (Fig. 5.4) suggest that the tunnel size can be decreased further to gain an even better performance, at the cost of some increase in control activity. The data state nothing about any *margins*, or *limits*. Although Wilckens (1973) hypothesized a deterioration of

performance when decreasing the tunnel size beyond a certain level, no further analysis has been reported. The cybernetic approach *does* allow such a control-theoretic analysis. Consider Fig. 5.13(a) in which performance (expressed in the STD of the position error) is shown as a function of the combined outer loop crossover frequency. For the larger tunnels, performance is low and so are the crossover frequencies. Decreasing the tunnel size increases the bandwidth of the position error feedback, yielding an increased performance. This relation, however, is non-linear: the bandwidth must increase more and more to obtain an equivalent increase in performance. A further reduction in tunnel size does not lead to an improved performance at all: the pilot/aircraft system becomes *saturated*. Fig. 5.13(b), showing the performance as a function of the combined outer loop phase margin, marks a significant reduction in closed loop stability for smaller tunnels. Recall that a phase margin of 20 [deg] is generally considered a minimum, even in single-axis compensatory disturbance tasks (van der Vaart, 1992). Hence, from a stability point of view, further decreasing the tunnel size is undesirable and should be avoided.

Summarizing, stability and performance must be regarded as equally important. A tunnel size that is too small yields ill-damped closed loop control dynamics that should be prevented from a stability (and thus performance), but especially a *safety* point of view. In such critical tasks as approach and landing considerable – robustness – margins should exist with respect to the stability of the pilot/aircraft control system. The cybernetic approach can be used to obtain guidelines concerning performance and stability requirements with a tunnel display in a conceptual manner (Mulder & Mulder, 1998).

5.6.2 Conclusions and recommendations

Conclusions

- The experimental findings support the hypotheses that a reduction of tunnel size leads to increasing performance, control activity, and workload.
- The aircraft velocity affects pilot control behaviour in a predictable fashion, having only a marginal effect on system performance and stability.
- The MLMs are relatively simple descriptive models of pilot control behaviour that are able to *describe* the time and frequency domain data in a satisfactory manner, with only a limited number of parameters.
- The modelling approach using the OCM was problematic for reasons of parameter identifiability. The problem that the OCM is overparameterized can only be circumvented by restricting the model parameters according to some *inevitably subjective* assumptions.
- The modelling efforts allow the determination of the principal feedback loop closures including their bandwidth and stability properties. This extends the understanding of pilot control behaviour beyond the knowledge obtained with conventional methods.
- The modelling results indicate that decreasing the tunnel size yields an increasing position error control bandwidth. This demands a considerable increase in the inner and middle loop bandwidth as well. While the stability of the latter two feedback loops remains

fairly constant, the stability of the position error feedback deteriorates for smaller tunnels.

- The MLMs show that pilot adaptation in the outer loop feedbacks is consistent. The inner loop equalization variation suggests that considerable freedom exists in closing the attitude control loop. This variation, even in an elementary experiment as considered here, impedes the generalization of the experimental findings.

- No attempt was made to explicitly include the pilot's observation process and the effects of the tunnel characteristics on this process in the models applied here. Although the models provide additional quantitative evidence for *inferring* the effects of tunnel design parameters on pilot behaviour, the inference procedure remains a difficult task.

- Tunnel size guidelines must specified according to two principles. First, the pilot/aircraft system should have a *consistent* performance. Second, the pilot/aircraft system should inherit a *sufficient level of stability*. The cybernetic approach can be used to obtain performance and stability guidelines in a conceptual fashion.

Recommendations

- Additional experiments should be conducted in a moving-base flight simulator. The presence of motion has a number of consequences. First, it improves the realism of the task, facilitating the generalization of the experimental results. Second, because pilots use the motion cues to improve their inner loop attitude control, the additional feedbacks should be modelled too (van der Vaart, 1992; Hosman, 1996). It can be hypothesized that the 'extra' phase margin in the attitude feedback allows a higher bandwidth. The outer loops can take advantage of the enhanced attitude control, improving performance.

- Guidelines concerning the selection of a tunnel size in a particular situation must be obtained for an array of different aircraft, aircraft configurations and types of aircraft control augmentation systems, including effects of weather.

- The applicability of the cybernetic approach must be assessed in other situations than the one described here. For instance, the effects of larger, heavier – and thus lower bandwidth – aircraft on the identification techniques need to be examined further.

- The modelling approach does not succeed in identifying the cue dominance hierarchies. These effects can be examined by properly *isolating* cues from others through a clever manipulation of the display. This procedure will be applied in Chapters 7, 8 and 10.

Chapter 6

The effects of the viewing distance

6.1 Introduction

A fundamental issue of pilot behaviour with a tunnel display is that of *preview*. Although it can be hypothesized that pilots focus their attention on some part of the tunnel ahead, this is a coarse abstraction of reality. Rather, findings in literature suggest that they tend to use the entire preview of the trajectory ahead (Gordon, 1966b; Grunwald & Merhav, 1976; Land & Horwood, 1995). A pilot can be *forced* to put attention on a limited part of the trajectory some distance ahead, however, by constraining the display *viewing volume* to that particular viewing distance. This will be the approach adopted here, with the purpose of examining the consequences of showing such a highly-limited part of the tunnel for pilot control behaviour. In §6.2 the background of the research into the viewing distance will be discussed, clarifying the objectives of the investigation. Experiment X2 (§6.3) is set identical to the one discussed in the previous chapter. Instead of varying the tunnel size, now the viewing distance is manipulated, allowing a comparison between the *full-preview* situation and the situation in which the preview is *limited* to only a very small part of the tunnel. The experimental results and the modelling efforts are described in §6.4 and §6.5, respectively, followed by a retrospective in §6.6.

6.2 Background

Previous studies

The viewing distance is closely related to the concept of *preview*, discussed in Chapter 2. The preview of the trajectory ahead mainly serves the human's need for *anticipatory information*. This finding is supported by many experimental research efforts that showed that

drivers shift their gaze from looking close-by in order to align their vehicle with the road, to looking farther away to anticipate future course deviations and changes in the trajectory. The *dual-mode* driver modelling concept has become a standard approach, incorporating a compensatory and an anticipatory controller (Weir & McRuer, 1968; McRuer et al., 1977; Donges, 1978; Reid, 1983).

The aimpoint model Despite the fact that drivers tend to use the whole preview ahead of their vehicle, many modelling attempts applied only a single viewing distance (Wohl, 1961; McRuer et al., 1977; Baxter & Harrison, 1979). This concept is rooted in the hypothesis that drivers adopt a viewing distance D_v ahead of their vehicle that is proportional to the vehicle velocity U_0 and the so-called mean response time τ, i.e. $D_v = \tau U_0$ (Wohl, 1961). It is generally referred to as the *aimpoint* model of driver control (Baxter & Harrison, 1979), in which a driver responds to the angular deviation of the road's centerline from the vehicle's present heading at some viewing distance ahead. The aimpoint model has received much attention and showed considerable success in describing automobile driver behaviour (Reid et al., 1981). The relationship between the preview distance D_v and the vehicle's velocity is examined in many studies with either confirming (Kondo & Ajimine, 1968; Land & Horwood, 1995) or negating (Gordon, 1966a; McLean & Hoffmann, 1973) results. Furthermore, the preview times reported varied also with the type of the changes in the trajectory to be followed: for straight trajectories the preview times were larger and more consistent (7–9 [s]) than for trajectories that contained tight curves (2–4 [s]) (Kondo & Ajimine, 1968; McLean & Hoffmann, 1973).

The *one-point* viewing model The aimpoint model corresponds with the *one-point* viewing model of Grunwald and Merhav (1976). The linearized expression for the displacement of the projected trajectory, ϵ, at distance D_v, on the viewplane is given by:

$$\epsilon = \kappa \left(\psi_e + \frac{x_e}{D_v} \right). \tag{6.1}$$

This quantity is determined by the track-angle error ψ_e and the cross-track error x_e, with the latter scaled by the viewing distance. κ is a projection-related gain, see §3.3.1. Grunwald and Merhav (1976) reported that the one-point viewing model is sufficient to describe pilot behaviour for fixed (and restricted) distance viewing, but not for the full-preview task. In this task, a *two-point* viewing model was developed which improved the description of pilot control behaviour considerably. This is not surprising, however, since perceiving the angular deviation ϵ at two viewing distances would enable a pilot to *differentiate* between the track-angle error ψ_e and the cross-track error x_e, allowing them to successively close these *two* feedback loops, corresponding with the 'normal' pilot control strategy (Mulder, 1994). The relative success of the single-point viewing or aimpoint models can be attributed to the *quickening*-qualities (Birmingham & Taylor, 1954) of Eq. 6.1: closing the ϵ-loop is similar to a well-damped feedback of the lateral position error. This characteristic is the main virtue of several alternative pictorial display designs (Adams & Lallman, 1978; Hynes, Franklin, Hardy, Martin, & Innis, 1989).

(a) limiting the viewing volume

D_v [m] $\rightarrow$

| 100 | 200 | 400 | 800 |

(b) tunnel images for a limited viewing volume
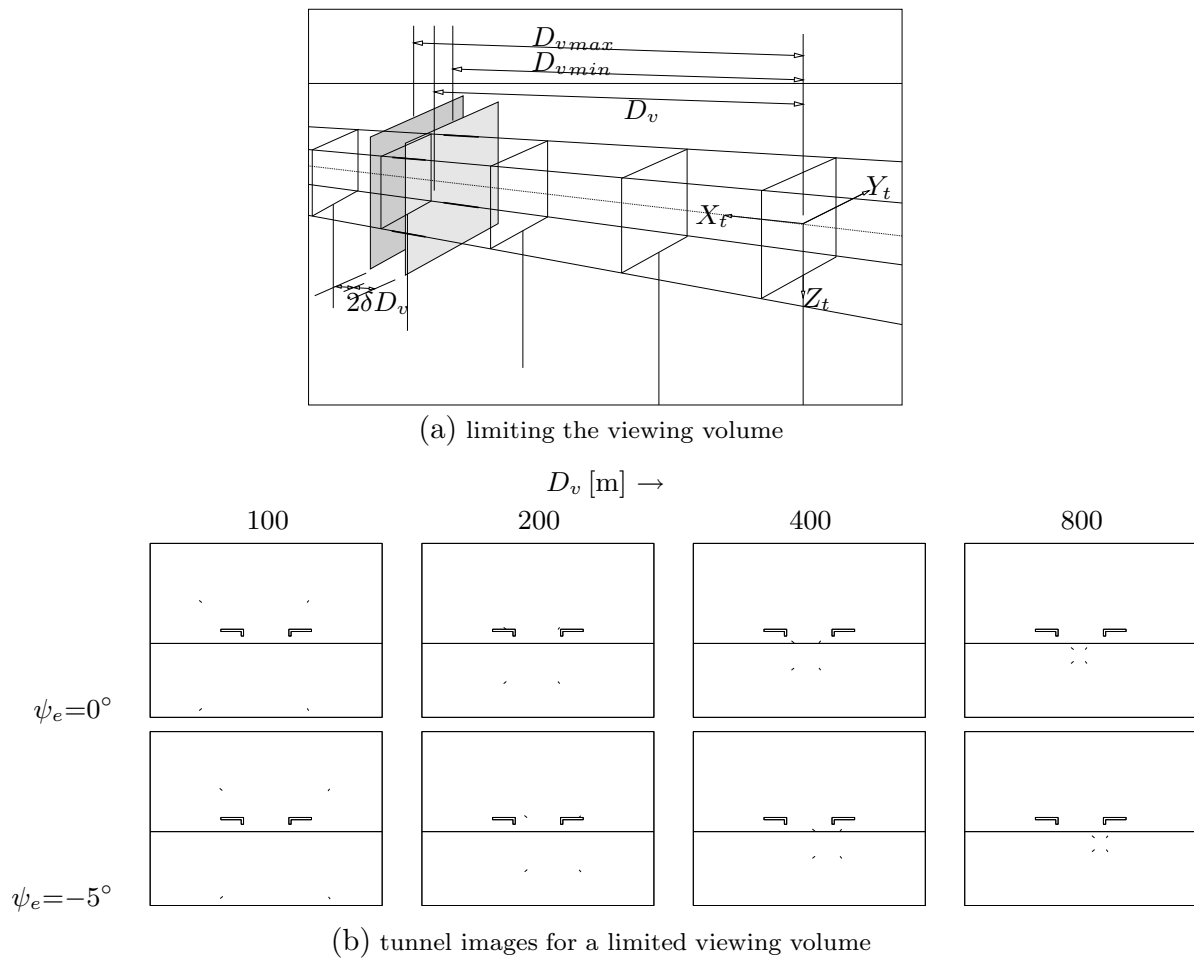
Figure 6.1: Limiting the viewing volume of the tunnel display to a small area around a viewing distance D_v (top). Defining the minimum and maximum viewplanes at a distance δD_v from D_v yields the projection on the viewplane of only the four line segments, resulting in the display images of the two bottom rows. The figures depict a situation for four viewing distances D_v (x_e=+5 [m]; ψ_e= 0, -5 [deg]; W_t=H_t=40 [m]).

Limiting the viewing volume

The viewing distance as a design variable   The available trajectory preview is determined by the minimum and maximum viewing distances D_{vmin} and D_{vmax}. The discussion of the optical cues in Chapter 3 revealed that the aircraft position errors with respect to the trajectory are conveyed by the translation of *nearby* sections of the tunnel on the display. The aircraft attitude errors are coded in the translation of sections of the tunnel that are located *far* away. Hence, D_{vmin} determines the *resolution* with which the position error, x_e, is presented on the display and D_{vmax} determines the perceivability of the heading angle error ψ_e. Despite the fact that providing a full trajectory preview seems advantageous, there are some constraints. First, presenting the entire trajectory to be flown can lead to *display clutter*. Second, when the position measurement functions of
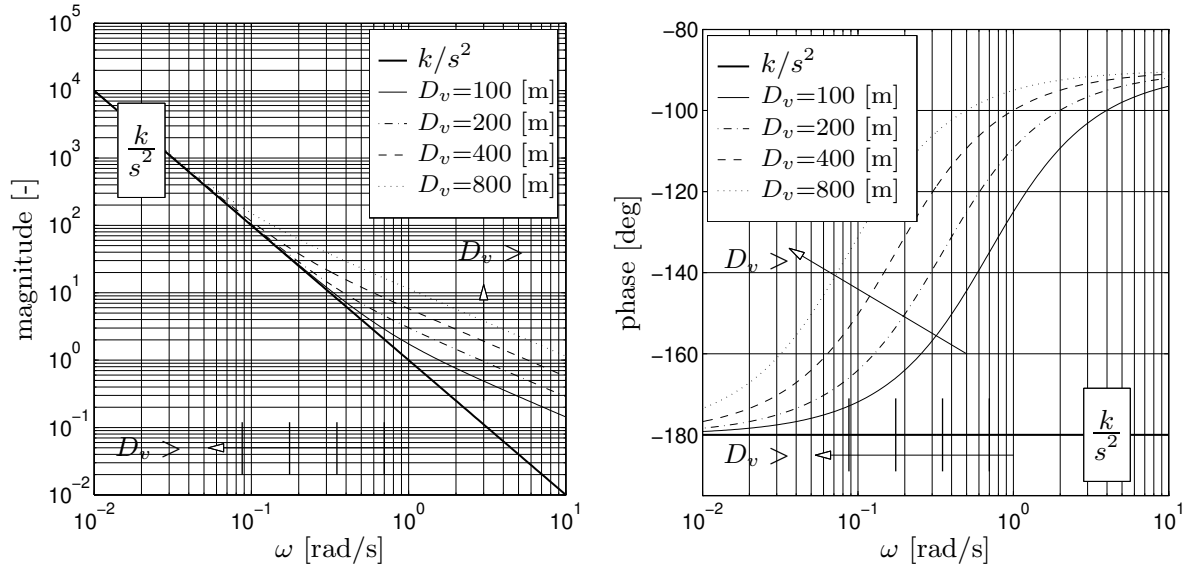
Figure 6.2: The equivalent outer loop ϵ dynamics for a velocity of 70 [m/s], as a function of the viewing distance D_v.

the aircraft avionics systems are too in-accurate (or too slow), this can lead to *jittering* motions of the tunnel on the display, especially at smaller viewing distances. These factors could lead to a tunnel display design in which the preview ahead is limited.

A single viewing distance   Presenting only a part of the tunnel corresponding with a particular viewing distance D_v yields a *one-point* viewing situation (Fig. 6.1(a)). The displacement of the restricted tunnel image with respect to the viewplane center is characterized by ϵ. Fig. 6.1(b) shows the tunnel image restricted around a set of viewing distances D_v. The effect of a position error is strongest for the small viewing distances and is attenuated when the viewing distance increases, Eq. 6.1. The heading angle error is apparent especially for larger viewing distances. For a smaller viewing distance the effects of a position error and an attitude error are summed. Some combinations of x_e and ψ_e result in a displacement ϵ that is zero: $x_e = -D_v\psi_e$, or, since $\dot{x_e} = V_{tas}\psi_e$ (when $\beta = 0$, i.e. no slip): $\frac{x_e}{\dot{x_e}} = -\frac{D_v}{V_{tas}}$. This expression will be discussed further below.

Dynamic properties of the one-point viewing distance   In the *one-point* viewing or aimpoint model, the operator applies the angular deviation ϵ of the visible part of the trajectory as the outer loop. Because the outer loop aircraft dynamics have a direct relationship between the track-angle error and the cross-track error ($\dot{x_e} = V_{tas}\psi_e$), the ϵ loop closure is similar to a *quickened* loop closure of the lateral position error:

$$\epsilon = \psi_e + \frac{x_e}{D_v} = \frac{\dot{x_e}}{V_{tas}} + \frac{x_e}{D_v} \overset{\text{Laplace}}{\Longrightarrow} \frac{\epsilon(s)}{x_e(s)} = \frac{1}{D_v}\left(1 + \frac{D_v}{V_{tas}}s\right). \tag{6.2}$$

A pilot's strategy of minimizing ϵ yields an exponential convergence to the path with a lag time of $\frac{D_v}{V_{tas}}$. Thus, for a fixed velocity V_{tas} a reduction in viewing distance D_v decreases

the time to correct for a position error. This also requires, however, a higher pilot tracking bandwidth that could increase workload. When the aircraft roll angle feedback (inner loop) satisfies the crossover theorem (i.e. $H_{CL}^{in} \approx 1; \omega < \omega_c^{in}$), the equivalent system to be controlled in the *outer* loop equals (Appendix E):

$$H_{CL}^{in} \frac{g_0}{D_v} \frac{1}{s^2} \left(1 + \frac{D_v}{V_{tas}} s\right) \approx \frac{g_0}{D_v} \frac{1}{s^2} \underbrace{\left(1 + \frac{D_v}{V_{tas}} s\right)}_{lead}.$$

The *lead* to stabilize the double integrator of the aircraft middle and outer loops (due to the turn co-ordination and path integration poles) is provided by the displacement cue ϵ itself[1] (Grunwald & Merhav, 1976) and a pilot can close the loop with a *gain* to comply with the crossover theorem requirements. The ϵ dynamics are illustrated in Fig. 6.2 which shows the equivalent outer loop system as a function of the viewing distance D_v. For larger viewing distances the system becomes an elementary integrator that is easy to control. When the viewing distance becomes too small, the pilot must increase his crossover frequency to obtain this situation. When the aircraft velocity increases, a similar situation results, with the difference that the frequencies at which the dynamics change are higher. Thus, for higher velocities the situation will be increasingly difficult for smaller viewing distances.

Conclusive remarks   When considering the motion of a restricted part of the tunnel on the viewplane, it is important to realize that the *dynamics* of the 'equivalent' system under control change as a function of viewing distance (Eq. 6.2). In other words, by focusing one's attention to the motion of a restricted part of the tunnel, one can *change* the dynamics of the control task. It can be hypothesized that, for a given aircraft velocity there could exist a (range of) viewing distance(s) that are *preferred* by a pilot. This preference can further be assumed to be a *function* of, or at least depending on, the velocity of the aircraft Wohl (1961). As far as modelling pilot behaviour in the restricted viewing situation is concerned, two models can be proposed. First, there is the *conventional* model as applied in the previous chapter, consisting of the successive feedbacks of the aircraft roll angle, the track-angle error and the lateral position error. An alternative model would be to maintain the inner loop roll angle feedback and to replace the middle (ψ_e) and outer (x_e) loop feedbacks with a single outer loop feedback of ϵ. This model, referred to as the ϵ-*model*, is similar to the *one-point* viewing model of Grunwald and Merhav (1976).

6.3   Experiment X2

Experiment X2 had three objectives. First, the effects of the viewing distance on pilot behaviour are to be examined, i.e. 'how do pilots adapt their control strategy?'. Second, the effects of the *interaction* between the viewing distance and the aircraft velocity on this behaviour must be assessed, i.e. 'does the pilot adaptation depend on the velocity?'.

---

[1]Note that this is only true when the viewing distance D_v is not too small. Generally, for a velocity V_{tas}, the viewing distance must be such that $\frac{V_{tas}}{D_v} \ll \omega_c^{out}$ to provide sufficient outer loop lead.

Table 6.1: Experimental conditions (X2).

	1	2	3	4	5	6	7	8	9	10	11	12
V_{tas} [m/s]	50	50	50	50	70	70	70	70	100	100	100	100
D_v [m]	100	200	400	800	100	200	400	800	100	200	400	800

Third, the pilot behaviour in the restricted viewing situation must be compared with the behaviour in the *full preview* situation of Experiment X1. For this purpose, the experimental definition was set identical to that of Experiment X1.[2] Note that it is <u>not</u> the goal of the experiment to postulate a *one-point* viewing distance model equivalent of the full preview operator model. The fundamental differences between both the control situations have been analyzed by Grunwald and Merhav (1976).

METHOD

Experiment X2 is identical to Experiment X1, except that the viewing distance is manipulated. The discussion will be concise; for details the reader is referred to §5.3.

Experimental conditions and design The experiment conditions (Table 6.1) result from a factorial combination of the two principal independent variables:

(i) The *viewing distance D_v* (4 levels): 100, 200, 400 and 800 [m].
(ii) The *aircraft velocity V_{tas}* (3 levels): 50, 70 and 100 [m/s].

The experiment procedure, design and subjects were identical to those in X1.

Dependent measures The same dependent measures as in Experiment X1 were measured, extended with the tunnel image displacement ϵ and its derivative $\dot{\epsilon}$.

Description of the experiment simulation

Tunnel geometry The tunnel was identical to that of X1, with the tunnel size W_t fixed to 40 [m]. As illustrated in Fig. 6.1(b), the tunnel geometry is displayed around a viewing distance D_v. D_{vmin} and D_{vmax} were chosen such that the *absolute* size of the visible elements of the tunnel geometry was constant for all viewing distances. Since all other simulation characteristics were identical to those of Experiment X1, the experimental findings can be compared to those reported before (conditions 2, 6 and 10 of X1).

Experiment hypotheses

The hypotheses are straightforward. First, it is hypothesized that the position errors increase and the heading angle errors decrease for larger viewing distances. Second, because

---

[2]Another objective was to test the model identification methods in an elementary multi-loop control task. Due to the specific character of the control situation examined here, the modelling and identification issues are rather straightforward. In fact, Experiment X2 was the first experiment conducted of all experiments. It proved to be advantageous, however, to discuss its results after those of Experiment X1.

Table 6.2: Pilot questionnaire (X2): realism of the simulation. The pilot judgements for Experiment X1 are shown in brackets for ease of reference.

How would you describe the level of *realism* of the simulated aircraft *dynamics*?					
	very realistic	realistic	average	unrealistic	very unrealistic
$V_{tas}=$ 50 [m/s]	·(·)	1(1)	·(·)	2(2)	·(·)
$V_{tas}=$ 70 [m/s]	·(·)	1(2)	1(1)	1(·)	·(·)
$V_{tas}=$ 100 [m/s]	·(·)	2(3)	1(·)	·(·)	·(·)
How would you describe the level of *realism* of the simulated aircraft *disturbances*?					
	very realistic	realistic	average	unrealistic	very unrealistic
$V_{tas}=$ 50 [m/s]	·(·)	·(·)	·(1)	3(2)	·(·)
$V_{tas}=$ 70 [m/s]	·(·)	·(1)	1(1)	2(1)	·(·)
$V_{tas}=$ 100 [m/s]	·(·)	·(·)	1(·)	2(3)	·(·)

the ϵ outer loop dynamics are easier to control for larger viewing distances, it is hypothesized that for these conditions pilot control activity decreases as well as the magnitudes of the aircraft roll angle. The anticipated effects of the velocity are twofold. A higher velocity means that the control of the lateral displacement cues become increasingly difficult for small viewing distances. Furthermore, since the control of the aircraft becomes easier for the larger velocities it is expected that control will be smoother for these conditions. The viewing distance and the aircraft velocity *both* determine the equivalent ϵ outer loop dynamics, and the possibility exists of a viewing distance that is *preferred* by pilots for a particular aircraft velocity. Hence, it is hypothesized that, third, these *preferred* D_vs indeed exist and, fourth, that they increase for larger aircraft velocities.

6.4 Results

6.4.1 The pilot questionnaire

Below, only the questionnaire data of subjects A–C will be discussed (Table 6.2).

Realism of the simulation Subjects preferred the high-velocity vehicle dynamics (Table 6.2). The atmospheric turbulence was considered unrealistic for all velocity conditions. Especially the lower frequencies of the disturbance were commented to be too strong and demanded too much pilot compensation. In normal flight the high-frequency content of the turbulence becomes dominant when the aircraft velocity increases. The objective of maintaining a constant level of turbulence over the experimental conditions, however, conflicts with this argument. The comments are similar to those of Experiment X1 (shown in brackets). Tentatively, the level of realism was judged somewhat lower here, which could be attributed to the fact that in Experiment X1 the whole tunnel was displayed instead of only four small line segments on the display.
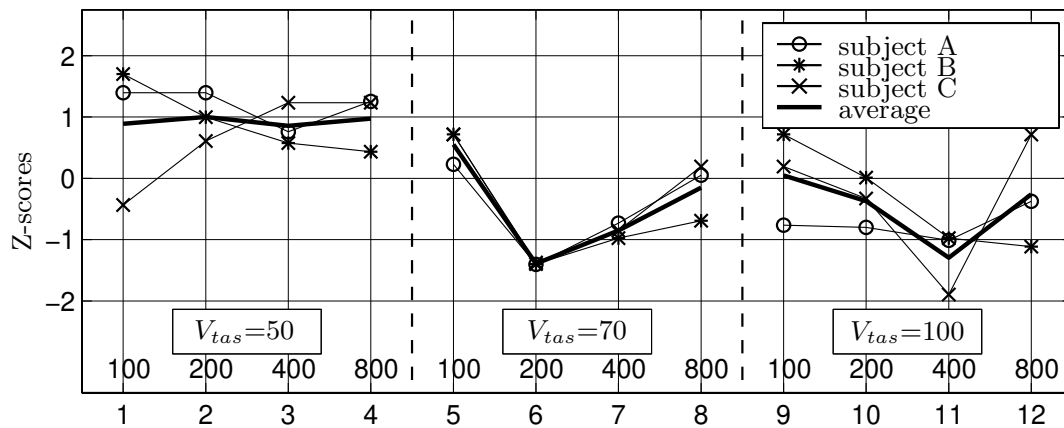
Figure 6.3: Z-scores of the effort ratings for all 12 conditions of Experiment X2. Here, and in the following, the insets show the three velocity conditions (in [m/s]). The numbers 100–800 in the bottom of the figure mark the viewing distances (in [m]) and the numbers 1-12 below the figure indicate the experimental configurations of Table 6.1.

Display characteristics   In describing the sources of information used in conducting the task, subjects reported to put their efforts on centering the visible elements of the tunnel image around the aircraft reference symbol. The control situation for the smallest viewing distance was found annoying, because it forced them to shift their attention out of the preferred display center to the outer limits of the screen.

Effort ratings   The pilot effort ratings decrease for larger velocities (Fig. 6.3). The relatively high ratings for the low-velocity condition correspond well with the poor flying characteristics as commented by the subjects. For the higher two velocity conditions, the ratings show a minimum for a certain viewing distance (V_{tas}=70 [m/s]: D_v=200 [m] and V_{tas}=100 [m/s]: D_v=400 [m]). The ratings for the low-velocity condition are independent of the viewing distance.

6.4.2   Time domain data: statistical analysis

A full-factorial mixed-model Analysis of Variance was conducted for the time domain experimental data. The independent measures were the aircraft velocity (V) (3 levels) and the viewing distance (D) (4 levels). The ANOVA results are summarized in Table 6.3.

Pilot control activity   Pilot control activity, Figs 6.4(a) and 6.4(b), decreases for the higher velocities (δ_a: $F_{2,6}$=541.187, p <0.01; $\dot{\delta}_a$: $F_{2,6}$=223.268, p <0.01). It also decreases for larger viewing distances (δ_a: $F_{3,9}$=33.703, p <0.01; $\dot{\delta}_a$: $F_{3,9}$=0.745, not significant), but only for the lower velocity conditions, causing the significant V×D-interaction (δ_a: $F_{6,18}$=11.566, p <0.01; $\dot{\delta}_a$: $F_{6,18}$=3.167, p=0.027). Post-hoc tests (NK, p=0.05) showed that for $\dot{\delta}_a$ only the differences between the low and the high-velocity conditions were sig-

Table 6.3: Results of a full-factorial ANOVA (X2). In this table '★★', '★' and '○' represent chance levels of $p \leq 0.01$, $0.01 < p \leq 0.05$ and $0.05 < p \leq 0.10$, respectively.

	control activity		inner loop measures		path-following performance		visual cue effects	
	δ_a	$\dot{\delta}_a$	$\dot{\phi}$	ϕ	ψ_e	x_e	ϵ	$\dot{\epsilon}$
main effects								
V	★★	★★	○	·	★★	·	★★	★★
D	★★	·	★★	★★	○	★★	★★	★★
2-way interaction								
V×D	★★	★	★★	○	★★	○	★★	·

nificant. For δ_a only the value for the smallest viewing distance was significantly different.

Inner loop measures Figs 6.4(c) and 6.4(d) illustrate that the higher aircraft velocity conditions lead to somewhat higher values of $\dot{\phi}$ ($F_{2,6}$=4.2136, p=0.072), whereas they have no significant effect on the roll angle itself. An increasing viewing distance leads to lower values of the roll angle ($F_{3,9}$=18.935, p <0.01), almost independent of the velocity as judged by the borderline significance of the V×D-interaction. The same effect of viewing distance is apparent for the roll angle derivative ($F_{3,9}$=18.202, p <0.01), but holds only for the two lower velocity conditions (V×D-interaction: $F_{6,18}$=10.458, p <0.01).

Path-following performance The track-angle error (Fig. 6.4(e)) decreases for the higher velocity conditions ($F_{2,6}$=51.672, p <0.01), an effect that is significant for all velocities (NK, p=0.05). For each velocity condition, a different trend is apparent: ψ_e increases for the low-velocity condition, whereas for the other two velocities there appears to be a minimum (V_{tas}=70 [m/s]: D_v=200 [m] and V_{tas}=100 [m/s]: D_v=400 [m]). These findings account for the borderline significance of the viewing distance and the highly significant V×D-interaction. The cross-track error (Fig. 6.4(f)) is not affected by the aircraft velocity, but increases significantly for larger viewing distances ($F_{3,9}$=29.746, p <0.01). The V×D-interaction is caused by the relatively constant values of x_e for small viewing distances of the high-velocity condition. The effect of the viewing distance is different for the three velocity conditions. Post-hoc tests (NK, p=0.05) showed that the differences in x_e for the viewing distances are all significant for the low-velocity conditions, whereas for the other two velocities only the two largest viewing distances are different from the rest.

Visual cue effects Both the displacement ϵ and its derivative $\dot{\epsilon}$ (Figs 6.4(g) and 6.4(h)) decrease for the higher velocity conditions (ϵ: $F_{2,6}$=51.974, p <0.01; $\dot{\epsilon}$: $F_{2,6}$=56.703, p <0.01). Furthermore, $\dot{\epsilon}$ decreases significantly for larger viewing distances ($F_{3,9}$=40.086, p <0.01), independent of the aircraft velocity. The trends in ϵ depend on the aircraft velocity: for the low velocity conditions, ϵ remains relatively constant, whereas for the other velocity conditions, there appears to be a minimum (V_{tas}=70 [m/s]: D_v=200 [m] and V_{tas}=100 [m/s]: D_v=400 [m]). These trends yield a significant effect of viewing distance ($F_{3,9}$=33.500, p <0.01) and a significant V×D-interaction ($F_{6,18}$=8.909, p <0.01).
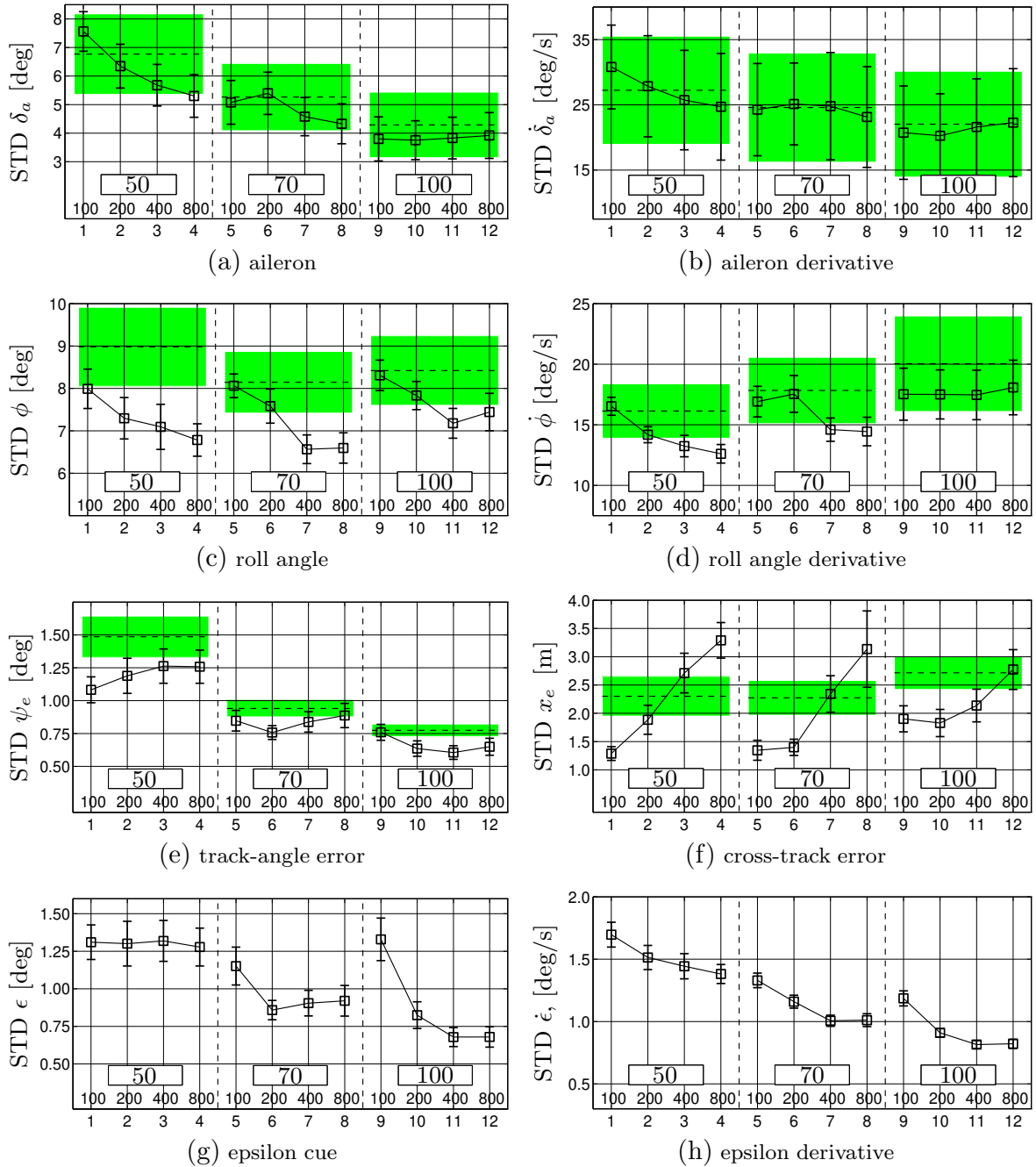
Figure 6.4: Means and 95% confidence limits of the STDs of the dependent measures (all subjects). The dashed lines and the shaded areas show the values of these quantities of Experiment X1.
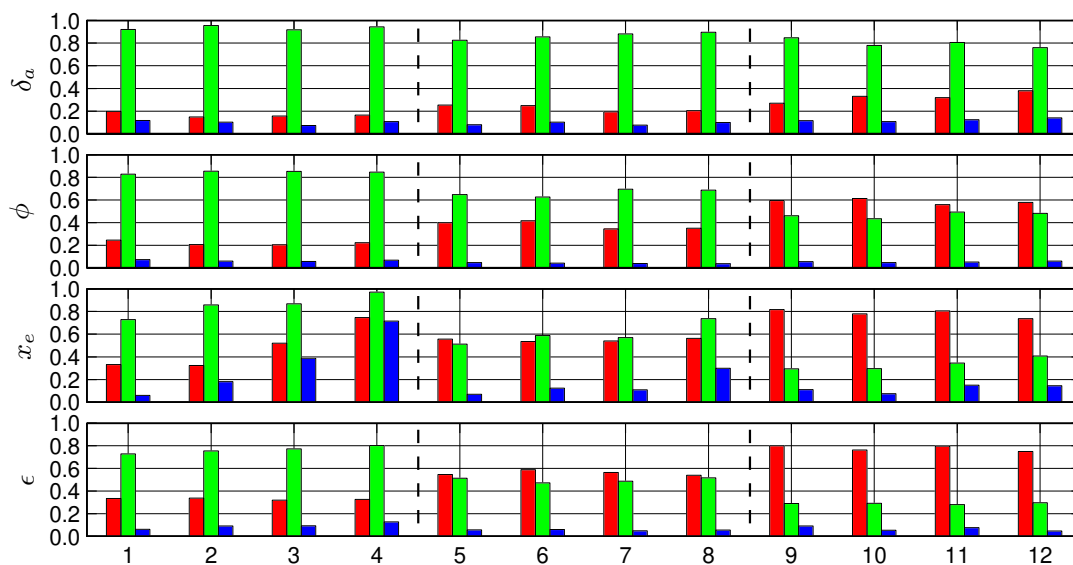
Figure 6.5: Relative noise ratios (one subject, all conditions). The three bars for each condition represent the RNRs computed at frequencies i_1 (left), i_2 (middle) and $i_1 \& i_2$ (right).

6.4.3 Frequency domain data

Relative noise ratios There are two alternative models available for the non-parametric identification of the multi-loop system: the conventional model and the ϵ-model. The RNRs for the outer loop signals x_e and ϵ show significant lower values for the latter outer loop signal (Fig. 6.5). This indicates that the ϵ signal contains much less noise at the frequency sets of i_1 and i_2 than x_e, suggesting that the pilot indeed uses ϵ rather than x_e (and, implicitly, ψ_e). Note that the lower RNRs for the ϵ signal also indicate higher SNRs for the non-parametric identification. Thus, the RNRs suggest that the ϵ-model is indeed the model that is most relevant in this experiment, which was the case for all pilots.

Crossover frequencies and phase margins The inner and outer loop crossover frequencies and phase margins can be obtained by combining the estimated pilot frequency responses and the aircraft models. The discussion for these quantities for the ϵ-model will be postponed to §6.5.2. The crossover frequencies and phase margins of the *combined* outer loop of the conventional model are shown in Fig. 6.6. The phase margins increase for larger viewing distances, for all velocities. With respect to the phase margins of X1, the values of this experiment overlap them, tentatively for higher viewing distances when the velocity increases. The crossover frequencies $\omega_c^{out^c}$ are considerably smaller for larger viewing distances for the low-velocity condition, whereas the other two velocity conditions show a clear maximum. These maxima lie between 100 and 200 [m] for the V_{tas}=70 [m/s] condition, and between 200 and 400 [m] for the V_{tas}=100 [m/s] condition.
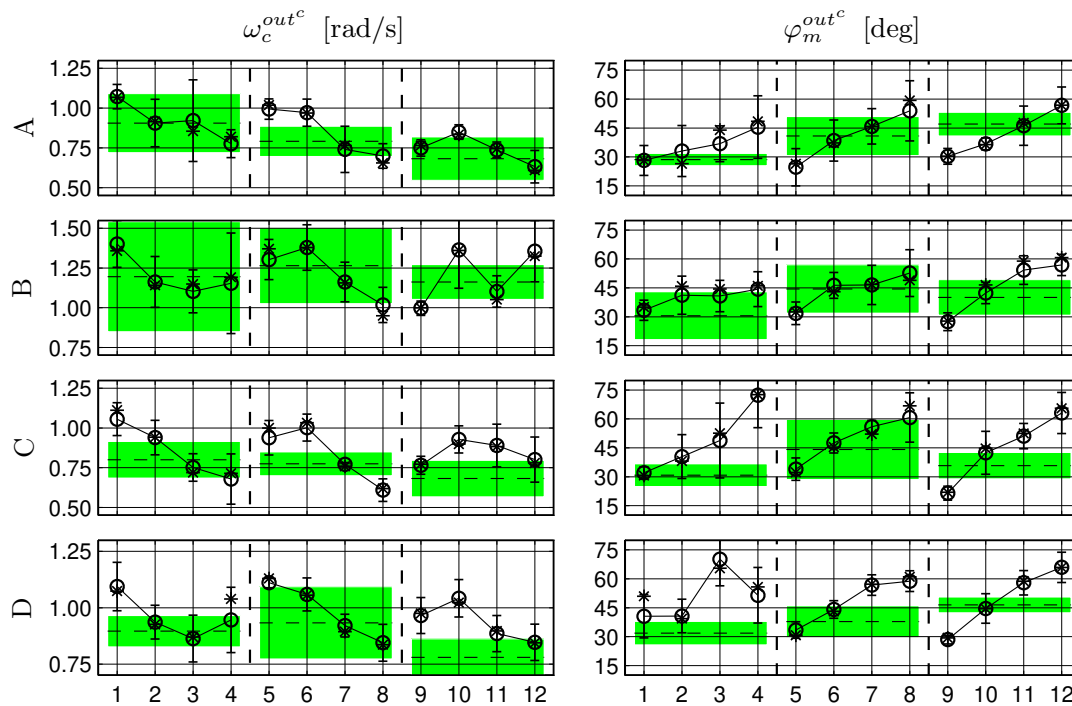
Figure 6.6: Crossover frequencies and phase margins for the conventional model (all subjects, all conditions). In this figure, the 'o'-symbols and the cross-hairs show the mean and standard deviations of these quantities for the estimated frequency responses for all 5 replications. The '*'-symbols show them for the averaged response. The filled rectangles and the dashed lines show the values of these quantities for the *full preview* situation of Experiment X1.

6.5   Modelling efforts

Two modelling approaches, i.e. the MLM (§6.5.1) and the OCM (§6.5.2) are applied for two pilot models, i.e. the ϵ-model and the conventional model. Whereas the ϵ-model was found superior in describing pilot control behaviour, the conventional model facilitates the comparison between the limited viewing situation considered here and the *full preview* case of Experiment X1. The discussion below will focus in particular on the ϵ model.

6.5.1   Multi-loop model

MLM model structure   The structure of the conventional model MLM is identical to that applied in Experiment X1. The structure of the ϵ-model MLM is similar, except for the single ϵ outer loop, that is closed with a proportional gain – $K_{p_{out}}^{\epsilon}$ – only.

MLM model parameters   The pilot model parameters for the ϵ-model are illustrated in Figs 6.7 and 6.8. Similar to the pilot adaptation in Experiment X1, a reduction of the pilot time delay and neuromuscular (nm) damping, as well as an increasing nm bandwidth occurs for the higher velocity conditions. The effects of the viewing distance vary consid-
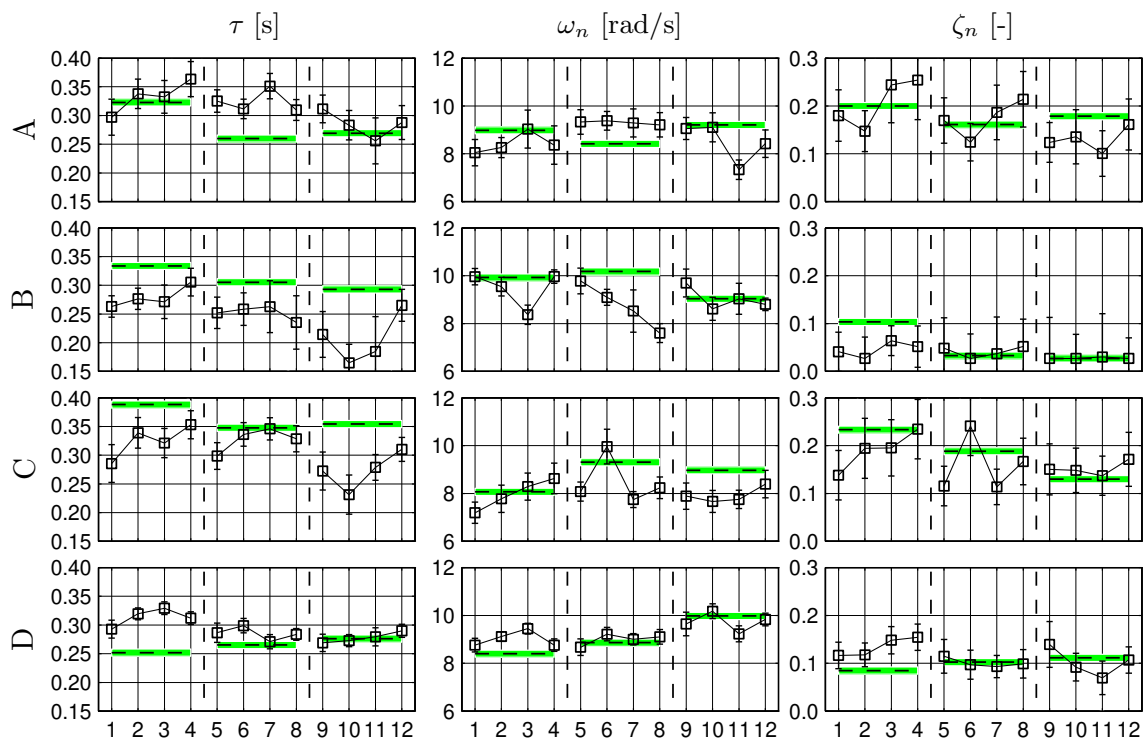
(a) time delay, neuromuscular bandwidth and damping
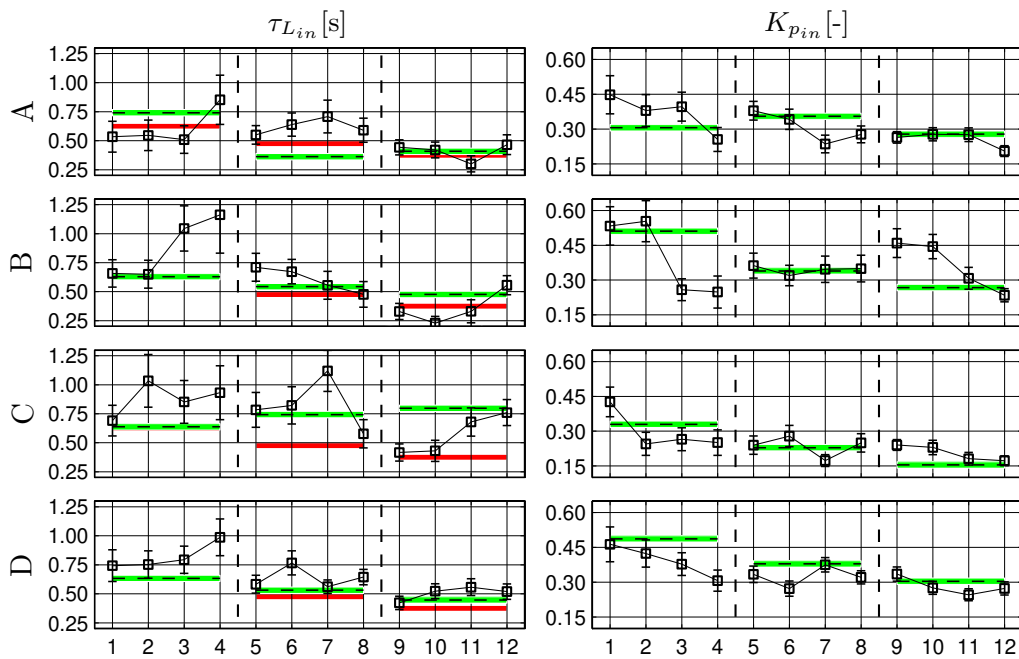
(b) inner loop lead and gain

Figure 6.7: Inner loop ε-model MLM variables (all subjects, all conditions). Here, and in the following, the cross-hairs show the parameter estimation uncertainties according to Cramer-Rao, whereas the horizontal light shaded areas show the parameter values for the *full preview* situation of Experiment X1. In the bottom left figure, the horizontal dark shaded areas show the values of the aircraft roll subsidence lag time constant, τ_ϕ.
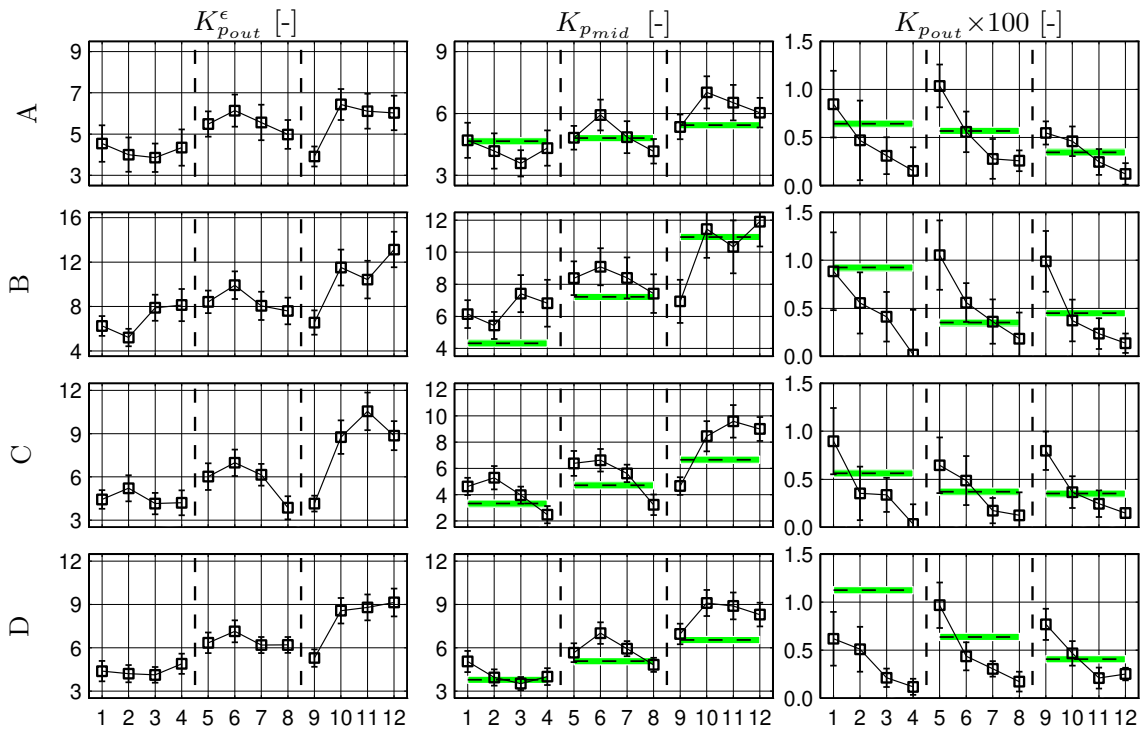
Figure 6.8: MLM pilot model parameters (all subjects, all conditions). The left column in this figure shows the outer loop gain of the ϵ-model. The two columns on the right show the middle and outer loop gains of the conventional model, respectively. The horizontal shaded areas and the dashed line show the values of these quantities for Experiment X1.

erably among subjects. Both the inner loop gain and lead decrease for the higher velocity conditions (Fig. 6.7(b)), an effect that can be attributed to the different aircraft handling characteristics for these conditions. The inner loop gain decreases for larger viewing distances for almost all pilots, a reduction that is accompanied by an increasing inner loop lead. This provides evidence for a strategy of lowering the bandwidth of the inner loop roll angle feedback to gain more inner loop phase margin. The ϵ-model outer loop gain $K_{p_{out}}^{\epsilon}$ has maximum values at D_v=200 [m] and around 400 [m] for the V_{tas}=70 and 100 [m/s] conditions, respectively (Fig. 6.8). A general trend is one of a lower gain for the small viewing distances and a higher gain for the larger viewing distances. This latter trend is not intuitive, but can be explained by examining the similar trend in the inner loop lead for these conditions. Such a correlation also exists for the other velocities, but to a lesser extent. These results suggest that especially for the low-velocity condition pilots increase their inner loop phase margin to enable them to increase the bandwidth of the outer loop. This could explain the higher (and relatively constant) pilot effort ratings for these conditions.

The inner loop pilot equalization and limitation parameters of the conventional model are
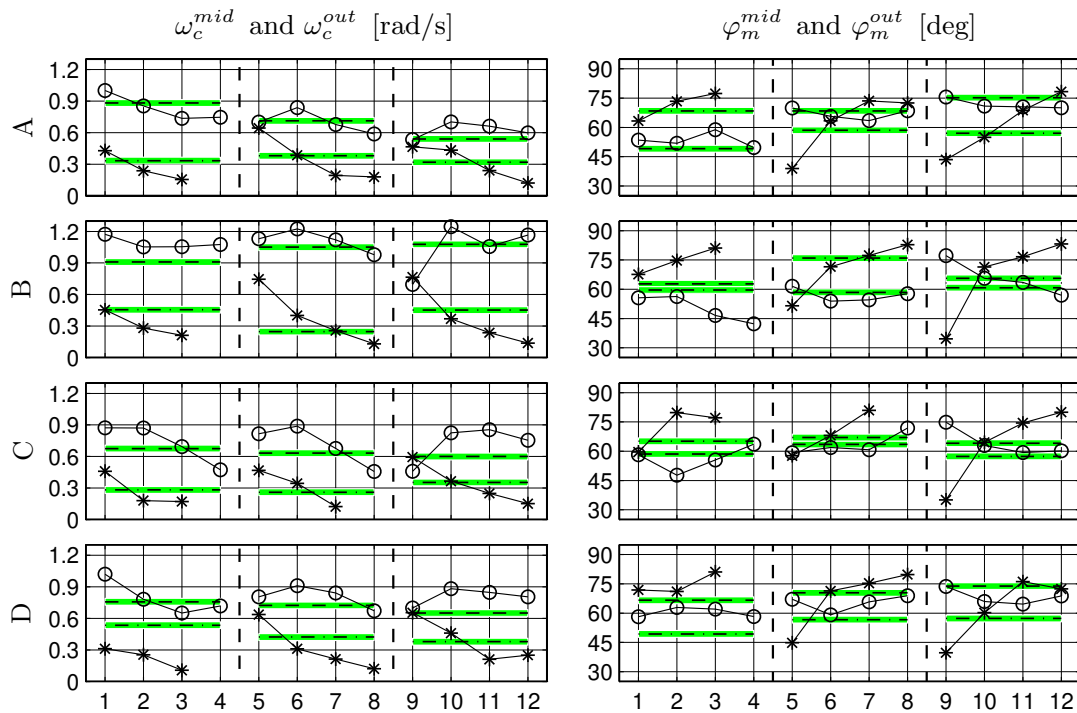
Figure 6.9: The middle ('o') and outer ('*') loop crossover frequencies and phase margins (all subjects, all conditions) for to the conventional MLM. The dashed and the dash-dot lines in the shaded areas show the quantities computed in Experiment X1.

similar to those of the ϵ-model. The middle and outer loop gains for the conventional model are shown in Fig. 6.8. The outer loop feedback of the position error decreases considerably for the larger viewing distances. The middle loop gain, determining the bandwidth of the heading angle error feedback, shows similar trends as those of the outer loop gain of the ϵ-model. Compared to the *full preview* situation of Experiment X1, Fig. 6.8 shows that the middle loop gain is generally higher in this experiment, whereas the outer loop gain is higher for the small viewing distances and considerably lower for the higher viewing distances. The middle and outer loop crossover frequencies and phase margins corresponding with the conventional model are illustrated in Fig. 6.9. The middle loop quantities show different effects of the viewing distance depending on the velocity condition. For the low-velocity condition, they decrease for larger viewing distances. The two high-velocity conditions show to have maximum crossover frequencies (and minimum phase margins) for a certain viewing distance. These maxima appear at larger viewing distances when the aircraft velocity increases. The outer loop feedback bandwidth decreases for larger viewing distances, irrespective of the aircraft velocity. For some configurations the outer loop feedback disappears completely, i.e. it becomes unmeasurable. With respect to the *full preview* situation of Experiment X1, the outer loop crossover frequencies resemble those corresponding with larger viewing distances for increasing velocities.
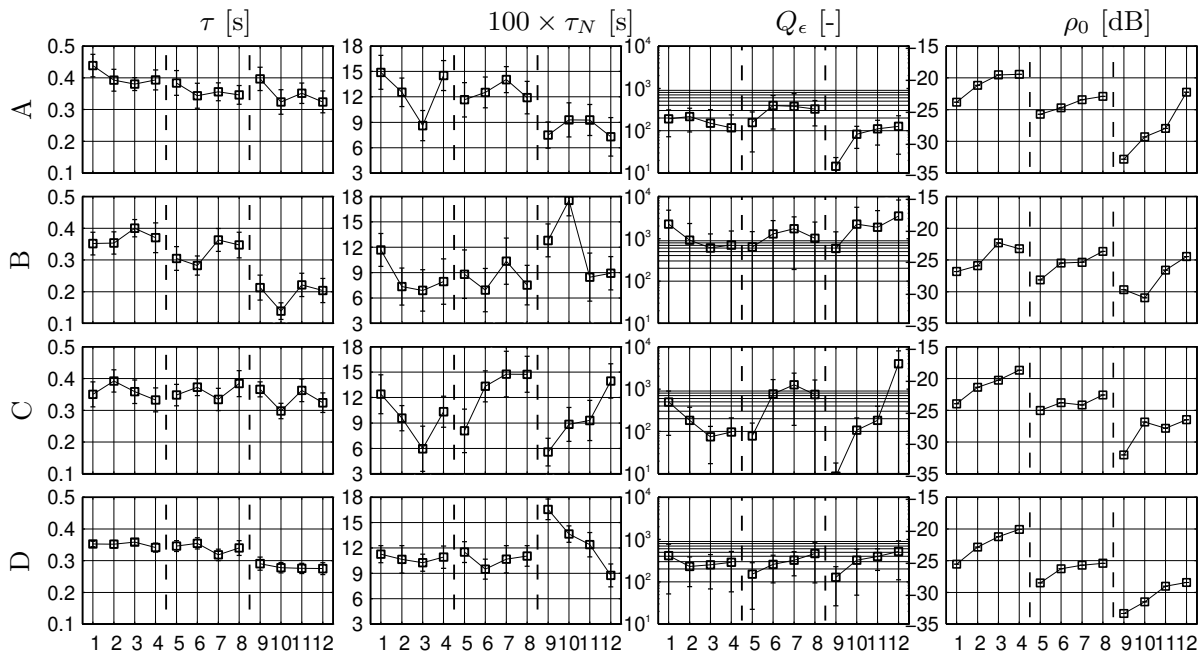
Figure 6.10: The OCM parameters τ, τ_N, Q_ϵ and ρ_0 of the ϵ-model (all subjects, all conditions). In the left three columns the cross-hairs show the uncertainties according to Cramer-Rao.

6.5.2 Optimal control model

Again, there were considerable problems in the estimation of the OCM parameters for the conventional model. Those of the ϵ-model could be determined rather well.

OCM model structure The OCM model structure for the ϵ-model is simple. The two variables of interest are the aircraft angle of roll (inner loop) and the tunnel image displacement ϵ (outer loop). The implicit OCM assumption that also the derivatives are observed results in an observation vector with four components. The OCM application requires twelve parameters to be specified: the time delay τ, the neuromuscular lag τ_N, the motor noise ratio ρ_u, four observation noise ratios ρ_{y_i}, the control input weighting R and four elements of the weighting matrix Q_{y_i}. It was not possible to obtain a consistent estimate of all these parameters, forcing a reduction of the number of model parameters.

Limiting the number of OCM model parameters The first parameter to be fixed is the motor noise ratio ρ_u (to -25 [dB]). Parametric studies revealed that only the *ratio* between the weighting on the pilot's output δ_a, R, and that on the input ϵ, Q_ϵ, had an effect on the fit to experimental data. Thus, R was fixed to '1' and all elements of the weighting matrix were set to zero except for the weighting on ϵ, which was set free. The resulting OCM application had only seven parameters that could all be estimated satisfactory. The uncertainty in estimating the parameters[3] is smaller compared to the application of the

---

[3]The computation (Cramer-Rao) of these uncertainties were based on the frequency domain data only.

OCM in Experiment X1 (Fig. 6.10). A number of trends appears. First, the time delay and the neuromuscular lag decrease and the observation noise ratios of the inner loop variables increase for the higher velocity conditions. The inner loop can be controlled in a smoother fashion for those velocity conditions, corresponding to the MLM results. The weighting on ϵ increases considerably for the two higher velocity conditions and decreases for the lower velocity conditions when the viewing distance increases. This also corresponds with the findings of the MLM models. The uncertainty in these weighting parameter estimates, however, is rather large. All observation noise ratios increase for larger viewing distances, which can be illustrated best in examining the *nominal* observation noise ratio ρ_0 (Fig. 6.10). The trend in the data corresponds with the increasing weight on the displacement cue ϵ, which merely changes the *balance* in the model with respect to the weighting of the input signal. The *fractions* of attention (not shown), §E.3.4, revealed that, again, the OCM predicts that most (> 80 %) of the pilot attention is put on controlling the *inner* loop. This is surprising because the task of the pilots (as expressed in the OCM by manipulating the weight on ϵ) is to minimize ϵ, irrespective on the inner loop measures. The OCM predicts that for the larger velocities, the attention to the outer loops reduces further and also that more attention is given to the derivative of ϵ than to this value itself. This is rather strange because the MLM models did *not* use the derivative of the outer loop variable at all.

Summarizing, although this time the OCM parameters could be estimated consistently, the results remain difficult to interpret. For instance, how can one possibly explain the increasing observation noise ratios of the inner loop variables? Because the structure of the OCM has been restricted beforehand by limiting some of the parameters, this could result in a *wrong* adaptation of the model to the experimental results. The possibility that other choices of the OCM parameters exist that *do* yield less paradoxal results, cannot be excluded. The question of *what* selection of OCM parameters solves these difficulties, however, remains unanswered. The overparameterization of the OCM does not allow the right model parameters to be selected on the basis of *objective* data alone. This puts serious doubts upon the model applicability, even in the elementary task studied here.

MLM and OCM results: crossover frequencies and phase margins The crossover frequencies and phase margins (ϵ-model) of the inner and outer loop MLM and OCM models are illustrated in Fig. 6.11. The trend in the inner loop variables is a reduction in crossover frequency and an increasing phase margin for larger viewing distances. With respect to the full-preview situation (X1) the inner loop phase margins are somewhat higher. Again, the inner loop crossover frequencies are higher for the higher velocity conditions, supporting the pilot comments of the questionnaire. The outer loop quantities show a clear trend for all pilots of a decreasing crossover frequency and an increasing phase margin for larger viewing distances. For the two high velocity conditions, the crossover frequency has a maximum value at viewing distances between 100 and 200 [m], and 200 and 400 [m], respectively. For the ϵ-model these quantities represent the *true* outer loop, not the combined middle and outer loops as in the conventional model. Both the

(a) inner loop

(b) outer loop
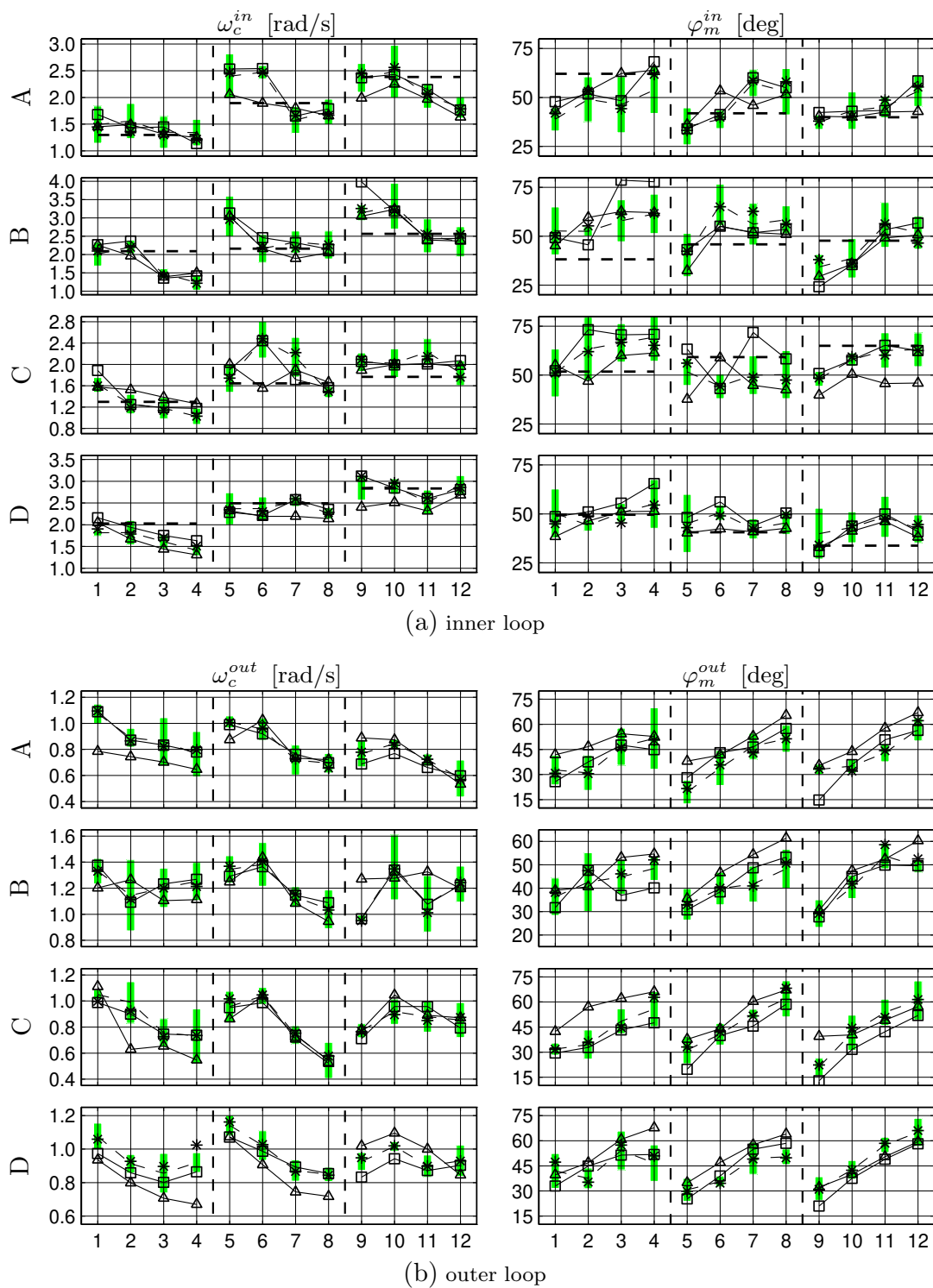
Figure 6.11: Crossover frequencies and phase margins of the ϵ-model (all subjects, all conditions). The filled areas show the uncertainty regions of the raw frequency response data, with the averages connected with the dashed line. The '*'-symbols show the quantities for the frequency responses of the *averaged* data, whereas the squares and triangles show them according to the MLM and OCM models, respectively. The thick, horizontal, dashed lines show the inner loop quantities computed in Experiment X1 (MLM, conventional), for the matching conditions.

models account for the main trends in the data, with some preference for the MLM model, although they both have difficulty in modelling the inner loop phase margin. The OCM generally leads to an underestimation of the outer loop crossover frequency accompanied by an outer loop phase margin that is too large. Both the models show maxima for the outer loop crossover frequencies at increasing viewing distances for larger velocities.

6.6 Retrospective

6.6.1 Discussion of the results

Analysis

The elementary objectives of Experiment X2 yielded a basic experimental set-up, providing a good starting point of the cybernetic approach. The hypothesized effects of the viewing distance, stated in §6.3, could almost all be confirmed. Most importantly, it is shown that the different *dynamics* of the limited visible parts of the tunnel force pilots to *adapt* their control behaviour. The dynamic characteristics of the tunnel image result in *preferred* viewing distances, which increase for larger aircraft velocities. This result has important consequences for the design of the tunnel display viewing volume.

A *preferred* viewing distance and its relation with the aircraft velocity   The dynamic characteristics of the displacement ϵ of a limited part of the tunnel on the viewplane are a function of both the aircraft velocity V_{tas} and the distance D_v to that part. One of the experimental hypotheses was that for a given aircraft velocity, pilots *prefer* a certain viewing distance. The experimental results provide evidence for this hypothesis and also for the hypothesis that the *preferred* viewing distances become larger when the aircraft velocity increases. The pilot effort ratings (Fig. 6.3) show that whereas pilots have no preference for the low-velocity condition, they do prefer the 200 and 400 [m] viewing distances for the 70 and 100 [m/s] velocity conditions, respectively. The ratings correspond well with the objective data, such as the courses of the STDs of the heading angle error ψ_e, the displacement ϵ and its derivative $\dot{\epsilon}$ (Figs 6.4(e), 6.4(g) and 6.4(h)). The frequency domain data also support the hypotheses, as can be seen from the inner and outer loop crossover frequencies (Figs 6.6 and 6.11), especially those of the higher two velocity conditions. For the small viewing distances the bandwidth of the outer loop first increases and then decreases when the viewing distance increases, resulting in a *maximum*. The inner and outer loop phase margins increase monotonously for larger viewing distances. These findings were further supported in the analytical analysis using both the MLM as the OCM models. The low-velocity condition does *not* show an optimum viewing distance. A possible reason is that the smaller viewing distance (100 [m]) is already beyond the preferred viewing distance, resulting in the monotonous decrease in outer loop bandwidth for even larger D_vs (Fig. 6.11(b)). Another cause could be that, because of the relative difficulty of controlling the aircraft for this velocity condition, all viewing distances resulted in a control situation of the same difficulty. The pilot ratings (Fig. 6.3) and the adaptation of

the inner loop MLM models (Fig. 6.7) show evidence for the latter option. Concerning the aircraft velocity, similar effects were found as in the *full preview* experiment of the previous chapter, illustrating that also the adaptation of the pilot to the aircraft handling characteristics must be studied. This adaptation can be anticipated beforehand using the crossover model theorem.

The limited viewing condition vs. the *full preview* situation A second theme in the analysis is the comparison of pilot behaviour between the *full preview* situation studied in the previous chapter and the limited *one-point* viewing condition of this experiment. Subjects commented that the experiment was very *abstract* which, even though the experimental set-up was identical, led to lower ratings of the experiment realism and to higher effort ratings (not shown). In general, pilot control activity (δ_a, $\dot{\delta}_a$) and inner loop measures (ϕ, $\dot{\phi}$) were lower than those of experiment X1, independent of the aircraft velocity (Figs 6.4(a) – 6.4(d)). Only for the smallest viewing distance the control activity was similar to that measured in X1. These findings are supported by the inner loop crossover frequencies and phase margins (Fig. 6.11(a)) that were generally lower and higher, respectively. The STDs of the heading angle error were smaller than those observed in X1, corresponding with the higher crossover frequencies of the middle feedback loop (Figs 6.4(e) and 6.9). Contrary to the results of Grunwald and Merhav (1976), the heading angle error did *not* become smaller for larger viewing distances, except for the high velocity condition. The path-following performance was considerably better for the small viewing distances and the low velocity conditions whereas for the high-velocity condition the path-following performance was better for all viewing distances (Fig. 6.4(f)). These results were supported by the higher outer loop crossover frequencies for the small viewing distances (Fig. 6.9). The fact that the performance was better for the high velocity conditions can be attributed to the higher bandwidth of the heading angle error feedback loop for increasing D_vs. Maintaining such a tight middle loop closure is possible due to the characteristics of the displacement ϵ for larger viewing distances (Eq. 6.1). This automatically brings us to the meaning of the ϵ outer loop closure, the properties of which determine the relative importance of the heading angle error and the position error feedback. For small viewing distances, ϵ is a function of both the heading error ψ_e and the position error x_e, whereas for the large viewing distances the effects of a position error are attenuated in ϵ. The results of this experiment suggest that not only the *perceivability* of these two aircraft state elements (i.e. in ϵ) is what matters, but rather their *usability* which is also determined by their *dynamic* characteristics.

A *preferred* viewing distance in the *full preview* situation? The experiment provides evidence for the hypotheses that, first, in a limited viewing situation a particular viewing distance is preferred over others, and, second, that this *preferred* viewing distance increases with velocity. In the comparison between the results of the limited viewing experiment as opposed to the *full preview* situation of Experiment X1, it was shown that there are some differences but also some resemblances in pilot behaviour and performance. For instance, whereas the level of control activity is lower in the limited viewing experiment,

the path-following performance matches the performance of the full preview experiment. An interesting question would be whether a comparison of the experimental results indicates a *preferred* viewing distance in the *full preview* situation and, if so, whether this viewing distance is also a function of velocity. Regarding the experimental results, some evidence for this hypothesis can indeed be found in comparing the trends in especially the outer loop and the combined outer loop crossover frequencies ω_c^{out} and $\omega_c^{out^c}$, respectively (Figs 6.11(b) and 6.9). Their values, depending on both the viewing distance and the aircraft velocity, are in the same range of values of the full preview experiment for increasing viewing distances at larger velocities. Although the trends in the pilot adaptation provide some additional evidence, not much other empirical data exist for the hypothesized relation. This stresses the difficulty in explaining the hypothesis across the available experimental data. Experiment X2 *did* show the impact of the dynamic characteristics of a highly-limited viewing volume on pilot behaviour. These properties are not any different in the *full preview* situation, except for the fact that in the latter case there exists an infinite number of viewing distances that can be used, not to mention the other optical cues that become available, such as the optical splay angles.

Synthesis

The experimental results suggest that limiting the viewing volume could have significant consequences for pilot behaviour. It is shown that the usability of a part of the tunnel at a distance D_v from the viewplane depends on the velocity with which the aircraft travels through the tunnel. This understanding is fundamental when determining the viewing volume, i.e. values for D_{vmin} and D_{vmax}. In Fig. 6.12 the STD of the position error is shown vs. the combined outer loop crossover frequency (a) and phase margin (b). The effect of the viewing distance on the relation between the performance and the outer loop crossover frequency is relatively small. The stability margins show a clear trend, caused by the viewing distance, of a lower phase margin and higher performance for the small viewing distances. Limiting the viewing volume to that part of the tunnel that is close to the viewplane leads to improved path-following accuracy, higher levels of workload and reduced system stability. Limiting the viewing volume to that part of the tunnel that is positioned far away leads to degrading path-following accuracy and a higher level of stability, but does not necessarily lead to lower levels of pilot workload. Obviously, both options are less desirable than the *full preview* situation. They do suggest, however, a number of possibilities and limitations for constraining the viewing volume. Basically, all that matters is the presentation of aircraft heading and position errors. The heading angle error can be shown by just presenting the part of the tunnel that is located at very large distance – the *infinity point* – or with an elementary symbol such as a heading angle error bug. This could limit the viewing volume considerably by decreasing the maximum viewing distance. The experimental data show the importance of the near-by part of the tunnel for path-following performance. For the higher velocity conditions, however, showing only the part of the tunnel that is too close leads to decreasing system stability
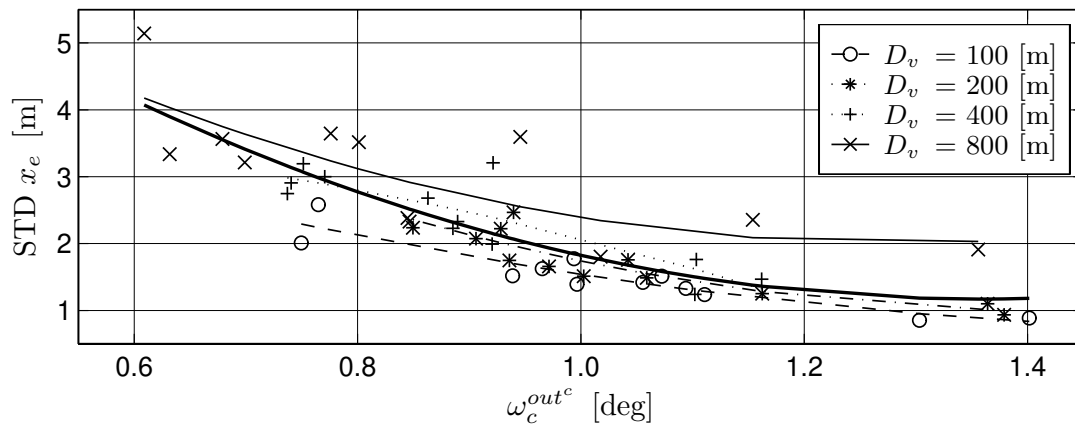
(a) performance vs. the combined outer loop crossover frequency
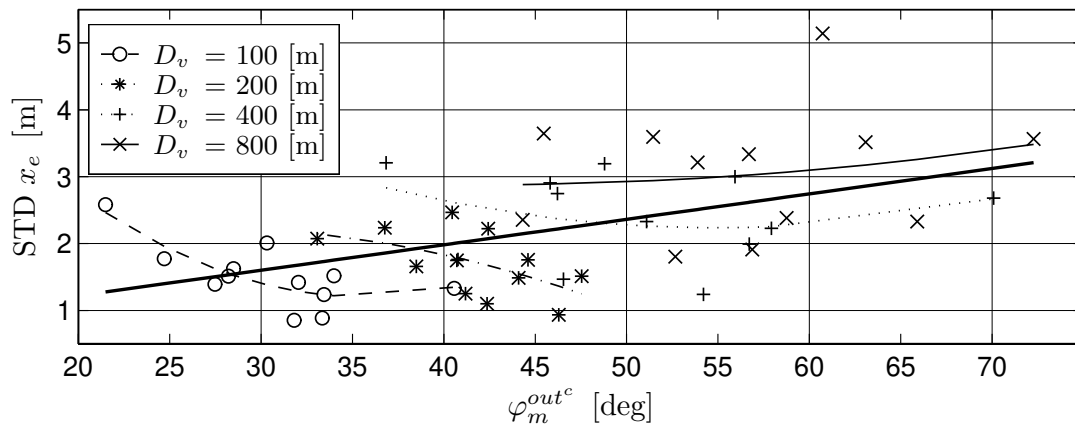
(b) performance vs. the combined outer loop phase margin

Figure 6.12: Pilot performance vs. the combined outer loop bandwidth and stability (all subjects, all conditions). The various lines illustrate a best (LS) fit of the data for the individual viewing distances (see legend) and for all data together (thick line).

and higher workload. Hence, for these velocities the minimum viewing distance can be increased too. One should keep in mind, however, that by increasing the minimum viewing distance one also limits the *dynamic information* of the visible part of the tunnel that is off-central. This dynamic information could be mandatory when side-slip and wind effects are included, for in those situations the aircraft heading does not determine the direction of motion relative to the path. The latter problem can be solved by showing a flight-path vector, which is the subject of Chapter 9. Tunnel images for a low and high-velocity flight condition, based on these design rules are shown in Figs 6.13(a) and 6.13(b), respectively. Based on the analysis of this chapter it is hypothesized that path-following accuracy, pilot workload and system stability characteristics are not inferior to those of the *full preview* situation of Experiment X1. The amount of the trajectory that is shown, however, is considerably smaller here, which limits the problems of display clutter and a low-accuracy or slow-updating aircraft avionics position measurement. Reducing the visible part of the

(a) low velocity flight condition   (b) high velocity flight condition
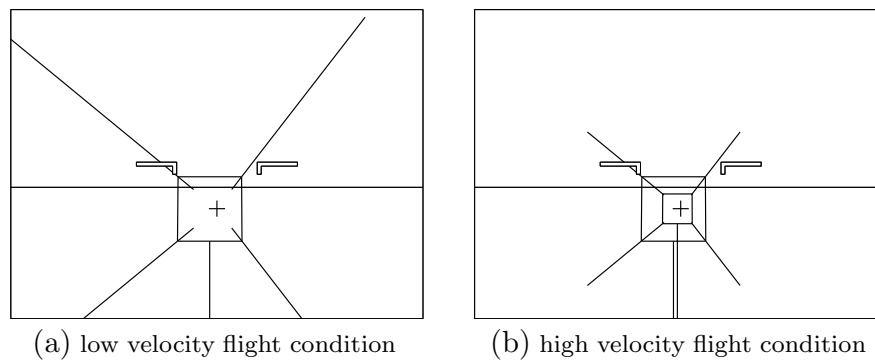
Figure 6.13: Tunnel images with a limited viewing volume for two velocity conditions. In these figures the cross symbol explicitly shows the *infinity point*, allowing pilots to directly perceive their heading with respect to the trajectory.

future trajectory that is far away has indeed been applied successfully by Wickens et al. (1989), who presented the tunnel upto a fixed distance ahead, followed by a line showing the rest of the future trajectory to be flown.

6.6.2   Conclusions and recommendations

Conclusions

- The mathematical analysis of a limited viewing condition shows that the tunnel dynamic characteristics are determined by the viewing distance and the aircraft velocity.
- In the limited viewing situation pilots adapt their control behaviour to the dynamic characteristics of the displacement cue ϵ.
- In a limited viewing control task pilots prefer a particular viewing distance over others. The preferred viewing distance depends on the aircraft velocity with a trend of an increasing viewing distance for larger velocities.
- The path-following performance in the limited viewing situation for small viewing distances is superior to the performance in the *full preview* case. This is accompanied by a higher workload and a reduction of system stability.
- The comparison of the experimental results with the *full preview* situation of Experiment X1 is difficult. Although the observed trends indicate a similar preference for a certain viewing distance as a function of velocity, the results are not convincing.
- The MLM modelling efforts show a consistent adaptation in the outer loops, whereas the inner loop equalization shows more variation. The effects of the aircraft velocity on pilot control behaviour can be anticipated beforehand.
- The identification and modelling attempts according to the ϵ-model are superior to those of the conventional model. The latter model facilitates the comparison between the limited viewing and the full preview conditions.
- The OCM application was more successful than in the previous experiment, although again the number of model parameters had to be limited considerably to allow a successful

parameter estimation. The OCM results remain difficult to interpret.

- The experiment showed that in the specification of viewing volume design guidelines the effects of the aircraft velocity should be incorporated. An alternative for showing the complete trajectory could be the combination of showing the tunnel from small to intermediate viewing distances and a symbolic presentation of the motion relative to the path, e.g. by means of a flight-path vector.
- Increasing the minimum viewing distance – presenting the tunnel from a distance ahead – could deteriorate the perceivability of the dynamic motion cues. This effect is attenuated for higher velocities.
- Decreasing the maximum viewing distance – presenting the tunnel up to a distance ahead – could deteriorate system stability. This effect can be mitigated by showing the relative motion with respect to the trajectory by means of some symbol.
- Decreasing the maximum viewing distance – restricting the preview – could have a negative impact on *situation awareness*. Showing the future trajectory by means of a perspective line could mitigate this problem as has been shown in (Wickens et al., 1989).

Recommendations

- The experiment could be conducted with the addition of a side-slip disturbance, which could lead to a degrading performance and a higher control activity. Especially the usefulness of the tunnel at large viewing distances should be examined for this situation.
- The limited tunnel and symbology display (Fig. 6.13) could be examined experimentally. By manipulating the visible part of the tunnel, the effect of the aircraft velocity can then be examined for a situation that is closer to the full-preview situation.
- The recommendations of the previous chapter concerning the addition of motion cues and the use of other (e.g. heavier) aircraft models apply in this experiment too.

The results of the OCM modelling approach disappointed once again, putting serious doubts upon its applicability in the experiments studied here. Even for the elementary situations examined in this and the previous chapter, the model parameters could only be estimated successfully after limiting the number of OCM parameters. A theoretical analysis of the applicability and, especially, the identifiability of the OCM (van Wijk & Kok, 1977), has already shown these problems. It is strange – if not to say disturbing – that in the many applications of the OCM this fact is often ignored. This can partly be attributed to the fact that, in most cases, the model is validated only in the time domain (e.g. (Grunwald & Merhav, 1976, 1978; Korn, Gully, & Kleinman, 1982)). Tentatively, it can be postulated that the intellectual attractiveness of the OCM, with its appealing regulator and observer structure, has often *dazzled* its users. A thorough re-examination of the usability, applicability, and validity of the OCM, especially in multi-loop control tasks is seriously recommended. This analysis is beyond the scope of this thesis and the OCM will not be applied again in the following chapters.

Chapter 7

Cues in straight tunnel sections

7.1   Introduction

In the previous two experiments, especially the one investigating the effects of the tunnel size, an important conclusion was that the cybernetic approach does not succeed in determining the *relative* usefulness of various optical cues when they are presented simultaneously. An alternative could be to manipulate the tunnel display geometry such that a particular design conveys only one of the prominent sets of optical cues. Then, the characteristics of pilot behaviour can be determined for each one of these sets, allowing a *comparison* of these properties. This will be the approach followed in the current chapter. As has been hypothesized in Chapter 3 the principal optical cues conveyed by the tunnel display that refer to a position error with respect to the reference trajectory are those of *optical splay* and *optical density*. The relative usefulness of these two sets for the control of an aircraft through a straight tunnel section is the subject of this chapter. Based on the discussion of Chapter 3, which is recapitulated shortly in §7.2, Experiment X3 has been designed to assess the functionality of splay and density (§7.3). The results of this experiment and the efforts to describe the observed control behaviour mathematically are discussed in §7.4 and §7.5, respectively. The chapter ends with a retrospective in §7.6.

7.2   Background

In this section some the main findings of Chapter 3 – in particular §3.4 – are summarized, emphasizing the properties of the cues of optical splay and optical density.

Optical splay and optical density   Central in Gibson's ecological approach to visual perception is the locomotion of an observer with respect to a surface (Gibson, 1986). As has been discussed in §3.2.2, the optical concomitants of the observer's locomotion are the changing texture gradients. The perspective projection of lines parallel to the viewing direction conveys optical splay angle information. The perspective projection of lines per-
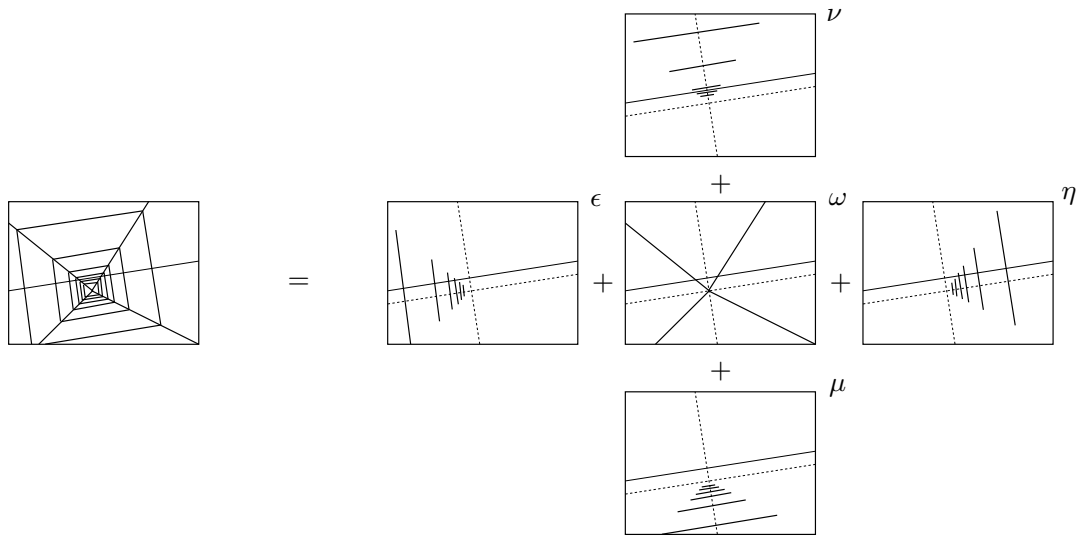
Figure 7.1: A generic tunnel (left) dissected in a number of entities (right), showing either optical splay – ω – or optical density – η, ϵ, μ, ν – information. The dashed lines represent the horizontal and vertical pseudo-horizons through the infinity point.

pendicular to the viewing direction conveys optical density information. Both the variables are isolated components of the *global* optical expansion pattern that results from an approach to a surface, and represent the perspective gradient and the compression gradient, respectively (Flach et al., 1992). In the guidance task with a tunnel-in-the-sky display the aircraft always approaches two of the four tunnel planes. Because the tunnel geometry is presented by a perspective wireframe, conveying the texture gradients introduced above, it is hypothesized that these cues are essential in examining pilot behaviour with the tunnel display.

Mathematical cue analysis   The approach of Chapter 3 has been to dissect the tunnel geometry into a number of base entities, illustrated in Fig. 7.1. Recall that the attitude of the aircraft with respect to the tunnel trajectory is depicted by the position of the *infinity point* on the display. Furthermore, extending the planes of the top and bottom tunnel walls results in a *horizontal pseudo-horizon*, parallel to the real horizon. Extending the planes of the left and right tunnel walls yields a *vertical pseudo-horizon*. The projection of the longitudinal lines connecting the individual tunnel frames convey four **optical splay angles** $\omega_1 \ldots \omega_4$. For a square tunnel the following *linearized* expressions can be obtained (substitute $H_t = W_t$ in Eqs 3.12-3.15):

$$\omega_1 = -\frac{v_e}{W_t} - \frac{x_e}{W_t}; \qquad \omega_3 = +\frac{v_e}{W_t} + \frac{x_e}{W_t};$$
$$\omega_2 = -\frac{v_e}{W_t} + \frac{x_e}{W_t}; \qquad \omega_4 = +\frac{v_e}{W_t} - \frac{x_e}{W_t}.$$

The optical splay angles have a number of distinct properties. First, any splay angle is a function of *both* the lateral and the vertical position error relative to the trajectory:

the position error is shown in a *coupled fashion*. Second, they provide strong cues for symmetry: when either x_e or v_e is zero, the splay angles are symmetric with respect to the vertical and horizontal pseudo-horizons, respectively. Third, because the angle is a property of the whole line, the change in splay angle is the same for all points on that line, i.e. the *splay gain* is independent on which part of the line is perceived. Fourth, the optic splay angles create no optic flow information specifying forward motion. The derivatives of the splay angles are a function of the flight-path angle error in *both* the lateral (χ_e) and the vertical (γ_e) direction.

The displacements of the horizontal and vertical tunnel frame line segments on the display are also shown in Fig. 7.1. The *relative* displacements of these frame lines with respect to the horizontal and vertical pseudo-horizons convey **optical density** information. For a frame i at a distance D_i the following expressions hold for the lateral optical densities:

$$\epsilon_{i\infty} = \epsilon_i - \epsilon_\infty = \kappa \left(\frac{W_t + 2x_e}{2D_i} \right); \quad \eta_{i\infty} = \eta_i - \eta_\infty = \kappa \left(\frac{W_t - 2x_e}{2D_i} \right),$$

and the vertical optical densities:

$$\mu_{i\infty} = \mu_i - \mu_\infty = \kappa \left(\frac{H_t - 2v_e}{2D_i} \right); \quad \nu_{i\infty} = \nu_i - \nu_\infty = \kappa \left(\frac{H_t + 2v_e}{2D_i} \right).$$

The optical densities have a number of characteristics. First, they show the position error in an *uncoupled* fashion, i.e. the lateral and vertical densities are only a function of the lateral and the vertical position error, respectively. Second, the relative change in density depends on the position of the particular elements that are involved, i.e. the *gain* depends on the distances from the observer to the particular local elements, D_i. Third, when the aircraft moves through the tunnel, the tunnel frames approach the observer: the displacement of the frames lines on the screen are affected by the forward motion. The observer must perceive a change in the relative displacements *on top* of the displacements due to the forward motion itself. Fourth, the derivatives of the density gradients in a particular direction, are only a function of the flight-path angle error in that particular direction. Similar to the relative displacements, however, and probably worse, the rates of the changes in relative displacements must be perceived on top of the motion of the local elements due to the forward motion.

Assessing cue functionality   The texture gradients of optical splay and optical density are a function only of the position of the aircraft relative to the tunnel centerline. The relative virtues of these two principal sets of cues to estimate a position error on a straight section of the trajectory are recapitulated above. It appears that, basically, two effects are fundamental in assessing the functionality of these cues in a comparative way.

First, the position error is shown in a *coupled* fashion with optical splay, and in an *uncoupled* fashion with optical density. A change in any splay angle can be the result of a change in position in either the vertical or lateral direction, or both. A change in an optical density in a direction can only be caused by a change in position in that particular direction. Thus, when controlling the lateral dimension only – as in the previous experiments – both

cues could do equally well. When both the channels are to be controlled simultaneously, however, the analysis predicts a clear advantage for the use of optical density cues. Note that this holds equally well for the derivatives of both cues, conveying information about flight-path relative to the trajectory.

The second issue of interest is that of forward motion, i.e. the motion parallel to the reference trajectory. Whereas the optical splay angles are useful referents for the lateral and vertical motion – i.e. in a plane perpendicular to the reference trajectory – they do not present *any* information about the forward motion. The optical density cues, conveyed by the displacements of the tunnel frame line segments with respect to the pseudo-horizons, are affected by the aircraft motion in all directions. The longitudinal motion leads to tunnel frame motion towards the observer, and a change in the optical density must be perceived *on top* of the expanding frames. Thus, in the theoretical case that the aircraft could *hover* and there would be no forward motion, the optical density perception is relatively unambiguous. When forward motion is active – the normal condition – a pilot must intermittently shift his attention towards a new set of frames when the 'old' ones approach the borders of the viewplane. The shifting of pilot's gaze forwards and backwards in the tunnel also leads to increased uncertainty about the perceived position errors. Recall that the optical depression gain depends on the *local* elements involved, depending strongly on the distance to these elements. Hence, intermittently changing attention forwards and backwards into the tunnel also leads to intermittent changes in the estimates of the position errors. The optical splay angles are independent of the forward motion and, because the angle is a property of the whole line, they yield unambiguous information about the position error. Again, these characteristics also hold for the derivatives of the texture gradients. In the Experiment X3 special interest will be paid to these effects.

7.3   Experiment X3

Experiment X3 investigates the effects of providing different sets of optical cues – most prominently, those of optical splay and optical density – on pilot performance and pilot control behaviour. The analysis of the characteristics of these cues revealed that special interest should be paid to, on the one hand, the effects of forward motion and, on the other hand, the degrees of freedom of the lateral/vertical motion. In the following, it will become clear that the latter interest leads to the incorporation of a *dual* axis control task. That is, the lateral/longitudinal *roll* axis task conducted in the previous chapters will be extended with the vertical/longitudinal *pitch* axis task. Because this is the first – and the last – application of this material in this thesis, the discussion will emphasize this point.

METHOD

Subjects and instructions to subjects　　　Four subjects (A – D) participated in the experiment. They were instructed to control the aircraft through the tunnel as accurately

(a) Display **A**   (b) Display **B**   (c) Display **C**
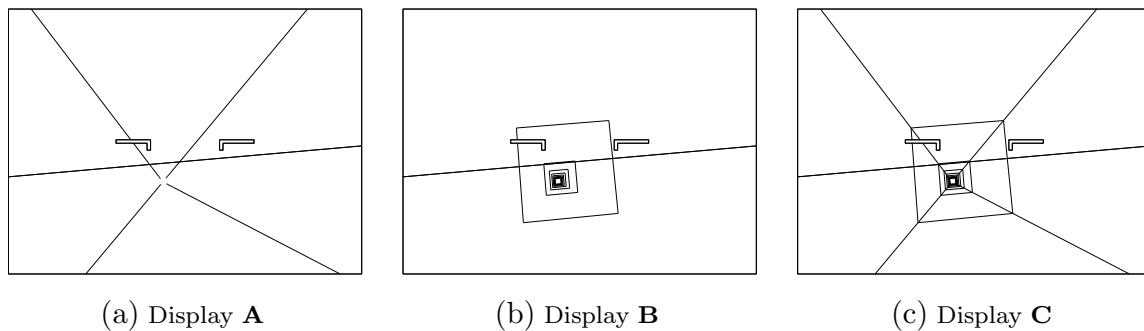
Figure 7.2: The three displays of Experiment X3: Display **A**, the splay-only tunnel; Display **B**, the density-only tunnel; Display **C**, the combination of Displays **A** and **B**.

Table 7.1: Experimental conditions (X3).

	1	2	3	4	5	6	7	8	9	10	11	12	13	14	15	16	17	18
display	**A**	**A**	**A**	**A**	**A**	**A**	**B**	**B**	**B**	**B**	**B**	**B**	**C**	**C**	**C**	**C**	**C**	**C**
channel	R	P	D	R	P	D	R	P	D	R	P	D	R	P	D	R	P	D
motion	·	·	·	M	M	M	·	·	·	M	M	M	·	·	·	M	M	M

as possible. In other words, subjects had to minimize all the position and attitude errors, despite the effects of the disturbances acting on the aircraft.

Apparatus   The Human-Machine Laboratory was used, described in Appendix A.

Independent variables   Three independent variables were defined. First, three different <u>displays</u> were defined that are all abstractions of the basic tunnel (Fig. 7.2): (i) Display **A**, showing only the longitudinal lines connecting the tunnel frames; (ii) Display **B**, showing only the tunnel frames themselves, and (iii) Display **C**, a combination of Displays **A** and **B**. Obviously, Display **A** conveys only optical splay information, Display **B** conveys only optical density information, and Display **C** provides both. No altitude poles were presented. To analyze the usefulness of the optical cues, two additional variables were manipulated in the experiment. The second independent variable was the <u>control channel</u>. Three control channels were applied: (i) *roll* (R), where only the lateral/longitudinal motion must be controlled; (ii) *pitch* (P), where only the vertical/longitudinal motion must be controlled, and (iii) *dual* (D), where the roll and pitch channels must be controlled simultaneously. The third independent variable was the status of the longitudinal or <u>forward motion</u>. Two situations were examined: (i) *no forward motion* (·), in which the longitudinal position of the aircraft was fixed, resulting in a *hovering* task[1], and (ii) *forward motion* (M), in which the longitudinal position was set free, resulting in the conventional tunnel tracking task. Summarizing, the independent measures are the *display* (3 levels), the *control channel* (3 levels) and the *forward motion* condition (2 levels).

---

[1]In this situation the aircraft moves (in lateral and/or vertical direction) in a plane perpendicular to the tunnel centerline.

Experimental design A full-factorial within-subjects design was applied, consisting of a total of 18 conditions (Table 7.1). The conditions were randomized over the experiment. Each subject conducted eight familiarization sessions (144 runs) before completing six replications of all experimental conditions (108 runs) that served as the measurements.

Procedure During the course of two and a halve days a subject conducted 252 experimental runs, divided in 42 blocks of six runs each. A single run lasted 120 [s], consisting of a run-in time T_i of 15 [s] and a measurement time T_m of 105 [s]. The pace of the experiment was such to allow sufficient time for subject preparation and to prevent fatigue.

Dependent measures For both the roll and the pitch channel five performance variables were selected, representing pilot control activity, inner loop activity and path-following performance. In the roll channel, these were the aileron control signal (δ_a) and its derivative ($\dot{\delta}_a$), the aircraft roll angle (ϕ), the heading angle error (ψ_e) and the lateral position error (x_e). In the pitch channel, these were the elevator control signal (δ_e) and its derivative ($\dot{\delta}_e$), the aircraft pitch angle (θ), the vertical flight-path angle error (γ_e) and the vertical position error (v_e). All *error* variables are defined with respect to the reference trajectory. The STDs of these ten variables acted as the dependent measures.

Description of the experiment simulation

Tunnel display geometry A generic tunnel was used consisting of square frames ($H_t = W_t = 40$ [m]) connected with longitudinal frame lines. The display format was one of the independent measures, yielding the three displays of Fig. 7.2. The reference trajectory was straight and had a downslope Γ_t of 3 [deg]. The intermediate frame distance $\triangle D$ was fixed at 350 [m]. No flight-path vector or other symbology was presented.

Aircraft models The linearized symmetric (pitch) and asymmetric (roll) dynamics of a Cessna Citation I were simulated. The aircraft dynamics were fully *uncoupled* for the two channels. The velocity was fixed at 70 [m/s]. The roll channel dynamics were identical to those applied in the previous experiments. The pitch channel dynamics are illustrated in Fig. 2.10(b). The dynamics in both channels consist of a concatenation of three elementary transfer functions connecting the pilot's input signal with the aircraft inner (*attitude*: roll and pitch angle), middle (*flight-path*: flight-path azimuth and angle of climb) and outer (position) loops. When the roll axis control task is active, all state variables of the pitch axis are fixed to their initial condition, and vice versa (Appendix C).

Atmospheric disturbances The lateral and vertical channels are both disturbed with two independent input signals each: i_1 and i_2 for roll and i_3 and i_4 for pitch. The four input signals were each computed as a sum of 12 sinusoids and are listed in Table 7.2. In order to identify pilot control behaviour in both the roll and the pitch channel simultaneously, the frequencies of the four input signals were chosen as 12 groups consisting of 4 components each, distributed over the frequency range of interest (Fig. 7.3). Grouping four frequency components closely together was problematic especially for low frequencies, and led to

Table 7.2: Definition of the input signals i_1, i_2 (roll) and i_3 and i_4 (pitch).

	roll channel							
	input signal i_1				input signal i_2			
	k_{1_i}	ω_{1_i}	A_{1_i}	ϕ_{1_i}	k_{2_i}	ω_{2_i}	A_{2_i}	ϕ_{2_i}
i	[-]	[rad/s]	[deg]	[deg]	[-]	[rad/s]	[deg]	[deg]
1	4	0.2396	0.4000	-8.7396	5	0.2992	2.0954	161.0276
2	11	0.6582	0.4130	-131.0308	12	0.7181	1.9941	-112.8963
3	19	1.1369	0.4402	-123.4390	21	1.2566	1.7939	113.1471
4	27	1.6157	0.4758	150.6975	28	1.6755	1.6241	111.9376
5	35	2.0944	0.5147	-149.1154	37	2.2141	1.4202	108.8338
6	47	2.8125	0.5680	26.5673	49	2.9322	1.1939	91.4982
7	65	3.8896	0.6144	-42.8377	66	3.9494	0.9572	53.4347
8	82	4.9069	0.6142	153.3283	83	4.6671	0.7914	44.0517
9	111	6.6422	0.5553	-62.1594	113	6.7619	0.6009	-19.6409
10	145	8.6768	0.4679	-59.7727	146	8.7366	0.4728	40.2383
11	193	11.5491	0.3698	12.8682	194	11.6089	0.3597	-145.7304
12	251	15.0198	0.2907	-143.8011	252	15.0796	0.2786	-123.6679

	pitch channel							
	input signal i_3				input signal i_4			
	k_{3_i}	ω_{3_i}	A_{3_i}	ϕ_{3_i}	k_{4_i}	ω_{4_i}	A_{4_i}	ϕ_{4_i}
i	[-]	[rad/s]	[deg]	[deg]	[-]	[rad/s]	[deg]	[deg]
1	6	0.3590	1.1841	-36.1717	7	0.4189	1.8966	-110.0366
2	13	0.7779	0.9929	-179.8160	15	0.8976	1.5302	100.8650
3	22	1.3165	0.7061	168.0954	23	1.3763	1.2087	67.0291
4	29	1.7354	0.6281	147.5793	31	1.8550	0.9757	-10.9675
5	38	2.2739	0.5064	75.3704	39	2.3338	0.8099	172.9186
6	50	2.9919	0.3988	40.4268	51	3.0518	0.6403	133.6905
7	67	4.0093	0.3045	-102.3458	68	4.0691	0.4907	-157.7298
8	85	5.0864	0.2427	135.7491	86	5.1462	0.3922	-63.7353
9	115	6.8816	0.1809	151.8412	116	6.9414	0.2932	-80.4634
10	147	8.7965	0.1421	-118.4814	148	8.8563	0.2307	-141.2839
11	196	11.7286	0.1069	10.3814	197	11.7885	0.1738	-103.6693
12	253	15.1395	0.0829	9.4847	254	15.1993	0.1349	83.4947

a considerable increase in the measurement interval T_m from the usual 81.92 [s] to 105 [s]. The amplitudes of the forcing functions were determined by the input signal shaping filters. For the roll channel, these filters were the same as those applied in Experiments X1 and X2. To reduce the subject task demand load, however, the *intensity* of forcing function i_1 was chosen to be 4.54 [deg^2] instead of the common 10.0 [deg^2]. This hampers a comparison between the results of this experiment and those of others. The amplitudes of the pitch channel forcing functions were determined by the following shaping filters:

$$H_{w_3}^{i_3}(s) = \frac{1}{1 + \tau_3 s}; \quad \text{and} \quad H_{w_4}^{i_4}(s) = \frac{1}{1 + \tau_4 s}, \tag{7.1}$$

with τ_3 and τ_4 the time constants that are both set at 1.0 [s]. The input density of i_3 is set at 4.0 [deg^2] and that of i_4 to 10.0 [deg^2]. Note that both the pitch channel shaping filters do not compensate for the aircraft pitch dynamics. A well-chosen combination of
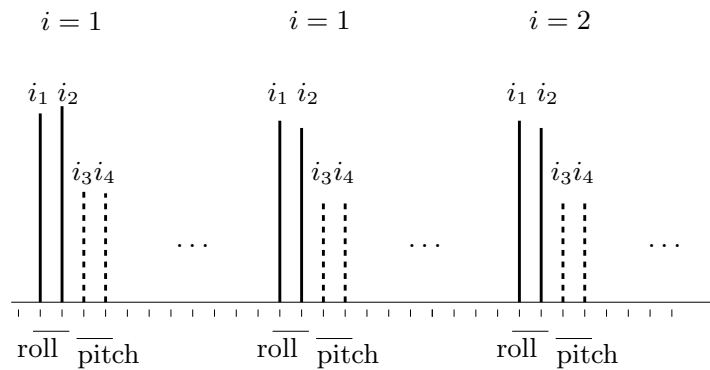
Figure 7.3: The distribution of the *frequencies* of the four forcing functions $(i_1 \ldots i_4)$, i.e. k_{1_i}, k_{2_i}, k_{3_i} and k_{4_i} (Table 7.2). The figure illustrates the fact that the frequencies are *clustered*, in twelve groups of four frequency components (the first three clusters are shown, i.e. $k_{1_1} = 4$, $k_{2_1} = 5$, etc.).

the system dynamics, the disturbance signals' spectra and their intensities is crucial in the experiment (Mulder, 1996). The settings defined above were chosen according to the input signal design rules of Appendix F and after extensive pre-experimental validation.

Initial condition   Before the start of each run, the aircraft was positioned in the center of the tunnel with zero position and attitude errors. The initial longitudinal position of the aircraft on the tunnel reference trajectory was randomized. This could lead to an artifact for Display **C** and especially Display **B**, in the *no forward motion*-conditions. Here, the perception of the optical density conveyed by the tunnel frames could be hampered when the first visual frame is located either very near the aircraft or very far away. This effect was countered by limiting the randomization of the longitudinal position – relative to the first visible frame – within boundaries determined in the pre-experimental analysis.

Identification issues

Dual axes vs. simple axis tasks   When both the vertical and the lateral axis are controlled, the pilot model in principle has six input signals and two output signals (6×2). A common assumption applied throughout this thesis, is to combine the estimation of the middle and outer loop pilot feedbacks, yielding a model with only four input signals (4×2). In Appendix F the identification method for estimating all pilot feedbacks and the potential *cross-couplings* between both the control channels is discussed. One could also assume, however, that all cross-channel interactions are zero, resulting in two parallel and independent pilot models for each control channel, each with only two input signals and one output signal (2×1). In the latter case, the effects of the cross-couplings are incorporated in the identification method as an increase in the estimated pilot noise.

The perceivability of the aircraft flight-path   As has been discussed in Chapter 4, the addition of a disturbance signal to the aircraft's flight-path angle disturbs the

relation between the aircraft's direction of motion and its attitude relative to the trajectory. This seriously affects the use of the tunnel display, because in this case the direction of motion is not fixed any more relative to the aircraft's Body axis – the display principal axis. Because the pilot's middle (flight-path) and outer (position) feedback loops can be identified simultaneously, the addition of a third disturbance signal in each control channel is unnecessary. This procedure has been used throughout this thesis – except in Chapter 9 – and applies well in the roll channel control task. Here, the aircraft direction of motion, the flight-path angle, equals the heading angle relative to the trajectory, which can be estimated using the location of the *infinity point* on the display.

In the pitch channel control task, however, this situation no longer holds. The location of the infinity point is a function of the aircraft's *attitude*, not its flight-path. In the roll channel – without slip – these are the same. In the pitch channel, even without a disturbance on the flight-path, they are not. In most aircraft, changing the pitch angle results in a lagged response of the angle of climb, that could lead to significant task difficulty in controlling the latter variable. Hence, the addition of a forcing function (i_4) on the aircraft vertical attitude angle makes things even worse: the angle of climb still lags the angle of pitch, but the latter is also disturbed by an unknown, random noise signal.

Summarizing, it can be expected that the control of the pitch channel is difficult for two reasons. First, and most important, the direction of vertical motion – the angle of climb – cannot be estimated *directly* from the display, but must be *inferred* from the changing perspective of the tunnel. Second, the control of the angle of climb is hampered due to the lagging response and the addition of an unknown random disturbance signal. This Catch-22 situation (Heller, 1961) emerged in the pre-experimental analysis. Adding a flight-path vector symbol could solve the problem but is conflicting with the purpose of the experiment. Removing the second disturbance signal in the pitch channel could also partially solve the problem, but would have made the identification of pilot behaviour in the pitch channel impossible.

Experiment hypotheses

The experiment hypotheses are straightforward when considering the pre-experimental cue analysis of §7.2. First, it is hypothesized that whereas the presence of forward motion has no effect at all on the performance with Display **A**, it deteriorates performance with Display **B**. Second, it is hypothesized that whereas adding another control channel deteriorates performance with Display **A**, performance remains more or less the same with Display **B**. The latter assumption will probably be hard to prove because a dual axes task will *inherently* be more difficult to control than a single axis task. The effects of the independent measures on Display **C** are expected to be a mixture of the effects on Displays **A** and **B**. Because it is a combination of both displays, the relative virtues and characteristics of the combined sets of cues could compensate for each other.

The effects of the explicit or implicit perceivability of the direction of motion in the roll and pitch channels, respectively, cannot be predicted beforehand. The experimental re-

sults could shed a light on the question whether either optical splay or optical density is suitable for estimating the direction of motion. It is clear, however, that because of the implicit nature of the flight-path information in the pitch channel, control of this channel can be expected to be more difficult than that of the roll channel.

7.4   Results

7.4.1   The pilot questionnaire

Because subject D was involved in the definition and set-up of the experiment, only the comments of subjects A to C will be discussed.

Realism of the simulation   The simulated roll dynamics were considered realistic; the simulated pitch dynamics were judged less realistic but still satisfactory (Table 7.3). The realism of the disturbances acting on the vehicle were judged satisfactory for the pitch channel but less realistic for the roll channel. Subjects had no further comments.

Experienced egomotion and perceived depth   Subjects considered Display **A** as a two-dimensional shape and lost their sense of egomotion completely (Table 7.3). This can be attributed to the fact that the splay-only display conveys no flow information about *forward* motion whatsoever. In the frame-only display, **B**, the sense of depth and the experienced egomotion increases dramatically when forward motion is active. The same holds for the combined display, **C**. Concluding, for all displays the experienced egomotion is negligible when the forward motion is inactive and – except for Display **A** – increases dramatically when actually moving through the tunnel. The perceived depth also gains much from adding forward motion except for Display **A**. For Display **B** and especially Display **C** the perceived depth is average even when the forward motion is turned off.

Sources of information and control strategies   Subjects were aware of and applied the two different sets of cues, splay and density, for Displays **A** and **B**, respectively. Although Display **B** implicitly showed four splay angles through 'virtual' lines connecting the tunnel frame vertices, subjects gave no comments whatsoever on this *hidden* splay information. For the combined display, **C**, the comments were mixed. Two subjects tended to use the splay lines continuously and used the approaching frames momentarily to check their position relative to the tunnel. The other subject used the frames as a primary cue and the splay angles as a check. Subjects unanimously judged the splay angles to be useful in the pitch channel control task, because it allowed them to improve their estimate of the vertical motion. Subjects judged the forward motion to be detrimental for Display **B**. Because they preferred to focus their attention to the center of the display, the expansion of the approaching frames forced them to intermittently change their attention. One subject stated that the perspective of the approaching frames allowed the aircraft dynamics to be 'visualized', which was useful for damping control inputs. Finally, all subjects commented on the difficulty of controlling the pitch channel dynamics, especially because of the lack of a reference or datum point showing their motion relative to the tunnel. One pilot

Table 7.3: Summary of results from a pilot questionnaire (X3).

How would you describe the level of *realism* of the simulated aircraft [–] *dynamics*?				
	very realistic	realistic	average	unrealistic	very unrealistic
roll	·	2	1	·	·
pitch	·	1	1	1	·

How would you describe the level of *realism* of the simulated aircraft [–] *disturbances*?				
	very realistic	realistic	average	unrealistic	very unrealistic
roll	·	·	1	2	·
pitch	·	·	2	1	·

How would you describe the strength of the experienced *egomotion*, i.e. did you have a strong feeling you were moving through a three-dimensional world or did you not?				
	very strong	strong	average	weak	very weak
A, no motion	·	·	·	·	3
A, motion	·	·	·	·	3
B, no motion	·	·	·	·	3
B, motion	·	2	1	·	·
C, no motion	·	·	·	1	2
C, motion	1	2	·	·	·

How would you describe the strength of the sense of *depth* in the display, i.e. did you have a strong feeling you were looking ahead into a three-dimensional world or did you not?				
	very strong	strong	average	weak	very weak
A, no motion	·	·	·	1	2
A, motion	·	·	·	1	2
B, no motion	·	·	1	1	1
B, motion	·	2	1	·	·
C, no motion	1	1	1	·	·
C, motion	2	1	·	·	·

commented that the applied pitch axis control strategy was not very realistic, especially when aircraft vertical load factors would be concerned.

Effort ratings   The effort ratings (Fig. 7.4) show that the roll control task is less difficult than the pitch control task, and that the dual axis task is more difficult than the single axis tasks. These findings are independent of the forward motion condition. Whereas the effect of the display is negligible between Displays **A** and **B**, control with the combined Display **C** is preferred. Although subjects commented that forward motion affected their control strategy with Display **B**, no such trend can be seen in the ratings.
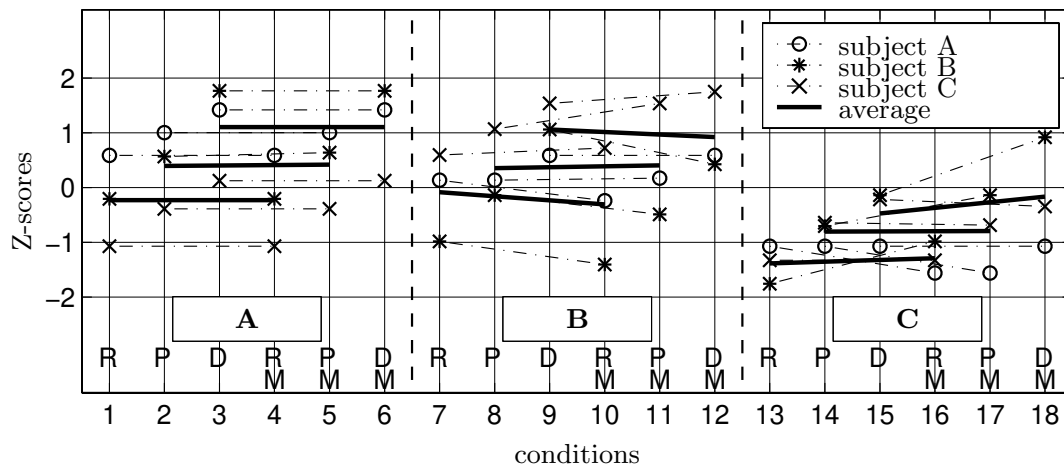
Figure 7.4: Z-scores of the effort ratings for all 18 conditions of Experiment X3. In this figure
and in the following, the insets show the three displays, the strings 'R/P/D' show
the control channel, and 'M' depicts the motion condition. The numbers below the
figure show the experimental conditions.

7.4.2   Time domain data: statistical analysis

A full-factorial mixed-model Analysis of Variance was conducted for the time domain data
of the roll and pitch channels. Three independent measures were defined: the display (D)
(3 levels), the control channel (C) (2 levels) and the forward motion condition (M) (2
levels). For a particular dependent measure, the channel measure merely compares the
single vs. the dual axis control task, i.e. 'R' vs. 'R+P' for the roll axis variables and 'P'
vs. 'P+R' for the pitch axis variables. The ANOVA results are summarized in Table 7.4.

Roll channel variables   The means and 95% confidence intervals for the aileron control
signal and its derivative are illustrated in Figs 7.5(a) and 7.5(b). It is clear that control
activity decreases when the pitch channel is added. Both variables show only a significant
D×M-interaction (δ_a: $F_{2,6} = 5.673$, $p=0.041$; $\dot{\delta}_a$: $F_{2,6} = 5.942$, $p=0.038$), caused by the
fact that whereas motion has no effect on Display **A**, it does affect Displays **B** and **C**
significantly. For the latter two displays control activity decreases when motion is added.
This can be verified by dividing the data into three categories according to the display
variable, and computing an ANOVA for each of them.

Quite the opposite holds for the roll angle (Fig. 7.5(c)), that increases when the pitch
channel is added. Again, a significant D×M-interaction is found ($F_{2,6} = 6.415$, $p=0.032$),
caused by the different effects of motion on Display **A** vs. Displays **B** and **C**.

The path-following accuracy, expressed in terms of the heading angle error ψ_e (Fig. 7.5(d))
and the lateral position error x_e (Fig. 7.5(e)) shows some clear effects. Surprisingly,
none of the independent measures causes significant effects for the heading angle error.
Independent of the other measures, ψ_e is smallest for Display **B**, where the results for
Displays **A** and **C** are equivalent. The addition of the pitch control channel leads to an
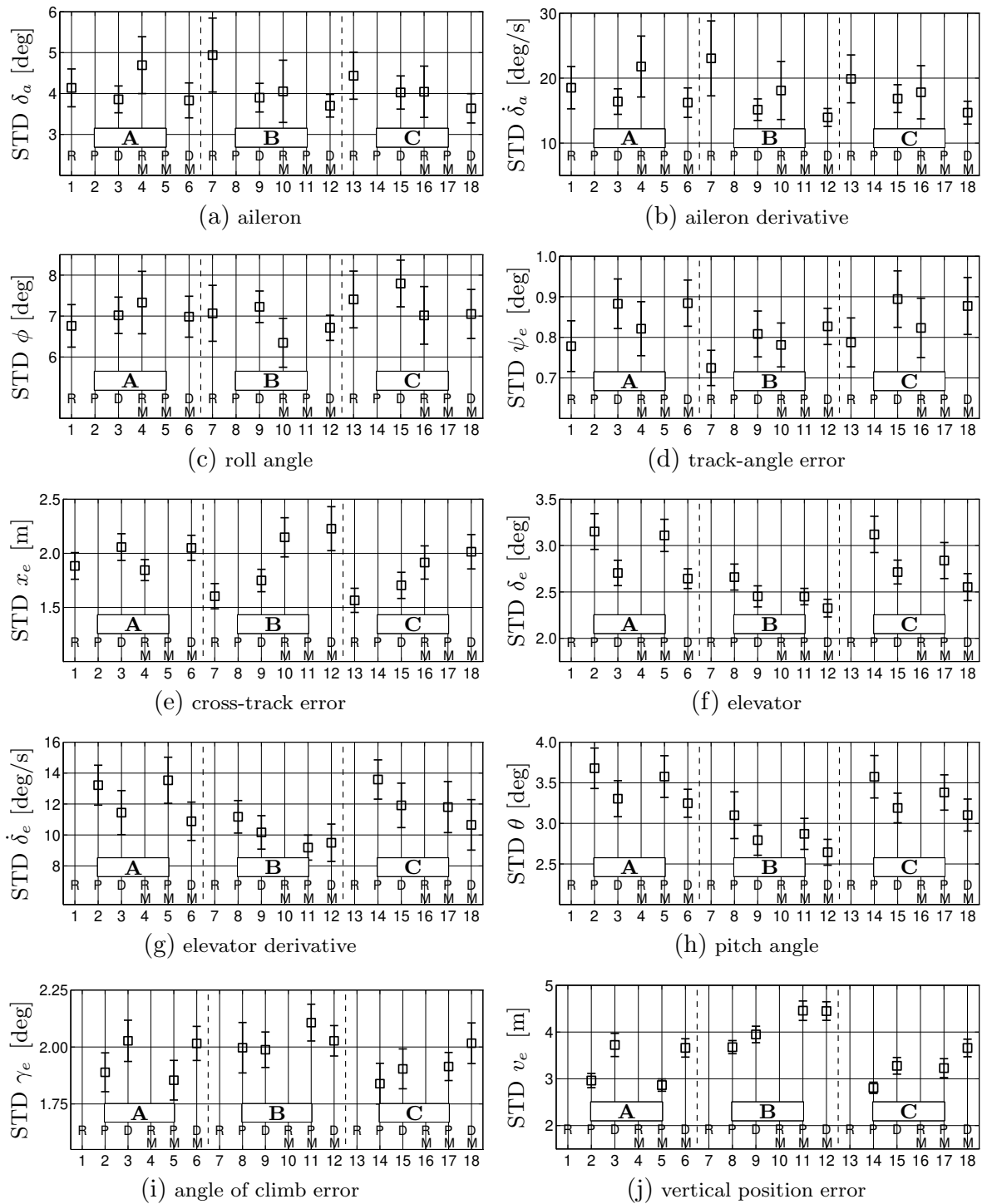
Figure 7.5: Means and 95% confidence limits of the STDs of the dependent measures (all subjects).

Table 7.4: Results of a full-factorial ANOVA (X3) on the dependent measures involving control activity, inner loop activity and path-following accuracy (in this table '$\star\star$', '$\star$' and '$\circ$' represent significance levels of $p \leq 0.01$, $0.01 < p \leq 0.05$ and $0.05 < p \leq 0.10$, respectively).

	roll channel					*pitch channel*				
	δ_a	$\dot{\delta}_a$	ϕ	ψ_e	x_e	δ_e	$\dot{\delta}_e$	θ	γ_e	v_e
main effects										
D	·	·	·	·	$\circ$	$\star\star$	$\star\star$	$\star\star$	$\star\star$	$\star\star$
C	·	·	·	·	$\circ$	$\star$	$\star$	$\star$	$\star$	$\star\star$
M	·	·	·	·	$\star$	·	·	·	·	$\star\star$
2-way interactions										
D×C	·	·	·	·	·	$\star\star$	$\star\star$	·	$\star$	$\star\star$
D×M	$\star$	$\star$	$\star$	·	$\star$	·	·	·	·	$\star\star$
C×M	·	·	·	·	·	·	·	·	·	·
3-way interaction										
D×C×M	·	·	·	·	·	·	·	·	·	$\circ$

increasing heading angle error. Motion has a small but not significant effect on Displays **B** and **C**. The cross-track error is smallest for Display **C** in almost all conditions, causing a display effect of borderline significance ($F_{2,6} = 3.591$, $p=0.094$). Motion has no effect on Display **A**, but it leads to decreasing performance with Displays **B** and **C**. This causes the significant effect of motion ($F_{1,3} = 12.117$, $p=0.040$) and the significant D×M-interaction ($F_{1,3} = 8.863$, $p=0.016$). The addition of the pitch control task leads to an increasing cross-track error ($F_{1,3} = 9.797$, $p=0.052$).

Pitch channel variables Table 7.4 indicates that the variation in the independent measures leads to much stronger effects on the pitch channel variables relative to the roll channel variables. The means and 95% confidence limits of the elevator control signal and its derivative are shown in Figs 7.5(f) and 7.5(g). Control activity is smallest for Display **B** and decreases when the roll channel is added, causing the significant effects of display (δ_e: $F_{2,6} = 28.306$, $p <0.01$; $\dot{\delta}_e$: $F_{2,6} = 15.436$, $p <0.01$), and control channel (δ_e: $F_{1,3} = 33.057$, $p=0.011$; $\dot{\delta}_e$: $F_{1,3} = 14.937$, $p=0.031$). The effect of the control channel is not significant for Display **B**, causing the significant D×C-interaction (δ_e: $F_{2,6} = 32.125$, $p <0.01$; $\dot{\delta}_e$: $F_{2,6} = 33.561$, $p <0.01$). Forward motion has no effect on Display **A**. It leads to a decrease in control activity for Displays **B** and **C**, that is not significant.

The pitch angle (Fig. 7.5(h)) has similar effects. First, it is smallest for Display **B**, independent of the other measures, causing the significant effect of display ($F_{2,6} = 24.749$, $p <0.01$). Second, the addition of the roll axis yields a decreasing pitch angle variance, also independent of the other measures, causing the significant channel effect ($F_{1,3} = 29.733$, $p=0.012$). Whereas forward motion has no effect on Display **A**, it does lead to a decrease – but not significant – for Displays **B** and **C**.

The path-following accuracy, expressed in the vertical position error v_e and the angle of

climb error γ_e, is shown in Figs 7.5(j) and 7.5(i). Performance is superior for Display **C**, both in terms of v_e and γ_e. Performance is worst with Display **B**. The display effect is significant (v_e: $F_{2,6} = 22.390$, $p <0.01$; γ_e: $F_{2,6} = 23.488$, $p <0.01$). Furthermore, the addition of the roll axis task deteriorates performance with Display **A**, independent of the motion condition, and Display **C**. The effect does virtually not exist for Display **B**. These effects together cause the significant effect of the control channel (v_e: $F_{1,3} = 40.281$, $p <0.01$; γ_e: $F_{1,3} = 13.177$, $p=0.036$), the D×C-interaction (v_e: $F_{2,6} = 11.475$, $p <0.01$; γ_e: $F_{2,6} = 9.652$, $p=0.013$) and the D×C×M-interaction of v_e ($F_{2,6} = 3.793$, $p=0.086$). Whereas forward motion has no effect on Display **A**, it leads to a deteriorating performance for Displays **B** and **C**, but only in terms of v_e. This causes the significant effect of motion ($F_{1,3} = 67.717$, $p <0.01$) and the D×M-interaction ($F_{1,3} = 15.522$, $p <0.01$).

7.4.3 Frequency domain data

Relative noise ratios   Seven RNRs can be computed of the control, inner loop and outer loop signals of both the pitch and roll channels: four RNR's for each individual frequency ($i_1 \ldots i_4$), two RNR's of the set of frequencies of each channel ($i_1 \& i_2$ and $i_3 \& i_4$) and a RNR for all frequencies at a time ($i_1 \& i_2 \& i_3 \& i_4$). The RNRs provided insight into what could be expected in the procedure of estimating the frequency responses. First, they showed that in the dual axes tasks the distribution of variance due to the potential cross-couplings between both channels was negligible. For a particular signal, the dual axes task only led to an increase in the RNRs at the corresponding frequencies of the particular signal channel. Second, whereas the RNRs marked a clear increase in the noise variance in the dual axes task for Display **A**, this effect was marginal for Displays **B** and **C** (see Fig. 7.6, that shows characteristic values of the roll channel RNRs of one subject). Third, whereas the RNRs showed a clear increase in the noise variance when forward motion was added for Display **B**, this effect was smaller for Displays **A** and **C**.

Estimated frequency responses   Recall that the frequency responses were estimated for two operator models, i.e. the (4×2) parallel model *combining* the pitch and roll channels, and the common (2×1) parallel model where the estimation in both channels is separated (Appendix F). The estimates support the findings of the RNRs. Fig. 7.7 shows typical estimated inner loop frequency responses of the (4×2) parallel feedback model. Four frequency responses are estimated, consisting of the two *within*-channel responses $H_{\phi\delta_a}$ and $H_{\theta\delta_e}$ and the two *between*-channel responses $H_{\phi\delta_e}$ and $H_{\theta\delta_a}$. The figures show two different estimates: (i) the averaged frequency response estimations using the *raw* time histories (squares) and the variance in the estimates (cross-hairs), and (ii) the frequency response estimations using the *averaged* time histories (circles). The figures illustrate that whereas the two estimates are similar for the within-channel responses, they are not for the cross-couplings. The estimates of the between-channel responses are *not consistent*. First, the large variance in these estimates indicate that they change considerably between trials. Second, the averaged estimates are not the same as the estimates using the
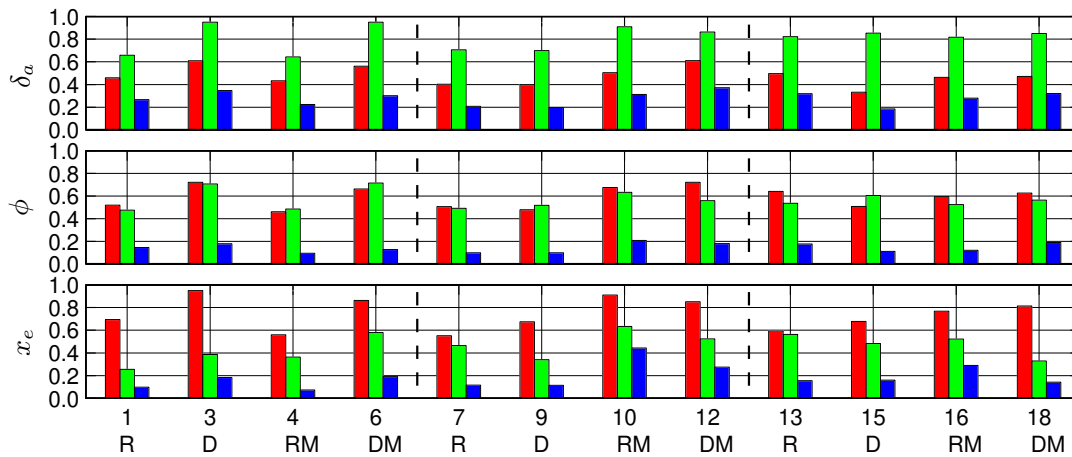
Figure 7.6: Relative noise ratios (one subject, *roll* conditions). The three bars for each condition represent the RNRs computed at frequencies i_1 (left), i_2 (middle) and $i_1\&i_2$ (right).

averaged data. Third, the estimated frequency responses do not correspond to a *normal* system. The estimates of the within-channel responses – the direct couplings – show an opposite trend. First, they are consistent between trials as judged by the comparatively small uncertainties. Second, the averaged estimates resemble those computed with the averaged data closely. And third, the estimates portrait a normal linear system.

In conclusion, the RNRs as well as the estimates of the frequency responses suggest that the dual axes tasks can be regarded as *two single axis tasks operating in parallel*, i.e. a dual (2×1) instead of a single (4×2) feedback process. In the frequency response estimation procedure, it can be assumed that both control channels can be treated independently of each other. The cross-couplings appear only as an increase in the noise components of a particular signal, leading to larger uncertainties of the estimates.

7.5   Modelling efforts

The pre-modelling data (RNRs etc.) indicated that the pilot behaviour in the dual axes tasks could be modelled as two single axis controllers running in parallel. Therefore the results for both the roll and the pitch channel are discussed separately.

Roll channel

Model structure   The MLM model structure in the roll channel is identical to the structure applied in Experiments X1 and X2. The model consists of three feedback loops representing pilot control of aircraft attitude, flight-path and position.
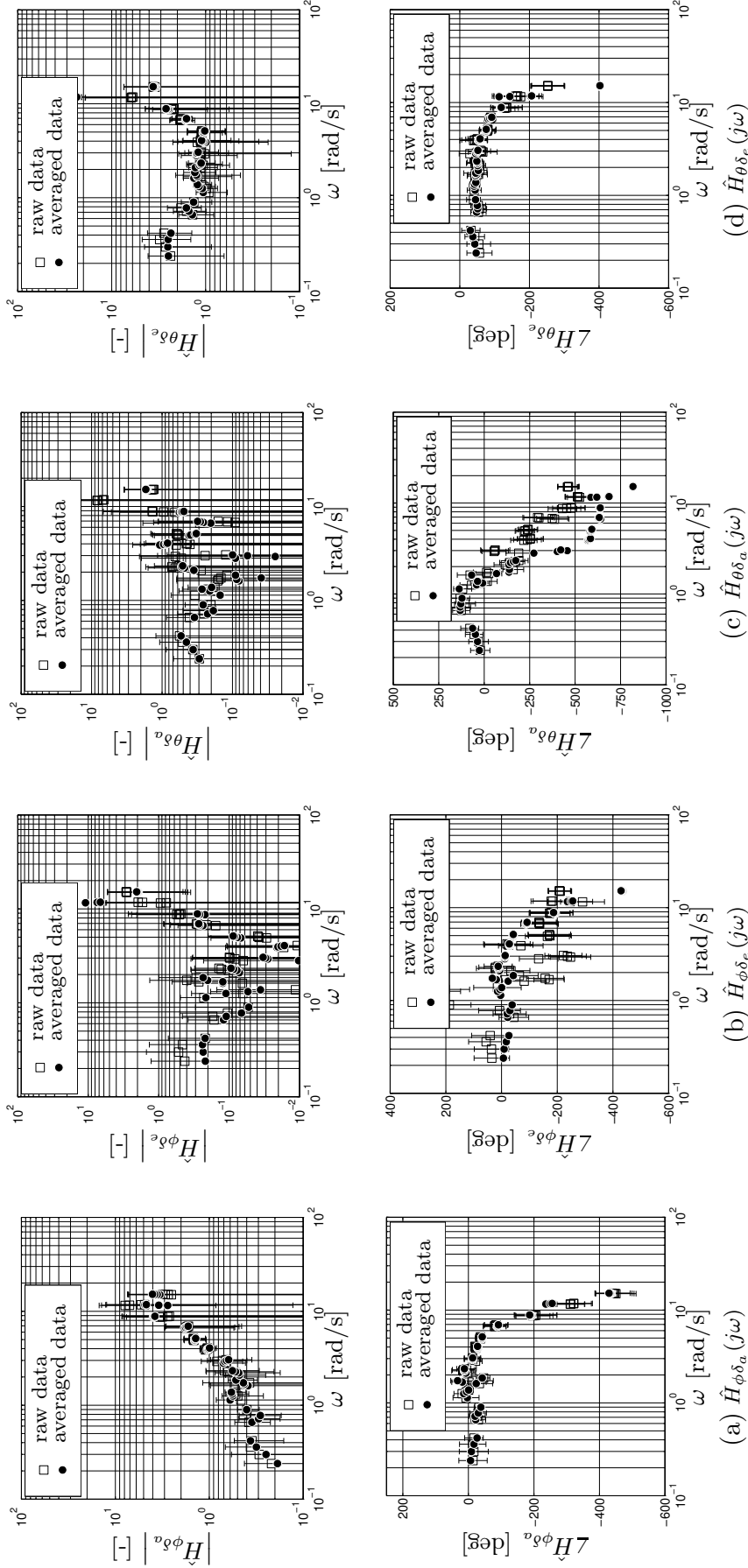
Figure 7.7: Estimates of the inner loop frequency responses, using the 4×2 parallel model structure (one subject, one condition). The left and right columns show the two *within*-channel responses, and the two middle columns show the *between*-channel responses. That is, $H_\phi^{\delta_a}$ depicts the pilot frequency response relating the aircraft inner loop signal, ϕ, with the pilot control signal, δ_a, for the *roll* channel control task. The same holds for $H_\theta^{\delta_e}$ in the aircraft pitch channel control task. $H_\phi^{\delta_e}$ is the pilot frequency response relating the aircraft inner loop signal in the roll channel, ϕ, with the pilot control signal, δ_e, in the pitch channel.

(a) time delay, neuromuscular bandwidth and damping

(b) inner loop lead and gain
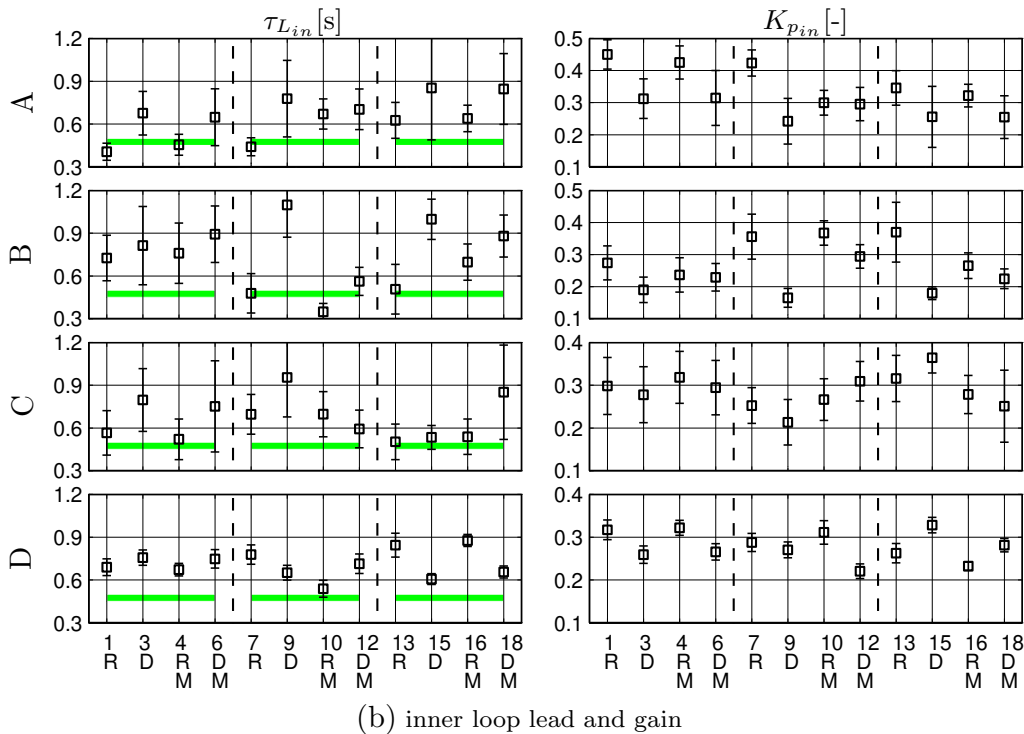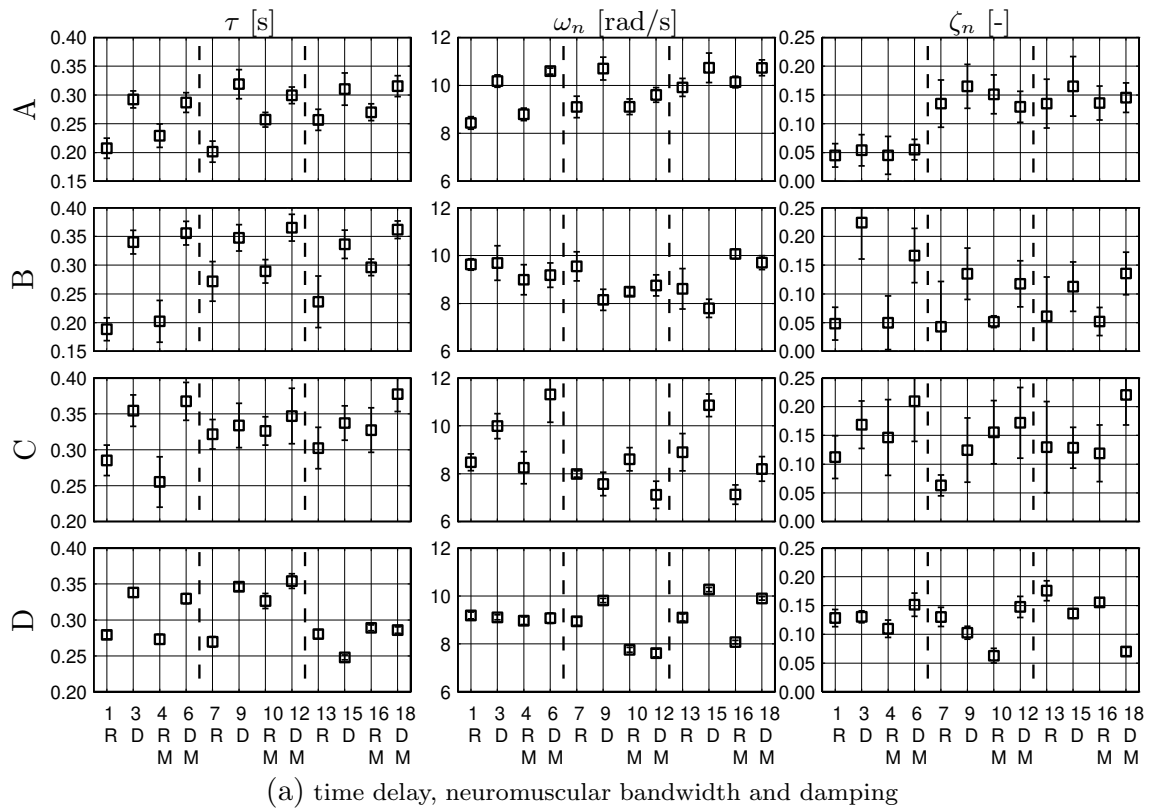
Figure 7.8: Roll channel inner loop MLM pilot model variables (all subjects, all conditions). Here, and in the following, the cross-hairs show the parameter estimation uncertainties according to Cramer-Rao. In the bottom left figure, the horizontal shaded areas show the values of the aircraft roll subsidence lag time constant, τ_ϕ.

Model parameters   The MLM model parameters are identical to those applied in Experiment X1. It is hypothesized that all pilot equalization efforts are put in the control of the inner loop (attitude). The middle and outer loops are fed back with two proportional gains which merely determine the bandwidth of the two feedback loops. Here only the inner loop variables are discussed.

The estimated inner loop parameters are illustrated in Figs 7.8(a) and 7.8(b) for the pilot limitation and pilot equalization subsystems, respectively. The main trends in the pilot limitation data are, first of all, an increasing time delay, neuromuscular frequency and damping for the dual axes tasks. This is a clear and obvious effect of the fact that a pilot must control two channels simultaneously. Dividing attention over two channels leads to an increasing delay, which in turn causes a more conservative neuromuscular system dynamics. Second, the motion condition has no effect on parameters with Display **A**. Third, the trend in the parameters for Display **C** generally follows that of Display **A**. Fourth, the time delay is somewhat larger for Displays **B** and **C**, especially in the single axis conditions. Finally, the forward motion condition leads to increasing time delays for Displays **B** and **C**. These trends are not always clear, however, for all subjects.

The trends in the pilot equalization data show the antagonistic character of the inner loop lead and gain. First of all, the lead increases and the gain decreases for the double axis conditions. This illustrates a pilot's need to gain extra phase margin needed at these conditions to compensate for the increasing delay. Second, whereas the motion condition has no effect on Display **A**, it affects the data of the other displays. For Display **B** the lead becomes smaller and the gain increases when motion is added. Thus, the inner loop equalization network can not compensate completely for the increasing delay for the conditions with Display **B**. Again these trends are not always clear for all subjects.

MLM results: crossover frequencies and phase margins   The measured and modelled crossover frequencies and phase margins of the inner loop and the combined outer loop are illustrated in Figs 7.9(a) and 7.9(b), respectively. The dual axes tasks lead to a decreasing inner loop bandwidth and an increasing phase margin for all displays. Whereas the forward motion condition has no effect on Display **A**, it leads to lower inner loop phase margins for Display **B**. In the dual axis tasks, the inner loop bandwidth is smallest for Display **B**. The addition of motion in these conditions increases bandwidth somewhat. Finally, the largest phase margins are found for Display **C**. The combined outer loop bandwidth is smaller (larger phase margin) for the dual axes tasks, for all displays except Display **B**. Whereas the addition of motion has no effect on Display **A**, it leads to a smaller bandwidth and higher phase margins for Displays **B** and **C**. In the combined outer loop, the trends in Display **C** resemble those of Display **B**. Display **C** yields the highest values of the combined outer loop bandwidth, accompanied by the lowest values of the phase margin. The estimation of the MLM middle and outer loop gains allows the combined outer loop to be dissected in the middle and outer feedback loops. The bandwidth and stability margins of these loops are shown in Fig. 7.10. The dual axes tasks lead to lower values of the middle
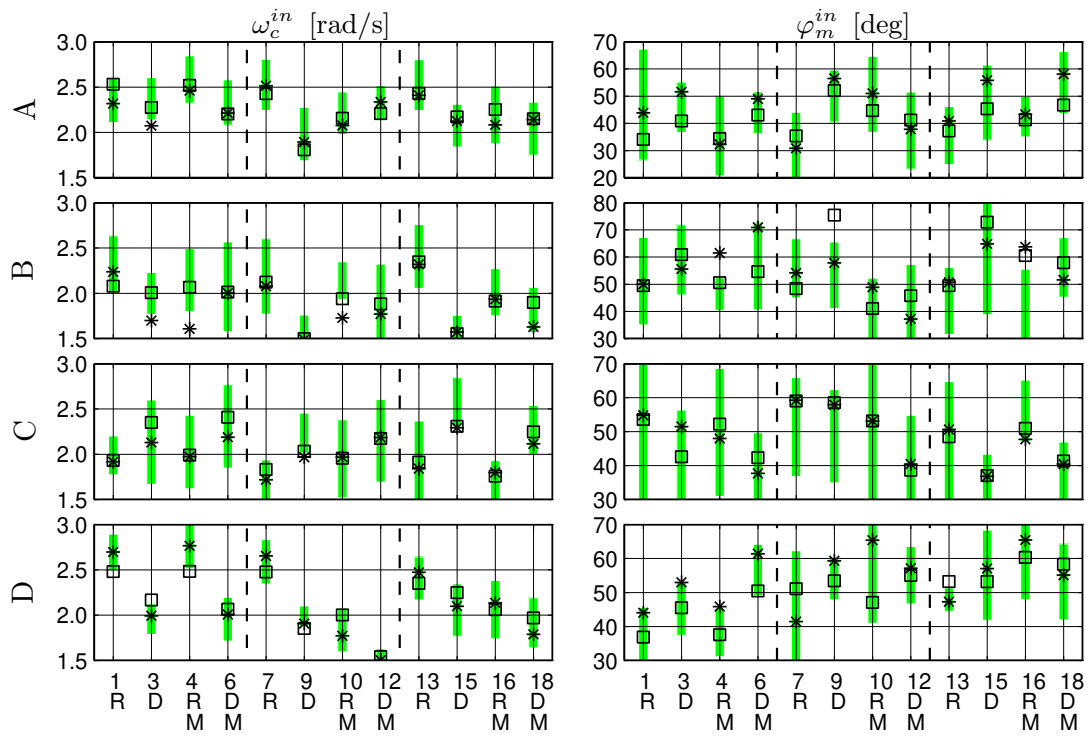
(a) inner loop
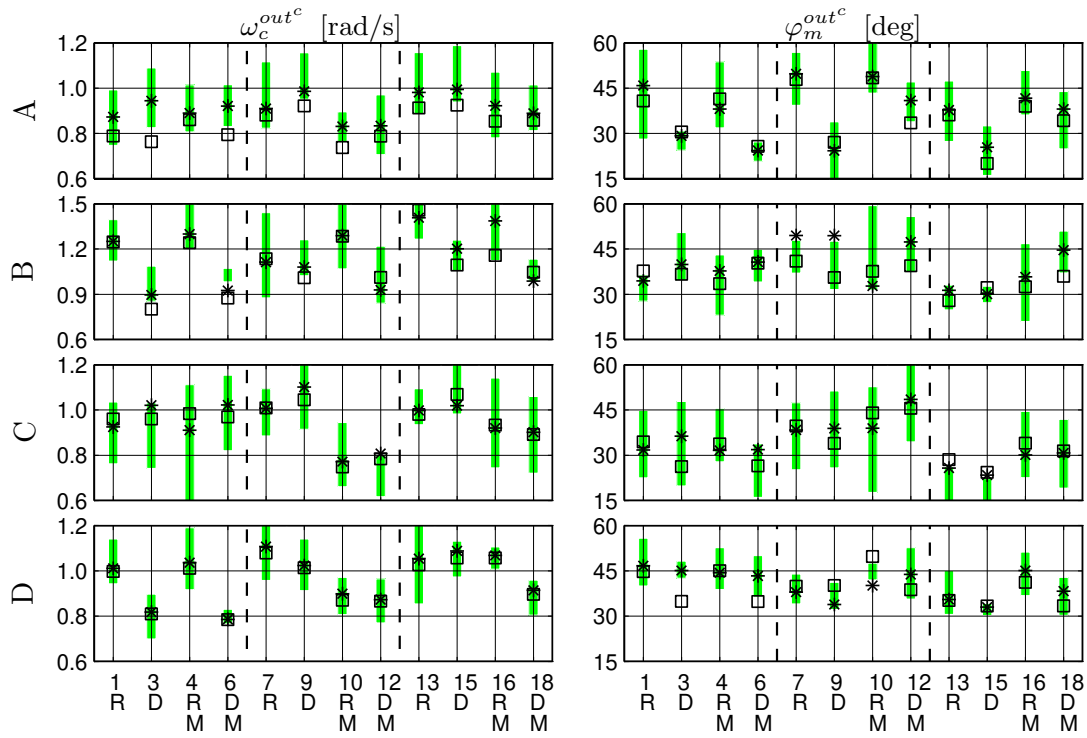
(b) outer loop (combined)

Figure 7.9: Roll channel crossover frequencies and phase margins (all subjects, all conditions).
The shaded areas show the uncertainty regions of the raw frequency response data.
The '*'-symbols show the quantities for the averaged frequency responses; the
squares show them for the MLMs.
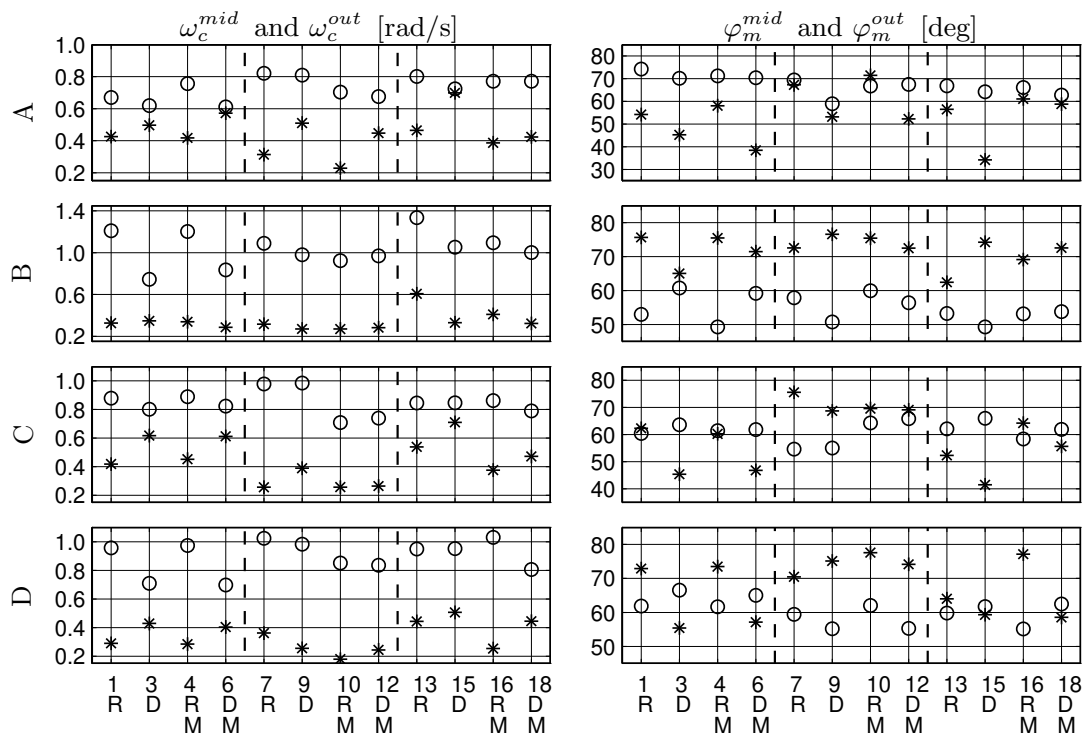
Figure 7.10: Roll channel crossover frequencies and phase margins of the middle ('o') and outer ('*') loops, following the MLM analysis (all subjects, all conditions).

loop bandwidth for all displays, especially Display **A**. The effect on phase margin is less clear and depends on the display: for Display **A** bandwidth increases, whereas for Display **B** it decreases for the dual axes tasks. The forward motion does not influence Display **A**, but leads to lower values of the middle loop bandwidth and increasing phase margins for Display **B**. The effects of adding another control channel and forward motion have only marginal influence on Display **C**. Bandwidth is highest and stability margins smallest for this display. The trends in the outer loop variables are clear. First, the dual axes tasks lead to higher bandwidths and lower phase margins. This contradicts to what could be expected and will be explained later. The forward motion affects Display **C** and especially Display **B**, decreasing the bandwidths (higher stability margins). Generally, bandwidth is highest for Display **C** and lowest for Display **B**, except for the conditions with forward motion where Display **A** is superior. The stability margins are lowest for Display **B**.

Pitch channel

In all other experiments of this thesis, the single axis roll channel control task is examined and the states of the symmetric aircraft motion are fixed to their initial conditions. Experiment X3 is the only experiment where pilots had to control the aircraft in the vertical dimension. The symmetric aircraft dynamics are described in detail in Appendix C. Below, the pilot model in the pitch channel will be elaborated.
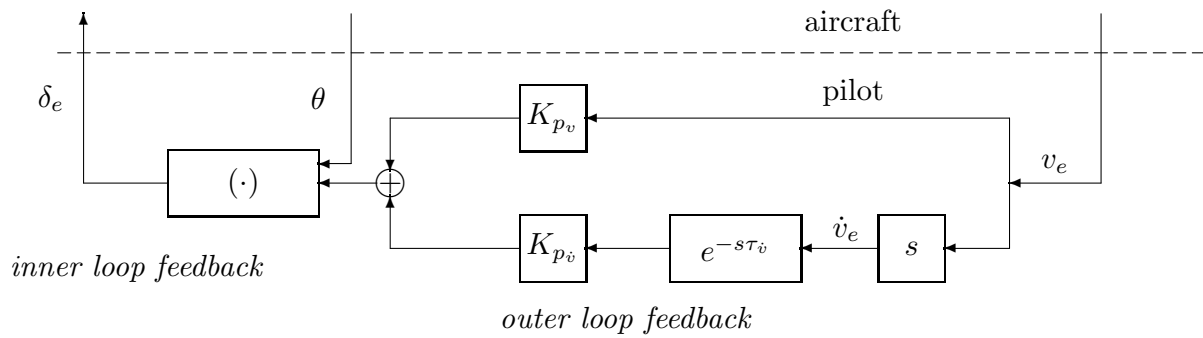
Figure 7.11: MLM model structure of the pitch channel outer loop. Here, the upper path marks a proportional feedback of the vertical position error. The lower path shows a proportional feedback of a delayed estimate of the vertical position error rate.

MLM model structure   The model structure of the inner loop is similar to that of the roll channel, except for the inclusion of the pilot lag time constant $\tau_{I_{in}}$. Recall that the inner loop aircraft dynamics are simplified by an elementary integrator, yielding a proportional relation between the aircraft pitch rate and the pilot elevator deflection. The estimated frequency responses revealed that the lag parameter $\tau_{I_{in}}$ was necessary to describe the low-frequency lag adopted by pilots to dampen their pitch-rate response.

The model structure in the outer loop is completely different from that of the roll channel. Recall that whereas in the roll channel the flight-path ψ_e is directly visible from the display (through the infinity point), this is not the case in the pitch channel. Here, the flight-path angle error γ_e must be estimated, through perceiving the *derivatives* of the cues for a position error – optical splay and optical density. A model structure was applied – illustrated in Fig. 7.11 – that incorporated the *indirectness* of controlling vertical flight-path. It consists of two paths. The first path is a proportional feedback of the vertical position error v_e, K_{p_v}. The second is a proportional feedback of the estimated vertical position error rate $\dot{v}_e$, $K_{p_{\dot{v}}}$. Because this rate must be perceived from the changing perspective geometry, a time delay is added in the second path, $\tau_{\dot{v}}$. The resulting model structure could describe the measured pilot control behaviour in the vertical dimension quite well. One of the virtues of the cybernetic approach is that, when mistakenly applying a pilot model like the one used in the roll channel, i.e. with an *explicit* feedback of flight-path, the results would be dramatic. Hence, the frequency domain estimates provide a strong link with the analysis of cue functionality, and vice versa.

MLM model parameters   The inner loop variables are illustrated in Figs 7.12(a) and 7.12(b) for the pilot limitation and equalisation subsystems, respectively. As one can see from Fig. 7.12(a), the estimation of the `nm` damping was problematic, forcing this variable to be fixed at its lower bound – 0.045 [s] – for almost all conditions and subjects. The badly damped `nm` system and the relatively low time delay – as compared

(a) time delay, neuromuscular bandwidth and damping

(b) inner loop lead and gain
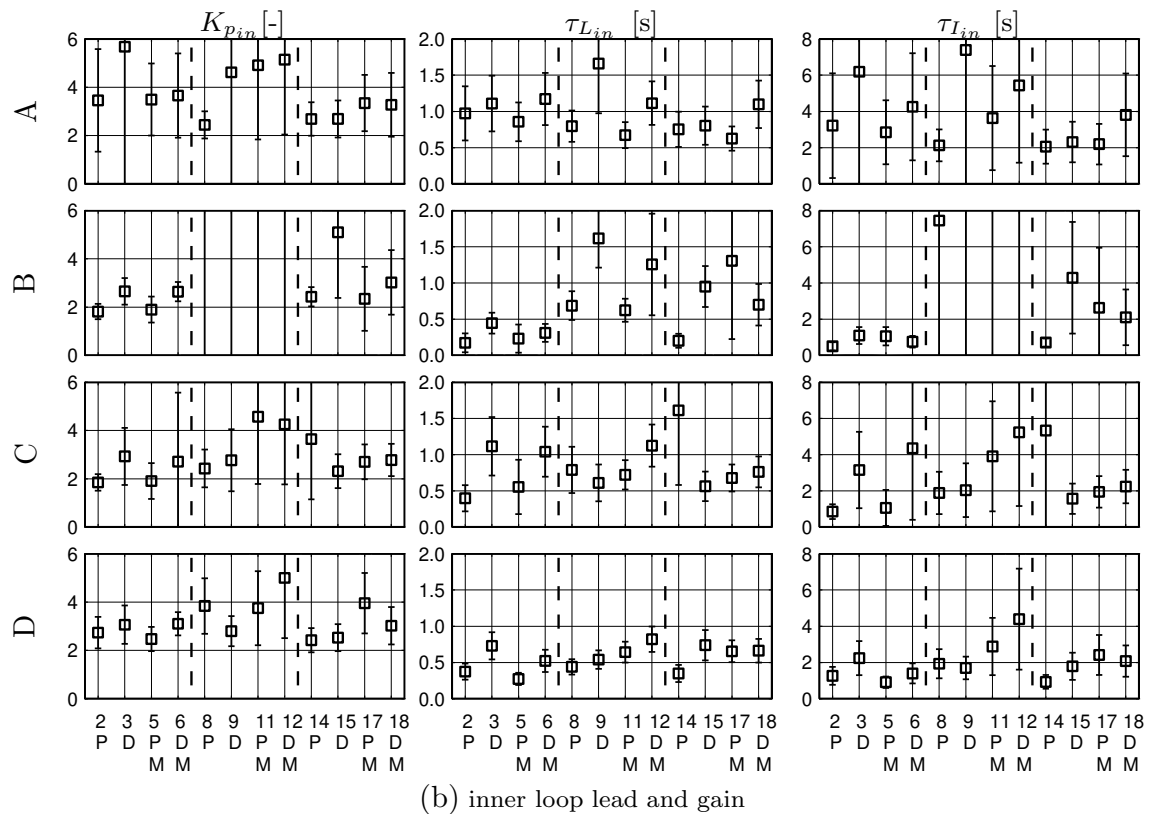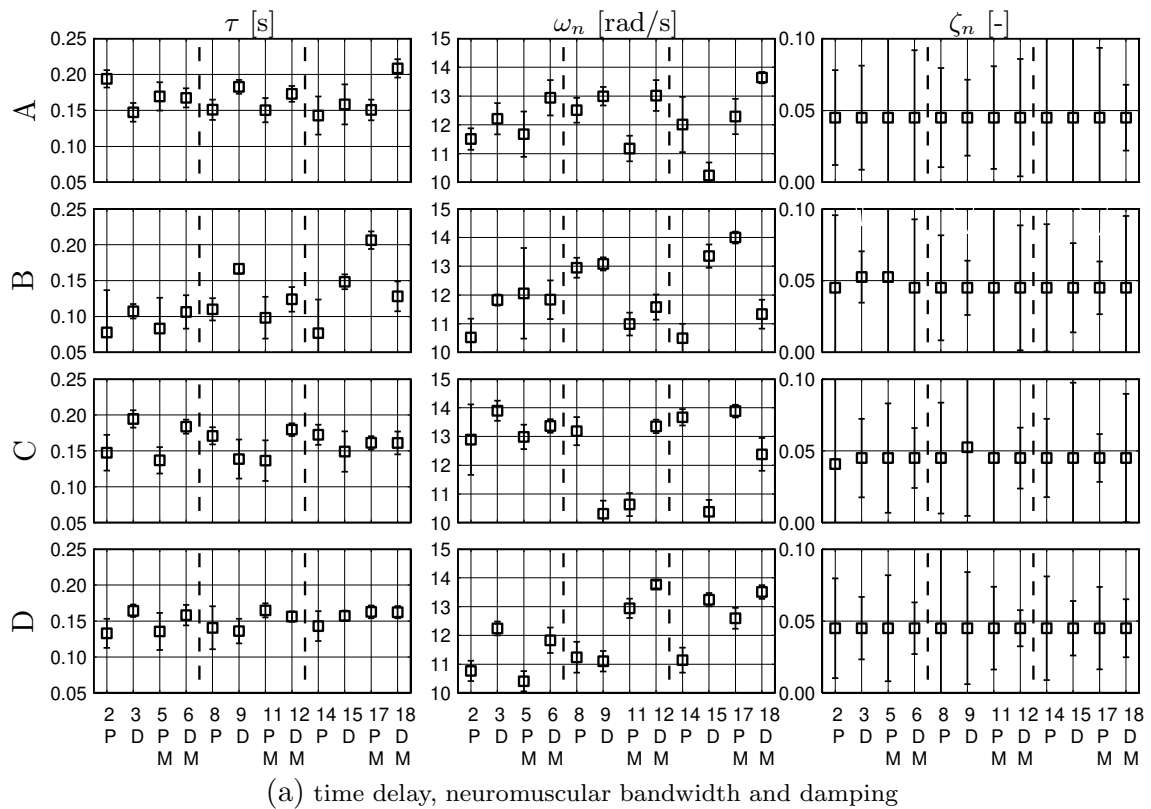
Figure 7.12: Pitch channel inner loop MLM pilot model variables (all subjects, all conditions).
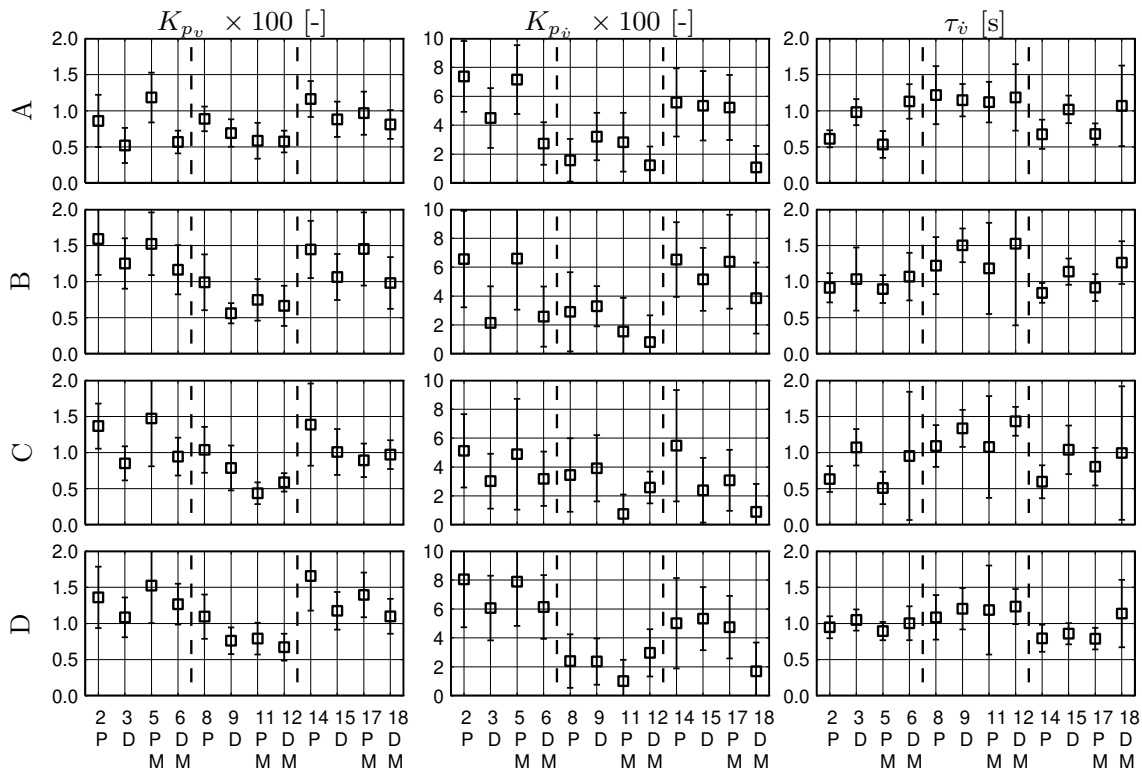
Figure 7.13: Pitch channel outer loop MLM variables (all subjects, all conditions).

to the roll channel – are signs of a strong pilot need for phase margin at the middle and high-frequency regions. The effects on τ and ω_n are not very clear, although they both increase for almost all dual axes conditions. Whereas motion had no effect on Display **A**, it results in an increasing delay for Display **C**. The equalization variables also have a rather scattered appearance. Especially the inner loop gain and lag time constant are difficult to estimate in the conditions with Display **B** (subject B). Generally, the dual axes tasks lead to increasing values of all equalization variables. Furthermore, all variables appear to be larger for Display **B** especially in the forward motion conditions. The network variables $\tau_{L_{in}}$ and $\tau_{I_{in}}$ have almost identical trends. The increasing lead time constants for the dual axes tasks are an obvious attempt to compensate for the increasing delay at these conditions. The effects for Display **C** are less clear. Summarizing, the estimation of the inner loop variables was difficult and showed considerable differences between subjects.

The outer loop – the vertical position error feedback – parameter estimation was more successful (Fig. 7.13). First of all, the motion conditions had no effect on the parameters with Display **A**. The gains of both the position error and derivative feedbacks decrease for Displays **A** and **C** when the roll task is added. This effect is smaller for Display **B**. The addition of motion leads to decreasing gains for Displays **B** and **C**. For the conditions without motion, the position derivative feedback gains increase for Display **B**. Generally, K_{p_v} and $K_{p_{\dot v}}$ are highest for Displays **A** and **C**, especially for the single axis conditions.

These gains are smallest for Display **B**, especially when motion is added. The time delay $\tau_{\dot{v}}$ – modelling the time needed to *implicitly* derive position error derivative (flight-path) information – is rather high, i.e. 0.5 to 1.5 [s], especially for Display **B**. For all displays this variable increases for the dual axes conditions. Motion appears to have no effect at all for any of the displays. The trends for Display **C** are similar to those of Display **A**.

MLM results: crossover frequencies and phase margins The inner loop and outer loop bandwidth and stability margins are shown in Figs 7.14(a) and 7.14(b), respectively. The effects are as they were anticipated. Concerning the inner loop variables, the inner loop bandwidth decreases for the dual axes conditions for Displays **A** and **C**, whereas they increase for Display **B**. The opposite trends hold for the phase margin that increases for Displays **A** and **C** and decreases for Display **B**. The forward motion has no effect on Display **A**, it leads to lower bandwidths and higher phase margins for Display **B**, and has a mixed effect on Display **C**. Generally, the inner loop bandwidth is lowest with Display **B** and highest with Display **A**. The opposite holds for the phase margin, except for Display **A** in the dual axes configurations. Concerning the outer loop variables, these show some interesting trends. Display **A** is independent of the motion condition, and is only affected by the dual axis configurations, leading to lower bandwidths and higher stability margins. For Display **B**, the effects of the dual axes tasks are less strong. Control with this display is harmed most by the addition of forward motion, judged by the lower bandwidths and higher phase margins in these conditions. The trends in Display **C** seem to be mixed versions of those with the other two displays, and depend also on the subjects involved. Generally, the outer loop crossover frequency is lowest for Display **B** and highest for Display **A**, especially for the single axis conditions. The phase margins are lowest for Displays **A** and **C** and highest for Display **B**, especially when the forward motion is active.

7.6 Retrospective

7.6.1 Discussion

The main optical sources of information conveyed by a tunnel-in-the-sky display that refer to a position error with respect to the reference trajectory are those of optical splay and optical density. The relative usefulness of these two sets of cues for the control of an aircraft along a straight tunnel trajectory has been the subject of this chapter. By manipulating the tunnel display geometry, Experiment X3 has isolated the two sets of cues, allowing a comparison of the measured pilot performance and pilot control behaviour. Three displays have been applied: one conveying only splay information (**A**), one showing only density information (**B**) and one presenting both (**C**). The pre-experimental cue analysis of §7.2 revealed that special attention should be put on two aspects that could affect the functionality of the optical cues. First, the analysis predicts that the display showing only splay information could be vulnerable when more than one aircraft degree of freedom is controlled simultaneously. Second, the display showing only density information
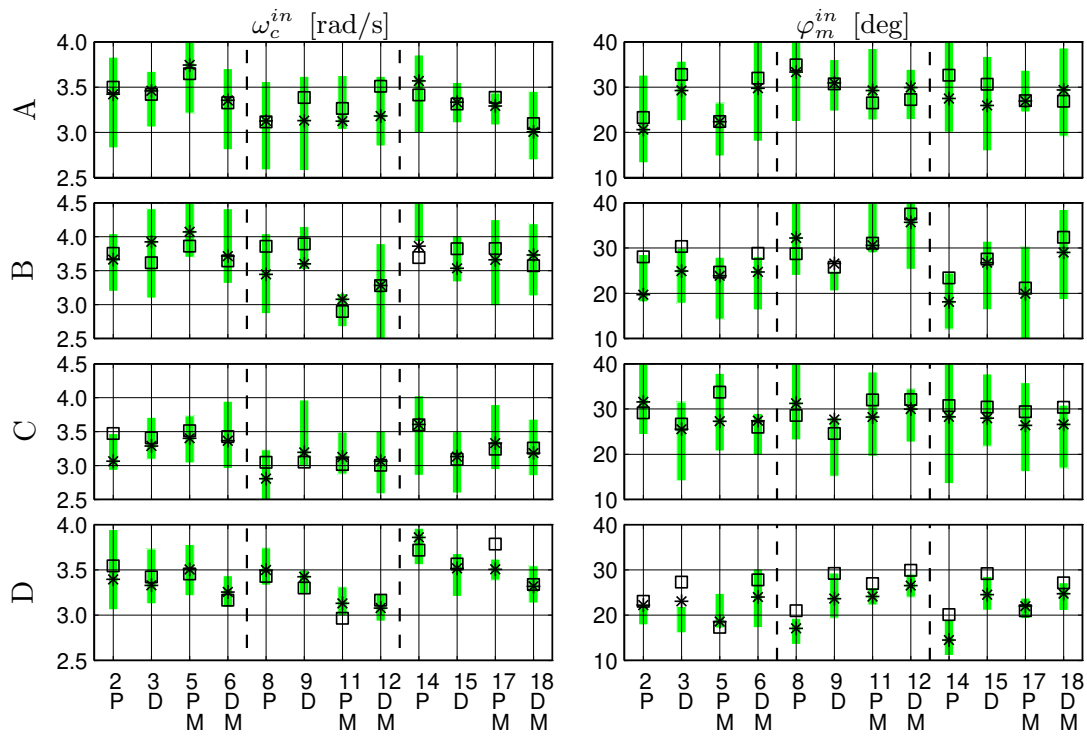
(a) inner loop
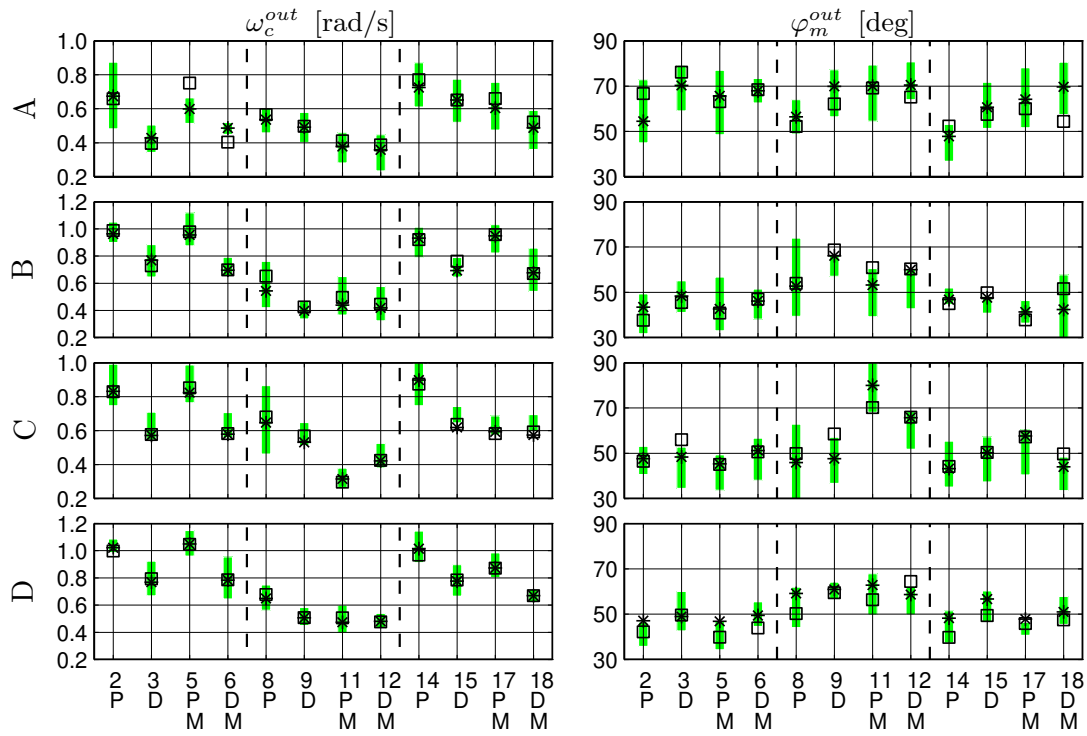
(b) outer loop

Figure 7.14: Pitch channel crossover frequencies and phase margins (all subjects, all conditions). The shaded areas show the uncertainty regions of the raw frequency response data. The '*'-symbols show the quantities for the averaged frequency responses; the squares show them for the MLMs.

could be affected by the fact that the perceivability of these cues are hampered by the forward aircraft motion. These two aspects led to the incorporation of two independent measures in the experiment, i.e. the *channel* measure depicting either the single axis (roll or pitch) or the dual axis (roll and pitch) control tasks, and the *motion* measure, depicting either the hovering aircraft motion or the conventional traversing aircraft motion.

In the definition of the experiment according to the design objectives stated above, it became clear that yet another variable could affect pilot performance, i.e. the presentation of flight-path. In the roll channel the lateral direction of motion relative to the tunnel trajectory could be estimated either *directly* from the position of the infinity point, or *indirectly* through the changing tunnel perspective, i.e. through the derivatives of optical splay and density. In the pitch channel, pilots had no alternative but to estimate the vertical direction of motion relative to the tunnel trajectory *indirectly* from the changing tunnel perspective. Thus, whereas flight-path information is *explicit* in the roll channel and can be perceived directly, this information is *implicit* in the pitch channel and must be estimated indirectly from the tunnel motion perspective. Solutions to this undesirable difference in both the pilot's task and the task difficulty between both channels were impracticable for a number of reasons. Rather, it was decided to *use* this difference of explicit vs. implicit flight-path information as an extension of the experimental design.

In the following, the experimental results will be elaborated further in an attempt to obtain insight into the relative functionality of splay and density. Central in the discussion will be the validity of the experimental hypotheses, the consequences of the explicit vs. the implicit presentation of aircraft flight path, and the possible existence of a cue dominance hierarchy between splay and density (Mulder et al., 1999b).

The experimental hypotheses

The experimental data provides an abundance of affirmative evidence for the experimental hypotheses stated in §7.3.

The effects of forward motion No differences in pilot performance and control behaviour whatsoever have been found for Display **A** when manipulating the aircraft forward motion condition. Clearly, the aircraft motion parallel to the longitudinal lines conveying the splay angle information is not coded in any way in these splay angles. The pilot questionnaire revealed that pilots regard the splay-only display as a transforming two-dimensional shape: they experienced no egomotion with this display. The opposite holds for Displays **B** and **C**, for which pilots commented a strong increase in the experienced egomotion and sense of display three-dimensionality when forward motion is added. Pilots also found control more difficult in traversing motion, especially with Display **B**. Furthermore, pilot performance with the density-only display (**B**) deteriorates strongly when traversing aircraft motion is active. It leads to a decreasing control activity, lower inner loop attitude variation and a clear increase in the position errors in both channels. The modelling results show an increase in pilot variation, i.e. pilot noise (RNRs), markedly larger time delays and decreasing bandwidths in all feedback loops when motion

is added. The higher levels of pilot equalisation in the roll and pitch channels cannot fully compensate for the increasing pilot delays in the forward motion conditions, leading to a more conservative control strategy: pilots offer performance (bandwidth) for stability (phase margin). On the other hand, in the hovering tasks the roll channel performance was best with the density-only display, leading to higher levels of control activity, higher bandwidths and lower stability margins. This superiority could not be found in the pitch channel, which can possibly be attributed to the implicit instead of explicit flight-path information in this channel. The effects of forward motion on Display **C** – showing both density as splay information – are less clear. In both control channels the trends of the data – especially the performance-related data – for Display **C** resemble those of Display **B** (density). These effects, however, are smaller and show more variation between subjects.

The effects of control channel Adding another control channel generally leads to a decreasing pilot control activity and performance with all displays, irrespective of the forward motion condition. The modelling results reveal that the main cause is most probably the increase in pilot time delay. Controlling both channels simultaneously forces a pilot to divide attention across channels, increasing processing time and pilot variation, and leading to a more conservative control strategy, i.e. a lower bandwidth and a higher stability margin. For all displays, but especially Display **A**, pilots offer performance to regain a sufficient stability margin. For all displays, control activity decreases as well as inner loop attitude variation, and flight-path and position control performance decreases. Generally, Display **B** is less affected by the dual axes task conditions, whereas the effects for Display **C** lie between those for **A** and **B**. When the aircraft is hovering, performance is best with Displays **B** and **C** in the roll channel, and Displays **A** and **C** in the pitch channel. When traversal motion is added, however, performance with Display **B** decreases rapidly, leading to the superiority of Displays **A** and **C** in both channels, irrespective of the number of channels to be controlled. In both channels the increasing processing time delay is countered by pilots through increasing their inner loop lead. This creates more inner loop stability margin and compensates partly for the increasing processing time delay. In the dual axes tasks, the roll channel bandwidths of the middle (flight-path) and outer (position) feedback loops approach each other for Displays **A** and **C**, indicating that in these conditions pilots go further in maintaining a higher bandwidth and allowing the stability margins to drop. The fact that this could not be found in the pitch channel could be attributed to the fact that – due to the lack of explicit flight-path information in that channel – control was reported to be more difficult, supported by the pilot ratings. Thus, the easier aircraft control in the lateral dimension provided pilots the opportunity to maintain a relatively high performance by sacrificing more stability margin, a strategy that was impossible in the control of the aircraft vertical motion (Mulder, 1996).

The effects of explicit vs. implicit flight-path information

In the pitch channel control task, pilots had to estimate the aircraft vertical direction of motion with respect to the reference trajectory with the changing tunnel perspective,

i.e. through the cues of splay-rate and/or density-rate. The application of a conventional middle loop and outer loop (flight-path and position) pilot model in this task turned out to be impossible, leading to the development of a pilot model where the time-consuming indirect estimation of flight-path is incorporated through the use of a time delay $\tau_{\hat{v}}$. The measured pilot performance data and the modelled pilot control behaviour in the pitch channel provides substantial evidence for the statement that – as far as the estimation of flight-path is concerned – the use of splay-rate leads to superior results. First, control activity and outer loop performance are highest for the splay-only display, **A**. Second, the vertical flight-path estimation time delay is lowest for Display **A**, especially in the single axis conditions. Third, the highest bandwidths of the outer loop feedback are measured for the splay-only display. Although the addition of another channel leads to a marked decrease in performance and control activity with Display **A**, these variables still exceed those that were measured for the density-only display.

In the roll channel, the superiority of splay vs. density in the estimation of lateral flight-path could not be found. Rather, here the performance was best with the displays conveying optical density cues, Displays **B** and **C**. One should keep in mind, however, that the lateral flight path can most easily be estimated through the infinity point. Pilots do not necessarily have to consider the optical rate cues emerging from the changing tunnel perspective, they can simply have a quick look at the infinity point and continue their efforts on estimating the position error. The directly visible lateral flight path could be the main reason for the fact that pilots found the roll channel control task easier than the pitch channel task, as judged by their comments and effort ratings.

Cue dominance: optical splay vs. optical density

The pilot questionnaire supported the hypothesis that with Displays **A** and **B**, pilots would apply the cues of, respectively, optical splay and density in controlling their aircraft. For Display **C**, the comments were less clear and they depend on the pilot involved, indicating that no cue was dominant over the other when the two were combined. This is supported by the majority of the experimental and modelling data, where the trends for Display **C** most often laid between those of Displays **A** and **B**. It can be stated that whereas Display **A** is affected mostly by the degrees of freedom of the task, and Display **B** is affected by the aircraft motion, Display **C** is affected by both. Generally, however, these effects are not as strong as with the other displays, which is a clear sign for a more *robust* performance with the combined display.

When considering the differences in pilot performance and control behaviour between the splay-only display (**A**) and the density-only display (**B**), a marked difference exists between the roll and pitch channels. Again, generally, in the roll channel performance is best with Display **B**, especially in the hovering condition. In the pitch channel, however, performance is superior with Display **A**, irrespective of the fact whether an additional channel is added or not. This could be caused by the 'hidden' experimental variable of explicit of implicit flight-path information.

Consider once again the properties of the optical cues of splay and density. Optical splay is a property of the whole line and, as a consequence, has a fixed gain depending only on the tunnel size. It is unaffected by forward motion. Optical density is a property of a particular line relative to the pseudo-horizon and, as a consequence, has a variable gain that is reciprocal to the distance from the observer to the particular line segment. It is affected by forward motion. Now, first suppose that flight path can be estimated directly from the display. Then, in the hovering task the best alternative would be to use density with the maximum achievable gain, i.e. using the tunnel frame closest to the observer and located towards the borders of the viewplane. When motion is added, however, the use of this frame would be impractible because of the high velocity with which it disappears from the screen. In this case, pilots must use a frame that is located farther away into the tunnel, decreasing the density gain. This could explain what is found in the roll channel where flight path could be estimated directly from the position of the infinity point. Second, suppose that flight path can not be estimated directly from the display, but must be perceived through either splay rate or density rate. Although the gain of the density rate would be highest when perceiving the frame closest to the observer, the relatively large velocity of this frame causes a pilot to choose a frame located farther away, with a lower gain. This is not necessary for the splay rate that can be perceived anywhere on the display with a fixed gain. Thus, in the hovering task both cues could in principle do equally well, depending on how a pilot would be able to use the higher gains of density. It is clear, however, that in traversal motion the pilot would certainly have to look even farther in the tunnel – decreasing the density gain – because of the fact that the translation due to the lateral/vertical motion is added upon the translation due to the longitudinal motion. This could explain what happened in the pitch channel control tasks.

Summarizing, when flight-path is directly coded in the display, the data of Experiment X3 show that pilots use splay and density for purposes of estimating the position error only. In this case, the density information has a clear advantage when traversal motion is inactive, because a pilot can select the frame with the highest perceivable gain. When flight path must be estimated from the display, the splay rate leads to superior results especially because it is a property of the whole line. Furthermore, as would have been the case when optical density is the only available cue, and especially in the case when motion is added, pilots are not forced to select a frame farther away, with a lower density gain.

7.6.2   Conclusions and recommendations

Conclusions

•   The experimental data support the hypotheses that were based on the pre-experimental cue analysis of §7.2. That is, performance with a display presenting only optical splay information is unaffected by the traversing motion parallel to the lines conveying the splay information. Performance with the splay-only display decreases when more than one direction of motion has to be controlled simultaneously, which can be attributed to the fact

that splay information shows the motion referents in a coupled fashion. Performance with a display presenting only optical density information decreases when traversing motion is active. Although the performance with this display is also affected detrimentally by the dimensions of the control task, these effects are smaller than for the splay-only display. This can be attributed to the fact that density information shows the motion referents in an uncoupled fashion.

• The splay-only display conveys no information whatsoever on the state of the forward, traversing motion. As a result, subjects regard this display as a transforming two-dimensional shape, giving rise to no sensation of egomotion at all.

• The density-only display conveys a multitude of information regarding three-dimensionality. When traversing through the density-only tunnel the experienced egomotion and the sense of perceived depth is satisfactory for all pilots. Thus, the optical density cues are essential in providing a pilot the sense of forward motion through the tunnel.

• The frequency domain identification methods show that in the dual axis control tasks, potential cross-couplings between both control channels, are not consistent. It can be concluded that, in this experiment, these cross-couplings do not indicate real pilot behaviour, but merely an increase in pilot control behaviour variation and noise.

• The frequency domain identification method directly shows the correctness of a certain proposed pilot model. Because the proposed models result from the analysis on optical cue functionality, the success of the identification method for a proposed pilot model structure can be used as an indication of support for a particular property of an optical cue.

• The modelling results show that the main cause for the increasing task difficulty in the dual axis tasks is the increasing pilot time delay. This forces pilots to increase their inner loop equalization in order to compensate for the loss in stability margin. Generally, pilots offer performance to re-establish a certain level of closed loop stability.

• When flight-path is directly visible from the display, e.g. through the infinity point, pilots will always be able to use this cue, independent of the type and characteristics of other potential sources of information for flight-path, such as splay-rate or density-rate. When flight-path is *not* directly visible from the display, the real differences in functionality of the other potential sources of information become clear.

• The modelling results support the notion of indirectness of vertical flight-path information by demanding a different pitch channel pilot model structure, incorporating a significant outer loop time delay. This time delay is quite large (0.5-1.5 [s]) for all displays, but especially for the density-only display.

• When flight-path information is not directly coded in the display, the experimental data support the notion that in this case, optical splay leads to the best performance.

• When flight-path information is not directly coded in the display, the task difficulty as experienced by pilots increases dramatically.

• What is probably the most important virtue of optical splay information vs. optical density information is that it is a property of the *whole* line, i.e. it has a constant *gain* independent of the pilot's gaze. As a consequence, pilots do not have to re-direct their

gaze when traversing through the tunnel.

- When flight-path information is directly coded in the display, leading to an easier control task, pilots have more freedom in maintaining performance and further sacrificing their stability margin. This is not possible in the more difficult tasks where flight-path information can not directly be perceived from the display.

- Evidence for an unequivocal cue dominance strategy could not be found when the optical splay and optical density cues were presented simultaneously. It depends on the particular situation whether one of the cues becomes dominant. The relative attractiveness of these cues for a pilot to conduct the task can be predicted rather well by conducting an extensive pre-experimental cue analysis.

- The effects of the experiment independent measures on the display presenting both the optical density as the optical splay information are a mixture of those found for the splay-only and density-only displays. Because the effects on the combined display are smaller, it can be concluded that both the cues compensate for their deficiencies, leading to a more *robust* performance with the combined display

Recommendations

- The experiment would have had considerable benefit when conducted in a moving base simulator. Especially the experienced level of realism in the pitch channel would be enhanced, which could have led to smaller elevator control inputs and more reasonable levels of the aircraft vertical load factors.

- The combination of the texture gradients of perspective and density is a strong one. Whereas both the individual gradients have their own virtues and shortcomings, the experiment suggests that both cues combined compensate for each other. The manner of and under what conditions this compensation takes place should be examined further.

- The cues of optical splay and density were examined here in a task of following a straight trajectory. The information analysis of Chapter 3 revealed that these cues have different properties when a curved trajectory needs to be followed. This will be further elaborated in Chapter 8.

- Although the experiment allows many different comparisons to be made concerning the effects of the independent measures and those of flight-path presentation, a number of follow-up experiments could be planned. For instance, an experiment could focus on the effects of explicit vs. implicit flight-path information, keeping dynamics and disturbances in both the roll and pitch channel the same. A similar experiment, but in a different context, will be reported in Chapter 9 discussing the effects of a flight-path vector presentation.

Chapter 8

Cues in curved tunnel sections

8.1 Introduction

The investigation presented here resembles the one discussed in the previous chapter. Again, the relative usefulness of the two primary cues – optical splay and optical density – will be examined, but now for the pilot guidance task of following a trajectory that is *circular* (Mulder, 1998). As has been shown in Chapter 3, the curvi-linear aircraft motion condition is much more difficult to examine than the recti-linear motion condition. For example, as will be discussed in the background section §8.2, *presentation biases* occur in presenting curved sections of the trajectory. These biases refer to the fact that, under some marked conditions, the information conveyed by the tunnel display does not accurately reflect the exact position and attitude of the aircraft with respect to the tunnel centercircle. Together with the main goal of assessing the effectiveness of splay and density information in following curved trajectories, Experiment X4, defined in §8.3, is conducted with the secondary objective of examining the presentation biases. The experimental results and pilot control behaviour modelling efforts are stated in §8.4 and §8.5, respectively. All findings are summarized and discussed in detail in the retrospective, §8.6.

8.2 Background

Kinematics of a stationary horizontal non-slipping turn

The aircraft guidance task of following a circular trajectory, depicted in Fig. 8.1(a), requires a pilot to maintain a constant track angle rate $\dot{\chi}_c$. In a stationary horizontal non-slipping ($\beta=0$) turn the horizontal component of the aircraft lift force L equals the centrifugal force F. The following relations hold for the *stationary* flight condition of flying along a circular trajectory, with radius R_c, and with a velocity V_{tas} (Etkin, 1972):

$$\phi_c = \arctan\left(\frac{V_{tas}^2}{g_0 R_c}\right); \quad \dot{\chi}_c = \frac{V_{tas}}{R_c}; \quad n = \frac{1}{\cos\phi_c}, \tag{8.1}$$
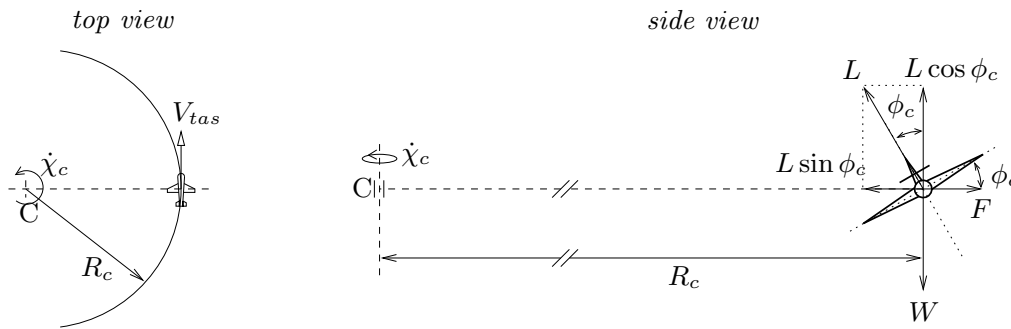
(a) geometry of a stationary horizontal turn ($\beta=0$)
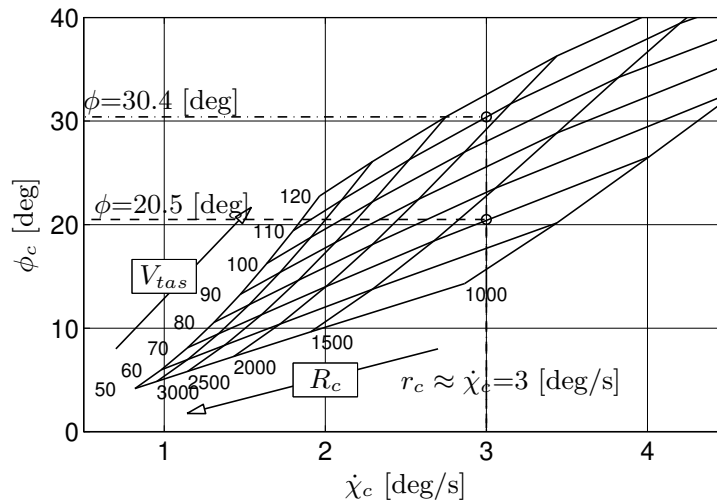
(b) relations between the aircraft roll angle ϕ_c, the velocity V_{tas} (in [m/s]), the yaw rate r_c and the curve radius R_c (in [m])

Figure 8.1: Kinematics of a stationary horizontal non-slipping turn.

with ϕ_c the reference aircraft roll angle, g_0 the gravitational acceleration and n the aircraft load factor. Fig. 8.1(b), depicting the relations between ϕ_c, R_c, V_{tas} and $\dot{\chi}_c$ ($\approx r_c$), shows that the aircraft manoeuverability decreases at higher velocities: increasing the velocity from 70 to 110 [m/s] for a fixed track angle rate of 3 [deg/s] requires a larger aircraft roll angle (30.4 vs. 20.5 [deg]) and yields a larger curve radius (2101 vs. 1337 [m]).[1] In (Brockhaus, 1994) it is argued that the main problem of the flight control system in controlling the aircraft along the FMS-defined circular trajectories is the changing direction and magnitude of the wind vector. Secondary effects are the atmospheric turbulence, the decreasing aircraft mass – due to fuel consumption – and the non-constant aircraft velocity.

Earlier research

None of the investigations concerning tunnel displays conducted in the past has focused exclusively on the pilot guidance task of flying a co-ordinated steady turn. Whereas only

---

[1] Pilots are aware of these relationships and use the following rule of thumb to estimate the required aircraft roll angle for a one-rate-turn, i.e. for a yaw rate r_c of 3 [deg/s]: $\phi_c \approx 2 \cdot \frac{V_{tas}}{10} + 7$.

straight trajectories were applied in the theoretical as well as the experimental research efforts reported in (Wilckens & Schattenmann, 1968; Wilckens, 1973), the trajectories flown in the experiments of (Grunwald et al., 1981; Grunwald, 1984; Theunissen & Mulder, 1995b) consisted of a concatenation of straight and curved segments.

As has been discussed in §2.2.2 the tunnel display of Grunwald is essentially a combination of the basic tunnel geometry and a flight-path predictor. With a well-tuned predictor the task of following a curved trajectory becomes one of keeping the predictor symbol inside the predictor reference square, moving ahead of the observer at a distance $D = T_p/V_{tas}$ (T_p is the prediction time interval). In the experiments reported on using the tunnel-and-predictor display, no special emphasis was put on the task of flying a co-ordinated turn. All performance measures of interest were computed for the *whole* trajectory including the straight segments and, more importantly, including the *transitions* between the straight and curved segments. Hence, these performance measures as such are not worthwhile to reconsider here. An interesting novelty introduced in (Grunwald, 1984), however, is the concept of a *banked tunnel*. The discussion in the previous subsection showed that flying a co-ordinated horizontal turn with a constant velocity (neglecting the effects of wind and turbulence) requires a constant aircraft roll angle ϕ_c. Maintaining a constant roll angle yields a constant track angle rate $\dot{\chi}_c$ and a curvi-linear motion condition with a fixed radius R_c. Flying along a circular trajectory with a *commanded* radius R_c and accompanying yaw rate $\dot{\chi}_c$ can be achieved by rolling the aircraft with an appropriate roll angle ϕ_c. Grunwald inventively applied this property in the tunnel geometrical design by *banking the tunnel as a whole* with the required, or, commanded aircraft roll angle ϕ_c, Fig. 8.2(c): a nice example of a *pictorial* solution. Fig. 8.2(c) illustrates that in a steady turn with roll angle ϕ_c the tunnel frames appear parallel with the viewplane borders. The inclined horizon provides the *only* actual aircraft bank angle information. In (Grunwald, 1984) the banked tunnel was one of the designs investigated in an experiment of manually flying curved trajectories. It was found that pilot performance with the banked tunnel was similar to that with the non-banked tunnel. Grunwald concluded that the pictorial bank angle command information provided by the banked tunnel elements did not contribute much to the path-following performance and was ignored in most cases. Later in this chapter a possible explanation will be given for this finding. Although the hypothesized performance improvements were not achieved, this setback did not stop Grunwald in applying the banked tunnel concept in later studies (Grunwald, 1996b).

A similar experiment investigating pilot performance in following a complex curved trajectory was reported in (Theunissen, 1993b). The independent measures were the tunnel size and the type of symbology, i.e. the use of a flight-path vector vs. a flight-path predictor. Subjects were instructed to accurately follow a single approach trajectory consisting of three straight segments and two curves. An analysis of the performance measures computed over the *whole* trajectory yielded similar findings as those reported in (Grunwald et al., 1981; Grunwald, 1984). Later, the performance data were *re*-analyzed for the straight and curved segments of the trajectory (Theunissen, 1997). Although it is

contour + frames   *contour*   *frames*

(a) straight trajectory

(b) curved trajectory

(c) curved trajectory (banked tunnel)
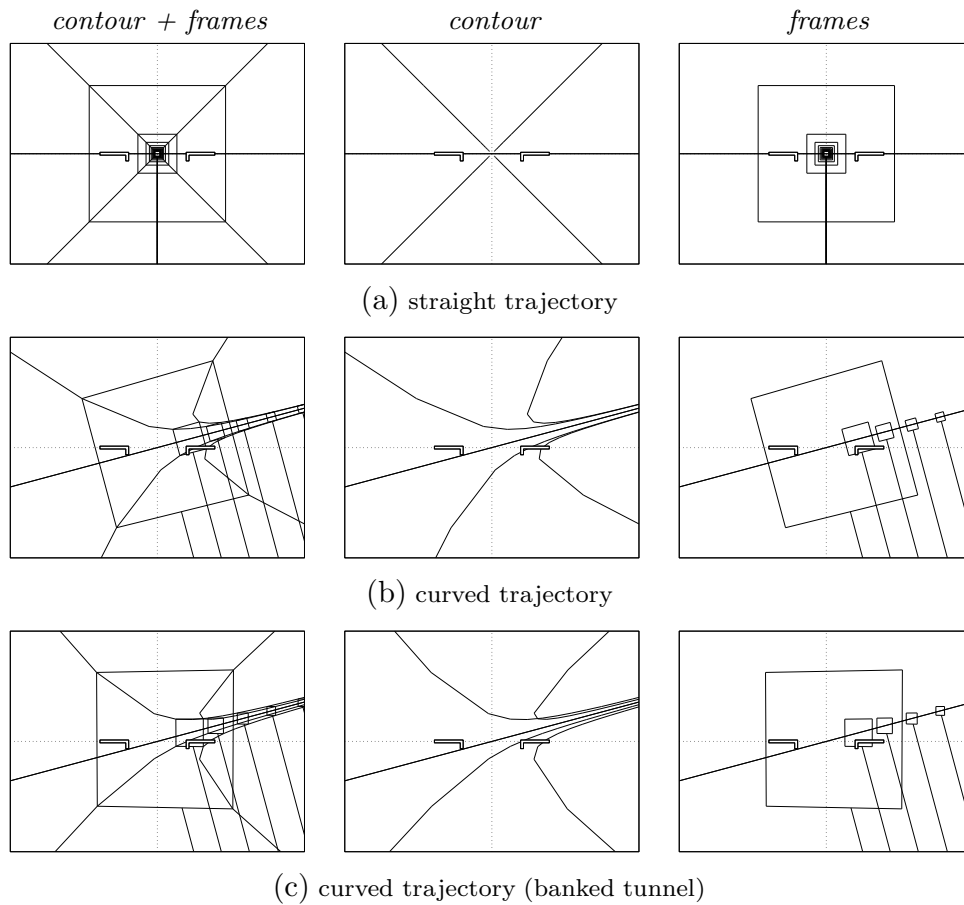
Figure 8.2: The tunnel display images corresponding to an aircraft recti-linear motion condition along a straight trajectory (top) and an aircraft curvi-linear motion condition along a circular trajectory (middle and bottom rows). The tunnel images are shown for the total display (left), the contour-only display (middle) and the frames-only display (right). The dotted lines represent the screen center. The aircraft attitude and position errors with respect to the trajectory are zero.

not described *how* the data were re-computed, most probably the trajectory itself served as a criterion whether a data point belonged to either a straight or curved segment of the trajectory. This is a questionable procedure, however, a statement that requires some explanation. Recall that the task of following a trajectory consisting of straight and curved sections implies that pilots have to anticipate oncoming changes in the trajectory, yielding *transition manoeuvres* between straight and curved sections. These transition manoeuvres lead to a conflicting interest between on the one hand the need to roll into (or out of) the curve well before the curve starts (ends) and on the other hand the need to optimize path-following performance. Although rolling into the curve some time before the curve begins is mandatory to overcome the lagging aircraft motions, the moment the aircraft starts rolling it also starts drifting away from the reference trajectory to the inner side of the curve. This leads to the so-called *corner-cutting* phenomenon, that is reported

as a significant problem in all previous investigations on following curved trajectories (Grunwald et al., 1981; Grunwald, 1984, 1996a). The curve transition manoeuvre is the subject of Experiment X6, and, as will be discussed in Chapter 10, corner-cutting leads to considerable position errors towards the inner side of the curve. Hence, computing path-following performance in tasks of following either a straight or a curved segment of the trajectory can not be done properly when the recorded data contains traces of behavioural responses belonging to curve transition manoeuvres, as these could lead to considerable biases in the data. Therefore, the results reported in (Theunissen, 1997) must be ignored.

Tunnel display information analysis for curved trajectories

Differences between cues in straight and curved tunnels The optical cues in curved tunnel sections have been analyzed in §3.6. Similar to the discussion of optical cues in straight tunnels in §3.6 and §7.2, it is hypothesized that the *gradients of optical splay and optical density* are essential in understanding pilot behaviour. The properties of these optical gradients do not change much when a circular rather than a straight tunnel trajectory is presented on the display. There are, however, some important differences in presenting circular rather than straight tunnel sections that affects the functionality of the gradients. Most importantly, the visible part of the trajectory – the preview – is limited with circular tunnels which has a number of consequences. First, whereas for straight trajectories the pilot can perceive the projection of the trajectory at very large viewing distances, yielding the *infinity point*, for curved trajectories the tunnel is bended towards one of the sides and is cut off by the viewing volume at larger viewing distances. Second, whereas the presentation of a straight trajectory on the display yields a clear *symmetrical condition*, Fig. 8.2(a), the curved trajectory representation does not, Fig. 8.2(b). Such a symmetrical image condition can be expected to be very useful in controlling the aircraft along the trajectory. Third, whereas the representation of a straight trajectory on the display yields a singular infinity point and, most importantly, the *horizontal and vertical pseudo-horizons*, the curved trajectory presentation does not. Rather, an infinity point emerges for each curve segment s_i, and no pseudo-horizons exist at all. Fourth, recall that due to the perspective projection the nearest part of the tunnel is not presented on the display (Fig. 8.3). For straight tunnels this causes no problems because the direction of the trajectory does not change. The attitude and position of the aircraft relative to the tunnel centerline can be perceived equally well from the presentation of the tunnel geometry at some distance ahead. For curved tunnels, however, the trajectory bends off into the curve. The aircraft attitude and position become more difficult to perceive from the first visible part of the tunnel because this part will be bended off with respect to the tangent of the tunnel centercircle where the aircraft is positioned, Fig. 8.3. This leads to *presentation biases*, analyzed in Appendix D.

Summarizing, presenting curved rather than straight tunnel segments has important consequences for the pilot. All effects mentioned above can be expected to have some detrimental effect on pilot performance. In the following these effects will be discussed further.

straight tunnel trajectory   *curved tunnel trajectory*
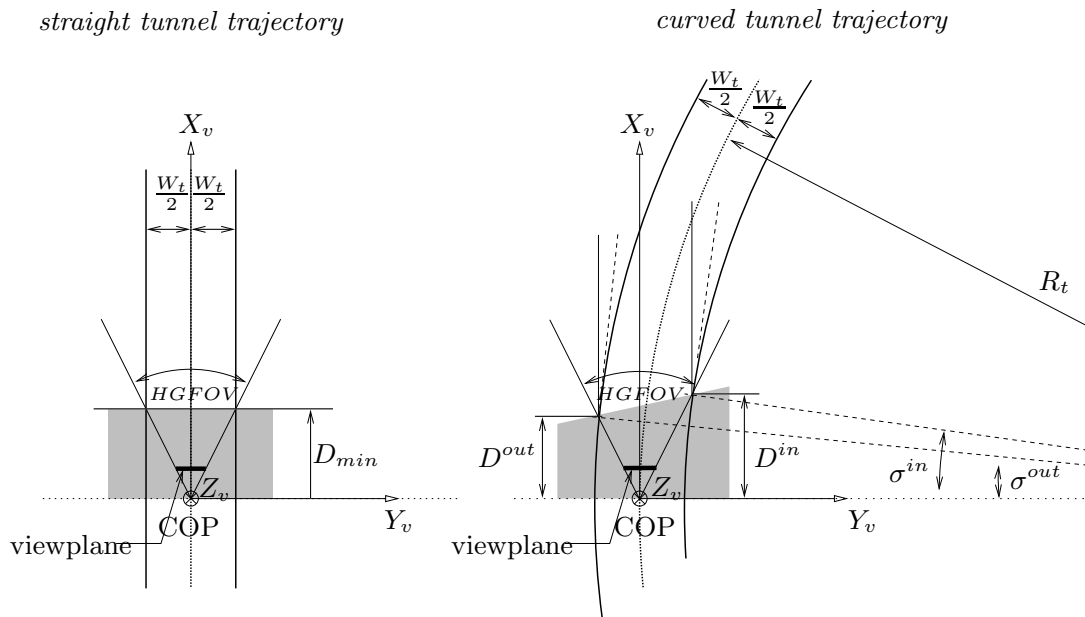
Figure 8.3: The effects of *not* showing the nearest part of the trajectory – due to the perspective projection method – for a straight (left) and curved (right) trajectory. The shaded areas indicate the part of the trajectory that is not visible for a pilot. The aircraft Body axes are positioned on and aligned with the tunnel centerline or centercircle.

Optical splay   In straight trajectories the pilot perceives the splay angles of only four lines stretched until infinity, intersecting at the infinity point. Because the splay angle is an attribute of the entire line, the optical splay information is independent of the viewing distance and it does not matter whether the first part of the trajectory is shown or not. The curved trajectory presentation, however, yields a *set* of optical splay angles and an infinity point *for each segment s_i* of the trajectory. Due to the trajectory curvature the values of these splay angles and the position of the infinity points *change* as a function of the viewing distance. Comparing Figs 8.2(a) and 8.2(b) one can see that the clear symmetry in presenting zero aircraft position and attitude errors, which does appear for the straight trajectory, is lost completely. The curved tunnel presentation for zero position and attitude errors is markedly more difficult for the pilot to use as a reference condition in controlling the aircraft. As has been shown in Chapter 3 the properties of the optical splay gradient remain fairly similar. They are a function only of the aircraft position relative to the centercircle, whereas their derivatives, the optical splay angle rates, depend only on the aircraft motion relative to the centercircle. An important difference with the straight trajectories, however, is that the splay angle gains change as a function of the viewing distance into the curve, σ_{s_i} (Appendix D). The splay angles – and their derivatives – of segments closest to the viewplane (small σ_{s_i}) are affected most by the lateral/vertical aircraft position relative to the centercircle (van der Hoek, 1997b).

Concluding, the presentation of a curved trajectory does *not* provide a symmetrical condition that is easy to use as a reference for control. Nonetheless, optical splay angles and their derivatives do convey very useful information about the aircraft position and motion with respect to the tunnel centercircle, especially at smaller viewing distances.

Optical density   In straight tunnel sections the optical density gradient depicts the compression of the 'texture' elements[2] of the four tunnel walls with respect to the vertical and horizontal pseudo-horizons. The singular infinity point marks the cross-point of the horizontal and vertical pseudo-horizons, forming the primary reference for vertical and lateral control, respectively. The position of the frames relative to the pseudo-horizons, or, equivalently, the *relative* compression of the texture elements on the left/right and top/bottom tunnel walls provides an intuitive symmetrical condition, Fig. 8.2(a). In curved trajectories the tunnel presentation consists of a concatenation of straight segments with a regularly changing heading relative to the world. The outer and inner curve tunnel walls are most probably *not* perceived as walls. Rather, it are the relative displacements of the *local* elements that must be perceived. A *set* of infinity points emerges instead of a singular point. The pseudo-horizons are not available in curves and, as a consequence, no intuitive symmetry condition can be used as a reference for control. In Chapter 3 it is shown that the properties of the optical density gradient remain fairly similar. The relative displacements and their derivatives are a function only of the aircraft position and, respectively, the aircraft motion relative to the centercircle. An important difference with straight sections, however, is that only the relative displacements of the frame elements closest to the viewplane (small σ_{s_i}) convey information about position and relative motion. The displacements of frames positioned farther away are only a function of the aircraft's attitude relative to the centercircle (van der Hoek, 1997b).

Concluding, the presentation of a curved trajectory does *not* provide a symmetric condition that is easy to use. The absence of the useful and important pseudo-horizons hampers the use of the lateral displacement cues considerably. Information about the position and motion relative to the tunnel centercircle can be obtained by perceiving the relative displacements of local elements of the tunnel geometry, at smaller viewing distances.

Presentation biases in curved trajectories   The presentation biases in curved trajectories are analyzed in Appendix D through investigating the effects of two entities of the tunnel geometry, the tunnel *contour* and the tunnel *frames*. Concerning a possible bias in presenting the aircraft heading with respect to the tunnel centercircle, this analysis shows that the optical information conveyed by *both* the geometrical entities leads to an impression that the *aircraft is heading towards the outer side of the curve.* Concerning a bias in presenting the aircraft lateral position with respect to the tunnel centercircle, the analysis reveals a more complex situation. First, the lateral displacement of the tunnel contour as a whole to the inner side of the curve leads to an impression of the *aircraft being positioned towards the outer side of the curve.* This effect increases for larger tunnels and for smaller curve radii. Second, whereas the lateral displacements of the tunnel frames relative to the

---

[2]These 'texture' elements are in fact the lateral and vertical tunnel frame line segments.

viewplane center lead to a presentation bias with the same effect, the *relative* lateral displacements of the two or three tunnel frames nearest to the viewplane lead to an opposite effect. Thus, the tunnel frames convey *two* presentation biases *with opposite signs*, i.e. they could possibly compensate for each other. Third, an important difference between the presentation biases caused by either the contour lines or the frames is their dependency upon the *longitudinal* aircraft position along the tunnel centercircle. In a steady horizontal turn the tunnel contour lines maintain a *steady state* on the viewplane, and the presentation biases caused by these contour lines are *continuous in time* and do not depend on the aircraft position along the centercircle. The tunnel frames, however, move towards the observer during a steady turn along trajectories on the viewplane depicted by the tunnel contour. Here, the presentation biases are *not constant in time*. Rather, the analysis in §D.5 revealed that the presentation biases caused by presenting the tunnel frames *all decrease* when approaching the first visible tunnel frame.

***Banked tunnels*: effects of the tunnel rotation**   The cue analysis conducted above must be reconsidered in the light of Grunwald's suggestion of rotating the tunnel geometry as a whole, i.e. the so-called *banked* tunnel (Grunwald, 1984). The effects of rotating the tunnel on the usefulness and functionality of the primary cues of splay and density, is nil. The splay angles of a segment s_i rotate on the viewplane with respect to the infinity point of that particular segment. As far as the density gradients are concerned, the local elements of the geometry are all rotated with similar angles. Hence, for both sets of cues only the *reference* conditions change – they are rotated on the viewplane – as well as the direction of the *relative* changes in the optical cues providing their functionality. The properties of these changes in terms of magnitude in both sets of cues, however, remain identical, leading to no significant change in their functionality whatsoever.

When considering the effects of tunnel geometry rotation on presentation biases, Figs 8.2(b) and 8.2(c) illustrate that especially the tunnel contour lines convey a dramatic change in reference condition. Whereas the tunnel frames as such appear to be simply rotated around their centers (as they are in fact), the contour as a whole appears rotated towards a more central position on the viewplane, i.e. to similar positions as in straight trajectories. At a first glance, it can be hypothesized that pilots interpret the rotated tunnel contour information as being located towards the inner side of the curve, i.e. contrary to the presentation bias caused by the non-rotated tunnel. The validity of this hypothesis must be evaluated experimentally. As far as the presentation bias in conveying aircraft heading information, these biases are unaffected by the rotation of the tunnel geometry.

The need for Experiment X4   In this thesis it is assumed that in curved as well as in straight sections of the trajectory the two primary optical sources of information are those of optical splay and optical density. Experiment X3 has shown that both information sources have their weaknesses and strengths. For instance, whereas splay is superior over density when the aircraft moves forward through the tunnel, the opposite holds when the aircraft vertical and lateral motion relative to the tunnel must be controlled simultaneously. Because the characteristics of these optical cues are similar for straight and curved sections

of the trajectory, it is hypothesized that the findings of Experiment X3 also hold for the pilot task of following a circular trajectory. The experimental measures of *forward motion* and *control channel* as applied in Experiment X3 can be abandoned for further analysis, allowing Experiment X4 to focus on other phenomena, especially those marking the differences between the optical information in straight and curved sections. As will be put forward in §8.3, Experiment X4 assesses primarily the relative usefulness of showing the tunnel contour lines – providing splay information – vs. the tunnel frames – providing density information. The second main interest is the effect of presentation biases for these different tunnel geometries. As is discussed above, it are especially the tunnel contour lines that lead to significant biases, whereas the tunnel frames themselves yield different biases with opposite signs. Third, to analyze the effects of frames vs. contour one step further, also the *positioning* of these frames along the circular trajectory is analyzed, i.e. what are the effects of putting these frames at irregular inter-frame distance? The fourth interest will be the effects of rotating the tunnel geometry as a whole, the banked tunnel of (Grunwald, 1984), on pilot performance. Finally, the path-following performance in curved sections will be compared to the performance in straight sections of the trajectory.

8.3 Experiment X4

Experiment X4 resembles Experiment X3 in the sense that it investigates the effects of providing different sets of optical information – mainly those of optical splay and optical density – on pilot performance and control behaviour (van der Hoek, 1997a).

METHOD

Subjects and instructions to subjects   Four subjects (A – D) participated in the experiment. They were instructed to control the aircraft through the tunnel as accurately as possible, i.e. all occurring attitude and position errors must be minimized, despite the effects of the disturbances acting on the vehicle.

Apparatus   The Human-Machine Laboratory was used, described in Appendix A.

Independent measures   Three independent variables were manipulated in the experiment. First, five different displays were defined that are all abstractions of the basic tunnel-in-the-sky display (Fig. 8.4). Display **A** is the baseline tunnel. Displays **C** and **D** are the same as **A** except that Display **C** shows no tunnel frames, whereas Display **D** shows no tunnel contour. Displays **B** and **E** are the same as, respectively, Displays **A** and **D**, except that the tunnel frames are separated with a randomized inter-frame distance. The main characteristics of the experimental tunnel geometries are summarized in Table 8.1. The second independent measure was the fact whether the tunnel geometry was rotated as a whole, or not. This variable was introduced to study the effectiveness of pictorially presenting the reference aircraft roll angle, discussed in §8.2. The third independent measure was the aircraft velocity. Two velocities were simulated, 70 and 110 [m/s], representing
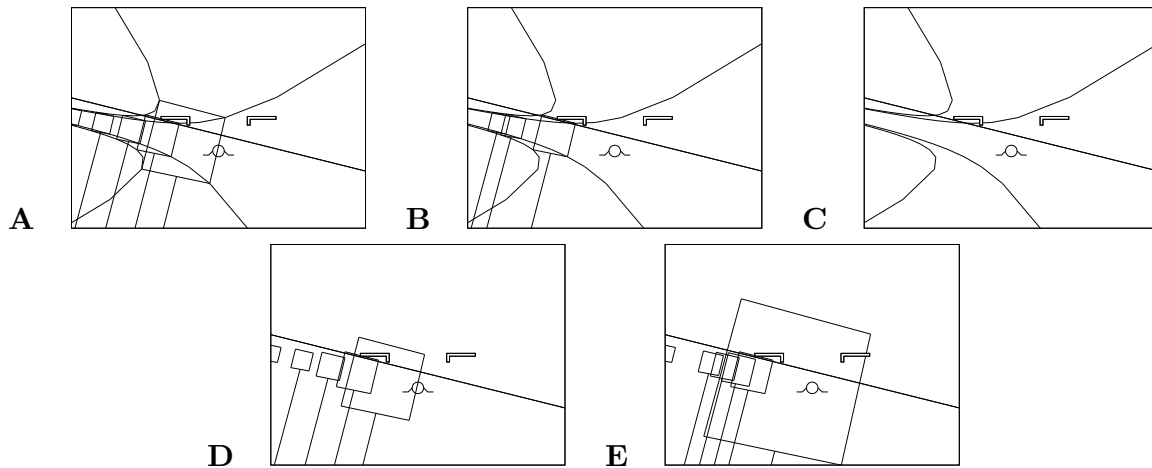
Figure 8.4: The experimental tunnel display characteristics (no rotation of the tunnel).

Table 8.1: Experimental tunnel geometries (X4).

$display \rightarrow$	**A**	**B**	**C**	**D**	**E**
tunnel contour	yes	yes	yes	no	no
tunnel frames	yes	yes	no	yes	yes
tunnel frame positioning	regular	random	-	regular	random

an approach and cruise velocity, respectively. Recall that the aircraft velocity determines both the aircraft handling characteristics as the magnitude of the dynamic cues stimuli. Finally, to prevent boredom the trajectories were curved either to the left or to the right on a fifty/fifty basis. The introduction of this independent measure (`direction`), however, did not lead to any statistically significant change in pilot performance at all (van der Hoek, 1997a). Summarizing, the independent measures of interest here are the `display` (5 levels), the `rotation` of the tunnel (2 levels) and the aircraft `velocity` (2 levels).

Experimental design   A full-factorial within-subjects design was applied, consisting of a total of 20 conditions ($5 \times 2 \times 2$). The conditions were randomized over the experiment. Each subject conducted six (three to the left, three to the right) familiarization sessions (120 runs) before completing six replications (three to the left, three to the right) of all experimental conditions (120 runs) that served as the measurements.

Procedure   During the course of two days a subject conducted 240 experimental runs, divided in 30 blocks of eight runs each. A single run lasted 101.92 [s], consisting of a run-in time T_i of 20 [s] and a measurement time T_m of 81.92 [s]. The pace of the experiment was such to allow sufficient time for subject preparation and to prevent fatigue.

Dependent measures   A number of variables were selected as dependent measures: (i) the pilot's control signal δ_a and its derivative $\dot{\delta}_a$; (ii) the difference ϕ_e between the aircraft angle of roll ϕ and the reference angle of roll ϕ_c, and its derivative $\dot{\phi}_e$; (iii) the heading angle error ψ_e, and (iv) the cross-track error x_e. The STDs of these signals were used in the statistical analysis. Because in some conditions the cross-track error was

considerably *biased*, both the standard deviation x_e-S as well as the root-mean square x_e-R were computed, yielding a total of seven dependent measures.

Description of the experiment simulation

Tunnel geometry The five displays of Fig. 8.4 originate from the baseline tunnel, **A**, having square frames (W_t=H_t=40 [m]) positioned on altitude poles and connected with longitudinal frame lines. The reference trajectory was circular and had a downslope Γ_t of 3 [deg]. The curve radius R_t depends on the required yaw rate r_c and the aircraft velocity V_{tas} see Eq. 8.1. Fixing the yaw rate r_c at 2 [deg/s] yields radii of 2002.6 [m] and 3146.9 [m] for the two velocity conditions of 70 and 110 [m/s], respectively. The reference aircraft roll angle ϕ_c is then 14.3 and 22.4 [deg] for the two velocity conditions, respectively. If applicable, the tunnel geometries were rotated with these angles. The tunnel displays were augmented with a green flight-path vector showing the instantaneous direction of motion. Because the atmospheric disturbances did not lead to a side-slipping motion of the aircraft, the flight-path vector did not show any additional information of interest for this experiment, and could have been left out from the start.

Concerning the positioning of the tunnel frames the following procedure was adopted. The circular trajectory is approximated by concatenating a series of straight tunnel segments s_i bridging a constant angular distance $\triangle\Psi$ (Fig. 3.10). The tunnel frames f_i can then only be positioned at the connections of these segments. Hence, the distance – measured along the centercircle – between frames is a function of the (fixed) angular distance between segments: $\triangle S^f = c \triangle S^s = cR_t \triangle \Psi$ (§3.6.1). In the experiment $\triangle\Psi$ was set at 5 [deg]. Furthermore, for the displays with *regular* frame positioning (**A** and **D**), c was constant at 2.[3] For the displays with *irregular* frame positioning (**B** and **E**), c was defined as a random integer with a normal distribution: $c \sim \mathcal{N}(2, 1.5)$.[4] For each velocity condition (70 and 110 [m/s]) and irregular frame display five trajectories were generated, yielding twenty quasi-random trajectories that were randomized over these experimental conditions.

Aircraft model The same aircraft model (of a Cessna Citation I) was used as applied in the experiments discussed before. As will be discussed in Appendix C the model was obtained by linearization around a stationary co-ordinated turn. Again, only the asymmetric motion was simulated (zero side slip), whereas the aircraft symmetric motion states were fixed at their initial condition values. Thus, the aircraft moved along the circular

---

[3]With a fixed yaw rate r_c of 2 [deg/s] for both velocity conditions the time required to move between two consecutive frames, for displays with a regular inter-frame distance, was constant at 5 [sec]. A fixed $\triangle\Psi$ results in the situation that the number of visible frames on the display remains the same.

[4]Putting the intermediate distances between successive tunnel frames in a vector $\underline{c}$ results in:

Displays **A** and **D**: $\underline{c}^T = [2\ 2\ 2\dots2]\ \rightarrow \mu_{\underline{c}} = 2;\ \sigma_{\underline{c}} = 0$.
Displays **B** and **E**: $\underline{c}^T = [1\ 4\ 2\dots3]\ \rightarrow \mu_{\underline{c}} = 2;\ \sigma_{\underline{c}} = 1.5$.

tunnel with a downslope Γ_t of 3 [deg] through the vertical center of the tunnel.

Atmospheric disturbances   Two independent reference signals were inserted in the control loop, i_1 and i_2, that were defined identical as the ones applied in Experiments X1 and X2. To allow a comparison between the two aircraft velocity conditions the input signal spectra were compensated for the aircraft model characteristics. As a consequence, the results for the 70 [m/s] velocity condition can be compared one-on-one with those obtained in Experiments X1 (for the W_t=40 [m] condition) and X2, for the same velocity.

Initial condition   Before the start of each run, the aircraft was positioned in the center of the tunnel with zero position and attitude errors. The initial longitudinal position of the aircraft on the tunnel reference trajectory was randomized.

Experiment hypotheses

In Table 8.2 a qualitative summary is given of what can be considered as an application of the theoretical findings from the information analysis of §8.2 to the experimental displays. In other words, based on the cue inventarisation this table reflects the hypotheses of Experiment X4 focusing on the independent measures of `display` and `rotation`. Regarding the optical information on the aircraft roll angle error ϕ_e, Table 8.2 shows that it can be hypothesized that tunnel rotation leads to superior performance in maintaining a small ϕ_e for all displays except Display **C**. It can be hypothesized further that tunnel rotation has no effect at all on pilot path-following performance, expressed in ψ_e and x_e. Concerning the aircraft heading angle error ψ_e, Table 8.2 indicates that for displays showing the tunnel contour lines, optical splay is hypothesized to be most effective. In these displays particularly also the tangent point and the infinity points could be helpful, especially in Display **C** where the pilot must focus fully on the tunnel contour. For displays containing frames the density gradients are hypothesized to be useful too, especially when the tunnel frames are spaced at regular distances. In the latter case, pilots could obtain an accurate estimate of S_t^{max}, especially when also the contour is available. When no contour is available, the performance in ψ_e is expected to decrease significantly. All displays are hypothesized to convey the same presentation bias in ψ_e. In the last row of the ψ_e-section of Table 8.2, the hypothesized *relative performances* in maintaining a small ψ_e are stated, which can be regarded as a summary of the individual cue hypotheses listed above.

Similar hypotheses are stated for the *relative* usefulness of the optical cues for controlling the aircraft lateral position error x_e. It is hypothesized that presentation biases in x_e are smallest for displays containing frames, especially when these frames are spaced regularly. It is further hypothesized that these displays provide accurate density information and allow pilots to use the movements of the frames nearest to the viewplane. When only the tunnel contour is presented, the bias in x_e is expected to be largest. The last row of the x_e-section of Table 8.2 contains the hypothesized relative performances in minimizing x_e.

Table 8.2: Qualitative summary of the findings from the information analysis conducted in Chapter 3 and §8.2 (van der Hoek, 1997a). In this table the symbols '--', '-', 'o', '+' and '++' reflect the qualifications 'very bad', 'bad', 'neutral', 'good' and 'very good', respectively. A '.' means that such a qualification is not applicable.

optical information for the aircraft roll angle error ϕ_e										
	not-rotated					rotated				
	A	B	C	D	E	A	B	C	D	E
horizon line	+	+	+	+	+	+	+	+	+	+
tunnel frames	o	o	.	o	o	++	++	.	++	++
optical information for the aircraft heading angle error ψ_e										
	not-rotated					rotated				
	A	B	C	D	E	A	B	C	D	E
splay rates	+	+	++	.	.	+	+	++	.	.
density rates	+	o	.	o	−	+	o	.	o	−
frame displacements*	+	o	.	o	−	+	o	.	o	−
infinity points	o	o	+	.	.	o	o	+	.	.
tangent point	o	o	+	.	.	o	o	+	.	.
max. viewing distance S_t^{max}	+	o	o	o	--	+	o	o	o	--
$\longrightarrow$ *relative performance*	+	o	++	−	--	+	o	++	−	--
optical information for the aircraft position error x_e										
	not-rotated					rotated				
	A	B	C	D	E	A	B	C	D	E
splay	+	+	+	.	.	+	+	+	.	.
density	+	o	.	+	o	+	o	.	+	o
frame displacements**	+	o	.	+	o	+	o	.	+	o
tangent point	+	+	+	.	.	+	+	+	.	.
$\longrightarrow$ *relative performance*	++	+	o	o	−	++	+	o	o	−
*presentation biases***										
	not-rotated					rotated				
	A	B	C	D	E	A	B	C	D	E
bias in ψ_e	−	−	−	−	−	−	−	−	−	−
bias in x_e	+	o	--	o	−	+	o	--	o	−

---

* At *large* viewing distances.

** At *small* viewing distances.

*** Here, the '+' and '-' labels (etcetera) should be read as 'leading to a small bias', and 'leading to a large bias', respectively.

8.4   Results

8.4.1   The pilot questionnaire

Because subject D was involved in the definition and set-up of the experiment, only the comments of subjects A to C will be discussed.

Realism of the simulation   The simulated aircraft responses were judged rather realistic, especially for the high velocity condition, Table 8.3. The realism of the disturbances acting on the aircraft was judged less realistic. One subject mentioned even that the disturbances *spoiled* the realism of the simulation. Once again the need to stimulate a

Table 8.3: Summary of results from a pilot questionnaire (X4).

How would you describe the level of *realism* of the simulated aircraft *dynamics*?					
	very realistic	realistic	average	unrealistic	very unrealistic
V_{tas}= 70 [m/s]	·	1	1	1	·
V_{tas}=110 [m/s]	·	2	1	·	·
How would you describe the level of *realism* of the simulated aircraft *disturbances*?					
	very realistic	realistic	average	unrealistic	very unrealistic
V_{tas}= 70 [m/s]	·	1	1	1	·
V_{tas}=110 [m/s]	·	1	1	1	·

How would you describe the strength of the experienced *egomotion*, i.e. did you have a strong feeling you were moving through a three-dimensional world or did you not?					
	very strong	strong	average	weak	very weak
Display **A**	1(1)*	2(2)	·	·	·
Display **B**	1(1)	2(1)	·(1)	·	·
Display **C**	·	·	·	2(2)	1(1)
Display **D**	·	2(1)	1(2)	·	·
Display **E**	·	·	2(2)	1(1)	·

How would you describe the strength of the sense of *depth* in the display, i.e. did you have a strong feeling you were looking ahead into a three-dimensional world or did you not?					
	very strong	strong	average	weak	very weak
Display **A**	1(2)	2(1)	·	·	·
Display **B**	1(1)	2(2)	·	·	·
Display **C**	·	·	·	2(2)	1(1)
Display **D**	·	1(2)	2(1)	·	·
Display **E**	·	1(2)	2(1)	·	·

* Here, the numbers inside and outside the brackets show the subject responses for the rotated and not-rotated tunnel geometries, respectively.

measurable subject response contradicted with the need for a realistic simulation.

Experienced egomotion and perceived depth   As before, the perception of depth was highly correlated with the experienced sense of egomotion (Table 8.3). The rotation of the tunnel geometry with the reference aircraft roll angle did not influence the experience of egomotion nor the sense of depth. The absence of the tunnel contour (Displays **D** and **E**) decreased both entities considerably. Placing the tunnel frames at irregular distances further decreased these variables, but only when the tunnel contour was not presented. In the absence of tunnel frames (**C**) the experienced egomotion was weak. All subjects mentioned that in this case only the movements of the vertices of the concatenated curve segment lines provided some sense of depth and egomotion. This is in agreement with the judgements given in Experiment X3 for Display **A** – the splay-only display – which was regarded by subjects as a two-dimensional image. Note that decreasing the angular

segment length $\triangle\Psi$ could attenuate the effects of egomotion even further. In conclusion, the tunnel frames provided the strongest cues in conveying a sense of egomotion.

Sources of information and control strategies   Although stated in different terms, subjects were consistent in their comments regarding the use of information in the experimental displays. For all displays and independent of the tunnel rotation, subjects used the tunnel projection at large viewing distances to judge aircraft heading. Stated to be helpful for *all* displays, the rotation of the tunnel emphasized the need to maintain a tight control on aircraft roll angle, and thus yaw rate. The tunnel frames were commented as important for a proper control of the aircraft flight-path and position errors. Subjects judged the movement of the two frames closest to the viewplane useful in controlling lateral motion. Especially the *relative* lateral displacements of these two frames and the fact whether the center of the closest frame moved towards the center of the viewplane were mentioned as the main cues. When the frames were regularly spaced, subjects reported using a *sequencing* behaviour concerning their attention towards either one of the first two frames: they *synchronized* the relative movements of these frames to control their focus of attention. Irregular frame spacing limited the use of this strategy and forced subjects to switch and cross-check the relative movements of the frames only temporarily. Subjects did not like the frame irregularity, especially when the tunnel contour was not presented: for Display **E** (relative to **D**), frame irregularity was found to be very detrimental for performance, whereas for Display **B** (relative to **A**) frame irregularity was judged to have no effect of importance. Finally, subjects stated that regular frame spacing was important to obtain a consistent estimate of the velocity of their forward motion. When no frames were presented (**C**) subjects fully concentrated on the position and the movement of the tunnel contour lines on the viewplane. Especially the position of these lines relative to the *fixed* elements of the display, i.e. the aircraft symbol and the screen edges, proved to be useful. All subjects stated that rotation of the tunnel was useless in this condition, *simply because it was hardly noticeable.* In the absence of the tunnel contour (**D** and **E**) all subjects commented on putting more effort in controlling the aircraft roll angle. Therefore, it is not surprising that the effect of frame rotation was judged to be very useful for these displays: providing the reference roll angle pictorially, allowed subjects to maintain a correct value of this roll angle, and, more importantly, their yaw rate. One subject stated that in this particular task with the strong turbulence, the effectiveness of the banked tunnel presentation decreased considerably: maintaining the reference roll angle did not necessarily result in the best path-following performance, the main pilot task.

More pilot comments on tunnel rotation and frame irregularity   Although subjects liked the rotation of the tunnel geometry with the reference roll angle, they were rather sceptical on the use of this feature in real flight. The fact that when flying a co-ordinated turn the reference roll angle *changes continuously* as a function of airspeed and turn rate could lead to pilot confusion. They doubted the use of frame rotation when a steady crosswind would be present, as this would require a *changing reference* roll angle when moving through the tunnel. It could also lead to confusion when one of the aircraft flight
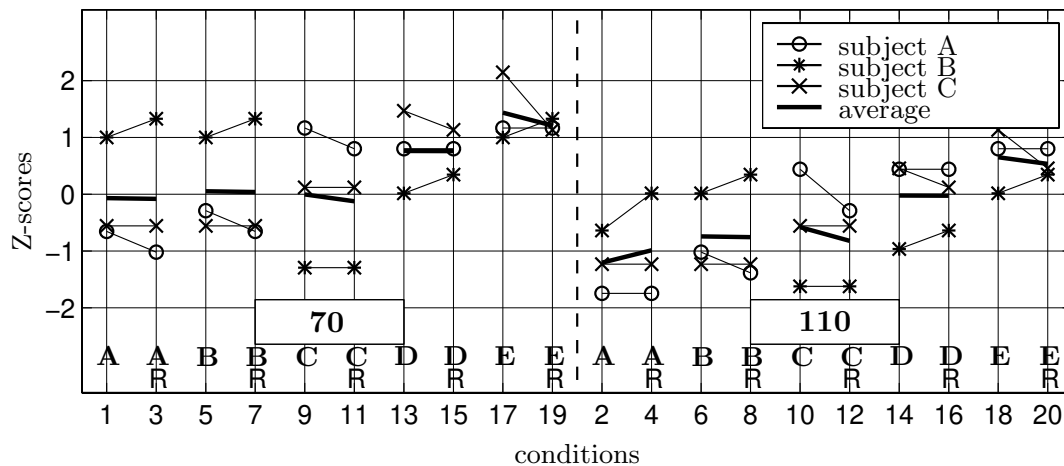
Figure 8.5: Z-scores of the effort ratings for all 20 conditions of Experiment X4. In this figure
and the following, the insets show the two velocity conditions (70 & 110 [m/s]). The
codes of the five displays are shown at the bottom, whereas the 'R' depicts whether
the tunnel geometry is rotated or not. The numbers below the figure depict the
experimental conditions.

control systems or engines fails. Subjects *did* suggest the use of a gradually changing
tunnel rotation at the entry or exit of curved trajectory segments. Subjects disliked the
irregular frame positioning, merely because it forced them to be continuously alert on
the effectiveness of their control strategy. They judged frame regularity essential during
the execution of a certain task and suggest that regularity should only change in-between
tasks. They further suggested a decreased frame distance in situations where accurate
manoeuvering is required, such as attitude level-offs, turns and in steep curves.

Effort ratings   The effort ratings show that the control task was judged easier for the
high velocity condition, Fig. 8.5. The aircraft velocity does not affect the overall trends.
Rotating the tunnel geometry has no effect on the effort ratings. As far as the tunnel
geometries are concerned, there appear to be no differences between Displays **A**, **B** and
C. The task is judged more difficult for Display **D** and especially Display **E**.

8.4.2   Time domain data: statistical analysis

A number of mixed-model Analysis of Variance computations has been conducted for
the time domain data. First, a full-factorial ANOVA with all independent measures –
including the `direction` (left/right) of the curve – was done, which revealed that this
variable did not result in any statistically significant effect of importance (van der Hoek,
1997a). The `direction` measure could therefore be abandoned in the analysis. In the
following the other ANOVA results will be discussed.

(a) aileron

(b) roll angle

(c) roll angle derivative

(d) heading angle error

(e) STD position error

(f) RMS position error

Figure 8.6: The means and 95% confidence limits of the STDs of the dependent measures (all subjects). The dotted line and the shaded area show these quantities for Experiment X1, i.e. for the task of following straight tunnel trajectories.

Table 8.4: Results of a full-factorial ANOVA (X4) on the dependent measures involving control activity, inner loop measures and path-following accuracy (in this table '$\star\star$', '$\star$' and '$\circ$' represent chance levels of $p \leq 0.01$, $0.01 < p \leq 0.05$ and $0.05 < p \leq 0.10$, respectively).

	control activity		*inner loop measures*		*path-following performance*		
	δ_a	$\dot{\delta}_a$	ϕ_e	$\dot{\phi}_e$	ψ_e	x_e-S	x_e-R
main effects							
D	$\star\star$	$\circ$	$\cdot$	$\star\star$	$\star$	$\star\star$	$\star$
R	$\cdot$	$\cdot$	$\star$	$\cdot$	$\cdot$	$\cdot$	$\cdot$
V	$\star\star$	$\star$	$\star\star$	$\cdot$	$\star$	$\star$	$\cdot$
2-way interactions							
D×R	$\cdot$	$\cdot$	$\cdot$	$\cdot$	$\cdot$	$\cdot$	$\cdot$
D×V	$\cdot$	$\star$	$\circ$	$\cdot$	$\circ$	$\circ$	$\cdot$
R×V	$\star$	$\circ$	$\cdot$	$\cdot$	$\cdot$	$\cdot$	$\cdot$
3-way interaction							
D×R×V	$\cdot$	$\cdot$	$\cdot$	$\cdot$	$\cdot$	$\cdot$	$\star\star$

Table 8.5: Results of a full-factorial ANOVA (X4) on the dependent measures involving control activity, inner loop measures and path-following accuracy (in this table '★★', '★' and '○' represent chance levels of $p \leq 0.01$, $0.01 < p \leq 0.05$ and $0.05 < p \leq 0.10$, respectively).

	control activity		inner loop measures		path-following performance		
	δ_a	$\dot{\delta}_a$	ϕ_e	$\dot{\phi}_e$	ψ_e	x_e-S	x_e-R
main effects							
C	○	·	·	○	·	○	·
R	·	·	○	·	★★	★★	★★
V	★★	★	★★	·	★	★	·
2-way interactions							
C×R	·	·	·	·	·	○	○
C×V	·	○	·	·	·	★	·
R×V	·	·	·	·	○	★	★★
3-way interaction							
C×R×V	·	·	·	·	·	·	·

Full factorial: `display` × `rotation` × `velocity`

The means and 95% confidence limits of the dependent measures are shown in Fig. 8.6. Three independent measures are defined: `display` (D) (5 levels), `rotation` (R) (2 levels) and `velocity` (V) (2 levels). The ANOVA results are summarized in Table 8.4.

The main finding of this ANOVA is that the `rotation` measure leads to no statistically significant change in pilot performance. The only exception is that it *does* lead to a statistically significant ($F_{1,3}=17.158$, $p=0.026$) decrease in roll angle error ϕ_e for all displays except Display **C**, Fig. 8.6(b). The performance increase in ϕ_e is especially strong for the displays that did not show the tunnel contour (**D** and **E**). All other visible differences in performance, such as the increase for almost all displays of δ_a, x_e-S and x_e-R, are *not* statistically significant. The only other measures involving rotation that are rather significant are the R×V-interactions for δ_a ($F_{1,3}=10.500$, $p=0.048$) and $\dot{\delta}_a$ ($F_{1,3}=9.628$, $p=0.053$), caused by the fact that for the low velocity conditions these two variables increase when the tunnel geometry is rotated, whereas for the high velocity conditions they do not.

These findings led to the decision of abandoning the `rotation` variable in the further analysis, and to concentrate on the two remaining independent measures. For this purpose, the displays were classified in two different manners depending on the geometrical definitions used in Table 8.1. Three ANOVAs were conducted to examine the usefulness of the tunnel frames vs. the tunnel contour, and the effects of positioning the frames at regular vs. irregular distances. The starting point of these ANOVAs were the re-computed means and 95% confidence limits of the dependent measures, shown in Fig. 8.7.

(a) aileron

(b) roll angle

(c) roll angle derivative
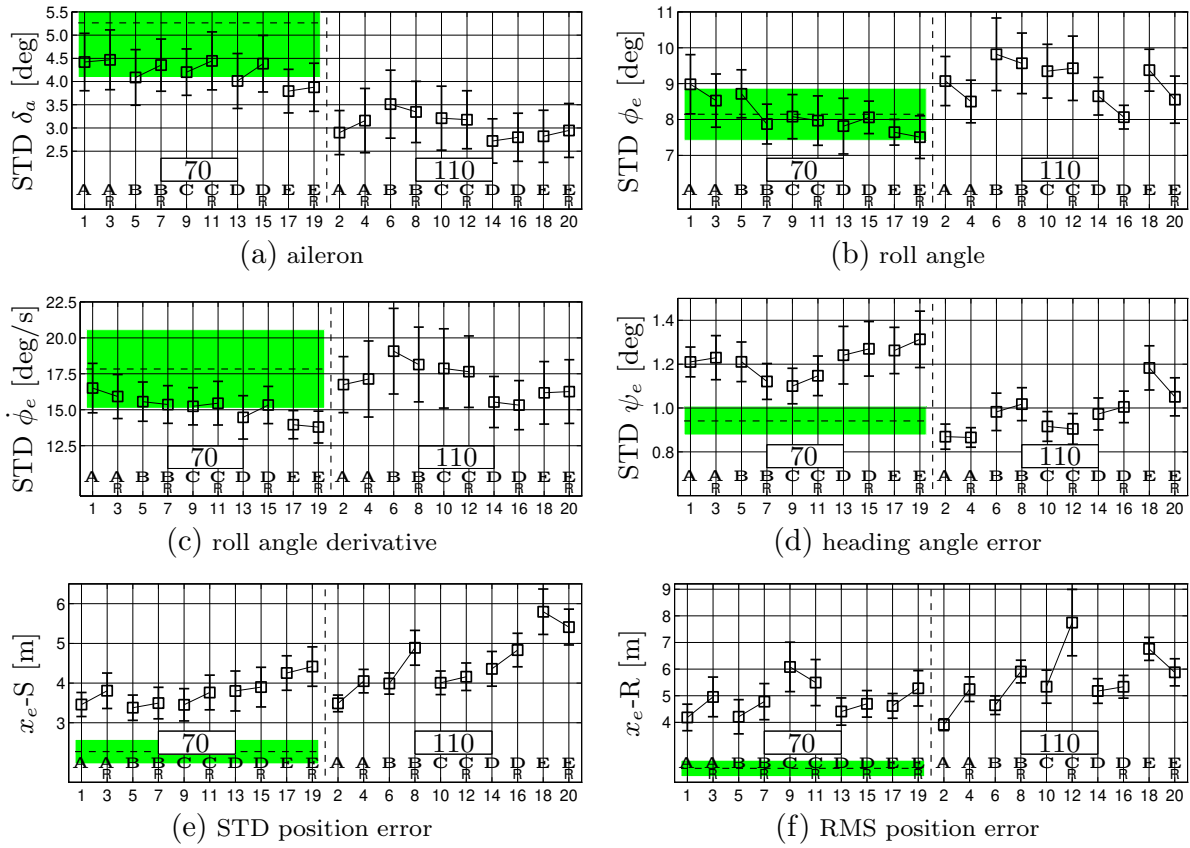
(d) heading angle error

(e) STD position error

(f) RMS position error
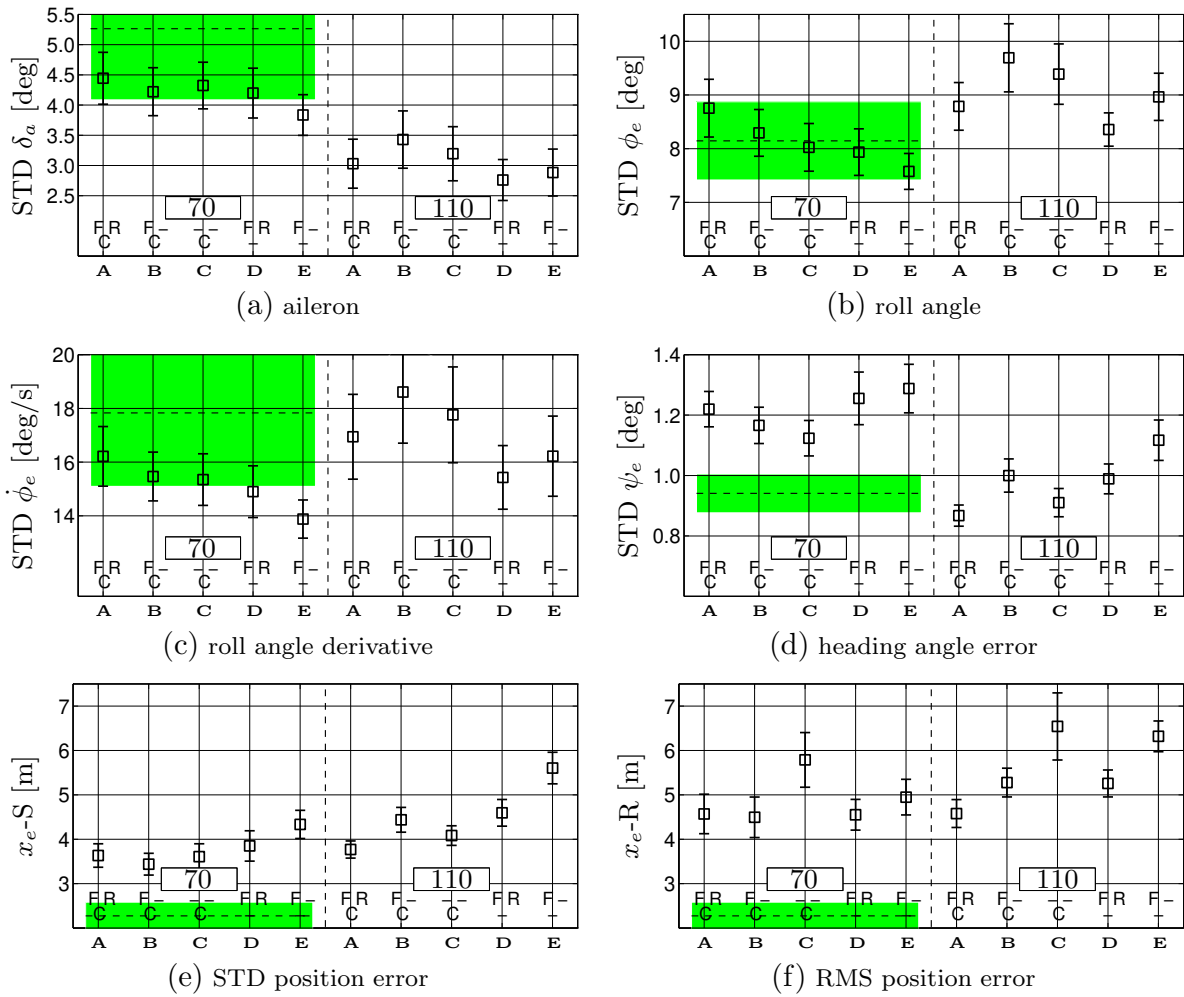
Figure 8.7: The means and 95% confidence limits of the STDs of the dependent measures (all subjects). The codes at the bottom indicate whether frames 'F' and/or the contour 'C' are shown, and the fact whether the frames are positioned at regular 'R' intervals, or not (Table 8.1).

The tunnel contour and the regularity of frames

Consider the displays containing tunnel frames, i.e. all displays except Display **C**. The two measures of interest are, first, the fact whether the tunnel contour (C) is shown (**A**, **B**) or not (**D**, **E**) (2 levels) and second, the fact whether the frames are positioned at regular (R) distances (**A**, **D**) or not (**B**, **E**) (2 levels). Together with the aircraft velocity (V) a three-way ANOVA has been conducted, yielding Table 8.5.

With respect to the low velocity conditions the high velocity leads to decreasing control activity (δ_a: $F_{1,3}$=99.386, p <0.01; $\dot{\delta}_a$: $F_{1,3}$=23.234, p=0.017), higher roll angle errors ϕ_e ($F_{1,3}$=83.021, p <0.01), smaller heading angle errors ψ_e ($F_{1,3}$=27.405, p=0.014) and higher position errors (x_e-S: $F_{1,3}$=28.923, p=0.013). The presence of the tunnel contour leads to higher control activity δ_a ($F_{1,3}$=9.602, p=0.053) and roll rates $\dot{\phi}_e$ ($F_{1,3}$=8.828,

Table 8.6: Results of a full-factorial ANOVA (X4) on the dependent measures involving control activity, inner loop measures and path-following accuracy (in this table '★★', '★' and '○' represent chance levels of $p \leq 0.01$, $0.01 < p \leq 0.05$ and $0.05 < p \leq 0.10$, respectively).

	control activity		inner loop measures		path-following performance		
	δ_a	$\dot{\delta}_a$	ϕ_e	$\dot{\phi}_e$	ψ_e	x_e-S	x_e-R
main effects							
C	○(○)*	·(·)	·(·)	○(○)	·(○)	·(★)	·(·)
F	·(·)	·(·)	·(·)	·(·)	·(·)	·(·)	○(·)
V	★★(★)	★(★)	★★(★)	·(·)	★(★)	○(★)	·(○)
2-way interactions							
C×F ⁵	-	-	-	-	-	-	-
C×V	·(·)	·(·)	·(·)	·(·)	·(·)	★(·)	·(·)
F×V	·(·)	·(★)	·(·)	·(·)	·(·)	·(·)	·(·)
3-way interaction							
C×F×V ⁵	-	-	-	-	-	-	-

---
* Here, the symbols inside and outside the brackets show the significance levels for the displays with irregular and regular frame positioning, respectively.

$p{=}0.059$). Whereas Figs 8.7(a) - 8.7(c) show that frame regularity yields higher values of δ_a, ϕ_e and $\dot{\phi}_e$, these effects are *not* significant. The regularity of frames leads to considerably lower values of the heading angle error ψ_e ($F_{1,3}{=}57.167$, $p < 0.01$), especially at high velocities resulting in the R×V-interaction. Although Fig. 8.7(d) shows that presenting the tunnel contour has a positive effect on heading performance, this effect is not significant. Concerning position performance, the presence of the tunnel contour leads to smaller values of the STD position error ($F_{1,3}{=}7.904$, $p{=}0.067$) and the RMS position error (not significant), especially when the frames are put at irregular distances, causing the significant C×R-interactions. Furthermore, the effect of the tunnel contour is larger for the high velocity conditions, yielding the C×V-interaction of x_e-S. Irregular frame positioning leads to a decreasing performance (x_e-S: $F_{1,3}{=}50.086$, $p < 0.01$; x_e-R: $F_{1,3}{=}62.727$, $p < 0.01$), especially at high velocities, causing the significant R×V-interactions for both variables. Summarizing, the tunnel contour has a positive but not always significant effect on path-following performance. Frame irregularity has a significant detrimental effect on performance. Both trends are stronger for the high velocity conditions.

The tunnel contour and tunnel frames for *regular* frame positioning

To examine the effects of showing the tunnel contour vs. showing the tunnel frames two ANOVAs must be computed. This is caused by the manipulation of the positioning of the frames, which makes no sense for Display **C** which has no frames. The effects were examined for displays with regular frames (**A** and **D**), discussed here, or with irregular frames (**B** and **E**), discussed later. The two independent measures of interest are the fact

whether the contour (`C`) is shown (**A** and **C**) or not (**D**) (2 levels), and the fact whether the frames (`F`) are shown (**A** and **D**) or not (**C**) (2 levels). Together with the aircraft velocity (`V`) (2 levels) a three-way ANOVA was conducted, Table 8.6.[5]

The presence of the tunnel contour leads to higher control activity (δ_a: $F_{1,3}$=7.473, p=0.072), higher roll angle errors (not significant) and roll rates ($\dot{\phi}_e$: $F_{1,3}$=7.327, p=0.073), to lower ψ_e's and x_e-S's (both not significant), especially at high velocities causing the `C`×`V`-interaction. It is also clear from Fig. 8.7(f) that when only showing the tunnel contour (**C**) the x_e-R is significantly larger than the x_e-S, which is caused by a considerable *bias* in the position error. Thus, the presence of the tunnel frames leads to a significantly lower RMS position error (x_e-R: $F_{1,3}$=6.408, p=0.085). This is the only significant effect, however, of the tunnel frames, emphasizing the relative importance of this measure with respect to the presentation of the tunnel contour lines for pilot performance.

The tunnel contour and tunnel frames for *irregular* frame positioning

The ANOVA introduced above was repeated for the displays with irregular frame positioning, yielding the results shown in brackets in Table 8.6. The presentation of the tunnel contour affects pilot performance to a larger extent than in the case with regular frame positioning. Control activity is higher (δ_a: $F_{1,3}$=9.723, p=0.053) as well as the roll angle error (not significant) and roll angle rates ($\dot{\phi}_e$: $F_{1,3}$=7.775, p=0.069) when the contour is presented. Furthermore, the heading angle error as well as the STD position error increase significantly when the contour is not shown (ψ_e: $F_{1,3}$=6.063, p=0.091; x_e-S: $F_{1,3}$=16.757, p=0.026). Again, x_e-R is significantly higher than x_e-S for the contour-only Display (**C**). The presence of the tunnel frames leads to no important effects on performance, which can be attributed to the relative dominance of the tunnel contour measure.

Comparison of Experiments X4 and X1

The current experimental definition, in terms of simulation variables such as the aircraft models and disturbances, is identical to the one applied in Experiment X1 (W_t=40 [m], V_{tas}=70 [m/s]: condition '6'). A comparison of pilot performance in the tasks of following a trajectory that is straight (X1) or circular (X4) is therefore allowed, especially for the baseline tunnel (**A**) configuration. Hence, in Figs 8.6 and 8.7 the means and 95% confidence limits of configuration '6' of Experiment X1 are also included. Although it is impossible to apply a statistical analysis to compare the data of both experiments objectively, the visible trends are crisp and clear. First, pilot control activity, expressed in STD δ_a and $\dot{\delta}_a$, is considerably lower when following the circular trajectory. This is accompanied by lower aircraft roll rates, whereas the aircraft roll angle errors remain the same. Concerning path-following performance, the heading angle error ψ_e is almost twice as large in the circular trajectory tracking task, illustrating the difficulty of pilots in perceiving ψ_e

---

[5]Combining frames (yes/no) and contour (yes/no) factorially would lead to a display condition 'without frames and without contour'. Because this condition was not examined experimentally, the two-way interaction of frames and contour and the three-way interaction of all measures could not be computed.
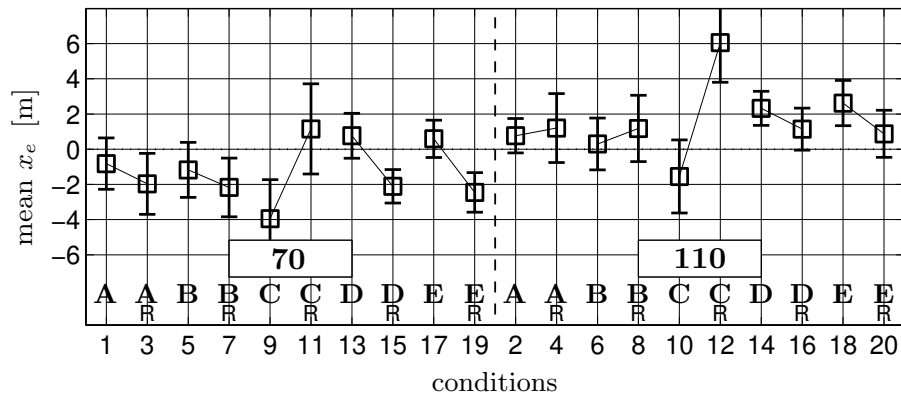
Figure 8.8: The means and 95% confidence limits of the *average* aircraft lateral position error
x_e (all subjects). A negative sign means that the aircraft is positioned towards the
inner side of the curve.

in these conditions. A consequence is that the lateral position errors are also considerably
larger, both in terms of x_e-S and x_e-R. *Biases*, i.e. non-zero means, in the position errors
only exist in the circular trajectory following task, showing pilot difficulties in perceiving
their position relative to the centercircle. The detrimental effects of the perceptual biases
emerging in the presentation of curved tunnels are thus clearly demonstrated.

The effects of presentation biases

The presentation biases in ψ_e and x_e in curved tunnels are one of the main causes for
the significant decrease in path-following performance as compared to the task of follow-
ing straight tunnel trajectories. All displays convey a presentation bias in presenting the
aircraft track angle with respect to the trajectory, leading to a considerable increase in
variations in ψ_e. The time histories of ψ_e, however, do not contain any traces of biases
in the aircraft heading angle error, as these would lead to a continuously increasing air-
craft lateral position error. The time histories of x_e, however, show consistent biases,
illustrated in Fig. 8.8.[6] On the average, the biases in x_e are small, except for Display **C**
where these biases reach values up to 6 [m]. A three-way full-factorial ANOVA (the inde-
pendent measures were `display` (5 levels), `rotation` (2 levels) and `velocity` (2 levels))
revealed a number of trends. First, whereas for the low velocity conditions the aircraft is
generally positioned towards the inner side of the curve, the opposite holds for the high
velocity condition ($F_{1,3}=64.066$, $p <0.01$). Tunnel rotation leads to a shift in the position
error bias towards the inner side of the curve, except for Display **C** that has the opposite
effect (causing a significant `D`×`R`-interaction: $F_{4,12}=47.496$, $p <0.01$) and for Displays **A**
and **B** for the high velocity condition (causing a significant `R`×`V`-interaction: $F_{1,3}=11.207$,
$p =0.044$). For both velocity conditions the position error bias of Display **C** differs signifi-

---

[6]The position error time histories for Experiment X1 – the straight trajectory following task – contain
no traces of these biases at all, i.e. the mean aircraft position errors are zero.

cantly (NK, p=0.05) from the others. In fact, the differences between x_e-S and x_e-R were found to be significant (t-test, p=0.05) only for Display **C** (van der Hoek, 1997a). When the tunnel geometry is rotated the position error biases for all displays except Display **C** are the same. When the tunnel geometry is not rotated the average bias for Displays **D** and **E** are more towards the outer side of the curve than for Displays **A** and **B**.

Fig. 8.8 illustrates that the presentation biases in x_e caused by the tunnel contour and the tunnel frames confirm the experimental hypotheses. Without rotation, the largest bias is found for the contour-only display, **C**, towards the inner side of the curve. For the frames-only displays the biases are directed towards the outer side of the curve. The effects of both biases *compensate* for each other when both the frames and the contour lines are presented simultaneously. As expected, when the tunnel geometry is rotated as a whole, the x_e-bias for the contour-only display changes dramatically to a considerable bias towards the *outer* side of the curve. The opposite effect holds for the frames-only displays, an effect, however, which can not be explained from the information analysis. Again, the effects of the presentation biases caused by both the frames-only and the contour-only presentations *compensate* for each other when they are presented at the same time.

8.5 Modelling efforts

The measured pilot control behaviour is captured in a mathematical model, a descriptive multi-loop model introduced in Chapter 4. Below the main findings are discussed.

Model structure   The MLM model structure is identical to the one applied in Experiments X1, X2 and X3 (roll channel). Recall that this model consists of three feedback loops representing pilot control of aircraft attitude, flight-path and position.

Model parameters   The MLM model parameters are also identical to those applied in Experiments X1, X2 and X3 (roll channel). It is hypothesized that all pilot equalization efforts are concentrated in the control of the aircraft inner loop (attitude). The aircraft middle and outer loops are fed back with two proportional gains that merely determine the bandwidth of these two feedback loops. Here only the inner loop variables are discussed. The estimated inner loop parameters are not shown. The main trends in the pilot *limitation* data are, first, a greater τ and a smaller ω_n for the low velocity conditions. Second, rotation generally leads to a lower ζ_n and ω_n and a smaller delay for Displays **D** and **E**. No trends are clear in the data when considering the display measure alone. Finally, in comparison to the data of Experiment X1, the time delays are larger and ω_n is smaller. The *equalization* parameters show that, generally, $\tau_{L_{in}}$ is larger and $K_{p_{in}}$ is smaller than the values of Experiment X1. Furthermore, $\tau_{L_{in}}$ is considerably larger than the lead necessary to compensate for the aircraft roll response lag τ_ϕ. These effects indicate that pilots generate more lead to obtain the necessary phase margin in their inner loop feedback, an indirect proof of the hypothesized difficulty in this task as compared to that of following a straight trajectory. In the low velocity conditions more lead is generated than in the high velocity conditions, which can be explained by the favourable aircraft handling for the

latter conditions. No clear trends are apparent in the data as far as the display measure is concerned, a disappointing finding caused by the rather large between-subject variation.

MLM results: crossover frequencies and phase margins   The measured and modelled crossover frequencies and phase margins of the inner loop and the combined outer loop are illustrated in Fig. 8.9. Whereas the inner loop bandwidths ω_c^{in} are clearly lower (φ_m^{in} higher) than those measured in Experiment X1, the bandwidths (and phase margins) of the combined outer loop are about the same. Only the values of the latter variable are considerably lower for Displays **D** and **E**, i.e. the displays without the tunnel contour lines. Fig. 8.9(a) shows that ω_c^{in} increases (φ_m^{in} decreases) when the tunnel geometry is rotated, for all conditions: pilots put more effort in maintaining a small roll angle error ϕ_e. No other effects concerning the display measure can be seen in these figures. The combined outer loop bandwidth shows an opposite effect when the tunnel is rotated: here, the bandwidth $\omega_c^{out^c}$ decreases ($\varphi_m^{out^c}$ increases) for all displays. Thus, pilots put less effort on path-following performance to allow them to increase their performance in minimizing ϕ_e. The aircraft velocity has no effect at all on the data. Fig. 8.9(b) shows that the combined outer loop bandwidth is largest for the displays presenting the tunnel contour lines. Clearly, bandwidth is low for Displays **D** and **E**, showing only the tunnel frames. The positioning of the tunnel frames themselves leads to no overall trend, whatsoever.

The estimation of the MLM middle and outer loop gains allows the combined outer loop to be dissected into the middle and outer feedback loops. The bandwidths and stability margins of these loops, illustrated in Fig. 8.10, reveal a number of trends. First, whereas the bandwidths of the middle loop for the displays showing the tunnel contour are about the same as those found in Experiment X1, their phase margins are considerably lower. The opposite holds for the displays showing only frames, **D** and **E**. Clearly, the control of aircraft heading is considerably more difficult than in the task of following a straight trajectory. This can also be stated for the outer loop where bandwidths ω_c^{out} are lower (φ_m^{out} higher) than for Experiment X1. Second, whereas higher middle loop bandwidths ω_c^{mid} (lower φ_m^{mid}) are found for the low velocity conditions, the opposite holds for the outer loop bandwidths. Thus, irrespective of the other measures, pilots put more effort in controlling their position errors when the aircraft velocity increases. Third, rotation leads to lower middle loop bandwidths ω_c^{mid} (higher φ_m^{mid}) for all conditions. It leads to lower outer loop bandwidths ω_c^{out} (lower φ_m^{out}) for the high velocity conditions, whereas for the low velocity conditions the outer loop bandwidth increases when the tunnel geometry is rotated. Finally, the displays presenting the tunnel contour lines allow pilots to maintain a relatively high middle loop bandwidth ω_c^{mid} (lower φ_m^{mid}), for all conditions, and a rather high outer loop bandwidth, only for the high velocity conditions. When the frames are not positioned regularly, the outer loop bandwidth decreases (and φ_m^{out} increases) considerably, especially for the low velocity conditions.
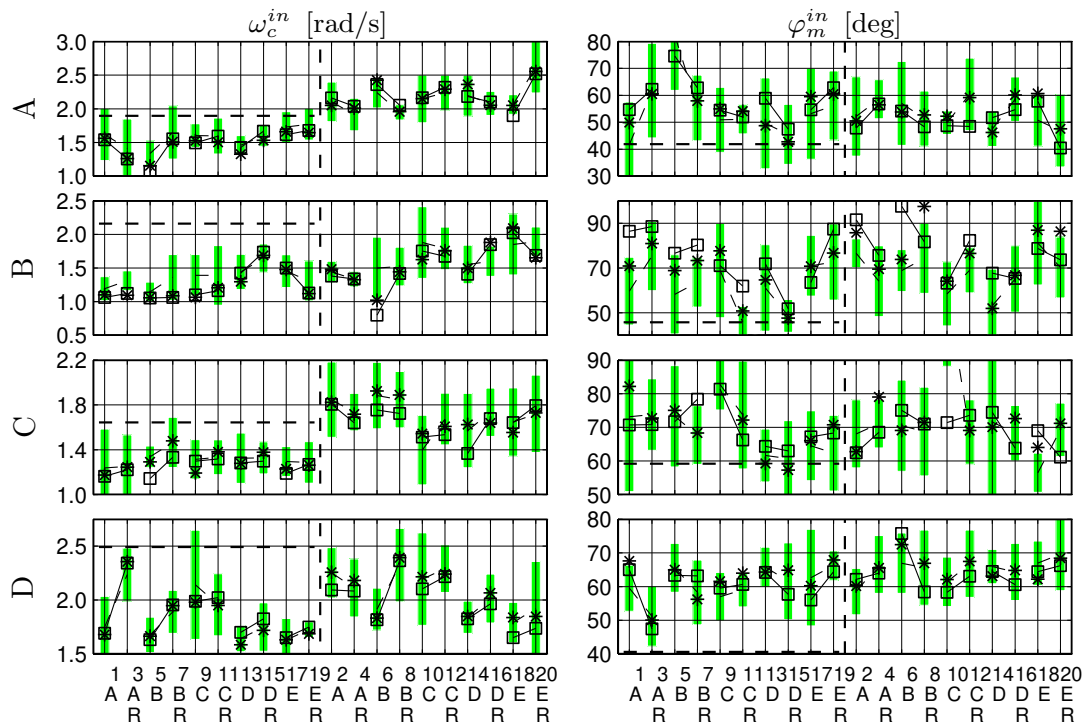
(a) inner loop
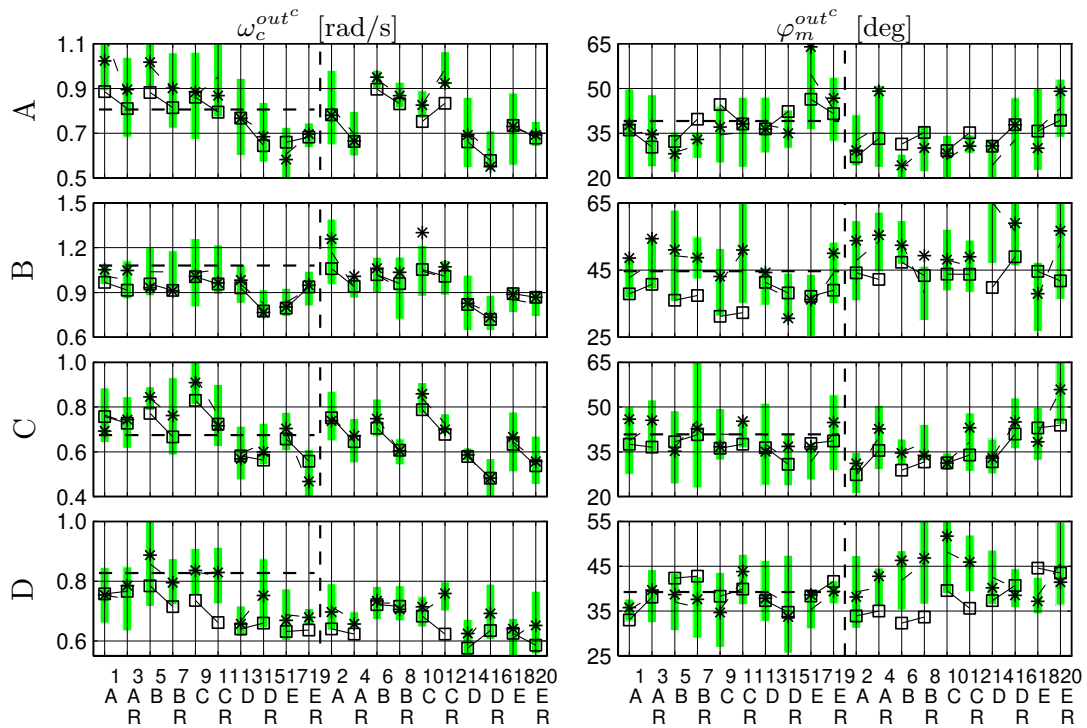
(b) outer loop (combined)

Figure 8.9: Crossover frequencies and phase margins (all subjects, all conditions). The shaded areas show the uncertainty regions of the raw frequency response data, their averages connected with the dashed line. The '*'-symbols show the quantities for the averaged frequency responses; the squares show them for the MLMs. The horizontal dashed lines show the values of these quantities for Experiment X1.
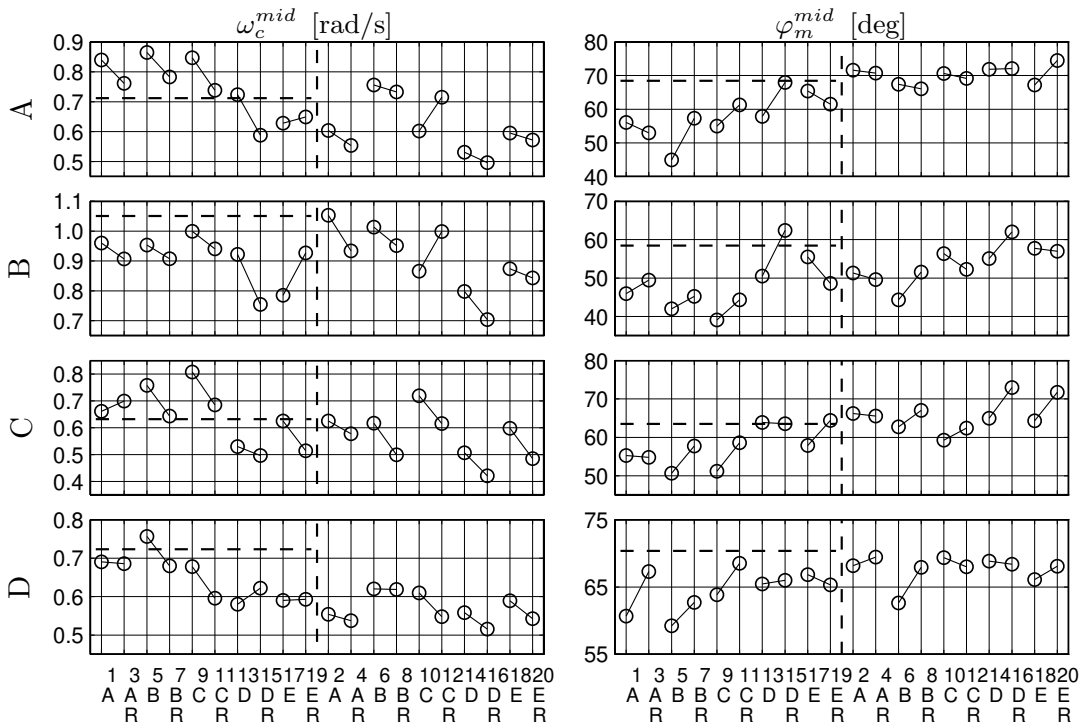
(a) middle loop crossover frequencies and phase margins
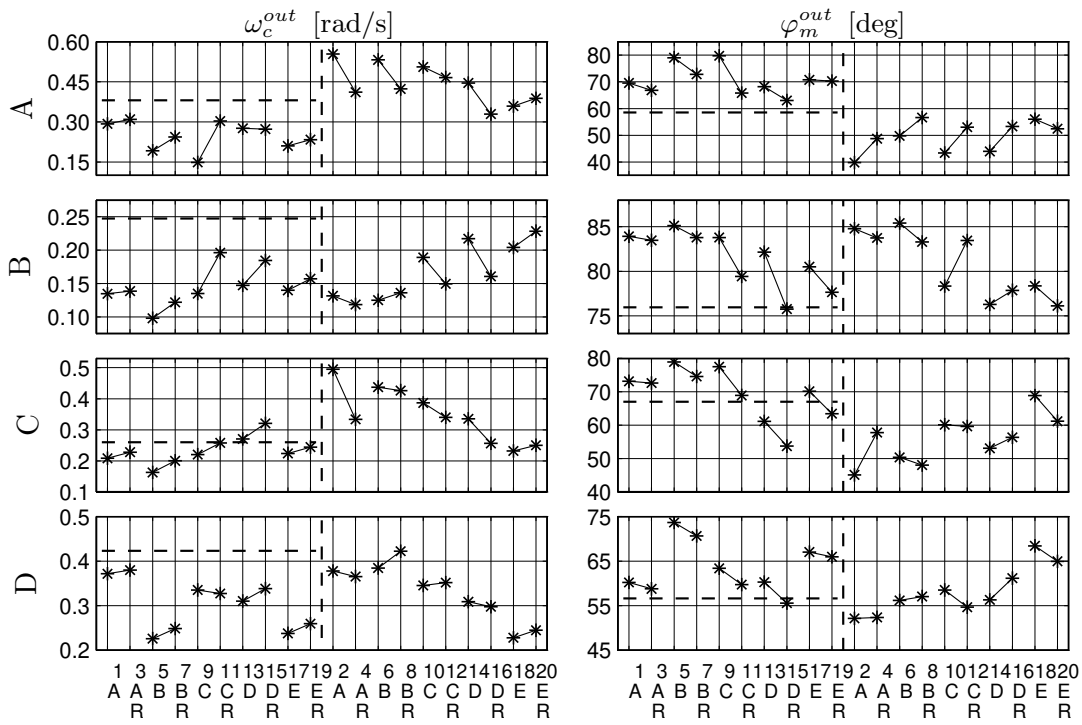
(b) outer loop crossover frequencies and phase margins

Figure 8.10: Middle and outer loop crossover frequencies and phase margins, following the MLM analysis (all subjects, all conditions). The horizontal dashed lines show the values of these variables for Experiment X1.

8.6 Retrospective

8.6.1 Discussion

A central theme in this thesis is the analysis of a pilot's use of optical information conveyed by the tunnel display, in particular the optical gradients of splay and density. The investigation in the previous chapter clearly demonstrated the relative usefulness of these two gradients in the task of following a straight trajectory. In §8.2 it was argued that, although significant differences exist in the optical information between this task and the circular trajectory following task, the main findings of Experiment X3 also apply here. This allowed Experiment X4, defined in §8.3, to focus on other phenomena that are important, and some of them unique, for the pilot task of tracking circular trajectories. Initially, three displays were designed: the baseline tunnel (**A**), the contour-only display (**C**) conveying only splay information, and the frames-only display (**D**) conveying only density information. In addition the distance between frames was manipulated, yielding Displays **B** and **E** derived from Displays **A** and **D**, respectively. Inspired by the investigation in (Grunwald et al., 1981), all five experimental displays were analyzed in a *banked* and a *non-banked* version. In the banked tunnel the frames and the contour lines are *rotated* around the centercircle with an angle equal to the aircraft reference roll angle needed to fly the turn. Experiment X4 investigated the effects of the various tunnel geometrical definitions on pilot performance, control activity and control behaviour. In the following, the experimental findings reported in §8.4 and §8.5 are elaborated further in an attempt to put them in a unified perspective. Central in the discussion will be the validity of the experimental hypotheses, the relative usefulness of splay and density information, the differences between the tasks of following straight and curved trajectories and the effects of presentation biases in the latter task (Mulder et al., 1999a).

The pre-experimental hypotheses

Similar to Experiment X3 the experimental data provide an abundance of affirmative evidence for almost all pre-experimental hypotheses stated in §8.3. Again this shows the strength, usefulness and above all the importance of an extensive pre-experimental information analysis, conducted in §8.2 and summarized qualitatively in Table 8.2.

Tunnel frames versus tunnel contour lines The optical density information conveyed by the tunnel frames must be perceived at small viewing distances in order to be useful for the control of the aircraft flight-path and position. This is confirmed by the questionnaire where pilots stated that especially the first two or three frames were used for control purposes. The same holds for the optical splay information provided by the tunnel contour lines. Similar to the findings in Experiment X3, the pilot questionnaire revealed that, contrary to the contour-only display, the tunnel frames are essential for an experience of egomotion. It was hypothesized that the aircraft heading with respect to the trajectory, in this experiment equal to the lateral motion, can be perceived best from the tunnel contour

lines. The aircraft lateral position relative to the tunnel centercircle was hypothesized to be perceived best from the tunnel frames. These hypotheses could both be confirmed. The effort ratings indicated that not showing the tunnel contour leads to a considerable increase in pilot effort. The time domain data revealed that the displays with the tunnel contour yielded the best path-following performance. Displays showing the tunnel contour led to higher pilot control activity, higher inner loop activity, smaller heading angle errors and smaller position error variations, x_e-S. The contour-only display (**C**), however, led to the worst performance in terms of x_e-R, which can be attributed to the existence of consistent biases in the lateral position error with this display. Here, the presence of tunnel frames is mandatory to achieve an acceptable performance. The presentation of the tunnel contour led to a positive effect on performance, especially when the tunnel frames were put at irregular distances. The modelling data indicated that displays showing tunnel contour lines allow pilots to maintain a high bandwidth of both their flight-path angle as well as their lateral position error feedback loops.

Summarizing, the splay information conveyed by the tunnel contour lines is essential to control the aircraft flight-path relative to the trajectory, and allows pilots to increase the bandwidths of their feedback loops determining path-following performance. The density information and the relative motion of the tunnel frames give pilots a sensation of forward motion, and they are important for their perception of the correct aircraft lateral position relative to the centercircle. The experimental findings clearly demonstrate that showing either one of the basic tunnel geometrical entities does not lead to the best performance. Rather, both the elements are mandatory in this respect: the tunnel contour lines for flight-path information and the tunnel frames for position information.

The effects of regular/irregular frame positioning   Putting the frames at irregular distances between each other is hypothesized to hamper the use of the density gradient considerably, negatively affecting the path-following performance. The comments in the pilot questionnaire showed that this assumption is correct: pilots definitively disliked the irregular frame positioning, especially when the tunnel contour lines were left out (examine the ratings for Display **E**). Irregularity of frames further led to a weakening pilot sense of egomotion. The time domain data revealed that frame irregularity had significant detrimental effects on path-following performance (ψ_e, x_e), especially at the high velocity conditions. The presence of the tunnel contour lines on the display led to a significantly increasing performance, in particular for the display with irregular frames. The modelling data showed that when the frames are put at irregular distances, pilots put relatively more effort in controlling the aircraft flight-path: whereas the bandwidth of this feedback loop increases, the bandwidth of the position error feedback loop decreases.

Summarizing, putting frames at irregular distances is especially harmful for pilot performance when no tunnel contour lines are available. When the tunnel contour is presented on the display, pilots can always fall back on using the information provided by the contour lines, allowing them to maintain an acceptable level of performance. When no tunnel contour is available, the random positioning of tunnel frames could mean that, until an

arbitrary frame moves closer, pilots temporarily have no accurate information about their current position and flight-path at all.

Rotating the tunnel geometry Because the cue analysis revealed that banking the tunnel has no effect at all on the presentation of ψ_e and x_e, it was hypothesized that this measure had no effect on path-following performance. As it *does* provide a clear reference for the required roll angle, however, a performance increase in terms of a small roll angle error was also hypothesized. The pilot questionnaire revealed that pilots interpreted the rotation of the tunnel geometry as an additional motivation for a tight control of the aircraft roll angle. The ratings showed no effects of rotation at all, reflecting the general pilot comment that rotating the tunnel did not help them in any way in improving their performance. An interesting finding is that pilots generally ignored the rotation of the tunnel in case of the contour-only display (**C**), simply because they *hardly noticed any difference with the non-rotated version*. Because the tunnel display applied in the experiments of Grunwald (1984) resembled the contour-only display of this experiment, this could explain the finding that tunnel rotation did not help pilots in improving their performance. The time domain data further supported the experimental hypotheses and the pilot comments. Although path-following performance clearly *decreased* for the rotated tunnels, these effects were not statistically significant. Rotation did yield a significant increase in terms of ϕ_e-performance for all displays, especially Displays **D** and **E**, but except for Display **C**. The modelling efforts showed a considerable increase in bandwidth of the feedback of the roll angle error for all displays. At the same time, the bandwidth of the combined outer loop decreases when the tunnel is rotated, leading to the decreasing path-following performance stated above. These effects are all markedly smaller for Display **C**. Apparently, the *balance* in pilot effort between the inner and outer loops changes when the tunnel is rotated, for the benefit of the inner loop. Hence, one could speak of a somewhat confusing situation for a pilot: whereas the rotated tunnel *suggests* pilots to maintain a small roll angle error, it does in fact not help them in improving their path-following performance. These results support those of Grunwald et al. (1981).

The effects of presentation biases

Caused by the trajectory curvature and the limited viewing volume accompanying the perspective projection, the information conveyed by the presentation of curved trajectories on the tunnel display does not accurately reflect the aircraft position and attitude relative to the centercircle. The presence of presentation biases in the projection of curved tunnel trajectories is one of the main differences between the tasks of following a straight and a curved trajectory. The cue analysis conducted in §D.5 and summarized in §8.2 indicated that different presentation biases exist for the two main tunnel geometrical entities, the frames and the contour lines. Based on this investigation, it has been hypothesized that presentation biases lead to the worst performance in terms of the lateral position error for the contour-only display (**C**). The experimental data confirm this hypothesis and support the other findings of the cue analysis. First of all, a consistent bias of considerable mag-

nitude was found for Display **C**, directed towards the inner side of the curve. Apparently, the strong position error bias conveyed by the contour lines is interpreted by pilots as if they were positioned towards the outer side of the curve, causing them to compensate for the bias through flying towards the inner side. Rotating the tunnel geometry yields a dramatic shift in the position error bias for Display **C** towards the *outer* side of the curve. Recall that the questionnaire revealed that pilots were generally unaware of the geometry being rotated for this display. Hence, they interpret the rotation of the contour line splay angles as a cue for being positioned towards the inner side of the curve, and compensate for this bias through flying towards the *outer* curve wall. Second, the position error biases for the frames-only displays are considerably smaller and are directed towards the outer side of the curve. The presentation biases in this case are caused by two biases with opposite signs (Appendix D), and apparently the bias leading to an impression of being located to the inner side of the curve – the relative lateral displacements of the frames – dominates. When the tunnel geometry is rotated the position error bias changes sign, an effect unexplained by the cue analysis and, considering Figs 8.2(b) and 8.2(c), which is rather counter-intuitive. Third and final, when both the tunnel contour as well as the tunnel frames are presented, the position error biases are smaller. Tentatively, the effects of the various presentation biases *compensate* for each other when both tunnel geometrical entities are presented simultaneously. Rotating the tunnel geometry has only a small effect on the position error biases with the combined displays. An interesting phenomenon is that when the tunnel geometry is rotated, the position error biases for all displays containing frames, i.e. all displays except Display **C**, are the same.

Comparison of the curved/straight trajectory following tasks

The cue analysis in Chapter 3, summarized in §8.2, led to the hypothesis that it is much more difficult for pilots to obtain an accurate perception of the aircraft position and attitude relative to the tunnel trajectory, causing a significant decrease in path-following performance. The experimental data support this hypothesis. Compared to the pilot performance variables obtained in the straight trajectory following task of Experiment X1, here the pilot control activity is lower, the aircraft roll rates are higher, the heading angle error is almost twice as large, and the lateral position errors are considerably higher. The modelling efforts provide additional insight into these findings. The pilot time delays are considerably higher in the curved trajectory tracking task, requiring an increase in pilot inner loop lead to maintain sufficient phase margin in the inner loop. Generally, the bandwidth of the inner loop is smaller and the phase margins are higher, indicating that pilots sacrifice inner loop bandwidth to be able to put more effort in the outer loops to maintain path-following performance. This is supported with the result that the bandwidth of the combined outer loop is about the same, except for the frames-only displays, **D** and **E**. Hence, pilots successfully attempt to maintain a high bandwidth but fail to do so for the displays without a tunnel contour. The middle and outer loop data shed a further light on this. Whereas the bandwidths of the middle loop – aircraft

flight-path ψ_e – approximate those of Experiment X1, the phase margins are considerably lower. This indicates that pilots have difficulty in perceiving ψ_e causing a larger delay and lower phase margins. An exception forms the displays without contour lines, where the phase margins are about the same as those in Experiment X1, but the bandwidths are considerably lower. Because the ψ_e-information is lacking seriously for these displays, a tentative explanation would be that pilots simply have to sacrifice bandwidth to obtain a more stable feedback of ψ_e. Finally, the bandwidths of the outer loop – aircraft lateral position error x_e – are markedly lower than those measured in X1 for all displays. This further exemplifies the apparent difficulty in perceiving the lateral position error in curved trajectories, for *all* geometric tunnel variations investigated here.

8.6.2 Conclusions and recommendations

Conclusions

- The experimental data support the hypotheses that were based on the pre-experimental cue analysis of §8.2. The relative usefulness of optical splay and density information for control purposes in the pilot task of following a curved trajectory is demonstrated.

- The aircraft *heading* with respect to the curved trajectory, in the experiment equivalent to the aircraft lateral motion, can be perceived best from the tunnel contour lines. The *optical splay information conveyed by these contour lines is essential for the perception and control of aircraft flight-path with respect to the trajectory.*

- The aircraft *position* with respect to the curved trajectory can be perceived best from the tunnel frames. The *optical density information conveyed by the tunnel frames is essential for the perception and control of aircraft position with respect to the trajectory.*

- The experiment indicates that both the optical density information as the optical splay information must be perceived at small viewing distances in order to use this information for the control of aircraft flight-path and position relative to the trajectory.

- Putting the tunnel frames at irregular distances between each other hampers the use of the optical density gradient and leads to a degrading path-following performance. The effects of frame positioning are larger when no tunnel contour lines are presented.

- The moving tunnel frames and not the tunnel contour lines give pilots a sensation of forward motion through the tunnel.

- Rotating the tunnel geometry provides pilots *pictorial* information about the required, or *commanded*, aircraft roll angle to fly the curve. Although pilots are aware that it does not help them in improving their path-following performance, rotation causes an increase in pilot motivation to maintain the right roll angle. Hence, the balance between the inner and the outer loop performance changes for the benefit of the inner loop.

- Rotating the tunnel geometry has no effect on the presentation of the aircraft flight-path and position relative to the trajectory. In the curved trajectory tracking task in the presence of disturbances considered here, tunnel rotation even leads to a *reduction*, but not significant, of pilot path-following performance.

• Rotation of the tunnel in the contour-only display is ignored by pilots because they hardly notice any difference with the non-rotated version. As a consequence, they interpret the information as a shift in aircraft position towards the inner side of the curve, causing a significant lateral position bias.

• Due to the limited viewing volume of the perspective projection, the tunnel display does not convey the exact aircraft position and attitude relative to a curved trajectory. These presentation biases lead to a significant decrease in path-following performance.

• The presentation biases lead to considerable errors in the aircraft lateral position relative to the centercircle. Although pilots attempt to smoothly and accurately control their aircraft through the circular tunnel they are not aware that they are in fact not flying through the tunnel center. The position error biases are largest for the display showing only the tunnel contour lines, and decrease considerably when the tunnel frames are presented. Furthermore, when both tunnel geometrical entities are shown at the same time the presentation biases *compensate* for each other leading to the best performance.

• Although displays showing the tunnel contour lines yield the best path-following performance, the tunnel frames must be presented as well to minimize the effects of the presentation biases.

• Pilot control of aircraft curvi-linear motion along a circular trajectory is markedly more difficult than the control of aircraft recti-linear motion along a straight trajectory. This is caused by the degrading information when presenting curved rather than straight sections of the trajectory on the display, both in a quantitative as a qualitative manner. Not only the number of optical cues becomes smaller, also the usefulness of the available cues decreases. Hence, it is much more difficult for pilots to obtain an accurate perception of the aircraft position and attitude relative to the tunnel trajectory, causing a significant decrease in path-following performance and increase in pilot effort.

Recommendations

• An experiment could be done to analyze the effects of limiting the viewing distance on pilot control behaviour in the task of following a curved trajectory. The current investigation revealed that in curved tunnels the information needed for control purposes must be perceived in particular at *small viewing distances*. Hence, limiting the tunnel display viewing volume can be expected to be detrimental in curved tunnel sections.

• The possibilities of the pictorial aircraft bank angle command information provided by a rotated tunnel geometry (in turns with constant curve radius) should be analyzed further. Especially the effects of a constantly changing aircraft reference bank angle, yielding a constantly changing tunnel geometry rotation, should be analyzed in terms of pilot performance and control behaviour, but also in terms of pilot confusion.

• The pre-experimental cue analysis showed that the presentation biases in curved trajectories depend on the size of the tunnel and the radius of the curve. These effects should be investigated further, if possible through experimental validation.

Chapter 9

Symbology: a flight-path vector

9.1 Introduction

The experiments discussed in the previous chapters have two things in common. First, the main subjects of interest are the tunnel *geometry* design variables. Second, in all experiments, except for the pitch channel control task of Experiment X3, the aircraft's direction of motion relative to the tunnel, χ, could be perceived *directly* from the display, namely through the position of the infinity point with respect to the display center, depicting ψ. In other words, although atmospheric turbulence was simulated that disturbed the aircraft motions, none of the turbulence components actually perturbed the aircraft *flight-path*, i.e. $\chi = \psi$. The investigation of this chapter differs in both ways. A *generic* tunnel geometry is chosen that remains the same throughout the experiment. Furthermore, the aircraft direction of motion will be perturbed with a disturbance on the lateral component of the aircraft velocity vector. Since in this case the aircraft heading angle ψ and track angle χ are not equal any more, the aircraft direction of motion can no longer be perceived *directly* from the display. Rather, it must be estimated from the changes in time of the perspective projection of the tunnel geometry on the viewplane, the ecological cues of motion perspective. The discussion in Chapter 3 revealed that this has often proved to be a challenging task. The task can be alleviated considerably, however, by augmenting the tunnel display with a so-called *Flight-Path Vector* (FPV) symbol. By explicitly showing the aircraft flight-path, the FPV restores the possibility of *directly* perceiving the direction of aircraft motion with respect to the trajectory. The essential background information on this basic form of synthetic display augmentation will be discussed in §9.2. Experiment X5, defined in §9.3, is conducted to assess the usefulness of providing explicit aircraft flight-path information on pilot behaviour, dependent on the various characteristic properties of the atmospheric turbulence and the velocity of the aircraft motion. The experimental results and pilot control behaviour modelling efforts are discussed in §9.4 and §9.5, respectively. All findings are summarized and discussed thoroughly in the retrospective, §9.6.

9.2   Background

9.2.1   Three tunnel display augmentation principles

Irrespective of the cockpit displays mediating the aircraft state to the pilot, the main issues that are of concern to the pilot in the aircraft guidance task are probably the questions of 'where am I?' and 'where am I going?'. The advantage of electronic displays over their (electro-)mechanical predecessors is that they can be *augmented with synthetic symbology* designed in particular to help pilots in conducting their tasks and to improve their performance. The synthetic enhancements are generally a form of *augmenting cues*, which can be defined as *"a perceptual event auxiliary to the basic display that is used to enhance an important characteristic of the display"* (Eberts, 1987). The synthetic nature of the tunnel-in-the-sky display allows these virtual enhancements to be integrated in a way that is compatible with the guidance task. In the past, numerous investigations have been conducted addressing the usefulness of synthetic symbology in two-dimensional (Gold, 1965; Merhav & Grunwald, 1978; Hynes et al., 1989) and three-dimensional (Grunwald & Merhav, 1978; Roscoe & Jensen, 1981; Jensen, 1981; Grunwald et al., 1981) aircraft guidance displays. The fact that visually presented augmenting cues have often shown to considerably improve human performance can be understood using two basic principles (Eberts, 1987):

1. a well-designed display augmentation transforms the task at hand from a *computational* to a *perceptual* task[1]; and,

2. it provides a means of establishing or improving the *compatibility* between the display and the operator's mental model of the system and the corresponding task.

Below, the three main forms of tunnel display augmentation, i.e. the flight-director, the flight-path vector, and the flight-path predictor, will be investigated. As it will become clear, these three forms represent elementary display augmentation principles of providing synthetic command, status and predictive information, respectively.

Augmenting with *command* information: the flight-director   In Chapter 1, the Flight-Director (FD) was introduced as an example of augmenting the conventional Primary Flight Display (PFD) with *command* information. Based on the requirements of the guidance task, the pilot selects an FD control mode and defines the FD controller setpoints. The FD computer algorithm then integrates the information and generates two control signals appropriate to fulfil the task requirements. The control signals drive the FD 'roll' and 'pitch' command bars on the PFD. The remaining task of a pilot operating with a FD is to move the control device – column or stick – in correspondence with the FD command signals, according to the rule of 'follow-the-needle'.

In the light of the two principles defined above two comments can be made. First, with a conventional set of planar flight displays the pilot is required to mentally combine the

---

[1]In terms of Ecological Interface Design (EID), the display provides the information needed for control in a form that exploits the power of perception (Vicente & Rasmussen, 1990).
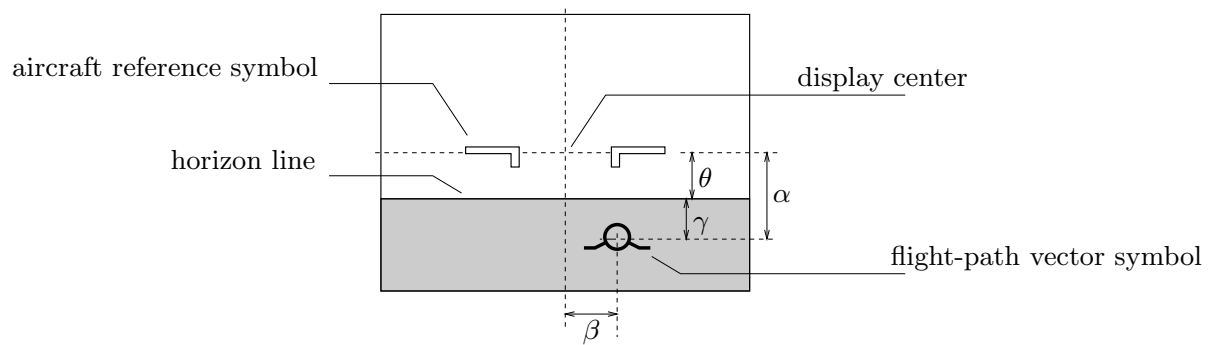
Figure 9.1: The flight-path vector: basics. The FPV shows the attitude (α, β) of the aircraft velocity vector (the Aerodynamic reference frame $\mathcal{F}^a$) with respect to the aircraft longitudinal axis (the Body reference frame $\mathcal{F}^b$) depicted by the display center.

status information and integrate the data into a mental representation of the aircraft's spatio-temporal situation. With a FD the *integration* of information is conducted by the FD algorithms. The FD relieves the pilot from the demanding *computational* integration task and provides the appropriate control action directly on the display. The resulting pilot behaviour is a typical psycho-motor task of reading a display and moving a control device. Second, the FD command indicators represent something that has no reference, or *meaning*, regarding the aircraft's spatio-temporal situation with respect to the commanded flight-path. The augmentation does certainly not help the pilot in improving awareness of the aircraft state itself and is therefore *not compatible* with any sensible mental model.

Not many examples exist of augmenting the tunnel display with a flight-director (Funabiki, 1997), most probably because the two concepts have been developed from totally different, possibly contradicting perspectives. Recall that one of the reasons for developing the tunnel display was to provide pilots an intuitive representation of the aircraft's spatio-temporal situation with respect to the commanded flight trajectory, allowing them to *directly* perceive the guidance information. Putting the FD command bars on the tunnel display means that two *abstract* entities, which have no meaning at all in the *pictorial* three-dimensional environment, must be integrated once again by the pilot. Whereas a tunnel display allows a more 'natural' control strategy, compatible with the situation as if the outside-world information would be continuously available through the windshield, the FD forces a pilot to adopt a two-axis compensatory tracking strategy. Hence, although certainly applicable, this is a doubtful combination of concepts. Rather, the aim of designing forms of augmentation for the tunnel display should be to investigate symbology that *is* compatible with the pictorial tunnel display format, and that is *compatible with the pilot's mental model*. Two of these possibilities are discussed next.

Augmenting with *status* information: the flight-path vector   The flight-path vector (FPV) has become almost a standard feature of the modern cockpit Primary Flight Display (PFD) and the Head-Up Display (HUD). It shows the attitude of the aircraft

velocity vector with respect to the longitudinal Body axis, Fig. 9.1, allowing a pilot to directly perceive the aircraft's angle of attack α and angle of slip β. This is aircraft *status* information that can be measured with any common on-board sensor (Kayton & Fried, 1997). To estimate the vertical direction of the aircraft motion relative to a horizontal plane, the angle of climb γ, a pilot can simply *perceive* the vertical deflection of the FPV with respect to the horizon line. To estimate the lateral direction of the aircraft motion relative to a ground track, the aircraft track angle χ, $(=\psi + \beta)$, the pilot must *mentally combine* the angle of slip (β) information from the PFD with the heading information (ψ) obtained from the Navigation Display (ND). The FPV symbol has proved to be very useful in many ground-referenced aircraft manoeuvering tasks (Hynes et al., 1989). For instance, when approaching the runway the pilot can simply steer the FPV symbol to the desired touchdown point on the runway (Gold, 1965). Or, to fly a horizontal turn at constant altitude, the pilot only has to keep the FPV on the horizon line.

In contrast to the flight-director command bars, the FPV symbol *can* be regarded as a natural addition to the basic display, enhancing an important characteristic of that display. Up to some point this holds for the application of a FPV on a standard, *planar*, PFD, since it allows a pilot to establish a one-to-one mapping of the aircraft flight-path to a symbol on the display moving with respect to the horizon. But it is certainly true for the presentation of a FPV on the *pictorial* three-dimensional tunnel-in-the-sky display. Recall that the spatial information mediated by the tunnel display allows a pilot to directly perceive the motion of the aircraft relative to the tunnel, a ground-referenced element of the artificial world. From the discussion in §3.4.3 and §3.5, however, it is clear that obtaining an accurate estimate of the direction of the aircraft motion relative to the tunnel is not that simple. The direction of one's egomotion relative to the environment is directly coded in the *changing* optical array mediated by the spatial display: it is a *feature* of the display. Either the *indirect* dynamic cues, i.e. the derivatives of the gradients of optical splay and optical density, or the *direct* dynamic cues of the optic flow field allow a pilot to perceive the direction of motion. There remains some dispute, however, regarding the accuracy of the human visual motion perception and, as a result, the functionality of this perception in manoeuvering tasks (Johnston et al., 1973; Warren et al., 1988; Warren & Hannon, 1990; Grunwald & Kohn, 1993). Presenting the direction of egomotion *explicitly* on the display can therefore be expected to be a *very useful synthetic enhancement of the natural environment*. The FPV allows a *direct* perception of the aircraft direction of motion from the display, even from a *static* representation, with the optical gradients of motion perspective as alternative cues. In the light of the two principles stated above it is clear that by showing where the aircraft is going, the FPV is certainly compatible with any pilot mental model that makes sense. The presentation of a FPV is not expected to change the way in which pilots control the aircraft with a tunnel display. The reason is that the flying task with a tunnel display is already highly perceptual and intuitive in nature, with only a very limited cognitive effort. An FPV will not change this significantly.

(a) 1st order prediction (b) 2nd order prediction
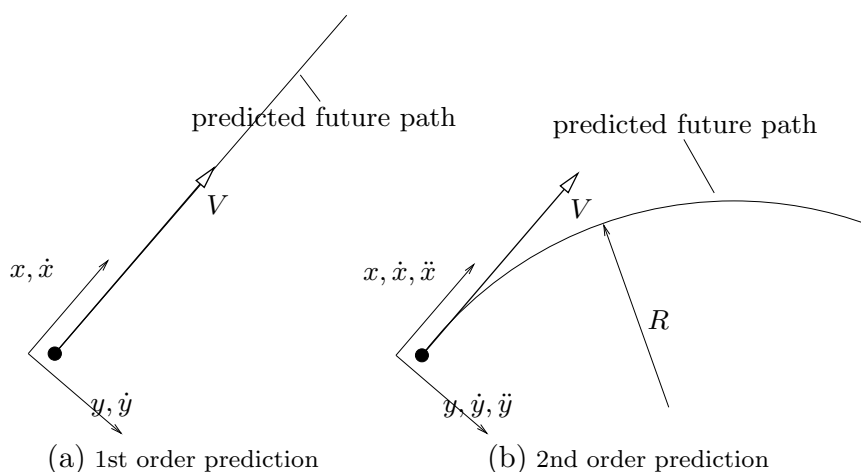
Figure 9.2: Two algorithms for predicting the aircraft future position. In this simplified figure, V represents the vehicle velocity and R the radius of the predicted circular future vehicle path. A first order algorithm (left) uses the aircraft position (x, y) and velocity $(\dot{x}, \dot{y})$ in the inertial reference frame. A second order algorithm (right) extends the first order prediction by incorporating the vehicle accelerations $(\ddot{x}, \ddot{y})$.

Augmenting with *predictive* information: the flight-path predictor   Consider the aircraft recti-linear motion condition, where the aircraft moves along a straight line through the environment. In this case the FPV, showing the instantaneous direction of the aircraft motion, explicitly indicates where the aircraft will be in the near future. In terms of the information analysis of §3.4.3, it marks the location of the focus of radial outflow (FRO) on the display, Fig. 3.8. A condition of recti-linear motion is interesting from a theoretical perspective, but less from a practical viewpoint. Rather, it must be regarded as a special case of a more general aircraft motion condition of curvi-linear flight. In curvi-linear motion the FPV shows the instantaneous direction of the aircraft motion, i.e. the velocity vector tangential to the locally circular trajectory, Fig. 3.13. The FPV shows *status* information, which can generally not be used for purposes of anticipating oncoming changes in the task demands (Kelley, 1967). To provide the information that could facilitate pilots in their anticipation behaviour, the so-called *Flight-Path Predictor* (FPP) concept is propagated in (Grunwald & Merhav, 1978; Grunwald et al., 1981). A FPP shows the predicted aircraft position some fixed time T_p ahead, usually a couple of seconds, as a two-dimensional (Grunwald et al., 1981; Korn et al., 1982; Wickens et al., 1989) or three-dimensional (Grunwald, 1984) symbol in the synthetic environment. Some authors recommend to show the future trajectory (Knox & Leavitt, 1977; Grunwald & Merhav, 1978; Viken & Burley, 1992; Below et al., 1995) or a set of equi-distant points of the future trajectory (Jensen, 1981). In most cases, also a predictor reference frame is displayed, moving ahead of the aircraft along the tunnel wireframe, with respect to which the motions of the FPP must be monitored, see Fig. 2.3(b). Predictive information has

often proved to be useful for human operators in a large variety of tasks (Kelley, 1967), ranging from submarines (McLane & Wolf, 1968) and super tankers (Stassen, 1994) to space applications (Breedveld, 1997). Directly presenting the aircraft future position on the tunnel display allows pilots to compare the predicted position with the future guidance constraints depicted by the tunnel, facilitating control and allowing to smooth anticipate future changes in the trajectory. It is clear that the flight-path predictor is compatible with a sensible pilot mental model of his task. It relieves the pilot from the task of mentally computing the future flight trajectory while at the same time coding this information in a format that is compatible with the other spatial information conveyed by the display. The future aircraft flight path can be determined using various computer algorithms (Grunwald, 1985; Mulder, 1992). In these algorithms the *order of prediction* dictates the use of higher order aircraft state variables. Fig. 9.2(a) illustrates that a first order prediction algorithm uses only the aircraft current inertial position and velocity to predict a recti-linear flight trajectory. A second order algorithm extends the first order prediction by incorporating acceleration terms, which could for instance yield the curvi-linear flight-path illustrated in Fig. 9.2(b). So, in essence, a first order FPP provides the same information as a flight-path vector symbol. Even in curvi-linear flight, i.e. with a centripetal acceleration perpendicular to the velocity vector, the predictor symbol will be positioned on a straight line directed along the FPV. Thus, it takes – at least – a second order predictor algorithm to present curvi-linear predictive guidance information. A theoretical framework to assess the relative usefulness of the FPV and the FPP has been developed in (Grunwald & Merhav, 1978). Here, it is concluded that this usefulness is determined by the vehicle dynamics and by the spectrum of the disturbances acting on the vehicle. A FPV is found very effective for fast vehicle dynamics and rather ineffective for slow vehicle dynamics. A FPP is very effective for slow dynamics but less effective for fast dynamics and fast disturbances. This will be discussed further in §9.2.2.

The application of a FPP has important consequences for the control task of a pilot. With a FPV the flight-path can be perceived directly from the display, facilitating the pilot in closing one of the three main feedback loops of attitude, flight-path and position. With a FPP, however, the control task of the pilot becomes one of maintaining the FPP symbol in the center of the accompanying predictor reference frame. With an accurate prediction, minimizing the displacements of the predictor symbol relative to the predictor reference frame (lateral: ϵ_ℓ/D, vertical: ϵ_v/D, Fig. 2.4(a)), both moving in front of the pilot, means that – the prediction time interval T_p later – the aircraft will also fly through the center of the tunnel. Hence, whereas the basic aircraft motion referents remain essential in the aircraft control with a FPV, they become of secondary importance for a pilot when the FPP is presented on the display. In the latter case the pilot control task becomes a two-axis pursuit tracking task of minimizing ϵ_ℓ and ϵ_v. For a discussion of the characteristics and applications of the combination of the tunnel display and flight-path predictor symbology, the reader is referred to the literature (Knox & Leavitt, 1977; Grunwald & Merhav, 1978; Grunwald et al., 1981; Jensen, 1981; Roscoe & Jensen, 1981; Grunwald, 1984; Viken &

Burley, 1992; Theunissen & Mulder, 1995b; Grunwald, 1996a, 1996b).

Conclusions   The flight-director, flight-path vector and flight-path predictor symbology exemplify three widely accepted display augmentation principles. From the discussion above it is clear that, first, the combination of the flight-path predictor and the tunnel display is the most promising one. In previous investigations it is shown that it indeed allows path-following performance with the same level of performance as a FD (Grunwald et al., 1981; Grunwald, 1984, 1996b). The FPP is compatible with a pilots' mental model but does force them to adopt (or should it be *allow*) a two-axis pursuit tracking strategy. Second, the flight-director command symbols represent *command* information, generated by a computer algorithm, that does *not* exist in the real world and that is nothing but a feature of the *artificial* pilot environment. It is not compatible with a pilot mental model and forces pilots to adopt a two-axis compensatory tracking strategy. Finally, the FPV symbol explicitly shows elements of the aircraft state – *status* information – that have meaning in the real world and which could, with the proper spatial representation of that world, in principle be perceived with some degree of accuracy by the pilot. The augmentation enhances the display by explicitly showing a feature of the *real* world that *is* useful for the task at hand. It is compatible with a pilot mental model and, other than the two other augmentation forms, it helps pilots in adopting the 'common' control strategy – the feedback of attitude, flight-path and position – similar to the one discussed in the previous chapters. Because this similarity allows a comparison with and an expansion of the previous results, the FPV will be the only augmentation form investigated in this thesis and forms the subject of the remainder of this chapter.

9.2.2   Variables affecting the use of a flight-path vector

Introduction   For a pilot in manual control of the aircraft an important piece of information is the relative motion of the aircraft relative to the surrounding air mass. The air mass itself, however, may move relative to the earth. Hence, since most aircraft guidance tasks are conducted with respect to ground-fixed references such as the runway or a virtual earth-fixed tunnel, it is essential for a pilot to be aware of the relative motion of the aircraft relative to the ground surface (Watler & Logan, 1981; Hynes et al., 1989). The advantage of a flight-path vector is that it may be used to show, in an intuitive fashion, either the relative motion of the aircraft with respect to the air mass or the relative motion with respect to the earth. Although the flight-path vector has become a standard feature on modern PFDs and HUDs, only a few studies have been conducted so-far addressing its functionality (Grunwald & Merhav, 1978). The obviousness and simplicity of the idea to present a flight-path vector may well be the reason for this. Another reason could be that the addition of a flight-path vector to the display is not expected to affect the control strategy of a pilot, as argued above.

Grunwald and Merhav's study on display augmentation   In (Grunwald & Merhav, 1978) the influence of the *vehicle dynamics* and the *bandwidth of the external disturbances*

on the effectiveness of different forms of synthetic symbology representing higher order aircraft state components was investigated. The manual control task used in the study was the remote control of the lateral-longitudinal motion of a flight vehicle using an elementary three-dimensional display. The vehicle response dynamics varied from 'slow', in terms of bandwidth, to 'fast'. The bandwidth of the turbulence shaping filter used to generate external disturbances varied between 0.1 and 3.2 [rad/s]. The experiment showed that a positive effect of a FPV and a FPP presentation on the performance of the closed loop pilot-vehicle system depends on the specific combination of vehicle dynamics and disturbance bandwidth, and the extent in which the FPV/FPP information is perturbed by the disturbances. The higher the order of the state elements of the vehicle dynamics, the more these state elements are influenced by the disturbances (Etkin, 1972). In case of slow vehicle dynamics the higher frequencies in the response of the vehicle and the presented symbology are much less prominent compared to the case of fast vehicle dynamics. In case of fast vehicle dynamics this results in rapid and unpredictable motions of those types of symbology that are driven by higher order state information, for example the flight-path predictor driven by a second order prediction algorithm.

Effects of turbulence   The work of Grunwald and Merhav (1978) showed the relevance of including effects *other* than those regarding the display presentation, such as turbulence. Consider the influence of the turbulence. The shaping filter for the disturbance v_g (or $\beta_g = v_g/V_{tas}$) on the *lateral* component of the aircraft velocity vector, v, is given by (Mulder & van der Vaart, 1994):

$$H_w^{v_g}(j\omega) = \sqrt{\frac{L_g}{V_{tas}}} \sigma_{v_g} \frac{1 + \sqrt{3}\dfrac{L_g}{V_{tas}}(j\omega)}{\left(1 + \dfrac{L_g}{V_{tas}}(j\omega)\right)\left(1 + \dfrac{L_g}{V_{tas}}(j\omega)\right)} \tag{9.1}$$

where V_{tas} is the aircraft velocity, L_g (in [m]) the so-called *scale length* of the turbulence, and $\sigma_{v_g}^2$ the *intensity* of the turbulence v_g which is independent of L_g and V_{tas}. The white noise w is coloured through the first order filter (zero at $s = -\frac{1}{3}\sqrt{3}\frac{V_{tas}}{L_g}$) concatenated with a second order low pass filter (two poles at $s = -\frac{V_{tas}}{L_g}$). The scale length indicates the *spatial extent of the correlation*. The quotient $\frac{V_{tas}}{L_g}$ determines the *bandwidth* of the turbulence and shows that this bandwidth is a function of the characteristics of the turbulence itself (L_g) and of the velocity of the aircraft moving through it. E.g., flying through a turbulence field (fixed L_g) with a smaller velocity yields a smaller bandwidth of the disturbances and thus less high-frequent perturbations. Because the aircraft velocity also determines to some extent the bandwidth of the aircraft dynamics (Appendix C), manipulating V_{tas} and L_g allows the experiment of Grunwald and Merhav (1978) to be repeated. There were some reasons that motivated this repetition. Grunwald and Merhav (1978) used the Optimal Control Model (OCM) to model their results without an attempt to *identify* the model from the experimental data. The previous experiments of this thesis showed that the cybernetic approach including the identification of pilot models leads to a much deeper understanding of the mechanisms behind the observed behaviour. Therefore

the present experiment, X5, was believed to increase the general understanding of how presenting a FPV influences pilot behaviour.

9.3   Experiment X5

Whereas in all experiments discussed so far the tunnel geometrical design has been the main subject of investigation, here only the *baseline* tunnel geometry is applied. Experiment X5 investigates the effects of showing the flight-path vector symbol on pilot behaviour. For this purpose the atmospheric turbulence applied in the previous experiments is extended by the introduction of a disturbance on the lateral component of the aircraft velocity vector: $v_g \neq 0$. In the previous section it has been described that the properties of this disturbance are determined on the one hand by the scale length L_g and intensity $\sigma^2_{v_g}$ of the turbulence field, and on the other hand by the aircraft velocity V_{tas}. Hence, in X5 the usefulness of the flight-path vector is examined for a variety of aircraft velocities and turbulence scale lengths for a turbulence field with a constant intensity $\sigma^2_{v_g}$.

METHOD

Subjects and instructions to subjects   Four subjects (A – D) participated in the experiment. They were instructed to control the aircraft through the tunnel as accurately as possible. All occurring aircraft attitude and position errors must be minimized, despite the effects of the disturbances acting on the vehicle.

Apparatus   The Human-Machine Laboratory was used, described in Appendix A.

Independent measures   Three independent measures were manipulated in the experiment. First, the *flight-path vector* symbol was either presented on the tunnel display or not. Second, three *scale lengths* L_g of the lateral turbulence were applied: 750, 250 and 85 [m]. The *intensity* of the turbulence field was kept constant at $\sigma^2_{v_g} = 1$ [m^2/s^2]. Third, the aircraft moved through the turbulence field with three velocities: 70, 100 and 130 [m/s]. The consequences of combining the three turbulence scale lengths and the three aircraft velocities on the properties of the disturbances are discussed below.
Summarizing, the independent measures were the `flight-path` vector symbol (2 levels), the turbulence `scale length` (3 levels) and the aircraft `velocity` (3 levels).

Experimental design   A full-factorial within-subjects design was applied, consisting of a total of 18 conditions ($2 \times 3 \times 3$). The conditions were randomized over the experiment. Each subject conducted four familiarization sessions (72 runs) before completing six replications of all experimental conditions (108 runs) that served as the measurements.

Procedure   During the course of two days a subject conducted 180 experimental runs, divided in 30 blocks of six runs each. A single run lasted 120 [s], consisting of a run-in time T_i of 15 [s] and a measurement time T_m of 105 [s]. The pace of the experiment was

Table 9.1: Definition of input signals i_1, i_2 and i_3 (X5).

	i_1		i_2		i_3	
	k_{1_i}	ω_{1_i}	k_{2_i}	ω_{2_i}	k_{3_i}	ω_{3_i}
i	[-]	[rad/s]	[-]	[rad/s]	[-]	[rad/s]
1	4	0.2394	5	0.2992	6	0.3590
2	10	0.5984	11	0.6582	13	0.7779
3	17	1.0173	18	1.0771	19	1.1370
4	23	1.3763	24	1.4362	25	1.4960
5	31	1.8550	32	1.9149	33	1.9747
6	41	2.4534	42	2.5133	43	2.5731
7	57	3.4109	58	3.4707	59	3.5306
8	75	4.4880	76	4.5478	77	4.6077
9	103	6.1635	104	6.2233	105	6.2832
10	137	8.1981	138	8.2579	139	8.3177
11	185	11.0704	186	11.1302	187	11.1901
12	251	15.0198	252	15.0796	253	15.1395

such to allow sufficient time for subject preparation and to prevent fatigue.

Dependent measures   Seven variables were selected as dependent measures: (i,ii) the subject's aileron control signal δ_a and its derivative $\dot{\delta}_a$; (iii,iv) the aircraft angle of roll ϕ and its derivative $\dot{\phi}$; (v) the heading angle error ψ_e; (vi) the track angle error χ_e, and (vii) the cross-track error x_e. Note that because of the disturbance on the lateral component of the aircraft velocity vector, v_g, the track angle error χ_e and <u>not</u> the heading angle error ψ_e represents the *true* aircraft lateral motion relative to the trajectory, i.e. $\chi_e = \psi_e + \beta_g$.

Description of the experiment simulation

Tunnel geometry   The baseline tunnel was applied, consisting of square frames ($W_t = H_t = 40$ [m]) positioned on altitude poles and connected with longitudinal frame lines. The reference trajectory was straight and had a downslope Γ_t of 3 [deg]. The intermediate frame distance $\triangle D$ was fixed at 350 [m]. If applicable, a green flight-path vector symbol was shown indicating the aircraft instantaneous direction of motion (χ).

Aircraft model   The asymmetric motions of a Cessna Citation I were simulated at the three velocity conditions introduced above. The lateral component of the aircraft velocity vector is perturbed by a turbulence signal i_3, defined below. The symmetric motion referents were fixed to their initial condition values (Appendix C). The aircraft moved in a plane with downslope 3 [deg] through the vertical center of the tunnel.

Atmospheric disturbances   Three independent sinusoidal reference signals – i_1, i_2 and i_3 – were inserted in the control loop (Table 9.1). The shaping filters and noise intensities of i_1 and i_2 are defined identical to the signals used in Experiments X1, X2 and X4. The insertion of a third reference signal i_3 impairs a comparison of this experiment results with those of others. The shaping filter of i_3 is defined according to Eq. 9.1. In order to allow a comparison of pilot performance in the experimental conditions, W_3 was defined such that

Table 9.2: Turbulence bandwidths and turbulence intensities as a function of the turbulence scale lengths L_g and aircraft velocities V_{tas} applied in Experiment X5.

| | turbulence scale length L_g (in [m]) | | | | | |
| | 750 | | 250 | | 85 | |
	bandwidth V_{tas}/L_g [rad/s]	intensity $\sigma^2_{\beta_g}$ [$\circ^2$]	bandwidth V_{tas}/L_g [rad/s]	intensity $\sigma^2_{\beta_g}$ [$\circ^2$]	bandwidth V_{tas}/L_g [rad/s]	intensity $\sigma^2_{\beta_g}$ [$\circ^2$]
V_{tas}=70 [m/s]	0.0933	0.6700	0.2800	0.6700	0.8235	0.6700
V_{tas}=100 [m/s]	0.1333	0.3283	0.4000	0.3283	1.1765	0.3283
V_{tas}=130 [m/s]	0.1733	0.1942	0.5200	0.1942	1.5294	0.1942

the variance $\sigma^2_{v_g}$ of the lateral disturbance *velocity* v_g is constant, at 1 [m^2/s^2]. This results in a *constant* lateral turbulence field through which the aircraft flies with three different velocities, resulting in the variances of β_g to decrease for larger aircraft velocities. It is now possible to examine the effect of the flight-path vector when flying through such a constant turbulence field at different velocities. An experimental combination was selected of three aircraft velocities and three turbulence scale lengths, resulting in the bandwidths V_{tas}/L_g and the variances of the side-slip turbulence signals β_g listed in Table 9.2.

Initial condition   Before the start of each run, the aircraft was positioned in the center of the tunnel with zero position and attitude errors. The initial longitudinal position of the aircraft on the tunnel reference trajectory was randomized.

Experiment hypotheses

It is hypothesized that, first, when a FPV is presented on the display, the pilot will apply a strong feedback loop on χ_e. Second, accordingly, when no FPV is presented the pilot is hypothesized to use the information on ψ_e, which is directly available from the display, as a first estimate of the track angle error. The motion perspective cues could help the pilot in improving this initial estimate. Furthermore, when the FPV is presented it is hypothesized that, third, due to the explicit information on χ_e the path-following performance will be superior. For smaller turbulence scale lengths L_g and higher aircraft velocities $V_{tas}$the bandwidth of the disturbance signal becomes larger, resulting in rapid motions of the FPV symbol on the display. Therefore, it is hypothesized that, fourth, pilot performance decreases in these conditions. Fifth, when no FPV is presented, it is hypothesized that pilot performance also deteriorates for smaller L_gs and for larger aircraft velocities, but to a significantly less extent than in the FPV conditions. This is because the effects of the turbulence are not directly visible from the display but must be perceived from the motion perspective cues. The implicitness of the flight-path angle error information leads to a decreasing pilot bandwidth of this variable. In other words, a pilot would ignore rapid changes in the flight-path angle error rather than rapidly trying to correct for them. Sixth, the effects of the bandwidth of the aircraft dynamics, determined by the aircraft velocity, are hypothesized to be similar to those found in earlier experiments of this thesis. That

Table 9.3: Summary of results from a pilot questionnaire (X5).

How would you describe the level of *realism* of the simulated aircraft *dynamics*?					
V_{tas} [m/s]	very realistic	realistic	average	unrealistic	very unrealistic
70	·	1	·	2	·
100	·	1	1	1	·
130	1	1	·	·	1

How would you describe the level of *realism* of the simulated aircraft *disturbances*?						
V_{tas} [m/s]	L_g [m]	very realistic	realistic	average	unrealistic	very unrealistic
70	750	·	·	·	2	1
	250	·	·	2	1	·
	85	·	1	·	2	·
100	750	·	·	1	1	1
	250	·	·	2	1	·
	85	·	1	1	1	·
130	750	·	1	1	·	1
	250	·	1	1	1	·
	85	1	1	1	·	·

is, at the high velocity conditions the performance in terms of ψ_e and χ_e will improve because for these conditions small changes in these quantities rapidly lead to large position errors. In this respect, the above mentioned fact that the aircraft velocity also affects the bandwidth of the disturbances acting on the vehicle could be of secondary importance.

9.4   Results

9.4.1   The pilot questionnaire

Because subject D was involved in the definition and set-up of the experiment, only the comments of subjects A to C are used.

Realism of the simulation   The simulated aircraft dynamics were judged unrealistic for the low velocity conditions but the simulation improved for higher velocities, Table 9.3. Pilot comments revealed that this was especially due to the rather large magnitude of the *disturbances* at the low velocities. The realism of the disturbances were judged similarly: it improved for higher aircraft velocities and also for smaller turbulence scale lengths, i.e. for larger bandwidths $\frac{V_{tas}}{L_g}$. Pilots considered the high velocity disturbances with smaller magnitudes as more realistic: "*nice bumps*". For the low velocity conditions the turbulence was too large in magnitude and required considerable pilot effort to maintain performance.

Sources of information and control strategies   The pilot comments were consistent. Without the FPV they claimed to use the relative displacements of the tunnel frames, ϵ_{ij} and η_{ij}, and especially the relative displacements of the altitude poles, π_{ij}, to perceive the lateral position with respect to the trajectory. The lateral aircraft motion is perceived
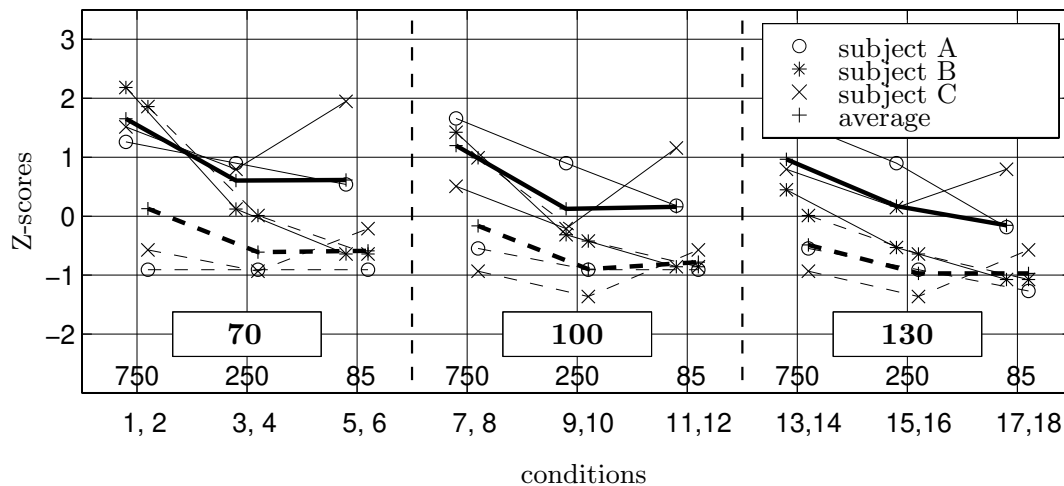
Figure 9.3: Z-scores of the effort ratings for all 18 conditions of Experiment X5. In this figure and in the following, the insets show the three velocity conditions (in [m/s]). The numbers 750-85 represent the turbulence scale lengths (in [m]). The dashed and the continuous lines represent the data with and without a flight-path vector, respectively. The numbers below the figure depict the experimental conditions.

primarily using the derivatives of the relative lateral displacements of the tunnel altitude poles, $\dot{\pi}_{ij}$. Surprisingly, no reference whatsoever was made by the subjects on the use of splay angles and their derivatives for controlling the aircraft. Subjects commented very favourably on the presence of a flight-path vector symbol. When the FPV is present, subjects considered their main task to keep the symbol positioned on the tunnel's infinity point ($\psi_e = \chi_e \longrightarrow \beta_g = 0$). Then, when this was achieved, the lateral position errors were estimated using in particular the relative displacements of the tunnel poles, π_{ij}. These position errors were corrected by positioning the FPV symbol away from the infinity point towards the more distant tunnel wall. Again, no reference was made upon the use of splay or splay-rate in these conditions. The aircraft velocity was believed to have no important effect at all on the control strategy. One pilot commented, however, that because of the larger aircraft pitch angle for higher velocities (Appendix C), the perception of the altitude poles' displacements became more difficult. Concerning the influence of the turbulence scale length no comments were made except that for the smaller L_gs (higher bandwidths), attending the relative movements of the FPV with respect to the tunnel's infinity point was considered to contribute to visual workload.

Effort ratings The effort ratings clearly show that the control task was judged considerably more difficult when the flight-path vector was not available, Fig. 9.3. The task was judged somewhat less difficult for the high velocity conditions. Furthermore, the effort ratings become *smaller* when the scale length of the turbulence decreases from 750 to 85 [m], for all velocities and independent of the presence of the flight-path vector.

Table 9.4: Results of a full-factorial ANOVA (X5) on the dependent measures involving control activity, inner loop measures and path-following accuracy (in this table '★★', '★' and '○' represent chance levels of $p \leq 0.01$, $0.01 < p \leq 0.05$ and $0.05 < p \leq 0.10$, respectively).

	control activity		inner loop measures		path-following performance		
	δ_a	$\dot{\delta}_a$	ϕ	$\dot{\phi}$	ψ_e	χ_e	x_e
main effects							
F	○	·	·	○	·	★	★
S	·	·	★★	★	·	★★	★
V	★★	★	★★	★	★★	★★	★
2-way interactions							
F×S	·	·	·	·	★★	★★	★★
F×V	·	·	·	·	·	★★	·
S×V	·	·	·	·	·	★	★
3-way interaction							
F×S×V	·	·	·	·	·	·	·

9.4.2 Time domain data: statistical analysis

A full-factorial mixed-model Analysis of Variance was conducted to analyze the time domain data. The independent measures were the presence of the flight-path vector (F) (2 levels), the turbulence scale length (S) (3 levels) and the aircraft velocity (V) (3 levels). The ANOVA results are summarized in Table 9.4. The means and 95% confidence limits of six of the seven dependent measures are shown in Fig. 9.4.

Pilot control activity   Pilot control activity, Fig. 9.4(a), decreases for the larger velocity conditions (δ_a: $F_{2,6}=15.233$, $p < 0.01$; $\dot{\delta}_a$: $F_{2,6}=7.481$, $p = 0.024$), increases when the FPV is presented (δ_a: $F_{1,3}=5.494$, $p=0.100$; $\dot{\delta}_a$: not significant) and increases only marginally when L_g decreases, Fig. 9.4(a). A post-hoc analysis (NK, $p=0.05$) revealed that the differences in control activity for the three velocity conditions are indeed all significant.

Inner loop measures   Figs 9.4(c) and 9.4(b) indicate that the roll angles and the roll rates increase for higher velocities (ϕ: $F_{2,6}=22.463$, $p < 0.01$; $\dot{\phi}$: $F_{2,6}=6.461$, $p = 0.032$) and for smaller turbulence scale lengths (ϕ: $F_{2,6}=16.022$, $p < 0.01$; $\dot{\phi}$: $F_{2,6}=5.542$, $p = 0.043$). The presence of a FPV symbol yields lower roll angle deviations (not significant) and higher roll angle rates ($F_{1,3}= 7.187$, $p = 0.075$). When the velocity increases the effect of the FPV on $\dot{\phi}$ becomes larger. Post-hoc analyses (NK, $p=0.05$) showed that the differences in ϕ and $\dot{\phi}$ for the three velocity conditions were indeed all significant. The roll angle differences between the smallest and the largest scale lengths are the only ones that are significant.

Path-following performance   The heading angle error and the track angle error decrease significantly for the high velocity conditions (ψ_e: $F_{2,6}=62.569$, $p < 0.01$; χ_e: $F_{2,6}=67.531$, $p < 0.01$), Figs 9.4(d) and 9.4(e). When the FPV is not presented, ψ_e is unaffected by the turbulence scale length. When the FPV is presented, ψ_e increases for

(a) aileron

(b) roll angle derivative

(c) roll angle

(d) heading angle error

(e) track angle error

(f) lateral position error
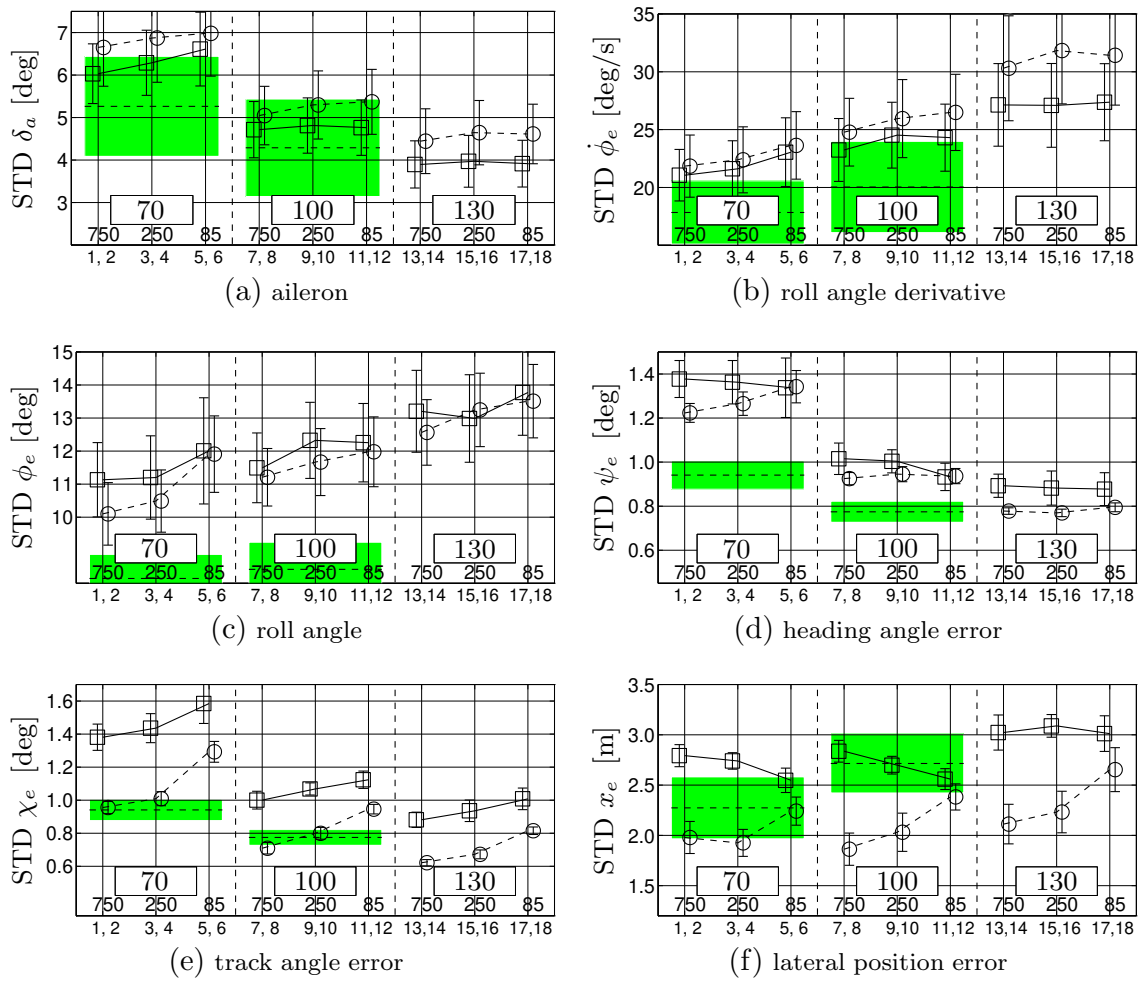
Figure 9.4: The means and 95% confidence limits of the STDs of the dependent measures (all subjects). Here, the squares connected with the continuous lines and the circles connected with the dashed lines represent the data for the configurations without and with a FPV, respectively. The horizontal dashed lines and the shaded rectangles show the values of these quantities for Experiment X1.

the smaller scales, especially at the low velocity conditions, leading to a significant F×S-interaction ($F_{2,6}$=16.643, p <0.01). Presenting the FPV leads to a significant decrease in track angle error χ_e and position error x_e (χ_e: $F_{1,3}$=16.022, p =0.028; x_e: $F_{1,3}$=27.437, p =0.014), i.e. performance improves significantly. Decreasing the turbulence scale length yields larger track angle errors χ_e and, at least when the FPV is presented, larger position errors (χ_e: $F_{2,6}$=69.091, p <0.01; x_e: $F_{2,6}$=5.411, p =0.045). When the FPV is not presented, the decreasing turbulence scale leads to *smaller* position errors, resulting in the significant F×S-interaction ($F_{2,6}$=30.363, p <0.01). The F×S-interaction of χ_e ($F_{2,6}$=33.973, p <0.01) is caused by the fact that when the FPV is presented the effects of changing the turbulence scale are somewhat larger. The effect of the scale length on χ_e is stronger for the low velocity conditions, yielding the significant S×V-interaction

($F_{4,12}$=5.093, p =0.012). The same holds for the presence of the FPV as indicated by the significant F×V-interaction ($F_{2,6}$=14.163, p <0.01). Finally, Fig. 9.4(f) shows clearly that position errors increase for the higher velocities ($F_{2,6}$=8.113, p =0.020). Post-hoc analyses (NK, p=0.05) indicated that the differences in χ_e as caused by the different velocities, the presence of the FPV symbol, and also those caused by the different turbulence scale lengths are all significant. The only exception is the effect of turbulence scale on χ_e when the FPV is not presented. Here, only the results for the smallest scale length differ significantly from the others. Furthermore, the position errors differ significantly only for the smallest scale length of 85 [m], independent of the presence of the flight-path vector.

Comparison of Experiments X5 and X1 The experimental definition for the lower two velocity conditions (V_{tas}=70 and 100 [m/s]) are similar to conditions '6' and '10' of Experiment X1 (W_t=40 [m]). Although in the current experiment a third noise signal is inserted into the loop, a rough comparison can be made to see what effects this additional disturbance has had on pilot performance. Fig. 9.4 illustrates that the disturbance on the aircraft flight-path has led to a considerable increase in pilot control activity (δ_a), roll angle errors and roll angle rates ($\phi, \dot{\phi}$), and a significant increase in the heading angle errors ψ_e. Path-following performance, in terms of χ_e and x_e, decreases significantly when no FPV is presented. When a flight-path vector is available, the χ_e-performance is similar to that found in terms of ψ_e in X1. This result indicates that when the aircraft direction of motion is directly perceivable from the display, no *real* performance differences have occurred between the two experiments, a comforting result from the perspective of comparing X5 with X1. Performance in terms of x_e is markedly better when a FPV is available, especially for the conditions of a small turbulence scale length. This is a remarkable result since the task is expected to become more difficult because of the insertion of a third disturbance signal. This finding will be commented on later in this chapter.

9.5 Modelling efforts

Recall that in all identification efforts discussed so far the middle and outer pilot feedback loops were identified as a single, *combined* outer loop which had to be dissected in the parametric estimation phase. The insertion of three independent forcing function signals in the closed loop allows the three primary pilot feedback loops to be estimated *directly*. Another difference with the previous investigations that results from inserting *three* signals in the loop is that the aircraft flight-path error equals the heading error added with the random disturbance signal: χ_e=ψ_e+β_g, where $\beta_g = i_3$. When i_3 equals zero the aircraft flight-path is identical to its heading which can be perceived directly from the display. Otherwise, the heading angle only *suggests* the direction of motion whereas the true direction of motion – the flight-path – must be estimated from the motion perspective of the wireframe tunnel. This has important consequences for modelling, as will be discussed next, at the hand of Fig. 9.5.
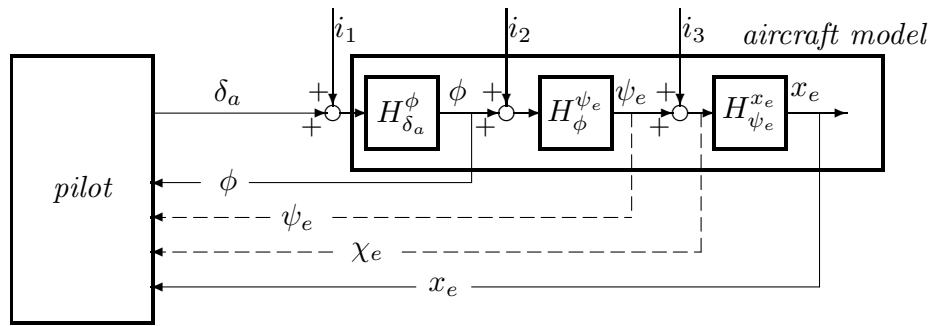
Figure 9.5: The composition of the three components of the aircraft dynamic model and the three disturbances inserted in the closed loop. This figure illustrates the fact that, dependent of the presence of the FPV symbol on the display, a pilot can close the middle loop using either ψ_e or χ_e, where $\chi_e = \psi_e + i_3$ and $i_3 = \beta_g$.

MLM models The non-parametric identification phase of estimating the pilot frequency responses from the experimental data revealed that the following findings were consistent for all pilots:

- when **no** *flight-path vector was presented* on the display the *pilots use the heading angle error feedback, ψ_e, to dampen their response to a position error x_e;*
- when *a flight-path vector was presented* on the display the *pilots use the flight-path angle error feedback, χ_e, to dampen their response to a position error x_e.*

This is an important result because it proves the hypotheses that, first, when no flight-path vector is available pilots are unable to perceive flight-path angle error *well enough* to use as their middle loop feedback, and they simply revert to the heading angle error for this purpose. Second, when a FPV is available pilots can directly perceive their flight-path angle from the display and use it as their middle loop feedback, leading them to basically ignore the heading angle error. In other words, when no FPV is available pilots successively close the ϕ, ψ_e and x_e loops – and χ_e is ignored. When a FPV is available pilots successively close the ϕ, χ_e and x_e loops – and ψ_e is ignored. From an identification perspective, these findings lead to the use of *two* pilot models. The first pilot model corresponds with the feedback of ϕ, ψ_e and x_e for the conditions without a flight-path vector. With this model the three pilot frequency responses can be identified *directly* in the frequency domain using the (3×1) identification method of Appendix F. The second pilot model corresponds with the feedback of ϕ, χ_e and x_e for the conditions with a flight-path vector. In this model the middle and outer loops are identified in the frequency domain as a single, *combined* outer loop, i.e. because $\dot{x}_e = V_{tas}\chi_e$, the same (2×1) identification procedure can be applied as in all previous experiments.

MLM parameters The parameters of the two MLM models are the same as those in previous MLM applications in the aircraft roll channel control task, see X1, X2 and X4, and
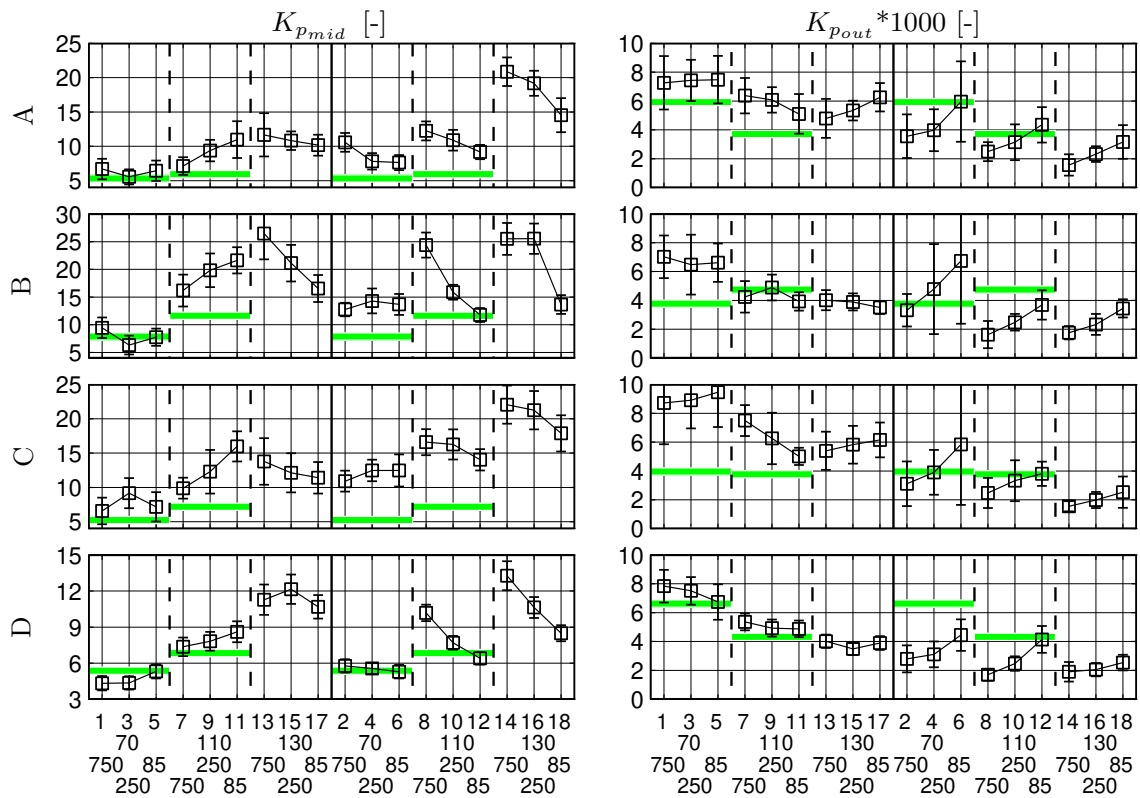
Figure 9.6: Outer loop MLM pilot model variables (all subjects, all conditions). Here, and in the following figures, the variables are shown for the conditions without a FPV (left, the odd numbers) and with the FPV (right, the even numbers). The horizontal shaded areas show the values of these quantities for the corresponding conditions of Experiment X1.

are thus unaffected by the use of two different models in the non-parametric identification phase. The uncertainties in estimating the limitation parameters (τ, ω_n, ζ_n, no figures shown) are large for the conditions without a FPV, indicating a lack of consistency in pilot inner loop control behaviour. Although the trends in the inner loop parameters are not consistent among subjects, some statements can be made. First, for increasing aircraft velocities the time delay τ decreases and the neuromuscular parameters increase. Second, when the FPV is available τ and ζ_n tend to be smaller and ω_n larger when compared to the situation without a FPV. No clear trends appear for the third independent measure, the scale length L_g. The equalization parameters show the, common, opposite trends. That is, $\tau_{L_{in}}$ is larger and $K_{p_{in}}$ smaller when a FPV is presented, especially for the low velocity conditions. For higher velocities *both* parameters decrease when the scale length becomes smaller and/or when the aircraft velocity increases. These trends indicate a lower inner loop bandwidth when the bandwidth of the flight-path disturbance ($\frac{V_{tas}}{L_g}$) becomes larger. Again, $\tau_{L_{in}}$ is considerably larger for all conditions compared to the lead time necessary to compensate for the aircraft roll response lag τ_ϕ: pilots generate more phase

margin for their inner loop feedback than necessary.

The two outer loop model parameters, $K_{p_{mid}}$ and $K_{p_{out}}$, are illustrated in Fig. 9.6. Recall that in the case no FPV is presented, $K_{p_{mid}}$ is the gain with which the *heading angle error* ψ_e is fed back. Similarly, when a FPV is presented, $K_{p_{mid}}$ represents the gain on the *flight-path angle error* χ_e. The outer loop parameters show some clear trends for all subjects. First, independent of the presence of a FPV, $K_{p_{mid}}$ increases and $K_{p_{out}}$ decreases when the aircraft velocity becomes larger. Second, $K_{p_{mid}}$ becomes considerably larger and $K_{p_{out}}$ smaller when the FPV is presented, indicating the importance of the explicit χ_e information. Third, the effects of the scale length L_g on both parameters are smaller (and less consistent) when no FPV is presented: they depend more on the aircraft velocity condition. When the FPV is presented, $K_{p_{mid}}$ decreases and $K_{p_{out}}$ increases considerably when L_g becomes smaller, for all subjects. Thus, it appears that with a flight-path vector the feedback of χ_e is considerably harmed when the bandwidth of the disturbance perturbing it increases.

MLM results: crossover frequencies and phase margins   The measured and modelled crossover frequencies and phase margins of the inner loop and the combined outer loop are illustrated in Figs 9.7(a) and 9.7(b), respectively. Recall that these variables for the latter loop can only be measured experimentally in case the *combined* middle and outer loop is estimated, i.e. in this case only for the conditions with the FPV presented and where the (2×1)-identification method is applied. Fig. 9.7(a) shows clearly that both ω_c^{in} and φ_m^{in} have opposite trends for the conditions with and without a FPV. That is, when no FPV is present, ω_c^{in} increases (φ_m^{in} decreases) for low velocities whereas ω_c^{in} decreases (φ_m^{in} increases) for the other velocity conditions. The opposite holds for the conditions with a FPV. Generally, the conditions where a FPV is presented have a phase margin φ_m^{in} that is considerably larger and an ω_c^{in} that is smaller than those without the FPV. These trends, however, are less clear as those for the variables marking the combined outer loop feedback, Fig. 9.7(b). Here, both $\omega_c^{out^c}$ as well as $\varphi_m^{out^c}$ decrease when the bandwidth of the disturbance ($\frac{V_{tas}}{L_g}$) increases, especially when L_g becomes smaller. Finally, it is clear that the pilot model results in a consistent underestimation of $\varphi_m^{out^c}$.

The crossover frequencies and phase margins of the pilot middle and outer loop feedbacks are illustrated in Figs 9.8(a) and 9.8(b), respectively. The trends in these data are clear, especially for the conditions where a FPV is presented on the display. For these conditions ω_c^{mid} decreases (φ_m^{mid} increases) and ω_c^{out} increases (φ_m^{out} decreases) when the bandwidth of the disturbance on flight-path increases (V_{tas} larger, but especially when L_g decreases). This indicates that pilots shift attention from the feedback of χ_e (middle loop) to that of x_e (outer loop) when the motions of the FPV on the display become rapid and less predictable. As compared to the data for the conditions without a flight-path vector, Fig. 9.8(b) illustrates that, independent of the other experimental measures, ω_c^{mid} is significantly larger (φ_m^{mid} smaller) and ω_c^{out} significantly smaller (φ_m^{out} larger) when a FPV is presented. Furthermore, the effects of varying L_g are much smaller, they are less consistent and depend more on the aircraft velocity when no FPV is present. Finally, the
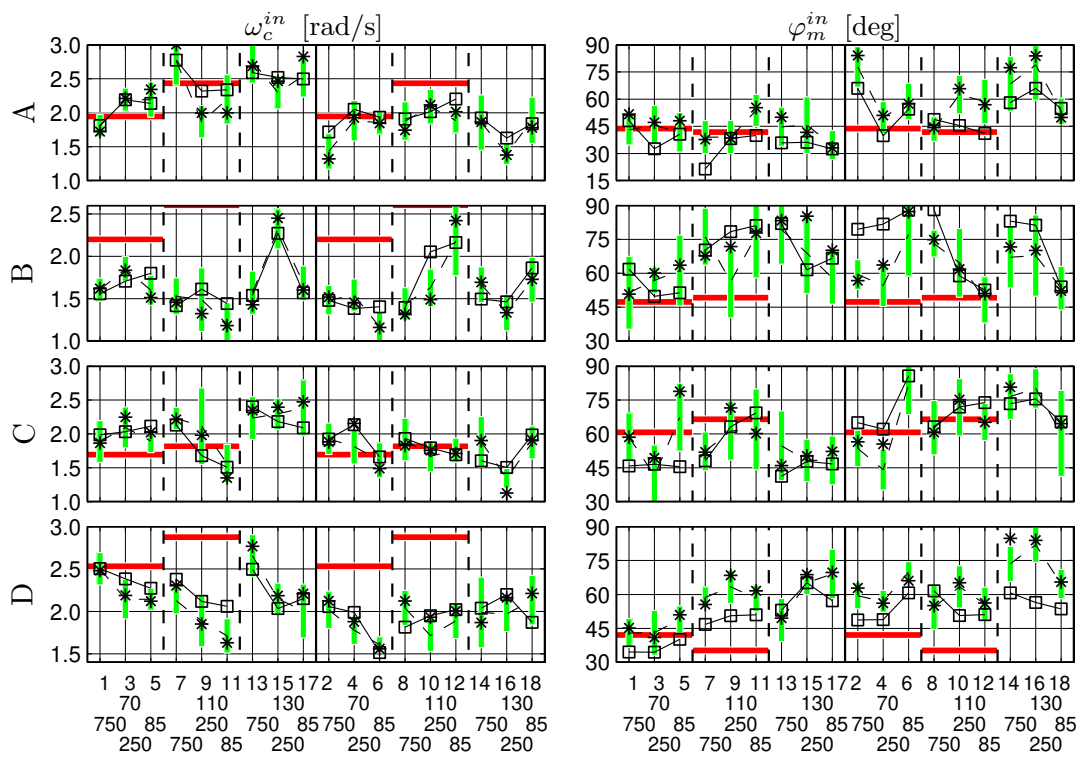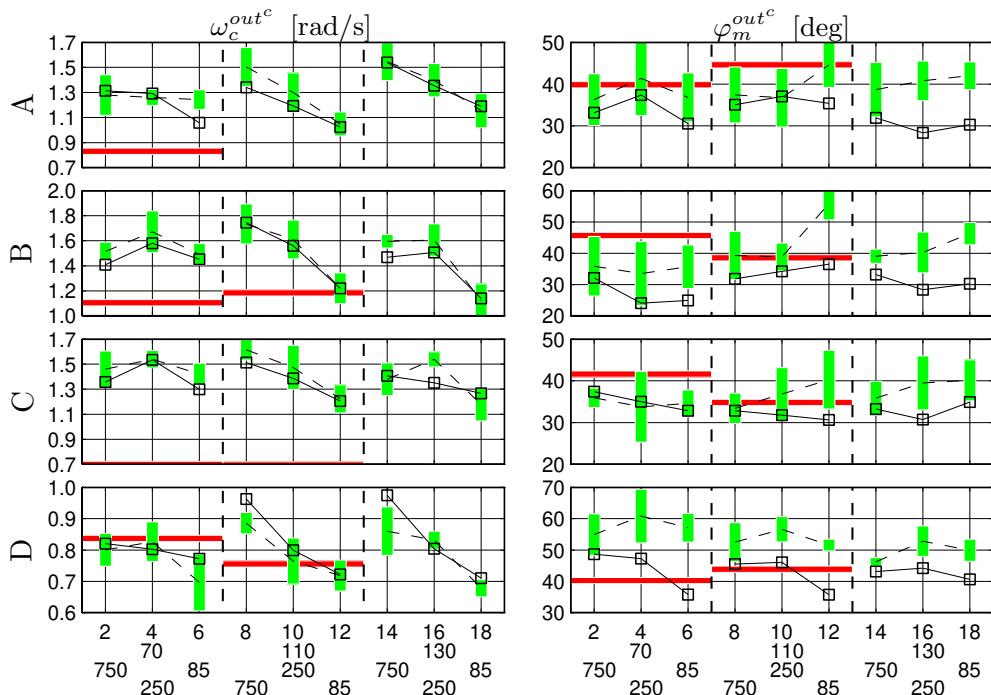
(a) inner loop

(b) outer loop (combined)

Figure 9.7: Crossover frequencies and phase margins (all subjects, all conditions). Here, and in the following figures, the shaded areas show the uncertainty regions of the raw frequency response data, their averages connected with the dashed lines. The '∗'-symbols show the quantities for the averaged frequency responses; the squares – connected with the continuous lines – show them for the MLMs. The horizontal shaded areas show the values of these quantities for the corresponding conditions of Experiment X1.
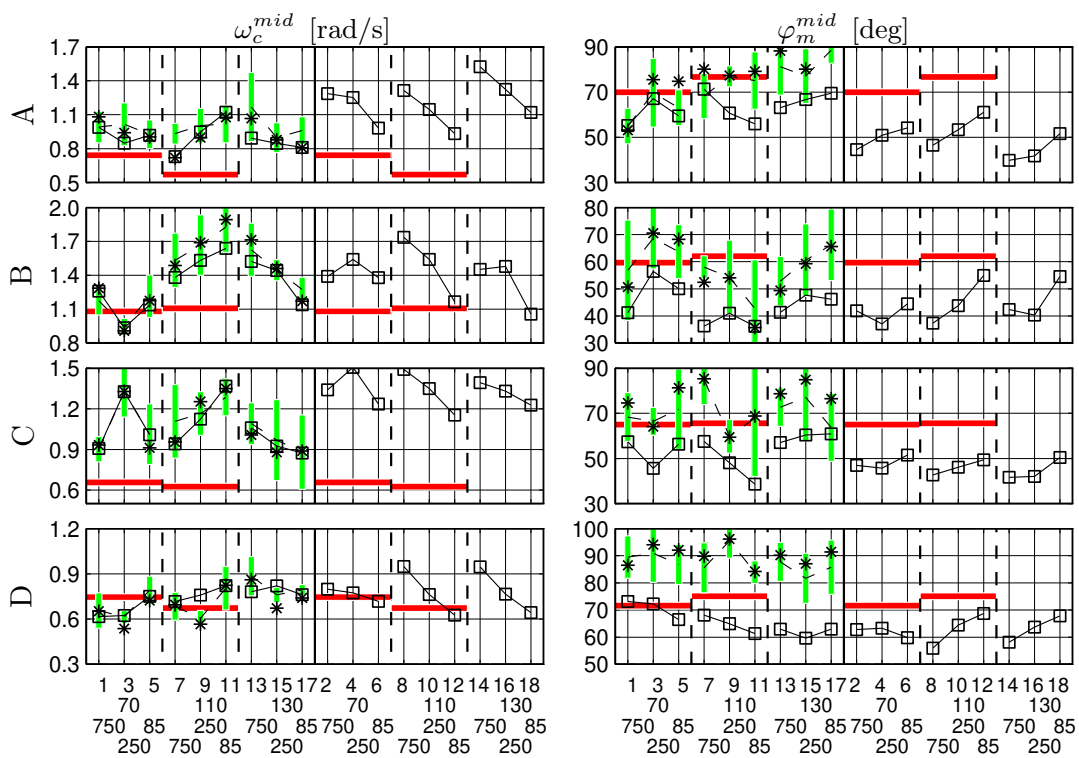
(a) middle loop crossover frequencies and phase margins
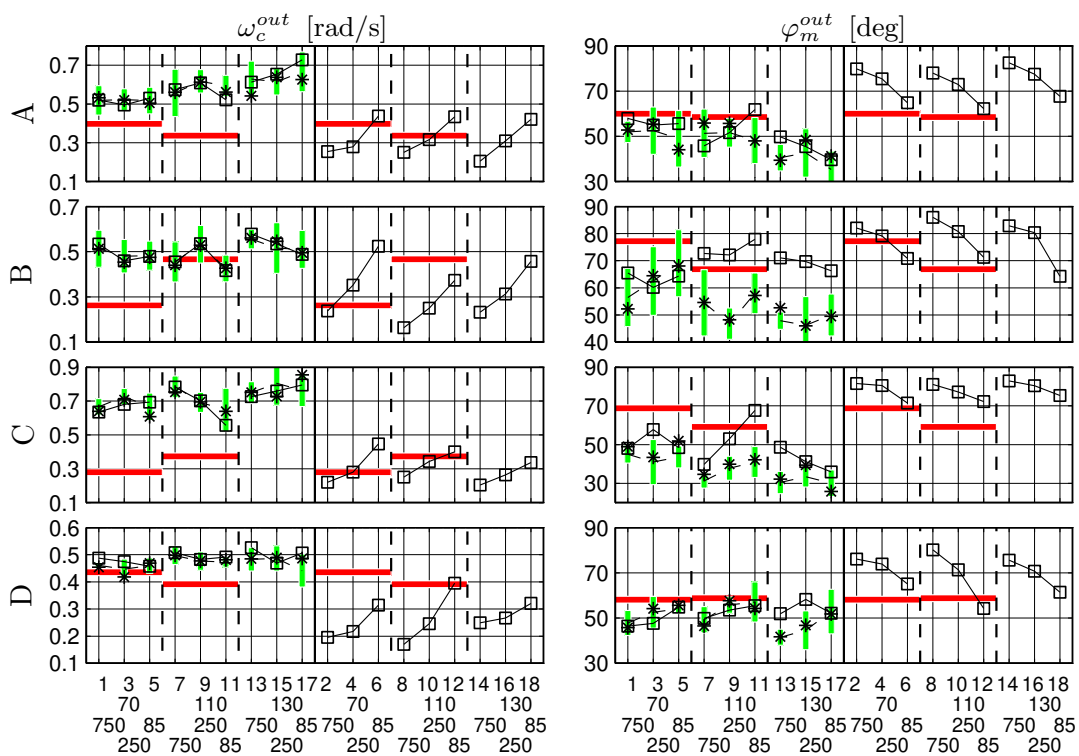
(b) outer loop crossover frequencies and phase margins

Figure 9.8: Middle and outer loop crossover frequencies and phase margins, following the MLM analysis (all subjects, all conditions). The horizontal shaded areas show the values of these quantities for the corresponding conditions of Experiment X1.

figure illustrates that the use of the pilot model leads to an underestimation of the middle loop phase margin and an overestimation of the outer loop phase margin. Because the bandwidths of these loops are consistent with the measurements, this could indicate that pilots generate some extra phase margin, e.g. through a lead in the middle loop feedback, that is not captured in the gain feedback of the model. Similarly, they could apply a lag or even be harmed with an additional delay in their outer loop feedback. In other words, although pilots definitely do *not* use the χ_e signal when no FPV is presented, they could apply some anticipatory control action on ψ_e instead. With the current data, however, this remains a matter of speculation.

Comparison of Experiments X5 and X1   In Figs 9.6 to 9.8 the MLM data of the corresponding conditions of Experiment X1 are indicated with the horizontal shaded areas. It appears that, compared to X1, whereas the pilot delay τ and the inner loop lead $\tau_{L_{in}}$ increase, the neuromuscular damping and the inner loop gain $K_{p_{in}}$ are much smaller (not shown). This indicates a rising need for pilots to increase their inner loop phase margin by generating more lead. Both the middle and outer loop feedback gains are considerably larger than those estimated in Experiment X1. The crossover frequencies and phase margins of the pilot loop closures clearly show that, compared to the findings of X1, much more pilot effort is put into increasing the bandwidth of the middle and outer loop feedbacks. That is, the inner loop crossover frequency ω_c^{in} has becomes significantly smaller (φ_m^{in} larger) whereas the bandwidths of the combined outer loop and the middle and outer feedback loops have become much larger (dito $\varphi_m^{out^c}$ and φ_m^{mid}, φ_m^{out}). For the conditions without a FPV both ω_c^{mid} and ω_c^{out} are significantly larger (φ_m^{mid}, φ_m^{out} smaller) than those found in X1. The conditions with a FPV show a spectacular increase in the bandwidth of the middle loop, at the cost, however, of a decrease in the outer loop bandwidth. When the bandwidth of the flight-path disturbance increases, however, both ω_c^{mid} and ω_c^{out} approximate the values found for X1, Fig. 9.8.

9.6   Retrospective

9.6.1   Discussion

The flight-path vector symbol has often demonstrated to be a very useful synthetic enhancement of the tunnel display. Of the three forms of display augmentation discussed in §9.2 only the flight-path vector does *not* change the common pilot control strategy of successively closing the aircraft attitude, flight-path and position feedback loops. Pilot control behaviour with a FPV is therefore not markedly different from the one investigated in the previous experiments of this thesis. The research reported in (Grunwald & Merhav, 1978) revealed that the effectiveness of the FPV is determined by a number of factors *other* than those concerning the display presentation, such as the vehicle dynamics and the bandwidth of the disturbances acting on the vehicle. To increase the general understanding of a pilot's use of the FPV and to extend the modelling efforts of Grunwald

and Merhav (1978), Experiment X5 has been conducted to investigate the usefulness of providing explicit aircraft flight-path information on pilot behaviour. In the following, the experimental findings of §9.4 and §9.5 will be elaborated along three themes of investigation (Mulder, 1999). These are, first, how does the presentation of the flight-path vector symbol affect pilot performance and control behaviour? Second, how is the pilot control behaviour affected by the characteristics of the flight-path disturbances? And third, what happens with pilot behaviour after the insertion of a disturbance on the aircraft flight-path in respect to the situation where this was not the case, i.e. how do the current results relate to those of Experiment X1?

The effects of showing a flight-path vector The experimental hypotheses concerning the use of a flight-path vector could be confirmed. Probably the most important finding of all has been that in determining the pilot model *structure* – the non-parametric identification phase of estimating the pilot frequency responses – it was found that *two* models had to be applied to describe the observed pilot control behaviour. That is, when no FPV is presented, a pilot successively closes the aircraft attitude, *heading angle error* and position error feedback loops. This is evidence for the hypothesis that *without the FPV pilots are unable to perceive the aircraft direction of motion relative to the tunnel trajectory (χ_e) well enough to use this information for purposes of control.* Rather, they revert to the best alternative for χ_e which *can* be perceived directly from the display, namely through the position of the infinity point, i.e. the heading angle error ψ_e. Second, when a FPV is presented, showing the aircraft flight-path angle error explicitly on the display, pilots use this flight-path information as their middle loop feedback, whereas the heading angle error can be ignored. Subjects stated that their aim was to continuously put the FPV symbol located on the tunnel's infinity point. The questionnaire revealed further that in particular the relative displacements of the tunnel altitude poles, π_{ij} and $\dot{\pi}_{ij}$, were used for position control. These findings demonstrate that the optical cues of motion perspective mediated by the generic wireframe tunnel are *not* salient enough for pilots to perceive the aircraft direction of motion *directly* from the display, at least not with the accuracy needed for purposes of control, and not with the current characteristics of the flight-path disturbances. This result has considerable theoretical implications and should be addressed further in future experiments.

The experimental findings provide evidence for the hypothesis that showing a flight-path vector significantly improves pilot performance. Pilot control activity, δ_a and $\dot{\delta}_a$, is considerably higher with a FPV as well as the magnitude of the aircraft roll angle rates. The heading angle errors have the same order of magnitude as those found for the conditions without a FPV. Hence, although this variable is not used for control purposes, the performance in terms of ψ_e is similar to that when the heading angle error *is* used for control. Path-following performance in terms of the flight-path angle error χ_e as well as the position error x_e becomes markedly better when the flight-path vector is presented. Furthermore, the pilot effort ratings are considerably lower when the FPV is available and pilots comment very favourably for the synthetic enhancement.

The MLM modelling efforts indicate for the conditions with a FPV a consistent shift in pilot attention to the feedback of flight-path angle error, at the cost of the position error feedback but especially the control of the inner loop of aircraft attitude. In other words, the bandwidth of the middle loop feedback is significantly higher and the bandwidth of the outer loop significantly lower in the case a FPV is presented. In the inner loop, bandwidth is sacrificed in order to gain extra phase margin when the FPV is presented, clarifying the results stated above that in these conditions the roll angle errors and roll angle rates increase significantly. The finding that the increase in pilot inner loop lead occurs mainly at the low velocity conditions, matches the relatively high effort ratings in these conditions.

The effects of the turbulence bandwidth   Recall that the bandwidth of the turbulence acting on the aircraft's flight-path is determined by the inverse quotient of the scale length L_g of the turbulence field and by the velocity V_{tas} of the aircraft moving through it. The questionnaire revealed that pilots judge the simulation more realistic for higher bandwidths ($\frac{V_{tas}}{L_g}$) of the flight-path perturbation. Although they did comment on a higher visual workload when bandwidth increased, the effort ratings show a contrary effect, independent on the presentation of the FPV, namely that of lower workload when the scale length decreases. The experimental data confirms the hypothesis that the pilot's use of the FPV is harmed when the bandwidth of the turbulence increases. Especially the scale length L_g affects pilot behaviour considerably, judged by the higher roll angles and roll angle rates but in particular the rapidly deteriorating performance in terms of χ_e, for smaller L_gs. The heading angle errors remain unaffected by the manipulation of L_g, which can be explained by the fact that with a FPV this variable is ignored, whereas in the conditions without the FPV this variable is *used for control*. The MLM data further support the finding that the feedback of χ_e deteriorates when the bandwidth of the disturbance acting on it increases, resulting to a shift in pilots' attention from the middle loop feedback (flight-path) to the outer loop feedback (position). Apparently, the rapid and unpredictable motions of the FPV on the display cause pilots to pay less attention to the FPV symbol. The bandwidth of the inner loop further deteriorates when L_g decreases indicating a further need of the pilots to put their efforts into controlling the two outer loops. When no FPV is presented, the effects of the bandwidth are smaller and less consistent among subjects. Not surprisingly, performance in terms of aircraft heading angle error is not influenced by the bandwidth. Whereas the flight-path angle error χ_e increases for higher bandwidths, independent of the presentation of a FPV, the position error performance *improves* in these conditions, a finding which contradicts the pre-experimental hypothesis. This improvement could be attributed to the fact that, first, the feedback of ψ_e applied in these conditions is not harmed at all by the increasing turbulence bandwidth, allowing subjects to maintain the bandwidth of their heading angle error feedback loop. Second, however, with a *fixed* turbulence intensity an increasing turbulence bandwidth yields larger amplitudes of the disturbance high-frequency components and lower amplitudes of the low-frequency components. Now, the fixed outer loop vehicle dynamics, an integrator-like system, acts as a low-pass filter weakening in particular the high-frequency components

of the disturbance, yielding smaller position errors. This artifact due to the design of the experiment, is *independent* of the presence of the FPV. As mentioned above, without the FPV the increasing bandwidth of the disturbances yields an improved path-following performance in terms of the position error, which makes sense. With a FPV, however, pilots apparently insist in correcting the rapid flight-path disturbances, decreasing the performance significantly: the FPV *harms* pilot performance in these conditions.

As has been hypothesized at the start of the experiment, the influence of the aircraft velocity V_{tas} is much smaller than that of the other variable marking the bandwidth of the flight-path disturbance, the scale length L_g. The experimental findings indicate that manipulating the aircraft velocity results in about the same effects on pilot behaviour as those found in the earlier experiments. That is, the higher velocity conditions are judged easier to control than the low velocity condition, although to a less degree than found earlier (Experiments X1, X2 and X4), which could indicate a mixture of the two effects that the velocity has on both the dynamics of the vehicle (making it easier for higher velocities) and the bandwidth of the disturbances (making it harder). The MLM data also shows such a mixture of effects caused by manipulating the aircraft velocity. For instance, the pilot middle loop feedback gain increases and the outer loop gain decreases when the velocity becomes larger. The turbulence scale length yields exactly the opposite effect when it decreases. So, obviously here the effects of the velocity on the vehicle dynamics dominate the effects it has on the bandwidth of the disturbances.

The effects of the disturbance on the aircraft flight-path   Although the additional disturbance on the aircraft flight-path complicates a comparison of the experimental results with those found in an earlier experiment, X1, with otherwise exactly the same definition (and subjects, of course), such a comparison could shed a light upon the effects that the insertion of this disturbance has had on pilot behaviour. Recall that without the flight-path disturbance the track angle equals the heading angle and the aircraft direction of motion can be perceived directly from the display using the infinity point. The *trends* in the data of Experiment X5 concerning the effects of manipulating the aircraft velocity are *exactly the same* as those found in X1. That is, independent of the presence of the flight-path vector symbol, when the aircraft velocity becomes larger the pilot control activity decreases, the aircraft roll angles and roll rates increase, the heading angle errors as well as the track-angle errors decrease and the position errors increase. The *magnitudes* of the performance data, however, are *markedly different*. Pilot control activity, δ_a and $\dot{\delta}_a$, is higher than that found in X1, as well as the roll angle rates and especially the roll angles themselves. The heading angle errors ψ_e are also considerably higher. Note that when the FPV is presented, performance in terms of χ_e equals the performance in terms of ψ_e found in Experiment X1, a finding that can be explained by the fact that in both cases the aircraft direction of motion with respect to the tunnel can be perceived directly from the display. The performance in χ_e deteriorates fast, however, when the bandwidth of the disturbances becomes larger. Generally, independent of the presence of the FPV, the pilot middle loop bandwidth is significantly higher and the pilot

inner loop bandwidth considerably lower than those found in X1, indicating the relative importance of controlling the aircraft direction of motion in the current experiment. When no FPV is presented, path-following performance, in terms of χ_e and x_e, is much worse than that found in X1, although the position performance data in X5 approximates that of X1 when the bandwidth of the turbulence increases. Surprisingly, when the FPV is presented, performance in terms of x_e is much better than that found in X1. This is a remarkable result because, due to the insertion of a third disturbance on the aircraft flight-path angle, the task as such was expected to become increasingly difficult. It could be caused by the fact that the feedback of the flight-path, the middle loop, is indeed so much stronger (higher bandwidth) as compared to the situation in X1 where the heading must be perceived through the position of the infinity point. Again, when the bandwidth of the flight-path disturbance increases, in particular when the scale length L_g decreases, the experimental data of Experiments X1 and X5 become approximately equal.

9.6.2   Conclusions and recommendations

Conclusions

- The common pilot control strategy with a perspective tunnel display, consisting of a feedback of the aircraft attitude, flight-path and position, does not change when the tunnel display is augmented with a flight-path vector symbol.
- The experimental data confirm the pre-experimental hypotheses regarding the effects of showing the FPV on pilot performance and control behaviour.
- The model-based analysis revealed that *two* pilot models had to be applied to describe the measured pilot control behaviour with and without the FPV.
- Without the FPV pilots are unable to perceive the aircraft direction of motion relative to the tunnel trajectory (χ_e) well enough to use this information for purposes of control. Rather, they revert to the best alternative for χ_e which *can* be perceived directly from the display, namely through the position of the infinity point, i.e. the heading angle error ψ_e. Hence, without the FPV the pilot successively closes the aircraft attitude loop, the *heading angle error* loop and the position error loop.
- When the FPV symbol is available, pilots optimize their performance by replacing the heading angle error loop with a direct feedback of the flight-path angle error, depicting the true aircraft direction of motion. The heading angle error is ignored.
- Presenting a FPV on the display significantly improves pilot performance, in particular of the flight-path angle error and the position error. The pilot effort ratings are considerably lower with a FPV.
- Presenting a FPV on the display leads to a consistent shift in pilot attention to the feedback of the flight-path angle error, at the cost of the position error feedback (the outer loop) but especially the control of the aircraft attitude (the inner loop).
- The pilot's use of the FPV is significantly harmed when the bandwidth of the turbulence, determined by the quotient of the aircraft velocity and the turbulence scale length,

increases. In particular the decreasing turbulence scale length leads to rapidly deteriorating path-following performance in terms of the flight-path angle error and the position error. The data even suggests that, in these high-bandwidth conditions, the pilots could perform *better without the FPV*.

• The model-based analysis indicates that when the FPV is presented on the display and the bandwidth of the turbulence is increased, pilots shift their attention from the middle loop feedback of χ_e to the outer loop feedback of x_e. Thus, the rapid and unpredictable motions of the FPV symbol on the display harms its use for purposes of control.

• The aircraft velocity affects both the aircraft dynamics as well as the bandwidth of the flight-path disturbance. The experiment shows that the first relation dominates the second in the effects manipulating the velocity have on pilot behaviour.

• The trends in the pilot performance data of the experiments with (X5) and without (X1) the disturbance on the aircraft flight-path angle, concerning the effects of the aircraft velocity are the same. The magnitudes of the data, however, are markedly different.

• The insertion of an additional disturbance on the aircraft flight-path leads to more pilot control activity and decreasing track-angle error performance, especially for the higher bandwidth conditions of the turbulence.

• As compared to the situation without the disturbance on flight-path, the pilot middle loop bandwidth is significantly higher and the bandwidth of the inner loop considerably lower, indicating the importance of firmly controlling the aircraft direction of motion in the current experiment.

• When a FPV is presented, performance in terms of x_e in Experiment X5 is markedly better than that of X1, *despite* the insertion of an additional forcing function in the first experiment. This indicates that the FPV dramatically improves the *direct* control of the aircraft direction of motion.

• When the bandwidth of the flight-path disturbance increases, especially due to a decreasing scale length, the performance in terms of x_e with and without a FPV approximate each other and they also become equal to the performance found in Experiment X1.

Recommendations

• The flight-path vector is useful in particular for the control of the recti-linear aircraft motion along a straight trajectory, because in this case it shows a *prediction* of the future aircraft trajectory. In curvi-linear motion along a curved trajectory, however, the FPV only shows the instantaneous direction of motion and the pilot has to mentally compute the future aircraft path. Hence, an experiment is needed to investigate the usefulness of showing a flight-path vector in curved tunnel sections and to assess whether the display augmentation in this task also improves pilot performance.

• The experiment provides evidence to conclude that, with the chosen level of disturbances, pilots are unable to perceive the aircraft's direction of motion directly from the display, at least not with an accuracy needed for control. Additional experiments are required to assess the generalizability of this finding, in particular in relation to the current

experimental set-up with more than one disturbance signal. For instance, one could investigate a similar task as conducted here but *without* the disturbances i_1 and i_2, focusing on the effects of the turbulence shaping filter and intensity of the flight-path disturbance i_3. Unfortunately, however, the absence of i_1 and i_2 prevents a model-based analysis because in this case the pilot frequency responses can not be identified.

• In the current experiment the aircraft velocity has had two different effects on the task difficulty. At higher velocities, the aircraft dynamics generally become easier to control. At the same time, however, the higher velocities increase the bandwidth of the flight-path disturbances, making the task harder to perform. A follow-up experiment should shed a light on this mixture of effects and should aim at separating them.

• The FPV has shown to dramatically improve pilot path-following performance in terms of the position error, even compared to the situation where there was no turbulence on flight-path at all, i.e. Experiment X1. This should be investigated further, for instance by repeating Experiment X1 with and without the flight-path vector symbol.

Chapter 10

Curve Interception

10.1 Introduction

The aircraft transition manoeuvre between a straight and a curved section of the reference trajectory is the subject of this chapter. Intercepting a curve is a task that is fundamentally different from the tasks previously addressed in this thesis. Instead of maintaining a certain aircraft stationary flight condition in the presence of disturbances, the pilot must control the aircraft from one stationary flight condition to another. Examining the interception of a curve addresses the first (and only) aircraft *manoeuvre* in this thesis. Because of the different nature of the task other cognitive, perceptual and control-theoretical issues are introduced that have not played a role of interest up until now. Central in the discussion will be the *timing* of the manoeuvre. Obviously, due to the inherent lags of the aircraft dynamics the pilot must initiate the manoeuvre well before the curve itself begins. But how far ahead? Pilots could for instance prefer a smooth manoeuvre that starts a relatively long time before the curve, or they could initiate a faster response just before the start of the curve. At first sight, the decision to begin the manoeuvre seems to be completely up to the pilot. It will be shown, however, that the curve interception manoeuvre is determined in the first place by the *manoeuverability constraints* of the aircraft. Within these constraints the pilot has some freedom in initiating the curve transition. The timing of the manoeuvre is then a matter of *decision making* and is determined mainly by the available visual information. Indeed, as will be shown in this chapter, different tunnel display designs have significant effects on the pilot timing strategy.

In §10.2 the findings of earlier studies on curve interception will be discussed, providing a background for the investigation. In §10.3 the effects of the aircraft dynamic characteristics on the transition response will be examined. In §10.4, the information-related properties of the tunnel display with respect to the task at hand will be examined. Based on these investigations, hypotheses on pilot timing strategies could be stated that were then evaluated experimentally. The experimental approach, described in §10.5, differs from previous ones: instead of conducting a closed loop regulation task, the subjects per-

formed an open loop anticipation task. The experimental results are described in §10.6, and the chapter ends with a retrospective, §10.7.

10.2   Background

Automobile driving research

Given the importance of such every-day driving tasks such as approaching and following road curves, it is surprising that relatively little is know about them: "*...despite evidence from accident studies that it might be an important area for countermeasures, driver behaviour in the approach to curves has been relatively seldom studied*" (Riemersma, 1988). Generally, two types of investigations are conducted. First, in *eye movement studies* the movements of the driver's eyes are measured and, in an attempt to identify patterns in driver fixation, analyzed with respect to the out-of-the-window visual scene (Rockwell, 1972). Second, *perceptual studies* examine the properties of the visual scene theoretically.

Eye movement studies: curve negotiation   A number of studies focused on examining driver visual scanning patterns in approaching and following a curved section of the road. An early study (Gordon, 1966b) reported that on straight sections of the road – well before a curve – the visual scanning shows a persistent pattern of eye fixation movements, forward to the limit of the perceivable road ahead and back to the vehicle. This *intermittent visual attention allocation process* is hypothesized to be a consequence of the dual requirements of *anticipation* and *vehicular alignment* (Gordon, 1966a). In (Kondo & Ajimine, 1968) it was reported that drivers actively control their sighting distance as well as their sighting angle when approaching and following a bend. As Fig. 10.1 shows, the look-ahead distance decreases well before the start of the curve and drivers fixate their gaze towards the turning direction. Thus, in approaching a curve, the driver's gaze changes direction from the longitudinal (...far–close–far...) motion laterally inwards into the curve. These anticipatory lateral eye movements preceding a bend in the road are considered to be a part of the so-called *curve negotiation* process (Shinar et al., 1977). Scanning the curve ahead may serve an anticipatory mechanism that constructs a *scheme* of the characteristics of the curve in terms of curvature, length and elevation.

Although these results suggest that drivers, when approaching and following a bend in the road, focus their attention primarily to a region close to the car on the inner side of the curve, later studies reported a *saw-tooth* visual scanning pattern during curve following (Jurgensohn, Neculau, & Willumeit, 1991; Osaka, 1991). A driver fixates a point in front of the car, continues to fixate that point for some time and then, when the fixation point comes near the car, chooses another fixation point further away. This so-called *driver-nystagmus* can probably be explained as the optical pursuit of the driver for local texture elements in apparent motion (Kramer & Neculau, 1986); optic flow needs some *carrier texture* (Landwehr, 1991). These findings are supported by a study of Land (1993). The approach to a curve is characterized by *ranging* saccades that probably help the visual
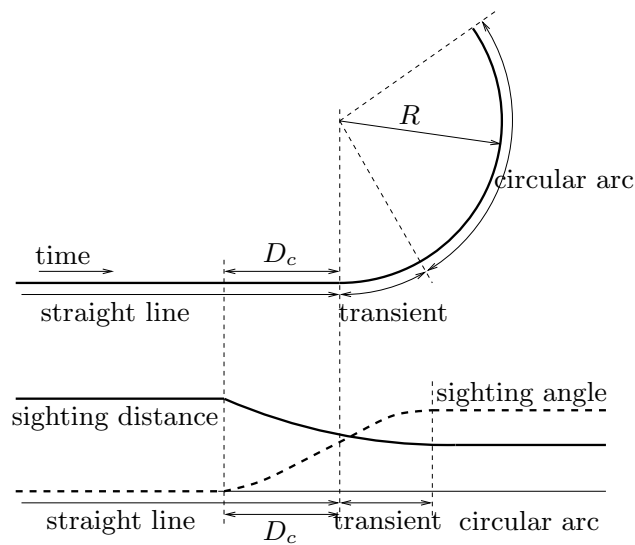
Figure 10.1: Eye movement pattern as reported in (Kondo & Ajimine, 1968).

system in forming an estimate of the *curvature* of the bend ahead. This is not unlikely for two reasons. First, the curvature determines the amount with which the steering wheel must be turned to follow the bend (Godthelp, 1986). Second, the timing of the lateral eye movements corresponds well to the availability of information about the curvature of the bend (Land, 1993). Summarizing, eye movement studies suggest that in approaching a curve, drivers tend to look into the curve while decreasing their forward looking distance. During curve-following the driver will continue to focus his gaze inwards the curve in an intermittent fashion, dependent on the characteristics of the visual scene.

Perceptual studies: the tangent point   Early theoretical studies have investigated the automobile driving task (Gordon, 1965, 1966a; Biggs, 1966; Fry, 1968). In (Riemersma, 1988, 1991) a theoretical analysis is presented of potential cues for the curve characteristics when approaching a curve, the perception of which is commonly recognized as causing the anticipatory lateral eye movements discussed above. Fig. 10.2 shows the geometry of a horizontal road curve viewed from the top as well as seen by the driver. The road curve is determined by the radius of the curve, R, and the curve deflection angle, α, that are independent. Several cues are considered useful for the perception of the deflection angle from the perspective scene viewed by the driver (Riemersma, 1988): (i) the distance between the two vanishing points P_1 and P_2, which equals $\tan \alpha$ and is independent of the distance to the beginning of the curve D_c; (ii) the angle Δ that depends on the deflection angle α and the distance to the curve D_c : $\Delta = \arctan \left(\frac{D_c}{H} \tan \alpha \right)$, with H the height above the ground. Riemersma suggests that for the perception of the curve radius the so-called *reversal point*, or *tangent-point* (TP) can be used, defined as "*the point at which the perspective of the inner edge line has a minimal horizontal visual angle with the vanishing point of the extended straight section*". The location of this point is independent of the deflection angle. In a passive viewing experiment it was found
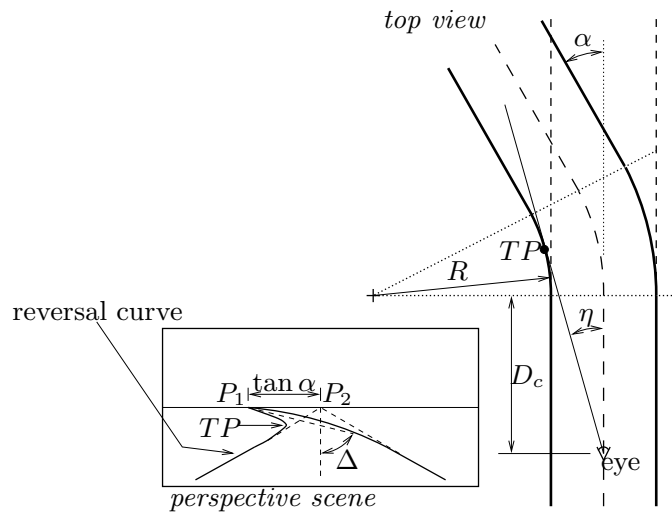
Figure 10.2: Perspective view and top view of the road scene examined in (Riemersma, 1988).

that subjects were indeed able to discriminate between curves of different deflection angle and radius (Riemersma, 1981). It was also concluded, however, that the visual cues for curve radius have a substantial impact only at shorter distances before the start of the curve. This finding was supported in a later study (Riemersma, 1991) that also showed that the usability of the cues depends on a reliable estimate of the distance remaining to the curve. The potential use of the reversal point in curve perception was originally reported by Brummelaar (1975), where it was suggested that an important aspect of a road curve was the shape of the inside edge line of the road, i.e. the *reversal curve.* Drivers were reported to underestimate the curvature of the road when radius increased, a phenomenon that is generally believed to be caused by the relative sharpness of the reversal curve (Brummelaar, 1983; Fildes & Triggs, 1986). The notion of the *reversal point* was supported in several later studies (Land & Lee, 1994; Brown, 1994). The tangent point of the inside edge of a curve was found to be very useful in following a twisting road (Land & Lee, 1994). Using cameras, the road ahead and the driver's direction of gaze was monitored. It was found that in approaching the bend, drivers suddenly fixed their eyes onto the tangent point, shortly before they started to turn the wheel. This corresponds well with the findings of the other eye movement studies that did not, however, attribute the change of gaze to a particular characteristic of the curve. It was reported further that it could in fact not be the tangent point itself that is crucial, but the angle η between the direction of movement and the line of sight towards the tangent point (see Fig. 10.2). It is hypothesized that drivers try to keep this angle η small: as the driver approaches a curve, this angle starts to increase (the bend *opens up*). Once a certain threshold is reached, the driver starts turning the steering wheel. Due to the resulting curvi-linear motion of the car, the angle η stops growing and may start to diminish. The effect is to trace a curve of approximately constant radius. The latter could attribute for the increasing difficulty in following a curve of changing radius, as reported in several other studies (Kondo &

Ajimine, 1968; Jurgensohn et al., 1991). The potential of the tangent point in modelling driver behaviour in curve negotiation has been shown in (Boer, 1996).

Research on perspective flight-path displays

The curve transition manoeuvre with a tunnel-in-the-sky display has not been the subject of many studies. Nonetheless, in one of the first experimental evaluations of tunnel display (Grunwald et al., 1980) the manoeuvre was concluded to be of major concern: "*transients to and from curved sections of the path were too sudden (...) This resulted from the fact that the curvature along the trajectory was varied in steps, without transients from one section to the other*". It was recommended that "*the functions for trajectory curvature and commanded bank angle are continuous and are matched to the average vehicle response*" (Grunwald, 1984). In (Grunwald, 1996a, 1996b) improvements to the original tunnel display for curved trajectory following are presented. One of the main shortcomings in the original tunnel display that was addressed is the poor performance in transitions between straight and curved trajectory sections, especially for large and sluggish aircraft. Generally, the degraded path-following accuracy was attributed to *corner cutting*, resulting from banking the aircraft well before its actual entry in the curve. This was also reported in (Theunissen & Mulder, 1995b). Because Grunwald's tunnel concept is essentially the combination of a tunnel and a vehicle path predictor, the corner-cutting phenomenon is countered with a more advanced predictor guidance scheme. An experimental validation showed a superior performance in transitions to and from curved trajectory sections with the improved predictor guidance scheme (Grunwald, 1996b).

Concluding remarks

Based on a literature survey, the perceptual mechanisms in approaching and following a bend in the trajectory have been discussed. Most – if not all – efforts in understanding human behaviour in this task originate in automobile driver research. The characteristics of the visual scene allow a driver to conduct the anticipatory actions at curve entrance. The curve negotiation phenomenon reflects a driver's need to obtain information about the properties of the bend, probably its curvature. The resulting anticipatory steering actions play a dominant role in the curve entrance phase (Godthelp, 1986). The compensatory actions that start after the initial open loop steering actions could be a function of the motion of the curve tangent point or, equivalently, the angle between the direction of the vehicle's motion and the curve tangent. In §10.4 it will be discussed if and how these phenomena apply to the curve interception manoeuvre with a tunnel-in-the-sky display.

10.3   Influence of the aircraft dynamics

Before the potential sources of information in the display are examined, it is important to identify first the constraints set by the dynamic characteristics of the aircraft. The results
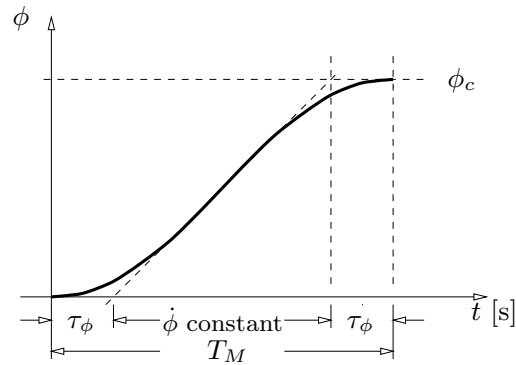
Figure 10.3: Response of the aircraft roll angle during a conventional roll-in manoeuvre.

of a *paper-pilot, paper-aircraft* simulation study will be discussed below. The simulation study allows the aircraft manoeuverability constraints to be examined conceptually, and introduces some variables that will prove to be useful in understanding the experimentally measured pilot behaviour.

Fundamentals of curve interception   The interception of a curve from a straight section of the trajectory involves a step change in the aircraft reference angle of bank (from 0 to ϕ_c), or, equivalently, a step change in the aircraft's yaw rate (from 0 to r_c). For almost all aircraft the *roll subsidence* mode (lag time constant τ_ϕ, Appendix C) is the principal descriptor of this manoeuvre. The total manoeuvre time T_M (in [s]) needed for an aircraft to achieve a step change in bank angle can be approximated by (Fig. 10.3):

$$T_M \quad \approx \quad 2\tau_\phi + \frac{\phi_c}{\dot{\phi}}. \tag{10.1}$$

Thus, the larger the roll-rate $\dot{\phi}$, the smaller T_M will be. Furthermore, when the roll-rate is constant, T_M is determined by the lag time constant τ_ϕ, a variable that depends mainly on aircraft inertial and aerodynamic characteristics and that does not depend much on the velocity of the aircraft (Etkin, 1972). The roll-in manoeuvre yields a yaw rate that is constant for a stationary horizontal turn without side-slip (Etkin, 1972). A step change in the commanded trajectory from a straight to a curved section with constant radius involves a discontinuity in the curvature function. It takes some time for an aircraft to achieve the desired angle of bank. The same holds for the yaw rate that evolves simultaneously. Due to the integration of the yaw rate into heading (no slip) and the subsequent integration of heading into the lateral position, a non-zero yaw rate yields a change in lateral position. The aircraft starts to move away from the straight trajectory in the direction of the curve, causing the *corner-cutting* phenomenon mentioned above. Hence, because it takes some time for an aircraft to roll-in, the accuracy in following the path will decrease. A solution could be to design the entrance into (and out of) a curved section of the trajectory based on the specific kinematic and dynamic characteristics of an aircraft (Grunwald, 1984).

Table 10.1: Characteristics of the two aircraft types for the two velocity conditions.

		Cessna Citation 500		Airbus A300	
		approach	cruise	approach	cruise
Main aircraft parameters					
velocity	[m/s]	59.9	121.3	77.0	131.5
mass	[tons]	4.5	4.7	130.0	130.0
wing-span	[m]	13.4	13.4	44.8	44.8
wing-area	[m^2]	24.2	24.2	260.0	260.0
Roll subsidence time constant τ_ϕ					
τ_ϕ	[s]	0.42	0.47	1.09	0.97
Properties of the curved flight (r_c= 1.5 [deg/s])					
ref. bank ϕ_c	[deg]	9.2	18.6	11.8	20.1
curve radius	[m]	2288.0	4633.3	2941.2	5022.9
Symmetrical initial condition					
pitch angle	[deg]	4.7	1.2	4.8	1.0
angle of attack	[deg]	4.7	1.2	4.8	1.0

Paper-pilot, paper-aircraft simulation study

To investigate the effects of aircraft dynamics on the timing and control of the roll-in manoeuvre a simulation study was conducted. Two aircraft types were selected:

1. A Cessna Citation 500, a small business-jet representing a high-bandwidth aircraft.
2. The Airbus A300, a medium-large airliner representing a low-bandwidth aircraft.

Both the aircraft models were implemented for an *approach* and a *cruise* velocity condition. Some of the main aircraft properties are listed in Table 10.1. It shows that, first, the roll subsidence lag time of the Airbus is about twice as large as that of the Citation and, second, that this variable is almost independent of the aircraft velocity.

A simulation program was implemented in a Matlab/Simulink environment (van Oorschot, 1997b). The aircraft dynamics were modelled using the linear asymmetrical dynamic models (Etkin, 1972), augmented with a turn-coordinator and yaw-damper. The resulting stability-augmented aircraft models yielded a well-damped Dutch roll mode and negligible side-slip, and could be controlled with aileron only. An automatic controller – the *paper pilot* – was designed for the curve initiation manoeuvre, controlling the aircraft smoothly from an initial straight and level flight condition into a stationary horizontal turn with a fixed yaw rate r_c of 1.5 [deg/s]. Fixing the yaw rate leads to different reference angles of bank ϕ_c and different curve radii for all four conditions (Table 10.1). The only degree of freedom that was varied in the simulation is the *magnitude* of the initial 'pilot' aileron response. A small magnitude of this signal yields a slow roll-in manoeuvre, and a large magnitude a fast manoeuvre. For details, the reader is referred to (van Oorschot, 1997b).

Results: time histories   The simulations were done for all four configurations as a function of the magnitude of the initial anticipatory control response. The time histories of

(a) aileron

(b) roll-rate

(c) roll angle

(d) yaw rate
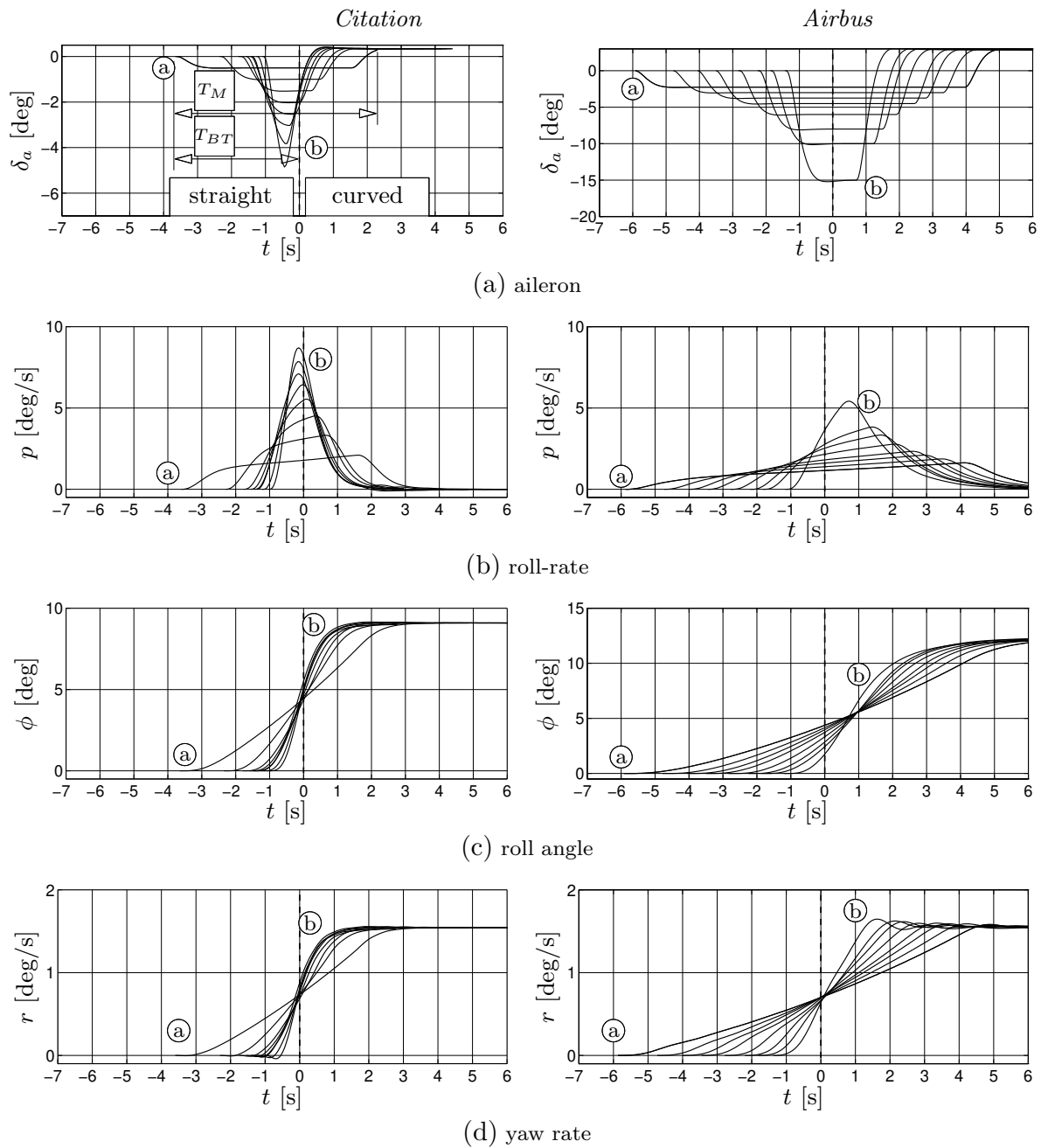
Figure 10.4: Time histories of the Cessna Citation 500 (left column) and the Airbus A300 (right column), plotted as a function of time relative to the start of the curve ($t=0$) (van Oorschot, 1997b). In this figure, the 'a' and 'b' circles mark the *slow* and *fast* responses, respectively. Note that the steady-state value of δ_a is non-zero and opposite to the initial deflection, a well-known idiosyncrasy of aircraft curve control.

the main response variables of the Cessna Citation and the Airbus, illustrated in Fig. 10.4, reveal that the paper pilot has considerable freedom in conducting the manoeuvre. In all cases pilots must initiate their control action well in advance of the start of the curve. The moment of this initiation can be characterized by the *Time-before-the-turn* T_{BT} (in [s]). The time interval a pilot continues to control the roll-in manoeuvre – i.e. until the reference bank angle ϕ_c has been achieved – equals the total manoeuvre time T_M introduced above. Both the quantities are illustrated in Fig. 10.4(a). Generally, the roll-in manoeuvre of the Airbus must be initiated earlier and will take more time than the Citation. The manoeuvre is approximately centered around the transition between the straight and curved section of the trajectory. It can be concluded that the required discontinuity in ϕ_c, or, equivalently, in r_c, cannot be matched, resulting in the aircraft drifting away from the reference trajectory towards the inner side of the turn (not shown).

Results: characteristic variables The time histories allow insight into the aircraft manoeuverability constraints. From each curve-interception manoeuvre a number of variables can be determined that are useful in quantifying these constraints:

(i) The total manoeuvre time T_M and the time-before-the-turn T_{BT}.

(ii) The maximum (absolute) values of the aileron deflection and aircraft roll-rate signals, i.e. $\delta_{a_{max}}$ and p_{max}.

(iii) The maximum (absolute) value of the lateral position error, $x_{e_{max}}$.

Fig. 10.5(a) shows that $T_M \approx 2T_{BT}$, indicating that almost all manoeuvres are conducted *symmetrical in time* with respect to the start of the curve. All other characteristic variables are illustrated as a function of the maximum aileron deflection in Fig. 10.5, emphasizing again the freedom in conducting the manoeuvre. A trade-off exists between the path-following accuracy and the roll-rates of the manoeuvre. From a path-following perspective, the best manoeuvres are those which are started just before the begin of the curve. The aircraft roll-rates, however, affecting passenger comfort and aircraft load factors[1], dictate a slower manoeuvre starting well in advance of the curve. Although the aircraft velocity does not have a large effect on the T_{BT}, the cruise-velocity conditions result in higher roll-rates and larger position errors for both the aircraft types. This can be attributed to the fact that for a fixed reference yaw rate r_c, the roll angle ϕ_c increases with velocity. Then, it follows from Eq. 10.1 that, for equal τ_ϕs and equal T_Ms, the roll-rates must be higher. Whereas the roll rates and path-following performance are higher for the Citation, the aileron deflections and the T_{BT} are larger for the Airbus.

10.4 Influence of the presented information

The curve interception manoeuvre executed by a pilot is determined by the aircraft dynamic properties and the nature of the presented visual information. The fact that the pilot

---

[1]The airframe and flight worthiness standards for a roll-change manoeuvre (FAR 23.157 (rate of roll)) indicate allowable levels of roll-rate of 10.6 and 8.6 [deg/s] for the Citation and Airbus, respectively.

(a) the total manoeuvre time T_M vs. the time-before-the-turn T_{BT}

(b) characteristic values for the Citation

(c) characteristic values for the Airbus
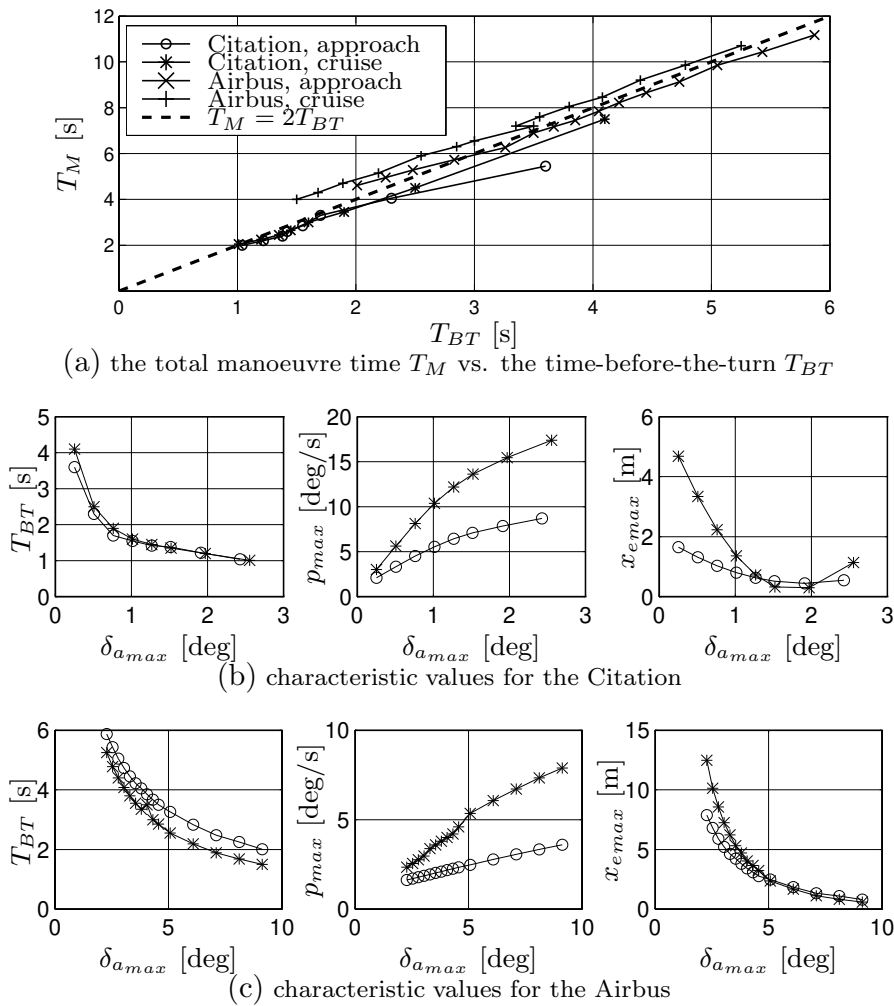
Figure 10.5: Characteristic values of the simulation study. The two bottom rows show the time-before-the-turn T_{BT}, the maximum roll-rate p_{max} and the maximum position error x_{emax} as a function of the maximum aileron deflection $\delta_{a_{max}}$. The circles and asterixes represent the approach and cruise velocity conditions, respectively.

can and will adapt his decision-making behaviour to the visually presented information has been shown in various other studies (Warren & Riccio, 1985; Reardon, 1988; Mulder et al., 1999). Below, the dynamic characteristics of the tunnel image when approaching a curved segment from a straight section will be investigated.

Characteristics of the tunnel when approaching a curve

Fig. 10.6(a) shows a top view of the situation considered here. A straightforward way of examining the properties of the tunnel projection when approaching a curve is simply to show the frozen frames of a hypothetical *moving picture*. The result is given in Fig. 10.6(b) for an aircraft approaching the curve with a velocity V_{tas} of 100 [m/s], start-

(a) bird's eye view of the situation

(b) frozen frames of a moving picture
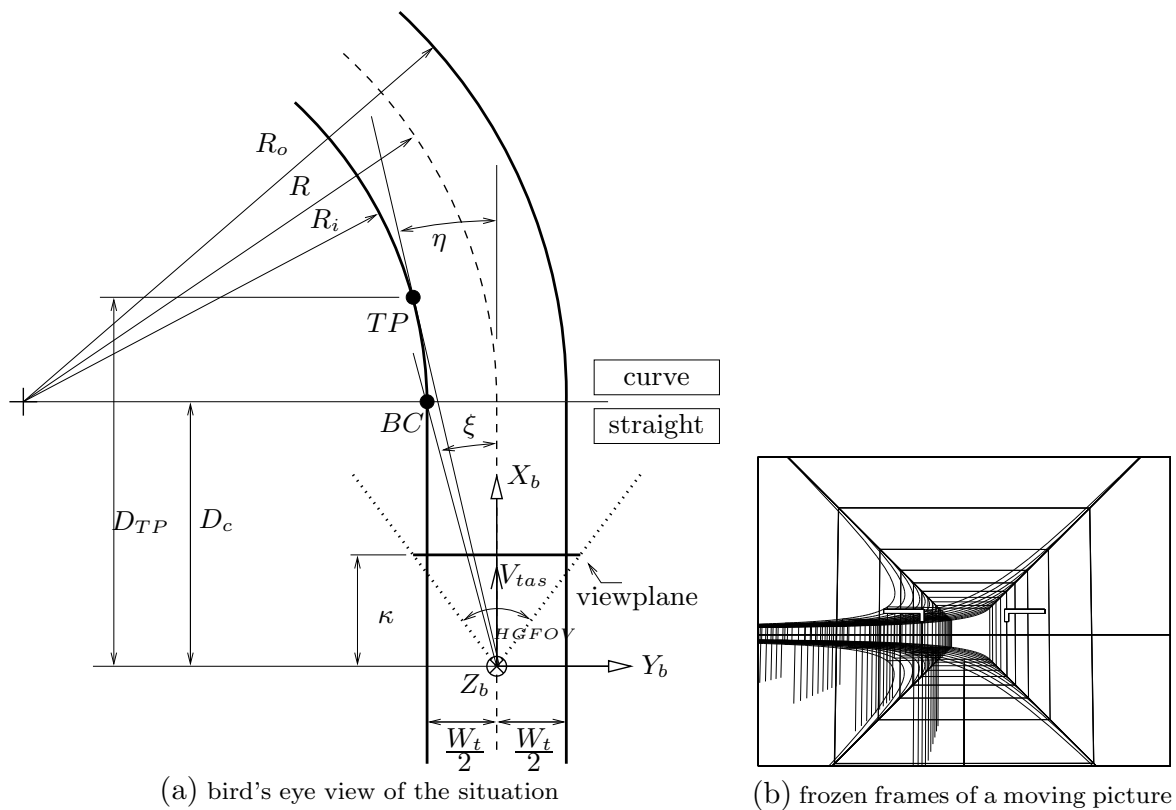
Figure 10.6: The approach of a curved section in the trajectory. The figure on the left shows a
bird's eye view of the situation. The aircraft is positioned at distance D_c before
the curve, with no position and attitude errors relative to the tunnel. Its Body
axes are aligned with the tunnel centerline. The aircraft moves along the tunnel
centerline towards the curve with constant velocity V_{tas}. The figure on the right
shows the frozen images of a 3-D *movie* showing the appearance of basic elements
of a generic tunnel display when approaching a curve.

ing at a distance D_c of 750 [m] before the curve, and showing the tunnel[2] display image
for 10 consecutive steps (0.75 [s]) time. Although the figure is cluttered, it is evident
that basically two things are happening: the tunnel frames expand and the outline of the
tunnel *opens up* when approaching the curve. These two effects can be illustrated better
when shown separately, as is done in Figs 10.7 and 10.8.

Fig. 10.7 shows only the tunnel *frames* and illustrates the expansion of these frames. As
will be discussed in detail below, it is known that humans are very susceptible to this kind
of information, because it provides information about the *Time-To-Contact* (TTC). A first
hypothesis is that pilots use TTC-information from the expanding tunnel frames to deter-
mine the moment to initiate the roll-in manoeuvre: a *time*-based approach (Strategy I).

Fig. 10.8 shows only the tunnel *outline* and illustrates the *opening* of the curve when ap-
proaching it. In this figure, the position in time of two particular points is shown: (i)

---

[2]Width and height 80 [m], intermediate frame distance 350 [m] and curve radius 2500 [m].

Figure 10.7: The frozen images of a 3-D *movie* showing the appearance of basic elements of the tunnel display when approaching a curve: tunnel-frames (and altitude poles) only.

the transition point between the straight and curved section of the trajectory, BC, and (ii) the so-called *reversal* or *tangent* point, TP, introduced in §10.2. Whereas the curve transition point translates along a straight line towards the observer, the trajectory of the tangent point is markedly different. After first following an identical straight line, the tangent point turns off into the direction of the curve. The trajectory of the tangent point is determined by the distance to the curve but is also affected by the size of the tunnel and the curve radius. This will be discussed in §10.4. A second hypothesis is that pilots use the tangent point of the tunnel outline to determine the moment to initiate the roll-in manoeuvre: a *distance*-based approach (Strategy II).

TTC-related information

In many experiments (Lee, 1974, 1980a; Lee, Young, Reddish, Lough, & Clayton, 1983; Mulder et al., 1999), a time-to-contact strategy for the onset of a control response has been demonstrated. Time-to-contact is defined as the time remaining to collision with an object if no corrective action is taken. Here, it is defined as the time remaining to the moment the aircraft passes a specific tunnel frame. The TTC to the frame marking the curve transition can be approximated by (Fig. 10.6(a)):

$$TTC = \frac{D_c}{V_{tas}} = \frac{\sin \xi \cos \xi}{\mathrm{d}\xi/\mathrm{d}t} \approx \frac{\xi}{\dot{\xi}}. \tag{10.2}$$

when ξ is small. The TTC is specified by an optical variable, *tau*, that describes the relative velocity of the optical image expanding across the retina (Lee, 1980a). Because the surfaces of the tunnel frames are perpendicular to the direction of motion, the optic
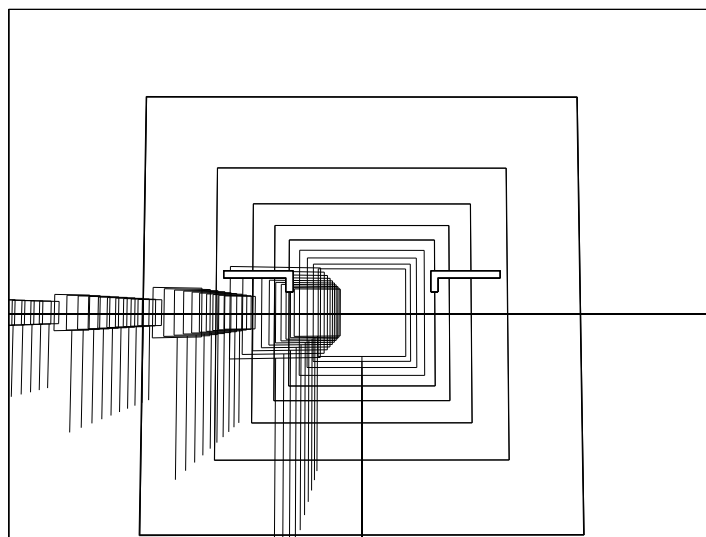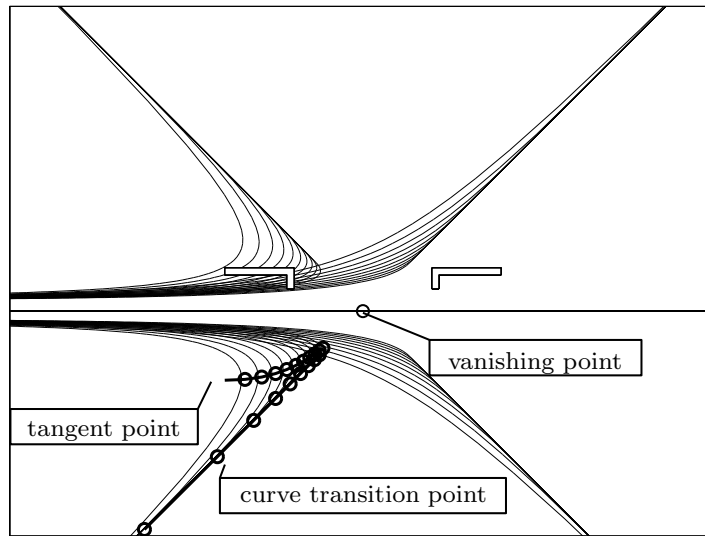
Figure 10.8: The frozen images of a 3-D *movie* showing the appearance of basic elements of the tunnel display when approaching a curve: tunnel-contour only. The movement of the tangent point (TP) is a cue for the approaching of the curve transition point (BC), which is less visible.

flow field expands isotropically (Koenderink, 1986). In this case the TTC can be perceived from *any* arbitrary point on the outline of the tunnel frame (Mulder et al., 1999).

Effect of the perspective projection   Experiments involving the perception of TTC are generally conducted for normal viewing conditions, i.e. two eyes looking into the outside world. Here, pilots perceive the TTC information from a screen showing a computer-generated perspective projection of a synthetic world, which has a number of consequences. First, as a result of the limited field-of-view of the projection, a tunnel frame *disappears* from the screen some time *before* the aircraft passes that particular frame, yielding a minimum TTC (Theunissen, 1997; van Oorschot, 1997a):

$$TTC_{min} = \frac{W_t/2}{V_{tas} \tan\left(HGFOV/2\right)}, \tag{10.3}$$

with W_t the tunnel width (in [m]), V_{tas} the velocity (in [m/s]) and $HGFOV$ the horizontal geometrical field-of-view (in [deg]). Because it is hypothesized that TTC information is important for the curve-interception manoeuvre, TTC_{min} should be much smaller than the TTC's in the experiment. A second topic that is of interest here is whether the perceived TTC information (following Eq. 10.2) equals the *real* TTC (given by D_c/V_{tas}), and whether this perceived TTC information depends on the position of the eye relative to the screen. Assume that the eye of a (monocular) observer is exactly positioned in the center of projection COP (δd=0 in Fig. 10.9(a)). Then, it can be shown that the perceived TTC, TTC_{cop} equals the real TTC, TTC_{real} until the distance of the COP to the frame, D_c, or, equivalently, the angle ξ subtended in Fig. 10.9(a), becomes too

large. Fig. 10.9(b), showing the quotient of TTC_{cop} and TTC_{real} vs. TTC_{real}, indicates that the TTC will be overestimated when the distance D_c to the frame becomes very small. Because the real TTC also becomes very small, however, this is only a marginal effect. When the eye of the observer is *not* positioned exactly in the COP ($\delta d \neq 0$ in Fig. 10.9(a)) perceptual biases may occur. These biases are caused by the fact that an observer in principle assumes that his eye position equals the position of the COP (the so-called *window assumption*) (McGreevy & Ellis, 1984). As indicated in Fig. 10.9(a), the true projector from a point P to the COP yields in a projection point p on the viewplane. The assumed or perceived projector, on the other hand, originating from the eye position and through the projection point p, maps the perceived point in space to the virtual point P'. The perceived TTC, TTC_{eye}, will now be based on the quotient of the angle ξ' and its derivative. It can be shown (van Oorschot, 1997a) that the perceived TTC from an eye position not equal to the COP (TTC_{eye}) leads to an underestimation of the TTC perceived when the eye position *would* be equal to the position of the COP (TTC_{cop}). In other words, the situation that the eye is positioned further away from the screen than the COP *compensates* the overestimation of the real TTC, as illustrated in Fig. 10.9(b). Summarizing, the tunnel display provides accurate TTC information. Due to the limited field-of-view, however, the TTC cannot be perceived for very small distances to a frame.

Characteristics of the tangent point

When no tunnel frames are presented and only the outline of the tunnel is available, other visual cues than the TTC must be used. The tunnel outline resembles the ordinary visual scene encountered in the automobile driving task to a high degree (compare Figs 10.2 and 10.8). Automobile driving research, discussed in §10.2, suggests that in this case two variables become important, i.e. the movement of the tangent point on the display and the estimate of the distance to the curve-transition point. In (Brummelaar, 1975), the following simplified but nonetheless accurate expression is derived for the longitudinal distance D_{TP} from the observer to the tangent point (Fig. 10.6(a)):

$$D_{TP} = \sqrt{R_i W_t + D_c^2}, \tag{10.4}$$

with R_i the inner curb curve radius, W_t the tunnel width, and D_c the distance to the curve (all in [m]). In case of no position and attitude errors of the aircraft relative to the tunnel centerline, the position of the tangent point on the display (u_{TP}, v_{TP}) becomes:

$$u_{TP} = \kappa \left(\frac{W_t + (D_{TP} - D_c)^2/R_i}{2D_{TP}} \right) = \kappa \left(\frac{D_{TP} - D_c}{R_i} \right) = \left. \kappa \sqrt{\frac{W_t}{R_i}} \right|_{D_c=0};$$

$$v_{TP} = -\kappa \left(\frac{W_t}{2D_{TP}} \right) = \left. -\kappa \frac{1}{2} \sqrt{\frac{W_t}{R_i}} \right|_{D_c=0}.$$

Figs 10.10(a) and 10.10(b) show the successive projections on the display of the tangent point (TP) and the point marking the beginning of the curve (BC) of the lower left tunnel

(a) top view of the situation

(b) the various quotients
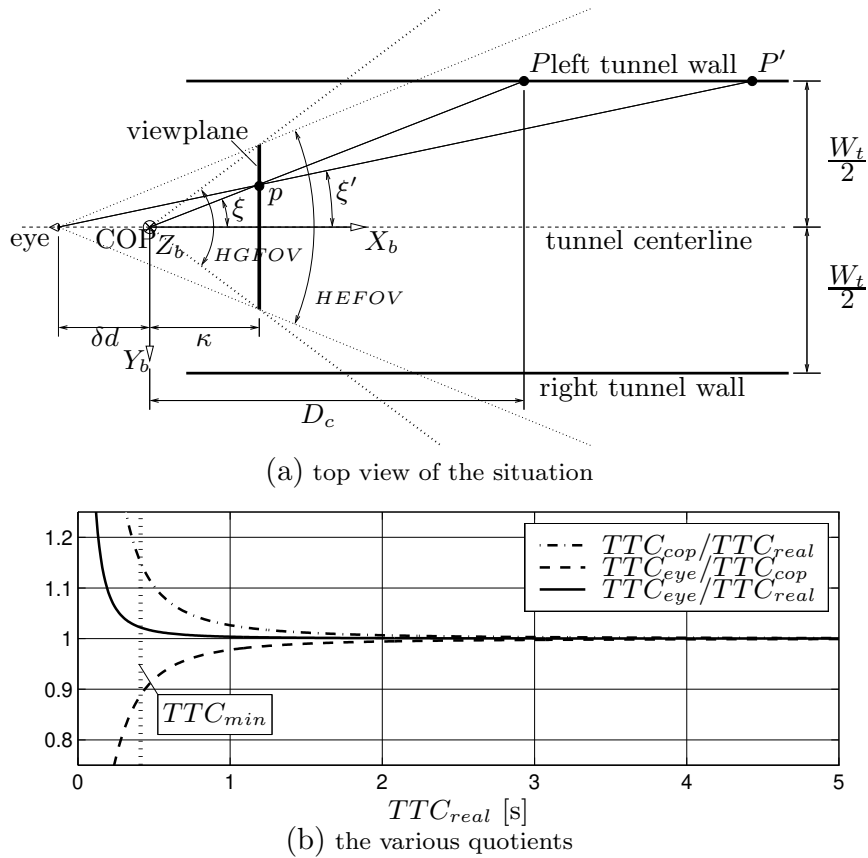
Figure 10.9: The top row of this figure shows the variables used to compute the various quotients of the bottom row. The values of the quotients TTC_{cop}/TTC_{eye}, TTC_{eye}/TTC_{cop} and TTC_{eye}/TTC_{real} as a function of the real TTC.

contour line in case the aircraft moves towards a curve directed to the left. The position of the start of the curve on the display is given by (no position and attitude errors):

$$u_{BC} = \kappa\left(\frac{W_t}{2D_c}\right); \quad \text{and} \quad v_{BC} = -\kappa\left(\frac{W_t}{2D_c}\right).$$

The point BC follows a straight line ($v = u$) when approaching the beginning of the curve. As has been discussed above (Fig. 10.8) the tangent point initially follows the same trajectory, but then starts to move in the direction of the curve (towards the line $v = u/2$ for very small D_cs). The figures show that, for equal curve radius, the tangent point drifts away from the BC-trajectory at *larger* distances before the curve (i.e. earlier) for larger tunnel sizes. For equal tunnel sizes, the tangent point drifts away from the BC-trajectory at *smaller* distances before the curve (i.e. later) for larger curve radii. Hence, although the motion of the tangent point on the display can be used to obtain knowledge about the distance to go to the start of the curve, this estimate is affected by the tunnel size and the curve radius. For equal curve radii, larger tunnel sizes will lead to an *under*estimation of the distance before the turn. For equal tunnel size, larger curve radii will lead to an *over*estimation of the distance before the turn.

(a) curve radius 2000 [m]

(b) curve radius 4000 [m]
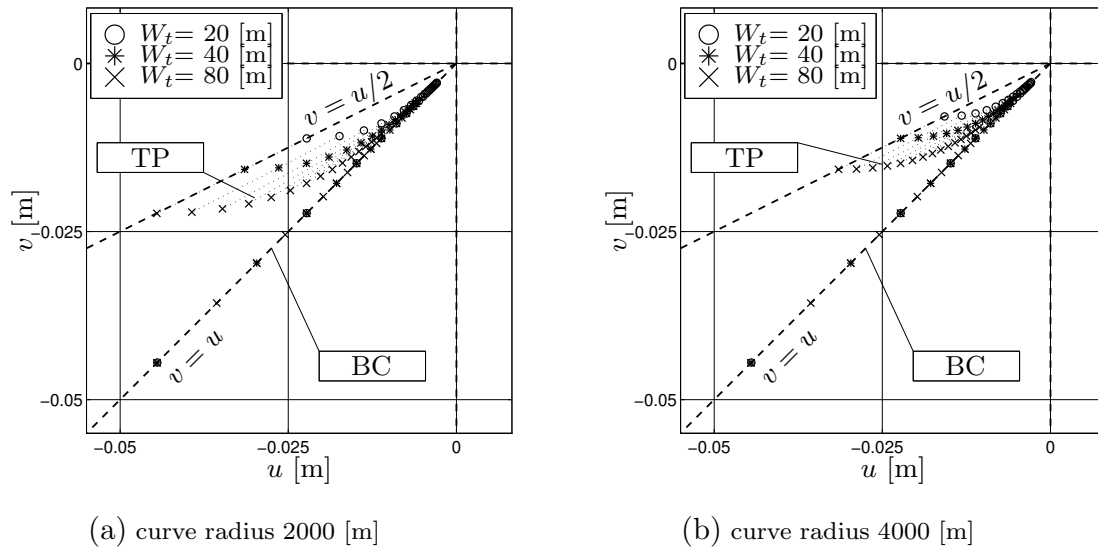
Figure 10.10: Successive projections of the tangent point (TP) and the point marking the beginning of the curve (BC). The curve is approached from an initial distance of 750 [m] to the start of the curve in steps of 75 [m]. Only the lower-left corner of the display is shown; the screen center is marked by the dashed lines ($u = v = 0$).

10.5 Experiment X6

Pilot decision making and control behaviour in the curve interception manoeuvre is determined by the dynamic properties of the aircraft and the characteristics of the presented visual information. Experiment X6 was conducted to examine the effects of both the aspects on the pilot timing strategies. The empirical study focuses on the anticipatory – open loop – curve interception behaviour, that requires an approach that is significantly different from the one applied in previous investigations reported in this thesis.

METHOD

Subjects and instructions to subjects   Five subjects (A-E) participated in the experiment. Their task was to control the aircraft through the tunnel during the transition from a straight to a curved trajectory. Subjects were instructed to be conservative in control activity and focus on a *well-timed* and *well-proportioned* curve interception manoeuvre.

Apparatus   The Human-Machine Laboratory was used, described in Appendix A.

Independent variables   The independent variables can be categorized in terms of the characteristics of the aircraft and the tunnel display. To examine the effects of the *aircraft characteristics*, two aircraft types were selected representing a large (sluggish) and a small (quickly responding) aircraft. Following the paper-pilot simulation study of §10.3, models of the Airbus A300 and the Cessna Citation 500 were used. Whereas the simulations indicated that the aircraft velocity did not affect the roll-in manoeuvre much, the investigation into the effects of the presented information stressed its importance in the timing

of the manoeuvre. Therefore, the aircraft types were both simulated at the two velocities of the simulation study, representing the *approach* and *cruise* conditions. Concluding, two aircraft types were simulated at two different aircraft velocities, yielding *four* independent experimental conditions based on the perspective of aircraft manoeuverability. As far as the *tunnel display characteristics* are concerned, the information analysis of §10.4 revealed that there exists a clear distinction between the function of the tunnel frames and the longitudinal lines connecting them. The expansion of the approaching frames conveys Time-to-Contact (TTC) – *time*-related – information. When no frames are presented, the tunnel contour allows a pilot to use the relative displacement of the curve tangent point on the display, the motion of which is determined by the *distance* to the curve transition. Based on these considerations, three different tunnel geometries will be applied in the experiment (Fig. 10.11):

1. <u>Disp</u>lay **A**, the *baseline* tunnel. In this display, the tunnel frames are positioned at equal distances from each other, and there is always a tunnel frame present in the transition plane between the straight and the curved section of the trajectory.

2. <u>Disp</u>lay **B**, the *trunk* tunnel. This tunnel has the same properties as Display **A**, except for the fact that <u>no</u> tunnel frames are displayed at all.

3. <u>Disp</u>lay **C**, a display similar to Display **A**, but with two distinct properties:

   (a) The distances between the individual frames are not fixed, but chosen in a (quasi-) random manner.
   (b) A tunnel frame is not always present at the transition plane between the straight and the curved section of the trajectory.

Another tunnel display property that is of interest is the tunnel size. The tunnel size could affect (i) the subjective velocity of egomotion (Chapter 3); (ii) the path-following accuracy (Chapter 5); (iii) the time at which an approaching tunnel frame disappears from the screen (TTC_{min}: Eq. 10.3); and (iv) the characteristics of the tangent point (§10.4). To examine these effects in a curve-transition task, two tunnel sizes – 20 and 40 [m] – were included in the experimental design. Concluding, three tunnel geometries and two tunnel dimensions are varied in the experiment, resulting in *six* independent experimental conditions based on the viewpoint of manipulating the visual sources of information.

Experimental design   A full-factorial of the four aircraft manoeuverability conditions and the six visual information conditions yields a total of 24 experimental conditions.

Procedure   The experiment focuses on the timing of the curve interception manoeuvre. Earlier experience in studying pilot timing strategies (Mulder et al., 1999) learned that in order to achieve satisfactory statistical evidence, the number of measurement runs should be rather large. Therefore, a measurement run must be designed such that many of them can be conducted within a reasonable amount of time. Because the simulation study showed that the roll-in manoeuvre is generally completed within 10 to 15 seconds, there is no reason to make the measurement run too long. The procedure is explained

(a) Display **A**   (b) Display **B**   (c) Display **C**
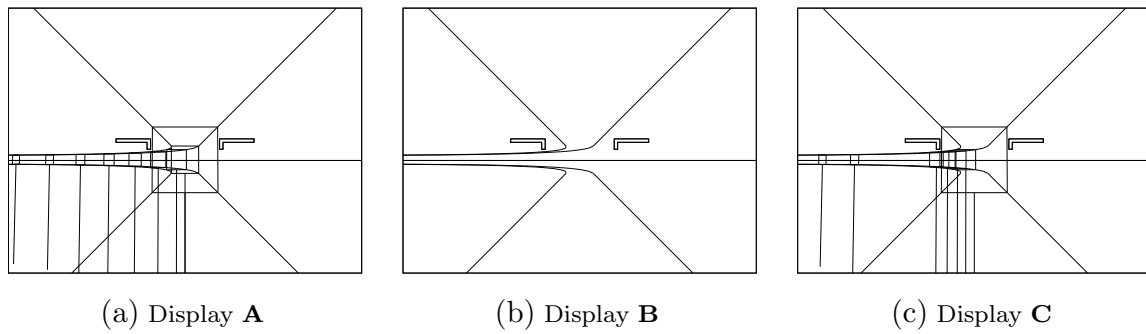
Figure 10.11: The displays of Experiment X6: Display **A**, the default tunnel; Display **B**, the tunnel without frames; Display **C**, the tunnel with frames at irregular distances.
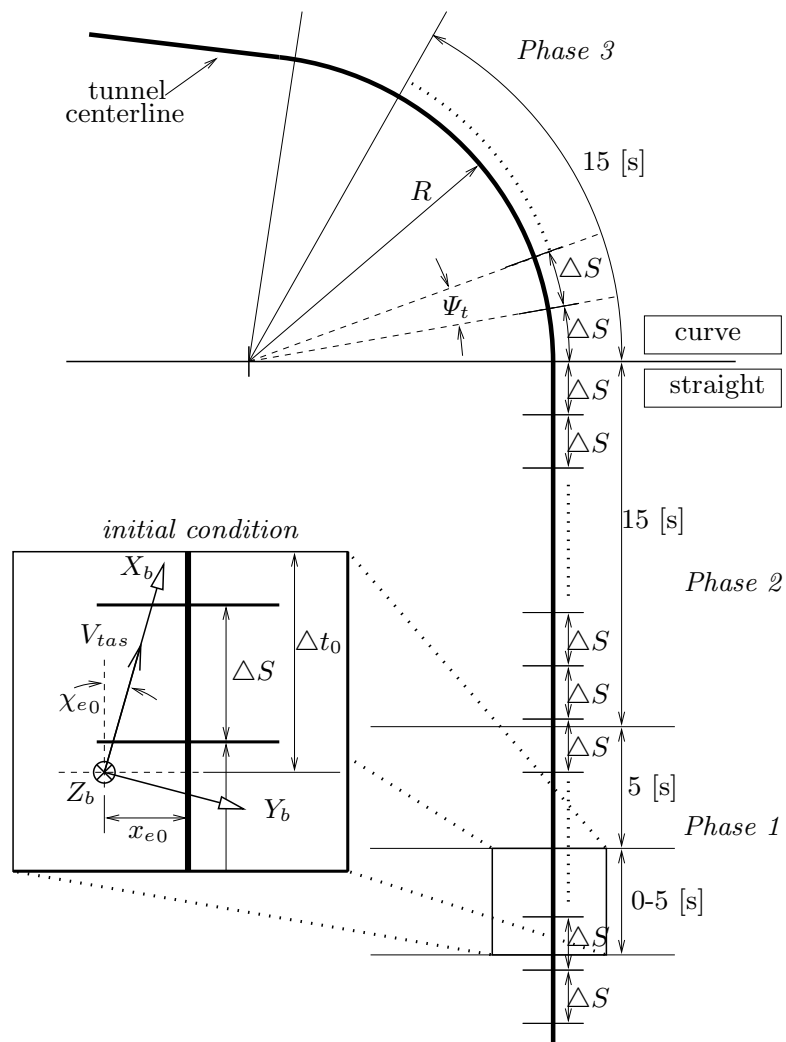

Figure 10.12: Bird's eye view of the tunnel geometry and the definition of the initial condition.

using Fig. 10.12, that shows a bird's eye view of the situation. At the start of every run, the aircraft is positioned well in advance of the curve on a straight section of the trajectory. A non-zero initial condition of the asymmetrical motion is chosen randomly over all conditions, as will be discussed below. Because of the non-zero initial condition, a pilot must first stabilize the aircraft motion with respect to the reference trajectory, resulting in a stationary recti-linear flight condition (*Phase 1*). With the curve approaching, a pilot determines the time at which the curve interception manoeuvre is initiated (*Phase 2*). After initiation of the manoeuvre, the aircraft rolls into the turn to follow the constantly curved section, leading to a stationary curvi-linear flight condition (*Phase 3*).

Dependent measures   The pilot task is to conduct a well-timed curve initiation manoeuvre with maximum performance. Three categories of dependent measures are defined:

 (i) *Performance*-related data, that can give an indication on the accuracy of the manoeuvre and the control activity of the pilot. These are similar to the time-domain data (standard deviations etc.) discussed in previous chapters.

 (ii) *Timing*-related data, depicting the moment of initiating the manoeuvre relative to the start of the curve, measured in time (T_{BT}) or distance (D_{BT}).

 (iii) *Manoeuvering*-related data, typifying the curve initiating manoeuvre. These variables will be introduced below.

The three categories characterizing the pilot response all contain several variables – introduced below – that will act as the dependent measures in the statistical analysis.

Description of the experiment simulation

Aircraft models   The two aircraft types were simulated using the *stability-augmented* models applied in the simulation study. Only the asymmetric (lateral-horizontal) aircraft motions were simulated; the symmetric aircraft motions and the aircraft velocity were fixed to their initial conditions (Table 10.1). Because the stability-augmented aircraft showed only negligible side-slip, pilots could control the aircraft using aileron only.

Atmospheric disturbances   No external disturbances (wind or turbulence) acted on the aircraft. This allowed pilots to fully concentrate on the curve transition manoeuvre.

Initial condition   When the initial distance to the curve is fixed for all conditions, pilots could in theory *cheat* their way through the experiment by simply starting to count (1, 2, 3, ...) when a run begins. To prevent this, the aircraft was positioned at a random distance $D_0 = (20 + \triangle t_0)\, V_{tas}$ (in [m]) before the curve (Fig. 10.12). The time interval $\triangle t_0$ is chosen randomly from a uniform distribution ($\triangle t_0 \sim \mathcal{U}(0.0, 5.0)$ [s]). The 20 [s] interval acts as a buffer to provide the pilot enough time to achieve a recti-linear stationary flight condition well before the turn. The initial condition has a lateral position error x_{e0} and a track-angle error ψ_{e0} that are both randomly selected from uniform distributions ($x_{e0} \sim \mathcal{U}(-2.5, 2.5)$ [m]; $\psi_{e0} \sim \mathcal{U}(-1.5, 1.5)$ [deg]). An additional constraint is that both

the variables have unequal signs, i.e. at the start of each run the aircraft will always move towards the reference trajectory. The aircraft roll angle has a zero initial value ($\phi_0 = 0$).

Measurement interval   All variables of interest were recorded during a 30 [s] interval: 15 [s] before and 15 [s] after the start of the curve (Fig. 10.12). A single run takes approximately 35 to 40 [s]. All 24 experimental conditions were repeated 12 times: four training runs and eight measurement runs. The experiment lasted one day for each subject.

Tunnel geometry   The main variable of interest in the geometrical definition of the tunnel is the positioning of the tunnel frames, defined in terms of the intermediate frame-distance $\triangle S$ (in [m]). In Chapter 3 it has been discussed that a curved section of the tunnel display is not really curved, but is approximated by a set of straight lines connecting points on the curve as determined by the relative change in heading Ψ_t. Although a smaller Ψ_t improves the accuracy of the projected curve, making this quantity too small would lead to unacceptably low display update-rates. Here Ψ_t is set to 2.5 [deg] yielding a minimum intermediate frame distance $\triangle S$ of $2.5\frac{\pi}{180}R$ with R the curve radius depending on the aircraft/velocity conditions (Table 10.1). When $\triangle S$ is known, for every aircraft/velocity condition the evenly spaced and *potential* positions of the tunnel frames can be computed, starting from the transition between and into the direction of the straight and curved sections of the trajectory (see Fig. 10.12). Depending on the experimental (display-) condition a frame is placed at that position. In case of Display **A**, the tunnel frames are positioned at an intermediate distance of $3\triangle S$, starting with the frame marking the curve transition and subsequently into the curved and straight sections of the trajectory. The situation is different for Display **C**, where the frames are positioned at intermediate distances $k\triangle S$, with k a random integer, such that the mean and standard deviation of all intermediate distances will be $3\triangle S$ and $1.5\triangle S$, respectively.[3] The (quasi-) random positioning of the tunnel frames yields a tunnel geometry with irregular frame distances. To prevent a pilot to adopt his control strategy to any specific irregular frame positioning (especially near the curve transition), five different tunnel geometrical definitions were generated for each of the four aircraft/velocity combinations for Display **C**. These geometries where randomized over the experiment. Display **B** has no tunnel frames at all and frame irregularity is not important. Summarizing, for Displays **A** and **B** four different tunnel geometries were generated, and 20 different tunnel geometries were generated for Display **C** (five for each of the four aircraft/velocity combinations).
Finally, only curves to the left were conducted. The tunnel downslope angle Γ_t was zero.

Estimation of the *timing* and *manoeuvering*-related quantities

The variables involving *timing* are not as simple to measure as the performance variables. In common stimulus-response (SR) experiments where subjects have to press a button or keyboard to trigger some response, the subject of measuring response timing is trivial

---

[3]Putting the intermediate distances between successive tunnel frames in a vector results in:
$\underline{d}_A = [3\ 3\ 3\ 3\ldots 3]\triangle S$ for A ($\mu(\underline{d}_A) = 3\triangle S, \sigma(\underline{d}_A) = 0$), and:
$\underline{d}_C = [3\ 2\ 1\ 4\ldots 2]\triangle S$ for C ($\mu(\underline{d}_C) = 3\triangle S, \sigma(\underline{d}_C) = 1.5\triangle S$).
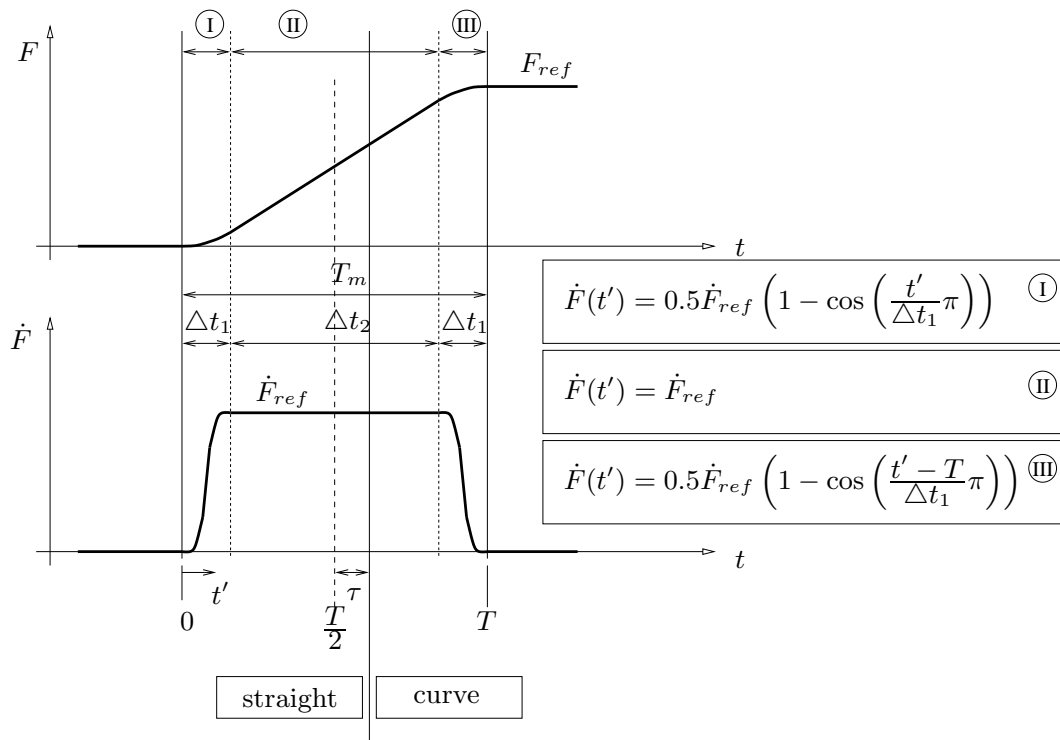
Figure 10.13: The reference function F (top) used to determine the time-related quantities. The reference function F is defined using its derivative $\dot{F}$ (bottom), with the definition of the latter function in time as indicated in the formula-boxes.

(Mulder et al., 1999). In the experiment studied here, however, a pilot is continuously controlling the aircraft and the open loop initiation of the curve interception manoeuvre is summed with the pilot closed loop regulating response (Mulder, 1995). It is clear that in this particular experiment it is important to obtain a reliable estimate of the time at which a pilot decides to start the manoeuvre. To obtain this estimate, a number of variables was considered as candidates: (i) the aileron control signal that is in fact the *only* real pilot output signal measured, and (ii) the aircraft roll angle, or, equivalently, the aircraft yaw rate, which are the *only* aircraft states that require a clear change in reference condition. Experiments showed that the aileron control signal did neither lead to accurate nor reliable results. The main reason was that the signal was rather noisy and although the pilot curve interception response could be identified visually from a particular aileron control time history, it was difficult to determine the exact moment the response started. Therefore, the other two signals were used in an attempt to develop a computer algorithm that could provide a reliable estimate of the T_{BT}.

Computer algorithm   The algorithm is based on fitting a reference function F to a measured time response R of either one of the two variables ϕ or r. The reference function of Fig. 10.13 served this goal reasonably well. It is based on (and therefore closely resembles) the default roll angle response of Fig. 10.3. F is defined using its derivative $\dot{F}$,

and can be characterized by the following three variables (all in [s]):

(i) T_M, the total time of the response,

(ii) $\triangle t_1$, the time interval in which the reference function derivative increases to (start of response) or decreases from (end of response) a constant level[4], and,

(iii) $\triangle t_2$, the time interval in which the reference function derivative is constant.

Because $T_M = 2\triangle t_1 + \triangle t_2$, only two of the three variables need to be computed to obtain the reference function. When F and $\dot{F}$ are used to fit the measured time response R, one additional variable is needed to *connect* the time-base t' of the reference function to the time instant the aircraft passes the curve transition: τ (in [s]). The τ-variable marks the difference in time between the symmetry-point of the reference function and the trajectory transition point, and is defined positive when the symmetry point lies before the transition point (Fig. 10.13). Using τ, the time histories are centered around the time at which the aircraft passes the transition. The T_{BT}, an estimate of the time-before-the-turn, i.e. the time before the transition point at which the reference function *starts* can then be computed as: $T_{BT} = T_M/2 + \tau$.

Curve fitting procedure   The parameter vector in the fitting procedure contains the three variables necessary to fit the reference function to the measured response:

$$\underline{\theta}^T = [T_M \ \tau \ \triangle t_1]; \quad \text{or} \quad \underline{\theta}^T = [\text{T}_M \ \tau \ \triangle t_2]; \quad \text{or} \quad \underline{\theta}^T = [\tau \ \triangle t_1 \ \triangle t_2].$$

The criterion to be minimized is computed using the squared differences between the reference function and the measured response and their derivatives:

$$J(\underline{\theta}) = \int_{-12}^{+12} [R(\sigma) - F(\sigma)]^2 \mathrm{d}\sigma + \int_{-12}^{+12} [\dot{R}(\sigma) - \dot{F}(\sigma)]^2 \mathrm{d}\sigma. \tag{10.5}$$

The parameter-vector $\underline{\theta}$ will be computed by minimizing $J(\underline{\theta})$:

$$\underline{\theta}^{opt} = \arg\min_{\underline{\theta}} J(\underline{\theta}), \tag{10.6}$$

using a SIMPLEX algorithm (Press, Teukolsky, Vetterling, & Flannery, 1992).

Performance of the algorithm   The algorithm was examined in terms of accuracy (bias and variance) and robustness of the estimation. The time histories of the *simulation study* were used for this purpose. The algorithm showed some slight dependence on the initial condition $\underline{\theta}_0$ of the parameter vector, a problem that could be solved by repeating the fitting procedure 20 times with 20 random initial condition vectors. The final parameter estimate is defined as the median of the resulting parameter estimates. The accuracy of the estimation of the T_{BT} was satisfactory, with timing errors generally smaller than 0.15 [s]. The accuracy deteriorated slightly for the extremely slow (T_{BT} very large) or extremely fast (T_{BT} very small) manoeuvres, yielding timing errors up to 0.30 [s]. Obviously, this was due to the fact that these manoeuvres differed most from the default or

---

[4]$\dot{F} = \dot{F}_{ref}$ with $\dot{F}_{ref} = \frac{F_{ref}}{\triangle t_1 + \triangle t_2}$.

'standard' response as dictated by the reference function. The application of the yaw rate signal as the reference signal led to smaller errors in estimating the time-before-the-turn. In conclusion, the algorithm performed satisfactory for the paper-pilot simulation responses. The applicability of the algorithm for the analytic responses does not imply the same for the experimental responses. As the experimental results will show, however, there is not much of an alternative to the approach taken here. The *yaw rate response* as measured in the experiment will be used in the algorithm.

Experiment hypotheses

Based on the pre-experimental analysis discussed in the previous two sections, hypotheses can be stated which will be evaluated in the experiment described at hand. First, it can be hypothesized that due to the different handling qualities, the roll-in manoeuvre is initiated earlier for the Airbus than for the Citation. Second, due to the different tunnel geometries applied in the experiment, two distinct timing strategies are expected: one based on TTC – Strategy I – for the displays with tunnel frames (**A** and **C**) and one based on the distance to the turn – Strategy II – for the display without tunnel frames (**B**) . Third, the influence of the dimension of the tunnel can be expected to show more ambiguity due to the already mentioned fact that it affects both the subjective velocity of egomotion as the time a tunnel frame leaves the screen (TTC_{min}). Because the subjective velocity of egomotion is influenced by both the real aircraft velocity and the tunnel size, it is difficult to hypothesize beforehand what the effect of manipulating the velocity will be. It could be that when the timing of the manoeuvre is conducted using TTC, the effect of velocity is negligible. When no TTC information is available and the timing strategy is related to the distance before the turn, the velocity might have a considerable effect.

10.6   Results

10.6.1   The pilot questionnaire

Because subjects D and E were directly involved in the set-up of the experiment, only the comments of subjects A–C are used.

Realism of the simulation   The Citation model was judged (Table 10.2) to be quite realistic except for the approach-velocity condition, which was considered to lack the usual level of inherent stability. The Airbus model was judged to be less satisfactory, mainly because the roll-rates were rather small with respect to the deflection of the stick.

Sense of egomotion and perceived depth   The similarity between the level of the experienced egomotion and the sense of depth is clear from Table 10.2. Especially Display **B** resulted in a low sense of egomotion and depth. All subjects commented on a positive influence of a higher velocity, which can be attributed to the increasing magnitudes of the dynamic stimuli. No effects were reported concerning the tunnel size. The irregularity

Table 10.2: Summary of results from a pilot questionnaire (X6).

How would you describe the level of *realism* of the simulated [aircraft] dynamics?						
		very realistic	realistic	average	unrealistic	very unrealistic
Citation	approach	·	1	1	1	·
Citation	cruise	1	1	·	1	·
Airbus	approach	·	1	1	1	·
Airbus	cruise	·	·	1	2	·

How would you describe the strength of the experienced *egomotion*, i.e. did you have a strong feeling you were moving through a three-dimensional world or did you not?						
	width	very strong	strong	average	weak	very weak
Display *A*	20 [m]	1	2	·	·	·
	40 [m]	1	2	·	·	·
Display *B*	20 [m]	·	·	1	2	·
	40 [m]	·	·	·	3	·
Display *C*	20 [m]	·	1	2	·	·
	40 [m]	·	1	2	·	·

How would you describe the strength of the sense of *depth* in the display, i.e. did you have a strong feeling you were looking ahead into a three-dimensional world or did you not?						
	width	very strong	strong	average	weak	very weak
Display *A*	20 [m]	2	1	·	·	·
	40 [m]	2	1	·	·	·
Display *B*	20 [m]	·	·	1	2	·
	40 [m]	·	·	1	2	·
Display *C*	20 [m]	1	2	·	·	·
	40 [m]	1	2	·	·	·

of the tunnel frames (Display **C**), leading to larger time periods in which no frames are passed, was commented as to decrease the sense of forward motion.

Display characteristics   Concerning the *timing strategies*, all subjects reported a strategy of estimating the time before passing the frame marking the beginning of the curve for Display **A**. They did not mention any influence of either the velocity or the tunnel size. The timing of the Airbus manoeuvre was somewhat more conservative – earlier – than that of the Citation. Subjects reported a mixture of two strategies for Display **B**. They commented on the useful motion of what is in fact the tangent point, especially with respect to the aircraft symbol. Another source of their interest was the estimate of the start of the curve, an estimate that improved for smaller tunnels. The timing strategy with Display **C** was reported to be similar as that with Display **A**, i.e. subjects tried to estimate the time left to passing the beginning of the curve. When a frame was present on the transition point, the task was considered easier. When no frame was present near the curve transition, subjects reported to use the experience gained with Display **B**, i.e.
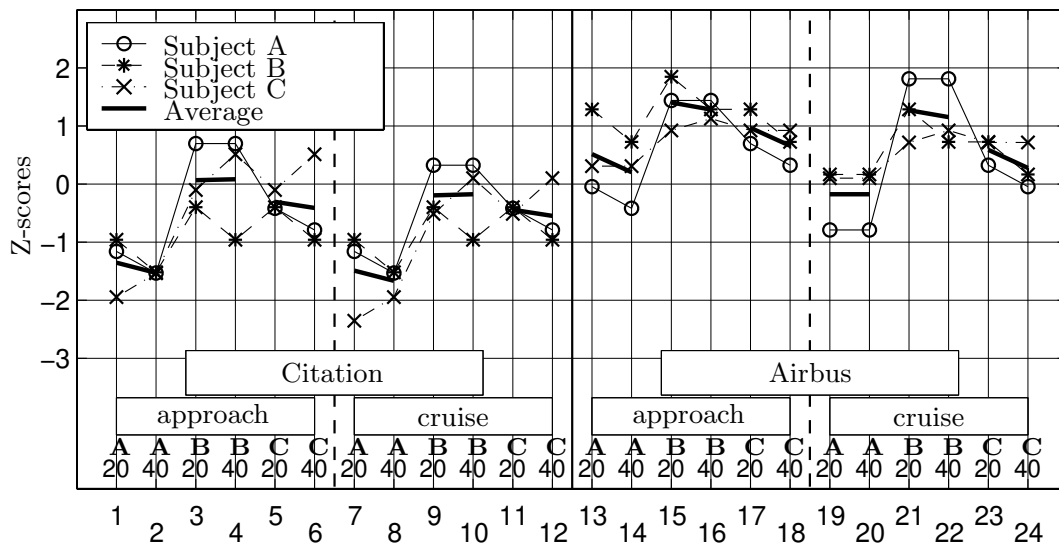
Figure 10.14: Z-scores of the effort ratings for all conditions of Experiment X6. In this figure and the following, the insets show the two aircraft types and the two velocity conditions for each aircraft. The codes **A** to **E**, representing the display types, and the tunnel widths are shown in the bottom of the figure. The experimental conditions are illustrated below the figure.

to estimate the start of the curve and also to use the motion of the tangent point. Generally, subjects did not appreciate the randomization of the intermediate frame distances in Display **C**. They continued to use the time-related strategy anyway, even when there were no frames positioned near the curve transition. In the latter case, subjects reported to use the distance-related information as a backup.

Effort ratings   Because the ratings for the Airbus are considerably higher than those for the Citation (Fig. 10.14), the Airbus was more difficult to control. For all aircraft/velocity conditions the ratings for Display **B** are higher than those of Display **C** and substantially higher than those of Display **A**. This clearly shows the increasing difficulty in performing the task with respect to the default tunnel (**A**), when the frames are positioned on irregular distances (**C**), or when there are no frames presented at all (**B**). Only marginal differences exist for (i) the lower effort for the cruise-velocity conditions vs. the approach-velocity conditions, and (ii) the increasing effort for the small tunnel conditions.

Pilot suggestions   With respect to the experiment itself, subjects commented on the lack of accurate roll angle information. They found this especially important because a well-performed manoeuvre required an accurate control of roll angle and roll rate. Although the horizon did explicitly show this information, pilots recommended the use of an additional analog roll pointer display. Three suggestions were made, having in common the *explicit* presentation of the moment of initiating the curve interception manoeuvre:

(i) The use of an additional frame with a different colour, positioned on the exact

location where the manoeuvre should be started.

(ii) The gradual rotation of the tunnel frames with a roll angle that equals the roll angle necessary for a proper roll-in manoeuvre. In other words, the tunnel frames should be rotated to provide a pictorial reference of the roll angle in a spatio-temporal format. This alternative was discussed in (Grunwald, 1984).

(iii) The use of a *flight-path predictor* that pictorially presents the necessity to take action when approaching the curve. This option has been discussed in (Grunwald, 1984, 1996a, 1996b).

In short, pilots prefer a clear *command* with respect to the timing of the manoeuvre. Because subjects reported a rather high level of task difficulty, such command information could indeed be mandatory for an acceptable level of pilot workload.

10.6.2 Time histories

The time histories of the main aircraft state variables as recorded during the experiment are shown in Fig. 10.15. Although quite some variation is present in these responses, they are similar to those obtained in the paper-pilot simulation study. The figure exemplifies the difficulty in determining the moment the pilot initiates the curve transition manoeuvre from the aileron deflection signal δ_a. Therefore, the yaw rate responses are used to determine this moment, using the response-fitting procedure discussed in §10.5. When examining the responses closer it appears that, generally, the motion of the aircraft is well-aligned with the straight section before the curve ($\psi_e \approx 0$). Pilots tend to initiate the leftward curve with the aircraft positioned slightly to the right of the centerline, yielding a *decreasing* position error when the curve-transition manoeuvre is initiated, an effect that has also been reported in automobile driving research (Boer, 1996). In following the curved section of the trajectory, the aircraft is positioned to the inside of the curved tunnel centerline, illustrating the corner-cutting phenomenon discussed above. This behaviour is typical for all subjects and configurations in the experiment. It could be a result of the fact that only curves to the left are flown resulting in adaptation of the subjects to a given trajectory, as reported in (Grunwald, 1996a; Theunissen, 1997).

10.6.3 Statistical analysis

A mixed-model Analysis of Variance is conducted with the variable *pilot* (5 levels) acting as a random variable. All other independent measures, i.e. the aircraft type (A) (2 levels), the aircraft velocity (V) (2 levels), the (D) (3 levels) and the tunnel size (W) (2 levels) acted as fixed variables. Table 10.3 summarizes the results of the full-factorial mixed-model ANOVA for all performance, timing and manoeuvering-related variables. Effects involving replication were not significant for any of the variables examined, which indicates that no significant changes in pilot behaviour occurred over time.
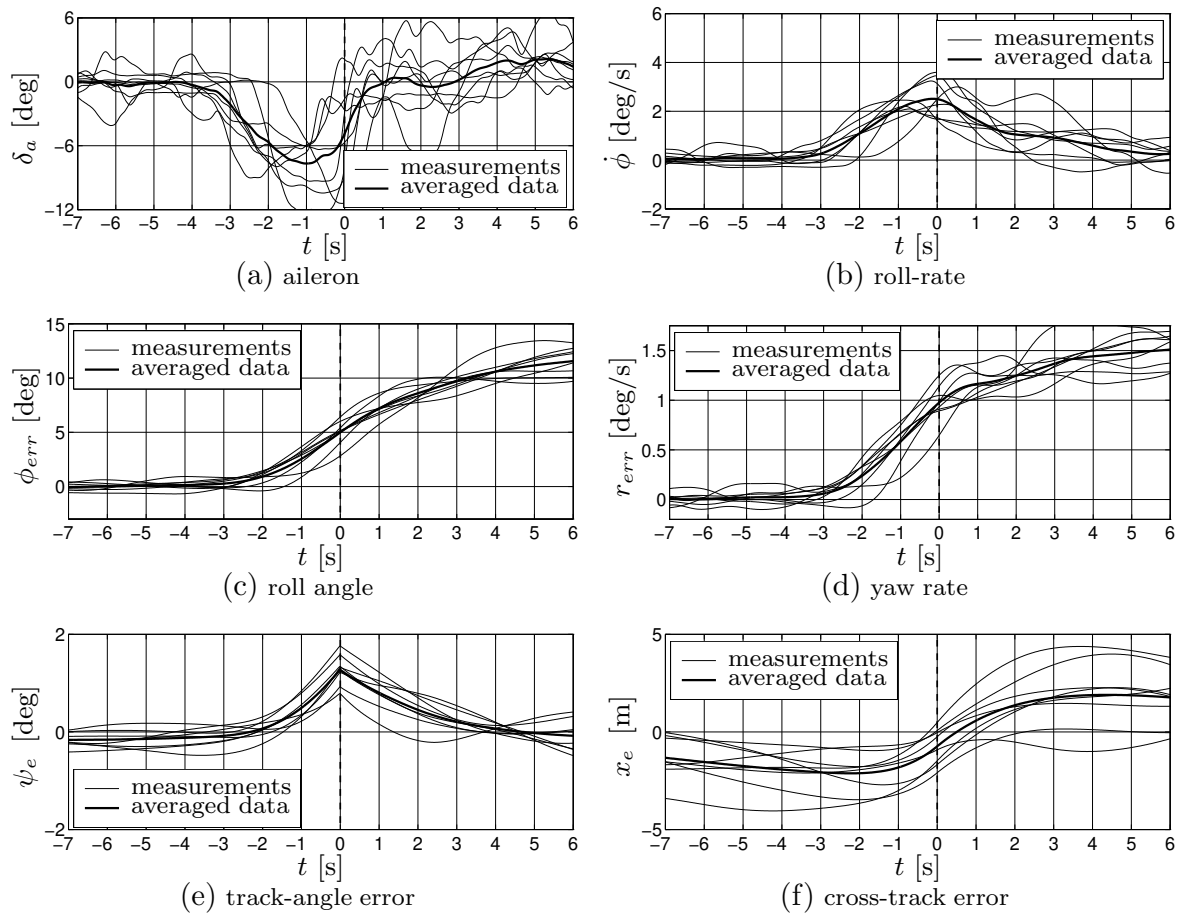
Figure 10.15: Time histories of measured and averaged data. Subject A, configuration 13 (Airbus A300, approach velocity, Display **A**, tunnel size 20 [m]).

Performance-related data

The following seven variables were recorded during the 30 [s] measurement interval:

- The aileron control signal δ_a (in [deg]) and its derivative $\dot{\delta}_a$ (in [deg/s]), depicting *pilot control activity*.

- The aircraft roll-rate $\dot{\phi}$ (in [deg/s]), the roll angle error ϕ_{err} (in [deg]) and the yaw rate error r_{err} (in [deg/s]), all illustrating *curve-transition accuracy*.

- The track-angle error ψ_e (in [deg]) and cross-track error x_e (in [m]), representing *path-following accuracy*.

The roll angle error signal ϕ_{err} is defined as the difference between the measured roll angle response and the *ideal* step response function as dictated by the curve (from 0 to ϕ_c at curve transition). The same holds for the yaw rate error signal r_{err} (from 0 to r_c = 1.5 [deg/s] at curve transition). Because experience with following curved trajectories (Chapter 8) showed that biases might evolve in the cross-track error, both the standard

Table 10.3: Results of a full-factorial ANOVA on the variables involving performance, timing, and manoeuvering-related data (in this table '★★', '★' and '∘' represent significance levels of $p \leq 0.01$, $0.01 < p \leq 0.05$ and $0.05 < p \leq 0.10$, respectively).

	performance								timing		manoeuvre	
	δ_a	$\dot{\delta}_a$	$\dot{\phi}$	ϕ_{err}	r_{err}	ψ_e	$x_e\text{-S}$	$x_e\text{-R}$	T_{BT}	D_{BT}	$\triangle t_1$	$\triangle t_2$
main effects												
A	★★	∘	★	·	∘	∘	·	·	∘	★	★	·
V	★	·	★★	★★	★	★★	·	·	·	★	·	★
D	·	·	∘	∘	∘	·	·	★	·	·	∘	·
W	★	★	★★	·	·	★★	★★	★★	★★	★★	★	★
2-way interactions												
A×V	★	·	·	·	★	★★	·	·	·	·	·	★★
A×D	·	·	·	·	·	·	·	∘	★	★	·	★
A×W	★	·	★	★★	★	·	·	·	·	·	·	·
V×D	·	·	·	·	·	·	★	★★	★	·	·	·
V×W	·	·	·	·	·	∘	·	★	·	★	·	·
D×W	·	·	★	·	★	·	★	★★	★★	★★	∘	★★
3-way interactions												
A×V×D	·	·	·	·	·	·	·	·	·	·	·	·
A×V×W	∘	·	·	·	·	·	·	·	·	·	·	·
A×D×W	·	·	·	·	·	·	·	·	·	·	·	·
V×D×W	·	·	·	·	∘	∘	·	★★	·	·	·	·
4-way interaction												
A×V×D×W	·	·	∘	·	·	·	·	·	·	·	·	·

deviation as the root-mean-square of this variable will be examined. The means and the 95% confidence limits of the dependent variables are shown in Figs 10.16(a) to 10.18(b).

Pilot control activity   Fig. 10.16(a) shows that pilot control activity is higher for the Airbus than for the Citation (δ_a: $F_{1,4}=49.919$, $p < 0.01$; $\dot{\delta}_a$: $F_{1,4}=6.528$, $p=0.063$). The small tunnel also yields an increasing control activity (δ_a: $F_{1,4}=20.011$, $p=0.011$; $\dot{\delta}_a$: $F_{1,4}=10.359$, $p=0.032$). For the high-velocity conditions, the aileron STD is significantly lower ($F_{1,4}=11.071$, $p=0.029$), an effect that is stronger for the Airbus than for the Citation as judged by the A×V-interaction. Although pilot control activity is somewhat smaller for Display **B**, no effects involving the displays (D) were found statistically significant.

Curve-transition accuracy   Fig. 10.16(b) shows an increasing roll-rate for the high-velocity conditions ($F_{1,4}=37.809$, $p < 0.01$) and a decreasing roll-rate for the Airbus ($F_{1,4}=13.058$, $p=0.023$). Furthermore, the small tunnel size conditions lead to higher roll-rates ($F_{1,4}=37.334$, $p < 0.01$). Only a marginal effect of the displays (D) was found ($F_{2,8}=3.761$, $p=0.071$) that is due to a lower roll-rate for Display **B**, especially for the large tunnel (accounting for the D×W-interaction). As Figs 10.17(a) and 10.17(b) show, a larger velocity leads to an increasing roll angle error ϕ_{err} ($F_{1,4}=341.552$, $p < 0.01$) and to a decreasing yaw rate error r_{err} ($F_{1,4}=21.020$, $p=0.011$). For the low-velocity conditions, the Air-

(a) aileron

(b) roll rate
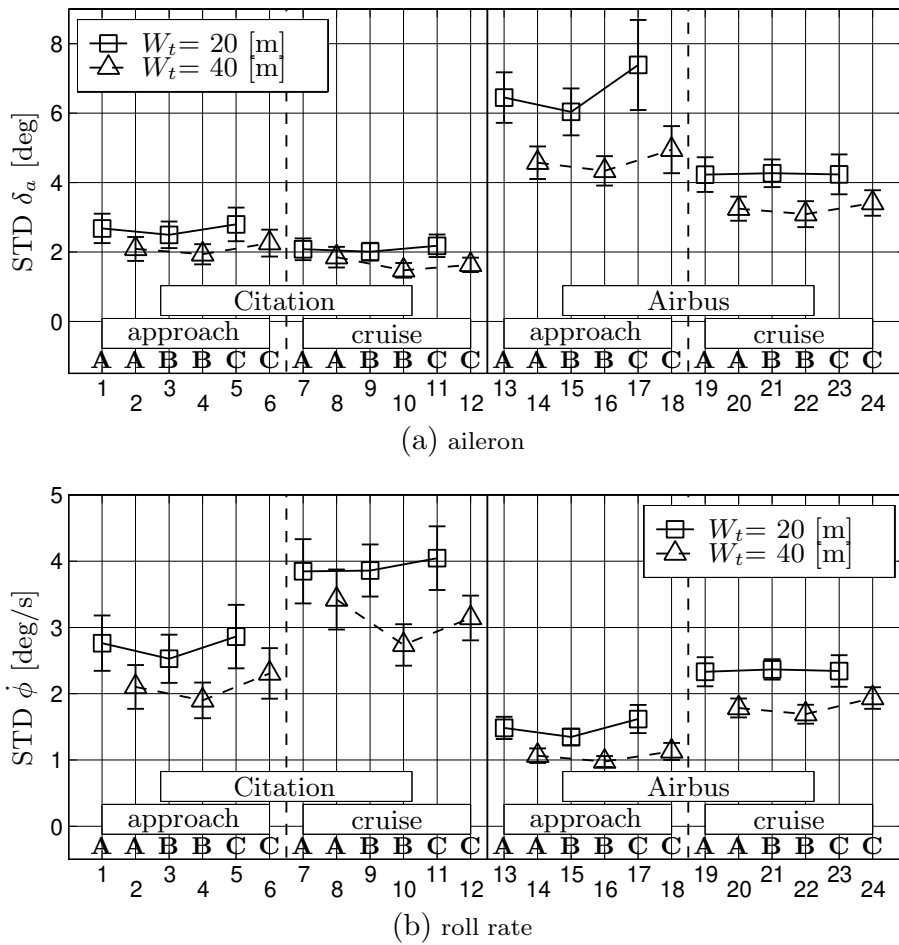
Figure 10.16: The means and 95% confidence limits of the STDs of the dependent measures (all subjects).

bus leads to smaller yaw rate errors (main effect A: $F_{1,4}=5.229$, $p=0.084$, and the A×V-interaction). Display **B** led to lower roll angle errors ($F_{2,8}=3.5439$, $p=0.079$) and yaw rate errors ($F_{2,8}=3.796$, $p=0.069$), both with only borderline significance. The A×W-interactions for both the roll angle error as the yaw rate error are caused by the fact that the effect of the tunnel size is strong for the Citation and virtually absent for the Airbus. The tunnel size had no influence at all for Display **B**, causing the D×W-interaction.

Path-following performance Figs 10.18(a) and 10.18(b) show the 95% confidence limits for the track-angle error ψ_e and the RMS of the position error (x_e-R), respectively. It follows from Table 10.3 that x_e-R has more pronounced effects of the independent variables than the STD of the position error (x_e-S). A smaller tunnel yields improved path-following performance in terms of both x_e-S ($F_{1,4}=45.125$, $p<0.01$) and x_e-R ($F_{1,4}=50.850$, $p<0.01$). The display has a significant effect on x_e-R ($F_{2,8}=6.150$, $p=0.024$), which is caused by the decreasing performance for Display **B** for the larger tunnel (D×W-interaction). The aircraft velocity has no effect on performance, except for Display **B** for the large tunnel, causing the W×V and D×W×V-interactions. There only exists

(a) roll angle error

(b) yaw rate error
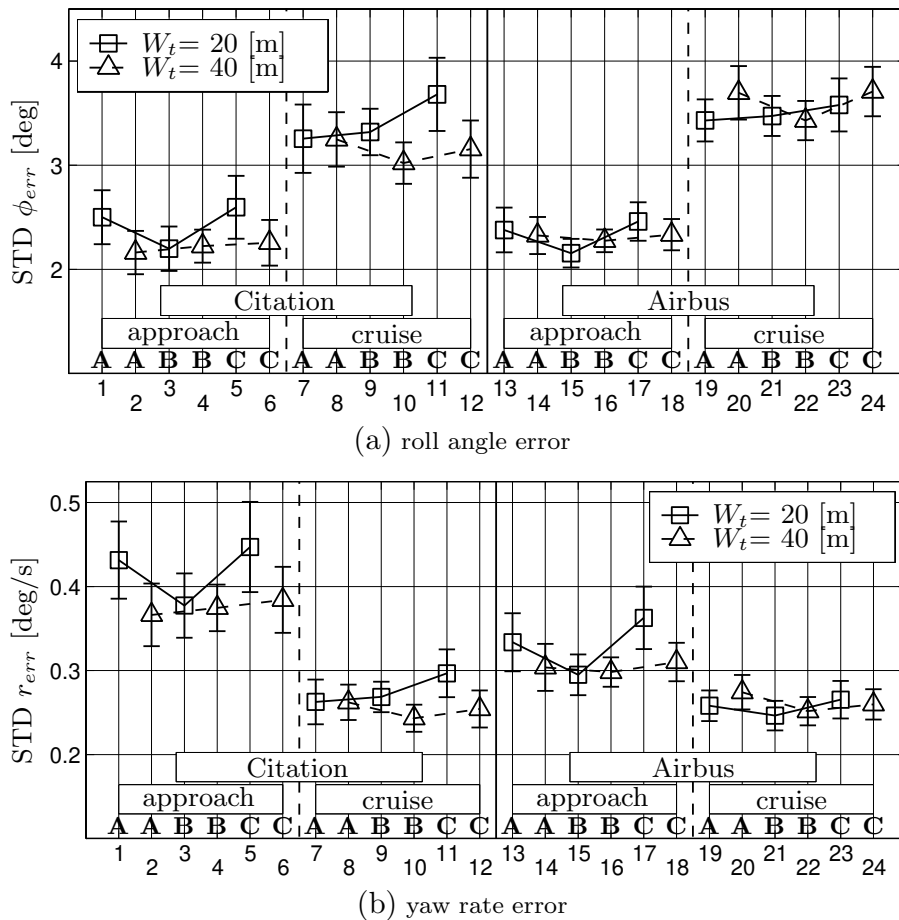
Figure 10.17: The means and 95% confidence limits of the STDs of the dependent measures (all subjects).

a statistically significant difference between x_e-S and x_e-R for the low-velocity conditions with Display **B**.

The track-angle error ψ_e decreases significantly for the small tunnels ($F_{1,4}$=27.167, p <0.01) and a significant decrease for the high-velocity conditions ($F_{1,4}$=36.775, p <0.01). Furthermore, the ψ_e for the Airbus is significantly lower ($F_{1,4}$=6.381; p=0.065), but only for the low-velocity conditions (A×V-interaction: $F_{1,4}$=37.895, p <0.01). Although ψ_e performance improves with Display **B**, this is only marginally significant for the small tunnel, low-velocity conditions (interactions V×W and D×W×V).

Timing-related data

The moment a pilot initiates the curve-transition manoeuvre can be related to the start of the curve in terms of time (T_{BT}, Fig. 10.19(a)) as well as in distance (D_{BT}, Fig. 10.19(b)).

The time-before-the-turn   The differences in the T_{BT} are relatively small, except those representing Display **B**, which are quite large indeed. They are significantly larger for the large tunnels ($F_{1,4}$= 26.555, p <0.01) and are somewhat larger for the Airbus ($F_{1,4}$=6.996;

(a) track angle error

(b) cross-track error (RMS)
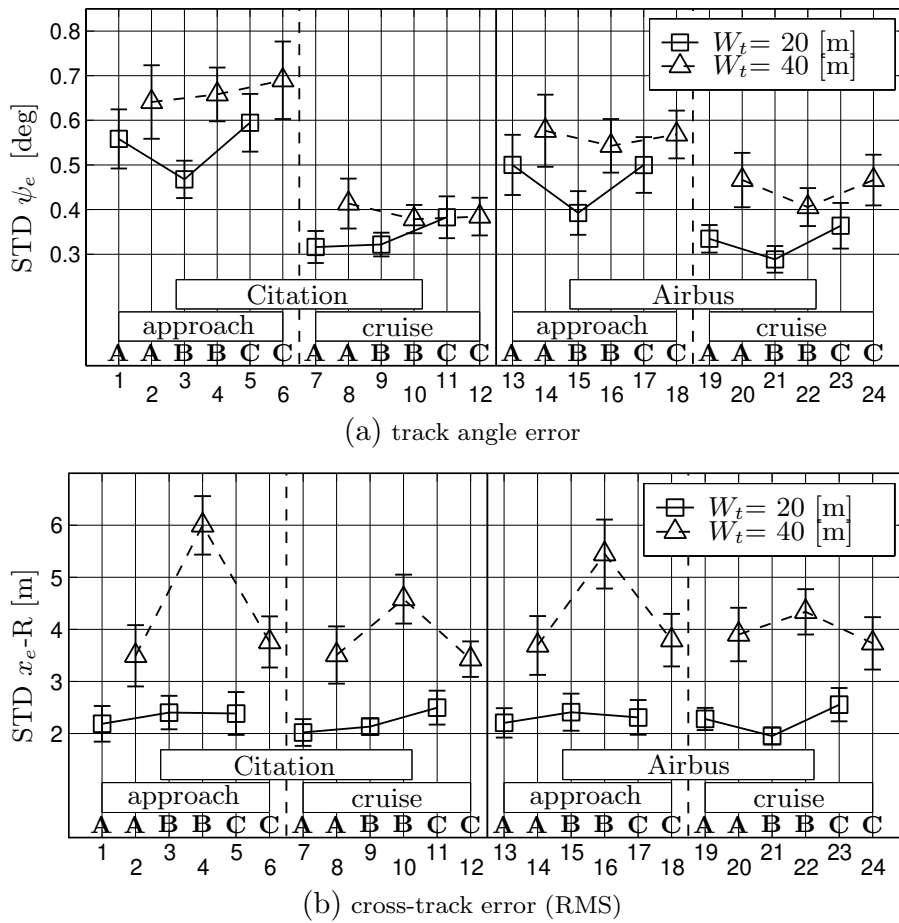
Figure 10.18: The means and 95% confidence limits of the STDs of the dependent measures (all subjects).

p=0.057). For all aircraft/velocity conditions, the T_{BT}s for Displays **A** and **C** are similar for the different velocities and become larger for the larger tunnel size conditions. On the one hand, for the small tunnel the T_{BT}s for Display **B** are similar to those of Displays **A** and **C**, but decrease significantly for the higher velocity conditions. On the other hand, for the large tunnel the T_{BT}s are markedly larger than those of Displays **A** and **C**, irrespective of the velocity. These effects cause the three significant two-way interactions. Especially Display **B** has a large effect on the T_{BT}. Moreover, the T_{BT}s for Display **B** show to be much more affected by the independent measures W and V. Some of these effects can be elucidated by examining the companion of the T_{BT}, the distance-before-the-turn D_{BT}.

Distance-before-the-turn Fig. 10.19(b) shows somewhat more variation in the D_{BT} for all displays. It increases for smaller tunnels ($F_{1,4}$=24.163, p <0.01), for the Airbus conditions ($F_{1,4}$=16.918, p=0.015), and for the high-velocity conditions ($F_{1,4}$=13.806, p=0.021). The effect of the displays (D) becomes clear when examining the significant D×W-interaction ($F_{2,8}$=15.272, p <0.01), that shows that the tunnel size only influences the D_{BT} for Display **B**. For the small tunnel the D_{BT} decreases for Display **B**, whereas for

(a) time-before-the-turn

(b) distance-before-the-turn
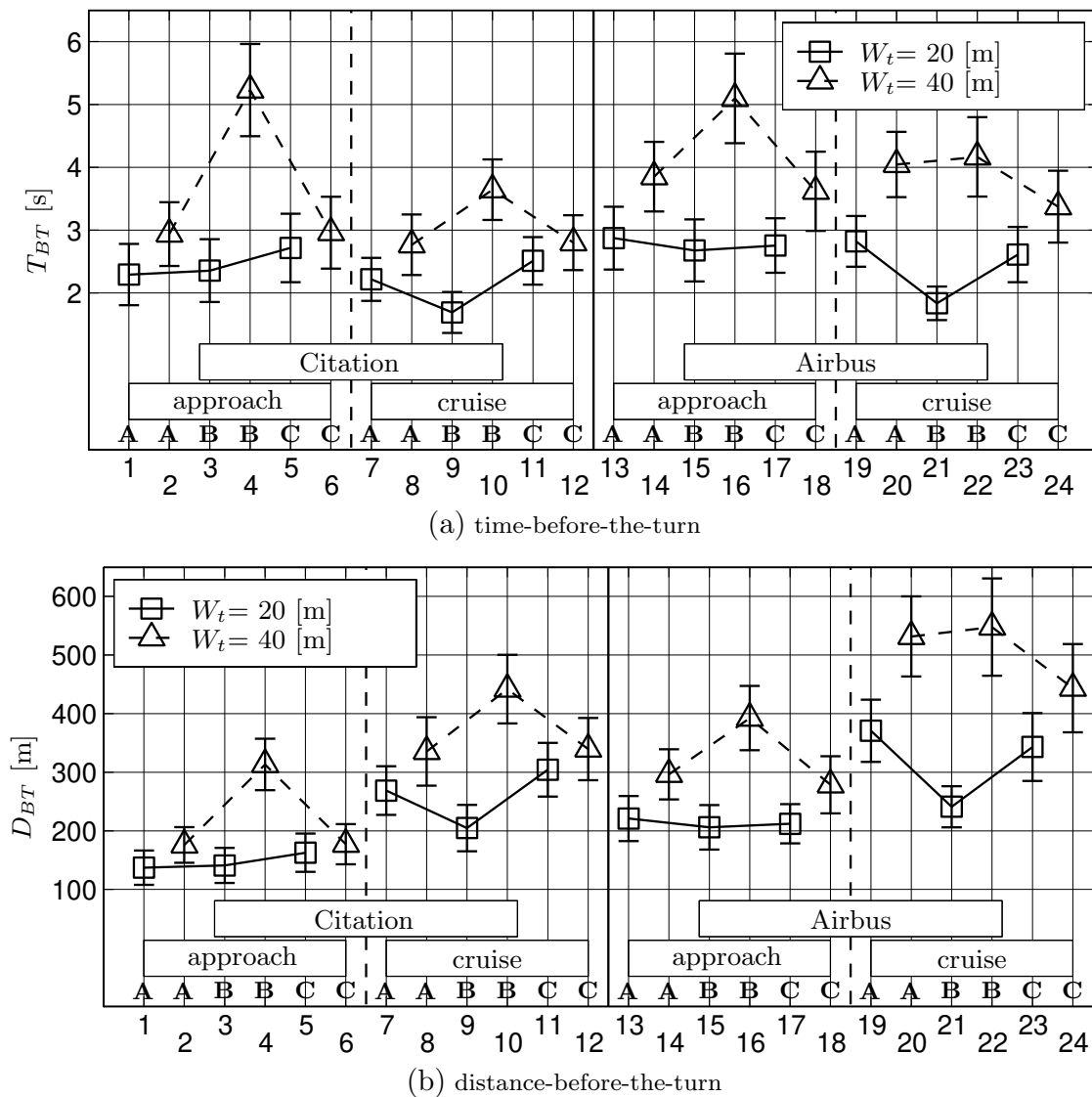
Figure 10.19: The means and 95% confidence limits of the dependent measures (all subjects).

the large tunnel the D_{BT} increases for Display **B**. The tunnel size shows no significant effects on the distance-to-the-turn for Displays **A** and **C**, although the D_{BT} becomes larger in all cases, especially in the high-velocity conditions. The relatively small differences in the D_{BT} for Display **B** illustrate a pilot tendency to initiate the manoeuvre at equal distances, dictated by tunnel size. This is especially clear for the small tunnels, for which the D_{BT} for Display **B** is more or less constant, irrespective of the aircraft or velocity conditions. The same trend, but less convincing, can be found for the large tunnels.

Manoeuvering-related data

The method of determining the time-before-the-turn from the measured yaw rate response yielded four variables ($T_M, \tau, \triangle t_1$ and $\triangle t_2$) that typify the manoeuvering style. Although

(a) manoeuvre variable $\triangle t_1$

(b) manoeuvre variable $\triangle t_2$
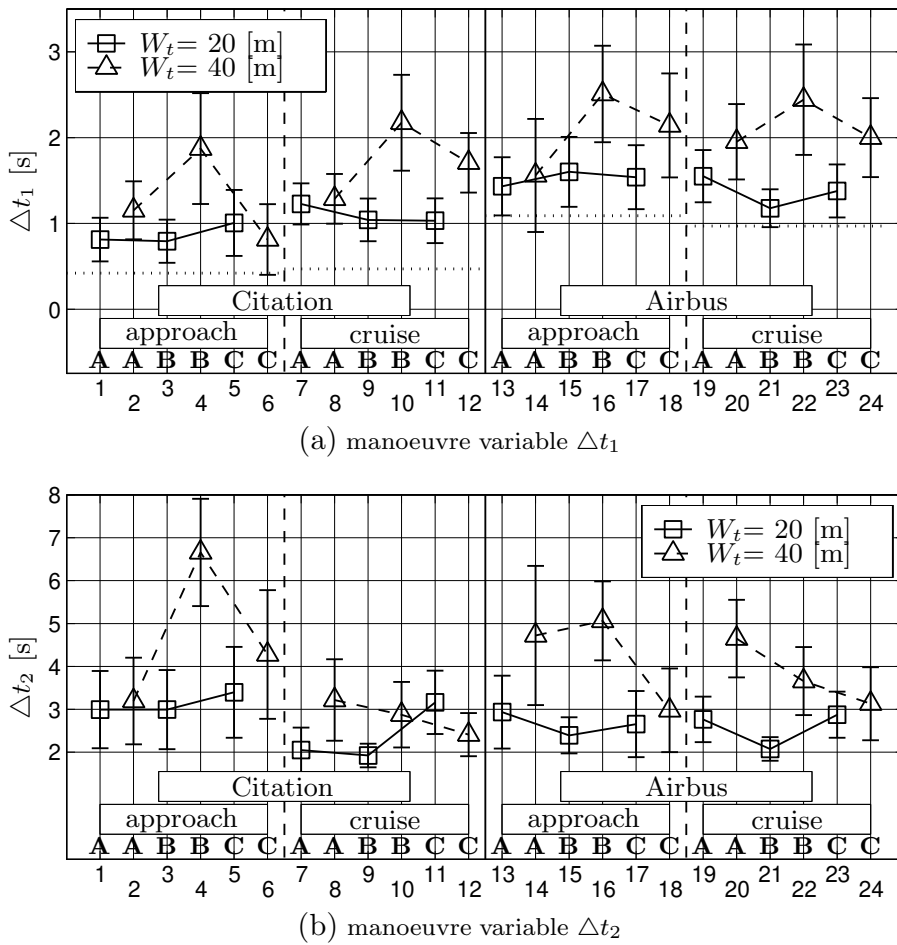
Figure 10.20: The means and 95% confidence limits of the dependent measures (all subjects). In the top figure the values of the aircraft roll subsidence time constant τ_ϕ of all four aircraft/velocity conditions are shown with the dotted lines.

the validity of these variables depends on the response-fitting procedure, on the average they provide a useful insight on the type of manoeuvre initiated by the pilot. The τ variable was generally very small (mean -0.079 [s]), indicating that on the average the *symmetry-point* of the response lay near the actual curve transition. It was independent of the type of display and the tunnel size, and was only affected, but not significantly, by the aircraft/velocity conditions. The fact that τ is almost zero is also reflected in the high correlation between the T_M and the T_{BT} (linear correlation coefficient $r = 0.961$). Hence, T_M can be approximated as twice the time-before-the-turn T_{BT}: $T_M \approx 2T_{BT}$.

Figs 10.20(a) and 10.20(b) show the means and 95% confidence limits of the variables $\triangle t_1$ and $\triangle t_2$. The values of $\triangle t_1$ are higher than the time constants τ_ϕ of the roll-subsidence modes, indicating that pilots did not control the curve-transition in a step-like manner. The onset of the roll-in manoeuvre is conducted slower (larger $\triangle t_1$) with the Airbus ($F_{1,4}$=13.531, p=0.021) than with the Citation. For smaller tunnels the manoeuvre is initiated more abruptly as indicated by the significantly lower values for $\triangle t_1$ ($F_{1,4}$=12.486,

p=0.024). Another trend is that the manoeuvre is initiated less abruptly for Display **B** for the large tunnel conditions (main effect D: $F_{2,8}$=3.542, p=0.079; D×W-interaction: $F_{2,8}$=3.730, p=0.072). The results for the variable $\triangle t_1$ match well with those of variable $\triangle t_2$, that marks the time interval during which the (fitted) yaw rate derivative is constant. Larger tunnels lead to smaller values of $\triangle t_2$ ($F_{1,4}$=15.634, p=0.017), i.e. they yield smaller values of the yaw rate (as determined by the roll-rate). Furthermore, $\triangle t_2$ decreases with the high-velocity conditions ($F_{1,4}$=11.046, p=0.029), especially for the Citation (as judged by the significant A×V-interaction). The display (D) interactions are all caused by Display **B** that yields increasing values of $\triangle t_2$, especially for the low-velocity and large tunnel conditions (D×W-interaction).

Finally, for all roll-rate and aileron responses the maximum (absolute) values were recorded and analyzed in identical manner (no figures shown). Results indicate that (i) the Airbus leads to lower roll-rates ($F_{1,4}$=15.699, p=0.017) and higher aileron deflections ($F_{1,4}$=46.529, p <0.01); (ii) the high-velocity conditions lead to larger roll-rates ($F_{1,4}$=18.650, p=0.013), and (iii) the small tunnels lead to higher roll-rates ($F_{1,4}$=33.325, p <0.01) and larger aileron deflections ($F_{1,4}$=29.321, p <0.01). No interactions of any importance were found.

10.7   Recapitulation

10.7.1   Discussion

Evaluation of the experimental hypotheses

The experimental data will be discussed in the context of the experimental hypotheses. The effects of the independent measures on the qualitative and the quantitative data are treated sequentially, focusing on the general findings.

Effects of the aircraft type   The data support the experimental hypotheses well. The roll-in manoeuvre is initiated earlier (larger T_{BT} and D_{BT}) and is conducted slower (lower $\dot{\phi}$, $\triangle t_1$ and $\triangle t_2$) for the Airbus than for the Citation. Pilot ratings suggest more difficulty in performing the manoeuvre with the Airbus. These effects can be attributed to the different aircraft handling characteristics.

Effects of the aircraft velocity   The timing of the curve interception manoeuvre, as expressed in T_{BT}, is not affected by the aircraft velocity for Displays **A** and **C**. The velocity does have a significant effect on the distance to the turn, D_{BT} with these displays. This provides strong evidence for a TTC-strategy (Strategy I) with these displays which was one of the main hypotheses of the experiment. The opposite holds for Display **B**, where the T_{BT} decreases, and the D_{BT} increases for higher velocities. For the higher velocity conditions, performance in terms of track-angle error and yaw rate error is better than for the lower velocity conditions, at the cost of more inner loop activity (larger $\dot{\phi}$ and ϕ_{err}).

These findings resemble those of the curve regulation experiment (X4, Chapter 8).

Effects of the tunnel size   As has been hypothesized, a decreasing tunnel size leads to an improved performance (smaller x_e and ψ_e), at the cost, however, of increasing control activity (larger δ_a and $\dot{\delta}_a$), a less smooth manoeuvre (smaller $\triangle t_1$ and $\triangle t_2$), and higher effort ratings. These results are similar to those reported in Chapter 5. For the large tunnels, the timing of the manoeuvre is somewhat earlier (larger T_{BT}s) for Displays **A** and **C** with respect to the small tunnel. This effect is probably caused by the fact that for larger tunnels the tunnel frames disappear from the viewplane earlier, yielding a small bias in the moment of initiating the manoeuvre.

Effects of the tunnel geometry   No significant differences in pilot timing behaviour and performance were found between Displays **A** and **C**. Timing with these displays was similar and quite consistent over the other experimental conditions. The hypothesis that a TTC-strategy has been applied for these displays can indeed be supported with the experimental data. Display **B** was affected significantly by the independent measures. Compared to Displays **A** and **C**, the roll-in manoeuvre with Display **B** was smoother (lower $\dot{\phi}$, larger $\triangle t_1$ and $\triangle t_2$), with superior performance in following the curve (ψ_e, r_{err} and ϕ_{err} smaller), but also with far worse accuracy in path-following (larger x_e-S and x_e-R). These findings correspond well with the results of the curve regulation Experiment X4 of Chapter 8. As far as *timing* is concerned, the results of Display **B** show a somewhat less convincing but still sufficient argument for the use of a distance-related strategy (Strategy II), i.e. using the tangent point and the estimate of the distance to the curve transition. This can be seen when examining the significant effects of aircraft velocity and tunnel size on the timing data. Assume that a pilot initiates the manoeuvre when the position of the tangent point on the screen exceeds a certain threshold. Then, from the discussion in §10.4 it is known that: (i) for equal curve radii (and thus equal velocity), a larger tunnel would lead to an earlier response (T_{BT} larger), and (ii) for equal tunnel size, a smaller radius (and thus smaller velocity) leads to the same effect. This corresponds well with what has been found in the experiment. Independent of tunnel size, the T_{BT} decreases for the higher velocity conditions (larger radius). Independent of aircraft velocity, the T_{BT} increases for larger tunnels. When investigating the effects together with those for the distances to the turn – the D_{BT}s – sufficient evidence is found for the distance-related strategy hypothesis, especially for the small tunnel size conditions. The pilot effort ratings support the hypothesis of two pilot timing strategies: a time-based strategy for the tunnels with frames presented (Displays **A** and **C**) and a distance-based strategy for the tunnel without frames (Display **B**). As judged by these effort ratings, initiating the manoeuvre with Display **B**, i.e. applying the distance-strategy, is considerably more difficult.

TTC as a *context-independent* cue

The experimental data confirm the hypothesis that when enough frames are positioned near the curve transition, subjects use the expansion of the approaching frames to apply a time-to-contact timing strategy. When no frames are available at or near the transition,

subjects are no longer able to apply the TTC strategy and must adopt another, yet more vulnerable, distance-related strategy. Of course, in reality one would not consider using a tunnel without frames, but in this experiment the frame-less tunnel display serves well to prove a point about the superiority of TTC information (Mulder & van der Vaart, 1998b) The experimental data clearly show that timing with the TTC strategy is independent of almost all experimental variables. For a given aircraft type the curve interception manoeuvre was initiated at approximately the same T_{BT}, independent of the velocity of the aircraft (determining the curve radius), the size of the tunnel, and the fact whether the positions of the frames near the curve were randomized or not. Without exceptions, subjects showed a consistent timing behaviour when TTC information was available. Removing the frames from the tunnel display, i.e. showing only the contours of the tunnel trajectory to be followed, results in a situation where no TTC information is available at all. The experimental data show clearly that in this case another timing strategy is used that leads to a dramatic increase in pilot timing behaviour variation. Here, the timing is not consistent and depends on the velocity of the aircraft (and thus the curve radius) and especially the size of the tunnel. In this case, the pilots' timing behaviour depends strongly on the specific context of the environment, such as the tunnel geometry.

Summarizing, the TTC strategy is superior mainly because it is independent of the *context* of the environment. The consistent timing behaviour of pilots when TTC information is available strengthens the status of the TTC as a robust strategy for timing (complex) human behaviour. The tunnel geometrical design should support pilots in adopting the TTC strategy for intercepting curves by presenting sufficient tunnel frames near the curve transition (Mulder & van der Vaart, 1998a).

Evaluation of the pilot timing measurement method

In Experiment X6, it was argued that it is important to obtain a reliable estimate of the moment a pilot initiates the open loop curve interception manoeuvre. In various other experimental efforts on aspects of human timing behaviour (Lee et al., 1983; Mulder et al., 1999) the experimental approach has been one of a classical stimulus-response experiment. Pilots were confronted with a dynamic visual scene and were required to press a button to initiate some standard or (semi-)automated response. For instance, in an experiment examining the timing of the landing flare manoeuvre (Mulder et al., 1999), subjects had to press a button when they thought the aircraft must start the flare (nose up) manoeuvre, a short time before touchdown. When the button was pressed, the aircraft simulation started an automated response, allowing no further pilot interaction. Obviously, assessing timing in these kinds of experiments is trivial. Because the interaction of a pilot and his environment is highly limited in the experimental procedure, a number of questions always arises after completing these experiments. For instance – and most prominently – what if a pilot *could* have interacted more with the environment, would the observed timing behaviour be different? Usually this is a matter of pure speculation.

In this context it is important to recall one of the principal hypotheses in Gibson's ecolog-

ical approach to visual perception, which is that perceiving and acting have a reciprocal relationship. More specifically, perceiving is regarded as the active acquiring of information about which action strategy is appropriate. Actions are modulated in order to *control the informative variables of stimulation* (Gibson, 1986). In the light of Gibson's approach, the SR-experiments are too much of an abstraction of reality; they do not support subjects to really invest in optimizing their perception and action loops. The experimental approach applied here *does* provide subjects the freedom to behave *naturally*, i.e. to adopt the same natural perception and action patterns as they would have done in reality. Clearly then, a problem of both theoretical and practical interest arises in this approach, that became clear in the development of the experiment, returning to the question addressed at the beginning of this paragraph. The computational method developed here to obtain an estimate of pilot timing is an objective method, and does not require a time-consuming and often inevitably subjective visual inspection of the data. Basically, by taking one of the aircraft state variables – the yaw rate – as a reference signal, one *inverts* the pilot and aircraft system. Naturally, one could ask oneself whether there are any differences between the moment a pilot *decides* to begin the manoeuvre, the moment a pilot *initiates* the manoeuvre by moving the control manipulator, and the moment the aircraft itself starts to move into the turn. These topics, however, are of philosophical interest and will not be further elaborated. The method chosen is a compromise between what one actually wants to measure and that what is physically possible to measure at all. For the purposes of the experiment here, where the main objective was to *compare* timing strategies – and not to obtain an absolute estimate of pilot timing at all – the method proved to be satisfactory.

10.7.2 Conclusions and recommendations

Conclusions

- The aircraft dynamic properties determine an *envelope of manoeuverability*. Within these constraints, a pilot has considerable freedom to choose the moment of initiating the curve transition manoeuvre. The results of Experiment X6 indicate that the aircraft handling characteristics do not interfere with the effects on pilot timing behaviour caused by the various tunnel display designs.
- The timing of the initiation of the curve interception manoeuvre is significantly influenced by – and can therefore be manipulated by – the design of the tunnel.
- When the tunnel frames are presented, pilots adopt a timing strategy based on the *time* resting before the beginning of the curve. The experimental results provide strong evidence for a TTC strategy for these displays, essentially because timing with these displays is unaffected by the aircraft velocity. The expanding tunnel frames convey time-to-contact information that is independent of the geometric properties of the tunnel (size), as well as those of the curve (radius). The TTC-strategy is a *context-independent* and therefore a *robust* strategy to time the initiation of the manoeuvre: independent on the geometry of the tunnel involved, or the radius of the curve to be intercepted, timing

remains the same.

- When no tunnel frames are presented pilots adopt a timing strategy based on the *distance* resting before the beginning of the curve. The changing position of the curve *tangent point* on the screen serves as the principal optical event used to trigger the curve transition manoeuvre. The experimental data provide evidence for the use of the distance-strategy, especially because the trends in the date correspond with characteristics of the tangent point. Because this strategy *does* depend on the geometry of the tunnel (size) as well as the properties of the curve (radius) this timing strategy is *vulnerable*, i.e. not robust. This leads to variation in pilot timing behaviour caused by the properties of the environment.

- The pilot questionnaire supported the existence of the two timing strategies. Furthermore, it showed that pilots prefer the time-related Strategy I over the distance-related Strategy II; the latter strategy was judged considerably more difficult.

- The effects of randomizing the distance between the tunnel frames were marginal. Timing of the manoeuvre with these displays was similar and consistent over the experimental conditions. The pilot questionnaire revealed that the task was judged somewhat more difficult when the distances were random. Generally, the presence of the tunnel frames allowed pilots to adopt the preferred TTC-strategy.

- Generally, the effects of the other experimental variables – such as the tunnel width effects, the effects of the forward velocity, and the accuracy of following a straight or curved segment of the reference trajectory – were similar to those reported in the experiments of this thesis that investigated similar properties (Experiments X1, X3, X4).

- The computational method – developed in §10.5 to obtain an estimate of the instant in time pilots initiate the curve interception manoeuvre – served well for the objective in this experiment of examining the relative differences in pilot timing behaviour.

Recommendations

- The experiment clearly illustrated the superiority of the TTC strategy. To allow pilots to adopt the preferred and robust TTC strategy, the tunnel display design should provide enough tunnel frames near transitions in the trajectory.

- Pilots suggested that in order to improve the performance of the curve interception manoeuvre, the status of the aircraft roll angle should be clearly indicated, preferably with an additional roll pointer.

- Although beyond the scope of the present experiment, pilots suggested the incorporation of *explicit command* information concerning the timing of the curve interception manoeuvre. Additional experiments should be done to examine the virtues of the suggested improvements in terms of performance and workload.

- The scope of Experiment X6 could be enhanced considerably when conducted in a moving-base flight simulator. The presence of motion stimuli could have helped pilots in controlling especially the roll rates during the manoeuvre. This would probably lead to lower roll rates measured in this experiment, having a considerable impact on the timing and performance of the manoeuvre.

Chapter 11

Conclusions and recommendations

11.1 Conclusions

Consensus in the aviation community is growing that, at last, the flexibility gained with the introduction of programmable electronic cockpit displays in the 1980s must be exploited to the full extent. The primary flight display of the future should present the aircraft guidance and navigation information in a way that is *intuitively understandable*, that *improves the pilot's situation awareness*, and that is *compatible with the pilot's control and monitoring tasks*. A strong candidate to satisfy these demands in the current and future air navigation systems is the *Tunnel-in-the-Sky* display, a perspective flight-path display that shows the trajectory to be flown in a synthetic three-dimensional world. The usefulness of the tunnel display in the pilot manual control task of guiding the aircraft along a prescribed trajectory has been the subject of this thesis. In an attempt to complement the mainstream of tunnel-in-the-sky display research, which is generally confined to *empirical* comparisons of the new, perspective, tunnel display with the conventional, planar, formats, a *theoretical* study of the tunnel display is conducted from the perspective of *cybernetics*.

In **Chapter 1** the *cybernetic approach* is introduced as an integrated, four-stage, multi-disciplinary methodology to study the fundamental properties of pilot/display interaction, centered around a theoretical analysis of information, in particular the *information used for control*. The *first* stage of the approach consists of an analysis of the pilot's tasks and the information needs to fulfil these tasks. The *second* stage investigates the optical cues that, *theoretically*, are *available to* the pilot and that, *practically*, can be *used by* the pilot for purposes of control. The *third* stage consists of empirical studies into the effectiveness of the optical cues concerning pilot perception and control. The *fourth* stage attempts to describe the measured pilot behaviour with mathematical models. In the following, the main conclusions from the *theoretical* analysis and the *empirical* studies are summarized,

followed by some general conclusions regarding the *methodology* adopted in this thesis.

11.1.1 Theory

The task analysis is described in **Chapter 2**. With a tunnel display, the tasks of guiding an aircraft along a trajectory and controlling an automobile along a road have striking resemblances, and hence, one of the first hypotheses has been that pilot behaviour is similar to that of an automobile driver. The task of following a trajectory which is presented in a three-dimensional format, allowing a *preview* ahead, is *dual*. First, the operator must keep the vehicle aligned with the trajectory in the presence of disturbances, that act as the *stochastic* inputs to the pilot/vehicle control system. Second, the operator must anticipate oncoming changes in the trajectory, which is the *deterministic* forcing function for the control system. The *boundary control* task (i.e. staying within the constraints of the tunnel or road) yields a continuum between the control strategy of continuously compensating for all vehicle deviations from the trajectory and that of neglecting these errors as long as the spatial or temporal constraints remain satisfied. A second hypothesis has been that the most important pilot control task is that of flying the aircraft along the prescribed trajectory *as accurately as possible*. It was shown that the reference trajectories could be synthesized by a *concatenation of straight and circular segments*. In the pilot task of following these trajectories, *four sub-tasks* were distinguished: (i) following a straight segment; (ii) anticipating and intercepting the circular segment; (iii) following the circular segment, and (iv) anticipating and intercepting a straight segment. The first and third sub-tasks correspond with the two main aircraft stationary flight conditions of *recti-linear* and *curvi-linear* motion, respectively. Maintaining a stationary flight condition in the presence of disturbances is referred to as a *regulation* task. Controlling a transition manoeuvre between these two reference conditions is referred to as an *anticipation* task.

In conducting the aircraft control and guidance tasks a pilot needs information about the aircraft's motion state – in terms of its attitude, flight-path and position relative to the trajectory – and about the trajectory to be followed. A study of the control-related information conveyed by the tunnel display is the subject of **Chapter 3**. The pilot perception of the transforming three-dimensional tunnel geometry has been analyzed from the perspectives of *information transfer* and *information processing*. The principal hypothesis in the study, rooted in Gibson's ecological approach to visual perception (Gibson, 1986), was that *the main stimulus of the pilot when guiding the aircraft through a restricted environment such as depicted by the tunnel display is that of an approach to a surface*. In accordance with the task analysis the information presented by the display was analyzed for the two stationary flight conditions of *recti-linear* and *curvi-linear* motion. In both the conditions the aircraft attitude and position relative to the trajectory can be perceived through the cues of *linear perspective*, cues that emerge in a *static* tunnel image. The aircraft flight-path, velocity, and temporal status relative to the trajectory can be perceived through the cues of *motion perspective*, cues that emerge in the *dynamic* tunnel image.

The tunnel display conveys a substantial number of potentially useful optical cues. The information analysis addressed the effects of the tunnel geometrical design variables on the relative usefulness of these cues. In the task of following a straight trajectory, corresponding with the recti-linear aircraft motion, the most salient cues are the *optical splay* angles (the *perspective* gradient) formed by the longitudinal lines connecting the tunnel frames, parallel to the viewing direction, and the *optical density* information (the *compression* gradient) conveyed by the relative displacements of the lateral and vertical frame lines, perpendicular to the viewing direction. The projection of the tunnel at large viewing distances yields the *infinity point*, marking the cross-point of the lateral and vertical *pseudo-horizons* that serve as optical references for the optical density cues. Studying the task of following a circular trajectory, corresponding with the curvi-linear aircraft motion, is much more complex. Although in principle the same information is available as in straight tunnels, the optical splay and density cues are only useful at small viewing distances. Furthermore, because the projection of the curved trajectory on the viewplane does not yield the infinity point nor the pseudo-horizons and even results in *presentation biases*, the task of following curved trajectories was hypothesized to be markedly more difficult than that of following straight trajectories. Finally, one of the main general findings was that, since the display does not present any information other than the tunnel wireframe, it was considered to be questionable whether the cues of the *global* optic flow field (such as the focus of optic outflow) can be used by pilots to control the aircraft motion through the tunnel. Hence, it has been hypothesized that it are essentially the *local* cues conveyed by the dynamic transformation of the tunnel geometry that are used.

To assess the hypotheses originating from the control and information analysis, a number of empirical studies was conducted. A methodology of experimenting was developed, discussed in **Chapter 4**, that had two objectives. First, the experiments were designed to be *interactive* in the sense that pilots had to continuously control the aircraft motion through the tunnel using the *same* perception and action mechanisms as they would apply in real flight. Second, they were designed to allow an evaluation of pilot/display interaction not only in terms of performance, but also in a control-theoretical sense. This is *not* a trivial problem. If it is hypothesized that, when properly instructed, pilots attempt to *optimize* the aircraft path-following performance, a mathematical description can be obtained of pilot control behaviour. In the past several pilot models have been developed, most notably the *Crossover Model* (COM) (McRuer & Jex, 1967) and the *Optimal Control Model* (OCM) (Kleinman & Baron, 1971), and these models were both applied to describe pilot behaviour in the regulation tasks. It is shown that the pilot model identification methods put strict demands on the definition and the design of the experiment. The pilot's use of only a *subset* of the array of optical cues can be identified at the same time. The pilot loop closures of the main aircraft motion states, however, *can* be determined, yielding a *minimal representation* of pilot control behaviour. The pilot models are *not* the main result of the investigation. Rather, since their application allows the *adaptation* of the modelled pilot control behaviour to the experimental conditions to be analyzed, the mod-

els can be regarded as *tools* for studying the validity of the experimental hypotheses in a control-theoretical sense.

11.1.2 Experiments

Three experiments are discussed in which the effects of manipulating some of the main tunnel display design variables are studied, such as the *tunnel size*, the *viewing volume* and the presence of *flight-path vector* symbology. Another three experiments are described that investigate the fundamental characteristics of the *tunnel geometrical design* in the two pilot regulation tasks of following a trajectory that is either straight or circular, and in the pilot anticipation task of conducting a transient curve-interception manoeuvre.

In **Chapter 5** an important tunnel display design variable, the *tunnel size*, is examined. Previous tunnel display investigations showed unequivocally that the tunnel size *commands* the level of path-following accuracy to be adopted by the pilot (Wilckens, 1973; Grunwald et al., 1981). The information analysis showed that the tunnel size affects the presentation of the aircraft position error relative to the trajectory. It *scales* the magnitude with which this variable is conveyed by the optical density cues and in particular the optical splay angles. Hence, it was hypothesized that, first, by reducing the size of the tunnel the pilots can better perceive the aircraft position error, allowing them to increase the bandwidth of their position error feedback. Making the tunnel too small, however, could result in a reduction of the stability of this feedback, a second hypothesis. The experimental data supported the results from earlier tunnel display research. Reducing the tunnel size yields an improved path-following performance, but it also leads to higher levels of pilot control activity and workload. The validity of the two hypotheses stated above must be addressed with a model-based approach, and in this respect the current analysis extends the findings from the previous investigations. The modelling data indicated that decreasing the tunnel size indeed yields a larger position error feedback bandwidth, requiring a considerable increase in the bandwidths of the other pilot feedback loops as well. Whereas the stability of these loops remains fairly constant, the stability of the position error feedback deteriorates for smaller tunnels. Thus, the two main hypotheses could be confirmed. It was concluded that a tunnel size that is too small yields an ill-damped control situation that should be prevented from the perspectives of performance, closed loop stability, and especially a *safety* point of view. A general recommendation was that in critical tasks such as landing an aircraft considerable *robustness* margins should be incorporated. The model-based analysis allows guidelines concerning the tunnel size design variable to be specified from a human-centered perspective. Two principles must be kept in mind: (i) the tunnel size should allow a consistent level of *performance*, and (ii) the tunnel size should lead to a control situation with a sufficient level of *stability*.

An important virtue of the tunnel display is that it provides *preview* information. Although it is often hypothesized that, in vehicle control tasks, humans focus their attention on some part of the trajectory ahead, a literature survey suggested that the *entire* pre-

view of the trajectory is used. A pilot can be *forced* to put attention on a limited part of the trajectory by limiting the display viewing volume to a particular viewing distance (Grunwald & Merhav, 1976). This has been the approach followed in **Chapter 6**. The information analysis showed that, when considering the motion of a restricted part of the tunnel on the viewplane, the *dynamics* of the *equivalent* system (that is, the combination of the aircraft dynamics and the dynamics of the display) to be controlled by the pilot change as a function of two variables, the viewing distance and the aircraft velocity. The varying *dynamics* force pilots to *adapt* their control behaviour as a function of these two variables. The experimental results confirm the hypotheses that, first, pilots *prefer* a particular viewing distance over others, dependent on the aircraft velocity, and second, that the preferred viewing distance increases for larger aircraft velocities. Hence, limiting the tunnel display viewing volume could have significant consequences for pilot behaviour. It is shown that increasing the minimum viewing distance, presenting the tunnel from a distance ahead, deteriorates the pilot perception of the dynamic and temporal cues, an effect that is attenuated for higher aircraft velocities. Surprisingly, in the restricted viewing case for *small* viewing distances the path-following performance was superior to that found in the *full preview* case, discussed in Chapter 5. Decreasing the maximum viewing distance, presenting the tunnel up to a distance ahead, also leads to higher pilot workload and deteriorates system stability. This effect can be mitigated by explicitly presenting the direction of the aircraft motion with respect to the trajectory. An alternative for presenting the complete trajectory ahead could therefore be the combination of showing the tunnel from small to intermediate viewing distances and a flight-path vector symbol.

The relative usefulness of the various optical cues conveyed by the tunnel display is a difficult issue to be determined experimentally, especially because most of these cues are presented *simultaneously*. In **Chapter 7** it is described how the functionality of a selected set of cues can be studied by investigating these cues one at a time. The relative usefulness of the main information sources depicting the aircraft position error, *optical splay* and *optical density*, is investigated in the pilot regulation task of following a *straight* trajectory. The information analysis indicated that, in this respect, two issues required special attention. First, whereas the optical splay angles convey the aircraft lateral and vertical position errors in a *coupled* fashion, they are shown in an *uncoupled* fashion with the optical density. Hence, the first hypothesis is that, when both the position error variables must be controlled simultaneously, the optical density information yields the best performance. Second, the aircraft traversal motion causes the tunnel frames moving towards the pilot, and a *change* in the optical density due to a lateral or vertical position error must be perceived *on top* of the expanding frames. The optical splay angles do not convey *any* information regarding the forward motion. Hence, a second hypothesis is that, when the aircraft moves forward through the tunnel, the optical splay angle information yields the best performance. To assess the findings of the analysis experimentally, three tunnel display designs were examined: a *splay-only* display, a *density-only* display and a combination of the two, the baseline tunnel. Two independent measures were added in

the experimental design, the *channel* measure depicting either the single (roll or pitch) or the dual (roll and pitch) axis aircraft control task, and the *motion* measure, depicting either the hovering or the traversing aircraft motion. The experimental design introduced an essentially different presentation of the flight-path. Whereas in the roll channel the lateral direction of motion could be perceived *directly* via the position of the infinity point on the display, in the pitch channel the vertical direction of motion could be estimated only *indirectly* using the cues of motion perspective. The experimental data supported the hypotheses well. Performance with the splay-only display was unaffected by the traversing motion, but decreased when more than one channel had to be controlled simultaneously. Performance with the density-only display decreased when the aircraft traversing motion was active, whereas the effects of the control task dimension are smaller than for the splay-only display. Evidence for a cue dominance hierarchy could not be found when the splay and density cues were presented simultaneously. The data indicated that when the aircraft flight-path information is *not* directly coded in the display, the splay-only display yields the best performance. The principal virtue of the splay angle information relative to the density information was concluded to be the fact that the splay angle is a property of the *whole* line, it has a constant *gain* independent of where the pilot is looking at.

In **Chapter 8** the optical information conveyed by the tunnel display, most importantly the optical splay and the optical density information, is investigated in the pilot regulation task of controlling the aircraft along a *circular* trajectory. The analysis of Chapter 3 indicated that although, generally, the properties of the optical gradients remain the same, there are some important differences due to the presentation of a curved rather than a straight trajectory. The projection of curved tunnel sections on the display yields *no infinity point*, and the aircraft direction of motion must be perceived from the cues of *motion perspective* conveyed by the transforming tunnel image, especially at smaller viewing distances. Furthermore, since the projection of curved tunnels does not convey the pseudo-horizons, which act as the optical reference for the optical density cues, it is hypothesized that especially the optical splay angles are important for the perception and control of the aircraft *flight-path* relative to the trajectory. Furthermore, due to the trajectory curvature the aircraft position and heading relative to the trajectory is not accurately presented by the display. Because these so-called *presentation biases* are large in particular for the optical splay angles, a second hypothesis is that the optical density information is important for the perception and control of the aircraft *position* relative to the trajectory. As far as the optical density information is concerned, another issue was the *regularity* in the positioning of the tunnel frames that convey this information. It was hypothesized that, third, placing these frames at irregular distances results in a decreasing path-following performance, and fourth, that this performance decrease is especially large when no information other than the density cues is available. It is clear from the statements above, i.e. the ones that lead to the hypotheses, that the quality of the information in curved tunnel sections is much worse as compared to the information in straight tunnel sections. Hence, a fifth hypothesis has been that the task of controlling the aircraft along

circular trajectories is markedly more difficult than that of following straight trajectories. An experiment has been described that assessed the validity of the hypotheses. The same tunnel displays were applied as in the previous experiment, i.e. a splay-only display, a density-only display and the baseline tunnel display. For the displays presenting the tunnel frames (all displays except the splay-only display), an additional experimental measure was the positioning of these frames at regular or irregular distances. A final experimental variable, originating from previous tunnel display investigations (Grunwald, 1996a, 1996b), was the *rotation* of the tunnel geometry as a whole with the reference aircraft roll angle needed to fly the curve. Concerning this latter variable, the information analysis revealed no significant differences in the optical information conveyed by the display when the tunnel was rotated or not. Hence, it was hypothesized that rotating the tunnel does not help pilots much in improving their path-following performance. The experimental data and the model-based analysis confirmed *all* the hypotheses originating from the pre-experimental cue analysis.

An important advantage of electronic displays is that they can be *augmented with synthetic symbology* designed in particular to help pilots in conducting their tasks. In **Chapter 9** the usefulness of the *flight-path vector*, a symbol that explicitly shows the aircraft direction of motion to the pilot, has been investigated. In order to assess this usefulness the effects were investigated of perturbing the lateral component of the aircraft velocity vector, i.e. the aircraft flight-path angle. Without this side-slip disturbance the direction of the aircraft motion can be directly perceived through the position of the infinity point on the display (at least, for straight tunnels) and a flight-path vector symbol would be of only limited use in this situation. With the side-slip disturbance, however, the infinity point can not be used to perceive the flight-path angle and the flight-path vector symbol *can* be extremely useful. In this case it is hypothesized that the presentation of the FPV allows a direct perception of the aircraft direction of motion. Without the FPV, it was hypothesized that subjects would use the cues of motion perspective – the splay angle rates and the compression rates – to estimate their flight-path, considerably limiting the path-following performance. Previous investigations showed that the potential benefit of the various display augmentation forms depends on the dynamics of the vehicle to be controlled and on the characteristics of the disturbances acting on the vehicle (Grunwald & Merhav, 1978). These effects on the use of the flight-path vector were investigated experimentally through the combination of three turbulence scale lengths and three aircraft velocities, which yielded nine different turbulence *bandwidths*. It was hypothesized that the higher bandwidths of the flight-path disturbance considerably limits the usefulness of presenting the FPV. The experimental data showed that the common pilot control strategy with a perspective tunnel display, a feedback of the aircraft attitude, flight-path and position, does not change when the FPV is presented. An interesting finding was that in determining the pilot model structure, *two* models had to be applied in order to describe the observed pilot behaviour. Without the FPV, the pilots are found to be unable to perceive the aircraft direction of motion relative to the tunnel trajectory well enough to

use this information for purposes of control. Rather, they revert to the best alternative for the flight-path that *could* be perceived directly from the display, namely through the position of the infinity point, i.e. the heading angle error. This result was *not* expected beforehand. It suggests as if pilots are not able to use the cues of motion perspective in the task at hand, at least not as well as one would expect from such an ecological display as the tunnel display. It was recommended that a series of experiments were necessary to further investigate the effects of the characteristics of the flight-path disturbance on this – potentially far-reaching – finding. When the FPV symbol is available, pilots optimize their control behaviour by adopting a direct feedback of the flight-path angle error. This significantly improves the path-following performance and leads to considerably lower pilot effort ratings. Furthermore, the data confirmed the hypothesis that a pilot's use of the flight-path vector is harmed when the bandwidth of the turbulence increases, resulting in a significant deterioration of path-following performance. The model-based analysis indicated further that, when turbulence bandwidth increases, pilots shift attention from the middle loop feedback of flight-path to the outer loop feedback of position error. It was concluded that in the high-bandwidth conditions the rapid and unpredictable motions of the FPV symbol on the display hampered its use for purposes of control. The data even suggest that, in these conditions, pilots could have performed *better without* the FPV.

The aircraft transition manoeuvre between a straight and a curved section of the trajectory is investigated in **Chapter 10**. Intercepting a curve is the only *anticipation* task addressed in this thesis. Other cognitive, perceptual and control-theoretical concepts had to be examined, centered around the issue of the pilot *timing* of the manoeuvre. The curve interception manoeuvre is determined in the first place by the aircraft *manoeuverability constraints*. Within these constraints, pilots have considerable freedom in initiating the curve transition. In a simulation study the manoeuverability constraints were derived, yielding concepts that were useful later when examining the observed pilot behaviour. Based on a literature survey and an analysis of especially the *temporal* properties of the tunnel display, two hypotheses were stated concerning the timing of the manoeuvre. First, pilots could use *time-to-contact* (TTC) information from the expanding tunnel *frames*, a *time*-based approach. Second, pilots could focus on the motion of an emergent feature of the tunnel *outline*, the *tangent point*, a *distance*-based approach. The experiment varied the tunnel geometrical designs, the tunnel size, the aircraft dynamic models and the aircraft velocity. The experimental data proved that the timing of the curve interception manoeuvre is determined to a considerable extent by the tunnel geometry. When the tunnel *frames* are presented, pilots adopt the strategy based on the *time* resting before the beginning of the curve. The data provided strong evidence for such a TTC strategy, essentially because pilot timing was consistent and remained unaffected by the aircraft velocity. Since the TTC information conveyed by the expanding tunnel frames is independent of the geometric properties of the tunnel (size), as well as those of the curve (radius), the TTC-strategy is *context-independent* and therefore a *robust* strategy to time the initiation of the manoeuvre. In contrast, when no tunnel frames are presented, pilots

adopt the strategy based on the *distance* resting before the beginning of the curve. The motion of the tunnel *outline* tangent point on the viewplane serves as the principal optical event used to trigger the curve transition manoeuvre. The data provide evidence for the use of the distance-strategy, especially because the trends in the data correspond well with the characteristics of the tangent point. Since this timing strategy *does* depend on the geometry of the tunnel as well as the properties of the curve it is a *vulnerable* strategy, not robust, leading to considerable variation in pilot timing behaviour.

11.1.3 Methodology

Generally, it can be concluded that the cybernetic approach has been quite successful in pin-pointing the important characteristics of pilot/display interaction. For all experiments in this thesis, the experimental findings provided an abundance of affirmative evidence for the majority of the pre-experimental hypotheses. The methodology adopted here provides a *structured* approach to both a theoretical as well as an experimental assessment of the effects of varying the tunnel display design variables on pilot performance, control behaviour and mental workload. It allows possible artifacts to be identified in the pre-experimental stage of investigation. A number of general conclusions is stated below, focusing in particular on the experimental issues of including a model-based analysis in the experimental investigations.

- The development of a general, predictive model of pilot control behaviour with a tunnel display has shown to be a respectable, but unfortunately a too ambitious goal. The first reason for this setback is that the various sources of optical information conveyed by the tunnel display are entangled and can not be isolated into a set of *parallel* cues without severely altering the display geometry. There will always be some *redundancy* in the optical information, and any display design that is worthwhile to investigate experimentally will in general convey a specific motion referent in more than one fashion. Another additional reason is a matter of identification. In the aircraft control situation that was the subject of the study, the pilot model identification methods only allow two or at most three pilot feedback loops to be identified experimentally at a time. It is shown that only the *integral pilot response* to the various optical cues conveying a particular aircraft motion referent can be determined. So, in order to investigate the presence of cue dominance hierarchies, i.e. the relative usefulness of the optical cues, these cues must still be *isolated* from others through a clever design of the display. Although the optical *redundancy* is a problem common of basically *any* approach, the results in this thesis show that in this respect the additional value of a model-based analysis is small. It does certainly not lead to a significant breakthrough in solving this problem.

- The limited pilot model identification methods led to the approach of applying a relatively simple pilot model structure with a limited number of parameters that *can* be identified. Then, the *changes* in the pilot model parameters as a function of the independent measures of the experiment have been investigated. The experiments have proved that this approach can provide some useful insights into the manner in which

the modelled pilot behaviour is *adapted* to the experimental conditions. The pilot models allow considerable insight into *how* pilots could have adapted their behaviour, the question *why* this adaptation happens in the way it appears to be done, however, must still be inferred from the data. Although the models provide much additional quantitative data, the inference procedure itself, to be done by the experimenter, remains a difficult task.

- In most of the previous studies with (spatial) displays, the pilot's control task has been simplified to a single axis tracking task. The multi-loop character of the model-based analysis applied here allows the multi-loop pilot control behaviour to be investigated. When more than one pilot feedback loop is closed simultaneously the number of possibilities of adapting the control behaviour increases considerably. It is shown that this introduces considerable difficulties in interpreting the model-based results. Generally, the adaptation in the outer loop feedbacks was found to be consistent among the subjects. The adaptation of the inner loop feedbacks showed much more variation among subjects, which makes it difficult to relate the pilots' adaptation to the experimental conditions. This variation can be attributed to two causes. First, in the tasks considered the pilots were instructed to optimize especially their outer loop (aircraft path-following) performance. Second, the inner loops *serve* the outer loops and there exist many ways of doing this. In most cases, the model parameters just allowed the bandwidths and stability margins of the main pilot feedbacks to be determined.

- The model-based approach has been shown to be able to *complement* the common performance and workload-oriented analysis of human behaviour. Because the proposed pilot models are a direct result of the functional analysis of the optical cues, a successful application of the identification methods used in the model validation procedure provides direct, quantitative evidence for a particular property of an optical cue. The frequency domain identification methods sometimes explicitly show the validity of a pilot model for a particular control situation. One of the best examples is the pilot's use of the flight-path vector symbol, investigated in Chapter 9. Here, the model-based analysis provided clear evidence for the above mentioned fact that without the explicit presentation of the aircraft's direction of motion, pilots are unable to derive this information from the cues of motion perspective or, at least, they are unable to use this information for purposes of control. Without the model-based analysis it would have been impossible to draw such a conclusion, a conclusion that has theoretical interest.

- The multi-loop pilot models (the MLMs) successfully *describes* the observed pilot control behaviour and performance with a limited number (six to eight) of parameters. They can not be used, however, to *predict* pilot performance and control behaviour in situations other than those in which these models were validated experimentally. This considerably limits the value of these models.

- The application of the Optimal Control Model (OCM) has not been successful. Evidence is found for the problems of *over-parameterization* of the OCM. In two rather elementary experiments the model parameters could not be identified, even with the elaborate model validation methods adopted here and, in particular, even with the considerable

amount of experimental data, both in the frequency domain and the time domain, available for purposes of model validation. Tentatively, it can be concluded that the intellectual attractiveness of the OCM, with its appealing regulator and observer structure, has often 'dazzled' its users. A thorough re-examination of its usability, applicability, and especially its identifiability, especially in multi-loop control tasks is definitely recommended.

11.2   Recommendations

• A general recommendation would be to conduct the experiments in a more realistic environment. In particular the use of a moving-base flight simulator, providing motion cues to the pilots, is recommended. The motion stimuli are important for the aircraft attitude control, the inner loop, and the lack of these motion cues could have caused the variation in the experimentally observed pilot control behaviour in the inner loop. On the one hand, it can be hypothesized that the addition of motion cues will not significantly change the outcomes of the experiments in terms of pilot performance and control behaviour in the outer loops. The addition of motion will help pilots mainly in improving their inner loop aircraft attitude control. On the other hand, as has been shown by van der Vaart (1992) and Hosman (1996), one should definitely incorporate the human vestibular system feedback characteristics in modelling the inner loop aircraft attitude feedback of pilots.

• The results in this thesis showed that the effectiveness of a particular tunnel display design depends significantly on the definition of the other task variables. Hence, in investigating the properties of interaction of human subjects with (spatial) displays, factors other than the display geometrical design must be well-considered. An analysis of especially the influences of the *dynamics* of the system to be controlled and the characteristics of the *disturbances* acting on the closed loop system must be incorporated in the pre-experimental investigation. For instance, when considering the effects of the velocity of the aircraft motion through the virtual environment, attention is often focused completely on the relation between the velocity and the (global) optical flow field. One should realize, however, that *also* the aircraft dynamic properties, i.e. its control characteristics, change when the aircraft velocity is manipulated, possibly affecting the usefulness of certain optical sources of information considerably. This is an important avenue of further research where the insights from the (control) engineering sciences can complement those obtained in psychology.

• The tunnel display can be characterized as a *task-oriented display* because it allows the pilot to control the aircraft through the tunnel *directly* using the transformation of the tunnel image. Even without an advanced tunnel display, however, tremendous benefits can be achieved (in terms of pilot performance and mental workload) through the development of advanced flight control system algorithms (Hynes et al., 1989). Augmenting the aircraft with a flight-path oriented flight control system would allow pilots to *directly* control the aircraft direction of motion relative to the trajectory. This is characterized as a *task-oriented control*. It takes little imagination to hypothesize that the *combination* of the

task-oriented tunnel display, that intuitively shows the pilots where they are and where they are going, and a *task-oriented automatic flight control system*, which allows pilots to directly control the direction of their locomotion, is an extremely powerful concept. This concept is being pursued in an ongoing research project at Delft Aerospace, called *DREAM* (Delft Research into Enhanced Aircraft Manoeuvering concepts). The aim of this project is to make the pilot manual control of an aircraft along the complex, curved trajectories of the future air navigation system as *safe* and *easy* as that of an automobile driver.

Appendix A

Experimental apparatus

The experiments described in this thesis were conducted in the Human-Machine Laboratory (HML) of the Faculty of Aerospace Engineering. The laboratory has been designed and implemented by the author of this thesis in the summer of 1995 and consists mainly of hardware that belonged to the former moving base flight simulator of Delft Aerospace. It has been developed to provide a flexible, real-time, distributed simulation environment for fundamental research into human-machine interaction.

The lab consists of analog and digital hardware that together provide the real-time simulation environment. The laboratory and its components will be described on three levels, starting with a general description in §A.1. The functionality of the components is discussed in detail in §A.2 with the intention to examine possible time delays in the simulation process. The various components' technical specification is summarized in §A.3.

A.1   General description of the laboratory

The physical layout of the laboratory and its components is shown in Fig. A.1. This figure also shows the elementary flow of information in the simulation process pictorially.

Laboratory layout   The Human-Machine Laboratory consists of an experiment cabin and a simulation control area. Subjects are seated in an adjustable pilot chair in the noise-free and darkened *experiment cabin* (ground area 6 [m^2]). The tunnel display formats are presented by means of a 17 inch colour monitor in front of the subject. A two-axis electro-hydraulic servo-controlled side-stick is the control manipulator. Because the cabin is fixed to the floor, no motion cues can be simulated. Fig. A.2 shows an artist impression of the situation viewed from just behind the subject's head, facing the display.

The experimenter stays outside of the cabin in the so-called *simulation control area*. Two computers – the HOST computer and the EFIS computer – are placed here that are especially programmed to provide a flexible real-time research environment. The HOST computer controls the main simulation process. The primary task of this computer is
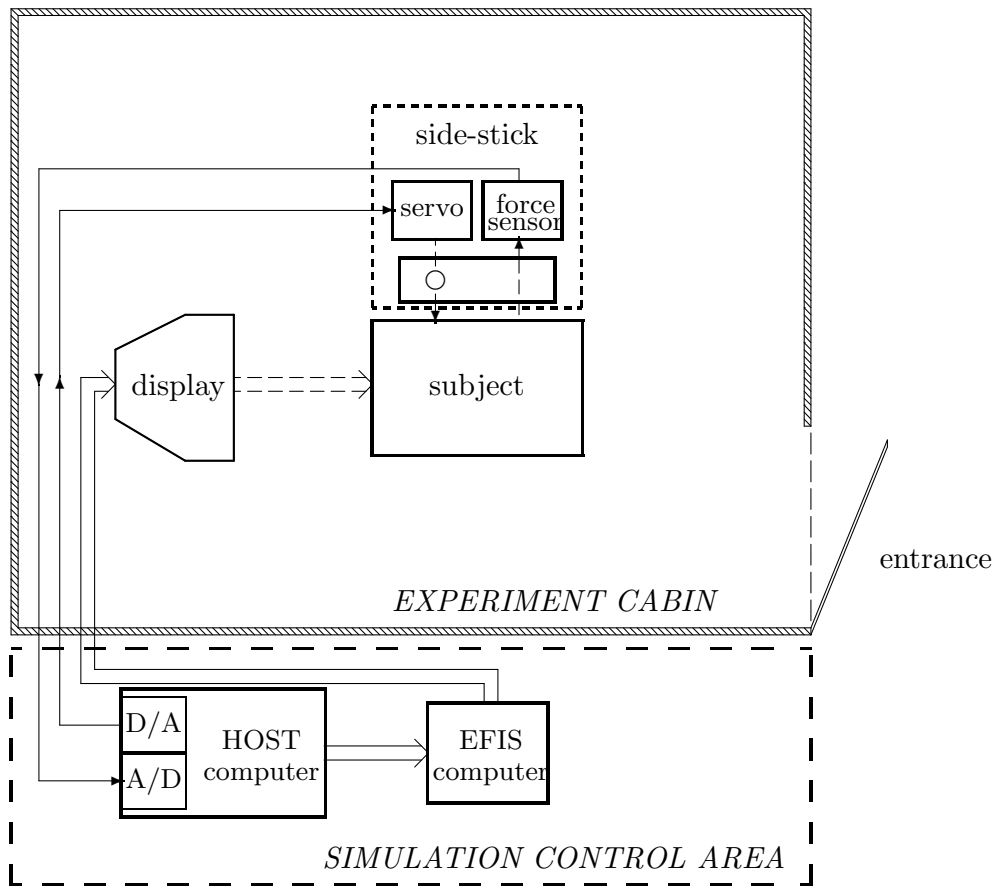
Figure A.1: Lay-out of the laboratory and a pictorial representation of the elementary informa-
tion flow in the simulation environment.

the real-time simulation of the side-stick model, the aircraft model and the atmospheric
disturbance models[1]. The secondary task of the HOST computer is the recording of all
experimental data. Via a digital connection an array of variables is sent to the EFIS
computer. The only task of the EFIS computer is to drive the tunnel-in-the-sky display.

Information flow in the simulation environment   The elementary flow of information
in the simulation environment can be described in general terms at the hand of Fig. A.1.
The pilot is acting in a closed loop. The information presented by the display is the
pilot's primary input. The pilot controls the aircraft by means of the side-stick. For
this purpose, the *force* that the pilot applies on the stick is measured and sent to the
HOST computer. The force is A/D-converted and used for the stick simulation model
that computes the updated stick position. The new position then acts as input signal for
the aircraft dynamic model, resulting in an update of the aircraft state.
Now, two things happen. First, the updated stick position is D/A-converted and sent to
the side-stick servo. The stick servo puts the stick into the commanded position. Second,

---

[1]These models are described in Chapter 4 and Appendix C.
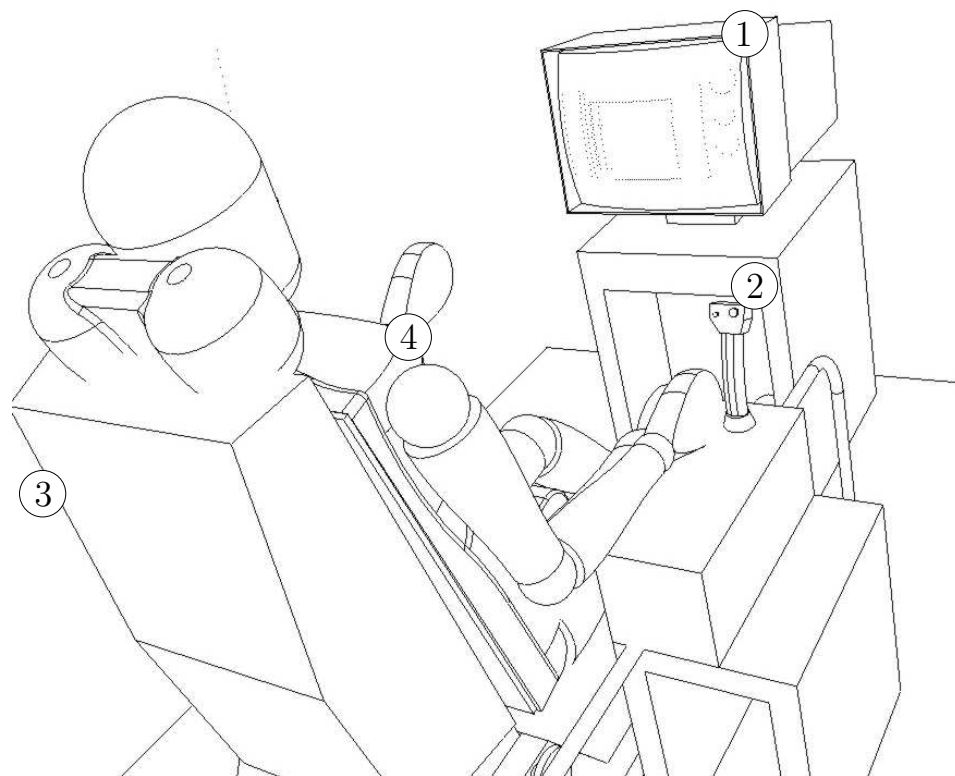
Figure A.2: Artist impression of the experiment cabin of the Human-Machine Laboratory. In this figure, ① indicates the tunnel display, ② the stick, ③ the chair and ④ the subject.

the updated aircraft state is sent via a digital connection to the EFIS computer. The EFIS computer uses this information to update the tunnel display.

In the following section, the simulation process will be discussed in more detail.

A.2 The real-time simulation process and the simulation time delays

A.2.1 Introduction

The simulation environment consists of a number of components introduced in the former section. The majority of these components is operating in a digital, discrete, manner. Generally speaking, the subject is one of the few *continuous* elements in the closed-loop human-machine system. Clearly, the simulation can be made *pseudo*-continuous by setting the simulation frequency at a very high level. However, a number of elements in the loop, in our case especially the display, makes this impossible. Because of this fact, time delays could emerge in the control loop that could have an effect on a subject's control behaviour.
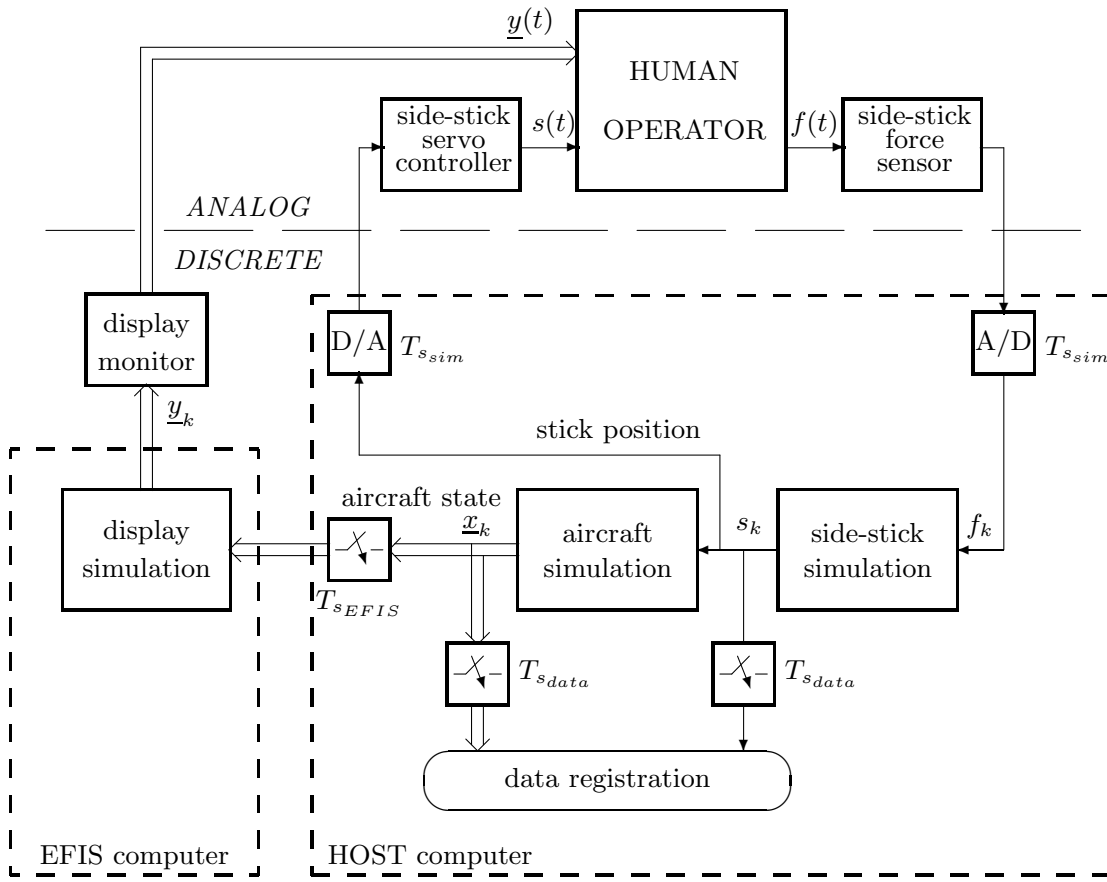
Figure A.3: Functional analysis of the experimental setup for a single-axis multi-loop tracking task. In this figure, $\underline{x}$ depicts the aircraft state, $\underline{y}$ the displayed variables, s the position of the side-stick and f the force exerted on the stick. The sample-times $T_{s_{sim}}$, $T_{s_{EFIS}}$ and $T_{s_{data}}$ are reciprocal to the general simulation frequency f_{sim}, the display update-rate f_{EFIS} and the data recording frequency f_{data}, respectively. The subscript $_k$ depicts a discrete-time variable, the (t) indicates a continuous-time variable.

Below, the presence of time delays in the simulation environment of the Human-Machine Laboratory will be investigated. For this purpose the real-time simulation process will be discussed in somewhat more detail.

A.2.2   Description of the real-time simulation process

In Figure A.3 the main elements of the real-time simulation process are illustrated for a single-axis control task. Naturally, the human controller is put central. The input signals of the subject are the displayed variables $\underline{y}(t)$, visual channel, and the position $s(t)$ of the side-stick, the proprioceptive channel. The output signal of the subject is the force $f(t)$ exerted on the side-stick.

The measured force on the side-stick is sent to the HOST computer. The HOST controls the real-time simulation process, running at the simulation frequency f_{sim} that is fixed for all experiments at 2000 [Hz]. The stick force is discretized, f_k, and used in the side-stick simulation model to compute a new position of the stick, s_k. The updated position of the stick and the outputs from the atmospheric disturbance models (not shown) serve as the input signals of the aircraft simulation model, resulting in an update of the aircraft state vector, $\underline{x}_k$.

All variables of interest are now computed in the HOST computer and are sent to the other components. First, the updated position of the side-stick, s_k, is converted to an analog signal and sent to the stick servo-controller, which puts the stick into the commanded position. Second, the updated aircraft state, $\underline{x}_k$, will be send to the EFIS computer via a digital connection. The latter transfer, however, cannot be done at the simulation frequency f_{sim}, simply because it is not possible to update the tunnel display at such a high frequency. The display simulation frequency, f_{EFIS}, is limited by (i) the display refresh-rate determined by display hardware, here 60 [Hz], and (ii) the display update-rate, determined by the display software and the computing power of the graphics processing card. With the hardware and software applied in this thesis, discussed in §A.3, a simplified tunnel display generally has a maximum update-rate of 20 [Hz]. Such a display update-rate means that only 1 of every 100 samples can be shown to the subject. Hence, a *decimation* of the simulation frequency f_{sim} is necessary. The digital information transfer from the HOST to the EFIS computer is therefore conducted with a frequency equal to the display update-rate, i.e. f_{EFIS}.

All experimental data are recorded in the HOST computer with frequency f_{data}, fixed for all experiments at 50 [Hz]. Hence, here also a decimation of the simulation frequency from 2000 [Hz] to 50 [Hz] is necessary. The detrimental effects of this decimation are countered by using a Finite Impulse Response (FIR) filter, described in (Aström & Wittenmark, 1984). Due to the use of a FIR filter the recorded variables are an undistorted copy of the variables in the simulation process.

Conclusion   In the simulation environment, three processes are running simultaneously at three different frequencies:

A The <u>kernel</u> of the simulation: The main program running on the HOST computer that controls the simulation of the side-stick model, the aircraft model and the atmospheric disturbance models:

$$
\begin{array}{lllll}
\text{simulation frequency} & : & f_{sim} & = & 2000.0 \quad [\text{Hz}]; \\
\text{sample time} & : & T_{s_{sim}} & = & 0.0050 \quad [\text{s}].
\end{array}
\tag{A.1}
$$

B The <u>periphery</u> of the simulation:

(i) The data recording process (HOST computer):

$$
\begin{array}{lllll}
\text{data recording frequency} & : & f_{data} & = & 50.0 \quad [\text{Hz}]; \\
\text{data sample time} & : & T_{s_{data}} & = & 0.020 \quad [\text{s}].
\end{array}
\tag{A.2}
$$

(ii) The simulation of the display (EFIS computer):

$$
\begin{array}{ll}
\text{display updaterate} & : \quad f_{EFIS}; \\
\text{display updatetime} & : \quad T_{s_{EFIS}}.
\end{array} \tag{A.3}
$$

Both the processes in the periphery are synchronized with the kernel simulation process.

A.2.3 Origin of the simulation time delays

The frequency of the kernel simulation process is very high, Eq. A.1, resulting in only a negligible time delay. Furthermore, as was mentioned above, the use of a FIR-filter suppresses the detrimental effects of the decimation necessary for the recording of all experimental data, Eq. A.2. This leaves us with the simulation of the tunnel display. The delay in the closed loop due to the simulation of the display can be approximated by:

$$
\tau_{EFIS} \approx \frac{3}{2}\frac{1}{f_{EFIS}} = \frac{3}{2}T_{s_{EFIS}} \quad \text{(in [s])}, \tag{A.4}
$$

with the constant of $\frac{3}{2}$ caused by summing two effects:

(i) A delay $T_{s_{EFIS}}$ equal to the update-time of the display.

(ii) A delay due to what can be regarded as the D/A-conversion of the presented data. This requires some further explanation. With a display refresh-rate of 60 [Hz] and a display update-rate of 20 [Hz], every image is shown 3 times to a subject. In other words: the display monitor acts as some sort of a Zero Order Hold (ZOH) circuit in the closed loop. When it is assumed that a subject watches the display continuously, the perceived image will *on the average* be $\frac{1}{2}$ times the display update-time $T_{s_{EFIS}}$ 'old'.

Hence, a relatively high display update-rate of 20 [Hz] already leads to a time delay in the closed loop of 75 [ms]. It is clear that a delay of this magnitude can not be neglected.

In conclusion, the time delays in the simulation process are primarily caused by the limited update-rate of the tunnel display. All other possible time delays can be neglected, because they are merely a fraction of the delay due to the display. Hence, the simulation time delay τ_{sim} equals:

$$
\tau_{sim} \approx \tau_{EFIS} \approx \frac{3}{2}T_{s_{EFIS}} \quad \text{(in [s])}. \tag{A.5}
$$

In the modelling and identification procedure the effects of the simulation time delay should be taken into account, which is discussed in detail in Appendix F.

A.3 Technical specification of the components

The technical specifications of the components are summarized in Table A.1.

Table A.1: Technical specification of the laboratory components.

computers		
	HOST computer	
	type	PC 486 DX-2 66MHz (1995)
	process timer	National Instruments AT-MIO-16E-10 (1995)
		DAQ-STC timer chip (20 MHz clock)
	A/D-conversion	National Instruments AT-MIO-16E-10 (1995)
		16 channels, 12 bits
	D/A-conversion	National Instruments AT-MIO-16E-10 (1995)
		2 channels, 12 bits
	digital connection	National Instruments AT-DIO-32F (1991)
	(to EFIS)	32 bit parallel high-speed I/O
	EFIS computer	
	type	PC 386 40MHz (1991)
	digital connection	National Instruments AT-DIO-32F (1991)
	(from HOST)	32 bit parallel high-speed I/O
	display hardware	TIGA 34020 SDB (1991)
		TMS 34020 GSP, 1Mb VRAM, 1Mb DRAM
	display software	DELPHINS
display monitor		
	type	NEC Multisync 5FGe colour monitor (1995)
	diagonal	17 inch
	aspect ratio	4 : 3
	screen size	1024 × 768 [pixels] (0.345 × 0.259 [m])
	refresh rate	55-60 [Hz]

A.3.1 Computers

HOST computer   The real-time simulation process is controlled by the HOST computer, a common 486 PC. For this purpose, two special hardware cards are installed.
A National Instruments AT-MIO-16E-10 card controls the timing of the simulation process and the A/Dand D/A-conversion of the analog side-stick signals. The AT-MIO card is programmed to a multiple scanning mode, in which the signals of the four channels of interest (force on the stick and position of the stick, both in pitch and roll direction) are A/D-converted (sample time interval set at 10 [μs], the board minimum). The scan time interval is set at 500 [μs], resulting in a fixed simulation frequency of 2000 [Hz].
A National Instruments AT-DIO-32-F high-speed digital I/O board provides a digital connection with the EFIS computer, in which a similar card is installed. The two AT-DIO boards are programmed so that the HOST computer sends the variables of interest at a fixed frequency. The EFIS computer waits until this information becomes available and acknowledges the receipt of the data via a digital handshaking protocol. As mentioned above, the frequency of this information transfer is determined by the update-rate of the

display. In all cases the maximum transfer rate was chosen that did not interfere with the main simulation process.

EFIS computer The task of the EFIS computer, a common 386 PC, is to control the display in the experiment cabin. It contains two special cards. The purpose of one of these cards, i.e. the AT-DIO board, has already been discussed above.

The second card that is installed is a Texas Instruments Graphics Architecture (TIGA) TMS 34020 graphical processing card. This card generates the images of the tunnel display. The display software accompanying the card has been developed at the Faculty of Electrical Engineering of the Delft University of Technology, in the context of the DELPHINS project (Theunissen, 1993a).

A.3.2 Side-stick

The manipulator used in the experiments is an electro-hydraulic servo-controlled side-stick. The stick has two axes: a roll axis (positive left) and a pitch axis (positive forward). Both axes can be controlled independently.

The stick's roll and pitch axes are driven by a rotating and a linear hydraulic motor respectively, that are both configured as position servos. As has been discussed above, two electric signals from the HOST computer command the position of the stick. Because the stiffness of the hydraulic servo is very large, the forces the subject applies on the stick have only a negligible effect on the position of the stick. The strain gauges in the handle of the stick measure these (sideways and longitudinal) forces and send these signals to the HOST computer. The HOST computes the new stick position based on the measured force and the stick simulation model.

The *de-coupling* of the position of the stick and the force (or moment) exerted on the stick is a unique property of the hydraulic side-stick. It enables the experimenter to simulate the properties of virtually *any* type of side-stick that makes it an excellent instrument for research into manual control behaviour. This has been demonstrated in research into the properties of the neuromuscular system (van Paassen, 1994).

A.3.3 Display

The display monitor is a NEC Multisync 5FGe, a regular off-the-shelf colour monitor. The average distance between the display screen and the subject's eyes is 0.80 [m].

A.3.4 Chair

The side-stick used in the experiments is mounted on an iron frame that also supports the subject's chair. The chair, a real co-pilot's chair (van Paassen, 1994), is adjustable in height and in forward-backward direction. This allows subjects to obtain a comfortable position with respect to the side-stick and the display.

Appendix B

Example pilot briefing and pilot questionnaire

In each experiment described in this thesis, subjects were extensively briefed beforehand. Several days before the start of a particular experiment, the subjects received a *pilot briefing* by mail. Such a briefing contained information on the purpose of the experiment, the specific task of the subject and a time schedule of the experimental trials. Before the experiment was actually started, the main contents of the pilot briefing were repeated verbally to a subject. An example of a pilot briefing is given in §B.1. It is a copy of the briefing used for Experiment X4, discussed in Chapter 8.

When all experimental trials were performed, the subjects were requested to complete a *pilot questionnaire*, containing a number of specific questions on the experiment. The objective for the use of the questionnaires was to obtain subjective, qualitative, data that could substantiate the merely quantitative experimental results. It was considered very useful and important to obtain the opinions of the subjects, all professional pilots, in a structural manner. An example of a pilot questionnaire is given in §B.2. It is a copy of the questionnaire used for Experiment X4, discussed in Chapter 8.

B.1 Example pilot briefing

Pilot Briefing Experiment X4

Pilot Performance and Control Behaviour on Curved Trajectories with a Tunnel-in-the-Sky Display

A.J. van der Hoek & Max Mulder

January 20, 1997

Introduction

At the Faculty of Aerospace Engineering of the Delft University of Technoloy, a research project is conducted in order to investigate pilot manual control behaviour with perspective flight-path displays. These displays are a promising candidate to become the primary flight display in future aircraft.

The present phase in the research project is focused on obtaining a better understanding of the manner in which pilots use such a display in case of curved tunnel sections. The current experiment, referred to as experiment X4, has been designed to examine the effects of *tunnel geometry, tunnel rotation* and *aircraft velocity* on pilot performance, pilot control activity and pilot control behaviour. The experiment will be conducted in February 1997.

Experiment

Experimental conditions

The experiment is focused on evaluating the effects of three independent variables:

- **Tunnel Geometry**, i.e. the characteristics of the tunnel display. Five display configurations will be tested (Figure 1):

1. **Display A**, showing the complete wireframe of the tunnel. The distances between the tunnel frames is kept constant.

2. **Display B**, showing the complete wireframe of the tunnel. The distances between the tunnel frames is randomized.

3. **Display C**, showing only the longitudinal lines connecting the tunnel frames.

1

Pilot Briefing Experiment X4

4. **Display D**, showing only the tunnel frames. The distances between the frames is kept constant.

5. **Display E**, showing only the tunnel frames. The distances between the frames is randomized.

- **Aircraft velocity**, the velocity with which the aircraft moves through the world. Two velocities are applied, i.e. 70 and 110 [m/s]. These velocities, together with the required aircraft's yaw rate, fixed at 2 [deg/s] in the experiment, result in reference bank angles ϕ_{ref} of 14.3 and 22.4 [deg] respectively.

- **Tunnel Rotation**, depicting the situation whether or not the tunnel is rotated with the required angle-of-bank ϕ_{ref}. Figure 1 shows the tunnel displays without rotation, while Figure 2 shows the displays with the rotated tunnel. The desired angle of bank can be computed from the aircraft's velocity and required yaw-rate, the latter fixed at 2 [deg/s] in the experiment.

These independent variables result in a total of 20 experimental conditions: 5 Displays × 2 Rotations × 2 Velocities. The tunnel trajectories will be curved either to the right or to the left, in a random manner.

Task of the pilot

The task of the pilot is *to control the aircraft through the tunnel as accurately as possible, i.e. to minimize all occurring position and attitude errors*. It is a single-axis tracking task, in which only the asymmetric aircraft dynamics have to be controlled. The symmetric aircraft dynamic properties are fixed to their initial condition.

The aircraft is a small business-jet, the Cessna Citation I, which will be simulated using a simplified linear aircraft model. The velocity of the aircraft is automatically kept constant at the appropriate level. Due to the use of different velocities, however, the aircraft will have slightly different flying characteristics for each of the two velocity conditions. For all models a yawdamper and a turn-coordinator are installed, resulting in a well-damped Dutch Roll and zero side-slip. As a consequence, the aircraft can be controlled satisfactory using aileron only.

The aircraft will be disturbed by atmospheric turbulence. The turbulence does not change the direction of the velocity with respect to the aircraft longitudinal axis, i.e. there is no side-slip.

Experimental design

The experiment, consisting of 20 conditions, will be designed according to the *full randomization* design principle: The replication of all 20 conditions are distributed randomly over the experiment.

2

Pilot Briefing Experiment X4

Figure 2: The tunnel display characteristics of experiment X4 (*rotation* of the tunnel with reference bank angle ϕ_{ref}).

4

Pilot Briefing Experiment X4

Figure 1: The tunnel display characteristics of experiment X4 (no rotation of the tunnel).

3

Pilot Briefing Experiment X4

09.00	Block 1
10.30	
10.45	Block 2
12.15	
	LUNCH
13.15	Block 3
14.45	
15.00	Block 4
16.30	

Figure 3. Experiment time schedule.

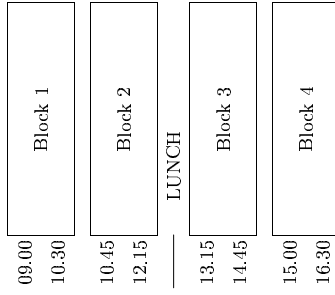The experiment consists of two parts:

1. *Learning phase*, in which the subjects have to get accustomed to the experiment. This phase must lead to a relatively constant level of performance, as expressed by the position error variance, at all conditions.

2. *Measurement phase*, in which all data are measured and recorded for a later analysis.

A single run takes approximately 100 seconds. All experimental conditions will probably be replicated 10 times, depending on the measured performance. The experiment will be conducted in two days. Each day will be divided into four blocks, each block consisting of 3 smaller sub-blocks of 8 runs each. After each sub-block the subjects have a 5 minute break, while in-between blocks a 15 minute break is available (see Figure 3).

Experimental setup

Subjects will be seated in an adjustable chair in a low-noise, darkened room. The tunnel display is shown by means of a 17 inch color monitor, placed in front of the subject. The control manipulator is an electro-hydraulic, servo-controlled, passive side-stick with one degree of freedom (aileron).
The display shows the tunnel as a grey wireframe on a black background. The aircraft symbol is a green outline. A yellow flight-path vector will be presented showing the instantaneous direction of motion.

B.2 Example pilot questionnaire

Pilot Questionnaire Experiment X4

Pilot Questionnaire Experiment X4

Pilot Performance and Control Behaviour on Curved Trajectories with a Tunnel-in-the-Sky Display

A.J. van der Hoek & Max Mulder

January 20, 1997

Name subject	
Date	

First of all, thanks a lot for your co-operation in the experiment!

As a subject in the experiment, you have controlled a small aircraft, the Cessna Citation I, along a constantly curved trajectory using a simplified *Tunnel-in-the-Sky* display. The experiment contained 20 conditions, consisting of 5 Displays, 2 aircraft Velocities (70 and 110 [m/s]) and the situation whether the tunnel as a whole was Rotated or not.

This questionnaire can provide very useful additional information upon the quantitative results of the experiment. Therefore, please answer the following questions as accurately as possible.

1

Realism of the simulation

1. How would you describe the level of *realism* of the simulated aircraft dynamics for the low-speed ($V_{tas} = 70$ [m/s]) condition:

   very realistic ☐ realistic ☐ average ☐ unrealistic ☐ very unrealistic ☐

   Comment:

2. How would you describe the level of *realism* of the simulated aircraft disturbances for the low-speed ($V_{tas} = 70$ [m/s]) condition:

   very realistic ☐ realistic ☐ average ☐ unrealistic ☐ very unrealistic ☐

   Comment:

3. How would you describe the level of *realism* of the simulated aircraft dynamics for the high-speed ($V_{tas} = 110$ [m/s]) condition:

   very realistic ☐ realistic ☐ average ☐ unrealistic ☐ very unrealistic ☐

   Comment:

4. How would you describe the level of *realism* of the simulated aircraft disturbances for the high-speed ($V_{tas} = 110$ [m/s]) condition:

   very realistic ☐ realistic ☐ average ☐ unrealistic ☐ very unrealistic ☐

   Comment:

2

Pilot Questionnaire Experiment X4

Display characteristics

7. Describe, if possible using the accompanying figures, what sources of information you used in controlling the aircraft. Take special notice of the effects of the type of display and the regularity of the frame distances.

Furthermore, try to draw two contour lines of visual attention in these figures, depicting the area of the display on which you focused approx. 50 and 90 percent of your attention (see example).

Example of contour lines of visual attention

A   Total tunnel, regular frame distances

B   Total tunnel, irregular frame distances

4

Pilot Questionnaire Experiment X4

Sense of egomotion and perceived depth

5. How would you describe the strength of the experienced *egomotion*, i.e. did you have a strong feeling you were moving through a three-dimensional world or did you not[1]:

		very strong	strong	average	weak	very weak
Display A	not-rotated	☐	☐	☐	☐	☐
	rotated	☐	☐	☐	☐	☐
Display B	not-rotated	☐	☐	☐	☐	☐
	rotated	☐	☐	☐	☐	☐
Display C	not-rotated	☐	☐	☐	☐	☐
	rotated	☐	☐	☐	☐	☐
Display D	not-rotated	☐	☐	☐	☐	☐
	rotated	☐	☐	☐	☐	☐
Display E	not-rotated	☐	☐	☐	☐	☐
	rotated	☐	☐	☐	☐	☐

Comment:

6. How would you describe the strength of the sense of *depth* in the display, i.e. did you have a strong feeling you were looking ahead into a three-dimensional world or did you not:

		very strong	strong	average	weak	very weak
Display A	not-rotated	☐	☐	☐	☐	☐
	rotated	☐	☐	☐	☐	☐
Display B	not-rotated	☐	☐	☐	☐	☐
	rotated	☐	☐	☐	☐	☐
Display C	not-rotated	☐	☐	☐	☐	☐
	rotated	☐	☐	☐	☐	☐
Display D	not-rotated	☐	☐	☐	☐	☐
	rotated	☐	☐	☐	☐	☐
Display E	not-rotated	☐	☐	☐	☐	☐
	rotated	☐	☐	☐	☐	☐

Comment:

[1]For an explanation of the coding of the displays (*A - E*) please refer to the illustrations presented in question 7 (not-rotated tunnel, pages 4-5) and question 8 (rotated tunnel, pages 6-7).

3

Pilot Questionnaire Experiment X4

A   Total tunnel, regular frame distances
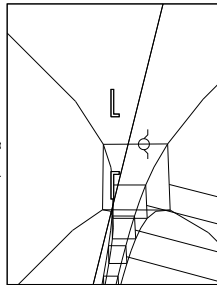
B   Total tunnel, irregular frame distances
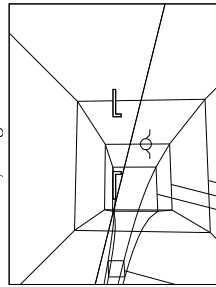
C   Longitudinal frame lines only
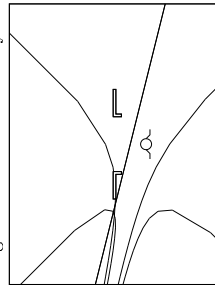
D   Tunnel frames only, regular frame distances
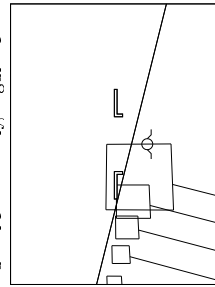
6

Pilot Questionnaire Experiment X4

C   Longitudinal frame lines only
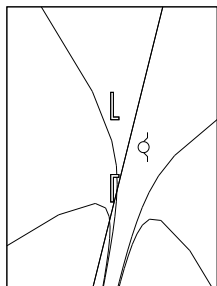
D   Tunnel frames only, regular frame distances
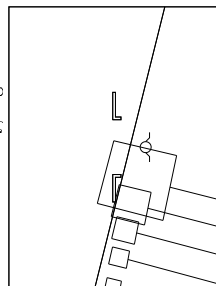
E   Tunnel frames only, irregular frame distances
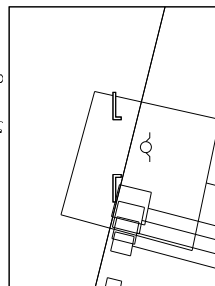
8. Describe, if possible using the accompanying figures, what sources of information you used in controlling the aircraft. Take special notice of the effects of the <u>rotation</u> of the tunnel.
Furthermore, try to draw two contour lines of visual attention in these figures, depicting the area of the display on which you focused approx. 50 and 90 percent of your attention.

5

Pilot Questionnaire Experiment X4

E   Tunnel frames-only, irregular frame distances
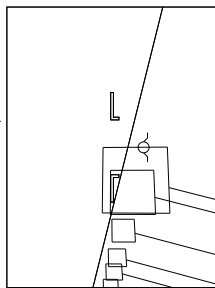
9. The following questions address the *ROTATION* of the tunnel as a whole.

   (a) How would you describe the usefulness of the *rotation* of the tunnel in the task at hand? In other words, did the rotation help you in any way to improve or maintain performance, or did it cause a detrimental effect:

	very useful	useful	no difference	detrimental	very detrimental
Display A	☐	☐	☐	☐	☐
Display B	☐	☐	☐	☐	☐
Display C	☐	☐	☐	☐	☐
Display D	☐	☐	☐	☐	☐
Display E	☐	☐	☐	☐	☐

   Comment:

   (b) The aircraft velocity was fixed at two levels: 70 and 110 [m/s]. Did the velocity of the aircraft have any effect on the relative usefulness of the rotation, i.e. on your answers on the previous question?

   (c) Your task was to follow a constantly curved trajectory. Could you think of other tasks or situations in which the rotation of the tunnel as a whole could be effective?

7

Pilot Questionnaire Experiment X4

10. The following questions address the *REGULARITY* of the intermediate distances between the individual tunnel frames.

    (a) How would you describe the usefulness of the *regularity* of the intermediate tunnel frame distances in the task at hand? In other words, did the regularity help you in any way to improve or maintain performance, or did it cause a detrimental effect:

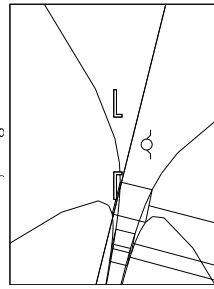 | | very useful | useful | no difference | detrimental | very detrimental |
    |---|---|---|---|---|---|
    | Display A | ☐ | ☐ | ☐ | ☐ | ☐ |
    | Display B | ☐ | ☐ | ☐ | ☐ | ☐ |
    | Display C | no frames are displayed in this condition | | | | |
    | Display D | ☐ | ☐ | ☐ | ☐ | ☐ |
    | Display E | ☐ | ☐ | ☐ | ☐ | ☐ |

    Comment:

    (b) The aircraft velocity was fixed at two levels: 70 and 110 [m/s]. Did the velocity of the aircraft have any effect on the relative usefulness of the frame distance regularity, i.e. on your answers on the previous question?

    (c) Your task was to follow a constantly curved trajectory. Could you think of other tasks or situations in which the regularity and/or irregularity of the tunnel frame distances could be either effective or detrimental?

11. The tunnel trajectories were either curved to the left or to the right. Did you experience any difference in difficulty in performing the task between tunnels to the left or to the right?

8

Pilot Questionnaire Experiment X4

Effort ratings

12. Depict on the following rating-scales the effort you experienced in performing the task ('0' is extremely easy, '10' is extremely difficult, and '5' is average). The five scales are grouped for each display. On every scale, place a cross and the number '70' to represent the 70 [m/s] velocity condition, '70R' for the same velocity but for a rotated tunnel, and the numbers '110' and '110R' to represent the 110 [m/s] velocity condition for the not-rotated and rotated displays respectively.

Please note that the ratings will be compared over all conditions.

Display A

0 1 2 3 4 5 6 7 8 9 10

effort $\longrightarrow$

Display B

0 1 2 3 4 5 6 7 8 9 10

effort $\longrightarrow$

Display C

0 1 2 3 4 5 6 7 8 9 10

effort $\longrightarrow$

Display D

0 1 2 3 4 5 6 7 8 9 10

effort $\longrightarrow$

Display E

0 1 2 3 4 5 6 7 8 9 10

effort $\longrightarrow$

9
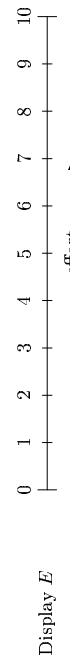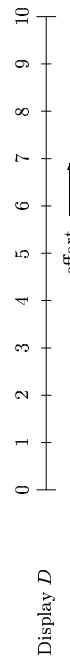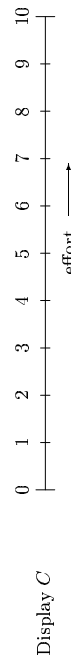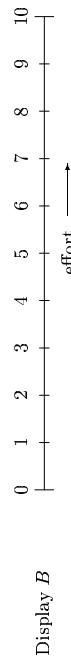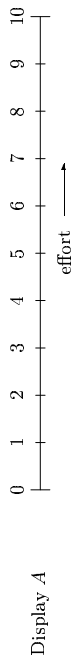
Pilot Questionnaire Experiment X4

Remarks

13. Do you have any remarks on the experimental setup ?

14. Do you have any remarks on the experiment that have not been addressed in this questionnaire ?

10

Pilot Questionnaire Experiment X4

Pilot characteristics

Name . . . .

Year of birth . . . .

Flying experience . . . .

Vision
☐ uncorrected
☐ corrected
☐ glasses
☐ lenses

Hand
☐ left
☐ ambidexter
☐ right

Thank you very much for filling in this questionnaire. Please check whether all questions have been addressed properly. Then send this questionnaire to:

T.U. Delft
Faculteit Luchtvaart- en Ruimtevaarttechniek

t.a.v. ir. M. Mulder
SIMONA-gebouw
Kluyverweg 4
2629 HS Delft

11

Appendix C

Aircraft kinematics and dynamics

The kinematic and dynamic characteristics of aircraft are discussed in this appendix, starting with a definition of reference frames and their transformations in §C.1. The aircraft kinematics and a definition of the aircraft *recti-linear* and *curvi-linear* stationary flight conditions are the subject of §C.2. The mathematical aircraft dynamic models are introduced in §C.3, focusing on the properties of those models that are applied in this thesis. The discussion will be elementary; for a thorough treatment of the topics discussed here, the reader is referred to (Etkin, 1972) and (Brockhaus, 1994).

C.1 Reference frames and transformations

C.1.1 Frames of reference

All frames of reference applied in this thesis are orthogonal and right-handed.

The Inertial frame of reference The Inertial frame of reference $\mathcal{F}^i$ is fixed relative to the Earth. The $O_i X_i Y_i$ plane is a horizontal plane with longitudinal axis X_i pointing towards the North. The Z_i axis points towards the center of the Earth. The origin of $\mathcal{F}^i$ can be defined arbitrarily. The World axes frame of reference $\mathcal{F}^w$ is identical to $\mathcal{F}^i$.

The Geodetical frame of reference The Geodetical frame of reference $\mathcal{F}^g$ is similar to the Inertial frame of reference, except that the origin of $\mathcal{F}^g$ moves along with the aircraft center of gravity. Its attitude remains coincident with $\mathcal{F}^i$.

The aircraft Body frame of reference The aircraft attitude relative to $\mathcal{F}^g$ is specified with the Body axes reference frame $\mathcal{F}^b$, the origin of which is positioned in the aircraft center of gravity. The longitudinal axis X_b is pointed forward, along the fuselage centerline, and lies within the aircraft plane of symmetry $O_b X_b Z_b$, with Z_b pointed downwards. The

lateral axis Y_b is perpendicular to the plane of symmetry and points to the right.

The Aerodynamic frame of reference The attitude of the aircraft velocity vector with respect to $\mathcal{F}^b$ is defined by the Aerodynamic frame of reference $\mathcal{F}^a$. The origin of $\mathcal{F}^a$ lies in the aircraft center of gravity. The longitudinal axis X_a coincides with the aircraft velocity vector. The lateral axis Y_a is perpendicular to X_a and is pointed to the right. The vertical axis Z_a is perpendicular to the $O_a X_a Y_a$ plane and is pointed downwards.

The Flight-Path frame of reference The attitude of the aircraft velocity vector with respect to $\mathcal{F}^g$ is defined by the Flight-Path frame of reference $\mathcal{F}^p$. The origin of $\mathcal{F}^p$ is the aircraft center of gravity. The longitudinal axis X_p coincides with the aircraft velocity vector. The lateral axis Y_p is pointed to the right and is perpendicular to the vertical (with respect to $\mathcal{F}^g$) plane $O_p X_p Z_p$, of which the vertical axis Z_p is positive downwards.

C.1.2 Co-ordinate transformations

General The orientation of any reference frame relative to another can be given by three angles that are the consecutive rotations about axes Z, Y and X (in that order) that carry the frame into coincidence with the other (Etkin, 1972). E.g. for reference frames $\mathcal{F}^x$ and $\mathcal{F}^y$ the transformation to align the latter with the former is given by:

$$T_y^x \;=\; R_X(\theta_x) \cdot R_Y(\theta_y) \cdot R_Z(\theta_z), \tag{C.1}$$

with:

$$\underbrace{\begin{pmatrix} 1 & 0 & 0 \\ 0 & \cos\theta_x & \sin\theta_x \\ 0 & -\sin\theta_x & \cos\theta_x \end{pmatrix}}_{R_X} ; \underbrace{\begin{pmatrix} \cos\theta_y & 0 & -sin\theta_y \\ 0 & 1 & 0 \\ \sin\theta_y & 0 & \cos\theta_y \end{pmatrix}}_{R_Y} ; \underbrace{\begin{pmatrix} \cos\theta_z & \sin\theta_z & 0 \\ -\sin\theta_z & \cos\theta_z & 0 \\ 0 & 0 & 1 \end{pmatrix}}_{R_Z} .$$

Because these matrices are all orthogonal, Eq. C.1 describes a *rigid body* transformation. The inverse of the transformation matrix equals its transpose: $T_x^y = T_y^{x-1} = T_y^{xT}$.

Body and Geodetical The attitude of the aircraft Body axes $\mathcal{F}^b$ with respect to $\mathcal{F}^g$ is determined by the three Euler angles, heading ψ, pitch θ and roll ϕ, Fig. C.1(a):

$$T_g^b \;=\; R_X(\phi) \cdot R_Y(\theta) \cdot R_Z(\psi). \tag{C.2}$$

The perspective projection method (Appendix D) is partly based on this transformation.

Aerodynamic and Body The attitude of the Aerodynamic reference frame $\mathcal{F}^a$ (the aircraft velocity vector) with respect to the aircraft Body axes is specified with the *angle of attack* α and the *angle of slip* β, Fig. C.1(b):

$$T_a^b \;=\; R_Y(\alpha) \cdot R_Z(-\beta). \tag{C.3}$$

Flight-Path and Geodetical The attitude of the Flight-Path reference frame $\mathcal{F}^p$ (the aircraft velocity vector) with respect to the Geodetical frame of reference $\mathcal{F}^g$ is specified with the *flight-path azimuth* angle χ and the *angle of climb* γ, Fig. C.1(c):

$$T_g^p \;=\; R_Y(\gamma) \cdot R_Z(\chi). \tag{C.4}$$

(a) Body in Geodetical

(b) Aerodynamic in Body

(c) Path in Geodetical
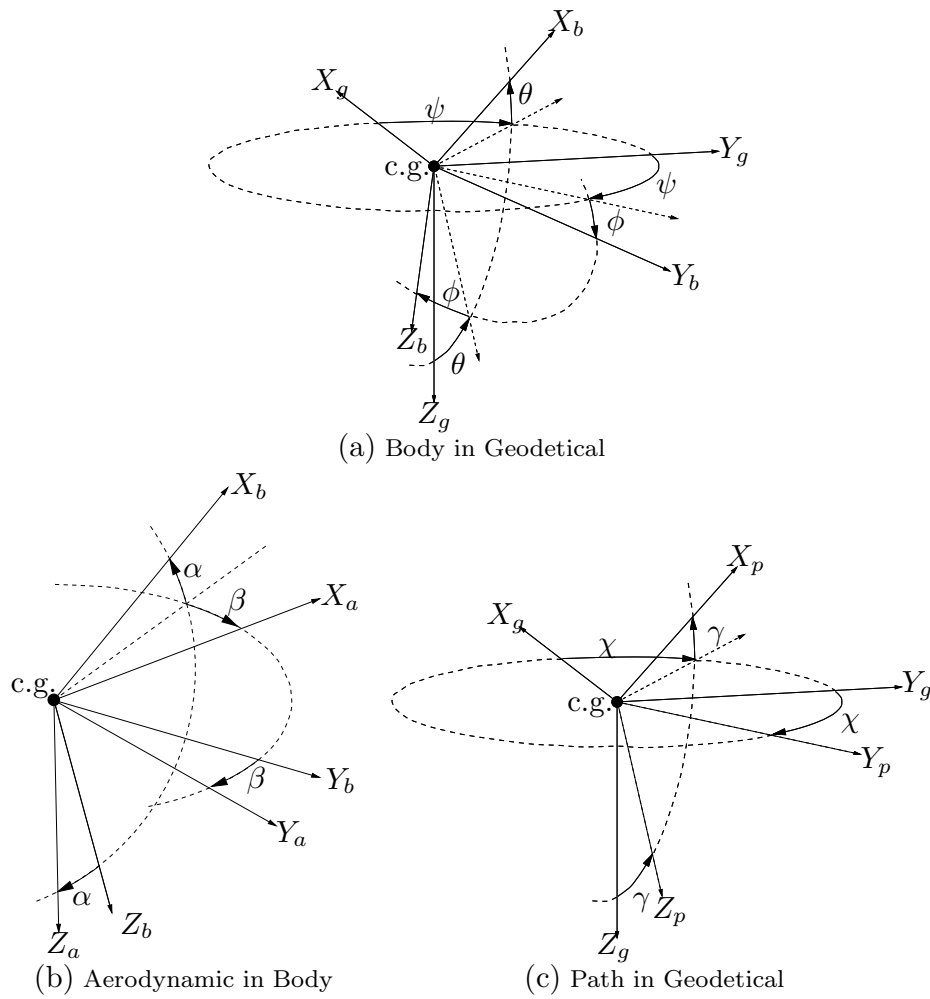
Figure C.1: The relation between the four main frames of reference.

Aerodynamic and Geodetical The attitude of the Aerodynamic reference frame $\mathcal{F}^a$ (the velocity vector) with respect to the Geodetical frame of reference $\mathcal{F}^g$ can also be specified with a combination of the Euler angles and the aerodynamic angles:

$$T_a^g \; = \; T_b^g \cdot T_a^b. \tag{C.5}$$

Because this expression is rather complex, generally Eq. C.4 is preferred.

C.2 Aircraft kinematics

C.2.1 Translational kinematics

The velocity of the aircraft in $\mathcal{F}^b$ ($\underline{V}_b = (u^b, v^b, w^b)^T$) is determined by the attitude of the velocity vector – defined by $\mathcal{F}^a$ – relative to $\mathcal{F}^b$:

$$\underline{V}^b = T_a^b \cdot \underline{V}^a = (V \cos\alpha \cos\beta,\; V \sin\beta,\; V \sin\alpha \cos\beta)^T. \tag{C.6}$$

The velocity of the aircraft in $\mathcal{F}^g$ ($\underline{V}_b = (u^g, v^g, w^g)^T$) is determined by the attitude of the velocity vector – defined by $\mathcal{F}^p$ – relative to $\mathcal{F}^g$:

$$\underline{V}^g = T_p^g \cdot \underline{V}^p = (V \cos\gamma\cos\chi,\ V\cos\gamma\sin\chi,\ -V\sin\gamma)^T. \tag{C.7}$$

As mentioned above, the velocity of the aircraft in $\mathcal{F}^g$ as specified by the attitude of the velocity in $\mathcal{F}^a$ relative to $\mathcal{F}^b$ is given by a complex relation. For small attitude angles, however, a useful approximation has been derived in (Brockhaus, 1994):

$$
\begin{aligned}
\beta &= (\chi - \psi)\cos\gamma\cos\phi + (\theta - \gamma)\sin\phi; \\
\alpha &= -(\chi - \psi)\cos\gamma\sin\phi + (\theta - \gamma)\cos\phi.
\end{aligned}
\tag{C.8}
$$

C.2.2 Rotational kinematics

The rotation rates of the aircraft Body axes ($\underline{\Omega}^b = (p^b, q^b, r^b)^T$) correspond with the time derivatives of the Euler angles ($\underline{\Omega}^g$) through a transformation that is *not* orthogonal:

$$\underline{\Omega}^b = R_g^b \cdot \underline{\Omega}^g \ \ ,\text{with}\ \ R_g^b = \begin{pmatrix} 1 & 0 & -\sin\theta \\ 0 & \cos\phi & \cos\theta\sin\phi \\ 0 & -\sin\phi & \cos\theta\cos\phi \end{pmatrix}. \tag{C.9}$$

C.2.3 Aircraft recti-linear motion

In the recti-linear motion condition the aircraft travels along a straight line. It is assumed that the aircraft rotation vector, all accelerations and the roll angle ϕ are zero. Furthermore, all attitude angles are small. In this flight condition, which forms the basis of the discussion in §3.4, one obtains $\beta = (\chi - \psi)$, $\alpha = (\theta - \gamma)$ and $\underline{V}^b = V(1, \beta, \alpha)^T$.

C.2.4 Aircraft curvi-linear motion

In the curvi-linear motion condition the aircraft travels along a circular path. The aircraft rotation vector in $\mathcal{F}^g$ is given by $\underline{\Omega}^g = (0, 0, V/R)^T$ with R the radius of the curve. For a velocity V, the curve radius in a stationary horizontal turn is determined by the aircraft roll angle according to the following expression (Etkin, 1972):

$$\tan\phi = \frac{V^2}{g_0 R} \ \ \rightarrow \ \ R = \frac{V^2}{g_0 \tan\phi}, \tag{C.10}$$

with g_0 the gravitational acceleration (9.80665 [m/s^2]). It is assumed that all accelerations are zero and that all angles except the roll angle are small. When the circular path is horizontal, one obtains the aerodynamic angles α and β with Eqs C.8 after substituting $\gamma = 0$. The rotation vector in $\mathcal{F}^b$ becomes:

$$\underline{\Omega}^b = R_g^b \cdot \underline{\Omega}^g = \left(\frac{g_0}{V}\right)(-\sin\theta\tan\phi,\ \cos\theta\sin\phi\tan\phi,\ \cos\theta\sin\phi)^T. \tag{C.11}$$

This flight condition forms the basis of the discussion in §3.6.

C.3   Aircraft dynamics

C.3.1   Linear aircraft models

Complex, non-linear aircraft models exist that are used for (flight) simulation purposes. For any stationary flight condition these models can be linearized, yielding linear time-invariant (LTI) descriptions of the dynamic aircraft system (Etkin, 1972; Brockhaus, 1994). These LTI systems can be used to design and evaluate automatic flight control systems. At the Faculty of Aerospace Engineering at the DUT an extensive program package – DASMAT – has been developed with which these linear models can be calculated for a large variety of flight conditions (van der Linden, 1996).

An important property of linear aircraft models is that the description of aircraft dynamic behaviour is separated in two independent parts. The symmetric linear aircraft models describe the aircraft longitudinal/vertical motion, i.e. the motion in the aircraft plane of symmetry. The inputs of the model are generally the elevator δ_e and the thrust δ_T. The symmetric aircraft model has two dominant modes: a low-frequent *phugoid* mode marking the exchange in potential and kinetic energy, and a relatively high-frequency *short period* mode describing the pitch attitude response. The asymmetric linear aircraft models describe the longitudinal/lateral motion, i.e. the motion perpendicular to the plane of symmetry. The inputs of the model are the aileron δ_a and the rudder δ_r. The asymmetric aircraft model has three dominant modes: a very slow and usually unstable *spiral divergence*, a relatively high-frequency *Dutch roll* and the *roll-subsidence* of which the latter mode describes the initial aircraft roll response. Both the asymmetric and the symmetric aircraft motion models can be extended with models incorporating the effects of turbulence (Mulder & van der Vaart, 1994).

In the experiments described in this thesis, the pilot could use only the aileron and elevator control signals. Therefore, the linearized aircraft models in both the dimensions were *augmented* with Automatic Flight Control System (AFCS). The symmetric models included an elementary *auto-throttle* system, using δ_T, that maintained a constant aircraft velocity. The asymmetric models were extended with a *yawdamper/turn-coordinator* system, using δ_r, that increased the damping of the Dutch roll mode and minimized the side-slip β.

The augmented linear aircraft models were used in the simulations of Experiment X6. The data of the Airbus A300 model was obtained from (Brockhaus, 1994), whereas the Cessna Citation 500 model was derived with DASMAT (van Oorschot, 1997b).

C.3.2   Simplified linear aircraft models

From the discussion of the philosophy of experimenting in Chapter 4, it follows that the pilot model identification procedure puts rather strict demands on the aircraft model:

(i) It must be a linear, time-invariant (LTI) system.

(ii) The aircraft model must be a *cascade* combination of transfer functions, serially connecting the main aircraft states. A cascade model structure is necessary for an

analytic computation of the bias and variance of the estimated frequency responses (Appendix F). Furthermore, such a structure provides the necessary freedom in inserting the forcing function signals.

(iii) The order of the cascaded aircraft transfer functions must be low and the bandwidth of these systems high to prevent an attenuation of the forcing function signals by the aircraft system itself. This could decrease the amount of energy inserted in the closed loop which has a detrimental effect on the identification. Compensating the forcing functions for the aircraft dynamics can partly solve this problem, as has been discussed in Chapter 4.

(iv) The aircraft model must allow a smooth control of the aircraft motion. The application of aircraft dynamics that are too sluggish would lead to pilot fatigue and varying pilot behaviour, having a negative effect on the pilot remnant.

(v) The aircraft flying characteristics must be such to allow the pilots sufficient freedom to choose their control strategy, i.e. for all loop closures a pilot should have the possibility to substantially vary the bandwidth and stability characteristics of the closed loop system.

Summarizing, these requirements on the one hand dictate the manner in which the aircraft dynamics are modelled – (i)-(ii) – and on the other hand determine the aircraft handling characteristics – (iii)-(v). Extensive experimentation revealed that the linear aircraft models of the Cessna Citation 500, that form the basis of the discussion below, satisfied all requirements except demand (ii). Hence, the augmented linear aircraft models as derived in §C.3.1 had to be simplified once again to obtain the cascaded system description of Chapter 4, in both the dimensions, that was used in the experiments.

Asymmetric model structure A well-designed yawdamper/turn-coordinator augmentation attenuates the effects of the Dutch roll and spiral divergence modes, leaving only the roll subsidence mode intact. Furthermore, the effects of side-slip β are minimized. The cascaded model describing the asymmetric aircraft dynamics, illustrated in Fig. 2.10(a), consists of the serial connection of three elementary linear transfer functions:

(i) The <u>Roll response</u>, representing the roll angle response to an aileron deflection (the roll subsidence mode):

$$H_{\delta_a}^{\phi}(s) = \frac{K_\phi}{s(1 + \tau_\phi s)}, \tag{C.12}$$

with K_ϕ ([-]) and τ_ϕ ([s]) the roll response gain and time constant, respectively. Both the variables depend on the velocity of the aircraft.

(ii) <u>Turn co-ordination</u>, representing the (steady-state) relation between the aircraft's heading angle rate and roll angle (§C.2):

$$H_{\phi}^{\psi_e}(s) = \frac{g_0}{V_{tas}} \frac{1}{s}, \tag{C.13}$$
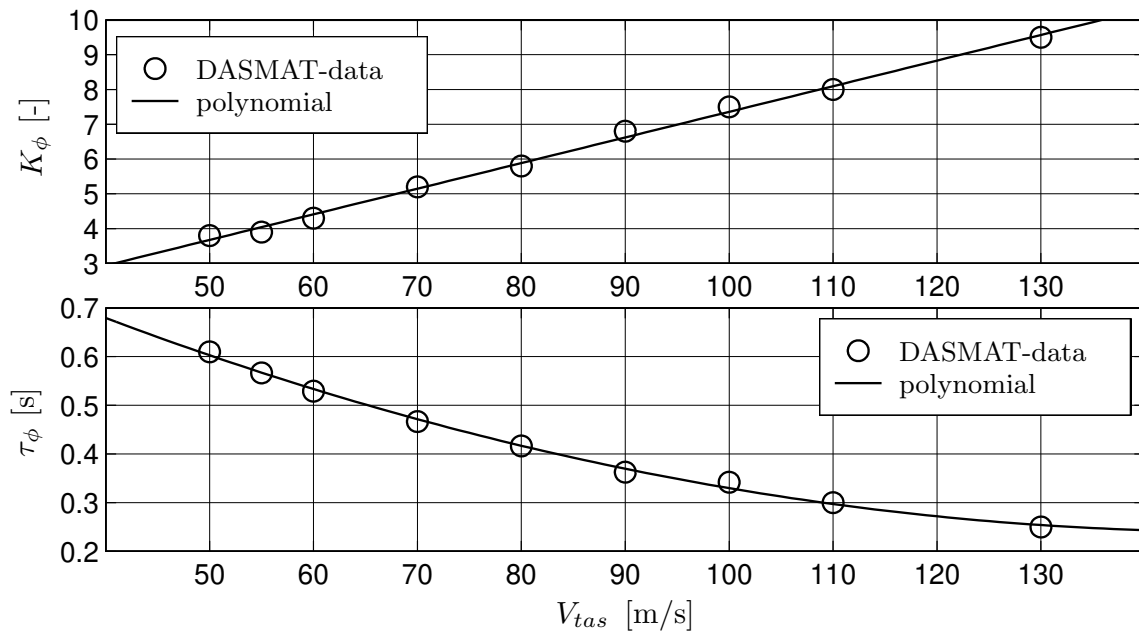
Figure C.2: The parameters of the simplified asymmetric aircraft model roll response (Eq. C.12) as a function of the aircraft velocity V_{tas} (Cessna Citation 500 – DASMAT).

with g_0 the gravitational acceleration ($[m/s^2]$) and V_{tas} ($[m/s]$) the aircraft velocity.

(iii) <u>Path integration</u>, representing the relation between the aircraft's lateral position and the heading angle (in this context with respect to the reference trajectory):

$$H_{\psi_e}^{X_e}(s) = V_{tas}\frac{1}{s}. \tag{C.14}$$

The simplified aircraft model for asymmetric motion has only a few parameters that depend mainly on the aircraft velocity. Using DASMAT, linear models describing asymmetric aircraft motion were obtained for a range of velocity conditions. The augmented linear models were then simplified to obtain the cascade structure. The resulting parameter values of K_ϕ and τ_ϕ for all velocity conditions are illustrated in Fig. C.2. From this figure it is clear that when the aircraft velocity decreases the aircraft dynamics become more sluggish, whereas for increasing velocities the dynamics are faster.

Symmetric model structure   A well-designed auto-throttle augmentation system attenuates the effects of the phugoid mode. The dynamics of the aircraft pitch attitude response in the mid-frequency area (i.e. between the phugoid mode and the short period mode) resembles an integrator. A further simplification yields the serial connection of three elementary linear transfer functions, illustrated in Fig. 2.10(b):

(i) The <u>Pitch response</u>, representing the pitch angle response to an elevator deflection:

$$H_{\delta_e}^{\theta}(s) = K_\theta\frac{1}{s}, \tag{C.15}$$
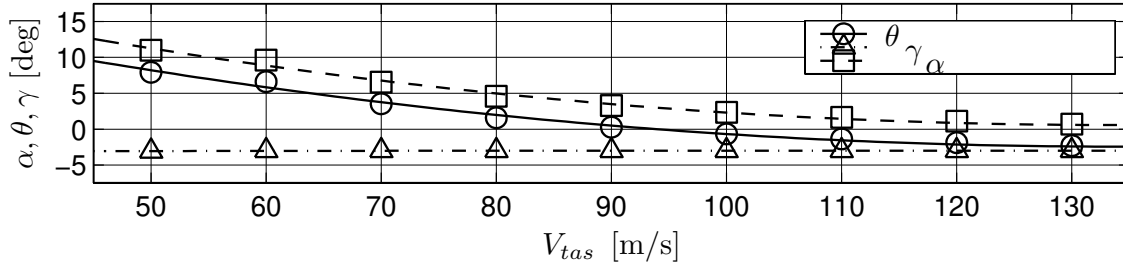
Figure C.3: The initial conditions of the aircraft angle of attack α, angle of climb γ and pitch attitude θ as a function of the velocity V_{tas} (Cessna Citation 500 – DASMAT).

with K_θ ([-]) the pitch response gain, dependent of the aircraft velocity.

(ii) <u>Flight-path response</u>, representing the relation between the aircraft pitch angle and the vertical flight-path angle (with respect to the reference trajectory):

$$H_\theta^{\gamma_e}(s) = \frac{K_\gamma}{(1 + \tau_\gamma s)}. \tag{C.16}$$

This is a lagged response with velocity-dependent parameters K_γ ([-]) and τ_γ ([s]).

(iii) <u>Path integration</u>, representing the relation between the aircraft's vertical position and the vertical flight-path angle (with respect to the reference trajectory):

$$H_{\gamma_e}^{V_e}(s) = V_{tas}\frac{1}{s}. \tag{C.17}$$

The simplified aircraft model for symmetric motion has only a few parameters that depend on the aircraft velocity. Because the symmetric model was used only in Experiment X3 (Chapter 7) for one flight condition (V_{tas}=70 [m/s]), a summary of parameter values suffices here: $K_\theta = 3$ [-]; $K_\gamma = 1$ [-]; $\tau_\gamma = 1.3$ [s].

Model initial condition   The initial conditions of all models were partly defined in DASMAT whereas some of them evolved from the linearization procedure itself. In all recti-linear motion conditions (X1–X3, X5) the initial condition was a stationary flight condition with an angle of climb γ of -3°. For the curvi-linear motion condition (X4), the stationary flight condition was defined with the same angle of climb, but with a pre-defined roll angle that depended on the aircraft velocity and the radius of the turn. The initial condition values of α and θ are shown in Fig. C.3 for all velocities of interest.

Appendix D

The calculation of optical cues

The properties of the optical information sources conveyed by the tunnel display were studied in Chapter 3, treating mainly the end-products of what has been an elaborate analysis. In this appendix the method of obtaining analytical expressions for an optical cue is discussed in §D.1 and §D.2. Analytic expressions are included for the most informative *static* cues in straight, §D.3, and curved, §D.4, tunnel sections. The characteristics of *presentation biases* in curved tunnels is the subject of §D.5.

D.1   The cue computation method

The ultimate goal of the cue computation method is to obtain expressions for optical cues that are *generic*. This means that, first of all, the primary elements of the aircraft state vector – attitude and flight-path angles and position error – must remain variable. Second, the expressions may not implicitly incorporate specific properties of a particular tunnel geometrical design or a particular perspective projection. A general projection method is applied (Foley et al., 1992) as well as a generic definition of the tunnel geometrical shape (§3.4.1 and §3.6.1). This approach yields an array of expressions for a set of optical cues that include the properties of all tunnel display design variables that could possibly affect the characteristics of that particular set of cues.

The properties of a particular optical cue are derived through what can be regarded as an *inversion* of the perspective projection (Chatterji, Menon, & Sridhar, 1994). When the tunnel geometry is projected on the viewplane all that is presented is a wireframe, a combination of lines and line segments. These line segments have a length and an orientation with respect to the viewplane frame of reference $\mathcal{F}^{vr}$, and also with respect to other lines. Most often optical cues emerge from relationships between line segments in terms of orientation and relative distance. When the two end-points of these line segments are known – and so are their projections on the viewplane – all properties of interest can be computed *analytically*. Then, with the help of advanced calculus programs, the non-linear expressions can often be brought into a more manageable form.

D.2 The perspective projection method

The perspective projection method, its main properties and all relevant terminology have been introduced in §3.3. The co-ordinates of an arbitrary point P in World axes $\mathcal{F}^w$ must be transformed to the Viewing axes $\mathcal{F}^v$ before projecting it onto the viewplane $\mathcal{F}^{vr}$. This is a rigid-body transformation. First, the co-ordinates of the point in $\mathcal{F}^w$ are corrected for the position of the COP (the origin of the Viewing axes) in $\mathcal{F}^w$ through a *translation.* Second, the reference frame $\mathcal{F}^w$ is aligned with $\mathcal{F}^v$ through a *rotation* with the three Euler angles. The co-ordinates of P in $\mathcal{F}^v$ can be computed with:

$$\underline{x}_p^v = T_w^v \left(\underline{x}_p^w - \underline{x}_{COP}^w \right), \tag{D.1}$$

with $\underline{x}_p^w$ and $\underline{x}_{COP}^w$ the co-ordinates of P and the COP in $\mathcal{F}^w$ and T_w^v the rigid body transformation matrix. Because $\mathcal{F}^v$ is identical to the aircraft Body axes $\mathcal{F}^b$, and $\mathcal{F}^w$ equals the Geodetical axis $\mathcal{F}^g$, T_w^v equals T_g^b of Eq. C.2. When the co-ordinates of P in $\mathcal{F}^v$ ($\underline{x}_p^v$) are known, the perspective projection yields the co-ordinates of the point in $\mathcal{F}^{vr}$:

$$u_p \;=\; \kappa \left(\frac{y_p^v}{x_p^v} \right); \quad v_p \;=\; -\kappa \left(\frac{z_p^v}{x_p^v} \right). \tag{D.2}$$

An important property of the perspective projection is that the denominator in Eq. D.2, x_p^v, is independent of the roll angle ϕ (substitute Eq. C.2 in Eq. D.1). This allows all geometric functions involving ϕ to be *excluded* from the perspective projection formulas, yielding Eq. 3.8. A rotation of the aircraft along X_b ($=X_v$) yields an *orthogonal* transformation of the tunnel geometry *within* $\mathcal{F}^{vr}$, preserving angles and distances.

D.3 Cues in straight tunnel sections

In §3.4 the aircraft recti-linear motion through a straight tunnel was studied. Below, analytic expressions of all *static* cues that form the basis of this investigation are listed.

(1) Position of the *infinity point* The co-ordinates of this point are given by:

$$u_\infty|_{\phi=0} = \lim_{D_t \to \infty} u_p \Big|_{\phi=0} \;=\; -\kappa \left[\frac{\cos \Gamma_t \sin \psi}{\cos \Gamma_t \cos \psi \cos \theta - \sin \Gamma_t \sin \theta} \right]; \tag{D.3}$$

$$v_\infty|_{\phi=0} = \lim_{D_t \to \infty} v_p \Big|_{\phi=0} \;=\; -\kappa \left[\frac{\cos \Gamma_t \cos \psi \sin \theta + \sin \Gamma_t \cos \theta}{\cos \Gamma_t \cos \psi \cos \theta - \sin \Gamma_t \sin \theta} \right]. \tag{D.4}$$

These co-ordinates are *independent* of the aircraft position with respect to the trajectory.

(2) The *optical splay angles* The following analytic expressions hold for the optical splay angles $\Omega_1 \ldots \Omega_4$, Fig. 3.5:

$$\tan \Omega_1 = \frac{+ (H_t - 2v_e) \cos \psi \qquad + (W_t + 2x_e) \sin \Gamma_t \sin \psi}{+ (H_t - 2v_e) \sin \theta \sin \psi \quad + (W_t + 2x_e)(\cos \theta \cos \Gamma_t - \sin \Gamma_t \sin \theta \cos \psi)};$$

$$\tan \Omega_2 = \frac{+ (H_t - 2v_e) \cos \psi \qquad - (W_t - 2x_e) \sin \Gamma_t \sin \psi}{- (H_t - 2v_e) \sin \theta \sin \psi \quad + (W_t - 2x_e)(\cos \theta \cos \Gamma_t - \sin \Gamma_t \sin \theta \cos \psi)};$$

$$\tan \Omega_3 = \frac{+ (H_t + 2v_e) \cos \psi \qquad + (W_t - 2x_e) \sin \Gamma_t \sin \psi}{+ (H_t + 2v_e) \sin \theta \sin \psi \quad + (W_t - 2x_e)(\cos \theta \cos \Gamma_t - \sin \Gamma_t \sin \theta \cos \psi)};$$

$$\tan \Omega_4 \quad = \frac{+\left(H_t + 2v_e\right)\cos\psi \quad -\left(W_t + 2x_e\right)\sin\Gamma_t\sin\psi}{-\left(H_t + 2v_e\right)\sin\theta\sin\psi \quad +\left(W_t + 2x_e\right)\left(\cos\theta\cos\Gamma_t - \sin\Gamma_t\sin\theta\cos\psi\right)}.$$

(D.5)

These expressions are *independent* of the aircraft roll angle, ϕ, the properties of the perspective projection, κ, and the distance into the tunnel, D_t. A similar expression holds for the fifth splay angle, Ω_5, of the *virtual* line connecting the tops of the altitude poles:

$$\tan \Omega_5 \quad = \frac{+\left(H_t - 2v_e\right)\sin\psi\sin\theta \quad -\left(2x_e\right)\left(\cos\theta\cos\Gamma_t - \sin\Gamma_t\sin\theta\cos\psi\right)}{+\left(H_t - 2v_e\right)\cos\psi \quad +\left(2x_e\right)\sin\Gamma_t\sin\psi}$$

(D.6)

This splay angle has the same properties as the other angles. Note that because splay angle Ω_5 is computed with respect to the vertical instead of the horizontal pseudo-horizon (as in $\Omega_1 \ldots \Omega_4$) the nominator and denominator of the expression appear to be swapped.

(3)–(5) The *lateral displacement* cues   Analytic expressions for ϵ_i (left), η_i (right) and π_i (altitude pole) of frame i can be derived directly from the perspective mapping formulas Eq. D.2. For small position errors and small attitude angles the following expression can be obtained for ϵ_i (with D_i the distance to frame i, measured along X_t):

$$\epsilon_i \quad = \quad \kappa \left[\frac{2D_i\sin\psi \quad + \quad \left(W_t + 2x_e\right)\cos\psi}{2D_i\cos\psi \quad - \quad \left(W_t + 2x_e\right)\sin\psi} \right].$$

(D.7)

Similar equations can be derived for η_i and π_i, expressions that together form the basis of the computation of all lateral displacement cues, listed in Table 3.1.

(6) The *vertical frame line* angles   The angles ζ_i (left) and ξ_i (right) of the vertical frame lines of frame i are defined in $\mathcal{F}^{vr}$. Assuming that all angles are small yields:

$$\zeta_i \quad = \quad \phi - \left(\frac{W_t + 2x_e}{2D_i}\right)\left(\theta + \Gamma_t\right); \quad \xi_i \quad = \quad \phi + \left(\frac{W_t - 2x_e}{2D_i}\right)\left(\theta + \Gamma_t\right).$$

(D.8)

(7)–(9) The *vertical displacement* cues   Analytic expressions for μ_i (bottom) and ν_i (top) of frame i can be derived in a similar way as for the lateral displacement cues:

$$\mu_i \quad = \quad \kappa \left[\Gamma_t + \left(\frac{2D_i\cos\psi\sin\theta \quad + \quad \left(H_t - 2v_e\right)\cos\theta}{2D_i\cos\psi\cos\theta \quad - \quad \left(H_t - 2v_e\right)\sin\theta} \right) \right].$$

(D.9)

A similar expression can be derived for ν_i. Together, these expressions form the basis of the computation of all vertical displacement cues, listed in Table 3.1.

(10) The *lateral frame line* angles   The angles ρ_i (bottom) and σ_i (top) of the horizontal lines of frame i are defined in $\mathcal{F}^{vr}$. Assuming that all angles are small yields:

$$\rho_i \quad = \quad \phi - \left(\frac{H_t - 2v_e}{2D_i}\right)\psi; \quad \sigma_i \quad = \quad \phi + \left(\frac{H_t + 2v_e}{2D_i}\right)\psi.$$

(D.10)

The angles of the lateral and vertical frame lines (Eqs D.8 and D.10) show a complex relationship between the aircraft position error in one dimension and the aircraft attitude in the other. They only convey information about these quantities for frames that are close to the viewplane: for larger distances D_i these angles approach the roll angle ϕ.

D.4 Cues in curved tunnel sections

In §3.6 the aircraft curvi-linear motion through a circular tunnel was studied. Below, analytic expressions of all *static* cues that form the basis of this investigation are listed.

(4) The optical splay angles   When θ and ψ are small, the following expressions hold for the optical splay angles $\Omega_1 \dots \Omega_4$ of segment s_i, Fig. 3.11:

$$
\begin{aligned}
\tan \Omega_{1_{s_i}} &= \frac{(H_t - 2v_e)\cos(\frac{\sigma_{s_i}+\sigma_{s_i-1}}{2})}{W_t \cos(\frac{\triangle \Psi}{2}) + 2x_e \cos(\frac{\sigma_{s_i}+\sigma_{s_i-1}}{2}) + 4R_t \sin(\frac{\sigma_{s_i}}{2})\sin(\frac{\sigma_{s_i-1}}{2})}; \\
\tan \Omega_{2_{s_i}} &= \frac{(H_t - 2v_e)\cos(\frac{\sigma_{s_i}+\sigma_{s_i-1}}{2})}{W_t \cos(\frac{\triangle \Psi}{2}) - 2x_e \cos(\frac{\sigma_{s_i}+\sigma_{s_i-1}}{2}) - 4R_t \sin(\frac{\sigma_{s_i}}{2})\sin(\frac{\sigma_{s_i-1}}{2})}; \\
\tan \Omega_{3_{s_i}} &= \frac{(H_t + 2v_e)\cos(\frac{\sigma_{s_i}+\sigma_{s_i-1}}{2})}{W_t \cos(\frac{\triangle \Psi}{2}) - 2x_e \cos(\frac{\sigma_{s_i}+\sigma_{s_i-1}}{2}) - 4R_t \sin(\frac{\sigma_{s_i}}{2})\sin(\frac{\sigma_{s_i-1}}{2})}; \\
\tan \Omega_{4_{s_i}} &= \frac{(H_t + 2v_e)\cos(\frac{\sigma_{s_i}+\sigma_{s_i-1}}{2})}{W_t \cos(\frac{\triangle \Psi}{2}) + 2x_e \cos(\frac{\sigma_{s_i}+\sigma_{s_i-1}}{2}) + 4R_t \sin(\frac{\sigma_{s_i}}{2})\sin(\frac{\sigma_{s_i-1}}{2})}.
\end{aligned}
\tag{D.11}
$$

When $R_t \to \infty$ ($\triangle \Psi$, σ_{s_i} and σ_{s_i-1} go to zero) these equations are identical to those for straight tunnels (Eq. D.5 with $\psi = \theta = \Gamma_t = 0$). When the number of segments becomes large ($\triangle \Psi \to 0$ and $\sigma_{s_i} \to \sigma_{s_i-1} \to \sigma_s$) the Eqs D.11 depict the angles of the lines tangent to the *circular* left and right tunnel walls at an angular viewing distance σ_s:

$$
\begin{aligned}
\tan \Omega_1(\sigma_s) &= \frac{(H_t - 2v_e)\cos(\sigma_s)}{W_t + 2x_e \cos(\sigma_s) + 2R_t(1 - \cos(\sigma_s))}; \\
\tan \Omega_2(\sigma_s) &= \frac{(H_t - 2v_e)\cos(\sigma_s)}{W_t - 2x_e \cos(\sigma_s) - 2R_t(1 - \cos(\sigma_s))}; \\
\tan \Omega_3(\sigma_s) &= \frac{(H_t + 2v_e)\cos(\sigma_s)}{W_t - 2x_e \cos(\sigma_s) - 2R_t(1 - \cos(\sigma_s))}; \\
\tan \Omega_4(\sigma_s) &= \frac{(H_t + 2v_e)\cos(\sigma_s)}{W_t + 2x_e \cos(\sigma_s) + 2R_t(1 - \cos(\sigma_s))}.
\end{aligned}
\tag{D.12}
$$

Linearizing the splay angle Eqs D.11 leads to expressions for the *change in splay* from the reference condition, listed in §3.6.2 as Eqs 3.43. The *gains* that result from the linearization depend on which splay angle is examined: the gains of splay angles 1 and 4 (outer curve wall) and those of 2 and 3 (inner curve wall) are equal. The following expressions hold:

$$
\begin{aligned}
K_{X^1_{s_i}} &= \frac{2H_t \cos^2(\frac{\sigma_{s_i}+\sigma_{s_i-1}}{2})}{H_t^2 \cos^2(\frac{\sigma_{s_i}+\sigma_{s_i-1}}{2}) + \left(W_t \cos(\frac{\triangle \Psi}{2}) + 4R_t \sin(\frac{\sigma_{s_i}}{2})\sin(\frac{\sigma_{s_i-1}}{2})\right)^2}; \\
K_{V^1_{s_i}} &= \frac{2\cos(\frac{\sigma_{s_i}+\sigma_{s_i-1}}{2})\left(W_t \cos(\frac{\triangle \Psi}{2}) + 4R_t \sin(\frac{\sigma_{s_i}}{2})\sin(\frac{\sigma_{s_i-1}}{2})\right)}{H_t^2 \cos^2(\frac{\sigma_{s_i}+\sigma_{s_i-1}}{2}) + \left(W_t \cos(\frac{\triangle \Psi}{2}) + 4R_t \sin(\frac{\sigma_{s_i}}{2})\sin(\frac{\sigma_{s_i-1}}{2})\right)^2}; \\
K_{X^2_{s_i}} &= \frac{2H_t \cos^2(\frac{\sigma_{s_i}+\sigma_{s_i-1}}{2})}{H_t^2 \cos^2(\frac{\sigma_{s_i}+\sigma_{s_i-1}}{2}) + \left(W_t \cos(\frac{\triangle \Psi}{2}) - 4R_t \sin(\frac{\sigma_{s_i}}{2})\sin(\frac{\sigma_{s_i-1}}{2})\right)^2};
\end{aligned}
$$
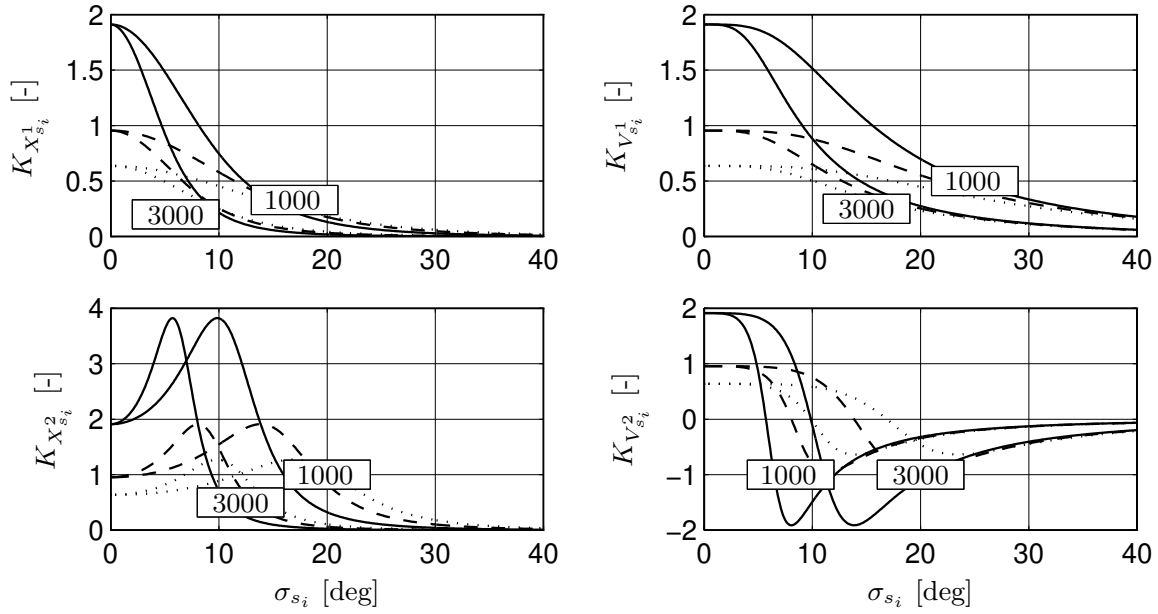
Figure D.1: Splay angle gains of the outer curve wall (top) and the inner curve wall (bottom) as a function of the viewing distance σ_{s_i}. It is assumed that the square tunnel ($H_t = W_t$) is a perfect circle ($\triangle\Psi = 0$, $\sigma_{s_i} = \sigma_{s_{i-1}}$). The lines represent the variables for two curve radii (1000 and 3000 [m]). The continuous, dashed and dotted lines represent tunnel sizes of 30, 60 and 90 [m], respectively.

$$K_{V_{s_i}^2} = \frac{2\cos(\frac{\sigma_{s_i}+\sigma_{s_{i-1}}}{2})\left(W_t\cos(\frac{\triangle\Psi}{2}) - 4R_t\sin(\frac{\sigma_{s_i}}{2})\sin(\frac{\sigma_{s_{i-1}}}{2})\right)}{H_t^2\cos^2(\frac{\sigma_{s_i}+\sigma_{s_{i-1}}}{2}) + \left(W_t\cos(\frac{\triangle\Psi}{2}) - 4R_t\sin(\frac{\sigma_{s_i}}{2})\sin(\frac{\sigma_{s_{i-1}}}{2})\right)^2}\ .$$

$$(D.13)$$

When $R_t \to \infty$ these gains become identical to those of straight tunnel sections, listed in §3.4.2 as Eqs 3.12-3.15. As illustrated in Fig. D.1, an important difference with the splay angle gains of straight tunnel sections, is that for circular trajectories these gains are *not constant*. Rather, they are a function of the *angular* viewing distance into the curve σ_{s_i}. The splay gains of the outer curve wall ($K_{X_{s_i}^1}$ and $K_{V_{s_i}^1}$) have their maximum values for small viewing distances and decrease monotonously when σ_{s_i} becomes larger. Hence, this splay angle information about the aircraft position relative to the centercircle is most useful for small viewing distances. The splay gains of the inner curve wall have their maximum values for a certain viewing distance ahead. Here, the splay information about position error is strongest around the inner bend of the curve, i.e. in the same region as the curve's tangent point. The splay gain $K_{X_{s_i}^2}$ of the inner curve lines, marking the change in splay due to a lateral position error x_e, varies from being equal to becoming twice as large as that of the outer curve lines. The sign of the splay gain $K_{V_{s_i}^2}$ of the inner curve lines, marking the change in splay due to a vertical position error v_e, even *changes its sign* when looking farther into the curve. This could lead to pilot confusion.

Because the gains $K_{V_{s_i}^1}$ of the outer curve lines do not show this phenomenon, the splay information conveyed by these lines are probably more suitable for vertical control.

Fig. D.1 shows that as the curve radius increases the maximum values of the splay angle gains move to shorter angular viewing distances. One should keep in mind, however, that for larger curve radii the same angular distance σ_{s_i} represents a larger *spatial* viewing distance S_{s_i} along the centercircle. The effect of the tunnel size is similar as for straight tunnels: it simply scales the splay angle gains. For the inner curve wall an additional effect of the tunnel size is that it changes the maximum values of the splay angle gains to larger viewing distances. This effect can be attributed to the fact that the area near the curve's tangent point moves forward when tunnels become larger, discussed below.

(7) The tangent point The position of the tangent point in $\mathcal{F}^{vr}$ is given by:

$$\eta^{TP}\big|_{\phi=0} = \kappa \left[\sqrt{\frac{W_t}{R_t}} \sqrt{1 - \frac{2x_e}{W_t}} - \psi \right]. \tag{D.14}$$

Linearization of this equation yields the expressions listed in Table 3.2.

D.5   Presentation biases in curved tunnel sections

Due to the perspective projection method, the nearest part of the tunnel that is shown on the display is always located some distance ahead of the viewplane. In circular tunnel sections the first visible part of the tunnel geometry is *bended towards the inner side of the curve* leading to a situation where, even when the aircraft is aligned with and located on the centercircle, the display conveys small deviations in these quantities, referred to as *presentation biases* (Mulder, 1998). Below, the presentation biases are discussed for two cases: (i) the tunnel trajectory is a perfect circle ($\triangle\Psi$=0); (ii) the circular trajectory is approximated by a concatenation of line segments (finite $\triangle\Psi$).

Biases in a *circular* tunnel

In a circular tunnel the segments are infinitely small, i.e. $\triangle\Psi$=0 and $\sigma_{s_i} = \sigma_{s_{i-1}} = \sigma_s$. Examining the circular tunnel is useful for analyzing the cues conveyed by the first visible parts of the tunnel geometry, i.e. the intersections of the tunnel contour lines with the viewing volume. Fig. D.2 shows the tunnel images for a right turn for three tunnel widths and two curve radii. At a first glance it appears as if the aircraft is heading outwards and, especially for larger tunnel sizes, is located towards the outer side of the curve.

The minimum viewing distances Consider Fig. D.3(a), showing a top view of the situation. From this figure it is clear that the first visible parts of the inner and outer curve tunnel walls are located some distance from the COP. First the outer curve tunnel wall intercepts the viewing volume (σ^{out}), and then the inner curve tunnel wall (σ^{in}):

$$\sigma^{out} = \arcsin\left(\frac{D^{out}}{R_t + W_t/2}\right); \quad \sigma^{in} = \arcsin\left(\frac{D^{in}}{R_t - W_t/2}\right), \tag{D.15}$$
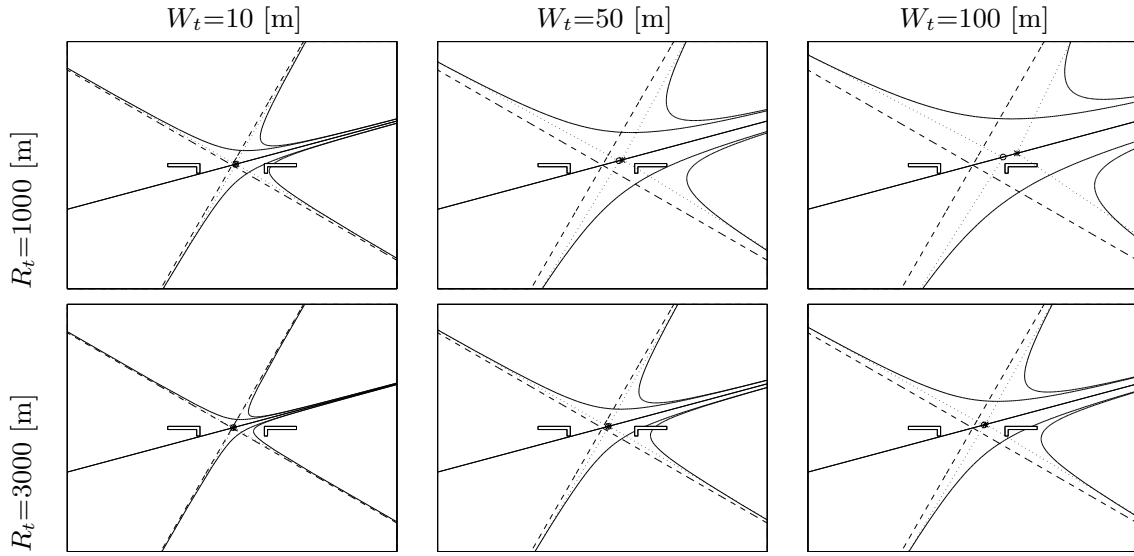
Figure D.2: Tunnel display images for a turn to the right. The aircraft attitude and position errors relative to the tunnel centercircle are zero. The dashed lines show the splay lines of the first visible elements of the tunnel geometry for an *imaginary* straight trajectory tangent to the centercircle. The dotted lines show the splay angles of the first visible elements of the tunnel geometry for the circular trajectory. These lines intersect at the infinity points of the inner (∘) and outer (∗) curve walls.

with: $D^{out} = \frac{\sqrt{R_t^2 + (1+1/\tau^2)W_t(R_t + W_t/4)} - R_t}{(\tau + 1/\tau)}$; and $D^{in} = \frac{R_t - \sqrt{R_t^2 - (1+1/\tau^2)W_t(R_t - W_t/4)}}{(\tau + 1/\tau)}$, where τ represents $\tan(HGFOV/2)$. The values of D^{out} and D^{in} are shown in Fig. D.3(b) for different combinations of R_t and W_t, with respect to the minimum viewing distance for straight trajectories, D_{min}, Eq. 10.3. It is clear that the outer curve wall intersects the viewing volume at a distance smaller than D_{min}, whereas the opposite holds for the inner curve wall: $D^{out} < D_{min} < D^{in}$. For larger curve radii the differences between D^{out} and D^{in} decrease, whereas these differences increase for larger tunnel sizes. These phenomena can be explained by the facts that for larger curve radii the trajectory curvature itself is smaller, and that for larger tunnels the tunnel geometry intersects the viewing volume at larger viewing distances, respectively.

Location of the infinity point   The location of the infinity point conveyed by the first visible splay angles follows from Eq. 3.40, with $\psi = \triangle\Psi = 0$: $u_\infty|_{\phi=0} = \kappa \tan(\sigma_s)$. Then, since σ_s is always positive ($\sigma^{in} > \sigma^{out} > 0$), the infinity point will always be located towards the *inner side* of the curve. Hence, the heading of the aircraft as conveyed by the first visible part of the trajectory on the tunnel display is *directed to the outer side of the curve*, even when the heading is tangential to the centercircle. Fig. D.2 illustrates that this presentation bias increases for larger tunnels and smaller curve radii.

Optical splay angles   The angles of the tangent lines of the first visible part of the circular trajectory can be computed with Eqs D.12 after substituting σ^{out} and σ^{in} and $x_e = v_e = 0$. It is clear that because $\sigma^{in} > \sigma^{out} > 0$ and because Ω_2 changes faster than

(a) top view of the situation

(b) D^{out} and D^{in}, relative to D^{min}
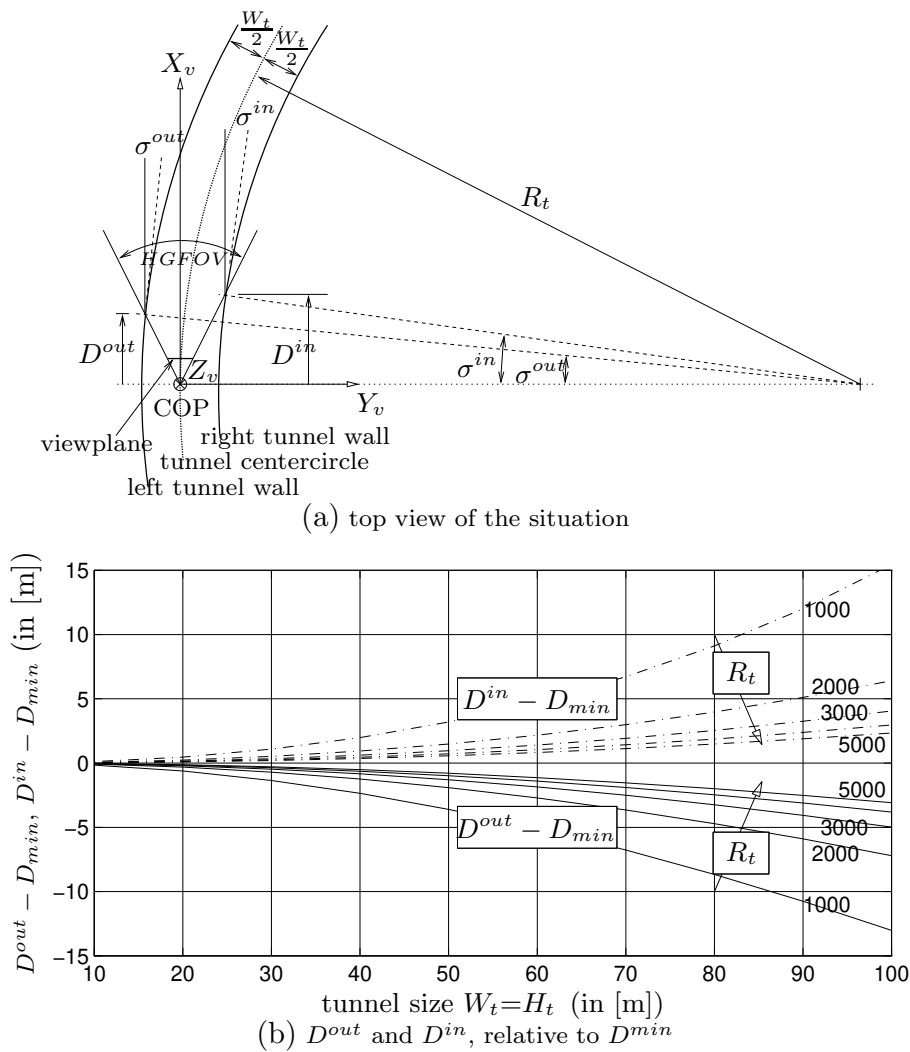
Figure D.3: The minimum viewing distances of the outer curve wall, D^{out}, and inner curve wall, D^{in}, shown with respect to the minimum viewing distance for a straight trajectory, D_{min}, as a function of the tunnel size W_t and the curve radius R_t (in [m]). The aircraft Body axes are aligned with the tunnel centercircle.

Ω_1 when looking farther into the curve the angles of the tangent lines convey an aircraft position towards the inner side of the curve. Compared to the splay angles as they would have been depicted for an imaginary straight trajectory tangential to the tunnel centercircle, shown by the dashed lines in Fig. D.2, the splays are slightly off-central. As indicated with the dotted lines in Fig. D.2, however, this is a marginal effect: it is small when the tunnel sizes are large and disappears for larger curve radii. Hence, although a pilot could interpret these first visible splay lines as if the aircraft would be positioned to the *inner side* of the curve, this can be regarded as only a secondary effect.

Lateral displacements Fig. D.2 clearly shows that the splay lines of the first visible part of the circular trajectory originate from positions on the viewplane borders that are off-central with respect to the splay lines corresponding with the imaginary straight

$\sigma_{f_i=1} = 10$ [deg] $\sigma_{f_i=1} = 6\frac{2}{3}$ [deg] $\sigma_{f_i=1} = 3\frac{1}{3}$ [deg]
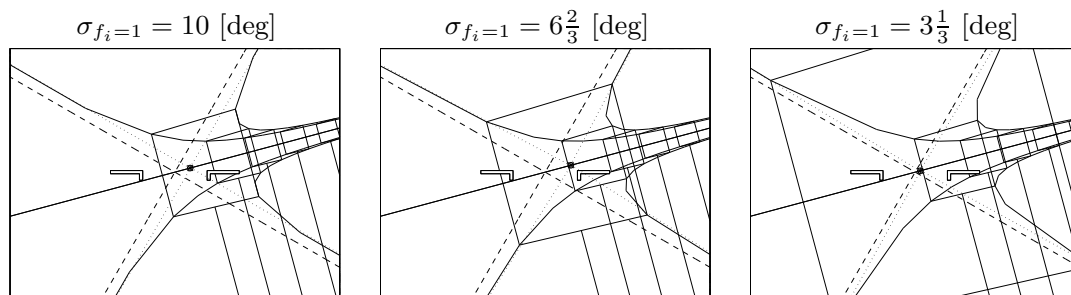
Figure D.4: Tunnel display images corresponding with a segmented right turn ($\triangle\Psi$=5 [deg], c=2, R_t=1000 [m], W_t=45 [m]). The aircraft attitude and position errors relative to the centercircle are zero. Recall that $\sigma_{f_i=1}$ depicts the angular viewing distance to the first visible frame. The dashed lines show the splay lines of an *imaginary* straight trajectory tangent to the centercircle. The dotted lines show the splay lines of the first visible elements of the tunnel geometry for the segmented trajectory, intersecting at the infinity points of the inner (o) and outer curve walls (∗).

trajectory. It appears as if the tunnel geometry as a whole is positioned slightly to the right, i.e. towards the *inner side* of the curve. Pilots could interpret this lateral displacement as if the aircraft would be positioned to the *outer side* of the trajectory. This presentation bias becomes larger for increasing tunnel sizes and for smaller curve radii.

Biases in a *segmented* tunnel

In a segmented tunnel the biases are similar to those found for circular tunnels. There are, however, some differences that depend on the granularity of the segmentation.

Location of the infinity point   Consider the location of the infinity point emerging from the first visible segment on the screen: $u_{\infty_{s_i}}\big|_{\phi=0} = \kappa\tan(\sigma_{s_i} - \triangle\Psi/2)$. When $\sigma_{s_i} > \triangle\Psi/2$ the infinity point will be located to the right of the screen, similar to the situation for circular tunnels. When $\sigma_{s_i} < \triangle\Psi/2$, however, the infinity point will be located to the left. Thus, when the tunnel segmentation would be rather coarse, i.e. $\triangle\Psi$ is large, the infinity point moves from the inner side of the curve towards the outer side of the curve when the aircraft travels to the end of the current segment s_i. In this case the presentation biases change as a function of the aircraft position along the centercircle relative to the segment through which the aircraft flies. To prevent this phenomenon the segmentation angle $\triangle\Psi$ should be defined smaller than $2\sigma^{in}$.

Optical splay angles   When the segmentation of the trajectory is not too coarse the optical splay angles lead to only a small presentation bias. The lateral displacements of the tunnel geometry as a whole towards the inner side of the curve, however, leads to a considerable presentation bias. Pilots could interpret this lateral displacement as if the aircraft would be positioned to the *outer side* of the trajectory. This presentation bias
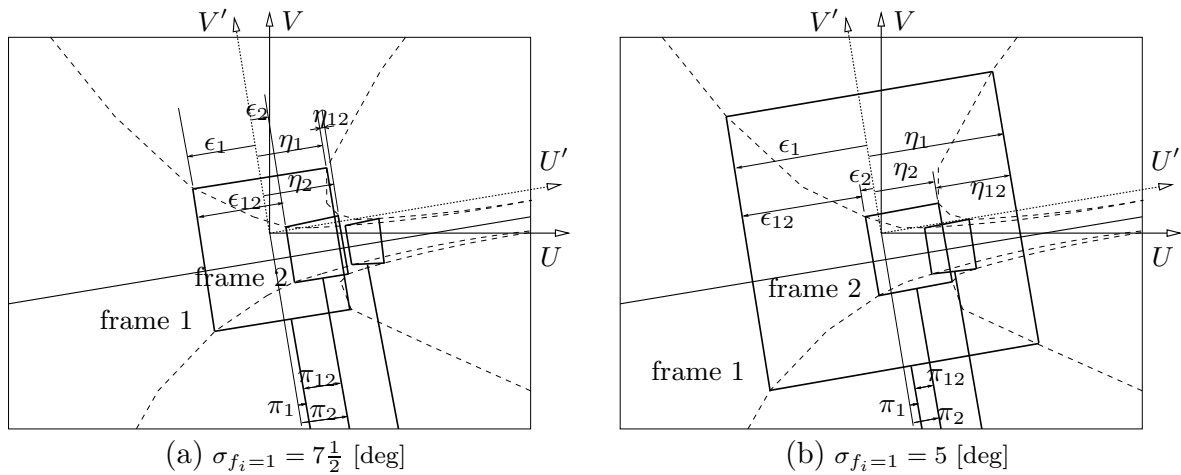
Figure D.5: Tunnel display images corresponding with a segmented ($\triangle\Psi$=5 [deg], c=2) turn to the right, for a curve radius of 1000 [m] and a tunnel width of 45 [m]. The attitude and position errors relative to the tunnel centercircle are zero. $\sigma_{f_i=1}$ depicts the angular viewing distance to the first visible frame. In this figure, ϵ_i, η_i, and π_i represent the lateral displacements of the lateral frame lines and altitude poles of frame i. ϵ_{ij} and η_{ij} mark the relative lateral displacements of frames i and j. (U, V) and (U', V') represent the not-rotated and rotated viewplane axes, respectively.

becomes larger for increasing tunnel sizes and for smaller curve radii.

Effects of tunnel frames Consider the lateral displacements (ϵ_i, η_i, π_i) of the tunnel frames with respect to the aircraft reference symbol, see Fig. D.5. Three effects can be distinguished. The frames appear off-central which could indicate an aircraft heading towards the outer side of the curve, the first effect, and/or an aircraft position towards the *outer side* of the centercircle, the second effect. When moving towards the first visible frame, this frame moves towards the center of the viewplane (compare Figs D.5(a) and D.5(b)). Hence, both effects decrease when the angular distance to that frame, $\sigma_{f_i=1}$, decreases. A third effect originates from the *relative* displacements of the first visible tunnel frames, ϵ_{ij} and η_{ij}. When taking the symmetrical condition of a straight trajectory as a reference, these relative displacements convey information that corresponds with being positioned to the *inner side* of the curve, i.e. $\epsilon_{12} \gg \eta_{12}$. When moving towards the first visible frame, the second visible frame moves towards the center of the first (compare Figs D.5(a) and D.5(b)), i.e. $\epsilon_{12} \longrightarrow \eta_{12}$. Hence, the relative displacement decreases and the third effect also becomes less important when approaching the first visible frame. All three effects increase for larger curve radii, essentially because – for the same segmentation $\triangle\Psi$ – the frames are located farther ahead and it becomes more difficult to relate them to the actual aircraft position relative to the centercircle.

Appendix E

Analytic pilot models

E.1 Introduction

The principal pilot modelling approaches applied in this thesis, introduced in §2.5.3, are:

- The <u>Multi-Loop Model</u> (MLM), a frequency domain descriptive model extending the structural-isomorphic model of McRuer and his colleagues (McRuer et al., 1965) to the multi-loop situation.

- The <u>Optimal Control Model</u> (OCM), a time domain normative model developed by Kleinman and his colleagues (Kleinman & Baron, 1971).

The main properties of both the models are described in §E.2 and §E.3, respectively.

E.2 The multi-loop pilot model

E.2.1 The quasi-linear pilot model

Research in the two decades following World War II resulted in the successful application of *quasi-linear* describing function theory to the problem of modelling human control behaviour in the elementary single-axis compensatory tracking task, Fig. E.1(a). In this task the operator minimizes the difference E between the output Y of the system to be controlled and a reference signal R. Experiments showed that, as long as the *task variables* remain constant, the operator control behaviour remains constant too (McRuer et al., 1965). It can be described by a *causal* model, a linear differential equation with constant coefficients and a time delay, and a *remnant* model, a stationary noise process. The result is a *quasi-linear pilot model*, Fig. E.1(b), where the describing function model accounts for the portion of the pilot's output that is *linearly* related to the input, and the remnant represents the difference between the causal model output and the experimentally measured output of the human controller.
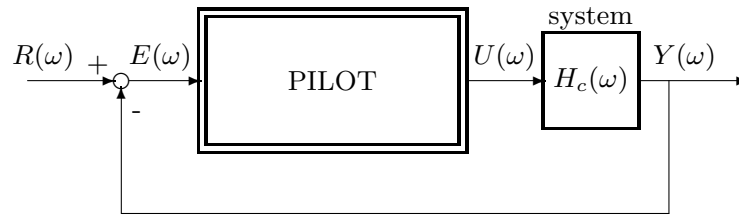
(a) single-axis compensatory tracking task
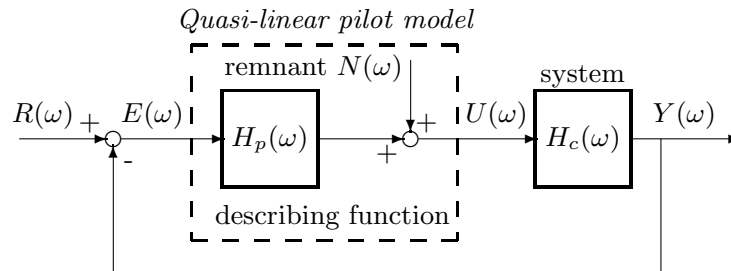
(b) quasi-linear pilot model

Figure E.1: The quasi-linear pilot model in the elementary single-axis compensatory tracking task. In this figure, H_c depicts the dynamics of the system to be controlled. R, E, U, and Y represent the reference signal, the displayed error signal, the pilot control signal and the system output signal, respectively. The quasi-linear pilot model consists of a describing function H_p and a remnant N.

E.2.2   The crossover model theorem

The research of McRuer and his colleagues generalized the *systematic* adaptation of human control behaviour with the postulation of their *crossover model* theorem (McRuer et al., 1965). According to this theorem, human operators *adjust* their control behaviour to the dynamics of the controlled element in such a way that the dynamic characteristics of the open loop transfer function in the crossover region can be described by:

$$H_{OL}(j\omega) \; = \; H_p(j\omega)H_c(j\omega) \; \approx \; \frac{\omega_c}{j\omega}e^{-j\omega\tau_e} \; , \tag{E.1}$$

with ω_c the crossover frequency – the frequency where the open loop magnitude equals 1 – and τ_e a time delay lumping the information processing lags of the operator. When the dynamics of the system to be controlled are known, Eq. E.1 allows a *prediction* of the human control characteristics. The parameters ω_c and τ_e are task-dependent and can be selected on the basis of the so-called *verbal adjustment rules* (McRuer & Krendel, 1974).

Model parameterization: structural-isomorphic models   The linear describing function of the quasi-linear pilot model takes on various forms depending on the precision with which one attempts to reproduce the characteristics of the measured pilot control behaviour. In its most extensive form, the so-called *precision model*, the linear describing

function can be described by (McRuer & Jex, 1967):

$$H_p(j\omega) = \overbrace{K_p}^{\text{gain}} \overbrace{\frac{1 + \tau_L j\omega}{1 + \tau_I j\omega}}^{\text{lead-lag}} \underbrace{\overbrace{\frac{\omega_n{}^2}{(1 + \tau_{N_1} j\omega)(\omega_n{}^2 + 2\zeta_n \omega_n j\omega + (j\omega)^2)}}^{\text{neuromuscular system}}}_{\text{pilot limitations}} \overbrace{e^{-j\omega\tau}}^{\text{time delay}} . \tag{E.2}$$

The parameters of the precision model reflect the pilot *adaptation* characteristics as well as the pilot *limitations* such as the time delay and the neuromuscular system. A well-known approximation of this model is the *simplified precision model* (McRuer & Jex, 1967):

$$H_p(j\omega) = K_p \left(\frac{1 + \tau_L j\omega}{1 + \tau_I j\omega} \right) e^{-j\omega\tau_e}. \tag{E.3}$$

Remnant Despite numerous efforts to obtain insight into the characteristics of the remnant (Levison, Baron, & Kleinman, 1969; Jex, Allen, & Magdaleno, 1971), only very general models have been developed for the SISO situation (McRuer & Krendel, 1974). In this thesis, no attempts were undertaken to further examine the remnant.

E.2.3 Multi-loop pilot models

Attempts to extend the single loop results to multi-loop or multiple loop situations have not been conducted very often. This can be attributed to the fact that multi-loop tasks are much more difficult to examine than single loop tasks. Whereas the tradeoffs between performance, stability and pilot equalization efforts are relatively clear-cut in the single loop task, the number of alternatives increases rapidly in multi-loop situations. Furthermore, the model identification and validation efforts are difficult in these situations. First, there is the problem of determining the feedback loops the operator will close: the model structure itself cannot be identified from experimental data (Stapleford et al., 1969). Second, there exists the conceptual difficulty of identifying systems operating in closed loop. The identification techniques for these closed loop multi-loop applications were not available until the pioneer work of (Stapleford et al., 1967, 1969), and it lasted until the late 1970s until they were formalized mathematically (van Lunteren, 1979). Hence, not many multi-loop operator models have been described in literature. Appendix F is attributed to the identification techniques for the multi-loop tasks described in this thesis.

Multi-loop model structure The human pilot evolves, in a learning and skill-development phase, a particular multi-loop system structure (Krendel & McRuer, 1960). The feedback connections are similar to those which would be selected for the development of an automatic controller and generally have the following properties (McRuer & Jex, 1967):

"(i) *To the extent possible, the feedback loops selected and the equalization adjustments made will be such as to allow wide latitude and variation in pilot characteristics.*

(ii) *The loop and equalization structure selected will exhibit the highest pilot rating of all practical loop closure possibilities. Preferably, the loops selected can be closed with a pure gain plus a large time delay.*

(iii) Delays due to scanning and sampling are minimized."

Thus, feedback selections that involve much equalization, or different equalization in each loop, seem to be avoided by the pilot (McRuer & Jex, 1967). The structure and the parameterization of the multi-loop models depend on the properties of the system to be controlled, the aircraft. Generally, only three elementary loops need to be closed by the pilot: the inner loop of aircraft attitude, the middle loop of aircraft flight-path, and the outer loop of aircraft position. These three loop closures lead to two potential structures of the human operator model: (i) a *parallel* model in which all loops are closed *simultaneously*, Fig. 4.1(a), and (ii) a *serial* model, in which the loops are closed *sequentially*, starting with the inner loop, Fig. 4.1(b). The two model structures are equivalent and can be transformed into each other[1]:

$$
\begin{aligned}
H^p_{p_{in}} &= H^s_{p_{in}}; \\
H^p_{p_{mid}} &= H^s_{p_{mid}} H^p_{p_{in}} &= H^s_{p_{mid}} H^s_{p_{in}}; \\
H^p_{p_{out}} &= H^s_{p_{out}} H^p_{p_{mid}} &= H^s_{p_{out}} H^s_{p_{mid}} H^p_{p_{in}} &= H^s_{p_{out}} H^s_{p_{mid}} H^s_{p_{in}}.
\end{aligned}
\tag{E.4}
$$

Parallel models are easier to be identified, whereas serial models contain less parameters (Stapleford et al., 1969; van Lunteren, 1979). The serial model with its explicit sequential loop closing structure, is more intuitive.

Multi-loop model parameterization

In multi-loop applications of the quasi-linear pilot model, it is generally assumed that *all pilot equalization is concentrated in the inner-most control loop*; the other loops are closed with proportional gains (McRuer & Jex, 1967; Stapleford et al., 1969; Weir & McRuer, 1972; Weir et al., 1972; Teper, 1972; McRuer & Krendel, 1974). The pilot loop closures of the middle and outer loops are then given by:

$$
H^s_{p_{mid}}(j\omega) = K_{p_{mid}} ,
\tag{E.5}
$$

and:

$$
H^s_{p_{out}}(j\omega) = K_{p_{out}} .
\tag{E.6}
$$

The aircraft attitude feedback includes all pilot equalization and depends on the dynamics of the inner loop asymmetric aircraft dynamics that are given by (Appendix C):

$$
H_{c_1}(j\omega) = \left(H^\phi_{\delta_a}(j\omega) \right) = \frac{K_\phi}{(1 + \tau_\phi j\omega)\, j\omega} ,
$$

with K_ϕ and τ_ϕ the aircraft roll response gain and lag time constant, respectively. It is clear that an inner loop pilot model given by:

$$
H^s_{p_{in}}(j\omega) = K_{p_{in}} \left(1 + \tau_{L_{in}} j\omega \right) e^{-j\omega\tau},
\tag{E.7}
$$

---

[1]In this equation the superscripts *p* and *s* indicate the *parallel* or *serial* model structure. The subscripts *in*, *mid* and *out* depict the inner, middle and outer loop, respectively.

leads to (for a well-chosen lead time constant $\tau_{L_{in}}$) the open loop characteristics as dictated by the crossover model, Eq. E.1. The experimental data revealed that the modelling accuracy could be improved by extending the description of the pilot limitations with the properties of the neuromuscular system. Hence, to *describe the pilot inner loop control behaviour the precision model is used*, Eq. E.2, with the lag time constant τ_I set to zero. Eqs E.2, E.5 and E.6 describe the multi-loop pilot model (MLM) for the control of asymmetric aircraft motion used throughout this thesis. The MLM used to describe pilot control behaviour in symmetric aircraft motion is discussed in Chapter 7.

MLM computation, identification and parameter variation The MLM transfer functions mimic the pilot frequency responses that are identified experimentally. The MLM does not incorporate a model for the remnant. Furthermore, it does *not include a model for the pilot observation process*: it quite simply assumes that the main aircraft state variables are perceived. The MLM parameter vector has eight components:

$$
\underline{\theta}^T \;=\; [\overbrace{K_{p_{in}} \; \tau_{L_{in}} \; \tau \; \omega_n \; \zeta_n \; \tau_{N_1}}^{\text{inner loop}} \; \vdots \; \overbrace{K_{p_{mid}}}^{\text{middle loop}} \; \vdots \; \overbrace{K_{p_{out}}}^{\text{outer loop}} \;]. \tag{E.8}
$$

Here, $K_{p_{in}}$, $K_{p_{mid}}$ and $K_{p_{out}}$ depict the pilot inner, middle and outer loop feedback gains. $\tau_{L_{in}}$ is the inner loop lead and τ is the pilot time delay; ω_n, ζ_n and τ_{N_1} depict the neuromuscular frequency, damping and lag, respectively, of which τ_{N_1} is neglected in almost all cases. The results of this thesis show that the multi-loop models can be identified and validated quite satisfactory.

E.2.4 Parameter sensitivity study

Model parameter identification yields insight into the manner in which pilots adapt their control behaviour to the experimental conditions. Although the adaptation process is determined by the experimental measures, it is also affected by constraints imposed by mere control-theoretical considerations such as the stability of the closed loop. Below, the effect of varying the MLM parameters on these control-theoretical properties are examined.

Model structure and loop closures The serial pilot model structure as introduced in §E.2.3 will be applied, combined with the linear cascaded aircraft model derived in Appendix C. Only the control of aircraft asymmetric motion will be discussed. The effect of a simulation time delay τ_{sim} as discussed in Appendix A is included. The effects of the atmospheric disturbances and the pilot remnant are neglected in the following, yielding a *deterministic* approach. The closed loop pilot/aircraft system is illustrated in Fig. E.2. The pilot closes three loops sequentially, yielding a serial pilot model with three inputs, $\tilde{\phi}, \tilde{\psi}_e$ and $\tilde{X}_e$, and one output, δ_a. The three input signals are delayed versions of the aircraft outputs due to the effect of the simulation time delay, modelled by $H_d(s) = e^{-s\tau_{sim}}$. The structure of the serial pilot model allows the computation of the bandwidth and the stability – determined by the crossover frequency and phase margin –
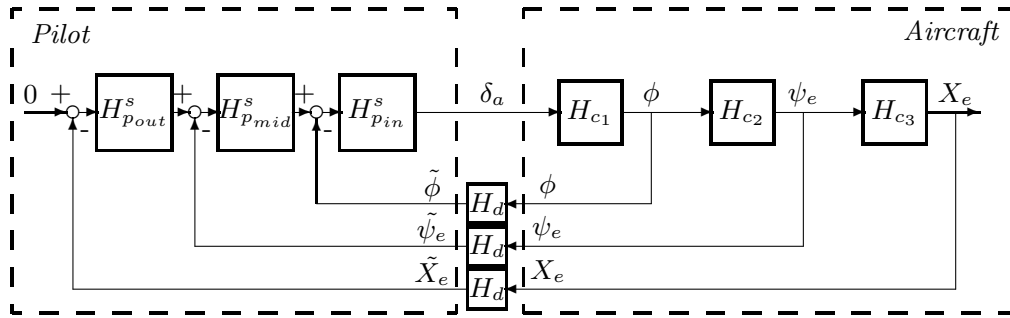
Figure E.2: Definition of the closed loop pilot/aircraft system of the sensitivity study. In this figure, H_{c_1}, H_{c_2} and H_{c_3} depict the aircraft inner, middle and outer loop dynamics. H_d indicates the simulation time delay that was present in the experiments of this thesis, see Appendix A. $H_{p_{in}}^s$, $H_{p_{mid}}^s$ and $H_{p_{out}}^s$ are the pilot inner, middle and outer loop feedback characteristics, according to a *serial* model structure.

of the three main feedback loops.

Analytic investigation   A considerable number of parameters exists that could play a role in the investigation: (i) the aircraft model parameters (V_{tas}, K_ϕ and τ_ϕ); (ii) the pilot model parameters (the parameter vector $\underline{\theta}$), and (iii) the simulation time delay τ_{sim}. To facilitate the analysis, it was assumed that: (i) the simulation time delay is zero; (ii) the neuromuscular lag time constant can be neglected; and (iii) the pilot time delay can be approximated by a second order Padé filter. The sensitivity study was preceded by an analytic investigation in which the characteristics of the loop closures of the closed loop system are examined without substituting parameter values. This investigation showed the importance of the inner loop zeros, remaining the same for the middle and outer loop closures. The position of these zeros can be manipulated by the pilot through the inner loop pilot lead time constant $\tau_{L_{in}}$ and, to a less extent, by the time delay τ. The analysis showed that because the system to be controlled simply adds an integrator pole in the middle and the outer loop closures, a well-chosen proportional feedback suffices in these loops, i.e. no further pilot equalization is necessary.

The parameter sensitivity study

Fixing the aircraft model parameters   Although pilots adapt their control behaviour to the dynamic characteristics of the aircraft to be controlled, the discussion below is limited to the velocity condition of 70 [m/s] (τ_ϕ=0.45 [s], K_ϕ=5.5 [-]). The effects of changing the velocity condition are then discussed shortly afterwards.

Fixing the pilot limitation model parameters   Two categories of pilot model parameters can be distinguished, i.e. (i) the *equalization* variables ($K_{p_{in}}$, $\tau_{L_{in}}$, $K_{p_{mid}}$ and $K_{p_{out}}$), and (ii) the *limitation* variables (ω_n, ζ_n and τ). These latter variables will be fixed at levels representative for those found in the experiments: $\omega_n = 9.0$ [rad/s], $\zeta_n = 0.10$ [-]

Figure E.3: The inner loop crossover frequency and phase margin as a function of the inner loop pilot gain $K_{p_{in}}$ for five levels of the pilot lead $\tau_{L_{in}}$. The dashed lines represent iso-$K_{p_{in}}$ lines (with levels marked in the insets) Here, and in the following, the filled rectangle contains approx. 90% of the values found in the experiments.

and $\tau = 0.30$ [s]. Two inner loop variables, $K_{p_{in}}$ and $\tau_{L_{in}}$, and two variables determining the middle and outer loop feedbacks, $K_{p_{mid}}$ and $K_{p_{out}}$, are to be varied in the analysis.

Inner loop   The inner loop lead is fixed at five different levels ($\tau_{L_{in}} = 0$, 0.25, 0.45, 0.75 and 1.0 [s]) and for each level the inner loop gain is varied. Fig. E.3 shows the resulting inner loop crossover frequencies ω_c^{in} and phase margins φ_m^{in}. Increasing the pilot lead for a fixed pilot gain generally leads to an increasing crossover frequency and phase margin, but only to a certain extent: when the lead is increased further, the phase margin will decrease. Increasing the pilot gain for a fixed lead always leads to an increasing ω_c^{in} and a decreasing φ_m^{in}. Hence, increasing φ_m^{in} while maintaining a constant ω_c^{in} generally requires a higher lead and a lower gain. Increasing ω_c^{in} while maintaining a constant φ_m^{in} requires a larger lead and a larger gain. A higher pilot lead puts heavier constraints on the pilot gain. It is a well-known fact that increasing lead is related with higher levels of mental workload (McRuer & Krendel, 1974). Hence, the pilot lead will be limited. In Fig. E.3 the shaded rectangle shows the iso-ω_c^{in} lines (levels 1.5, 2.0, 2.5 and 3.0 [rad/s]) that provide the basis for the middle and outer loop investigations.

Middle loop   The analysis is limited for three values of the inner loop pilot lead ($\tau_{L_{in}} = 0.25$, 0.45 and 0.75 [s]) and those cases that constitute fixed levels of the inner loop crossover frequency ω_c^{in} (1.5, 2.0, 2.5 and 3.0 [rad/s], with a lower limit on φ_m^{in} of 20 [deg]). Fig. E.4 shows the effects of varying the middle loop gain $K_{p_{mid}}$ on the middle loop crossover frequency and phase margin, for two values of the inner loop lead time constant
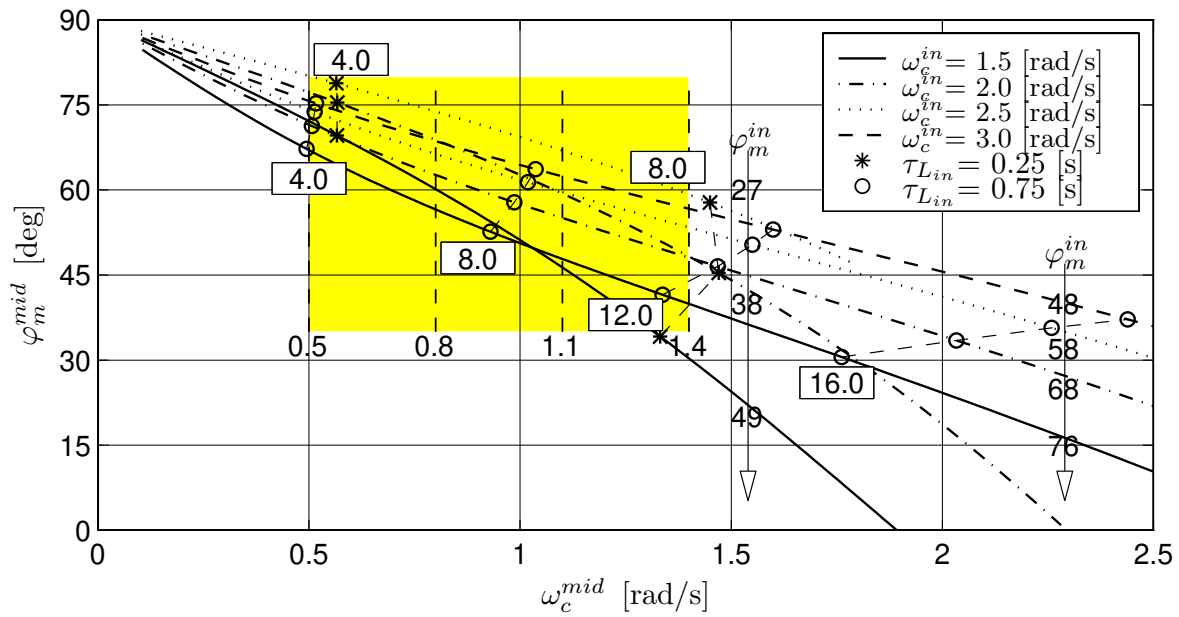
Figure E.4: The middle loop crossover frequency and phase margin as a function of the middle loop pilot gain $K_{p_{mid}}$ for four levels of the inner loop crossover frequency ω_c^{in} and two values of the inner loop pilot lead $\tau_{L_{in}}$. The values of $K_{p_{mid}}$ are shown in the upper and lower insets for the lead times $\tau_{L_{in}}$=0.25 and $\tau_{L_{in}}$=0.75 [s], respectively. The arrows show the inner loop phase margins for both the conditions.

(0.25 and 0.75 [s]) and the four levels of ω_c^{in}. To maintain a sufficient middle loop margin (φ_m^{mid}> 30 [deg]), ω_c^{mid} must be smaller than ω_c^{in}. Furthermore, for the larger values of $\tau_{L_{in}}$, ω_c^{mid} and φ_m^{mid} can obtain larger values with increasing $K_{p_{mid}}$. Higher levels of ω_c^{in} are advantageous for the middle loop. For constant levels of ω_c^{mid}, higher inner loop bandwidths lead to an increasing φ_m^{mid}. Also, for the same middle loop phase margin, an increased ω_c^{in} leads to a higher middle loop bandwidth. In Fig. E.4 a dashed and filled box marks the iso-ω_c^{mid} lines (levels 0.5, 0.8, 1.1 and 1.4 [rad/s]) that are used for the outer loop investigation.

Outer loop   The middle loop investigation supports the benefit of an inner loop lead that is larger than the aircraft roll subsidence lag time constant. Therefore, the outer loop case will be discussed for the $\tau_{L_{in}}$=0.75 [s]-case only. The outer loop crossover frequency and phase margin for the sixteen combinations of the four levels of ω_c^{in} and ω_c^{mid} are plotted in Fig. E.5 with the outer loop gain $K_{p_{out}}$ as parameter. The outer loop crossover frequencies and phase margins are strongly affected by ω_c^{mid} and hardly influenced by ω_c^{in}. Only for very large values of ω_c^{out} the influence of ω_c^{in} becomes apparent. The figure illustrates further that, in order to maintain sufficient outer loop phase margin (φ_m^{out}> 30 [deg]), it can be expected that ω_c^{out} will be smaller than ω_c^{mid}.

Effects of the aircraft velocity   The inner loop aircraft roll response lag time constant τ_ϕ decreases and the gain K_ϕ increases with increasing aircraft velocity (Appendix C).
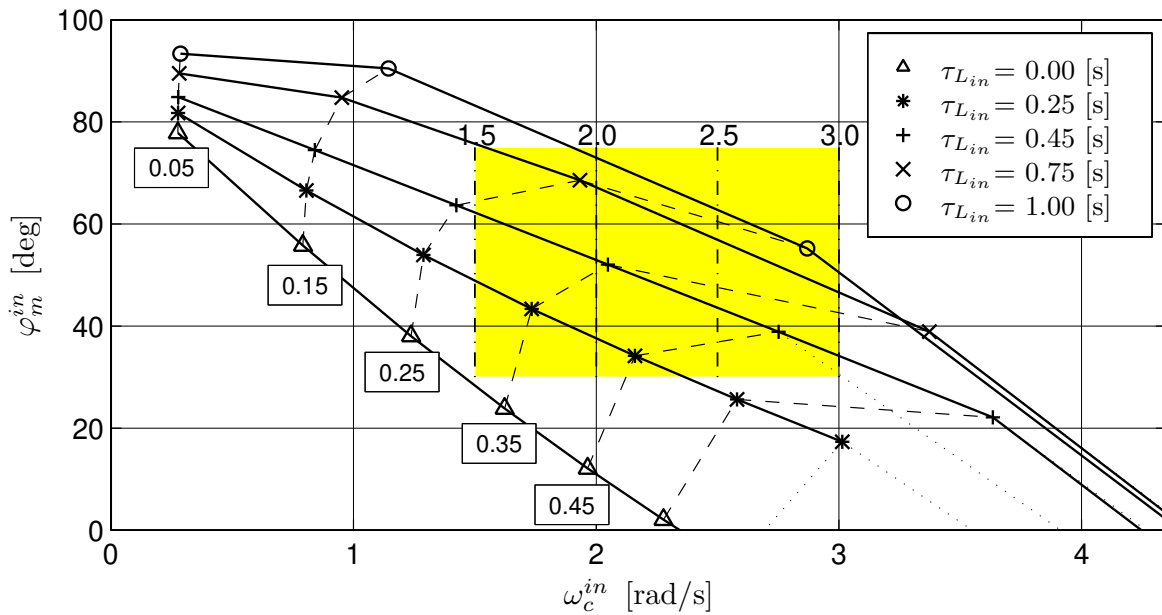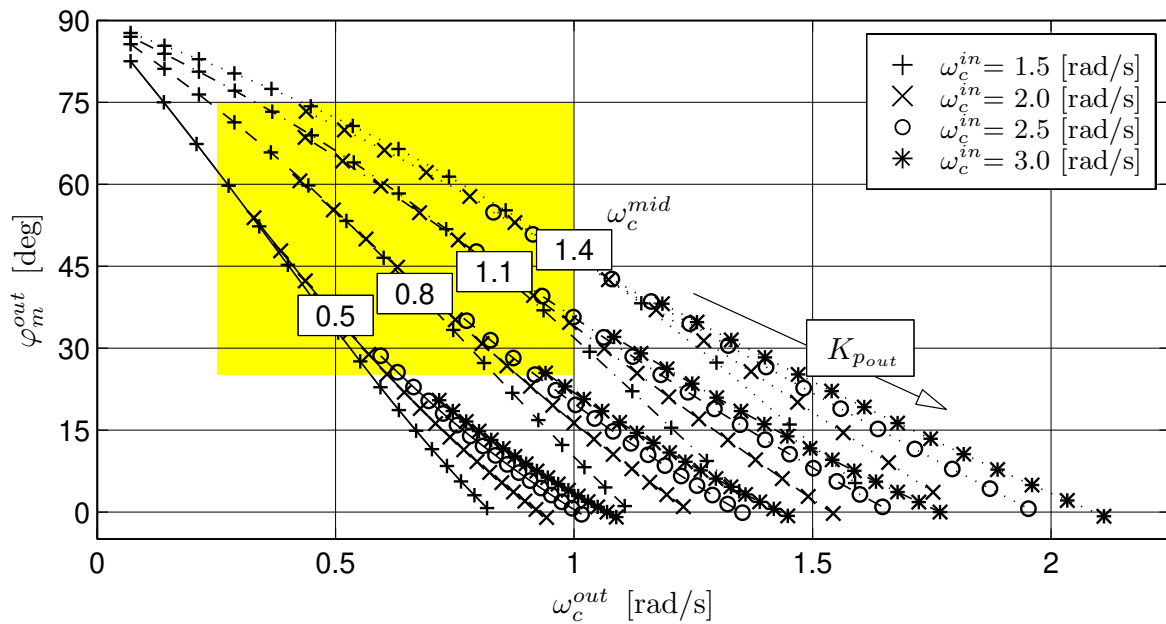
Figure E.5: The outer loop crossover frequency and phase margin as a function of the outer
loop pilot gain $K_{p_{out}}$ for four levels of the inner loop crossover frequency (legend)
and four values of the middle loop crossover frequency (insets). The diagonal arrow
shows the direction of increasing $K_{p_{out}}$.

Hence, the pilot lead time constant $\tau_{L_{in}}$ can become smaller for increasing aircraft velocity,
and the pilot inner loop gain will also decrease. The finding that it is advantageous to
maintain an inner loop lead that is somewhat larger than the aircraft lag time constant,
$\tau_{L_{in}} > \tau_\phi$, still holds. The middle loop aircraft gain ($\sim \frac{g_0}{V_{tas}}$) decreases for increasing
velocity. Because there is no reason to suspect a lower middle loop crossover frequency for
these velocity conditions, it can be expected that pilots increase their middle loop feedback
gain. A similar, but reciprocal effect can be hypothesized for the outer loop feedback. The
higher aircraft outer loop gain ($\sim V_{tas}$) for larger velocities must lead to a smaller outer
loop gain, for constant levels of the outer loop crossover frequency.

Conclusions   The sensitivity study exemplifies the difficulty in examining the multi-
dimensional control situation. Although considerable freedom exists in establishing the
inner loop equalization, it is advantageous for a pilot to maintain an inner loop lead that
is greater than or equal to the aircraft roll subsidence lag time constant, i.e. $\tau_{L_{in}} \geq \tau_\phi$.
This yields a sufficient phase margin interval, in which the inner loop crossover frequency
can obtain a reasonable level ($\approx$ 2–3 [rad/s]). The inner loop lead time constant, however,
must not be chosen too high because this results in a reduction in phase margin due to the
sharp increase in the inner loop crossover frequency. The middle loop feedback benefits
from an inner loop feedback with sufficient inner loop phase margin: the inner loop lead
(and thus the phase margin) determines the freedom of the pilot to choose the middle loop
crossover frequency. A tight but well-stabilized control of the inner loop(s) is advantageous

for the outer loops. A higher inner loop bandwidth allows a higher middle loop crossover frequency or phase margin. The middle loop gain itself has a straightforward effect on the middle loop feedback quantities. The same holds for the outer loop feedback, although here the influence of the inner loop is small relative to the effects of the middle loop.

E.3 The optimal control model

E.3.1 General description of the optimal control model

The principal assumption of the OCM is that *"the well-trained, well-motivated human operator behaves in an optimal manner, subject to his inherent limitations and to the requirements of the control task"* (Kleinman et al., 1970b). The OCM is a *normative* model, i.e. it prescribes what operators *should* do given their inherent constraints limiting their behaviour, and the extent to which they understand the task objectives. The OCM structure is shown in Fig. E.6. The operator task is to control a dynamic system (state $\underline{x}$) perturbed by external disturbances, $\underline{w}$. The outputs of the system, $\underline{y}$, are presented with a display. The operator uses the information gathered about the system state to generate a control signal, $\underline{u}$, that maintains a system reference state, compensating for the effects of the disturbances. The modelling through optimal control of the stationary input-output relation of the operator has the following starting points (Kok & van Wijk, 1978):

- The system to be controlled can be described as a linear time-invariant (LTI) system.
- The system outputs are an LTI combination of the system states.
- The operator minimizes a quadratic cost functional.
- The limitations of the operator can be modelled with:

  1. a <u>single time delay</u> τ, lumping the operator information-processing lags.
  2. an <u>observation noise</u> $\underline{v}_y$, a Gaussian white noise signal that represents operator uncertainties concerning the observed variables.
  3. a <u>motor noise</u> $\underline{v}_u$, a Gaussian white noise signal that represents operator uncertainties in generating the control input.
  4. a <u>neuromuscular lag</u> τ_N: representing the operator neuromuscular system.

- Operators have a *perfect* understanding of:

  - the dynamics of the system to be controlled,
  - the statistics of the system disturbances,
  - the relation between the observed outputs and the system state,
  - the task to be performed,
  - their own inherent limitations.

The *separation theorem* states that the optimum stochastic controller is realized by cascading an optimal state estimator (LQG) with a deterministic optimal controller (LQR) (Kwakernaak & Sivan, 1972). Hence, the OCM consists of two elements, an *optimal observer*, a cascade combination of a Kalman filter and a predictor, that use the available
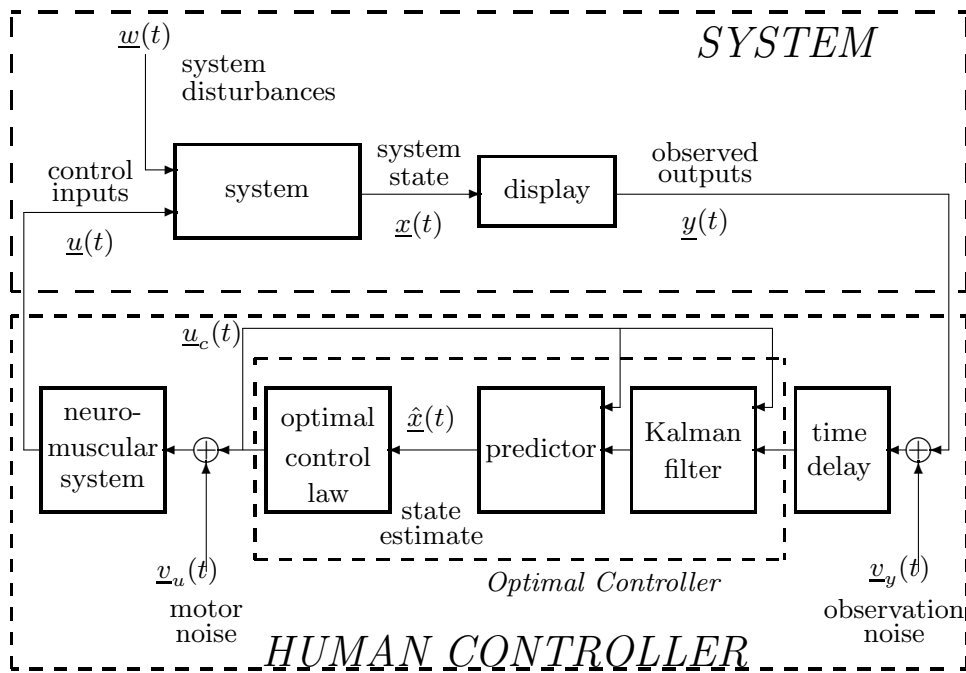
Figure E.6: Structure of the Optimal Control Model.

information to obtain an optimal estimate of the system state, $\hat{\underline{x}}$, and an *optimal regulator*, an optimal controller that transfers the state estimate into an optimal control signal, $\underline{u}_c$.

E.3.2 Mathematical formulation of the OCM parameters

A mathematical formulation allows a derivation of the model structure and the model computation, for which the reader is referred to (Kleinman & Baron, 1971).

System description   An LTI state description is applied:

$$\dot{\underline{x}}(t) = A\underline{x}(t) + B\underline{u}(t) + E\underline{w}(t) \ , \tag{E.9}$$

where $\underline{x}(t)$ is the $(n \times 1)$ state vector and $\underline{u}(t)$ are the ℓ inputs to the system. The $(k \times 1)$ disturbance vector is defined as an independent, zero-mean, Gaussian white noise vector with auto covariance: $\mathrm{E}\{\underline{w}(t)\underline{w}^T(t + \tau)\} = W\delta(\tau)$. It is assumed that several system outputs are presented to the human in a continuous way via some instrument panel:

$$\underline{y}(t) = C\underline{x}(t) + D\underline{u}(t) + H\underline{w}(t) \ , \tag{E.10}$$

with $\underline{y}(t)$ the $(m \times 1)$ observation vector representing the information set upon which the operator bases the control actions. It is assumed that if a quantity y_i is displayed, the derivative of that quantity – $\dot{y}_i$ – is perceived also: the observation vector contains *pairs* of variables explicitly displayed to, as well as those implicitly derived by the operator.

Human limitations   The inherent operator limitations are represented by: (i) a perceptual time delay τ; (ii) a neuromotor lag τ_N, and (iii) the observation and motor

noise vectors $\underline{v}_y$ and $\underline{v}_u$. The $(m \times 1)$ observation noise vector is defined as an independent, zero-mean, Gaussian white noise vector with auto covariance: $\mathrm{E}\{\underline{v}_y(t)\underline{v}_y^T(t+\tau)\} = \mathrm{diag}(V_y)\delta(\tau)$. The operator perceives a delayed, noisy replica of the system outputs:

$$\underline{y}_p(t) = \underline{y}(t-\tau) + \underline{v}_y(t-\tau) \ . \tag{E.11}$$

The perceived output is processed by the operator who generates a commanded control input $\underline{u}_c(t)$ that is considered *optimal* for the task at hand. A motor noise $\underline{v}_u(t)$ representing errors in executing the intended control movements, and the fact that the operator has no perfect knowledge of the system output $\underline{u}(t)$, is added to $\underline{u}_c(t)$:

$$\underline{u}(t) = \underline{u}_c(t) + \underline{v}_u(t) \ . \tag{E.12}$$

The $(\ell \times 1)$ motor noise vector is defined as an independent, zero-mean, 0 white noise vector with auto covariance: $\mathrm{E}\{\underline{v}_u(t)\underline{v}_u^T(t+\tau)\} = \mathrm{diag}(V_u)\delta(\tau)$.

Control task representation It is assumed that the task is reflected in the operator's choice of a feedback control $\underline{u}^*(\cdot)$ that, in steady-state, minimizes the cost functional:

$$J(\underline{u}) = \mathrm{E}\left\{ \sum_{i=1}^{m} q_i y_i^2 + \sum_{i=1}^{\ell} r_i u_{c_i}^2 + \sum_{i=1}^{\ell} g_i \dot{u}_{c_i}^2 \right\} \ , \tag{E.13}$$

conditioned on the perceived information $\underline{y}_p(\cdot)$. The rate of the control input is also weighted in the cost functional, introducing a first order lag in the optimal controller (Kleinman, Baron, & Levison, 1971). Hence, the control rate weighting matrix G is used to include a first order representation of the *neuromuscular system* in the model.

E.3.3 Model parameters, outputs, solution and identification

Model parameters In order to apply the OCM the following quantities must be defined: (i) the *system* parameters: the characteristics of the linear system (A, B, C, D, E, H), and the statistics of the system disturbance (W); (ii) the *task-related* parameters: the weightings of the cost functional (Q, R); and (iii) the *human response* parameters (τ, τ_N, V_y and V_u). The formulation of the characteristics of both the control task and the operator in mathematical terms is difficult. First of all, the task-related parameters – determining the *balance* of the model, or, equivalently, the control strategy of the operator – are hard to define beforehand. The OCM describes the operator as an optimal controller with respect to task-related quantities that do not necessarily relate to human-centered optimalization strategies. Second, the operator is assumed to have *perfect* knowledge of the system dynamics and the disturbance characteristics, and the OCM outputs must therefore be considered as the *best* possible operator performance.

Model outputs In contrast to the structural pilot models of §E.2, the OCM is a time domain model. Nonetheless, it provides results in both the domains. The *time domain* outputs are the variances of all signals in the closed loop, i.e. $\mathrm{E}\left\{u_i^2\right\}\big|_{i=1,\dots,\ell}$, $\mathrm{E}\left\{x_i^2\right\}\big|_{i=1,\dots,n}$,
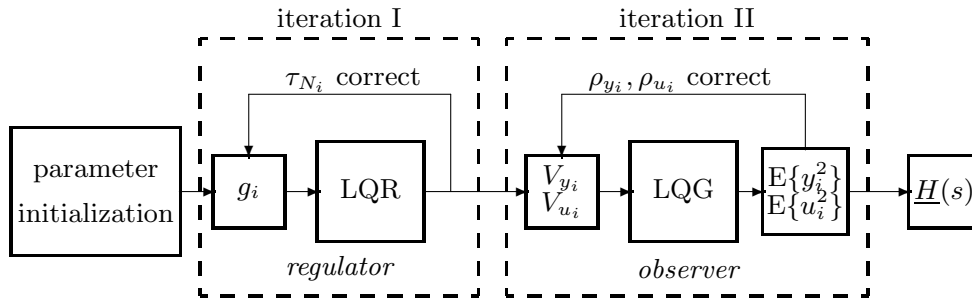
Figure E.7: Computation flow of the Optimal Control Model.

and $\mathrm{E}\left\{y_i^2\right\}\big|_{i=1,\ldots,m}$. Due to the incorporation of the pilot remnant through the observation and motor noises, these variances allow a direct comparison with the values obtained in the actual experiment. The *frequency domain* output is the multi-dimensional $(\ell \times m)$ transfer function matrix $\underline{H}(s)$, relating the m pilot inputs to the ℓ pilot outputs. The OCM assumes a *parallel* model structure: each of the operator outputs consists of the *sum* of the individual loop closures of the displayed variables. The *equivalent* frequency domain transfer function allows a comparison with the experimentally measured operator describing functions (Kleinman et al., 1970b, 1971).

Model solution

Parameter initialization Typical values used for the time delay τ are 0.15–0.35 [s] and for the neuromuscular lag τ_N 0.1 [s] (Kleinman et al., 1970a). The determination of the observation and motor noise intensities V_y and V_u is difficult. (Kleinman et al., 1970b, 1970a) suggested the following procedure:

$$V_{y_i} = \pi \rho_{y_i} \mathrm{E}\{y_i^2\}\big|_{i=1,2,\ldots,m} \quad \text{and} \quad V_{u_i} = \pi \rho_{u_i} \mathrm{E}\{u_{c_i}^2\}\big|_{i=1,2,\ldots,\ell} \tag{E.14}$$

The observation noise *ratio* ρ_{y_i}, defined as the noise intensity V_{y_i} normalized with respect to the signal variance, has a typical value of 0.01. In other words, the normalized observation noise intensity has a power density level of -20 [dB]. The motor noise ratio ρ_{u_i}, defined similarly as ρ_{y_i}, has a typical value of 0.003. Thus, the normalized motor noise intensity has a power density level of -25 [dB] (Kleinman et al., 1971; Baron, 1976).

Iterative OCM solution The OCM is computed in two iterations, Fig. E.7 (Thompson, 1987). First, the OCM *regulator* is computed. The ℓ diagonal elements g_i of G are computed iteratively until the lag time constants τ_{N_i} equal those defined by the user. Second, the OCM *observer* is computed. The observation and motor noise ratios are defined, and the model iteratively changes V_{y_i} and V_{u_i} – resulting in different variances – to obtain the defined ratios. In the application of the OCM in this thesis, the two iterations are conducted with a SIMPLEX and a first order gradient algorithm, respectively (Press et al., 1992).

Model identification

The OCM is known to be *overparameterized*, i.e. it contains more parameters than necessary to uniquely describe the input-output behaviour of the operator (Phatak et al., 1976; Kok & van Wijk, 1978). Due to this over-parameterization, the complete set of model parameters cannot be identified from experimental data alone (van Wijk & Kok, 1977). Identification methods have only been successful for OCM structures in which a subset of the parameter vector is either neglected (Phatak et al., 1976) or fixed (Wewerinke, 1979).

E.3.4   Allocation of attention

Theoretical background   Generally, human operators allocate their mental resources among several tasks and numerous displays. The characteristics of the displayed variables, the control tasks and the control task objectives determine the allocation of attention strategy of the operator. In (Baron & Levison, 1975) the effects of attention sharing are modelled by an increase in the so-called *nominal* observation noise ratio ρ_0 by:

$$\rho_{y_i} \;=\; \frac{\rho_0}{f_i} \quad (i = 1, 2, \ldots, m), \quad \text{subject to}: \quad \sum_{i=1}^{i=m} f_i \;=\; 1. \tag{E.15}$$

The nominal observation noise ratio is defined as the observation noise ratio when attention is not shared, and f_i represents the *fraction of attention* allocated to a display variable y_i. Then, ρ_{y_i} is the observation noise ratio associated with the ith display variable when attention is being *shared*. It is hypothesized that the operator divides attention among the displayed variables in an *optimal* manner. Then, only the nominal level of attention ρ_0 needs to be defined, and the model iteratively computes the *optimal* set f_i^* $(i = 1, \ldots, m)$, yielding the observation noise ratios ρ_{y_i} for all displayed quantities (Kleinman, 1976).

Inverse optimal allocation of attention   First, the m observation noise ratios ρ_i are identified. Then, a set of $(m+1)$ equations and $(m+1)$ unknown parameters results. The solution for the nominal level of attention is given by:

$$\rho_0 = \frac{1}{\left(\dfrac{1}{\rho_1} + \dfrac{1}{\rho_2} + \ldots + \dfrac{1}{\rho_m} \right)} \;, \tag{E.16}$$

which allows a computation of the fractions of attention f_i, using Eq. E.15.

Appendix F

Model identification and validation techniques

F.1   The two-stage identification procedure

The two-stage pilot model identification procedure, a common method in human-machine systems research and introduced in §4.2, is the subject of this appendix. The *first* stage of this method is a non-parametric identification of the pilot frequency responses, discussed in §F.2. The parameters of the pilot models are then estimated in the *second* stage, described in §F.3. In §F.4 a number of miscellaneous model validation issues is treated that accompany the application of the two-stage identification procedure in this thesis.

F.2   Stage I: Non-parametric identification

The non-parametric identification method is an *instrumental variable method* (IV) which prescribes that for each pilot frequency response to be estimated an uncorrelated input signal, a *forcing function*, must be inserted in the closed loop (van Lunteren, 1979). In the aircraft-control applications of this thesis, it is hypothesized that pilots feed back the aircraft attitude (inner loop), flight-path (middle loop) and position (outer loop). Hence, to identify these three loop closures with the IV-method, three forcing functions must be applied. In §4.2, however, it was stated that in most cases only two forcing functions can be inserted, and that the middle and outer loop closures must be estimated simultaneously. The intricacies of this assumption are discussed in §F.4.4. In this section, a generic identification method is discussed that can be applied for *all* non-parametric identification issues in this thesis, focusing on three cases:

- The identification of a pilot model with two input signals and one output signal (2×1), a method applied in almost all identification efforts (§F.2.1 and §F.2.2).
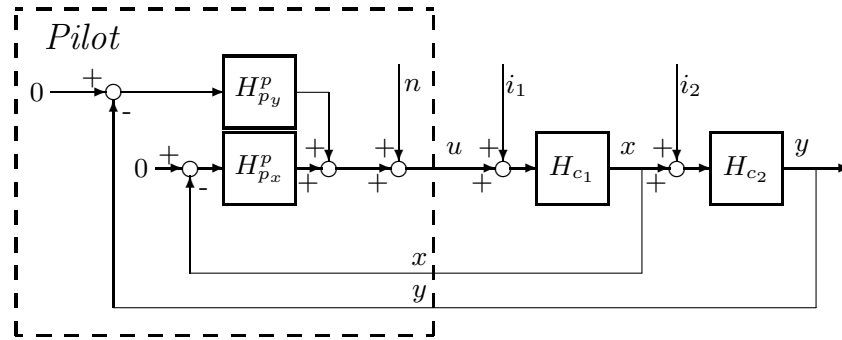
Figure F.1: The general situation of a *parallel* pilot model with two input signals and one output
signal in a disturbance task.

- The identification of a pilot model with three input signals and one output signal
  (3×1), a method that was used in Chapter 9 (§F.2.3).

- The identification of a pilot model with four input signals and two output signals
  (4×2), a method that was used in the dual-axis tasks of Chapter 6 (§F.2.4).

A further categorization applied in the discussion is that the structure of the pilot model
can be either a *parallel* or a *serial* model structure (§4.2).

F.2.1   The (2×1) parallel model

The identification procedure developed in (van Paassen, 1994) will be briefly summarized
below, a summary that facilitates the discussion of the *new* applications of this method
developed in this thesis, reported in §F.2.2 to F.2.4.

Definition of the situation   Fig. F.1 shows a general parallel pilot model with two
input signals and one output signal in a disturbance task. The linear part of pilot control
behaviour is characterized by the describing functions $H_{p_x}^p$ and $H_{p_y}^p$ that give the con-
tribution to the control signal u resulting from the feedback of the inner and outer loop
system outputs x and y, respectively. The non-linear part of pilot control behaviour is
characterized by the remnant n. Two forcing functions are applied: i_1 (at frequencies
$\underline{\nu}_{i_1} = \underline{k}_1 \nu_0$) and i_2 (at frequencies $\underline{\nu}_{i_2} = \underline{k}_2 \nu_0$) with ν_0 the ground frequency (Chapter 4).

Estimation of the describing functions   The measurable signals in the loop (u, x and
y) are discrete-Fourier transformed. For all frequencies ν_k the following expression holds:[1]

$$U(\nu_k; \zeta) = -H_{p_x}^p(\nu_k)X(\nu_k; \zeta) - H_{p_y}^p(\nu_k)Y(\nu_k; \zeta) + N(\nu_k; \zeta), \tag{F.1}$$

an expression that can be examined at an arbitrary frequency ν_{1_j} $(j = 1 \dots N_f)$ of i_1:

$$U_1 = -H_{p_x}^p(\nu_{1_j})X_1 - H_{p_y}^p(\nu_{1_j})Y_1 + N_1, \tag{F.2}$$

where U_1, X_1, Y_1 and N_1 are defined as the discrete-Fourier coefficients of these signals at
the frequencies ν_{1_j}. It is assumed that at these frequencies the contribution of the noise N_1

---

[1]Here, and in the following, a ζ indicates that a variable is a *realisation* of a stochastic process.

to the signal U_1 is small relative to the other contributions and can be neglected, yielding one equation with two unknowns at frequencies ν_{1_j}. A second equation can be obtained by *linear interpolation* of the signals from the neighbouring frequencies ν_{2_j}, where the second forcing function i_2 is acting (van Paassen, 1994). For example:

$$\tilde{U}_2 \;=\; \frac{\nu_{2_{j+1}} - \nu_{1_j}}{\nu_{2_{j+1}} - \nu_{2_j}} U(\nu_{2_j}; \zeta) + \frac{\nu_{1_j} - \nu_{2_j}}{\nu_{2_{j+1}} - \nu_{2_j}} U(\nu_{2_{j+1}}; \zeta), \tag{F.3}$$

where a ~ is used to indicate that a variable is obtained by *interpolation*. The $\tilde{X}_2$, $\tilde{Y}_2$, and $\tilde{N}_2$ signals are computed similarly, resulting in the second equation for the unknown describing functions at frequencies ν_{1_j}:

$$\tilde{U}_2 = -H^p_{p_x}(\nu_{1_j})\tilde{X}_2 - H^p_{p_y}(\nu_{1_j})\tilde{Y}_2 + \tilde{N}_2. \tag{F.4}$$

Again, it is assumed that at these frequencies the contribution of the *interpolated* noise $\tilde{N}_2$ to the signal $\tilde{U}_2$ is small and can be neglected. Then, a set of two equations with two unknowns is obtained, at frequencies ν_{1_j}:

$$\begin{pmatrix} U_1 \\ \tilde{U}_2 \end{pmatrix} = - \begin{pmatrix} X_1 & Y_1 \\ \tilde{X}_2 & \tilde{Y}_2 \end{pmatrix} \begin{pmatrix} H^p_{p_x}(\nu_{1_j}) \\ H^p_{p_y}(\nu_{1_j}) \end{pmatrix}. \tag{F.5}$$

Solving this set leads to expressions for the estimated pilot frequency responses at the N_f frequencies ν_{1_j} of i_1:

$$\hat{H}^p_{p_x}(\nu_{1_j}; \zeta) \;=\; \frac{U_1\tilde{Y}_2 - Y_1\tilde{U}_2}{\tilde{X}_2 Y_1 - \tilde{Y}_2 X_1} \;; \quad \text{and} \quad \hat{H}^p_{p_y}(\nu_{1_j}; \zeta) \;=\; \frac{X_1\tilde{U}_2 - U_1\tilde{X}_2}{\tilde{X}_2 Y_1 - \tilde{Y}_2 X_1}. \tag{F.6}$$

The same holds for the describing function estimations at the N_f frequencies ν_{2_j} of i_2:

$$\hat{H}^p_{p_x}(\nu_{2_j}; \zeta) \;=\; \frac{\tilde{U}_1 Y_2 - \tilde{Y}_1 U_2}{X_2\tilde{Y}_1 - Y_2\tilde{X}_1} \;; \quad \text{and} \quad \hat{H}^p_{p_y}(\nu_{2_j}; \zeta) \;=\; \frac{\tilde{X}_1 U_2 - \tilde{U}_1 X_2}{X_2\tilde{Y}_1 - Y_2\tilde{X}_1}, \tag{F.7}$$

with U_2, X_2 and Y_2 the Fourier coefficients of the signals u, x and y at frequencies ν_{2_j}, and $\tilde{U}_1, \tilde{X}_1$ and $\tilde{Y}_1$ their Fourier coefficients interpolated from frequencies ν_{1_j}.

Summarizing, the procedure leads to an estimation of the describing functions $H^p_{p_x}$ and $H^p_{p_y}$ at the $2N_f$ frequencies $\underline{\nu}_{i_1}$ and $\underline{\nu}_{i_2}$ of the two forcing functions. The main assumption is that at these two frequency sets the contribution of the noise to a particular signal is small relative to the contribution of the other signals. The consequences of this assumption for the bias and variance of the estimation are considered next.

Computation of the bias and variance in the estimation   A procedure for obtaining *analytical* expressions of the bias and variance in single-axis tasks has been reported (van Lunteren, 1979). The method was extended to the case of two-input signals in (van Paassen, 1994). The first step in this procedure is to obtain expressions for all signals *in the loop* (u, x and y) in terms of the signals *inserted* into the loop (n, i_1 and i_2). Then the frequencies ν_a ($a \in \underline{k}_1$) at which forcing function i_1 is acting are selected. At these frequencies the signals U, Y and X are expressed in terms of the injected noise N (referred to as N_1) and the disturbance signal I_1. The same holds for the frequencies ν_b ($b \in \underline{k}_2$)

at which i_2 is acting. Substituting the resulting sets of equations into Eq. F.6 yields the following expressions for the estimated describing functions (noting $U(\nu_k; \zeta)$ as U, etc., for brevity) (van Paassen, 1994):

$$\hat{H}_{p_x}^p = H_{p_x}^p - \left(H_{p_x}^p + \frac{1}{H_{c_1}} \right) \left(\frac{N_1}{I_1 + N_1} \right) - \frac{N_1 N_2}{I_2 (I_1 + N_1)} + \frac{N_2}{I_2}; \tag{F.8}$$

$$\hat{H}_{p_y}^p = H_{p_y}^p - H_{p_y}^p \left(\frac{N_1}{I_1 + N_1} \right) + \frac{N_1 N_2}{H_{c_2} I_2 (I_1 + N_1)} - \frac{N_2}{H_{c_2} I_2}. \tag{F.9}$$

These equations express the *estimated* describing functions, $\hat{H}_{p_x}^p$ and $\hat{H}_{p_y}^p$, in terms of the *true* describing functions $H_{p_x}^p$ and $H_{p_y}^p$, the controlled system dynamics H_{c_1} and H_{c_2}, and the Fourier coefficients of the forcing functions I_1 and I_2 and the noise signals N_1 and N_2. The Fourier coefficients of these noise signals are not known: they are *assumed* to be uncorrelated with zero means (van Lunteren, 1979).

Bias in the estimates   The bias of an estimator $\hat{\underline{\theta}}$ is defined as: $\text{Bias} \left(\hat{\theta} \right) = \text{E} \left\{ \hat{\theta} - \theta \right\}$ (Papoulis, 1991). Applying this formula for Eqs F.8 and F.9 results in:

$$\text{Bias} \left(\hat{H}_{p_x}^p \right) = \text{E} \left\{ -\frac{N_1 N_2}{I_2 (I_1 + N_1)} - \left(H_{p_x}^p + \frac{1}{H_{c_1}} \right) \frac{N_1}{I_1 + N_1} + \frac{N_2}{I_2} \right\};$$

$$\text{Bias} \left(\hat{H}_{p_y}^p \right) = \text{E} \left\{ \frac{N_1 N_2}{H_{c_2} I_2 (I_1 + N_1)} - H_{p_y}^p \frac{N_1}{I_1 + N_1} - \frac{N_2}{H_{c_2} I_2} \right\}.$$

Because N_1 and N_2 are assumed zero-mean and uncorrelated, the first and third terms at the right-hand side of both the equations are zero. The expected values of the second terms in both the equations, however, are not zero, and contribute to a bias in the estimates:

$$\text{Bias} \left(\hat{H}_{p_x}^p \right) = - \left(H_{p_x}^p + \frac{1}{H_{c_1}} \right) \text{E} \left\{ \frac{N_1}{I_1 + N_1} \right\}; \tag{F.10}$$

$$\text{Bias} \left(\hat{H}_{p_y}^p \right) = - \left(H_{p_y}^p \right) \text{E} \left\{ \frac{N_1}{I_1 + N_1} \right\}. \tag{F.11}$$

In both the equations an expectation expression emerges, referred to as E1, the computation of which involves the integration of the quotient of a complex stochastic variable and that same variable added to a deterministic variable. It is shown that this expectation can be computed as, at frequencies of i_1, (van Lunteren, 1979):

$$\text{E1}(\nu_{1_j}; \zeta) = \text{E} \left\{ \frac{N_1(\nu_{1_j}; \zeta)}{I_1(\nu_{1_j}) + N_1(\nu_{1_j}; \zeta)} \right\} = e^{-r_1(\nu_{1_j}; \zeta)}, \tag{F.12}$$

where r_1 depicts the *signal-to-noise ratio*, defined as the quotient of the power of the deterministic input signal I_1 and the power of the stochastic noise signal N_1, at frequencies ν_{1_j} of the input signal I_1 (van Paassen, 1994), see §F.2.5. For a practical calculation of the bias, the estimated frequency responses $\hat{H}_{p_x}^p$ and $\hat{H}_{p_y}^p$ of Eq. F.6 are substituted for the unknown describing functions $H_{p_x}^p$ and $H_{p_y}^p$.

Variance in the estimation of $\left| \hat{H}_{p_x}^p \right|$ The variance is defined as (Papoulis, 1991):

$$\text{Var} \left(\hat{\theta} \right) = \text{E} \left\{ \left(\hat{\theta} - \theta \right)^2 \right\} - \left(\text{Bias} \left(\hat{\theta} \right) \right)^2.$$

Table F.1: The calculation of the bias and variance of the estimated pilot frequency responses for the (2×1) parallel model.

$\hat{H}_{p_x}^p$	Bias	$-\left(\hat{H}_{p_x}^p + \frac{1}{H_{c_1}}\right)\text{E1}$	(F.16)
	Var$\lvert\cdot\rvert$	$\left\lvert\hat{H}_{p_x}^p + \frac{1}{H_{c_1}}\right\rvert^2 (\text{E2} - \text{E1}^2) + \frac{1}{r_2}(1 - 2\text{E1} + \text{E2})$	(F.13)
$\hat{H}_{p_y}^p$	Bias	$-\left(\hat{H}_{p_y}^p\right)\text{E1}$	(F.17)
	Var$\lvert\cdot\rvert$	$\left\lvert\hat{H}_{p_y}^p\right\rvert^2 (\text{E2} - \text{E1}^2) + \frac{1}{\lvert H_{c_2}\rvert^2 r_2}(1 - 2\text{E1} + \text{E2})$	(F.18)

Applying this formula for Eq. F.8 yields (van Paassen, 1994):

$$
\begin{aligned}
\text{Var}\left(\left\lvert\hat{H}_{p_x}^p\right\rvert\right) &= \left\lvert\hat{H}_{p_x}^p + \frac{1}{H_{c_1}}\right\rvert^2 \text{E}\left\{\frac{N_1^2}{(I_1 + N_1)^2}\right\} + \frac{1}{\tilde{r}_2}\left[1 - 2\text{E}\left\{\frac{N_1}{(I_1 + N_1)}\right\}\right. \\
&\quad \left. + \text{E}\left\{\frac{N_1^2}{(I_1 + N_1)^2}\right\}\right] - \left\lvert\text{Bias}\left(\hat{H}_{p_x}^p\right)\right\rvert^2.
\end{aligned}
\tag{F.13}
$$

The expected value of the first and fourth terms on the right-hand side of this equation can not be computed, since this would result in an integral with a solution of infinity. However, if a chance ϵ is accepted that the variance is underestimated this expectation, referred to as E2, can be computed with, at frequencies of i_1 (van Lunteren, 1979):

$$
\begin{aligned}
\text{E2}(\nu_{1_j}; \zeta) &= \text{E}\left\{\frac{N_1^2(\nu_{1_j}; \zeta)}{\left(I_1(\nu_{1_j}) + N_1(\nu_{1_j}; \zeta)\right)^2}\right\} \\
&= e^{-r_1+\delta} + e^{-r_1-\delta} - 1 + r_1 \int_\delta^{r_1} \frac{e^{p-r_1}}{p}\mathrm{d}p + r_1 e^{-r_1}\int_\delta^\infty \frac{e^{-p}}{p}\mathrm{d}p, \quad \text{(F.14)}
\end{aligned}
$$

where ϵ $(= 2e^{-r_1}\sinh(\delta))$ depicts the probability introduced above (usually, ϵ is set at 1%). In Eq. F.13 a second signal-to-noise ratio emerges, r_2, that is defined as the quotient of the power of the deterministic input signal I_2 and the power of the stochastic noise signal N_2, at frequencies ν_{2_j} of the input signal i_2. The $\tilde{}$ indicates that it is an *interpolated* SNR, a fact that will be discussed in §F.2.5.

Variance in the estimation of $\angle\hat{H}_{p_x}^p$ The variance of the estimate of $\angle\hat{H}_{p_x}^p$ can be approximated with, at frequencies of i_1 (van Paassen, 1994):

$$
\text{Var}\left(\angle\hat{H}_{p_x}^p\right)(\nu_{1_j}; \zeta) \approx \frac{\text{Var}\left(\left\lvert\hat{H}_{p_x}^p\right\rvert\right)(\nu_{1_j}; \zeta)}{\left\lvert\hat{H}_{p_x}^p(\nu_{1_j}; \zeta)\right\rvert^2}.
\tag{F.15}
$$

The variance in the estimation of $\left\lvert\hat{H}_{p_y}^p\right\rvert$ and $\angle\hat{H}_{p_y}^p$ can be conducted in a similar manner.
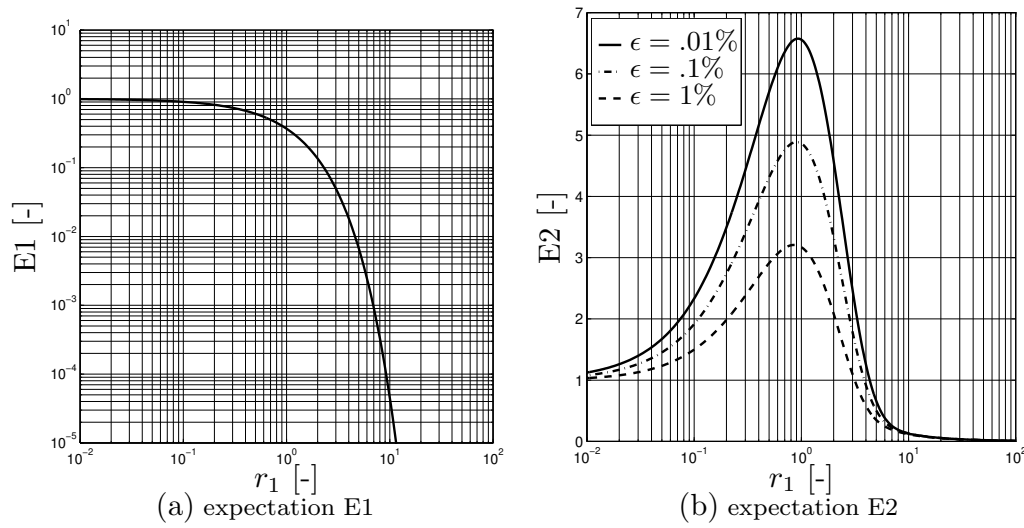
Figure F.2: The expectation quantities E1 and E2 as a function of the signal-to-noise ratio r_1. E2 is shown for three values of the probability variable ϵ (Eq. F.14).

Summary of the estimation method The describing functions $H_{p_x}^p$ and $H_{p_y}^p$ can be estimated at the set of frequencies of forcing functions i_1 and i_2 with Eq. F.6. The bias and variance of these estimated frequency responses can be computed *analytically* using Eqs F.16-F.17 and Eqs F.13-F.18, respectively (Table F.1). The bias and variance terms are mainly a function of the signal-to-noise ratios r_1 and r_2. Especially the signal-to-noise ratio r_1, determining the values for the expectations E1 and E2, is important (van Paassen & Mulder, 1998a). Figs F.2(a) and F.2(b), illustrating these expectations as a function of the signal-to-noise ratio r_1, show that when r_1 is large enough (>5), the variance and bias terms become small. Whereas the signal-to-noise ratio r_2 does not affect the bias terms, it is important in the computation of the variance terms. Because the system dynamics (H_{c_1} and H_{c_2}) are generally low-pass, Eq. F.18 shows that the estimation variance of the outer loop describing function $H_{p_y}^p$ can be expected to increase for the larger frequencies. It is clear that, in the design of the input signals, see §F.2.6, the goal should be to achieve large signal-to-noise ratios in the frequency range of interest.

F.2.2 The (2×1) serial model

Definition of the situation A general serial pilot model with two input signals and one output signal in a disturbance task is shown in Fig. F.3.

Estimation of the describing functions All measurable signals in the loop (u, x and y) are discrete-Fourier transformed. Similar to the discussion of the (2×1) parallel model expressions can be derived for the estimation of the two describing functions:

$$\hat{H}_{p_x}^s(\nu_{1_j};\zeta) = \frac{U_1\tilde{Y}_2 - Y_1\tilde{U}_2}{\tilde{X}_2Y_1 - \tilde{Y}_2X_1} \; ; \quad \text{and} \quad \hat{H}_{p_y}^s(\nu_{1_j};\zeta) = \frac{\tilde{U}_2X_1 - \tilde{X}_2U_1}{U_1\tilde{Y}_2 - Y_1\tilde{U}_2}, \tag{F.19}$$
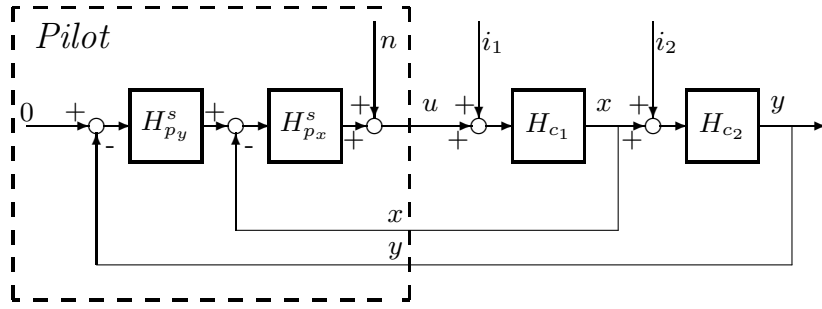
Figure F.3: The general situation of a *serial* pilot model with two input signals and one output signal in a disturbance task.

with U_1, X_1 and Y_1 the Fourier coefficients of the signals u, x and y at frequencies ν_{1_j} and $\tilde{U}_2$, $\tilde{X}_2$ and $\tilde{Y}_2$ their Fourier coefficients interpolated from frequencies ν_{2_j}. Similar expressions can be derived for the two estimated describing functions at frequencies of i_2.

Computation of the bias and variance First, all signals in the closed loop are described in terms of the signals that are inserted in the loop. These equations are then evaluated at the frequencies of i_1 and i_2 after which they can be substituted in Eq. F.19. The following expressions can be obtained for the estimated describing functions:

$$\hat{H}_{p_x}^s = H_{p_x}^s - \left(H_{p_x}^s + \frac{1}{H_{c_1}}\right)\left(\frac{N_1}{I_1 + N_1}\right) - \frac{N_1 N_2}{I_2(I_1 + N_1)} + \frac{N_2}{I_2}; \qquad \text{(F.20)}$$

$$\hat{H}_{p_y}^s = H_{p_y}^s - \frac{\left(H_{c_1} I_1 + H_{p_y}^s H_{c_2} H_{c_1} I_1\right) N_2 - \left(H_{p_y}^s H_{c_2} I_2\right) N_1}{H_{c_2}\left(\left(H_{p_x}^s H_{c_1} I_1 I_2\right) + \left(H_{c_1} I_1\right) N_2 - \left(I_2\right) N_1\right)}. \qquad \text{(F.21)}$$

These equations express the *estimated* frequency responses $\hat{H}_{p_x}^s$ and $\hat{H}_{p_y}^s$, in terms of the *true* describing functions $H_{p_x}^s$ and $H_{p_y}^s$, the controlled system dynamics H_{c_1} and H_{c_2}, and the Fourier coefficients of the forcing functions I_1 and I_2 and the noise signals N_1 and N_2. The estimation of $H_{p_x}^s$ is identical to the estimation of $H_{p_x}^p$, Eq. F.8, and the bias and variance of this estimated frequency response can be computed in the same way as for the inner loop frequency response of the parallel pilot model (Eqs F.16, F.13 and F.15). *No analytical expressions can be derived*, however, for the computation of the bias and variance for the estimate of the outer loop describing function $H_{p_y}^s$. An analytic computation of the expectation of Eq. F.21 implies the integration of the expression multiplied with the joint probability density function of N_1 and N_2. This integral can be solved analytically when the contributions of N_1 and N_2 to this integral are separated, which is impossible because both N_1 and N_2 are present in the denominator.

Concluding remarks The frequency responses $H_{p_x}^s$ and $H_{p_y}^s$ of the (2×1) serial pilot model can be estimated using Eq. F.19. The bias and variance can be computed analytically only for the estimated inner loop frequency response, a computation that is the same as for the (2×1) parallel model. The bias and variance of the estimated outer loop describing function can not be computed analytically. These quantities must
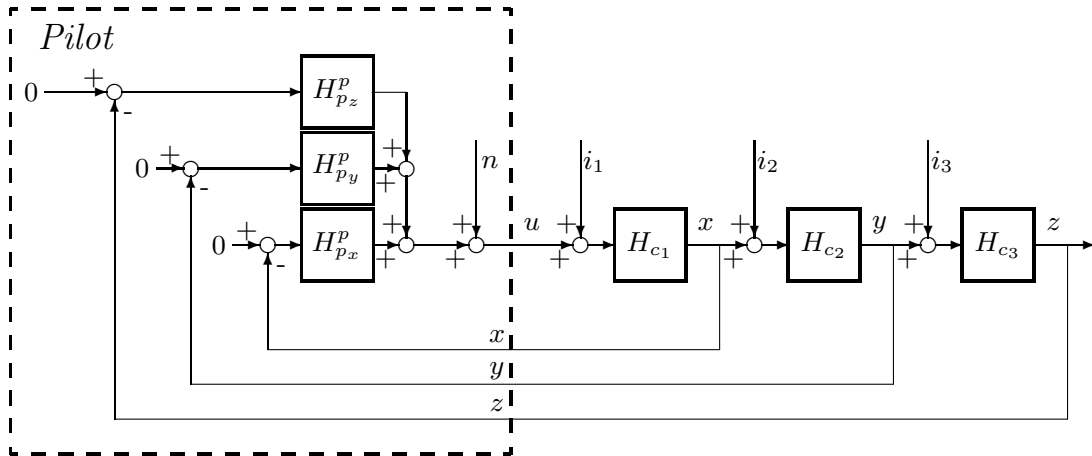
Figure F.4: The general situation of a *parallel* pilot model with three input signals and one output signal in a disturbance task.

then be estimated from the experimental data, substantially increasing the number of measurements. These difficulties also hold for the application of serial pilot models with more than two input signals, and it was concluded to apply only parallel models for identification purposes. This exemplifies the advantage of using a parallel pilot model structure from an identification point of view.

F.2.3 The (3×1) parallel model

Definition of the situation A general parallel pilot model with three input signals and one output signal in a disturbance task is shown in Fig. F.4. Three forcing functions are applied: i_1 (at frequencies $\underline{\nu}_{i_1} = \underline{k}_1 \nu_0$), i_2 ($\underline{\nu}_{i_2} = \underline{k}_2 \nu_0$) and i_3 ($\underline{\nu}_{i_3} = \underline{k}_3 \nu_0$).

Estimation of the describing functions All signals in the loop (u, x, y and z) are discrete-Fourier transformed. Through interpolation a set of three equations can be obtained for the three unknown describing functions, at frequencies of i_1:

$$\begin{pmatrix} U_1 \\ \tilde{U}_2 \\ \tilde{U}_3 \end{pmatrix} = - \begin{pmatrix} X_1 & Y_1 & Z_1 \\ \tilde{X}_2 & \tilde{Y}_2 & \tilde{Z}_2 \\ \tilde{X}_3 & \tilde{Y}_3 & \tilde{Z}_3 \end{pmatrix} \begin{pmatrix} H_{p_x}^p(\nu_{1_j}) \\ H_{p_y}^p(\nu_{1_j}) \\ H_{p_z}^p(\nu_{1_j}) \end{pmatrix}. \tag{F.22}$$

The same holds for the estimation of the three describing functions at the frequencies of signals i_2 and i_3. For these estimations the Fourier coefficients need to be interpolated from ν_{i_1} and ν_{i_3} to ν_{i_2} and from ν_{i_1} and ν_{i_2} to ν_{i_3}, respectively. The procedure yields an estimation of the pilot describing functions $H_{p_x}^p$, $H_{p_y}^p$ and $H_{p_z}^p$ at the frequencies $\underline{\nu}_{i_1}$, $\underline{\nu}_{i_2}$ and $\underline{\nu}_{i_3}$ of the three forcing function signals, i.e. at $3N_f$ frequencies.

Computation of the bias and variance in the estimation The following equations can be obtained for the estimated describing functions (skipping ν_k and ζ):

$$\hat{H}_{p_x}^p = H_{p_x}^p - \left(H_{p_x}^p + \frac{1}{H_{c_1}} \right) \left(\frac{N_1}{I_1 + N_1} \right) - \frac{N_1 N_2}{I_2 (I_1 + N_1)} + \frac{N_2}{I_2}; \tag{F.23}$$

Table F.2: The calculation of the bias and variance of the estimated pilot frequency responses for a (3×1) parallel model.

$\hat{H}^p_{p_x}$	Bias	$-\left(\hat{H}^p_{p_x} + \frac{1}{H_{c_1}}\right)\text{E1}$	(F.26)
	Var$|\cdot|$	$\left|\hat{H}^p_{p_x} + \frac{1}{H_{c_1}}\right|^2 \left(\text{E2} - \text{E1}^2\right) + \frac{1}{r_2}\left(1 - 2\text{E1} + \text{E2}\right)$	(F.27)
$\hat{H}^p_{p_y}$	Bias	$-\left(\hat{H}^p_{p_y}\right)\text{E1}$	(F.28)
	Var$|\cdot|$	$\left|\hat{H}^p_{p_y}\right|^2 \left(\text{E2} - \text{E1}^2\right) + \left(\frac{1}{r_3} + \frac{1}{|H_{c_2}|^2 r_2}\right)\left(1 - 2\text{E1} + \text{E2}\right)$	(F.29)
$\hat{H}^p_{p_z}$	Bias	$-\left(\hat{H}^p_{p_z}\right)\text{E1}$	(F.30)
	Var$|\cdot|$	$\left|\hat{H}^p_{p_z}\right|^2 \left(\text{E2} - \text{E1}^2\right) + \frac{1}{|H_{c_3}|^2 r_3}\left(1 - 2\text{E1} + \text{E2}\right)$	(F.31)

$$
\begin{aligned}
\hat{H}^p_{p_y} &= H^p_{p_y} - H^p_{p_y}\left(\frac{N_1}{I_1 + N_1}\right) - \frac{N_2 I_1}{H_{c_2} I_2 (I_1 + N_1)} - \frac{I_1 N_3}{I_3 (I_1 + N_1)}; & \text{(F.24)} \\
\hat{H}^p_{p_z} &= H^p_{p_z} - H^p_{p_z}\left(\frac{N_1}{I_1 + N_1}\right) + \frac{N_1 N_3}{H_{c_3} I_3 (I_1 + N_1)} - \frac{N_3}{H_{c_3} I_3}. & \text{(F.25)}
\end{aligned}
$$

The bias and variance terms can be computed similar as in §F.2.1, yielding expressions of Table F.2. Here, a *third* signal-to-noise ratio emerges, r_3, that is defined as the quotient of the power of the deterministic input signal I_3 and the power of the stochastic noise signal N_3, at frequencies ν_{3_j} of the input signal i_3. Again, the estimation bias and variance terms are mainly a function of the signal-to-noise ratios r_1, r_2 and r_3. Although r_2 and r_3 have no effect on the bias of the estimates, they must be large enough to allow a proper identification of the middle and outer loop frequency responses, Eqs F.29- F.31.

F.2.4   The (4×2) parallel model

Definition of the situation   A general two-axis dual-loop disturbance task is illustrated in Fig. F.5. In this task the pilot controls two channels simultaneously, with two parallel feedback loops and two cross-feeds in each channel, resulting in a pilot model with four input and two output signals. To estimate the pilot describing functions, four independent forcing functions (i_1, i_2, i_3 and i_4) must be inserted in the closed loop.

Estimation of the frequency responses   At an arbitrary frequency ν_k the following expressions hold (Fig. F.5):

$$
\begin{aligned}
U^1(\nu_k; \zeta) = & -H^p_{p_{x_{11}}}(\nu_k)X^1(\nu_k; \zeta) - H^p_{p_{y_{11}}}(\nu_k)Y^1(\nu_k; \zeta) \\
& -H^p_{p_{x_{21}}}(\nu_k)X^2(\nu_k; \zeta) - H^p_{p_{y_{21}}}(\nu_k)Y^2(\nu_k; \zeta) + N^1(\nu_k; \zeta);
\end{aligned}
\tag{F.32}
$$
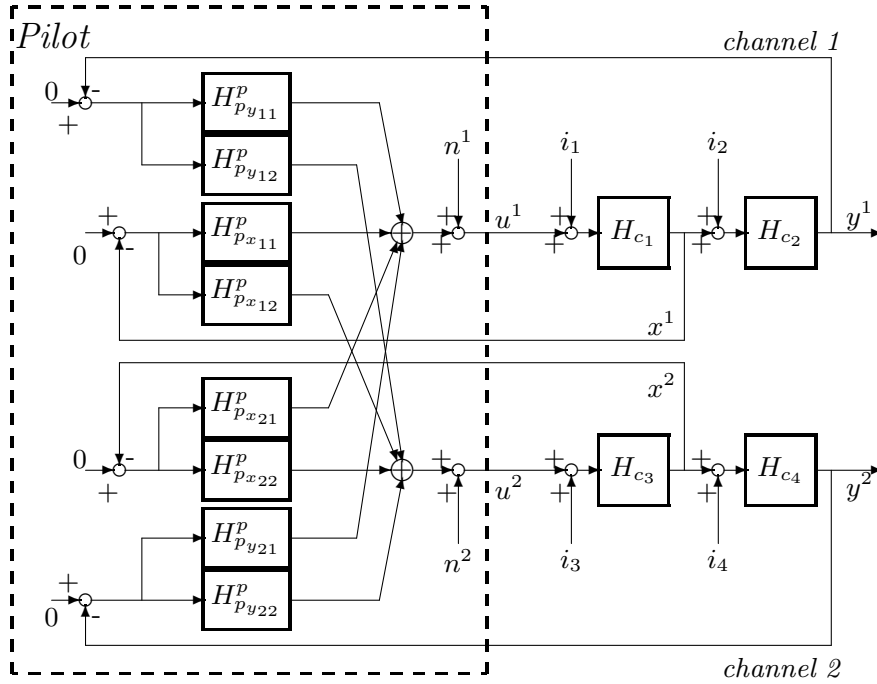
Figure F.5: The general situation of a *parallel* pilot model with four input signals and two output signals in a two-axis disturbance task. Two control channels can be distinguished that are controlled with two (2×1) parallel sub-models. The interference between both the channels is represented by the four cross-feeds.

$$
\begin{aligned}
U^2(\nu_k;\zeta) & = -H^p_{p_{x_{12}}}(\nu_k)X^1(\nu_k;\zeta) - H^p_{p_{y_{12}}}(\nu_k)Y^1(\nu_k;\zeta) \\
& \quad -H^p_{p_{x_{22}}}(\nu_k)X^2(\nu_k;\zeta) - H^p_{p_{y_{22}}}(\nu_k)Y^2(\nu_k;\zeta) + N^2(\nu_k;\zeta).
\end{aligned}
\tag{F.33}
$$

Two equations are obtained with eight unknowns. Similar as before, the expressions are evaluated at frequencies of the forcing function signals i_1 to i_4, where the contribution of the noise signals can be neglected. Interpolation of the Fourier coefficients yields a set of eight equations with eight unknowns for all $4N_f$ frequencies of the four forcing functions. E.g., at frequencies of forcing function i_1 the following set of equations holds:

$$
\begin{pmatrix} U_1^1 & U_1^2 \\ \tilde{U}_2^1 & \tilde{U}_2^2 \\ \tilde{U}_3^1 & \tilde{U}_3^2 \\ \tilde{U}_4^1 & \tilde{U}_4^2 \end{pmatrix} = - \begin{pmatrix} X_1^1 & Y_1^1 & X_1^2 & Y_1^2 \\ \tilde{X}_2^1 & \tilde{Y}_2^1 & \tilde{X}_2^2 & \tilde{Y}_2^2 \\ \tilde{X}_3^1 & \tilde{Y}_3^1 & \tilde{X}_3^2 & \tilde{Y}_3^2 \\ \tilde{X}_4^1 & \tilde{Y}_4^1 & \tilde{X}_4^2 & \tilde{Y}_4^2 \end{pmatrix} \begin{pmatrix} H^p_{p_{x_{11}}}(\nu_{1_j}) & H^p_{p_{x_{12}}}(\nu_{1_j}) \\ H^p_{p_{y_{11}}}(\nu_{1_j}) & H^p_{p_{y_{12}}}(\nu_{1_j}) \\ H^p_{p_{x_{21}}}(\nu_{1_j}) & H^p_{p_{x_{22}}}(\nu_{1_j}) \\ H^p_{p_{y_{21}}}(\nu_{1_j}) & H^p_{p_{y_{22}}}(\nu_{1_j}) \end{pmatrix}.
\tag{F.34}
$$

Solving this set of equations leads to estimates of the four parallel feedback loops and the four crossfeeds at the four sets of frequencies of the four forcing functions.

Computation of the bias and variance   Expressions can be derived for the *estimated* frequency responses in terms of the *true* frequency responses and the properties of the other elements in the closed loop. These expressions, however, do not allow an analytic computation of the bias and variance of the estimates, for similar reasons as discussed in §F.2.2, i.e. the contributions of the noise signals N^1 and N^2 can not be disentangled.

The bias and variance terms can only be computed by numerically evaluating a set of $\mathcal{C}^8$ complex integrals, which is beyond the scope of this thesis.

Concluding remarks The frequency responses of the four feedback loops and the four cross-feeds can be estimated from the measured data by solving Eq. F.34. The bias and variance of these estimates, however, cannot be computed analytically. It can be shown that this setback is true for *any* control task involving more than one control axis.

F.2.5 The signal-to-noise ratio SNR

Computation of the signal-to-noise ratios The signal-to-noise ratio r_1 is defined in §F.2.1 as the quotient of the variances of I_1 and N_1 at frequencies ν_{i_1} of the forcing function i_1. The *unknown* power of the stochastic noise signal is substituted by the experimentally determined variance of this signal, $s_{N_1}^2$, resulting in (van Paassen, 1994):

$$r_1(\nu_{1_j}; \zeta) = \frac{\left|I_1(\nu_{1_j})\right|^2}{s_{N_1}^2(\nu_{1_j}; \zeta)}, \tag{F.35}$$

where $s_{N_1}^2$ can be computed with (assuming a (2×1) parallel model structure):

$$s_{N_1}^2(\nu_{1_j}; \zeta) = s_{U_{N_1}}^2(\nu_{1_j}; \zeta) \left|1 + \hat{H}_{p_x}^p(\nu_{1_j}; \zeta) H_{c_1}(\nu_{1_j}) + \hat{H}_{p_y}^p(\nu_{1_j}; \zeta) H_{c_2}(\nu_{1_j}) H_{c_1}(\nu_{1_j})\right|^2.$$

Here, $s_{U_{N_1}}^2$ represents the *averaged* power of the pilot input signal at the neighbouring frequencies of ν_{1_j} (van Paassen, 1994):

$$s_{U_{N_1}}^2(\nu_{1_j}; \zeta) = \frac{1}{5} \sum_{\substack{m=k_{1_j}-3 \\ m \notin \underline{k}_1, m \notin \underline{k}_2}}^{m=k_{1_j}+3} |U(\nu_m; \zeta)|^2. \tag{F.36}$$

To allow a computation of this estimated variance there need to be a sufficient number of frequencies on both the sides of a forcing function frequency ν_{1_j} that is *not* a member of the two frequency sets $\underline{\nu}_{i_1}$ and $\underline{\nu}_{i_2}$. The same holds for the signal-to-noise ratio r_2 at frequencies ν_{2_j} and, for a (3×1) parallel model, for r_3 at frequencies ν_{3_j}.

Interpolation of the signal-to-noise ratios For the (2×1) parallel model structure, the pilot describing functions are estimated at both the sets of frequencies $\underline{\nu}_{i_1}$ and $\underline{\nu}_{i_2}$. Until now, the bias and variance of the estimates have been computed only at frequencies belonging to the set of i_1. To compute these quantities at frequencies of the second forcing function signal i_2, one can simply substitute the frequency components of ν_{2_j} for those of ν_{1_j} in the formulas. The signal-to-noise ratios, however, are defined only at their corresponding frequencies, i.e. r_1 at ν_{1_j} and r_2 at ν_{2_j}. Therefore, estimates are required for the signal-to-noise ratio r_1 at frequencies of i_2 and for r_2 at frequencies of i_1. The *interpolated* signal-to-noise ratio r_1 at frequencies ν_{2_j} is then defined as:

$$\tilde{r}_1(\nu_{2_j}; \zeta) = \frac{\left|\tilde{I}_1(\nu_{2_j})\right|^2}{\tilde{s}_{N_1}^2(\nu_{2_j}; \zeta)}, \tag{F.37}$$

with $\tilde{I}_1$ the interpolated Fourier coefficient of the forcing function I_1 and $\tilde{s}^2_{N_1}$ the inter-polated estimate of the variance of noise signal N_1. The same holds for the *interpolated* signal-to-noise ratio r_2 at frequencies ν_{1_j}.

F.2.6   Design rules for forcing function signals

The type and definition of the forcing function signals have been addressed in §4.2. The number of forcing functions that is applied in the control tasks of this thesis is 2 (X1–X4) or 3 (X5). They are each defined as a sum of sinusoids that have power at a limited set of frequencies, Eq. 4.1. As has been discussed in Chapter 4, there are several constraints on the use of the forcing function signals and their design is an important issue. Some guidelines are given here (van Paassen & Mulder, 1998a).

An important constraint is that the amount of *energy* that can be inserted in the closed loop is limited. Therefore, one should be economical in choosing: (i) the number of forcing functions; (ii) the number of frequencies per forcing function (N_f), and (iii) the distribution of the energy over the amplitudes of a forcing function. With a limited amount of energy an increase in any one of these variables automatically leads to a decrease in one of the others. The design should lead to a *balanced* insertion of energy that properly excites the elements of the system to be identified at the frequency range of interest.

The choice of the forcing function *frequencies* (i.e. $\underline{\nu}_{i_1}$) is determined by the demand that they cover the frequency range of interest. Generally a logarithmic separation between frequencies suffices. Although not necessary, a common procedure is to choose the various frequency components k_{1_j} in such a way that they cannot be an integer multiple of other frequency components of that or any other forcing function signal. Furthermore, to reduce the errors made in the various interpolations, Eq. F.3, the frequencies of the different forcing function signals should be close together. In general, it is attempted to put the pairs of frequencies next to each other, e.g. $\underline{k}_{i_2} = 1 + \underline{k}_{i_1}$. Finally, to allow an estimation of the variance of the noise signal near a particular frequency of a forcing function, Eq. F.36, there should be enough frequency components that are not used by a forcing function. Since all discrete frequencies are an integer multiple of the ground frequency ν_0, choosing the right frequency components is especially problematic in the low-frequency range.

Generally, for the *shaping filter* of the forcing function signals, determining the division of the signal power over the set of frequencies, a first or second order low-pass filter can be used. The bandwidth of the shaping filters should not be chosen too high, for this could result in *crossover regression* effects (McRuer & Jex, 1967). In the situation of a disturbance task, special notice should be taken of the attenuating effects of the system dynamics following the insertion of a forcing function. These effects can be reduced by compensating for these dynamics by pre-multiplying the shaping filter with the inverse of (part of) the aircraft dynamics, §4.5.1.

F.3   Stage II: Parametric identification

The parameter estimation techniques applied in this thesis are essentially *optimization* problems: a criterion is minimized that quantifies the mismatch between the modelled and measured data, Eq. 4.2. The minimization criteria and algorithms are discussed in §F.3.1 and §F.3.2, respectively. In this thesis a method is developed which allows the uncertainty in the estimated parameters to be computed with the Cramer-Rao lower bound, §F.3.3. The discussion will be limited to the case of two forcing functions.

F.3.1   Definition of criteria

The frequency domain criterion J_F J_F is a weighted least-squares (LS) criterion that quantifies the mismatch between the measured frequency responses ($\hat{H}_{p_x}^p(\nu_k; \zeta)$, $\hat{H}_{p_y}^p(\nu_k; \zeta)$) and the frequency responses of the model ($\tilde{H}_{p_x}^p(\nu_k; \underline{\theta})$, $\tilde{H}_{p_y}^p(\nu_k; \underline{\theta})$):

$$J_F(\underline{\theta}) = \frac{1}{2N_f} \sum_{k=1}^{k=2N_f} \left\{ \frac{\left| \hat{H}_{p_x}^p(\nu_{c_k}; \zeta) - \tilde{H}_{p_x}^p(\nu_{c_k}; \underline{\theta}) \right|^2}{\hat{\sigma}_{\left| \hat{H}_{p_x}^p \right|}^2(\nu_{c_k}; \zeta)} + \frac{\left| \hat{H}_{p_y}^p(\nu_{c_k}; \zeta) - \tilde{H}_{p_y}^p(\nu_{c_k}; \underline{\theta}) \right|^2}{\hat{\sigma}_{\left| \hat{H}_{p_y}^p \right|}^2(\nu_{c_k}; \zeta)} \right\}.$$

$$\text{(F.38)}$$

Here, $\underline{\nu}_c$ is defined as the *combined* set of frequencies of i_1 and i_2 ($\underline{\nu}_c = \underline{\nu}_{i_1} \cup \underline{\nu}_{i_2}$). In J_F the mismatch in modelling an estimated frequency response at a frequency ν_{c_k} is weighted by the estimated variance of that frequency response at that particular frequency. Thus, when the uncertainty in the estimation at a certain frequency is large, the error in matching this estimation does not contribute heavily to the cost function (and vice versa).

The time domain criterion J_T   Repeating an experimental condition yields an array of STDs of a particular variable, §4.4. The statistics, i.e. the estimated mean $\hat{\mu}_\sigma(\zeta)$ and standard deviation $\hat{\sigma}_\sigma(\zeta)$), of these arrays of STDs can then be used to compute J_T:

$$J_T(\underline{\theta}) = \frac{1}{N_v} \sum_{j=1}^{j=N_v} \frac{\left(\hat{\mu}_{\sigma_j}(\zeta) - \tilde{\sigma}_j(\underline{\theta}) \right)^2}{\hat{\sigma}_{\sigma_j}^2(\zeta)},$$

$$\text{(F.39)}$$

with N_v the number of time domain variables and $\tilde{\sigma}_j$ the STD of a particular variable according to the model. Again, the criterion weights the mismatch in modelling a variable with the uncertainty in experimentally measuring that particular variable.

Combining the frequency and time domain criteria   The application of a pilot model generally results in model outputs in the time domain as well as in the frequency domain. Although the data in both the domains are equivalent, the uncertainties in experimentally measuring them can be different. This could lead to a situation in which a criterion in one domain is insensitive to changing an element of the parameter vector, whereas the criterion in the other domain is not. Methods have been investigated that optimize a criterion function that operates in *both* domains. A two-step approach is developed.

First, the optimization is conducted in each domain separately, yielding minima for J_F (J_F^* for parameter $\underline{\theta}_F$) and J_T (J_T^* for parameter $\underline{\theta}_T$). Second, these minima are used as weighting factors to scale the contributions of both the criterions to the total criterion. Two definitions of the latter criterion were used:

1. Normalize the contributions of the criteria in both the domains with their minima:

$$J_{FT}^1(\underline{\theta}) = \lambda \frac{J_F(\underline{\theta})}{J_F^*(\underline{\theta}_F)} + (1 - \lambda) \frac{J_T(\underline{\theta})}{J_T^*(\underline{\theta}_T)}. \tag{F.40}$$

2. Normalize the *relative* contributions of the criteria with respect to their minima:

$$J_{FT}^2(\underline{\theta}) = \lambda \frac{J_F(\underline{\theta}) - J_F^*(\underline{\theta}_F)}{J_F(\underline{\theta}_T) - J_F^*(\underline{\theta}_F)} + (1 - \lambda) \frac{J_T(\underline{\theta}) - J_T^*(\underline{\theta}_T)}{J_T(\underline{\theta}_F) - J_T^*(\underline{\theta}_T)}. \tag{F.41}$$

For both the criterion functions the weighting factor λ was set to 0.5. The criterion functions J_{FT}^1 and J_{FT}^2 could be used well for the OCM and the MLM modelling approaches, respectively. This can be attributed to the fact that for the MLMs the time domain criterion in general was not convex, i.e. J_T could be minimized to very small values.

F.3.2 Criterion minimization procedures

Numerous algorithms are available for the minimization of a criterion function that depends on a set of variables. The SIMPLEX and BFGS optimization schemes are applied in this thesis. The *downhill simplex method* (Nelder-Mead) is a slow but robust minimization algorithm that does not require any derivative calculations. The BFGS (Broyden-Fletcher-Goldfarb-Shanno) algorithm is a quasi-Newton or variable metric method that resembles the Fletcher-Powell scheme (Press et al., 1992). The two optimization schemes were used in conjunction. First, the SIMPLEX method was applied to obtain a robust initial estimate of the parameter vector. Then, the BFGS algorithm was used to compute the final estimate. This procedure was generally repeated 3 to 5 times, with different initial conditions of the parameter vector, to increase the chance that a *global* rather than a *local* minimum was found. The minimization itself was implemented as a optimization problem with *constraints*, i.e. $\underline{\theta}_{min} < \underline{\theta} < \underline{\theta}_{max}$, preventing that elements of the parameter vector obtained values that were out of range.

F.3.3 The Cramer-Rao lower bound

When a criterion $J(\underline{\theta})$ is minimized an estimate $\hat{\underline{\theta}}$ of the true parameter vector $\underline{\theta}_0$ is obtained. The covariance of this estimate can be computed using the Cramer-Rao lower bound, Eq. 4.3, defined as the inverse of the Fisher information matrix, Eq. 4.4. In this thesis, a method is derived that allows a computation of the Fisher information matrix

for the use of a frequency domain criterion J_F, at the hand of (Klein, 1989).

Computation of the Fisher information matrix   The derivation starts with defining the frequency domain criterion for a SISO estimated frequency response $\hat{H}_p(\nu_k; \zeta)$:

$$J(\underline{\theta}) = \frac{1}{N_f} \sum_{k=1}^{k=N_f} \frac{\left| \hat{H}_p(\nu_{i_k}; \zeta) - \tilde{H}_p(\nu_{i_k}; \underline{\theta}) \right|^2}{\sigma^2_{\left| \hat{H}_p \right|}(\nu_{i_k}; \zeta)}, \tag{F.42}$$

with $\underline{\theta}$ the $(m \times 1)$ parameter vector, $\tilde{H}_p(\nu_{i_k}; \underline{\theta})$ the frequency response of the model and $\sigma^2_{\left| \hat{H}_p \right|}(\nu_{i_k}; \zeta)$ the variance in the estimated frequency response. A complex error signal e is defined as: $e(\nu_{i_k}; \underline{\theta}) = \hat{H}_p(\nu_{i_k}; \zeta) - \tilde{H}_p(\nu_{i_k}; \underline{\theta})$. It is assumed that, after the minimization of the criterion, e is a zero-mean Gaussian white noise signal. Substituting e in Eq. F.42, and differentiating this expression twice with respect to $\underline{\theta}$, yields:[2]

$$\begin{aligned}
\frac{\partial^2 J(\underline{\theta})}{\partial \underline{\theta} \partial \underline{\theta}^T} &= -\frac{2}{N_f} \mathrm{Re} \left\{ \sum_{k=1}^{k=N_f} \left(\left(\frac{\partial^2}{\partial \underline{\theta} \partial \underline{\theta}^T} \tilde{H}_p(\nu_{i_k}; \underline{\theta}) \right) \frac{1}{\sigma^2_{\left| \hat{H}_p \right|}(\nu_{i_k}; \zeta)} e^*(\nu_{i_k}; \underline{\theta}) \right. \right. \\
&\quad \left. \left. - \left(\frac{\partial}{\partial \underline{\theta}} \tilde{H}_p(\nu_{i_k}; \underline{\theta}) \right) \frac{1}{\sigma^2_{\left| \hat{H}_p \right|}(\nu_{i_k}; \zeta)} \left(\frac{\partial}{\partial \underline{\theta}} \tilde{H}_p(\nu_{i_k}; \underline{\theta}) \right)^* \right) \right\},
\end{aligned} \tag{F.43}$$

where * depicts the complex conjugate transpose. Taking the expectation of Eq. F.43 leads to the Fisher information matrix $M_{\underline{\theta}\underline{\theta}}$. Because e is assumed to be zero-mean Gaussian white noise, the first term on the right-hand side of Eq. F.43 becomes zero, giving:

$$M_{\underline{\theta}\underline{\theta}} = \frac{2}{N_f} \mathrm{Re} \left\{ \sum_{k=1}^{k=N_f} S(\nu_{i_k}; \underline{\theta}) \frac{1}{\sigma^2_{\left| \hat{H}_p \right|}(\nu_{i_k}; \zeta)} S^*(\nu_{i_k}; \underline{\theta}) \right\}, \tag{F.44}$$

with $S(\nu_{i_k}; \underline{\theta}) = \frac{\partial}{\partial \underline{\theta}} \tilde{H}_p(\nu_{i_k}; \underline{\theta})$ the *sensitivity function* $(\in \mathcal{C}^m)$, which can be computed using a symmetrized or balanced finite difference method (Press et al., 1992):

$$S^\ell(\nu_{i_k}; \underline{\theta}) = \frac{\partial \tilde{H}_p(\nu_{i_k}; \underline{\theta})}{\partial \theta_\ell} \approx \frac{\tilde{H}_p(\nu_{i_k}; \underline{\theta} + \triangle \underline{\theta}^\ell) - \tilde{H}_p(\nu_{i_k}; \underline{\theta} - \triangle \underline{\theta}^\ell)}{2 \triangle \theta_\ell}, \tag{F.45}$$

for $\ell = (1 \ldots m)$ with $\triangle \underline{\theta}^\ell = [0 \ldots 0 \ \triangle \theta_\ell \ 0 \ldots 0]^T$, resulting in:

$$S(\nu_{i_k}; \underline{\theta}) = \left(S^1(\nu_{i_k}; \underline{\theta}) \ \ldots \ S^m(\nu_{i_k}; \underline{\theta}) \right)^T. \tag{F.46}$$

The Cramer-Rao lower bound can be computed by inverting the Fisher information matrix.

Extending the computation to more than one frequency response   The method derived above can be extended in a straightforward manner to the situation with two estimated frequency responses, or more. Consider the situation for two frequency responses, where J_F is a summation of the contributions of the mismatch in modelling the estimated

---

[2]It is assumed that derivatives with respect to $\underline{\theta}$ are deterministic.

inner and outer loop frequency responses $\hat{H}_{p_x}^p$ and $\hat{H}_{p_y}^p$, respectively (Eq. F.38). Following the same procedure as above leads to the Fisher information matrix:

$$
\begin{aligned}
M_{\underline{\theta\theta}} \quad = \quad & \frac{2}{2N_f}\text{Re}\left\{\sum_{k=1}^{k=2N_f} S_x(\nu_{c_k};\underline{\theta})\frac{1}{\sigma^2_{\left|\hat{H}_{p_x}^p\right|}(\nu_{c_k};\zeta)}S_x^*(\nu_{c_k};\underline{\theta})\right\} \\
+ \quad & \frac{2}{2N_f}\text{Re}\left\{\sum_{k=1}^{k=2N_f} S_y(\nu_{c_k};\underline{\theta})\frac{1}{\sigma^2_{\left|\hat{H}_{p_y}^p\right|}(\nu_{c_k};\zeta)}S_y^*(\nu_{c_k};\underline{\theta})\right\},
\end{aligned}
\qquad \text{(F.47)}
$$

with the *two* sensitivity functions S_x and S_y defined similarly as above.

F.4   Miscellaneous topics in model validation

F.4.1   The relative noise ratio RNR

The insertion of deterministic forcing function signals in the closed loop with power at a limited set of frequencies has some advantages. As has been discussed in Chapter 4, it can be hypothesized that most of the power of an arbitrary signal in the closed loop at the frequency sets $\underline{\nu}_i$ is due to the forcing functions. At all other frequencies the power of those signals can only result from the pilot's noise signal n. The relative noise ratio (RNR) is a useful quantity that allows the computation of the *relative* contribution of the pilot noise to a signal's variance at such a particular set of frequencies:

$$
\text{RNR}(u;i_1) \quad = \quad \frac{\sum_{j=1}^{j=N/2}|U(\nu_j;\zeta)|^2 - \sum_{j=1}^{j=N_f}\left|U(\nu_{k_{1_j}};\zeta)\right|^2}{\sum_{j=1}^{j=N/2}|U(\nu_j;\zeta)|^2}.
\qquad \text{(F.48)}
$$

Here, $\text{RNR}(u;i_1)$ depicts the RNR of signal u, computed for the set of frequencies of forcing function i_1. The RNR is a positive number between 0 and 1. When the RNR of a signal at a set of frequencies equals 0, all power of that signal is concentrated at that particular set of frequencies. When the RNR of a signal at a set of frequencies equals 1 the power of that signal at those frequencies is zero. Hence, $\text{RNR}(i_1;i_2)=1$ and $\text{RNR}(i_1;i_1)=0$.

F.4.2   The effects of a simulation time delay

An analysis of the simulation environment (Appendix A) revealed that a considerable time delay τ_{sim} exists in the experimental set-up. Consider Fig. F.6. The signals u, x and y are recorded during a simulation run. The system output signals x and y are both presented to the pilot with a delay, represented by $H_d(s) = e^{-s\tau_{sim}}$. Thus, the pilot does not perceive the *recorded* system outputs, but the *displayed* outputs $\tilde{x}$ and $\tilde{y}$ that are delayed. In this case the frequency responses relating $\tilde{x}$ and $\tilde{y}$ to u can be computed using the estimated frequency responses $\hat{H}_{p_x}^p$ and $\hat{H}_{p_y}^p$ – using x and y – as follows:

$$
\hat{H}_{p_{\tilde{x}}}^p \quad = \quad \frac{\hat{H}_{p_x}^p}{H_d}; \quad \text{and} \quad \hat{H}_{p_{\tilde{y}}}^p \quad = \quad \frac{\hat{H}_{p_y}^p}{H_d}.
\qquad \text{(F.49)}
$$
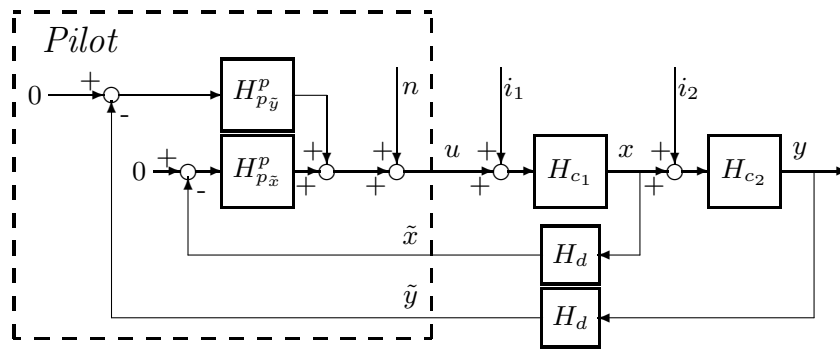
Figure F.6: The general situation for two forcing function signals with a time delay in the closed loop, represented by the blocks labelled H_d.

Since the delay is deterministic the bias and variance of the *true* describing functions $\hat{H}^p_{p\tilde{x}}$ and $\hat{H}^p_{p\tilde{y}}$ can be calculated using the bias and variance of the estimated describing functions $\hat{H}^p_{p_x}$ and $\hat{H}^p_{p_y}$.

F.4.3 Computing the crossover frequency and phase margin

The crossover frequency of a loop closure is defined as the frequency at which the magnitude of the open loop transfer function of that loop closure equals 1. The phase margin is defined as the difference between $-180°$ and the phase of that particular open loop transfer function at the crossover frequency. These definitions can be applied well with analytic, i.e. continuous, frequency transfer functions. In the application considered here, however, the frequency responses are known at a limited set of discrete frequencies ($\underline{\nu}_c \in \underline{\nu}_{i_1} \cup \underline{\nu}_{i_2} (\cup \underline{\nu}_{i_3})$) which means that the crossover frequency and phase margin must be obtained through *interpolation*. The application of an interpolation method generally provides satisfactory results for the frequency responses that were estimated using the averaged time domain data. The time-averaging procedure considerably attenuates the effects of the pilot remnant, leading to larger SNRs and an estimate that is reasonably smooth. Applying the interpolation method to the frequency responses that were estimated using the non-averaged time histories, however, can lead to problems in determining the crossover frequency. Therefore, a procedure was developed to improve the consistency of the estimate of the crossover frequency and phase margin quantities. It is based on the properties of the crossover model theorem, §E.2.2, that states that a pilot closes an arbitrary loop in such a way that the open loop equals an integrator and a time delay. When assuming that this theorem is valid for *all* loop closures, the estimated frequency responses will approximate an integrator-like function in the crossover region. This hypothesis is supported by the majority of the experimental data of this thesis. The method then simply fits an integrator – k/s – transfer function to the estimated frequency response in the least-squares sense, with the errors in matching the function weighted with the variances of the estimated frequency response. This weighted least-squares fitting procedure corresponds well with the empirical observation that the variance in the estimated

frequency response functions is minimal in the crossover region. The method uses the estimated frequency response at five pairs (or, in the case of three forcing functions, at five triples) of frequencies and required an initial estimate of the crossover frequency. After the fit was completed, the crossover frequency is defined as the frequency at which the *fitted* integrator function equals 1. The phase margin could be estimated similarly.

F.4.4 Parameterization of 3 loop closures with 2 input signals

In controlling the aircraft symmetric or asymmetric motion the pilot closes three feedback loops: attitude, flight-path and position. To identify the three frequency responses, the (3×1) parallel model of §F.2.3 is the most relevant model structure. In §4.2 it has been stated, however, that the addition of a forcing function to the aircraft flight-path could be conflicting with other experimental demands, a problem that can be circumvented by identifying the middle and outer loops simultaneously, i.e. as one *combined* outer loop.

Stage I: the non-parametric identification of the combined outer loop   There are two ways to obtain an estimate of the combined outer loop frequency response: (i) with the middle loop signal y, Fig. 4.2(a), or (ii) with the outer loop signal z, Fig. 4.2(b). In both cases the identification method of the (2×1) parallel pilot model can be applied.
Case I: using the middle loop signal   The identification method leads to an estimate $\hat{H}_{p_y}^{p^c}$ of the combined outer loop dynamics $H_{p_y}^{p^c}$, depicted by:

$$H_{p_y}^{p^c}(s) \;=\; H_{p_y}^{p}(s) + H_{p_z}^{p}(s)H_{c_3}(s). \tag{F.50}$$

Case II: using the outer loop signal   The identification method leads to an estimate $\hat{H}_{p_z}^{p^c}$ of the combined outer loop dynamics $H_{p_z}^{p^c}$, depicted by:

$$H_{p_z}^{p^c}(s) \;=\; H_{p_z}^{p}(s) + \frac{H_{p_y}^{p}(s)}{H_{c_3}(s)}. \tag{F.51}$$

In both cases the bias and variance of the estimates can be computed with the formulas of Table F.1. An important difference with the use of the middle loop signal is that when using the outer loop signal the dynamics of the outer loop system H_{c_2} are actually the dynamics of the *combined* middle and outer loop, i.e. $H_{c_{2,3}} = H_{c_2}H_{c_3}$. This has a consequence only for the variance computation of the combined outer loop frequency response $H_{p_z}^{p^c}$. The dynamics of the outer loop affect the contribution to the variance of the second term on the right-hand side of Eq. F.18. Recall that H_{c_3} reflects – in the aircraft control situation – the path integration dynamics. Therefore, in comparison with *Case I* the variance of the estimation of the (combined) outer loop frequency response can be expected to increase for higher frequencies and to reduce for lower frequencies.

Stage II: the parameterization of the combined frequency response   Here, it is important to distinguish between the two modelling approaches applied in this thesis.
Parameterization of the outer loops with the OCM pilot model   The outer loop aircraft dynamics are due to the path integration. The derivative of the position error is the flight-path angle error multiplied with the velocity of the aircraft, Eq. 3.28. Recall that one of

the main OCM assumptions is that when a variable is displayed and perceived, also the first derivative of that variable is perceived. When computing the transfer function of a certain loop closure the derivative feedback must be *included*, yielding the so-called *equivalent* transfer function, see §E.3.3. Thus, the notion of a combined outer loop frequency response is very similar to the definition of the *equivalent* transfer function of the OCM (§E.3.3). This property has been used in a similar manner in (Wewerinke, 1978).

Parameterization of the outer loops with the MLM pilot model   One of the main hypotheses in the definition of the MLM structure and parameters was that pilot equalization is conducted in the inner loop, and that all other loops are closed with proportional gains (§E.2.3). This means that the aircraft middle and outer loop feedbacks are closed with gains $K_{p_{mid}}$ and $K_{p_{out}}$, respectively. These gains can be determined via the estimated combined outer loop frequency responses in two steps. For *Case I* (using the middle loop signal), it can be shown that the serial counterpart of $H_{p_y}^{p^c}$ can be described as:

$$H_{p_y}^{s^c}(s) = \frac{V_{tas}}{s} K_{p_{mid}} K_{p_{out}} \left(1 + \frac{1}{V_{tas}K_{p_{out}}}s\right) = \frac{K_{p_{out}}^c}{s}\left(1 + \tau_{L_{out}}^c s\right). \qquad (F.52)$$

The parameters $K_{p_{out}}^c$ and $\tau_{L_{out}}^c$ are determined with the model parameter estimation algorithms of §F.3, marking the first step. In the second step the middle and outer loop gains are obtained from the combined outer loop lead and gain parameters as follows:

$$K_{p_{mid}} = K_{p_{out}}^c \tau_{L_{out}}^c; \quad \text{and} \quad K_{p_{out}} = \frac{1}{V_{tas}\tau_{L_{out}}^c}. \qquad (F.53)$$

The situation for *Case II* is, mutatis mutandis, solved in the same manner. In conclusion, the middle and outer loop pilot feedbacks can not be disentangled from the estimated combined outer loop frequency response, but must be determined by parameterization. This procedure is granted by the characteristics of the outer loop aircraft dynamics on the one hand and the properties of the two modelling approaches on the other.

F.4.5   Time domain results of frequency domain models

All pilot models were validated through comparing their outputs with the experimental data in both the frequency and time domains. Whereas the time domain OCM pilot model provides results in both the domains, the frequency domain MLM pilot model is commonly applied only in the frequency domain itself. Below, two (equivalent) methods are discussed that can be used to compute the time domain MLM outputs.

Method I: simulation of the pilot-aircraft system   When the parameters of the MLM are defined, all elements of the pilot/aircraft closed loop in Fig. F.1 are known, except for the pilot remnant signal n. The main assumption is that this signal can be neglected, an assumption that leads to an *underestimation* of the variances of the variables of interest with respect to the experimentally measured quantities.[3]   When remnant is neglected,

---

[3]Recall that the identification of the pilot models is conducted using the *averaged* time histories, §4.4, in which the effects of the remnant are reduced considerably. The assumption that the remnant is zero leads to an approximation of the variances of these averaged time histories.

the pilot/aircraft closed loop is completely *deterministic* and all its elements are known exactly. The frequency domain description of the pilot/aircraft system can be transformed into a state-space equivalent, with the forcing functions as deterministic input signals. The response of the system to these signals can then be computed, giving the time histories of Fig. 5.11 and allowing a computation of the STDs of all signals in the loop.

Method II: computation of the variances with the signal spectra Consider the situation for two forcing functions, Fig. F.1. In §F.2.1 it has been discussed how all signals in the loop (u, x, y) can be expressed in terms of the *external* signals that are inserted in the loop (n, i_1 and i_2). Similar to Method I, neglecting the unknown pilot remnant signal n yields a set of deterministic equations that express the Fourier coefficients of all variables in the loop in terms of the dynamics of all elements in the loop and the Fourier coefficients of the deterministic forcing functions. E.g. for the inner loop system output the following expression holds, for the (2×1) parallel model of §F.2.1:

$$X(\nu_k) = \left(\frac{H_{c_1}(\nu_k)}{\Delta(\nu_k)}\right) I_1(\nu_k) + \left(-\frac{H_{c_1}(\nu_k)H_{c_2}(\nu_k)H_{p_y}^p(\nu_k)}{\Delta(\nu_k)}\right) I_2(\nu_k), \quad \text{(F.54)}$$

with the denominator defined as: $\Delta(\nu_k) = 1 + H_{p_x}^p(\nu_k)H_{c_1}(\nu_k) + H_{p_y}^p(\nu_k)H_{c_2}(\nu_k)H_{c_1}(\nu_k)$. Substituting the modelled pilot frequency response functions for the *real* pilot frequency responses allows the power spectra of these signals to be computed analytically. These power spectra are zero except for the frequencies of the two sets of frequencies $\underline{\nu}_{i_1}$ and $\underline{\nu}_{i_2}$ of the two forcing functions. Because these signals are independent, their variances can be computed by simply adding the contributions of the spectra of all signals in the loop at these frequencies. For instance, continuing with Eq. F.54 leads to:

$$\hat{\sigma}_x^2 = \sum_{k=1}^{k=N_f} \left\{ \left|\frac{H_{c_1}(\nu_{1_k})}{\Delta(\nu_{1_k})}\right|^2 I_1^2(\nu_{1_k}) + \left|\frac{H_{c_1}(\nu_{2_k})H_{c_2}(\nu_{2_k})\hat{H}_{p_y}^p(\nu_{2_k})}{\Delta(\nu_{2_k})}\right|^2 I_2^2(\nu_{2_k}) \right\}. \quad \text{(F.55)}$$

The variances obtained with Method II are identical to those obtained with Method I. The second method, however, is faster and can be applied in a relatively simple manner. Because both methods neglect the pilot remnant, the MLM variances are smaller than those measured experimentally. The OCM pilot model, incorporating the contribution of the remnant through the pilot motor and observation noises (§E.3), however, does allow a comparison between the modelled and measured time domain data.

In the application of the time domain criterion J_T for the model parameterization efforts, the model variances are compared with the measured variances. It is clear that the MLM variances are always smaller than those of the experimental data. Therefore, in the application of this criterion for the MLM models the estimated mean and STD of the array of measured STDs ($\hat{\mu}_{\sigma_j}$ and $\hat{\sigma}_{\sigma_j}$) are *both* replaced by the mean of the averaged time histories, σ_j^a. Hence, the criterion J_T for the MLM models weights the *relative* amplitudes of the mismatch between the modelled and the *averaged* time domain variances.

References

Abbink, F. (1996). *Integrated Free Flight and 4-D Gate-to-gate Air Traffic Management, Possibilities, Promises and Problems* (NLR Technical Paper No. TP 96239 U). Amsterdam: National Aerospace Laboratory.

Adams, J. J., & Lallman, F. J. (1978). *Description and Preliminary Studies of a Computer Drawn Instrument Landing Approach Display* (NASA Technical Memorandum No. TM-78771). Washington (D.C.).

AGARD. (1996). *Flight Vehicle Integration Panel Working Group 21 on Glass Cockpit Operational Effectiveness* (AGARD-AR No. 349). Neuilly-sur-Seine, France: Advisory Group for Aerospace Research and Development.

Alfano, P. L., & Michel, G. F. (1990). Restricting the Field of View: Perceptual and Performance Effects. *Perceptual and Motor Skills*, *70*, 35–45.

Andersen, G. J., & Braunstein, M. L. (1985). Induced Self-Motion in Central Vision. *Journal of Experimental Psychology: Human Perception and Performance*, *11*(2), 122–132.

Andre, A. D., Wickens, C. D., Moorman, L., & Boschelli, M. M. (1991). Display Formatting Techniques for Improving Situation Awareness in the Aircraft Cockpit. *The International Journal of Aviation Psychology*, *1*(3), 205–218.

Aström, K. J., & Wittenmark, B. (1984). *Computer Controlled Systems: Theory and Design.* Englewood Cliffs (NJ): Prentice-Hall.

Awe, C. A., Johnson, W. W., & Schmitz, F. (1989). Inflexibility in Selecting the Optical Basis for Perceiving Speed. *Proceedings of the Human Factors Society – 33rd Annual Meeting – 1989*, 1440–1444.

Bajcsy, R., & Lieberman, L. (1976). Texture Gradient as a Depth Cue. *Computer Graphics and Image Processing*, *5*, 52–67.

Ballard, D., & Kimball, O. A. (1983). Rigid Body Motion from Depth and Optical Flow. *Computer Vision, Graphics, and Image Processing*, *22*, 95–115.

Barfield, W., & Rosenberg, C. (1992). The Effect of Geometric Field of View and Tunnel Design for Perspective Flight-Path Displays. *Society of Automotive Engineers*, *SAE Technical Paper 921131*, 1–6.

Baron, S. (1976). A Model for Human Control and Monitoring based on Modern Control Theory. *Journal of Cybernetics and Information Science*, *4*(1), 3–18.

Baron, S., & Levison, W. H. (1975). An Optimal Control Methodology for Analyzing the Effects of Display Parameters on Performance and Workload in Manual Flight Control. *IEEE Transactions on Systems, Man, and Cybernetics*, SMC-5(4), 423–430.

Batson, V. M., Harris, R. L., & Houck, J. A. (1992). Effect of Display Parameters on Pilot's Ability to Approach, Flare and Land. *AIAA-92-4139-CP*.

Baxter, J., & Harrison, J. Y. (1979). A Nonlinear Model Describing Driver Behavior on Straight Roads. *Human Factors*, *21*(1), 87–97.

Beall, A. C., & Loomis, J. M. (1996). Visual Control of Steering Without Course Information. *Perception*, *25*, 481–494.

Below, C., von Viebahn, H., & Hammer, M. (1995). 4D Flight Guidance Displays. *Proceedings of the SPIE Technical Conference "Synthetic Vision for Vehicle Guidance and Control". Aerosense, Orlando*, *2463*, 137–145.

Bennett, C. T., Johnson, W. W., Perrone, J. A., & Phatak, A. V. (1986). Synthetic Perspective Optical Flow: Influence on Pilot Control Tasks. *Proceedings of the Human Factors Society – 30th Annual Meeting – 1986*, 1–9.

Bennett, K. B., & Flach, J. M. (1992). Graphical Displays: Implications for Divided Attention, Focused Attention, and Problem Solving. *Human Factors*, *34*(5), 513–533.

Biggs, N. L. (1966). Directional Guidance of Motor Vehicles – A Preliminary Survey and Analysis. *Ergonomics*, *9*(3), 193–202.

Billings, C. E. (1991). *Human-Centered Aircraft Automation: A Concept and Guidelines* (NASA Technical Memorandum No. TM-103885). Moffett Field (CA): NASA Ames Research Center.

Billings, C. E. (1997). *Aviation Automation – The Search for a Human-Centered Approach.* Mahwah (NJ): Lawrence Erlbaum Associates, Inc.

Birmingham, H. P., & Taylor, F. V. (1954). A Design Philosophy for Man-Machine Control Systems. *Proceedings of the I.R.E.*, *42*, 1748–1758.

Blaauw, G. (1984). *Car Driving as a Supervisory Control Task.* Ph.D. dissertation, Institute for Perception TNO, Soesterberg.

Boer, E. R. (1996). Tangent Point Oriented Curve Negotiation. *IEEE Proceedings of the Intelligent Vehicles '96 Symposium, Tokio, September 19-20*.

Boff, K. R., Kaufman, L., & Thomas, J. P. (1986). *Handbook of Perception and Human Performance.* New York: John Wiley & Sons.

Brandt, T., Dichgans, J., & Koenig, E. (1973). Differential Effects of Central Versus Peripheral Vision on Egocentric and Exocentric Motion Perception. *Experimental Brain Research*, *16*, 476–491.

Breedveld, P. (1997). *The Design of a Man-Machine Interface for a Space Manipulator.* Ph.D. dissertation, Faculty of Mechanical Engineering, Delft University of Technology.

Brockhaus, R. (1994). *Flugregelung – Physikalische Grundlagen, Mathematisches Flugzeugmodell, Auslegungskriterien - Regelungssystemen, Entwurf von Flugregelungssystemen, Entwicklungslinien.* Berlin: Springer Verlag. (in German)

Brown, J. (1994). Moving Target Guides Drivers Round the Bend. *New Scientist, July*, 17.

Brummelaar, T. ten. (1975). Where are the Kinks in the Alignment? *Transportation Research Record, 556*, 35–50.

Brummelaar, T. ten. (1983). The Reversal Point in the Perspective Road Picture. *Australian Road Research, 13*(2).

Bruss, A. R., & Horn, B. K. P. (1983). Passive Navigation. *Computer Vision, Graphics, and Image Processing, 21*, 3–20.

Chatterji, G. B., Menon, P. K. A., & Sridhar, B. (1994). Machine-Vision Based Pilot Guidance for Night Operations. *AIAA-94-3691-CP*, 1332–1339.

Clocksin, W. F. (1980). Perception of Surface Slant and Edge Labels from Optical Flow: A Computational Approach. *Perception, 9*, 253–269.

Crossman, E. R. F. W., & Szostak, H. (1968). Man-Machine Models for Car Steering. *Proceedings of the Fourth Annual Conference on Manual Control, NASA SP-192*, 171–195.

Crowell, J. A., & Banks, M. S. (1993). Perceiving Heading with Different Retinal Regions and Types of Optical Flow. *Perception & Psychophysics, 53*(3), 325–337.

Crowell, J. A., & Banks, M. S. (1996). Ideal Observer for Heading Judgments. *Vision Research, 36*(3), 471–490.

Cutting, J. E., & Millard, R. T. (1984). Three Gradients and the Perception of Flat and Curved Surfaces. *Journal of Experimental Psychology: General, 113*(2), 198–216.

De Vriendt, K., Mulder, M., & van Paassen, M. M. (1999). Free Flight's Big Picture Displays. *Proceedings of the XVIIIth European Annual Conference on Human Decision Making and Manual Control, Loughborough, U.K., October 25-27.*

Denton, G. G. (1980). The Influence of Visual Pattern on Perceived Speed. *Perception, 9*, 393–402.

Donges, E. (1977). *Experimentelle Untersuchung und regelungstechnische Modellierung des Lenkverhaltens von Kraftfahrern bei simulierter Straßenfahrt.* Ph.D. dissertation, Technischen Hochschule Darmstadt. (in German)

Donges, E. (1978). A Two-Level Model of Driver Steering Behavior. *Human Factors, 20*(6), 691–707.

Dorighi, N. S., Ellis, S. R., & Grunwald, A. J. (1991). Evaluation of Perspective Displays on Pilot Spatial Awareness in Low Visibility Curved Approaches. *AIAA-91-3727-CP*, 153–158.

Dorighi, N. S., Grunwald, A. J., & Ellis, S. R. (1992). Perspective Format for a Primary Flight Display and its Effect on Pilot Spatial Awareness. *Proceedings of the 11th Digital Avionics Systems Conference, Seattle (WA), October 5-8, 1992*, 1–6.

Eberts, R. E. (1987). Internal Models, Tracking Strategies, and Dual-Task Performance. *Human Factors, 29*(4).

Eisele, J. E., Williges, R. C., & Roscoe, S. N. (1976). *The Isolation of Minimum Sets of Visual Cues Sufficient for Spatial Orientation During Aircraft Landing Approaches* (Aviation Research Laboratory Report No. ARL-76-16). Savoy, Illinois 61874: University of Illinois at Urbana-Champaign.

Endsley, M. (1995). Toward a Theory of Situation Awareness. *Human Factors*, *37*(1), 32–64.

Erkelens, L. J. J., & Dronkelaar, J. H. (1990). *Flight Simulator Evaluation of the Flyability of Curved MLS Approaches with Wide-Body Aircraft* (NLR Contractor Report No. CR 90238 L). Amsterdam: National Aerospace Laboratory.

Etkin, B. (1972). *Dynamics of Atmospheric Flight.* New York: John Wiley & Sons.

Fildes, B. N., & Triggs, T. J. (1986). An Illusion of Curvature in the Perception of Road Curves. In A. G. Gale, M. H. Freeman, C. M. Haslegrave, P. Smith, & S. P. Taylor (Eds.), *Vision in Vehicles* (pp. 409–412). Elsevier Science Publishers (North-Holland).

Flach, J. M. (1991). Control with an Eye for Perception: Precursors to an Active Psychophysics [Proceedings of a workshop held at NASA Ames Research Center, Moffett Field (CA), June 26 to July 14, 1989]. In W. W. Johnson & M. K. Kaiser (Eds.), *Visually Guided Control of Movement* (pp. 121–149). NASA Ames Research Center.

Flach, J. M., Hagen, B. A., & Larish, J. F. (1992). Active Regulation of Altitude as a Function of Optical Texture. *Perception & Psychophysics*, *51*(6), 557–568.

Flohr, E., & Huisman, H. (1997). Perspective Primary Flight Displays in the 4D ATM Environment. *Proceedings of the Nineth International Symposium on Aviation Psychology, Columbus (OH), April 28-30, 1997.*

Fogel, L. J. (1959). A New Concept: The Kinalog Display System. *Human Factors*, *1*, 30–37.

Foley, J. D., van Dam, A., Feiner, S. K., & Hughes, J. F. (1992). *Computer Graphics. Principle and Practice.* Reading (MA): Addison-Wesley Publishing Company.

Foyle, D. C., Ahumada, A. J., Larimer, J., & Sweet, B. T. (1992). Enhanced/Synthetic Vision Systems: Human Factors Research and Implications for Future Systems. *Society of Automotive Engineers*, *SAE Technical Paper 921968*, 59–66.

Fry, G. A. (1968). The Use of the Eyes in Steering a Car on Straight and Curved Roads. *American Journal of Optometry and Archives of American Academy of Optometry, June*, 374–391.

Funabiki, K. (1997). Tunnel-in-the-Sky Display Enhancing Autopilot Mode Awareness. *Conference proceedings of the 1997 CEAS Free Flight Symposium*, 29.1–29.11.

Galotti Jr., V. P. (1998). *The Future Air Navigation System (FANS)* (2nd. ed.). Aldershot (U.K.): Ashgate Publishing Company.

Gibson, J. J. (1950). *The Perception of the Visual World.* Boston (MA): Houghton Mifflin.

Gibson, J. J. (1954). The Visual Perception of Objective Motion and Subjective Movement. *Psychological Review*, *61*(5), 304–314.

Gibson, J. J. (1955). The Optical Expension Pattern in Aerial Locomotion. *The American Journal of Psychology*, *68*(3), 480–484.

Gibson, J. J. (1961). Ecological optics. *Vision Research*, *1*, 253–262.

Gibson, J. J. (1968). What Gives Rise to the Perception of Motion? *Psychological Review*, *75*(4), 335–346.

Gibson, J. J. (1986). *The Ecological Approach to Visual Perception.* Hillsdale (NJ): Lawrence Erlbaum Associates. (originally published in 1979)

Gibson, J. J., & Crooks, L. E. (1938). A Theoretical Field Analysis of Automobile Driving. *The American Journal of Psychology*, *51*(3), 453–471.

Gibson, J. J., Olum, P., & Rosenblatt, F. (1955). Parallax and Perspective During Aircraft Landings. *The American Journal of Psychology*, *68*(3), 372–385.

Godthelp, H. (1984). *Studies on Human Vehicle Control.* Ph.D. dissertation, Institute for Perception TNO, Soesterberg.

Godthelp, H. (1986). Vehicle Control During Curve Driving. *Human Factors*, *28*(2), 211–221.

Gold, T. (1965). Quickened Manual Flight Control with External Visual Guidance. *IEEE Transactions on Aerospace and Navigational Electronics*, *ANI-11*(9), 151–156.

Gordon, D. A. (1965). Static and Dynamic Visual Fields in Human Space Perception. *Journal of the Optical Society of America*, *35*(10), 1296–1303.

Gordon, D. A. (1966a). Experimental Isolation of Drivers' Visual Input. *Public Roads*, *33*(12), 266–273.

Gordon, D. A. (1966b). Perceptual Basis of Vehicular Guidance. *Public Roads*, *34*(3), 53–68.

Grunwald, A. J. (1984). Tunnel Display for Four-Dimensional Fixed-Wing Aircraft Approaches. *Journal of Guidance and Control*, *7*(3), 369–377.

Grunwald, A. J. (1985). Predictor Laws for Pictorial Flight Displays. *Journal of Guidance and Control*, *8*(5), 545–552.

Grunwald, A. J. (1996a). Improved Tunnel Display for Curved Trajectory Following: Control Considerations. *Journal of Guidance, Control, and Dynamics*, *19*(2), 370–377.

Grunwald, A. J. (1996b). Improved Tunnel Display for Curved Trajectory Following: Experimental Evaluation. *Journal of Guidance, Control, and Dynamics*, *19*(2), 378–384.

Grunwald, A. J., & Kohn, S. (1993). Flight-Path Estimation in Passive Low-Altitude Flight by Visual Cues. *Journal of Guidance, Control, and Dynamics*, *16*(2), 363–370.

Grunwald, A. J., & Merhav, S. J. (1976). Vehicular Control by Visual Field Cues – Analytical Model and Experimental Validation. *IEEE Transactions on Systems, Man, and Cybernetics*, *SMC-6*(12), 835–845.

Grunwald, A. J., & Merhav, S. J. (1978). Effectiveness of Basic Display Augmentation in Vehicular Control by Visual Field Cues. *IEEE Transactions on Systems, Man, and Cybernetics*, *SMC-8*(9), 679–690.

Grunwald, A. J., Robertson, J. B., & Hatfield, J. J. (1980). *Evaluation of a Computer-Generated Perspective Tunnel Display for Flight-Path Following* (NASA Technical Paper No. TP-1736). Washington (D.C.).

Grunwald, A. J., Robertson, J. B., & Hatfield, J. J. (1981). Experimental Evaluation of a Perspective Tunnel Display for Three-Dimensional Helicopter Approaches. *Journal of Guidance and Control*, *4*(6), 623–631.

Guo, K., & Fancher, P. S. (1983). Preview-Follower Method for Modeling Closed-Loop Vehicle Directional Control. *Proceedings of the Nineteenth Annual Conference on Manual Control*, 158–187.

Haskell, I. D., & Wickens, C. D. (1993). Two- and Three-Dimensional Displays for Aviation: A Theoretical and Empirical Comparison. *The International Journal of Aviation Psychology*, *3*(2), 87–109.

Heller, J. (1961). *Catch-22.* London: Vintage.

Hess, R. A. (1981). Aircraft Control-Display Analysis and Design Using the Optimal Control Model of the Human Pilot. *IEEE Transactions on Systems, Man, and Cybernetics*, *SMC-11*(7), 465–480.

Hess, R. A., & Modjtahedzadeh, A. (1989). A Preview Control Model of Driver Steering Behavior. *Proceedings of the IEEE Conference on Systems, Man, and Cybernetics*, 504–509.

Hettinger, L. J., Nelson, W. T., Brickman, B. J., Haas, M. W., & Roumes, C. (1995). Assessing Human Performance as a Design Aid for Airborne Applications of Virtual Environment Technology. *Proceedings of the Eighth International Symposium on Aviation Psychology, Columbus (OH), April 24-27, 1995*, 170–175.

Hicks, C. R. (1982). *Fundamental Concepts in the Design of Experiments* (3rd. ed.). New York: Holt, Rinehart and Winston.

Hills, B. L. (1980). Vision, Visibility and Perception in Driving. *Perception*, *9*, 183–216.

Horn, B. K. P., & Schunk, B. G. (1981). Determining Optical Flow. *Artificial Intelligence*, *17*, 185–203.

Hosman, R. J. A. W. (1996). *Pilot's Perception and Control of Aircraft Motions.* Ph.D. dissertation, Faculty of Aerospace Engineering, Delft University of Technology.

Hosman, R. J. A. W., & Mulder, M. (1997). Perception of Flight Information from EFIS Displays. *Control Engineering Practice*, *5*(3), 383–390.

Hynes, C. S., Franklin, J. A., Hardy, G. H., Martin, J. L., & Innis, R. C. (1989). Flight Evaluation of Pursuit Displays for Precision Approach of Powered-Lift Aircraft. *Journal of Guidance*, *12*(4), 521–529.

ICAO. (1992). *Operational Implications of Automation in Advanced Technology Flight Desks* (ICAO Circular No. 234-AN/142). Montreal, Canada: International Civil Aviation Organization.

Ineson, K. (1994). The DRA Virtual Cockpit Research Programme. *AGARD Conference Proceedings "Virtual Interfaces: Research and Applications"*, *CP-541*, 8.1–8.12.

Innocenti, M. (1988). The Optimal Control Model and Applications. *AGARD Lecture Series*, *157*, 7.1–7.17.

Jensen, R. S. (1978). The Effects of Prediction, Quickening, Frequency-Separation, and Percent of Pursuit in Perspective Displays for Low-Visibility Landing. *Proceedings of the Human Factors Society – 22nd Annual Meeting – 1978*, 208–212.

Jensen, R. S. (1981). Prediction and Quickening in Perspective Flight Displays for Curved Landing Approaches. *Human Factors*, *23*(3), 355–363.

Jex, H. R., Allen, R. W., & Magdaleno, R. E. (1971). Effects of Display Format on Pilot Describing Function and Remnant. *Proceedings of the Seventh Annual Conference on Manual Control, NASA SP-281*, 155–159.

Johnson, C., & Leibowitz, H. W. (1976). Velocity-Time Reciprocity in the Perception of Motion: Foveal and Peripheral Determinations. *Vision Research*, *16*, 177–180.

Johnson, W. W., Bennett, C. T., O'Donnel, K., & Phatak, A. V. (1988). Optical Variables Useful in the Active Control of Altitude. *Paper presented at the 23rd Annual Conference on Manual Control. Cambridge (MA).*

Johnson, W. W., & Kaiser, M. K. (Eds.). (1991). *Visually Guided Control of Movement* (NASA Conference Publication No. CP-3118). Moffett Field (CA): NASA Ames Research Center. (Proceedings of a workshop held at NASA Ames Research Center, Moffett Field (CA), June 26 to July 14, 1989)

Johnson, W. W., & Phatak, A. V. (1990a). Modeling the Pilot in Visually Controlled Flight. *IEEE Control Systems Magazine*, *10*, 24–26.

Johnson, W. W., & Phatak, A. V. (1990b). Optical Variables and Control Strategy Used in a Visual Hover Task. *Proceedings of the 1990 Conference on Systems, Man, and Cybernetics.*

Johnson, W. W., Tsang, P. S., Bennett, C. T., & Phatak, A. V. (1989). The Visually Guided Control of Simulated Altitude. *Aviation, Space and Environmental Medicine*, *60*, 152–156.

Johnston, I. R., White, G. R., & Cumming, R. W. (1973). The Role of Optical Expansion Patterns in Locomotor Control. *The American Journal of Psychology*, *86*(2), 311–324.

Jones, L. F., Schrader, H. J., & Marshall, J. N. (1950). Pictorial Display in Aircraft Navigation and Landing. *Proceedings of the I.R.E.*, 391–400.

Jurgensohn, T., Neculau, M., & Willumeit, H. P. (1991). Visual Scanning Pattern in Curve Negotiation. In A. G. Gale, M. H. Freeman, C. M. Haslegrave, P. Smith, & S. P. Taylor (Eds.), *Vision in Vehicles II* (pp. 171–178). Elsevier Science Publishers (North-Holland).

Kaiser, M. K., & Mowafy, L. (1993). Optical Specification of Time-to-Passage: Observer's Sensitivity to Global Tau. *Journal of Experimental Psychology: Human Perception and Performance*, *19*(5), 1028–1040.

Kappé, B. (1997). *Visual Information in Virtual Environments.* Ph.D. dissertation, University of Utrecht & Institute for Perception TNO.

Kayton, M., & Fried, W. R. (1997). *Avionics Navigation Systems* (2nd. ed.). New York: John Wiley & Sons.

Kelley, C. R. (1967). *Manual and Automatic Control. A theory of manual control and its application to manual and to automatic systems.* New York: John Wiley & Sons.

Kelly, R. J., & Davis, J. M. (1994). Required Navigation Performance (RNP) for Precision Approach and Landing with GNSS Application. *Navigation: Journal of the Institute of Navigation*, *41*(1), 1–30.

Klein, V. (1989). Estimation of Aircraft Aerodynamic Parameters from Flight Data. *Journal of Progress in Aerospace Sciences*, *26*, 1–77.

Kleinman, D. L. (1976). Solving the Optimal Attention Allocation Problem in Manual Control. *IEEE Transactions on Automatic Control*, *AC-21*(6), 813–821.

Kleinman, D. L., & Baron, S. (1971). *Manned-Vehicle Systems Analysis by Means of Modern Control Theory* (NASA Contractor Report No. CR-1753). Washington (D.C.).

Kleinman, D. L., Baron, S., & Levison, W. H. (1970a). An Optimal Control Model of Human Response. Part II: Prediction of Human Performance in a Complex Task. *Automatica*, *6*, 371–383.

Kleinman, D. L., Baron, S., & Levison, W. H. (1970b). An Optimal Control Model of Human Response. Part I: Theory and Validation. *Automatica*, *6*, 357–369.

Kleinman, D. L., Baron, S., & Levison, W. H. (1971). A Control Theoretic Approach to Manned-Vehicle Systems Analysis. *IEEE Transactions on Automatic Control*, *AC-16*(6), 824–832.

Knox, C. E. (1992). *Manual Flying of Curved Precision Approaches to Landing With Electromechanical Instrumentation* (NASA Technical Paper No. TP-3255). Washington (D.C.).

Knox, C. E., & Leavitt, J. (1977). *Description of a Path-in-the-Sky Contact Analog Piloting Display* (NASA Technical Memorandum No. TM-74057). Washington (D.C.).

Koenderink, J. J. (1986). Optic Flow. *Vision Research*, *26*(1), 161–180.

Koenderink, J. J., & van Doorn, A. J. (1981). Exterospecific Component of the Motion Parallax Field. *Journal of the Optical Society of America*, *71*(8), 953–957.

Kok, J. J., & Stassen, H. (1980). Human Operator Control of Slowly Responding Systems: Supervisory Control. *Journal of Cybernetics and Information Sciences. Special Issue on Man-Machine Systems*, *3*(1-4), 123–174.

Kok, J. J., & van Wijk, R. A. (1978). *Evaluation of Models Describing Human Operator Control of Slowly Responding Complex Systems.* Ph.D. dissertation, Faculty of Mechanical Engineering, Delft University of Technology.

Kondo, M., & Ajimine, A. (1968). Driver's Sight Point and Dynamics of the Driver-Vehicle-System Related to It. *Society of Automotive Engineers*, *SAE Technical Paper 680104*.

Korn, J., Gully, S. W., & Kleinman, D. L. (1982). Validation of an Advanced Cockpit Design Methodology via a Workload/Monitoring Tradeoff Analysis. *Proceedings of the Eighteenth Annual Conference on Manual Control*, 268–292.

Kramer, U., & Neculau, M. (1986). Driver's Display, Eye-movements, and Steering Behaviour: The Visual Basis of Car Driving. In A. G. Gale, M. H. Freeman, C. M. Haslegrave, P. Smith, & S. P. Taylor (Eds.), *Vision in Vehicles* (pp. 185–194). Elsevier Science Publishers (North-Holland).

Krendel, E. S., & McRuer, D. T. (1960). A Servomechanics Approach to Skill Development. *Journal of the Franklin Institute*, *269*(1), 24–42.

Kwakernaak, H., & Sivan, R. (1972). *Linear Optimal Control Systems.* New York: John Wiley & Sons.

Land, M. F. (1993). Eye-Head Coordination During Driving. *Proceedings of the IEEE Conference on Systems, Man, and Cybernetics*, *3*, 490–494.

Land, M. F., & Horwood, J. (1995). Which Parts of the Road Guide Steering? *Nature*, *377*, 339–340.

Land, M. F., & Lee, D. N. (1994). Where we look when we steer. *Nature*, *369*, 742–744.

Landwehr, K. (1991). Optical Guidance Revisited. In A. G. Gale, M. H. Freeman, C. M. Haslegrave, P. Smith, & S. P. Taylor (Eds.), *Vision in Vehicles II* (pp. 187–194). Elsevier Science Publishers (North-Holland).

Larish, J. F., & Flach, J. M. (1990). Sources of Optical Information Useful for Perception of Speed of Rectilinear Self-Motion. *Journal of Experimental Psychology: Human Perception and Performance*, *16*(2), 295–302.

Lee, D. N. (1974). Visual Information During Locomotion. In R. B. McLeod & H. Picks (Eds.), *Perception: Essays in Honor of J. J. Gibson.* Ithaca (NY): Cornell University Press.

Lee, D. N. (1980a). Visuo-Motor Coordination in Space-Time. In G. E. Stelmach & J. Requin (Eds.), *Tutorials in Motor Behaviour.* Amsterdam: North-Holland Publishing Company.

Lee, D. N. (1980b). The Optical Flow Field: the Foundation of Vision. *Philosophical Transactions of the Royal Society of London, Series B*, *290*, 169–179.

Lee, D. N., & Lishman, R. (1977). Visual Control of Locomotion. *Scandinavian Journal of Psychology*, *18*, 224–230.

Lee, D. N., & Reddish, P. E. (1981). Plummeting Gannets: A Paradigm of Ecological Optics. *Nature*, *293*, 293–294.

Lee, D. N., Young, D. S., Reddish, D. E., Lough, S., & Clayton, T. M. H. (1983). Visual Timing in Hitting an Accelerating Ball. *Quarterly Journal of Experimental Psychology*, *35A*, 333–346.

Lee, D. N., Young, D. S., & Rewt, D. (1992). How Do Somersaulters Land on Their Feet? *Journal of Experimental Psychology: Human Perception and Performance*, *18*(4), 1195–1202.

Levison, W. H., Baron, S., & Kleinman, D. L. (1969). A Model for Human Controller Remnant. *IEEE Transactions on Man-Machine-Systems*, *MMS-10*(4), 101–108.

Lintern, G., & Liu, Y. T. (1991). Explicit and Implicit Horizons for Simulated Landing Approaches. *Human Factors*, *33*(4), 401–417.

Lishman, J. R. (1981). Vision and the Optic Flow Field. *Nature*, *293*, 263–264.

Longuet-Higgins, H. C. (1984). The Visual Ambiguity of a Moving Plane. *Proceedings of the Royal Society of London, Series B*, *223*, 165–175.

Longuet-Higgins, H. C., & Prazdny, K. (1980). The Interpretation of a Moving Retinal Image. *Proceedings of the Royal Society of London, Series B*, *208*, 385–397.

Lovesey, E. J. (1977). The Instrument Explosion – A Study of Aircraft Cockpit Instruments. *Applied Ergonomics*, *8*(1), 23–30.

MacAdam, C. C. (1981). Application of an Optimal Preview Control for Simulation of Closed-Loop Automobile Driving. *IEEE Transactions on Systems, Man, and Cybernetics*, *SMC-11*(6), 393–399.

McDonnel, J. D. (1968). *Pilot Rating Techniques for the Estimation and Evaluation of Handling Qualities* (Technical Report No. AFFDL-TR-68-76). Wright-Patterson AFB (OH): Air Force Flight Dynamics Laboratory.

McGreevy, M. W., & Ellis, S. R. (1984). Direction Judgement Errors in Perspective Displays. *Proceedings of the Twentieth Annual Conference on Manual Control. NASA Conference Publication*, *2341*, 531–549.

McLane, R. C., & Wolf, J. D. (1968). Symbolic and Pictorial Displays for Submarine Control. *Proceedings of the Fourth Annual Conference on Manual Control, NASA SP-192*, 213–228.

McLean, J. R., & Hoffmann, E. R. (1973). The Effects of Restricted Preview on Driver Steering Control and Performance. *Human Factors*, *15*(4), 421–430.

McRuer, D. T., Allen, R. W., Weir, D. H., & Klein, R. H. (1977). New Results in Driver Steering Control Models. *Human Factors*, *19*(4), 381–397.

McRuer, D. T., Graham, D., Krendel, E. S., & Reisener Jr., W. (1965). *Human Pilot Dynamics in Compensatory Systems. Theory, models, and experiments with controlled element and forcing function variations* (Technical Report No. AFFDL-TR-65-15). Wright-Patterson AFB (OH): Air Force Flight Dynamics Laboratory.

McRuer, D. T., & Jex, H. R. (1967). A Review of Quasi-Linear Pilot Models. *IEEE Transactions on Human Factors in Electronics*, *HFE-8*(3), 231–249.

McRuer, D. T., & Krendel, E. S. (1974). *Mathematical Models of Human Pilot Behaviour* (Agardograph No. 88). AGARD.

Merhav, S. J., & Grunwald, A. J. (1978). Display Augmentation in Manual Control of Remotely Piloted Vehicles. *Journal of Aircraft*, *15*(3), 182–189.

Mulder, J. A., & van der Vaart, J. C. (1994). *Aircraft Responses to Atmospheric Turbulence.* Lecture notes D-47, Faculty of Aerospace Engineering, Delft University of Technology.

Mulder, M. (1992). *Aviation Displays and Flight Path Predictors.* Unpublished MSc. Thesis, Faculty of Aerospace Engineering, Delft University of Technology.

Mulder, M. (1994). *Displays, Perception and Aircraft Control. A survey of theory and modelling of pilot behaviour with spatial instruments* (Report No. LR-762). Delft: Faculty of Aerospace Engineering, Delft University of Technology.

Mulder, M. (1995). Towards a Control-Theoretic Model of Pilot Manual Control Behaviour with a Perspective Flight-Path Display. *Proceedings of the XIVth European Annual Conference on Human Decision Making and Manual Control, Delft, The Netherlands, June 14-16*, 1.2.1–1.2.13.

Mulder, M. (1996). Modelling Manual Control of Straight Trajectories with a Tunnel-in-the-Sky Display. *Proceedings of the XVth European Annual Conference on Human Decision Making and Manual Control, Soesterberg, The Netherlands, June 10-12*, 1.2.1–1.2.12.

Mulder, M. (1998). Tracking Curved Trajectories with a Tunnel-in-the-Sky Display. *Proceedings of the XVIIth European Annual Conference on Human Decision Making and Manual Control, Valenciennes, France, December 14-16*, 197–206.

Mulder, M. (1999). Flight-Path Vector Symbology in a Tunnel-in-the-Sky Display. *Proceedings of the XVIIIth European Annual Conference on Human Decision Making and Manual Control, Loughborough, U.K., October 25-27*.

Mulder, M., & Mulder, J. A. (1998). Tunnel Size in a Tunnel-in-the-Sky Display: A Cybernetic Analysis. *Proceedings of the Seventh IFAC/IFIP/IFORS/IEA Symposium on Analysis, Design and Evaluation of Man-Machine Systems, Kyoto Japan, September 16-18*, 335–340.

Mulder, M., Mulder, J. A., & Stassen, H. G. (1999a). Cybernetics of Tunnel-in-the-Sky Displays – Part II : Curved Trajectories. *Proceedings of the 1999 IEEE International Conference on Systems, Man, and Cybernetics, October 12-15, Tokyo, Japan.*

Mulder, M., Mulder, J. A., & Stassen, H. G. (1999b). Cybernetics of Tunnel-in-the-Sky Displays – Part I : Straight Trajectories. *Proceedings of the 1999 IEEE International Conference on Systems, Man, and Cybernetics, October 12-15, Tokyo, Japan.*

Mulder, M., Pleijsant, J. M., van der Vaart, J. C., & van Wieringen, P. C. W. (1999). The Effects of Pictorial Detail on the Timing of the Landing Flare: Results of a Visual Simulation Experiment. *The International Journal of Aviation Psychology.* (to be published)

Mulder, M., Stassen, H. G., & Mulder, J. A. (2000). A Cybernetic Analysis of the Tunnel-in-the-Sky Display. In L. J. Hettinger & M. W. Haas (Eds.), *Psychological Issues in the Design of Virtual and Adaptive Interfaces.* Lawrence Erlbaum Associates. (to be published)

Mulder, M., Theunissen, E., & van der Vaart, J. C. (1995). Perspective Flight-Path Displays and Time-to-Wall Crossing. In B. G. Bardy, R. J. Bootsma, & Y. Guiard (Eds.), *Studies in Perception and Action III* (pp. 203–206). Lawrence Erlbaum Associates, Inc.

Mulder, M., & van der Vaart, J. (1998a). Curve Interception with a Tunnel-in-the-Sky Display: Pilot Timing Strategies. *Proceedings of the Seventh IFAC/IFIP/IFORS/IEA Symposium on Analysis, Design and Evaluation of Man-Machine Systems, Kyoto Japan, September 16-18*, 341–346.

Mulder, M., & van der Vaart, J. (1998b). Flying Curves in the Air: Pilot Timing Strategies Using a Tunnel-in-the-Sky Display. *Proceedings of the Fifth European Workshop on Ecological Psychology (EWEP5), July 7-10, Pont-à-Mousson, France*, 105–109.

Naish, J. M. (1971). Control Information in Visual Flight. *Proceedings of the Seventh Annual Conference on Manual Control, NASA SP-281*, 167–176.

Nakayama, K., & Loomis, J. M. (1974). Optical Velocity Patterns, Velocity-Sensitive Neurons, and Space Perception: a Hypothesis. *Perception, 3*, 63–80.

NASA/DoD/FAA. (1995). *National Plan for Civil Aviation Human Factors: An Initiative for Research and Application* (1st ed.; Memorandum). Washington (D.C.): Federal Aviation Administration.

Oliver, J. G. (1990). Improving Situational Awareness Through the Use of Intuitive Pictorial Displays. *Society of Automotive Engineers, SAE Technical Paper 901829*, 1–6.

Osaka, N. (1991). Effects of Window Size and Eccentricity upon Eye Fixation and Reaction Time in Negotiation of Curves. In A. G. Gale, M. H. Freeman, C. M. Haslegrave, P. Smith, & S. P. Taylor (Eds.), *Vision in Vehicles II* (pp. 179–186). Elsevier Science Publishers (North-Holland).

Owen, D. H. (1990). Perception & Control of Changes in Self-Motion: A Functional Approach to the Study of Information and Skill. In R. Warren & A. H. Wertheim (Eds.), *The Perception and Control of Egomotion* (pp. 289–326). Hillsdale, N.J.

Owen, D. H., & Johnson, W. W. (1992). An Information-Based Approach to Simulation Research. In R. A. Feik (Ed.), *Proceedings of the future directions in simulation workshop* (pp. 1–10). Defense Science and Technology Organisation ARL-ASD, Melbourne (Australia).

Owen, D. H., & Warren, R. (1982). Optical Variables as Measures of Performance During Simulated Flight. *Proceedings of the Human Factors Society – 26th Annual Meeting – 1982*, 312–315.

Owen, D. H., Warren, R., Jensen, R. S., Mangold, S. J., & Hettinger, L. J. (1981). Optical Information for Detecting Loss in One's Own Forward Speed. *Acta Psychologica, 48*, 203–213.

Pallett, E. H. J., & Coombs, L. F. E. (1997). *Aircraft Instruments and Integrated Systems* (3rd. ed.). Harlow (UK): Addison Wesley, Longman Limited.

Palmer, E., & Wempe, T. (1971). Pilot Performance With a Simulated ILS-Independent Pictorial Display. *Proceedings of the Seventh Annual Conference on Manual Control, NASA SP-281*, 139–154.

Papoulis, A. (1991). *Probability, Random Variables, and Stochastic Processes* (3rd. ed.). New York: McGraw-Hill.

Parrish, R. V., Busquets, A. M., Williams, S. P., & Nold, D. E. (1994). *Spatial Awareness Comparisons Between Large-Screen, Integrated Pictorial Displays and Conventional EFIS Displays During Simulated Landing Approaches* (NASA Technical Paper No. TP-3467). Washington (D.C.).

Phatak, A. V., Weinert, H., Segall, I., & Day, C. N. (1976). Identification of a Modified Optimal Control Model for the Human Operator. *Automatica*, *12*, 31–41.

Poppen, J. R. (1936). Equilibratory Functions in Instrument Flying. *Journal of Aviation Medicine*, *6*, 148–160.

Prazdny, K. (1980). Egomotion and Relative Depth Map from Optical Flow. *Biological Cybernetics*, *36*, 87–102.

Prazdny, K. (1981). Determining the Instantaneous Direction of Motion from Optical Flow Generated by a Curvilinear Observer. *Computer Graphics and Image Processing*, *17*, 238–248.

Press, W. H., Teukolsky, S. A., Vetterling, W. T., & Flannery, B. P. (1992). *Numerical Recipes in C. The Art of Scientific Computing* (2nd. ed.). Cambridge: Cambridge University Press.

Prevett, T. T., & Wickens, C. D. (1994). *Perspective Displays and Frame of Reference: Their Interdependence to Realize Performance Advantages over Planar Displays in a Terminal Area Navigation Task* (Aviation Research Laboratory Report No. ARL-94-8). Savoy, Illinois 61874: University of Illinois at Urbana-Champaign.

Quinn, T. J. (1982). *Pictorial Formats Literature Review* (Technical Report No. AFWAL-TR-81-3156 (Volume III)). Wright-Patterson AFB (OH): Air Force Wright Aeronautical Laboratories.

RAND. (1993). *Airport Growth and Safety. A Study of the External Risks of Schiphol Airport and Possible Safety-Enhancement Measures* (Tech. Rep.). Santa Monica (CA): RAND.

Rasmussen, J. (1983). Skills, Rules, and Knowledge; Signals, Signs, and Symbols, and other Distinctions in Human Performance Models. *IEEE Transactions on Systems, Man, and Cybernetics*, *13*, 257–266.

Raviv, D., & Herman, M. (1994). A Unified Approach to Camera Fixation and Vision-Based Road Following. *IEEE Transactions on Systems, Man, and Cybernetics*, *24*(8), 1125–1141.

Reardon, K. A. (1988). The Effect of Nested Texture on a Landing-Judgement Task. *Proceedings of the Human Factors Society – 32nd Annual Meeting – 1988*, 10–14.

Regal, D., & Whittington, D. (1995). Guidance Symbology for Curved Flight Paths. *Proceedings of the Eighth International Symposium on Aviation Psychology, Columbus (OH), April 24-27, 1995*, 74–79.

Regan, D., Beverly, K., & Cynader, M. (1979). The Visual Perception of Motion in Depth. *Scientific American, 241*(2), 122–133.

Regan, D., & Vincent, A. (1995). Visual Processing of Looming and Time to Contact Troughout the Visual Field. *Vision Research, 35*(13), 1845–1857.

Reid, L. D. (1983). A Survey of Recent Driver Steering Behavior Models Suited to Accident Studies. *Accident Analysis and Prevention, 15*(1), 23–40.

Reid, L. D., Solowka, E. N., & Billing, A. M. (1981). A Systematic Study of Driver Steering Behavior. *Ergonomics, 24*(6), 447–462.

Reising, J., Barthelemy, K., & Hartsock, D. (1989). Pathway-in-the-Sky Evaluation. *Proceedings of the Fifth International Symposium On Aviation Psychology, Columbus (OH), April 1989.*

Rieger, J. H. (1983). Information in Optical Flows Induced by Curved Paths of Observation. *Journal of the Optical Society of America, 73*(3), 339–344.

Riemersma, J. B. J. (1981). Visual Control During Straight Road Driving. *Acta Psychologica, 48,* 215–225.

Riemersma, J. B. J. (1984). Perceptual Cues in Vehicle Guidance on a Straight Road. *Proceedings of the Fourth European Annual Conference on Human Decision Making and Manual Control,* 127–136.

Riemersma, J. B. J. (1988). Perceptual Factors in Driving. Perception of Characteristics of Horizontal Curves. *Proceedings of the Fourteenth Conference of the Australian Road Research Board, 4,* 121–125.

Riemersma, J. B. J. (1991). Perception of Curve Characteristics. In A. G. Gale, M. H. Freeman, C. M. Haslegrave, P. Smith, & S. P. Taylor (Eds.), *Vision in Vehicles II* (pp. 163–170). Elsevier Science Publishers (North-Holland).

Ritter, R. D. (1993). "And We Were Tired" – Fatigue and Aircrew Errors. *IEEE AES Systems Magazine,* 21–26.

Rockwell, T. H. (1972). Eye Movement Analysis of Visual Information Acquisition in Driving: An Overview. *Proceedings of the Sixth Conference of the Australian Road Research Board, 6*(3), 316–331.

Roscoe, S. N. (1948). The Effects of Eliminating Binocular and Peripheral Monocular Visual Cues upon Airplane Pilot Performance and Landing. *Journal of Applied Psychology, 32,* 649–662.

Roscoe, S. N. (1968). Airborne Displays for Flight and Navigation. *Human Factors, 10*(4), 321–332.

Roscoe, S. N., Corl, L., & Jensen, R. S. (1981). Flight Display Dynamics Revisited. *Human Factors, 23*(3), 341–353.

Roscoe, S. N., Hasler, S. G., & Dougherty, D. J. (1966). Flight By Periscope: Making Takeoffs and Landings; The Influence of Image Magnification, Practice, and Various Conditions of Flight. *Human Factors, 8*(2), 13–40.

Roscoe, S. N., & Jensen, R. S. (1981). Computer-Animated Predictive Displays for Microwave Landing Approaches. *IEEE Transactions on Systems, Man, and Cybernetics, SMC-11*(11), 760–765.

RTCA. (1995). *Final Report of RTCA Task Force 3 Free Flight Implementation* (Tech. Rep.). Washington (DC): RTCA, Inc.

Salvatore, S. (1968). The Estimation of Vehicular Velocity as a Function of Visual Stimulation. *Human Factors*, *10*(1), 27–32.

Sarter, N. B. (1991). The Flight Management System – Pilot's Interaction with Cockpit Automation. *Proceedings of the IEEE Conference on Systems, Man, and Cybernetics*, 1307–1310.

Sarter, N. B., & Woods, D. D. (1994). Pilot Interaction with Cockpit Automation II: An Experimental Study of Pilot's Model and Awareness of the Flight Management System. *The International Journal of Aviation Psychology*, *4*(1), 1–28.

Schattenmann, W., & Wilckens, V. (1973). *Vergleichende Simulatorstudien mit dem kontaktanalogen Kanal-Display und mit konventionellen Instrumentierungen* (Forschungsbericht No. FB 73-57). Deutsche Luft- und Raumfahrt. (in German)

Sheridan, T. B. (1991). Automation, Authority and Angst – Revisited. *Proceedings of the Human Factors Society – 35th Annual Meeting – 1991*, 2–6.

Shinar, D., McDowell, E. D., & Rockwell, T. H. (1977). Eye Movements in Curve Negotiation. *Human Factors*, *19*(1), 63–71.

Singh, A. (1991). *Optic Flow Computation: A Unified Perspective.* Los Alamitos, California: IEEE Computer Society Press Monograph.

Söderström, T., & Stoica, P. (1989). *System Identification.* Cambridge (UK): Prentice-Hall.

Stapleford, R. L., Craig, S. J., & Tennant, J. A. (1969). *Measurement of Pilot Describing Functions in Single-Controller Multiloop Tasks* (NASA Contractor Report No. CR-1238). Washington (D.C.).

Stapleford, R. L., McRuer, D. T., & Magdaleno, R. (1967). Pilot Describing Function Measurements in a Multiloop Task. *IEEE Transactions on Human Factors in Electronics*, *HFE-8*(2), 113–125.

Stassen, H. G. (1994). Measurement and Modelling, an Iterative Approach. In K. H. et al. (Ed.), *Measurement and Design* (pp. 83–110). Delft University of Technology.

Tanaka, K., & Matsumoto, K. (1986). A Hierarchical Model of Pilot's Procedural Behavior for Cockpit Workload Analysis. *Transactions of the Japan Society of Aeronautical and Space Sciences*, *28*(82), 230–239.

Teper, G. L. (1972). An Effective Technique for Extracting Pilot Model Parameter Values from Multi-feedback, Single-input Tracking Tasks. *Proceedings of the Eighth Annual Conference on Manual Control*, *Report AFFDL-TR-72-92*, 23–33.

Theunissen, E. (1991). *Perspective Displays for Three-Dimensional and Four-Dimensional Navigation. A literature review* (NLR Contractor Report No. CR 91364 L). Amsterdam: National Aerospace Laboratory.

Theunissen, E. (1993a). D^{3}S: The DELPHINS Display Design System. *Proceedings of the AIAA Flight Simulation Technologies Conference, Monterey (CA), August 9-11*, 62–67.

Theunissen, E. (1993b). A Primary Flight Display for Four-Dimensional Guidance and Navigation – Influence of Tunnel Size and Level of Additional Information on Pilot Performance and Control Behaviour. *Proceedings of the AIAA Flight Simulation Technologies Conference, Monterey (CA), August 9-11*, 140–146.

Theunissen, E. (1995). Influence of Error Gain and Position Prediction on Tracking Performance and Control Activity with Perspective Flight Path Displays. *Air Traffic Control Quarterly*, *3*(2), 95–116.

Theunissen, E. (1997). *Integrated Design of a Man-Machine Interface for 4-D Navigation.* Ph.D. dissertation, Faculty of Electrical Engineering, Delft University of Technology.

Theunissen, E., & Mulder, M. (1994). Open and Closed Loop Control With a Perspective Tunnel-in-the-Sky Display. *Proceedings of the AIAA Flight Simulation Technologies Conference, Scottsdale (AZ), August 1-3*, 32–43.

Theunissen, E., & Mulder, M. (1995a). Error-Neglecting Control with Perspective Flightpath Displays. *Proceedings of the Eighth International Symposium on Aviation Psychology, Columbus (OH), April 24-27, 1995*, 110–115.

Theunissen, E., & Mulder, M. (1995b). Pilot-in-the-Loop Studies into Manual Control Strategies with Perspective Flightpath Displays. *Proceedings of the XIVth European Annual Conference on Human Decision Making and Manual Control, Delft, The Netherlands, June 14-16*, 1.3.1–1.3.7.

Thompson, P. M. (1987). Program CC's Implementation of the Human Optimal Control Model. *Proceedings of the AIAA Guidance, Navigation and Control Conference, Monterey (CA), August 17-19.*

van der Hoek, A. J. (1997a). *Optical Cues in a Perspective Flight-Path Display. Part II: Empirical Evaluation of the Optical Cues in Curved Sections of the Tunnel-in-the-Sky Display.* Unpublished MSc. Thesis, Faculty of Aerospace Engineering, Delft University of Technology.

van der Hoek, A. J. (1997b). *Optical Cues in a Perspective Flight-Path Display. Part I: Theoretical Analysis of the Optical Cues in Curved Sections of the Tunnel-in-the-Sky Display.* Unpublished preliminary MSc. Thesis, Faculty of Aerospace Engineering, Delft University of Technology.

van der Linden, C. A. A. M. (1996). *DASMAT: the Delft University Aircraft Simulation Model and Analysis Tool* (Report No. LR-781). Delft: Delft University of Technology.

van der Vaart, J. C. (1992). *Modelling of Perception and Action in Compensatory Manual Control Tasks.* Ph.D. dissertation, Faculty of Aerospace Engineering, Delft University of Technology.

van Houtte, N. A. J. (1970). A Perspective Glideslope Indicating System. *Proceedings of the Sixth Annual Conference on Manual Control*, 117–131.

van Lunteren, A. (1979). *Identification of Human Operator Describing Function Models with One or Two Inputs in Closed Loop Systems.* Ph.D. dissertation, Faculty of Mechanical Engineering, Delft University of Technology.

van Oorschot, P. W. J. (1997a). *Cybernetische Aspecten bij Bochtinitiatie Tunnel-in-the-Sky.* Unpublished MSc. Thesis, Faculty of Aerospace Engineering, Delft University of Technology. (in Dutch)

van Oorschot, P. W. J. (1997b). *Simulaties voor Bochtinitiatie Tunnel-in-the-Sky.* Unpublished preliminary MSc. Thesis, Faculty of Aerospace Engineering, Delft University of Technology. (in Dutch)

van Paassen, M. M. (1994). *Biophysics in Aircraft Control. A model of the neuromuscular system of the pilot's arm.* Ph.D. dissertation, Faculty of Aerospace Engineering, Delft University of Technology.

van Paassen, M. M., & Mulder, M. (1998a). Identification of Human Operator Control Behaviour in Multi-Loop Tracking Tasks. *Proceedings of the Seventh IFAC/IFIP/IFORS/IEA Symposium on Analysis, Design and Evaluation of Man-Machine Systems, Kyoto Japan, September 16-18*, 515–520.

van Paassen, M. M., & Mulder, M. (1998b). The Cognitive Ecology of the Tunnel-in-the-Sky Display. *Proceedings of the Second International Conference on Engineering Psychology and Cognitive Ergonomics, October 28-30, Oxford, United Kingdom.* (to be published)

van Wijk, R. A., & Kok, J. J. (1977). Theoretic Aspects of the Identification of the Parameters in the Optimal Control Model. *Proceedings of the Thirteenth Annual Conference on Manual Control*, 27–34.

Vicente, K. J., & Rasmussen, J. (1990). The Ecology of Human-Machine Systems II: Mediating "Direct-Perception" in Complex Work Domains. *Ecological Psychology*, *2*(3), 207–249.

Vicente, K. J., & Rasmussen, J. (1992). Ecological Interface Design: Theoretical Foundations. *IEEE Transactions on Systems, Man, and Cybernetics*, *22*(4), 589–606.

Viken, S. A., & Burley, J. R. (1992). Predictive Nosepointing and Flightpath Displays for Air-to-Air Combat. *Proceedings of the International Society for Optical Engineering (SPIE), 'Helmet-Mounted Displays III' Conference*, *1695*, 154–165.

Warren, R. (1976). The Perception of Egomotion. *Journal of Experimental Psychology: Human Perception and Performance*, *2*(3), 448–456.

Warren, R. (1982). *Optical Transformation during Movement: Review of the Optical Concomitants of Egomotion* (Technical Report No. AFOSR-TR-82-1028). Bolling AFB (DC): Air Force Office of Scientific Research. (NTIS no. AD-A122 275)

Warren, R. (1988). Visual Perception in High-Speed Low-Altitude Flight. *Aviation, Space and Environmental Medicine*, *59*(Suppl. 11), A116–A124.

Warren, R., & Owen, D. H. (1982). Functional Optical Invariants: A New Methodology for Aviation Research. *Aviation, Space and Environmental Medicine*, *53*(10), 977–983.

Warren, R., & Riccio, G. E. (1985). Visual Cue Dominance Hierarchies: Implications for Simulator Design. *Society of Automotive Engineers*, *SAE Technical Paper 851946*.

Warren, W. H., & Hannon, D. J. (1990). Eye Movements and Optical Flow. *Journal of the Optical Society of America*, *7*(1), 160–169.

Warren, W. H., & Kurtz, K. J. (1992). The Role of Central and Peripheral Vision in Perceiving the Direction of Self-Motion. *Perception & Psychophysics*, *51*(5), 443–454.

Warren, W. H., Mestre, D. R., Blackwell, A. W., & Morris, M. W. (1991). Perception of Circular Heading From Optical Flow. *Journal of Experimental Psychology: Human Perception and Performance*, *17*(1), 28–43.

Warren, W. H., Morris, M. W., & Kalish, M. (1988). Perception of Translational Heading From Optical Flow. *Journal of Experimental Psychology: Human Perception and Performance*, *14*(4), 646–660.

Watler, J. F., & Logan, W. B. (1981). The Maneuvering Flight Path Display – An Update. *Proceedings of the Fifth Advanced Aircrew Display Symposium*, 138–162.

Weir, D. H., Heffley, R. K., & Ringland, R. (1972). Simulation Investigation of Driver/Vehicle Performance in a Highway Gust Environment. *Proceedings of the Eighth Annual Conference on Manual Control, Report AFFDL-TR-72-92*, 449–465.

Weir, D. H., & McRuer, D. T. (1968). Models for Steering Control of Motor Vehicles. *Proceedings of the Fourth Annual Conference on Manual Control, NASA SP-192*, 135–169.

Weir, D. H., & McRuer, D. T. (1972). *Pilot Dynamics for Instrument Approach Tasks: Full Panel Multiloop and Flight Director Operations* (NASA Contractor Report No. CR-2019). Washington (D.C.).

Wempe, T., & Palmer, E. (1970). Pilot Performance With a Simulated Pictorial Landing Display Including Different Conditions of Resolution and Udate Rate. *Proceedings of the Sixth Annual Conference on Manual Control*, 47–81.

Wewerinke, P. H. (1976). *An Analysis of In-Flight Helicopter Pilot Control Behaviour and Workload* (NLR Technical Report No. TR 76146 C). Amsterdam: National Aerospace Laboratory.

Wewerinke, P. H. (1978). *A Model of the Perception Process of the Outside World Useful for VFR Missions* (NLR Technical Report No. TR 78013 C). Amsterdam: National Aerospace Laboratory.

Wewerinke, P. H. (1979). *Visual Scene Perception – Frequency-Domain Data and Model Parameter Estimation Procedure* (NLR Memorandum No. MP 79009 U). Amsterdam: National Aerospace Laboratory.

Wewerinke, P. H. (1989). *Models of the Human Observer and Controller of a Dynamic System.* Ph.D. dissertation, Department of Applied Mathematics, University of Twente.

Wickens, C. D. (1992). *Engineering Psychology and Human Performance* (2nd. ed.). Harper-Collins.

Wickens, C. D., & Andre, A. D. (1988). Proximity Compatibility and the Object Display. *Proceedings of the Human Factors Society – 32nd Annual Meeting – 1988*, 1335–1339.

Wickens, C. D., & Andre, A. D. (1990). Proximity Compatibility and Information Display: Effects of Color, Space, and Objectness on Information Integration. *Human Factors, 32*(1), 61–77.

Wickens, C. D., Haskell, I. D., & Harte, K. (1989). Ergonomic Design for Perspective Flight-Path Displays. *IEEE Control Systems Magazine, 9*(4), 3–8.

Wiener, E. L. (1985). Beyond the Sterile Cockpit. *Human Factors, 27*(1), 75–90.

Wiener, E. L., & Curry, R. E. (1980). Flight-Deck Automation: Promises and Problems. *Ergonomics, 23*(10), 995–1011.

Wiener, N. (1961). *Cybernetics or Control and Communication in the Animal and the Machine* (2nd. ed.). New York: The MIT Press and John Wiley & Sons. (originally published in 1948)

Wilckens, V. (1971). On the Dependence of Information Display Quality Requirements Upon Human Characteristics and "Pilot/Automatics"-Relations. *Proceedings of the Seventh Annual Conference on Manual Control, NASA SP-281*, 177–183.

Wilckens, V. (1973). Improvements in Pilot/Aircraft-Integration by Advanced Contact Analog Displays. *Proceedings of the Ninth Annual Conference on Manual Control*, 175–192.

Wilckens, V., & Schattenmann, W. (1968). Test Results with New Analog Displays for All Weather Landing. *AGARD Conference Proceedings "Problems of the Cockpit Environment", CP-55*, 10.1–10.33.

Wohl, J. G. (1961). Man-Machine Steering Dynamics. *Human Factors*, *3*(4), 222–229.

Wolpert, L. (1988). The Active Control of Altitude over Differing Texture. *Proceedings of the Human Factors Society – 32nd Annual Meeting – 1988*, 15–19.

Wolpert, L., & Owen, D. (1985). Sources of Optical Information and their Metrics for Detecting Loss in Altitude. *Proceedings of the Third Symposium on Aviation Psychology, Columbus (OH)*, 475–481.

Wolpert, L., Owen, D. H., & Warren, R. (1983). *The Isolation of Optical Information and its Metrics for the Detection of Descent. Optical Flow and Texture Variables Useful in Simulating Self Motion (II)* (Final Technical Report for Grant No. AFOSR-81-0078). Columbus, OH: OSU, Dept. Psychology, Aviation Psychology Laboratory.

Zacharias, G. L., Caglayan, A. K., & Sinacori, J. B. (1985a). A Model for Visual Flow-Field Cueing and Self-Motion Estimation. *IEEE Transactions on Systems, Man, and Cybernetics*, *15*(3), 383–389.

Zacharias, G. L., Caglayan, A. K., & Sinacori, J. B. (1985b). A Visual Cueing Model for Terrain-Following Applications. *Journal of Guidance*, *8*(2), 201–207.

Zacharias, G. L., Miao, A. X., & Warren, R. (1995). Multistage Integration Model for Human Egomotion Perception. *Journal of Guidance, Control, and Dynamics*, *18*(5), 937–944.

Zeki, S. (1992). The Visual Image in Mind and Brain. *Scientific American*, *267*(3), 43–50.

Abbreviations and symbols

Abbreviations

2-/3-/4-D	Two-/Three-/Four-Dimensional
A/D	Analog-to-Digital
ADI	Attitude Director Indicator
AFCS	Automatic Flight Control System
ANOVA	Analysis of Variance
AP	Auto Pilot
ATC	Air Traffic Control
ATM	Air Traffic Management
CNS	Communication, Navigation, Surveillance
COM	Crossover Model
COP	Center of Projection
CRT	Cathode Ray Tube
D/A	Digital-to-Analog
DASMAT	Delft university Aircraft Simulation Model and Analysis Tool
DELPHINS	Delft Program for Hybridized Instrumentation and Navigation Systems
DFT	Discrete-Fourier Transform
DLR	Deutsche Luft- und Raumfahrt
DoD	US Department of Defence
DREAM	Delft Research into Enhanced Aircraft Manoeuvering concepts
DUT	Delft University of Technology
EFIS	Electronic Flight Instrument System
EFOV	Eye Field-Of-View
EID	Ecological Interface Design
EVS	Enhanced Vision System
FAA	Federal Aviation Administration
FANS	Future Air Navigation System
FAR	Federal Aviation Rules
FD	Flight-Director
FIR	Finite Impulse Response
FMS	Flight Management System
FPP	Flight-Path Predictor
FPV	Flight-Path Vector

FRO	Focus of Radial Outflow
FTS	Fast-Time Simulation
GPS	Global Positioning System
GS	Glide Slope
HCA	Human-Centered Automation
HDD	Head-Down Display
HGFOV	Horizontal Geometrical Field Of View
HMI	Human-Machine Interface
HML	Human-Machine Laboratory
HSC	Horizontal SCreen size
HSI	Horizontal Situation Indicator
HUD	Head-Up Display
ICAO	International Civil Aviation Organization
IFR	Instrument Flight Rules
ILS	Instrument Landing System
IMC	Instrument Meteorological Conditions
I/O	Input/Output
IRS	Inertial Reference System
IV	Instrumental Variable
KBB	Knowledge-Based Behaviour
LOC	Localizer
LTI	Linear Time-Invariant
LQG	Linear-Quadratic Gaussian
LQR	Linear-Quadratic Regulator
LS	Least-Squares
MA	Mode Awareness
MAG	MAGnetic heading
MFD	Multi-Function Display
MIMO	Multi-Input Multi-Output
MISO	Multi-Input Single-Output
MLM	Multi-Loop Model
MLS	Microwave Landing System
NA	Navigation Awareness
ND	Navigation Display
ND-CM	Navigation Display, Compass Mode
ND-MM	Navigation Display, Map Mode
NK	Newman-Keuls
NLR	National Aerospace Laboratory (the Netherlands)
OCM	Optimal Control Model
PCP	Proximity Compatibility Principle
PFD	Primary Flight Display
RBB	Rule-Based Behaviour
RMS	Root Mean Square
RNAV	Area (or Random) Navigation
RNP	Required Navigation Performance

RNR	Relative Noise Ratio
RTCA	Radio Technical Commission for Aeronautics
SA	Situation Awareness
SBB	Skill-Based Behaviour
SID	Standard Instrument Departure
SISO	Single-Input Single-Output
SNR	Signal-to-Noise Ratio
SOP	Successive Organisation of Perception
SR	Stimulus-Response
SRK	Skills-Rules-Knowledge
STAR	Standard Terminal Arrival Route
STD	STandard Deviation
SVS	Synthetic Vision System
TCAS	Traffic Collision Avoidance System
TIS	Tunnel-In-the-Sky
TLC	Time-to-Line Crossing
TMA	Terminal Manoeuvering Area
TNP	Trajectory-Negotiation Process
TP	Tangent Point
TTC	Time-to-Contact
TTP	Time-to-Passage
TWC	Time-to-Wall Crossing
US	United States
USAF	United States Air Force
VFR	Visual Flight Rules
VGFOV	Vertical Geometrical Field Of View
VMC	Visual Meteorological Conditions
VRP	View-Reference Point
VSC	Vertical SCreen size
VSD	Vertical Situation Display
WW	World War
ZOH	Zero-Order Hold

General notation

Latin symbols

A_{j_i}	amplitude # i of input signal j
Bias($\cdot$)	bias in estimation of variable ($\cdot$)
c	linear damping constant
$\mathcal{C}$	complex numbers
$\triangle D$	distance between two tunnel frames
D_c	distance to the start of the curved trajectory
D_t	distance of COP along tunnel longitudinal axis X_t

D_v	viewing distance
D_{BT}	distance-before-the-turn
D_{TP}	distance to the tangent point
$E\{\cdot\}$	expectation of variable $(\cdot)$
E1	pilot model identification expectation variable 1
E2	pilot model identification expectation variable 2
f	pilot force on side-stick
f_{data}	data recording frequency
f_i	tunnel frame number
f_i	pilot fraction of attention
f_s	sample frequency
f_{sim}	simulation frequency
f_{EFIS}	update-rate of EFIS display
$\mathcal{F}^a$	aircraft Aerodynamic frame of reference
$\mathcal{F}^b$	aircraft Body frame of reference
$\mathcal{F}^g$	aircraft Geodetic frame of reference
$\mathcal{F}^i$	Inertial frame of reference
$\mathcal{F}^p$	aircraft Flight-Path frame of reference
$\mathcal{F}^t$	Tunnel frame of reference
$\mathcal{F}^v$	display Viewing frame of reference
$\mathcal{F}^{vr}$	display Viewing Reference frame of reference
$\mathcal{F}^w$	World frame of reference
F	pilot timing reference function
F_{ij}	Snedecor F-distribution of two random variables with i and j degrees of freedom
g_0	Earth gravitational acceleration
G	pilot control-rate weighting matrix
h	aircraft horizontal position with respect to tunnel center
$H(j\omega)$	system transfer function (frequency domain description)
$H(s)$	system transfer function (Laplace description)
H_c	system transfer function
$H_{c_1}(s)$	system inner loop transfer function
$H_{c_2}(s)$	system middle loop transfer function
$H_{c_3}(s)$	system outer loop transfer function
H_d	approximated time delay transfer function
H_p	pilot transfer function
$H_{p_x}^p$	pilot inner loop transfer function (parallel model)
$H_{p_y}^p$	pilot middle loop transfer function (parallel model)
$H_{p_z}^p$	pilot outer loop transfer function (parallel model)
$H_{p_x}^s$	pilot inner loop transfer function (serial model)
$H_{p_y}^s$	pilot middle loop transfer function (serial model)
$H_{p_z}^s$	pilot outer loop transfer function (serial model)
$H_{p_y}^c$	pilot combined middle & outer loop transfer function (parallel model, using y)
$H_{p_z}^c$	pilot combined middle & outer loop transfer function (parallel model, using z)
H_t	tunnel height
$\underline{H}_p$	multi-loop pilot describing function

$i_1,\ i_2,\ i_3,\ i_4$	disturbance signal 1, 2, 3, 4
J	optimization criterion
k	linear spring constant
k_{j_i}	index # i of input signal j
$\underline{k}_j$	set of indices of Fourier coefficients of input signal j
K_γ	aircraft flight-path response gain
K_ϕ	aircraft roll response gain
K_θ	aircraft pitch response gain
$K_{p_{in}}$	pilot inner loop gain
$K_{p_{mid}}$	pilot middle loop gain
$K_{p_{out}}$	pilot outer loop gain
$K_{p_{out}}^\epsilon$	pilot outer loop gain (ϵ-model)
K_{p_v}	pilot vertical position error feedback
$K_{p_{\dot{v}}}$	pilot vertical position error rate feedback
$K_{V_{s_i}^1}$	splay angle #1 gain for a vertical position error (curved trajectory segment s_i)
$K_{V_{s_i}^2}$	splay angle #2 gain for a vertical position error (curved trajectory segment s_i)
$K_{X_{s_i}^1}$	splay angle #1 gain for a lateral position error (curved trajectory segment s_i)
$K_{X_{s_i}^2}$	splay angle #2 gain for a lateral position error (curved trajectory segment s_i)
L_g	turbulence scale length
m	mass
$\mathcal{M}$	model structure
$M_{\underline{\theta}\underline{\theta}}$	Fisher information matrix for a parameter vector $\underline{\theta}$
n	pilot remnant signal
$\underline{n}$	pilot remnant vector
$\mathcal{N}$	normal distribution
N	number of samples in data vector
N_f	number of frequencies in sinusoidal forcing function signal
N_v	number of variables in optimization criterion
p	chance level
p	aircraft rotation along the longitudinal Body axis
q	aircraft rotation along the lateral Body axis
Q	pilot observation vector weighting matrix
r	aircraft rotation along the vertical Body axis
r	signal-to-noise ratio
r_c	commanded yaw rate
$\mathcal{R}$	real numbers
R	pilot control input vector weighting matrix
R	curve radius
R_c	commanded trajectory circle radius
R_i	radius of the inner curve line
R_o	radius of the outer curve line
R_t	circular tunnel trajectory radius
R_X	x-axis rotation matrix
R_Y	y-axis rotation matrix
R_Z	z-axis rotation matrix

s	position of side-stick
s	Laplace variable
s_i	tunnel segment number
S	sensitivity function
$\triangle S^f$	distance between tunnel frames in segmented circular tunnel
$\triangle S^s$	length of circular tunnel segment
S_t	angular distance from COP along the tunnel centercircle
t	time
$\triangle t_1$	time interval in which the reference function derivative $\dot{F}$ increases/decreases to a constant level
$\triangle t_2$	time interval in which the reference function derivative $\dot{F}$ is constant
$\mathcal{T}$	transformation matrix
T_i	experiment run-in time
T_m	experiment measurement time
T_p	prediction time
$T_{s_{data}}$	data recording sample time
$T_{s_{sim}}$	simulation sample time
$T_{s_{EFIS}}$	EFIS display update time
T_{BT}	time-before-the-turn
T_M	total manoeuvre time
u	pilot control (system input) signal
u	aircraft velocity along the longitudinal Body axis
u_p	horizontal co-ordinate of the projection of point P on the viewplane
u_∞	horizontal co-ordinate of the infinity point on the viewplane
$u_{\infty_{s_i}}$	horizontal co-ordinate of the infinity point of segment s_i (circular tunnel) on the viewplane
$\triangle u_{\infty_{s_i,s_j}}$	relative horizontal co-ordinates of the infinity points of segments s_i and s_j (circular tunnel) on the viewplane
$\underline{u}$	pilot control (system input) vector
$\mathcal{U}$	uniform distribution
U	horizontal viewplane axis
U'	rotated horizontal viewplane axis
$U(\nu_k;\zeta)$	Fourier coefficient of a pilot control signal signal realization at frequency ν_k
v	aircraft velocity along the lateral Body axis
v_e	vertical position error
v_p	vertical co-ordinate of the projection of point P on the viewplane
v_∞	vertical co-ordinate of the infinity point on the viewplane
$v_{\infty_{s_i}}$	vertical co-ordinate of the infinity point of segment s_i (circular tunnel) on the viewplane
$\triangle v_{\infty_{s_i,s_j}}$	relative vertical co-ordinates of the infinity points of segments s_i and s_j (circular tunnel) on the viewplane
$\underline{v}_u$	pilot motor noise vector
$\underline{v}_y$	pilot observation noise vector
V	vertical viewplane axis
V'	rotated vertical viewplane axis

V_u	pilot motor noise intensity
V_y	pilot observation noise intensity
V_{tas}	true airspeed
$\underline{V}$	velocity vector
$\text{Var}(\cdot)$	variance in estimation of variable $(\cdot)$
w	aircraft velocity along the vertical Body axis
$\underline{w}$	disturbance vector
W	noise intensity
W_t	tunnel width
x	longitudinal position with respect to texture element
x	system inner loop output signal
$\underline{x}$	state vector
x_e	lateral position error
X	longitudinal axis
y	aircraft lateral position with respect to tunnel center
y	lateral position with respect to texture element
y	system middle loop output signal
$\underline{y}$	output vector
$\underline{y}$	optical cue vector
Y	lateral axis
z	height above a horizontal surface
z	system outer loop output signal
Z	vertical axis

Greek symbols

α	aircraft angle of attack angle
α	angular deflection angle
β	aircraft angle of slip angle
β_g	turbulence slip angle
γ	aircraft angle of climb angle
Γ_t	tunnel trajectory downslope angle
δ	optical depression angle
$\delta(\cdot)$	*change* in quantity $(\cdot)$
δ_a	aircraft aileron control signal
δ_e	aircraft elevator control signal
δ_r	aircraft rudder control signal
ϵ	chance level
ϵ	lateral displacement of a projected entity on the viewplane
ϵ_i	lateral displacement of vertical frame line (left) of tunnel frame i
ϵ_{ij}	relative lateral displacement of vertical frame lines (left) of tunnel frames i and j
$\epsilon_{i\infty}$	lateral displacement of vertical frame line (left) of tunnel frame i (w.r.t. vertical pseudo-horizon)
ϵ_ℓ	lateral displacement of predictor symbol with respect to predictor reference frame

ϵ_v	vertical displacement of predictor symbol with respect to predictor reference frame
ζ	realization of random variable
ζ_i	vertical frame line (left) angle of frame i
ζ_n	pilot neuromuscular damping
η	angle between the driver's line-of-sight and the tangent point
η_i	lateral displacement of vertical frame line (right) of tunnel frame i
η_{ij}	relative lateral displacement of vertical frame lines (right) of tunnel frames i and j
$\eta_{i\infty}$	lateral displacement of vertical frame line (right) of tunnel frame i (w.r.t. vertical pseudo-horizon)
θ	aircraft pitch angle
$\underline{\theta}$	parameter vector
κ	perspective projection method constant (distance to the screen)
$\mu(\cdot)$	average of random variable $(\cdot)$
μ_i	vertical displacement of lateral frame line (bottom) of tunnel frame i
μ_{ij}	relative vertical displacement of lateral frame lines (bottom) of tunnel frames i and j
$\mu_{i\infty}$	vertical displacement of lateral frame line (bottom) of tunnel frame i (w.r.t. horizontal pseudo-horizon)
ν_i	vertical displacement of lateral frame line (top) of tunnel frame i
ν_{ij}	relative vertical displacement of lateral frame lines (top) of tunnel frames i and j
$\nu_{i\infty}$	vertical displacement of lateral frame line (top) of tunnel frame i (w.r.t. horizontal pseudo-horizon)
ν_0	ground frequency
$\underline{\nu}_{i_k}$	set of frequencies of input signal i_k
ξ	angle
ξ_i	vertical frame line (right) angle of frame i
π_i	lateral displacement of tunnel altitude pole i
π_{ij}	relative lateral displacement of tunnel altitude poles i and j
$\pi_{i\infty}$	lateral displacement of tunnel altitude pole i (w.r.t. vertical pseudo-horizon)
ρ_0	pilot nominal observation noise ratio
ρ_i	lateral frame line (bottom) angle of frame i
ρ_u	pilot motor noise ratio
ρ_{y_i}	pilot observation noise ratio of system output signal i
$\sigma(\cdot)$	standard deviation of random variable $(\cdot)$
σ_{f_i}	angular distance to tunnel frame f_i in a segmented curved tunnel
σ_i	lateral frame line (top) angle of frame i
σ_{s_i}	angular distance to tunnel section s_i in a segmented curved tunnel
$\sigma^2(\cdot)$	variance of random variable $(\cdot)$
$\sigma^2_{\beta_g}$	variance of lateral turbulence field slip angle
$\sigma^2_{v_g}$	variance of lateral turbulence field velocity
τ	pilot time delay
τ_e	pilot equivalent time delay
τ_γ	aircraft flight-path response lag time constant
τ_ϕ	aircraft roll response lag time constant
τ_{sim}	simulation time delay
$\tau_{\dot{v}}$	pilot vertical position error rate feedback time delay

τ_{EFIS}	EFIS display time delay
$\tau_{I_{in}}$	pilot inner loop lag time constant
$\tau_{L_{in}}$	pilot inner loop lead time constant
τ_N	pilot neuromuscular lag time constant
ϕ	aircraft roll angle
ϕ_{j_i}	phase # i of input signal j
φ_m	phase margin
Φ	aircraft bank angle
χ	aircraft flight-path azimuth angle (track angle)
χ_c	commanded track angle
χ_t	tunnel trajectory track angle
ψ	aircraft heading angle
$\triangle\psi$	segmented tunnel curved trajectory heading angle difference
ω	frequency
ω_c	crossover frequency
ω_i	*change* in optical splay angle i
ω_{j_i}	frequency # i of input signal j
ω_n	pilot neuromuscular frequency
Ω	optical splay angle
Ω_{s_i}	optical splay angle of segment s_i (circular tunnel)
$\underline{\Omega}$	rotation vector

Subscripts

0	initial value
CL	closed loop
e	error
F	frequency domain (in optimization)
FT	frequency and time domains (in optimization)
in	inner loop
k	discrete-time variable
max	maximum
mid	middle loop
min	minimum
OL	open loop
out	outer loop
out^c	combined outer loop
p	pilot
s	side-stick
t	tunnel
T	time domain (in optimization)
u	with respect to pilot control u
x	with respect to aircraft inner loop variable x
y	with respect to aircraft middle loop variable y

| z | with respect to aircraft outer loop variable z |

Superscripts

$*$	optimal
a	averaged
in	inner loop
in	inner curve wall
mid	middle loop
out	outer loop
out	outer curve wall
out^c	combined outer loop
p	pilot
r	raw data

Other

$\hat{}$	estimated
$\tilde{}$	delayed
$\tilde{}$	interpolated
$\tilde{}$	modelled
$\dot{}$	first time derivative
$\ddot{}$	second time derivative
∂	partial derivative
$|(\cdot)|$	magnitude of complex variable $(\cdot)$
$\angle(\cdot)$	phase of complex variable $(\cdot)$
[dB]	decibel
°, [deg]	degrees
[ft]	feet
[Hz]	Hertz
[m], [km]	metre, kilometre
[min]	minute
[rad]	radians
[s]	second
(t)	continuous-time variable

Samenvatting

Het sterk groeiende aantal vertragingen van het luchtverkeer in Europa en de Verenigde Staten zijn een duidelijke indicatie voor het *capaciteits-probleem* van het luchtverkeersmanagement (ATM) systeem dat op dit moment operationeel is. Een veel efficienter gebruik van het luchtruim is noodzakelijk om het groeiende volume van het luchtverkeer te kunnen ondervangen. Een belangrijke stap naar een flexibel systeem dat een efficient gebruik maakt van het luchtruim zou zijn dat het principe van vaste vliegroutes wordt afgeschaft. Vliegtuigen zouden in staat moeten worden gesteld om in principe *elke* route te volgen, zo lang de separatie tussen de verschillende vliegtuigen is gegarandeerd. Om de veiligheid te waarborgen zullen deze vliegbanen gevolgd moeten worden met een hoge mate van precisie, niet alleen wat betreft de positie van het vliegtuig, maar ook deze positie in de tijd. Het volgen van de vier-dimensionale vliegbanen zal tot een verhoging van de werkbelasting van de vlieger leiden en vereisen verder dat de vlieger continu op de hoogte is van de toestand van het vliegtuig ten opzichte van de wereld. Onderzoek wordt uitgevoerd om de cockpit mens-machine interface dusdanig te verbeteren dat het de bemanning ondersteunt in het uitvoeren van de 4-D navigatie- en besturingstaken in een toekomstig luchtverkeersmanagement systeem.

Er bestaat steeds meer overeenstemming dat de nieuwe mogelijkheden in het ontwerpen van cockpit displays, verworven dankzij de introductie van programmeerbare, electronische displays in de jaren tachtig, volledig moeten worden benut. Een toekomstig vlieg- en navigatie-display zal de besturings- en navigatie-toestand van het vliegtuig moeten presenteren op een manier die intuitief te begrijpen is, die het toestands-bewustzijn van de vliegers ondersteunt, en die compatibel is met de verschillende taken. Een display dat aan deze eisen zou kunnen voldoen is het zogenaamde *Tunnel-in-the-Sky display*, een perspectivisch instrument dat de vliegbaan die moet worden gevolgd presenteert in een synthetische drie-dimensionale wereld. Onderzoek naar het gebruik van het tunnel display voor de vlieger handbesturingstaak van de geleiding van het vliegtuig langs de complexe vliegbanen van de toekomst is het onderwerp van dit proefschrift.

Het huidige onderzoek naar het tunnel display bestaat voornamelijk uit *empirische* studies die het display vergelijken met de conventionele cockpit instrumenten voor wat betreft de vlieger prestatie en mentale belasting. Met als doel dit gangbare tunnel display onderzoek te complementeren is er in dit proefschrift een theoretische en experimentele studie uit-

gevoerd vanuit het perspectief van de *cybernetica*. Een geïntegreerde, multi-disciplinaire methodologie is toegepast, bestaande uit vier stappen, waarmee de fundamentele eigenschappen van de vlieger/display interactie worden onderzocht. Een theoretische analyse van de door het tunnel display gepresenteerde informatie, en dan met name de *informatie die kan worden gebruikt voor de vliegtuigbesturing*, is het centrale thema. De *eerste* stap in de methode bestaat uit een analyse van de taken van de vlieger en de informatie die nodig is om deze taken uit te voeren. Bij de *tweede* stap worden de visuele bronnen van informatie onderzocht die, theoretisch gezien, beschikbaar zijn voor de vlieger en die, practisch gezien, gebruikt kunnen worden. De *derde* stap bestaat uit een reeks van experimentele studies die het gebruik van de verschillende optische informatiebronnen door de vlieger onderzoeken. Tenslotte worden bij de *vierde* stap pogingen ondernomen om het experimenteel gemeten vliegergedrag te beschrijven met mathematische modellen.

De *taak-analyse* wijst uit dat er bij de vlieger handbesturingstaak van het volgen van een complexe vliegbaan twee taken kunnen worden onderscheiden. Ten eerste is daar de besturingstaak waarbij de vlieger, omdat de gewenste vliegbaan (tijdelijk) niet verandert, slechts een stationair tunnel-beeld moet behouden en kleine verstoringen in dit beeld moet wegregelen. De twee belangrijkste stationaire vliegcondities zijn die waarbij het vliegtuig een *rechtlijnige* of een *circelvormige* vliegbaan heeft. De tweede besturingstaak is die waarbij de vlieger het vliegtuig, omdat de gewenste vliegbaan nu wel verandert, van de ene in de andere stationaire vliegconditie moet brengen.

De *informatie-analyse* is uitgevoerd met als uitgangspunt de door Gibson ontwikkelde ecologische theorie van de visuele waarneming. De hypothese is dat *de belangrijkste stimulus van de vlieger wanneer deze zich door een begrensde omgeving beweegt zoals weergegeven door het tunnel display, is die van het naderen van een plat vlak*. De informatie die door het tunnel display wordt gepresenteerd is onderzocht voor de stationaire vliegcondities waarbij het vliegtuig hetzij een rechtlijnige hetzij een circelvormige vliegbaan heeft. In beide vliegcondities kunnen de stand en de positie van het vliegtuig ten opzichte van de tunnel worden waargenomen door de *statische* informatiebronnen van het *lineair perspectief*. De richting van de vliegtuigbeweging ten opzichte van de tunnel, de vliegsnelheid en de temporele variabelen kunnen worden waargenomen door de *dynamische* informatiebronnen van het *bewegings-perspectief*. Een generieke methode is ontwikkeld die het mogelijk maakt de verschillende bronnen van visuele informatie te beschrijven in termen van het geometrisch ontwerp van het tunnel display, de parameters van de perspectivische projectie en de bewegingstoestand-variabelen van het vliegtuig. Met behulp van deze methode kunnen de karakteristieke eigenschappen van de verschillende optische informatiebronnen in het weergeven van de vliegtuig bewegingstoestand aan de vlieger worden onderzocht.

De beide *theoretische* studies leiden tot nieuwe inzichten hoe de variabelen die het geometrisch ontwerp van het tunnel display bepalen het gedrag van de vlieger kunnen beïnvloeden. Deze theoretische verbanden kunnen van belang zijn wanneer er display ontwerpregels moeten worden opgesteld waarbij de mens centraal staat. Om deze hypothetische relaties te onderzoeken worden er een aantal *experimenten* uitgevoerd. Het doel

van deze experimenten is te begrijpen hoe het variëren van een vooraf geselecteerde groep tunnel display ontwerpvariabelen invloed heeft op de prestatie, de werkbelasting en het stuurgedrag van de vlieger. De experimenten worden gedefiniëerd om het vliegergedrag te kunnen onderzoeken niet alleen in termen van de prestatie, maar ook betreffende meer regeltechnische aspecten. Dit is geen gemakkelijke opgave. De methoden die beschikbaar zijn om het stuurgedrag van de vlieger te identificeren zijn dusdanig beperkt dat alleen de vlieger terugkoppelingen van de stand, de bewegingsrichting en de positie van het vliegtuig kunnen worden bepaald, hetgeen leidt tot een minimale representatie van het vlieger stuurgedrag. De model-gerichte aanpak richt zich dan ook op het analyseren van de *aanpassing* van de beschrijvende vliegermodellen over de verschillende experimentele condities. Met andere woorden, de modellen worden gebruikt als *gereedschap* om de relaties tussen de verschillende tunnel display ontwerpen en het vlieger stuurgedrag te analyseren.

Drie experimenten worden beschreven waarin de gevolgen van het variëren van enkele belangrijke tunnel display ontwerpvariabelen, zoals de *grootte van de tunnel*, de *kijkafstand* en de presentatie van *vliegpad vector* symbologie. Daarnaast worden drie experimenten beschreven waarin enkele meer fundamentele eigenschappen van het *tunnel geometrisch ontwerp* worden onderzocht in de twee vlieger besturingstaken van het volgen van een referentie tunnelbaan die ofwel recht ofwel circelvormig is, en in de vlieger besturingstaak van het uitvoeren van een transiente manoeuvre die nodig is om, komende vanaf een rechte tunnelbaan, een circelvormige tunnelbaan te onderscheppen.

De *tunnelgrootte* is een ontwerpvariabele waarmee de presentatie van de positiefout van het vliegtuig ten opzichte van het tunnel referentiepad wordt geschaald. Het blijkt dat het verkleinen van de tunnelgrootte leidt tot een betere vliegerprestatie in volgen van de referentiebaan, maar ook tot een toename van de stuuractiviteit en werkbelasting van de vlieger. Een modelmatige analyse toont aan dat een te kleine tunnel leidt tot een slecht gedempt gesloten lus systeem. Het wordt dan ook aanbevolen om bij de keuze van een bepaalde tunnelgrootte in voldoende mate rekening te houden met grenzen ten aanzien van de robuustheid van het vlieger-vliegtuig systeem, grenzen die worden bepaald door de afweging tussen enerzijds de gewenste prestatie van de vlieger en anderzijds de stabiliteit van de besturing.
Het tunnel display toont de vlieger het verloop van de gewenste vliegbaan in de toekomst. Maar welk gedeelte van de toekomstige baan bevat nu de meest bruikbare informatie voor de vlieger? Door het zichtbare gedeelte van de gepresenteerde referentiebaan te beperken tot een klein gebied om een vooraf gekozen *kijkafstand*, wordt de vlieger gedwongen om het vliegtuig door de tunnel te sturen met informatie over alleen dat kleine stukje van de baan rondom die kijkafstand. De dynamica van het gepresenteerde stuk tunnel, een bepaalde kijkafstand vooruit, blijkt af te hangen van enerzijds de keuze van de kijkafstand zelf en anderzijds de snelheid waarmee het vliegtuig door de tunnel beweegt. Een experiment toont aan dat de vlieger zijn stuurgedrag aanpast aan deze twee variabelen. Afhankelijk van de vliegsnelheid prefereren vliegers de ene kijkafstand boven de andere, met een trend van een toenemende kijkafstand voor hogere snelheden van het vliegtuig.

Een groot voordeel van programmeerbare displays is dat ze kunnen worden uitgebreid met symbologie die speciaal ontwikkeld is om de prestatie van de vlieger te verbeteren. Zo laat het *vliegpad vector* (FPV) symbool de richting zien waarin het vliegtuig beweegt ten opzichte van de wereld. Het blijkt dat zonder het FPV symbool, de vliegers de bewegingsrichting van het vliegtuig niet nauwkeurig kunnen schatten, althans niet nauwkeurig genoeg om deze informatie te gebruiken voor de besturing van het vliegtuig. Het presenteren van de vliegpad vector stelt de vliegers in staat de bewegingsrichting direct te gebruiken voor de besturing van het vliegtuig, hetgeen leidt tot een verbetering van de prestatie en een verlaging van de werkbelasting. Echter, wanneer de bandbreedte van de atmosferische turbulentie werkend op de bewegingsrichting van het vliegtuig toeneemt, zal de bruikbaarheid van het vliegpad vector symbool afnemen. Bij deze grotere bandbreedtes van de verstoring is het zelfs zo, dat de vliegers beter af zouden zijn geweest wanneer de vliegpad vector in het geheel niet zou worden gepresenteerd.

De relatieve bruikbaarheid van de twee belangrijkste optische bronnen van informatie voor de vliegtuigpositie ten opzichte van de referentiebaan, de zogenaamde optische 'splay'-hoek (de hoek tussen de projectie van een lijn parallel aan de kijkrichting op het display en de projectie van de horizon op het display) en de optische dichtheid, is onderzocht in de taak van het besturen van de rechtlijnige vlucht van het vliegtuig langs een rechte tunnelbaan. Er wordt aangetoond dat waar de prestatie van de vlieger met een display dat alleen optische splay informatie presenteert niet beïnvloed wordt door de voorwaartse beweging van het vliegtuig, deze prestatie afneemt wanneer de verticale en laterale vliegtuigbewegingen tegelijkertijd moeten worden geregeld. Dit in tegenstelling tot de prestatie van de vlieger met een display dat alleen optische dichtheid informatie presenteert: de prestatie neemt af wanneer het vliegtuig vooruit beweegt en blijft nagenoeg constant bij de gelijktijdige besturing van de verticale en de laterale vliegtuigbeweging. Een voordeel van het gebruik van optische splay informatie ten opzichte van de optische dichtheid is dat de splay-hoek een eigenschap is van het gehele lijnsegment: de relatie tussen deze hoek en de positiefout die deze hoek representeert is constant en het maakt daarom niet uit welk deel van het lijnsegment de vlieger waarneemt.

Een vergelijkbare studie is uitgevoerd voor de taak van het besturen van de circelvormige vlucht langs een circelvormige tunnelbaan. Aangetoond wordt dat de optische informatie in gekromde tunnels de bewegingstoestand van het vliegtuig ten opzichte van de referentiebaan niet zo goed weergeeft als in rechte tunnels, waardoor de taak van het volgen van een circelvormige baan aanzienlijk moeilijker wordt. Zo kan de richting van de vliegtuigbeweging alleen worden waargenomen via de visuele informatiebronnen van het bewegingsperspectief, en dit alleen voor kleinere kijkafstanden. De optische splay-hoeken zijn vooral belangrijk bij de waarneming en het besturen van de bewegingsrichting van het vliegtuig ten opzichte van de tunnel. Door de laterale kromming van de referentiebaan worden de vliegtuig laterale positie en koershoek ten opzichte van deze baan niet exact weergegeven door het tunnel display. De afwijkingen in de presentatie van de positiefout zijn vooral aanwezig in de optische splay-hoeken, en het is om deze reden dat de optische dichtheid

informatie een belangrijke rol speelt bij de waarneming en de besturing van de positie van het vliegtuig ten opzichte van de gekromde tunnel.

De vliegtuig transitie manoeuvre tussen een rechtlijnig en een circelvormig stuk van de referentiebaan is de enige taak bestudeerd in dit proefschrift waarbij de vlieger het vliegtuig van de ene in de andere stationaire vliegtoestand moet brengen. Het gaat hierbij vooral om de *timing* van de manoeuvre. Twee hypotheses worden opgesteld. Ten eerste kunnen vliegers time-to-contact (TTC) informatie gebruiken die wordt gepresenteerd door de expansie van de tunnel frames (de rechthoeken gevormd door de lijnsegmenten loodrecht op de kijkrichting). Met andere woorden, vliegers maken een schatting van de *tijd* die hen nog rest voordat het vliegtuig de overgang tussen het rechtlijnige en het circelvormige gedeelte van de tunnelbaan passeert. Ten tweede wordt gesteld dat vliegers een specifieke eigenschap van de tunnel contour (gevormd door de lijnsegmenten in het verlengde van de kijkrichting) kunnen gebruiken, het zogenaamde *tangent punt*. Met behulp van de beweging van dit punt op het display kunnen vliegers inschatten welke *afstand* hen nog rest voordat het vliegtuig de overgang tussen de twee stukken van de referentiebaan bereikt. In verschillende experimentele condities kunnen beide hypotheses worden bevestigd. Omdat de TTC informatie onafhankelijk is van de geometrische eigenschappen van zowel de tunnel als die van de bocht, is de TTC strategie onafhankelijk van de context, hetgeen leidt tot een robuuste strategie van de vlieger om de transitie manoeuvre te initiëren.

De experimenten geven aan dat de cybernetische, informatie-gerichte aanpak er in slaagt om de belangrijkste eigenschappen van de interactie tussen vlieger, display en vliegtuig nauwkeurig aan te wijzen. Het gebruik van modellen van het vlieger stuurgedrag leidt tot meer inzicht in de manier waarop de vliegers zich aanpassen aan de experimentele condities. De model-gerichte aanpak complementeert de traditionele wijze van experimenteren die vooral gericht is op het analyseren van prestatie- en werkbelasting-gerelateerde data bij het onderzoek naar menselijk gedrag. Echter, ook de beperkingen en onmogelijkheden van een model-gerichte aanpak worden aangetoond. Allereerst kan alleen de *totale* vliegerrespsonsie op de verschillende bronnen van visuele informatie die een bepaalde bewegingstoestand representeren, worden geïdentificeerd. Omdat het tunnel display altijd een zekere redundantie heeft in de aangeboden informatie, leidt het gebruik van modellen dan ook niet tot het gewenste resultaat om langs deze weg bepaalde voorkeuren tussen de verschillende informatiebronnen aan te tonen. Ten tweede is de hoeveelheid manieren waarop de vliegers zich kunnen aanpassen aan de experimentele condities zeer groot wanneer men de klassieke vliegtuigbesturing onderzoekt, waarbij meerdere lussen tegelijkertijd worden gesloten door de vlieger. Deze vrijheid leidt tot aanzienlijke verschillen in de aanpassing van het stuurgedrag tussen de vliegers onderling, en dit vooral in de binnenlussen, hetgeen het generaliseren van de resultaten sterk bemoeilijkt.

Hoewel het onderzoek zich concentreert op het tunnel display, biedt dit proefschrift een uitgebreid en actueel overzicht van de finesses van het toepassen van een model-gerichte aanpak. Een manier van experimenteren is ontwikkeld met als doel de model-matige aanpak te integreren met de traditionele aanpak van het meten een verzamelen

van voornamelijk prestatie-gerelateerde gegevens. Er wordt beschreven hoe experimenten moeten worden opgezet en uitgevoerd waarvan de verkregen data geschikt zijn voor het analyseren van vliegergedrag vanuit een regeltechnisch perspectief. De beperkingen van de niet-parametrische identificatie methoden in meer-assige besturingstaken met voor iedere as meerdere terugkoppellussen worden beschreven. Er wordt aangetoond dat de analytische berekening van de onzuiverheid (bias) en variantie van de verkregen schattingen van het vlieger stuurgedrag alleen mogelijk is voor enkel-assige stuurtaken met gebruikmaking van een parallel vliegermodel. Het gebruik van verschillende criteriumfuncties in de parametrische indentificatie, zowel in het tijd- als het frequentiedomein, wordt beschreven. Daarnaast is er een methode ontwikkeld om de Cramer-Rao ondergrens van de variantie in de geschatte vliegermodel parametervector te berekenen. Tenslotte wordt de toepassing van de twee meest vooraanstaande modellen voor menselijk stuurgedrag beschreven, namelijk een meer-assige versie van het crossover model en het optimal control model. Het proefschrift bevat twee duidelijke voorbeelden van het feit dat het gebruik van het optimal control model sterk wordt bemoeilijkt doordat dit model meer parameters bevat dan strikt noodzakelijk om het gemeten vlieger stuurgedrag te beschrijven.

Acknowledgments

Conducting a Ph.D. sometimes requires the attitude of a lone wolf. Nonetheless, the support of many people meant a lot to me.

Above all, the love of Loes, my parents and my brother Hans have made life what it is.

I always felt very lucky and happy with my two promotors, Bob Mulder and Henk Stassen. Their antagonistic attitudes towards my work were an ideal mix. Bob had the courage to let me free in determining the research objectives and supported me all the way with his encouraging enthusiasm, pushing me a little further every time. Henk always insisted on clarifying my thoughts and plans before plunging into yet another area of research, stimulating me to keep on the right track. Bob and Henk have shown to me that a promotor is more than a thesis supervisor.

I was very lucky indeed to know a real *guru*, René van Paassen. René simply knows the unknowable and is able to solve the insoluble. He helped me when things became *really* difficult, at least, for me (and most other people).

As a member of the Human-Machine Systems project group I enjoyed working with Ruud Hosman, who warned me for some of the pitfalls in human-machine systems research. I am grateful to Hans van der Vaart for introducing me into the field of ecological psychology. He often surprised me with his gift of looking at things from a different perspective.

During the development Human-Machine Laboratory I received much valuable support from Adri Tak, especially with the side-stick hardware. Henk Lindenburg and Peter Kraan provided all the necessary computer hardware. My brother Hans was always there to help me in solving the low-level computer programming problems.

An essential element in this project have been the experiments. I am very grateful to the three professional airline pilots, Arun Karwal, Bart Benard and Eric Kruysen, who acted as subjects in all experiments described in this thesis. Although some of the experiments were rather tiring, they remained enthusiastic about their collaboration.

Concerning the identification and model validation issues described in this thesis I received much help from René van Paassen (non-parametric), Chu Qi Ping (parametric) and Coen van der Linden.

I enjoyed my role as a graduation project supervisor a great deal for many students. Of course, I am especially grateful to all students who have collaborated in the tunnel-in-the-sky project: Wim van Dorp, Wytse Hoos, Koen van Engelen, AJ van der Hoek (X4) and Peter van Oorschot (X6).

During the PhD period I joined a room, in fact several rooms, with Jan-Willem van Staveren, Steve Hulshoff and Paul van Gool. Jan-Willem helped me with some signal-processing issues and has demonstrated to me an admirable persistence in his efforts to keep on working in difficult times. I enjoyed the company of Steve, whose help considerably improved some of my publications (he simply re-wrote them when I took another sip of coffee). Paul, the Golem, besides singing Elvis songs, always assisted me with a large number of often trivial computer and LaTeX problems and provided me with a nice thesis format.

I would like to thank my family and friends whose support after the tragic death of Hans has made it possible for me to finish this thesis.

Max Mulder   Pijnacker, September 1999

Curriculum vitae

Max Mulder was born on a warm Sunday afternoon, May 28 1967, in 's-Hertogenbosch. From 1979 to 1985 he attended the Katholieke Scholengemeenschap in Etten-Leur (KSE) where he obtained the VWO (Atheneum B) certificate.

In August 1985 he became an *adelborst* at the Royal Netherlands Naval College (KIM, Den Helder) to join the officer training program of the Royal Dutch Navy.

After being discharged from military service in August 1986, Max started his university career at the Faculty of Aerospace Engineering of the Delft University of Technology. In August 1992 he obtained his M.Sc. degree (ir) in Aerospace Engineering with a study into aircraft flight-path prediction algorithms to be applied in tunnel-in-the-sky displays.

In November 1992 he joined the Control and Simulation division as a Ph.D candidate. The main objective of his research project was to investigate the suitability of tunnel-in-the-sky displays for pilot manual control. The results of this investigation are the subject of this thesis. The research was conducted under supervision of prof.dr ir J.A. Mulder, prof.dr ir H.G Stassen, dr ir R.J.A.W. Hosman and dr ir J.C. van der Vaart.

From March 1998 to August 1999 Max collaborated in the *SIMULTAAN* project, an initiative of the Dutch simulation industry and research institutes, aimed at developing an advanced software architecture for real-time distributed simulation.

Since January 1999, Max has been co-responsible for teaching two graduate courses at the Faculty of Aerospace Engineering, *Avionics* and *Aerospace Human-Machine Systems*. Currently, he is an Assistant Professor at the Control and Simulation division.